THE GEOLOGY OF THE MOUNT TAYLOR AREA

New Mexico Geological Society
Special Publication 14

GEOLOGY OF THE MOUNT TAYLOR AREA

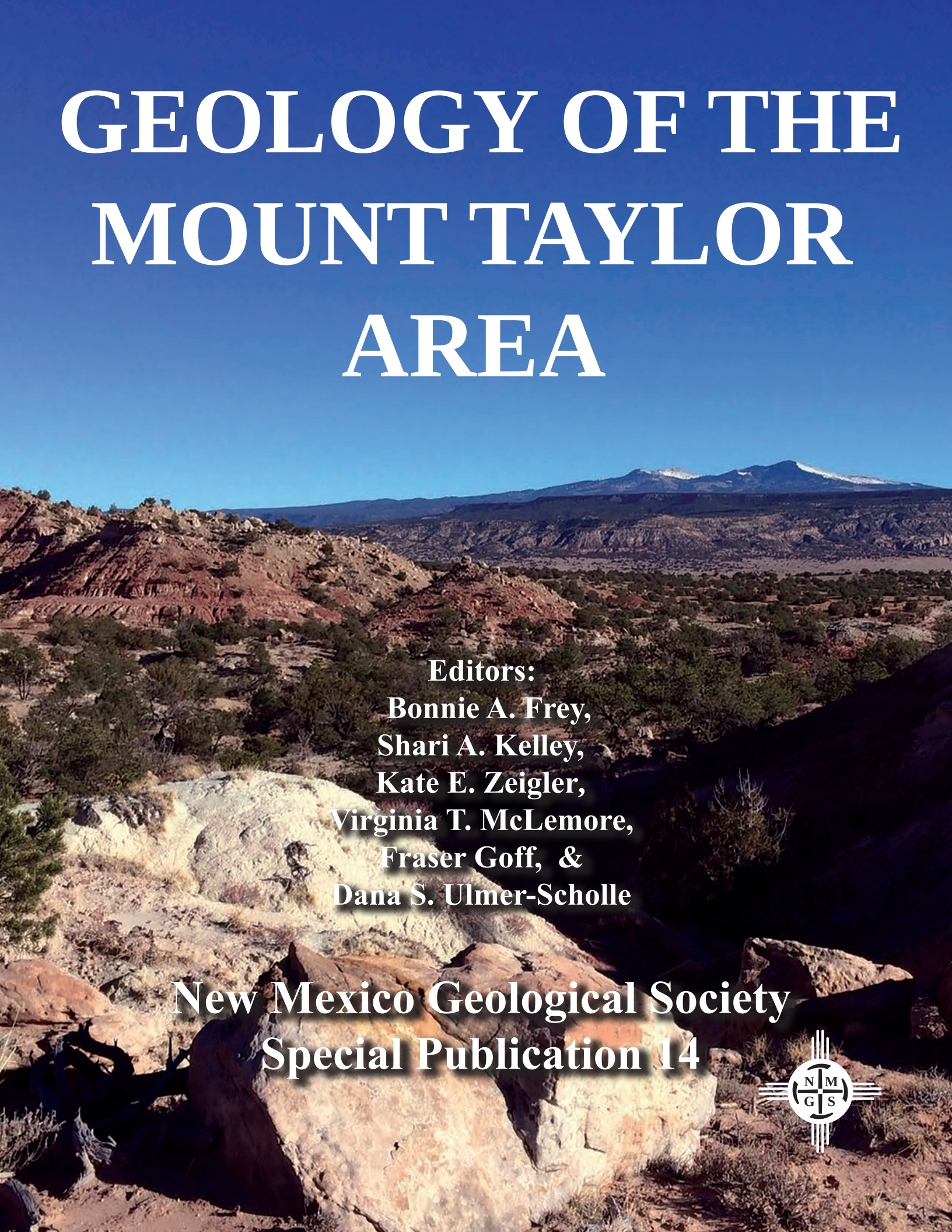

Editors:
Bonnie A. Frey,
Shari A. Kelley,
Kate E. Zeigler,
Virginia T. McLemore,
Fraser Goff, &
Dana S. Ulmer-Scholle

New Mexico Geological Society
Special Publication 14

The New Mexico Geological Society is a tax-exempt corporation registered in the State of New Mexico that promotes interest in geology and associated sciences, fosters scientific research and publications, encourages cooperation among its members, and stimulates interest in New Mexico geology. These goals are met through annual fall field conferences held in different locations in New Mexico or adjoining states and annual spring meetings, generally held in Socorro, New Mexico, where oral and poster presentations on different aspects of New Mexico geology are given.

NEW MEXICO GEOLOGICAL SOCIETY, INC.
801 LEROY PLACE
SOCORRO, NEW MEXICO 87801
https://nmgs.nmt.edu

Managing Editor: Dana S. Ulmer-Scholle
Design & Layout: Dana S. Ulmer-Scholle
Front Cover: Bonnie A. Frey
Title Page: Bonnie A. Frey
Back Cover: Bonnie A. Frey
Inside Back Cover: Kate E. Zeigler

ISBN NO. 1-58546-012-5
978-1-58546-012-0

https://doi.org/10.56577/SP-14

SPECIAL PUBLICATION 14
FIRST EDITION 2020

EDITORS' MESSAGE

We hope you will find New Mexico Geological Society Special Publication 14, which summarizes recent research in the Mount Taylor region, to be a useful resource. This publication was inspired by the 2019 publication of the geologic map of the Mount Taylor volcano by Fraser Goff and others and by recently completed investigations associated with "Energize New Mexico," a five-year, NSF-funded program that supported research in non-carbon emitting energy resources, including uranium resources.

The year 2020 has certainly been an interesting one. When the global coronavirus pandemic spread to the United States back in the spring, we were well along in the preparation of the 2020 NMGS Fall Field Conference road logs and guidebook papers. In June, we worked with the Executive Committee to make the decision to cancel the NMGS FFC for the first time in our organization's 71-year history. The decision was a hard one because of the uncertainty about how long the pandemic might last, but by June it was clear that the pandemic might linger into 2021. A virtual field trip was not really feasible. In the end, concern for the safety and health of our members guided us to postpone the field conference to September 2021. Since the guidebook papers had already been written, reviewed, and edited, and because many new thought-provoking data sets and ideas are presented in the papers, we decided to proceed with the publication of the technical papers as a digital special volume. Next year, the technical papers will be bundled with the road logs to be published as a paper guidebook, as usual.

Within this publication you will find papers about:

- the Mount Taylor volcano
- investigations regarding the ongoing impact of uranium mines
- historic reviews of uranium mining and milling activities in the Grants mining district
- discussions of regional stratigraphy and sedimentary provenance
- a review of Jemez lineament hypotheses
- the formation and geology of the Zuni Mountains
- and so much more!

Please join us in the exploration of the Mount Taylor region in 2021 year when our annual fall field conference returns.

DEDICATION

We gratefully dedicate this special publication about the geology of the Mount Taylor area to the Pueblo of Laguna. The Pueblo has supported and participated in both geologic and environmental research in and around Mount Taylor and Jackpile Mine. Mount Taylor is an important cultural site to the Laguna community. In addition, the Pueblo has been impacted by mining activities associated with uranium extraction in the area, including at Jackpile Mine.

The Pueblo of Laguna has been working with the New Mexico Bureau of Geology and Mineral Resources' mapping program for over a decade. Pueblo approval to access Laguna lands has facilitated the production of six STATEMAP geologic quadrangle maps. These maps were used to compile a geologic map of the Mount Taylor volcano, one of the featured works of the 2021 field conference.

The Laguna Environmental & Natural Resources Department (ENRD) also worked closely with several undergraduate and graduate students from New Mexico universities, whose studies focused on uranium mobility and the impact of mining activities at sites such as the Jackpile Mine in northern Laguna Pueblo. ENRD provided escorts, logistics, and site assistance to more than 10 university students and professionals who were participating in "Energize New Mexico," an NSF program dedicated to investigating energy industries that are not carbon emitters. This group of studies, which will also be featured during the 2021 field conference, was preceded by NMT soil and plant studies in the early 2000s and will continue with UNM and NMT health studies.

This research direction is indicative of the change in perspective toward mining that Laguna Pueblo has seen in the last one hundred years, from the 1950s "uranium capital of the world" to the modern focus on identifying hazards, remediating sites, and mitigating health effects, a focus described in McLemore et al. (this volume). Mining provided jobs for thousands in McKinley and Cibola counties, including members of the Laguna tribe. Mining also affected the health of citizens within the local communities.

The people of Laguna Pueblo have occupied the area since they migrated from Mesa Verde around 1300 A.D. or earlier. Their strong affinity with Mount Taylor, located only about 20 miles from the pueblo, is shared with many indigenous cultures, serving as a spiritual site and for hunting, grazing, farming, and collecting resources. Laguna Pueblo supported what became the successful 2008 designation of Mount Taylor as a Traditional Cultural Property, when the mountain became eligible for listing on the National Register of Historic Places.

Thanks to the Pueblo of Laguna for its dedication to this landscape and for their partnerships with the many groups working in the area.

The editors

PRESIDENT'S MESSAGE

What a year, huh? Normally, the NMGS president would begin an annual guidebook message by welcoming you to the 71st Fall Field Conference of the New Mexico Geological Society. But this is not a normal year. Instead, I am pleased to welcome you to Special Publication 14.

The 71st Fall Field Conference will be the first field conference to focus solely on the Mount Taylor area.

Some particularly compelling research on the impact of the uranium industry and the volcanic history of Mount Taylor is presented in the technical portion of the guidebook. Despite the delay of the field portion, we, the conference organizers and executive committee, felt that the technical material still needed to be published at this time, rather than waiting another year. The desire to release the current research has led to Special Publication 14, The Geology of the Mount Taylor Area.

As so many of you know, the goal of the Society is to promote interest in geology and foster scientific research in New Mexico. One of the primary ways the Society meets this objective is through the awarding of grants and scholarships. Despite not being able to meet face to face in 2020, the Scholarship Committee has been busy awarding the deserving and hardworking students of New Mexico colleges and universities with scholarships. This year the Society has awarded approximately $35,000 in scholarships to over 50 students. Awarding student scholarships is arguably the most rewarding component of Society involvement; none of which would be possible without the generous contributions of all of our members.

I will greatly miss seeing everyone this year and feeling the camaraderie that happens on the outcrop. While we wait another year to shake hands and share beers, I hope you will reach out to members you would normally only see once or twice a year and reconnect with them again this year, even if through a phone call or email. I am so proud to be part of this Society; a Society that produces extensive and impactful research for the state of New Mexico, and a Society with the most extraordinary members.

Until next time,

Shannon Williams

NEW MEXICO GEOLOGICAL SOCIETY FOUNDATION

The New Mexico Geological Society (NMGS) Foundation was established in 2003 with the mission of providing a source of funding for educational, and scientific objectives, which benefit the geologic profession in New Mexico and the general public. The NMGS has a distinguished history as one of the premier state geologic organizations in the country, dating to its founding 73 years ago in 1947. One of the primary attributes, that differentiates the NMGS from many state geological societies, is the ready access to world-class geologic outcrops and the effort to get young geoscience students out of the classroom and into this natural laboratory to gain hands-on experience during the annual Fall Field Conferences. NMGS Fall Field Conference organizers and presenters are at the forefront of their geoscience fields and use the latest technologies and applications that optimize students learning experiences and broaden their educational experience.

The NMGS Foundation was created as a Non Profit Organization (501(c)(3) Corporation) whose revenues are responsible for supporting activities that include the annual NMGS Fall Field Trip, NMGS Spring Meeting, numerous NMGS Grants-in-Aid to students undertaking geological research in the state of New Mexico, and scholarships to students attending 4-year colleges and research universities throughout New Mexico.

The objective of ensuring student participation in NMGS annual field trips and research events will continue the legacy of NMGS events as a premier nationwide destination for education in the geosciences. In that spirit, we invite you to join us in supporting the NMGS with a philanthropic gift. You can go https://nmgs.nmt.edu/donations to make your gift.

MEMORIAL

William (*Bill*) Lyman Chenoweth

In this volume, that features a location deep in uranium country, we memorialize one of the giants of uranium geology and a 66-year member of the New Mexico Geological Society (NMGS).

We remember Bill Chenoweth, who died in 2018, as the guy to go to if someone needed to know anything about uranium in the Western United States. Bill had a long career in the uranium industry, beginning as a student in New Mexico and culminating with nearly two decades working with the U.S. Atomic Energy Commission (AEC). He chaired the Nuclear Minerals Committee of the Energy Minerals Division of the American Association of Petroleum Geologists from 1983 to 1998 and spent his later years as a consultant to the Justice Department on the Radiation Exposure Compensation Act. His incredible memory for details and his meticulous record keeping were an invaluable resource to families of miners seeking compensation for radiation-related illnesses.

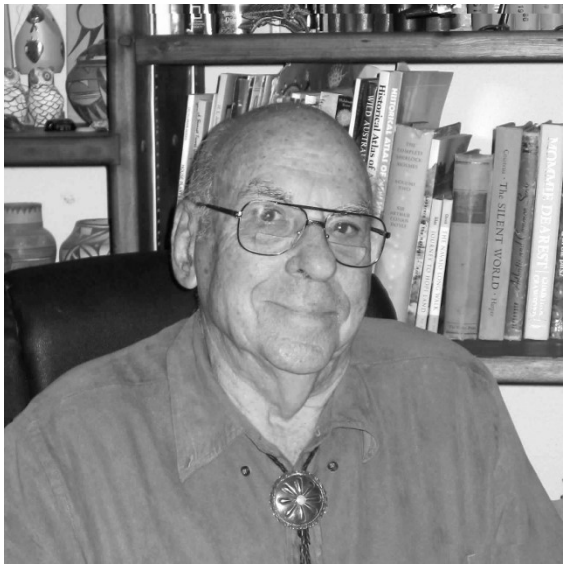

Bill received his bachelor's degree in geology from Wichita State University in 1951 and, while a student there, attended a summer field camp in the Zuni Mountains sponsored by the New Mexico School of Mines (now New Mexico Institute of Mining and Technology). After seeing New Mexico's geology, he decided to enroll in graduate school at the University of New Mexico, where he received a master's degree in geology in 1953. His thesis focused on the Morrison Formation in the southeastern part of the San Juan Basin, Valencia County, New Mexico – his first work funded by the AEC. After graduation, he worked on AEC uranium exploration drilling projects on, what was then called, the Navajo Indian Reservation, in northeastern Arizona and northwestern New Mexico, studying area uranium ore deposits for the next 11 years.

An added benefit of working in northwestern New Mexico was meeting his wife, Miriam (Polly) Pawlicki. They met in 1954 while she was the head nurse at the Indian Service Hospital in Shiprock, New Mexico. They were married on January 6, 1955, at Christ the King Mission in Shiprock. Their children, Mary and Martin, were born in Farmington, Peter in Flagstaff, and Paul in Grants.

In 1964, Bill was transferred from Grants to the AEC's main office in Grand Junction, Colorado. Although he was assigned to study uranium ore deposits in South Dakota and Wyoming, he continued to work on uranium deposits in New Mexico. Bill was appointed chief of the Geologic Branch in the Grand Junction office in 1970, responsible for the activities of the AEC geologists in the 14 western states. During this time, he examined all the major uranium mining areas in the United States. In 1983, his job was moved to Washington, D.C., by the Department of Energy. Rather than relocate, Bill began consulting and became a research associate at the New Mexico Bureau of Geology and Mineral Resources (NMBGMR), providing many unpublished mining records to the Bureau's mining archives and working with staff to compile the uranium mines databases now used by state and federal agencies.

Bill passed away in Grand Junction on July 23, 2018, at age 89. His legacy was extraordinary. He authored and co-authored more than 80 reports on uranium mining history, geology and resources in New Mexico, Arizona, Colorado and Utah. His most recent report – Uranium Resources, Volume C of Energy and Mineral Deposits in New Mexico, published as NMBGMR Memoir 50 and NMGS Special Publication 13 – won the 2018 Charles J. Mankin Memorial Award of the Association of American State Geologists). In 2019, Bill received a special tribute in a temporary historical photo exhibit in Grand Junction, where he had been secretary/treasurer of the Grand Junction Geological Society at the time of his passing. The exhibit marked the 75-year anniversary of that area's contribution to the Manhattan Project and the Cold War and recognized Bill for his research into the DOE's history in Grand Junction. Bill was inducted into the New Mexico Mining Association Hall of Fame on Sept. 5, 2019.

Virginia T. McLemore, NMBGMR

TABLE OF CONTENTS

VOLCANOLOGY/GEOCHRONOLOGY/GEOCHEMISTRY

ECONOMIC GEOLOGY

ENVIRONMENTAL GEOLOGY

STRATIGRAPHY

STRUCTURE

HYDROLOGY

NMGS COMMITTEES

2020 EXECUTIVE COMMITTEE

Shannon Williams, *President*.....Daniel B. Stephens & Associates
Dan Cadol, *Vice President*.....New Mexico Tech
Scott Baldridge, *Treasurer*.....Los Alamos National Laboratory
Brian Hampton, *Secretary*.....New Mexico State University
Dan Koning, *Past President*..... New Mexico Bureau of Geology and Mineral Resources

PUBLICATIONS COMMITTEE

David Lemke.....Retired Geoscientist
Virginia McLemore.....New Mexico Bureau of Geology and Mineral Resources
Barry Kues.....University of New Mexico
Adam Read.....New Mexico Bureau of Geology and Mineral Resources
Dana Ulmer-Scholle.....Scholle Petrographic, LLC
Steve Simpson.....New Mexico Tech
Chris Wolf.....Daniel B. Stephens & Associates

PUBLICATION SALES

Kelly Luster.....New Mexico Bureau of Geology and Mineral Resources
Elena Taylor.....New Mexico Bureau of Geology and Mineral Resources

SCHOLARSHIP

Kate Zeigler.....Zeigler Geologic Consulting
Susan Lucas Kamat.....New Mexico Environment Department
Dan Cadol.....New Mexico Tech

New Mexico Geological Society, Special Publication 14, Geology of the Mount Taylor Area, 2020, p. 1-15.

FACTS AND HYPOTHESES REGARDING THE MIOCENE–HOLOCENE JEMEZ LINEAMENT, NEW MEXICO, ARIZONA AND COLORADO

Fraser Goff[1] and Shari A. Kelley[2]

[1]Department of Earth and Environmental Science, New Mexico Tech, 801 Leroy Place, Socorro, NM 87801; candf@swcp.com
[2]New Mexico Bureau of Geology and Mineral Resources, 801 Leroy Place, Socorro, NM 87801

Abstract—The Miocene to Holocene Jemez Lineament (JL) consists of 10 volcanic fields stretching northeast from San Carlos in Arizona to Raton–Clayton in New Mexico and Colorado. We have tabulated data on volcanic style, magma composition, number of volcanic vents, age range, eruptive areas, eruptive volumes, presence of xenoliths and enclaves, significant sites, and significant references for all volcanic fields. The width of each field, based on total extent of mapped volcanic rocks perpendicular to the trend of the lineament, is highly variable; thus, as pointed out by others, magma ascent and volcanism cannot be controlled by a single fault or structure. Volcanic landforms are highly variable from field to field. Spatial-temporal trends are complex, and there is no systematic age progression in either direction; thus, the JL is not a hot-spot trend. There is also no compositional progression along the JL, although intermediate to silicic volcanism and tholeiitic basalts are most common toward the center of the lineament and the cross-cutting Rio Grande rift (RGR). Estimated surface areas and eruptive volumes of each field are highly variable. The Jemez Mountains volcanic field that formed at the intersection of the JL and RGR has erupted three times more volcanic products than all other volcanic fields combined. Recent geophysical studies have highlighted the presence of low-velocity (V_s<4.2 km/s) upper mantle all along the JL and have mapped stark differences in 2008–2010 JL seismicity on either side of the RGR. The only geothermal system along the JL with electrical potential (200–300°C) circulates within the 1.25 Ma Valles caldera (now a National Preserve), but low-temperature geothermal systems occur elsewhere along the JL. Two CO_2 gas fields are found at relatively shallow depths (≤1000 m) toward either end of the JL near the Springerville and Raton–Clayton volcanic fields. He- and C-isotopes indicate the gases are predominately derived from mantle sources. Extractable commodities have been perlite, pumice, sulfur and construction materials, and epithermal gold-silver was mined in the southeastern Jemez Mountains. The Grants uranium district underlies the Mount Taylor volcanic field, but a connection between remobilized (3 to 12 Ma) uranium deposition and magmatism has not yet been firmly established. Many researchers consider the older crustal structure beneath the JL to be a boundary between Proterozoic crustal provinces. Geophysical and geochemical observations support the idea that the Mesoproterozoic ancestry of this feature created fertile mantle lithosphere that has become part of the North American plate. Spacing between JL volcanic fields resembles volcano spacing found along many currently active subduction zones, although evidence for Paleoproterozoic arc-type volcanism is equivocal. Certainly, the alkaline affinity of volcanic rocks along much of the JL does not resemble the dominantly calc-alkaline magmatism of most subduction zones. Recent $^{40}Ar/^{39}Ar$ dating in the Raton–Clayton field indicates that the plate motion signal on time scales less than 1 Ma might constantly be present, but we currently do not have the spatial-temporal resolution to detect that pattern elsewhere along the JL.

INTRODUCTION

More than 60 years have passed since Mayo (1958) defined the Jemez Lineament (JL, aka, Jemez volcanic lineament) as an aid for mineral exploration (Fig. 1, Table 1). Simply stated, the JL is an apparent alignment of 10 volcanic centers stretching from east-central Arizona into the southeast corner of Colorado. The JL appears prominently on maps of late Cenozoic volcanic centers in New Mexico, Arizona and Colorado (Luedke and Smith, 1978a, b), which were designed for evaluations of igneous-related geothermal resources, volcanic hazards, volcano and volcano-tectonic studies and for general knowledge of volcanic rocks. Thereafter, the JL has been mentioned in numerous influential resource-, volcanic-, tectonic-, and seismic-focused papers about northern New Mexico (e.g., Chapin et al., 1978; Aldrich et al., 1981; Goff et al., 1981; Laughlin et al., 1982; Smith and Luedke, 1984; Aldrich, 1986; Spence and Gross, 1990; Magnani et al.,

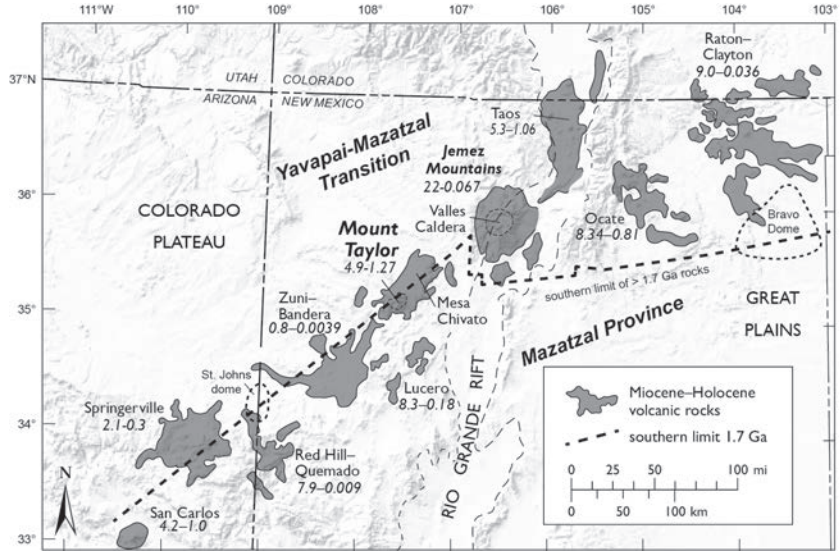

FIGURE 1. Index map showing the locations and age ranges (Table 1) of the volcanic centers that have been used to define the Jemez Lineament. The approximate boundary of the southern limit of 1.7 Ga metamorphic and igneous rocks (dashed line; Grambling et. al., 2015) and the Proterozoic provinces are also shown. The CO_2 gas fields along the JL are shown as dotted lines. The age units are Ma.

TABLE 1. General information on Miocene to Quaternary volcanic fields of the Jemez Lineament, Arizona, New Mexico and Colorado (Fig. 1).

Name, SW to NE	Volcanic Style	Magma Compositions	Number of Vents	Age Range	Eruptive Area (km^2)[1]	Estimated Volume (km^3)	Xenoliths & Enclaves	Significant Locations	References
San Carlos	Monogenetic flows, maar and diatreme	Basanite, alkali basalt and basaltic trachyandesite	3+	4.2 to 1 Ma?	≤50	≤1.5	Lherzolite	Peridot Mesa, Soda Springs vent and Black Hill	Wohletz, 1978; Holloway and Cross, 1978; Luedke and Smith, 1978a
Springerville	Monogenetic	Alkali basalt	405	2.1 to 0.3 Ma	3000	90	None reported	Cerro Hueco, Twin Knolls	Baldridge et al., 1989; Condit and Connor, 1996
(Mount Baldy)	(Alkalic shield)	(Trachyandesite to trachyte; minor basalt)	(20+)	(about 9 to 8 Ma)	335	33.5	(None reported)	(Mount Baldy and Mount Ord)	(Baldridge et al., 1989, p. 194)
Red Hill–Quemado	Monogenetic, some maars	Basanite, alkali basalt, basaltic andesite	40+	7.9 to 0.0094 Ma	≤200	≤6	None reported	Zuni Salt Lake (maar), Red Hill cone and maar	Crumpler and Aubele, 1990; McIntosh and Cather, 1994; Horning et al., 1996; Onken and Formen, 2017
Zuni–Bandera	Monogentic	Basanite, alkali to tholeiitic basalt; basaltic andesite	100+	0.8 to 0.0039 Ma	2460	75	Lherzolite	Bandera cone, El Calderon, McCarty's vent and flow	Laughlin et al., 1972; Luedke and Smith, 1978a; Laughlin et al., 1994; McIntosh, 1974
Lucero	Monogentic	Basanite, alkali basalt and tholeiitic basalt	25±	8.3 to 0.18 Ma	≤40	≤1.2	Lherzolite - granulite	Cerro Verde, Cerro Colorado, Black Mesa and Alkali Buttes	Baldridge et al., 1987, 1989; Zimmerer, person. comm., 2016
Mt. Taylor including Grants Ridge, Mesa Chivato and Puerco Necks	Stratovolcano of intermingled domes, flows, flanking monogenetic vents and plugs, and isolated domes	Basanite, basalt, trachybasalt, trachyandesite, trachydacite, trachyte, alkali rhyolite	300±	4.9 to 1.27 Ma	1700	≤120	Lherzolite, gabbro, norite, anorthosite, trochtolite, plus many mafic enclaves in andesitic–dacitic rocks	Mount Taylor, La Mosca, Grants Ridge, Cerro Chivato, Cerro Pelon, Cerro Redondo, Cerro Colorado, Cerro Aguila	Hunt, 1938; Lipman and Moench, 1972; Crumpler, 1980a, 1980b; Christiansen et al., 1983; Perry et al, 1990; Keating and Valentine, 1998; Goff et al., 2013, 2019, 2020
Jemez Mountains, Valles/Toledo calderas, Cerros del Rio and Santa Ana basaltic fields	Dome and flow complexes with intermingled lavas and tuffs, surmounted by two calderas with associated ignimbrites; flanked by three peripheral basaltic fields with some maars	Minor nephenlinite-basanite, alkali and tholeiitic basalt, trachyandesite, andesite, trachydacite, dacite, rhyolite and high-silica rhyolite	400 - 450	22 to 0.067 Ma	4400	2320	Granite, granulite, and other pre-caldera rocks in ignimbrites; mafic enclaves in andesitic-dacitic rocks	Valles caldera, Redondo Peak, Tschicoma Peak, Polvadera Peak, St. Peter's Dome, San Diego Canyon, Santa Clara Canyon, Battleship Rock, Cerro del Medio, Cerros del Rio, Montoso maar and Santa Ana Mesa	Smith and Bailey, 1968; Smith et al.,1970; Aubele, 1978; Eichelberger and Koch, 1979; Gardner et al., 1986; Self et al., 1986; Goff et al., 1989; Dunker et al., 1991; Gardner et al., 2010; Goff et al., 2011; Wolff et al., 2005, 2011; Kelley et al., 2013; Zimmerer et al., 2016
Taos Plateau	Broad basaltic shields, minor pillow basalt and maars with intermingled domes; very minor tuffs	Alkalic and tholeiitic basalts, basaltic trachyandesite, andesite, trachydacite, dacite and alkali rhyolite	150+	5.3 to 1.06 Ma	7000	420	None reported	Rio Grande Gorge, San Antonio Mtn, Taos Plateau, Black Mesa, Red Hill, No Agua dome, Cerro Chilfo, Cerro Negro	Lipman, 1969; Lipman and Mehnert, 1975; Dungan, 1987; Dungan et al., 1989; Thompson et al., 2015
Ocate (Mora)	Monogenetic flows and minor domes	Alkali basalt, minor andesite and dacite	45-50	8.34 to 0.81 Ma	1460	35	None reported	Wagon Mound fissure, Agua Fria, Cerrito Pelon, Cerro del Oro	Dungan et al., 1989; Nielsen and Dungan, 1985; O'Neill and Mehnert, 1988; Aubele and Crumpler, 2001
Raton–Clayton including Capulin	Monogenetic flows and cones of various ages intermingled with intermediate to silicic domes and flows	Basanite, alkali and tholeiitic basalt, trachybasalt, basaltic trachyandesite, trachyandesite and dacite; rare nephelinite	150+	9.0 to 0.036 Ma	3225 [2]	100	None reported	Capulin Mountain, Sierra Grande, Don Carlos Hills, Rabbit Ear Mountain, Carr Mountain	Stormer, 1972a, 1972b; Dungan et al., 1989; Aubele and Crumpler, 2001; Nereson et al., 2013; Zimmerer, 2019

[1]Measured from Luedke and Smith (1978a) or from sources cited in references column; estimated error ±20%.
[2]This area is the eruptive area from maps and GPS; see text.

2004, 2005; Schmandt and Humphreys, 2010; Nereson et al., 2013; Sosa et al., 2014; Channer et al., 2015). The objectives of this paper are to (1) describe the basic characteristics, (2) list some facts about the volcanic evolution, and (3) discuss some hypotheses about the origin and structure of the JL in order to place our new findings at Mount Taylor in a broader context (Goff et al., 2019, 2020).

FACTS REGARDING VOLCANISM ALONG THE JEMEZ LINEAMENT

Fact 1: Length of JL

When measured from the southeast edge of the San Carlos field (Peridot Mesa) to the northeast edge of the coalesced vent areas of the Raton–Clayton field, the JL is about 800 km long (Fig. 1; Luedke and Smith, 1978a, b). This length does not include long lava flows that extend into Oklahoma. The JL is not perfectly linear and has a pronounced right-stepping dogleg where it crosses the Rio Grande rift (RGR; Chapin et al., 1978). The JL west of the RGR follows the southeastern margin of the Colorado Plateau and the JL to the east cuts across the High Plains province.

Fact 2: Width of JL

The width of the JL is highly variable depending on the position and extent of coalesced vent and eruptive areas at each volcanic field (Fig. 1). For example, the maximum width based on total extent of mapped volcanic rocks perpendicular to the SW-NE trend of the JL is at the Springerville volcanic field (about 110 km wide) and at the Raton–Clayton field (about 125 km wide; Luedke and Smith, 1978a, b). However, the latter field has several pulses of volcanism and considerable open space among the various vents and flows (Stormer, 1972a; Dungan et al., 1989), thus an exact width of the field is equivocal. By comparison, the minimum width of the JL is at San Carlos (about 35 km wide).

Fact 3: The JL is not controlled by a single fault or set of structures

It should be clear from examination of Figure 1 and the remarks above that volcanic eruptions along the JL do not emanate from a single long fault, a narrow band of semi-parallel faults, an extended series of en-echelon faults, or a single deep-seated structure or zone of crustal weakness of northeast trend. JL volcanic fields and eruptive loci are too broad and too irregularly spaced to originate from a single structure or set of structures. We will elaborate on these points further in the "Proterozoic ancestry" section of this paper. Nonetheless, a few noteworthy but relatively short northeast-trending structures are found within the JL, such as (from southwest to northeast) the Cuates graben (N25E) in the Mount Taylor field (Goff et al., 2019), the El Malpais graben (N25E) in the Zuni-Bandera field, and the Jemez and Embudo fault zones (N55E) in the Jemez Mountains field (Aldrich, 1986). The Cuates graben contains 2.2 Ma monogenetic mafic vents and fault-controlled fissure vents (Goff et al., 2019), and the El Malpais graben is filled with the 3900-year-old McCartys and three older lava flows (Channer et al., 2015). The implied intersection of the Jemez and Embudo fault zones occurs beneath the Valles-Toledo caldera complex and associated rhyolitic volcanism.

Fact 4: The JL has a wide variety of volcanic landforms

The JL displays most if not all major volcanic landforms and structures (Table 1; Aldrich et al., 1981; Crumpler and Aubele, 2001; Crumpler, 2001): scoria cones, pahoehoe and a'a lava flows, lava shields, lava domes, blocky lava flows, extensive ignimbrites, volcanic necks and plugs, a large composite cone (Mount Taylor), many maar volcanoes, a few pillow basalts, the Valles-Toledo caldera complex, and two recognized diatreme (Wohletz et al., 1978; Goff et al., 2019). The only other stratovolcano along the JL is Sierra Grande, which is located in the center of the Raton–Clayton field and is primarily composed of two-pyroxene andesite flows that erupted 3.8±0.2 to 2.77±0.11 Ma (Stroud, 1997; Nereson et al., 2013). Sierra Grande, which is 10 km in diameter and has relief of 573 m above the Great Plains, is small in comparison to Mount Taylor but is a prominent landmark in this area. Truly, the variety of volcanic landforms along the JL contributes to New Mexico's oft-cited moniker as the "Volcano State."

Fact 5: Spatial-temporal patterns of volcanism are complex

The overall timing of volcanism along the JL from San Carlos to Raton–Clayton has no trend; thus the JL is not a hot spot track (Fig. 1; Luedke and Smith, 1978a; Aldrich, 1986), as stated by some researchers (e.g., Suppe et al., 1975; Morgan and Morgan, 2007). The youngest mafic rocks have erupted in the Zuni-Bandera volcanic field (McCartys and Bandera flows, about 4 and 10 ka, respectively; Laughlin et al., 1994; Dunbar and Phillips, 2004), and the youngest silicic eruptions formed in the Jemez Mountains volcanic field (East Fork Member rhyolites within Valles caldera at about 73–68 ka; Zimmerer et al., 2016). By comparison, the San Carlos field at the southwest end of the JL is 4.2 to 1.0 Ma (Wohletz, 1978; Holloway and Cross, 1978), whereas the youngest flow in the Raton–Clayton field is 36.6±6.0 ka (Zimmerer, 2019). Thus, the central JL has younger eruptions than the ends to the east and the west.

Interestingly, the increasing number of $^{40}Ar/^{39}Ar$ dates now available at individual volcanic fields reveals patterns indicating migration of activity toward the center of certain fields (Ocate, Raton–Clayton, Jemez; Olmstead and McIntosh, 2004; Nereson et al., 2013; Kelley et al., 2013, respectively). Recently published $^{40}Ar/^{39}Ar$ dates for nine vents in the Raton–Clayton volcanic field (368.2±7.3 ka to 36.6±6.0 ka) were combined with previously published dates to document a general pattern of eastward migration during the last 1.3 Ma that is not recognized in the older volcanic rocks in this field (Zimmerer, 2019).

Fact 6: The JL has no compositional progression

There is also no compositional progression of volcanism along the JL. Most volcanic products are alkaline to slightly alkaline (see Table 1 and references therein). Highly silica-undersaturated rocks erupted toward either end of the JL; nepheline-bearing trachytes are found in the Mount Baldy area of the Springerville field (Baldridge et al., 1989), and feldspathoidal lavas are observed in the Raton–Clayton field (Stormer, 1972b; Dungan et al., 1989). Some older nephelinite lavas were erupted in the southern Jemez Mountains volcanic field (Wolff et al., 2005), and a single nephelinite dike was discovered south of the Mount Taylor field (Goff et al., 2019). Some calc-alkaline rocks were produced toward the center of the JL at Mount Taylor (Goff et al., 2019; 2020), the Jemez Mountains volcanic field (Tschicoma Formation; Goff et al., 1989; Rowe et al., 2007; Kelley et al., 2013) and in the Taos field (Dungan, 1987; Dungan et al., 1989). Alkalic mafic rocks such as basanite are common within most of the JL but tholeiitic basalts are most common in the Jemez Mountains and Taos fields (Gardner et al., 1986; Wolff et al., 2005; Kelley et al., 2013; Dungan et al., 1989).

Fact 7: Surface areas of individual fields

The surface areas of most JL volcanic fields have been estimated previously (Table 1, see references) or by the current authors using available maps and other resources. For example, the area of Mount Baldy eruptions, sometimes included with the Springerville field, is calculated at 335 km^2 from the map in Baldridge et al. (1989, fig. 8). Some reported areas are unusually large. For example, the reported area of the Raton–Clayton field is 19,400 km^2 (Stormer, 1972b; Dungan et al., 1989, p. 474; Aubele and Crumpler, 2001), but examination of various maps (i.e., Luedke and Smith, 1978a) shows considerable open space between eruptive units. Most recently, Nereson et al. (2013) used GIS to calculate the total land-surface area covered by lava flows in the Raton–Clayton field to be 3225.5 km^2 and in the Ocate field to be 1457.6 km^2 (±20%). That being the case, we calculate the total surface area of eruptive products along the JL to be 23,870 km^2 (Table 1) with an estimated error of ±20%.

Fact 8: Erupted volumes of monogenetic fields

The erupted volume of most JL fields has not been calculated except for the Jemez Mountains and Mount Taylor, which have relatively large effusions of intermediate to silicic products (see below). The calculation of the volume of eruptive products is important in the assessment of volcanic hazards through the evaluation of the length of time, rates, and explosive behavior associated with past eruptions. These calculations are also valuable in estimating the flux of gases released during the formation of volcanic fields, as described later in this paper. Indeed, volumes are difficult to calculate because in most cases thickness is highly variable due to topography, and drill hole thicknesses over the given areas are not widely determined. For monogenetic lava fields, we have estimated an average thickness of 30 m based on our observations of variable lava flow thicknesses at many of these fields. In truth, most flows are not 30 m thick over broad areas, but this estimate accommodates increased thicknesses in ravines, vents and cones. Thus, the estimated volume of the Springerville field, considered to be one of the three largest monogenetic fields in the United States, is 90 km^3. For the Taos volcanic field, we have raised the average thickness to 60 m to accommodate canyon exposures along the Rio Grande gorge and the thicknesses of several large intermediate composition domes. The resulting estimate is 420 km^3. This estimate is not unreasonable, because Dungan et al. (1989) have calculated the volume of the extensive Servilleta Basalt component of this field at 200 km^3. Thus, the total erupted volume of (primarily) monogenetic fields is estimated at 880 km^3 with an estimated error of ±20%.

Fact 9: Erupted volumes of Mount Taylor and Jemez Mountains volcanic fields

Our estimate for the volume of the Mount Taylor stratovolcano is about 85 km^3 (Goff et al., 2020). Perry et al. (1990) estimated a volume of between 25 to 30 km^3 for monogenetic mafic lavas on surrounding mesas including Mesa Chivato. Recent detailed mapping on southwest Mesa Chivato (Goff et al., 2019) has recognized a 4-km-wide northeast-trending graben (Cuates graben) along the axis of Mesa Chivato that presumably contains previously unaccounted for ponded lavas. Additionally, Mesa Chivato contains a few trachyandesite to trachyte domes and flows (Crumpler, 1980a, b; Goff et al., 2019). The current authors generously estimate the volume of Grants Ridge Rhyolite center, associated mafic lavas, and the many volcanic necks along the Rio Puerco at ≤2 km^3. Thus, the total erupted volume of the Mount Taylor field is probably around 120 km^3.

Gardner (1985, p. 150) first calculated the volume of the main portion of the Jemez Mountains volcanic field at 2100 km^3. This total included 1000 km^3 for the "original" Keres group, 500 km^3 for the now-obsolete Polvadera Group (presently part of the Keres Group, see stratigraphic revisions in Goff et al., 2011, and Kelley et al., 2013), and 600 km^3 for the Tewa Group, mostly consisting of the Valles/Toledo calderas and the Bandelier Tuff. The volume of the Tewa Group, particularly the Bandelier Tuff, has since been raised to 800 km^3 because of geothermal drilling intercepts through intracaldera tuffs acquired in the 1980s and early 1990s (Goff, 2010; Goff et al., 2011). The volume of three monogenetic lava fields peripheral to the main Jemez Mountains field (El Alto, Cerros del Rio and Santa Ana Mesa) is estimated at ≤20 km^3 from maps and from the assumptions discussed above, insignificant when compared to the volume of the main Jemez Mountains field. Thus, the revised estimate for the Jemez Mountains volcanic field is 2320 km^3 or nearly 3 times greater than the combined erupted volume of all other volcanic fields along the JL.

Fact 10: JL P- and S-wave velocity anomalies

Several seismic experiments, including 2-D refraction and reflection lines and 3-D teleseismic arrays, have been deployed across the JL to assess the thermal state of the underlying mantle. These experiments include CD-ROM (Continental Dynamics–Rocky Mountains; Dueker et al., 2001; Yuan and Dueker, 2005; Zurek and Dueker, 2005, Magnani et al., 2004, 2005), LA RISTRA (Colorado Plateau–Rio Grande rift–Great Plains Seismic Transect; Gao et al., 2004; West et al., 2004; Wilson et al., 2005), and the Earthscope USArray transportable array (TA), which had a station spacing of 70 km across the United States. Over the years, several investigators have inverted various combinations of body and surface wave and receiver function information from all of these datasets to image the mantle and crust across the RGR and along the JL. Spence and Gross (1990) were the first to recognize low-velocity mantle beneath the JL using teleseismic data; these researchers were surprised to find that the mantle velocity anomaly beneath the JL was more robust than the signal from the RGR.

P- and S-wave travel time delays observed along the northwest-oriented LA RISTRA line were used by Gao et al. (2004) and West et al. (2004) to image an approximately 200-km-wide low-velocity zone centered on the RGR that extends to depths greater than 200 km, with S-wave velocities (V_s) as low as 4.2 km/s. This value is 6-7% below the global average and is indicative of partial melt. Wilson et al. (2005) used receiver functions to demonstrate that the small-scale convection associated with the RGR is restricted to the upper mantle. In contrast, the S-wave velocities beneath the JL where the LA RISTRA line passes across Mount Taylor (4.3–4.4 km/s at 70 km) are not as low as those beneath the RGR along this particular transect (Gao et al., 2004; West et al., 2004; Wilson et al., 2005). Here, the low mantle velocities associated with the RGR are the more robust signal.

The CD-ROM refraction line across the eastern JL (Fig. 2) indicates that the crust is thinner and that upper mantle velocities are lower under the JL compared to areas to the north in Colorado (Snelson et al., 2005; Levander et al., 2005). Other data collected as part of the CD-ROM experiment, including seismic reflection (Magnani et al., 2004, 2005) and passive seismic surveys (Yuan and Dueker, 2005; Zurek and Dueker, 2005), reveal complex crustal structure and low P- and S-wave velocities in the mantle beneath the JL near Las Vegas, New Mexico, along the northern edge of the Ocate volcanic field (Figs. 2, 3). Data from these profiles will be discussed further in the "Proterozoic ancestry" section.

More recent work by Schmandt and Humphreys (2010) used available body-wave data to show that, at a depth of 90 km, the entire JL and the southeastern margin of the Colorado Plateau are underlain by low-velocity mantle that extends down to at least 195 km. Lin et al. (2014) identified low S-wave velocities in the lower crust over a broad region that includes the southern Rocky Mountains, the western JL/eastern Colorado Plateau transitional boundary, and the High Plains of northeastern New Mexico. Fu and Li (2015) investigated mantle structure using radial anisotropy. Positive radial isotropy characterizes the JL

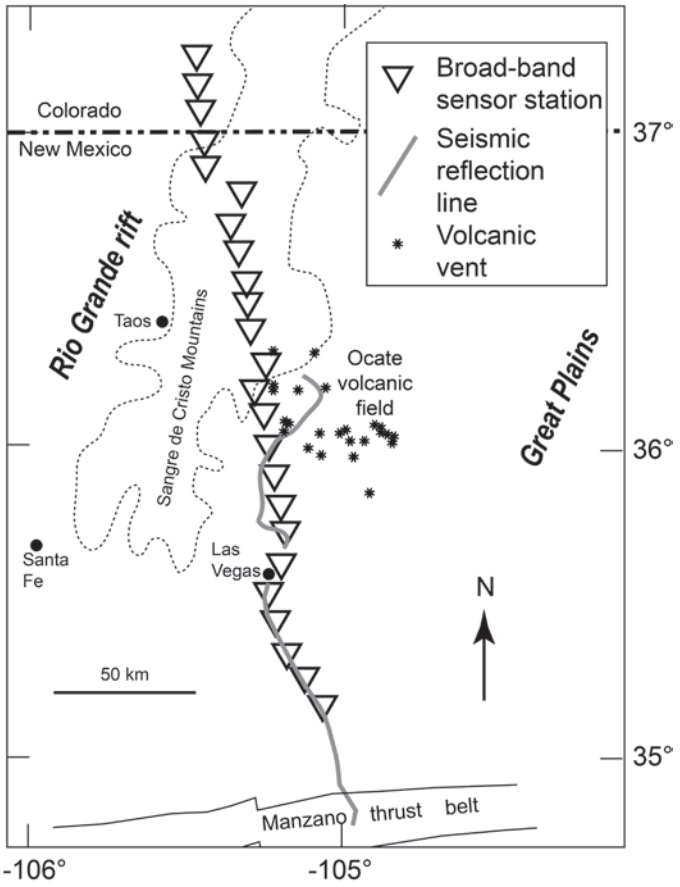

FIGURE 2. Map of the location of the CD-ROM seismic reflection line (Magnani et al., 2005) and the passive seismic array (Zurek and Dueker, 2005; Yuan and Dueker, 2005) relative to the Ocate volcanic field on the JL.

west of the RGR, indicating horizontal alignment of magma in the form of sills. In contrast, negative radial anisotropy is more common in the eastern lineament, suggesting the presence of vertical dikes or zones of migrating melts. Sosa et al. (2014) used LA RISTRA and TA data to create a 3-D model of the area surrounding the RGR. Like Gao et al. (2004) and West et al. (2004), Sosa et al. (2014) found low-velocity mantle at shallow depths below the RGR and low-velocity mantle along the eastern margin and below the Colorado Plateau.

Shen and Rizwoller (2016) inverted seismic data from the TA across the entire United States; this analysis identified well-known seismic velocity anomalies in the western United States, as described above, and discovered previously unrecognized anomalies in the midwestern and eastern United States. This inversion indicates that S-wave velocities are less than 4.2 km/s at depths greater than 70 km along the southeastern margin of the Colorado Plateau, along the RGR, and along the projection of the JL onto the High Plains as far east as the western edge of the Raton–Clayton volcanic field, near Capulin and the other young volcanic centers in that field. Based on recent experimental work by Takei (2017), Schmandt et al. (2019) note that V_s<4.2 km/s at 75 km is likely indicative of small percentages of partial melt.

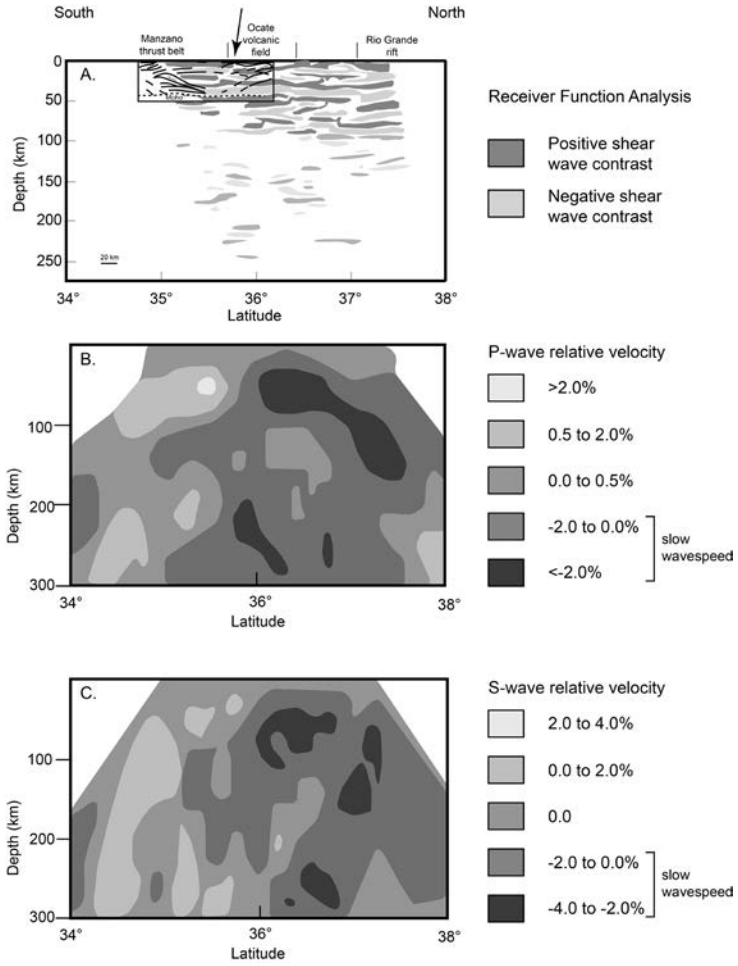

FIGURE 3. **A**) Receiver function inversion results of Yuan and Dueker (2005) and the interpretation of the seismic reflection data of Magnani et al. (2005; black lines in box near the surface between latitudes ~35° and ~36°) showing the duplex structure. The arrow points to a significant break in crustal layering, as discussed by Zurek and Dueker (2005). Note that the layering in the mantle that is imaged by the receiver function analysis is more prominent on the north end of the line. **B**) P-wave velocity inversion (Yuan and Dueker, 2005). **C**) S-wave velocity inversion (Yuan and Dueker, 2005). The darker shading in (B) and (C) highlights the relatively low P- and S-wave velocities in the mantle beneath the JL and the RGR, which are interpreted to represent mantle that is hot and/or contains partial melt. All four seismic data sets are at the same scale.

Fact 11: JL seismicity

Nakai et al. (2017) summarize seismicity in the vicinity of the JL during the timeframe when the Earthscope US Array TA and the CREST (Colorado Rockies Seismic Transect) seismic networks were deployed in Colorado and New Mexico between 2008 and 2010. The seismicity is starkly different in the western and eastern sections of the JL. Most notable is the aseismic nature of the eastern JL, which is bounded by areas of seismicity to the northwest and the southeast—a so-called "seismic halo." The seismicity to the northwest has been tied to coal-bed methane production in the Raton Basin (Rubenstein et al., 2014), but the band of seismicity to the southeast of the JL aligns with a zone of seismicity first recognized by Sanford et al. (2002). An earthquake recorded in 2010 in this area had a moment tensor indicative of strike-slip faulting. Possible hypotheses to explain the pattern of seismicity in the eastern JL will be discussed later in the "Proterozoic ancestry" section.

The alignment of seismicity along the JL west of the RGR is complex, alternating between N5E (rift structures) and N65E (Nakai et al., 2017). These authors note that the seismicity is inboard of the physiographic margin of the Colorado Plateau. Earthquakes are concentrated along the western JL, indicating complex deformation associated with the transition from northwest-southeast extension in the southeast Colorado Plateau and east-west extension within the Rio Grande rift. These authors point out the lack of seismicity in the Jemez Mountains. Sanford et al. (1991) and House and Roberts (2019) also note an absence of seismicity beneath the Valles caldera west of the RGR. Aprea et al. (2002) attribute this paucity to ductile deformation in proximity to a magma body.

An unusual northeast-trending swarm of 49 earthquakes (M_L 0.8–2.0) occurred over the course of a year (starting in November of 2008; most were within the first 60 days) in Zuni Canyon, which is on the north flank of the Zuni Mountain near the terminus of one of the Zuni-Bandera lava flows (Nakai et al. 2017). The activity migrated toward the southwest during the swarm. In the Mount Taylor region, the small earthquakes measured between 2008 and 2010 (M_L 1.0–2.5) form a diffuse, northeast-trending array on Mesa Chivato (Fig. 4). One swarm lies at the northeast tip of the mesa on a N25E-trending structure that parallels the faults of the Cuates graben of Goff et al. (2019).

Fact 12: JL electrical resistivity

Feucht et al. (2019) measured electrical resistivity of the crust and upper mantle using magnetotelluric methods along a profile line at latitude 36.25° that crosses the JL in the vicinity of the Ocate volcanic field and the very western end of the Raton–Clayton field. Both broadband and long period instruments were used. The phase-tensor azimuths are bimodal, striking northwest (N25W, paralleling the tipper strike) and northeast (N75E), indicative of anisotropy. The upper crust is resistive to depths of 15–25 km, and the middle to lower crust is conductive under the rift. The conductive zone is present both east (150 km) and west (100 km) of the rift. Measurements of the electrical fields are sensitive to north-south and east-west orientations of features along two-dimensional profiles, and the data collected during this study record strong anisotropy parallel to and perpendicular to the rift (Feucht et al., 2019). In detail, the electrical resistivity structure sensed by east-west electrical fields shows pockets of conductive material less than 50 ohm-m in the vicinity of the Ocate (40 km) and Raton–Clayton (25 km) volcanic fields. The short segment of the mantle lithosphere imaged beneath the High Plains north of the primary trend of the JL is resistive (100–1000 ohm-m).

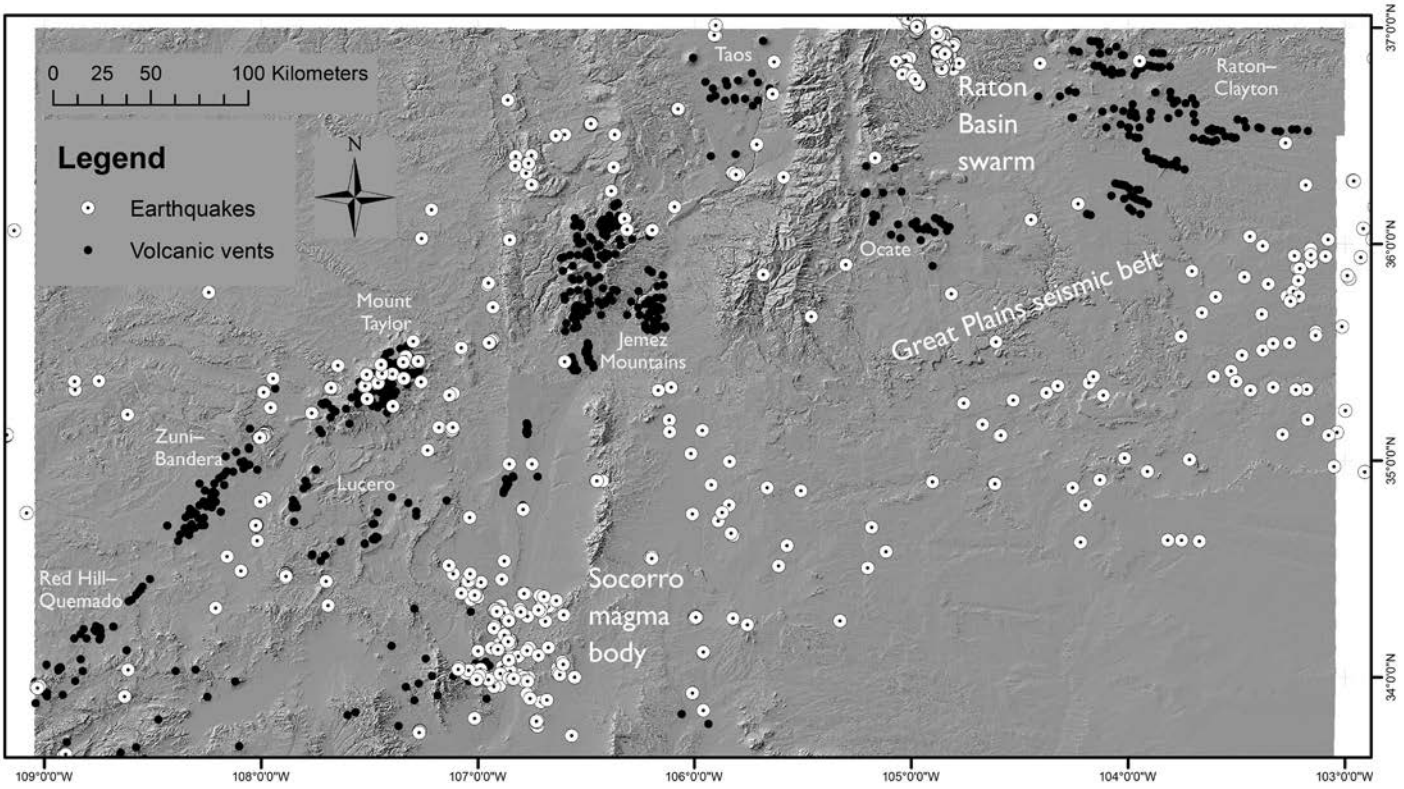

FIGURE 4. Earthquakes detected between 2008 and 2010 by Nakai et al. (2017) across northern New Mexico and volcanic vents in the JL. Note the clustering of earthquakes in the Raton Basin, which likely have an anthropogenic origin (Rubinstein et al., 2014), and the diffuse northeast-striking band of earthquakes south of the Ocate and Raton–Clayton volcanic fields. Also note the difference in the alignment of vents east and west of the RGR.

Fact 13: JL heat flow

Heat flow distribution and maps for the High Plains of northern New Mexico and southern Colorado were presented in a series of papers by Reiter et al. (1975), Edwards et al. (1978), and Swanberg (1979). A broad thermal anomaly that is characterized by an average heat flow value of 100 mW/m^2 (60–138 mW/m^2) has been observed at the boundary of the southern Rocky Mountains and the High Plains in the Raton Basin near Ocate and Raton–Clayton volcanic fields (Reiter et al., 1975; Edwards et al., 1978; Swanberg, 1979; Kelley, 2015). For comparison, heat flow on the Taos Plateau in the RGR is 115–130 mW/m^2 (Reiter et al., 1975).

Less is known about heat flow west of the RGR in the vicinity of the JL. Heat flow values in the general vicinity of Mount Taylor are 69–107 mW/m^2 (Eggleston and Reiter, 1984). Heat flow values in the Zuni-Bandera field are 75–191 mW/m^2 (Minier, 1987), and values in the Red Hill to Zuni Salt Lake region are highly variable at 43–170 mW/m^2. The 170 mW/m^2 value is associated with 13.4–9.9 ka Zuni Salt Lake maar (Onken and Forman, 2017). Recent work by Kelley et al. (2016) in the general vicinity of the 8.3 to 0.192 Ma Lucero volcanic field (Baldridge et al., 1987) suggests that two distinct bands of water wells located near the Hickman and Red Lake fault zones on the margins of the Acoma basin tap the San Andres-Glorieta aquifer and have elevated discharge temperatures of 34 to 52.8°C (depths 615 to 884 m).

In contrast, deep conductive heat flow in the central Jemez Mountains within the western Valles caldera is 200–400 mW/m^2 and can exceed 450 mW/m^2 (Sass and Morgan, 1988), which can only be caused by magma underlying the caldera at 7±1 km depth (Aprea et al., 2002). This is 2.7 times greater than maximum heat flow along the RGR and 4 to 5 times greater than heat flow along the rest of the JL.

Heat flow contour maps drawn by Edwards et al. (1978) and Blackwell et al. (2011) show elevated heat flow that roughly follows the JL. The elevated heat flow zone also wraps around the southeastern and southern edge of the Colorado Plateau. Elevated heat flow greater than 100 mW/m^2 associated with the RGR is also highlighted on these maps.

Fact 14: Geothermal systems along the JL

Considerable research since the middle 1970s shows that the only high-temperature geothermal system along the JL, and indeed in all of New Mexico, circulates within the southwest segment of the Valles caldera (Goff and Gardner, 1994; Goff and Janik, 2002). The Valles system consists of a near-boiling to boiling, gas-rich acid cap overlying a 200 to 300°C, chloride-rich brine at depths of 0.4 to 2 km. Although capable of producing modest amounts of electric power (20-30 MWe), the geothermal resource has been retired and is now part of the Valles Caldera National Preserve (Goff and Goff, 2017). Hot springs that discharge along the Jemez fault zone in Cañon de

San Diego are part of a hydrothermal outflow plume originating in the caldera and do not have high-temperature geothermal applications.

Several other hot springs and shallow thermal aquifers occur within the JL and its broad dogleg across the north-central RGR (Fig. 1; e.g., Goff and Goff, 2015; see Summers, 1976, for a comprehensive citation list). All such sites have had geothermal evaluations conducted at some time during the last 40+ years (Montezuma, Ojo Caliente, Taos area, San Ysidro/Jemez Pueblo, Lucero, Acoma Basin, Upper Frisco, Springerville). None of them have electrical potential, one is a successful commercial spa, one has possible green-house potential and most are currently "wild" (e.g., Stone, 1979; Vuataz et al., 1984; Albrecht et al., 2011; Goff and Goff, 2017; Blomgren et al., 2016).

An underground aquifer reported to be at least 40°C circulates at depths of ±1500 m in the large uranium mines flanking the northwest and east sides of the Mount Taylor volcanic field (Goff et al., 2019). This aquifer (or aquifers) has never been evaluated for geothermal potential, but the reported temperature and depth would match measured geothermal gradients in this region (25 to 35°C/km) and calculated heat flow of about 105 mW/m^2 (Nathenson et al., 1982). The age and volume of volcanic rocks in the Mount Taylor region are too old and too small (≥1.3 Ma; 120 km^3) to indicate much, if any, high-temperature geothermal reservoir potential (T≥200°C; Duffield and Sass, 2003).

Fact 15: CO_2 gas fields along the JL

Two carbon-dioxide (CO_2) gas fields, influenced by relatively young magmatism and high thermal gradients in the region, are located within the JL. The 3600 km^2 Bravo Dome CO_2 gas field is found in the southeastern portion of the Raton–Clayton volcanic field (Fig. 1; Broadhead, 1990, 2019; Sathaye et al., 2016; Brennan, 2017). The "discovery well" was drilled in 1916 to a depth of 763 m. Although this was an oil test well, 25 million cubic feet gas per day (MCFGPD) was produced from the Permian Tubb Sandstone. By the 1930s, a few wells from the field supplied gas to a processing plant that sold dry ice and bottled CO_2 to markets in Colorado and surrounding states. This enterprise went out of business long ago; now, the Bravo Dome field is unitized and supplies CO_2 gas by pipeline south to the Permian Basin oil fields of west Texas and southeastern New Mexico for enhanced oil recovery. About 47 trillion cubic feet of gas was produced between 2004 and 2018.

The gas in this field is nearly pure, greater than 98 mol-% CO_2 and is primarily produced from the Tubb Sandstone. The overlying Cimarron Anhydrite seals the reservoir. However, carbon and helium isotope studies show that the gases are mantle derived and rise in the north part of the field adjacent to the Raton–Clayton volcanics (Gilfillan et al., 2008; Brennan, 2017). The estimated pre-production volume of trapped gas at Bravo Dome is 1.3 Gt (Sathaye et al., 2016).

Although isotopic data indicates a mantle origin for the gases, the vast quantities of CO_2 in the Bravo Dome field have elicited controversy (Broadhead, 1990; Sathaye et al., 2014). Could all that CO_2 really come from the mantle or melts within it? Assume for the moment that the gas originated solely from degassed mafic magma along the JL in the Raton–Clayton volcanic field. The maximum solubility of CO_2 in tholeiitic to basanitic magma at 1100°C and 15 kbar (60 km) is roughly 4500 ppm (0.45 wt-%, Holloway and Blank, 1994, fig. 14A). The original volume of gas in the field (1.3 Gt) requires 290 x 109 metric tons of mafic magma to degas. The density of mafic magma is roughly 3 g/cm3 or 3 x 109 metric tons per km3. Thus, the original volume of unproduced gas could come from 96.6 km3 of mafic magma. Coincidentally, this volume is about the same as the volume of erupted products at the Raton–Clayton volcanic field (100 km3±20%, Table 1). Thus, deep magmatism along the JL is a plausible source for the CO_2 at Bravo Dome.

The 1800 km^2 St. Johns CO_2 gas field is located in east-central Arizona in the northwest part of the Springerville volcanics. Although the first gas well was drilled in 1939, this field is less studied than Bravo Dome (Rauzi, 1999; Gilfillan et al., 2008; Eastman and Muir, 2012). The main CO_2 reservoirs are in sandstones of the Permian Supai Formation (200 to 700 m deep) that directly overlie Proterozoic basement at depths of 800 to 1300 m. Intercalated anhydrite beds in the Supai provide localized seals or cap rocks to the CO_2. Since the mid-1990s, producers have intended to ship gas by pipeline to the Permian Basin for enhanced oil recovery, but financing for this endeavor was never successful. A secondary intent, also unsuccessful, was to separate and sell helium gas. More recently, a DOE-financed project intends to develop an enhanced geothermal (or "hot dry rock") project in Proterozoic basement using compressed CO_2 as the heat exchange fluid rather than water (Eastman and Muir, 2012). Gas compositions at the St. Johns field are variable, about 83 to 98 mol-% CO_2, yet the carbon and helium isotope values indicate a mantle origin for these constituents (Gilfillan et al., 2008). Presumably, the source for the gases is the Springerville magmatic system. Estimated CO_2 reserves are 445 billion m^3. This volume of gas is considerably smaller than the original volume of gas trapped at the Bravo Dome field (1.3 Gt); thus, degassing of deep mafic magma in the Springerville area of the JL is a reasonable source for the CO_2 trapped in the St Johns field.

Fact 16: Mineral/ore deposits associated with volcanism along JL

Ignoring sand, gravel, road metal, and cinder quarries, there are several locations along the JL where volcanism has formed extractable mineral deposits. Of course, pre-Puebloan and later Native American cultures mined obsidian from specific rhyolite domes and tuffs in the Jemez Mountains, Taos, and Mount Taylor volcanic fields (Shackley, 1998, 2005; Glascock et al., 1999; Shackley and Goff, 2016). Pumice has been mined extensively from both the basal pyroclastic fall deposits of the Otowi Member, Bandelier Tuff (Guaje Pumice Beds), and from the El Cajete Pyroclastic Beds in the Jemez Mountains volcanic field (McLemore and Austin, 2017). The pumice is used for construction, decorative stone, abrasives, and stone-

washed jeans. Small amounts of pumice were sporadically mined from the east end of Grants Ridge Rhyolite center in the Mount Taylor volcanic field during 1941 to 1967 (McLemore and Austin, 2017).

New Mexico is the leading producer of perlite in the United States. Perlite is extracted from several large mines in the No Agua rhyolite domes and flows of the Taos volcanic field. Perlite was mined from 1953 to 1991 at the Grants Ridge Rhyolite center in the Mount Taylor volcanic field. Perlite also occurs in older rhyolites and tuffs in the southern Jemez Mountains volcanic field but has not been mined (McLemore and Austin, 2017).

Epithermal gold-silver quartz veins and related base metals were explored and mined in the Cochiti mining district in the southeast Jemez Mountains volcanic field from the late 1880s until about 1916. Sporadic production continued into the 1940s (Hoard, 2007), and several mining companies reexamined the district into the 2000s. The ore is high-grade but low tonnage; gold values are highest near the tops of the veins. Mineralization is associated with 7 to 6 Ma Bearhead Rhyolite dikes, small intrusions, domes and flows (WoldeGabriel and Goff, 1989). An estimated $1.4 million dollars in gold, silver, copper, and lead was produced from 1894 to 1963, but the value of Jemez Mountains pumice (estimated $31 million) exceeds the value of precious metals (McLemore and Lueth, 2017). The forest fires of 2011 in the southeast Jemez Mountains have now made this mining district nearly inaccessible. Additional major gold-silver mining districts, such as the Old and New Placers, Cerrillos, and Elizabethtown-Baldy deposits (McLemore and Lueth, 2017), lie along the JL, but the ages of source volcanic and intrusive rocks pre-date the age of volcanism along the JL.

Until the 1980s, the Grants district was the largest uranium producing area in the United States and was possibly fourth worldwide. Two large mines lie on opposite sides of Mount Taylor; San Mateo is to the northwest and Jackpile is to the southeast. Several hundred bore holes were drilled through the volcanic rocks to trace uranium-bearing Jurassic strata, mostly the Westwater Canyon Member of the Morrison Formation, beneath the western and northern parts of the volcanic field (McLemore and Chenoweth, 2017; Goff et al., 2019). Renewed interest starting in 2007 sparked re-staking of claims in the Mount Taylor area, but the 2011 Fukushima nuclear accident caused a precipitous drop in uranium prices and demand. For the most part, uranium deposits have a Jurassic age of roughly 130 Ma, but there are a few redistributed uranium deposits that date as young as 3 to 12 Ma (McLemore and Chenoweth, 2017, table 7). It is presently not known if some redistributed uranium in the Grants area results directly from magmatic activity associated with the Mount Taylor volcanic field.

HYPOTHESES ABOUT THE FORMATION OF THE JEMEZ LINEAMENT

Proterozoic Ancestry

The JL has long been considered to be a boundary between Proterozoic crustal provinces (e.g., Cordell, 1978; Lipman and Mehnert, 1979; Aldrich et al., 1981). The aligned volcanic fields of the JL overlie a complex, NE-trending transition zone between two Proterozoic terranes that were accreted against Laurentia. The Yavapai province lies to the northwest and is comprised of several 1.80–1.70 Ga oceanic arcs that came together along the southern margin of the continent during the Yavapai orogeny at 1.71–1.68 Ga (Whitmeyer and Karlstrom, 2007). The Mazatzal province located to the southeast of the lineament is composed of 1.68–1.60 Ga rocks that formed in continental-margin and back-arc settings; these rocks were deformed during the 1.65–1.60 Ga Mazatzal orogeny (Whitmeyer and Karlstrom, 2007). The Mazatzal orogeny, which is related to subduction of the southern margin of the Yavapai block beneath the Mazatzal block, created a broad zone of mid-crustal folding and faulting that is preserved in modern mountain ranges in northern New Mexico and southern Colorado (Shaw and Karlstrom, 1999). The JL is considered to be a fundamental crustal boundary, because it marks the southern extent of 1.7 Ga rocks at the surface (Karlstrom and Humphreys, 1998), and lead isotope data in Arizona indicate different crustal compositions on either side (Wooden and DeWitt, 1991). The Paleoproterozoic crust was subsequently affected by widespread 1.45 to 1.35 Ga felsic volcanism.

Surface geologic mapping of Proterozoic rocks has yet to reveal the exact location of the boundary between provinces. Grambling et al. (2015) found that 1.4 Ga granites at the south end of the Sierra Nacimiento were derived from pre-1.7 Ga crust using hafnium isotope data, which indicates that Yavapai rocks extend further south than previously thought; thus the Proterozoic boundary is somewhere south of the Sierra Nacimiento. Similarly, Proterozoic rocks dated at 1.63 and 1.43 Ga (Strickland et al., 2003) are exposed in the core of the Zuni Mountains, which lie between the Zuni-Bandera volcanic field and Mount Taylor within the JL. Although a few scattered outcrops of ultramafic rocks that are chemically consistent with origin in ocean crust are preserved in the range, no clear evidence of the Mazatzal orogeny is preserved in the Zuni Mountains. Instead, the deformation that is preserved is 1.43 Ga (Strickland et al., 2003). The boundary must be north of the Zuni Mountains.

A seismic reflection line that was part of the CD-ROM experiment (Figs. 2, 3) images the Proterozoic boundary in the eastern JL in unprecedented detail, showing oppositely dipping reflection bands that converge near the volcanic lineament (Magnani et al., 2004; 2005). South of the latitude of Las Vegas, New Mexico, crustal reflectors at depths greater than 15 km dip north, whereas deep crustal reflectors north of Las Vegas dip south, forming what is interpreted to be a "doubly vergent crustal duplex." At shallower crustal levels, the north-vergent Manzano thrust zone near the south end of the line and north-vergent Pecos thrust and nappe near the north end of the line form prominent reflectors. The crustal boundary here is broad (~100 km) and diffuse because of the collision of a Mazatzal island arc with the Yavapai margin. As collision continued, the margin was subducted along a south-dipping zone, creating the bivergent convergence geometry. Notable sub-horizontal, fairly continuous, strong reflectors on the seis-

mic line at depths of 10–15 km are interpreted as mafic sills of possible Mesoproterozoic (Amarante et al., 2005) or late Cenozoic age. Given the fact that many of the lavas in the Raton–Clayton volcanic field show evidence of crustal contamination (e.g., Ramos et al., 2019), the latter interpretation is more likely.

Zurek and Dueker (2005) used receiver functions, which image sharp vertical changes in velocity, to map layering in the crust and the mantle across the JL (Figs. 2, 3). Many of the layers and truncations of layers in the receiver function image align nicely with features identified on the seismic reflection line (Fig. 3a), but one south-dipping truncation in the receiver function profile, highlighted by the arrow in Figure 3a, is not obvious in the reflection line because a data gap (the reflection line could not be run through the town of Las Vegas). Thus, the two methods complement one another and the receiver function image supports the "doubly vergent crustal duplex" interpretation. Note that this feature does not penetrate all the way through the crust; it probably soles into the brittle-ductile transition in the crust. The Moho is relatively flat at a depth of 40 km across this profile, with one small step up at the north end of the reflection line. Model resolution is poor north of latitude 37°.

The tomographic body-wave images of Yuan and Dueker (2005; Figs. 3b, 3c) show that both P- and S-velocities are reduced beneath and north of the Ocate volcanic field, in the same region of pronounced layering in the 100-km-thick mantle lithosphere. Zurek and Dueker (2005) and Yuan and Dueker (2005) attribute these observations to a juxtaposition of lithospheric materials of different chemical composition. Hydration of the mantle during Proterozoic subduction has resulted in the preservation of "sub-solidus material" in lithosphere that can more readily form partial melt (Yuan and Dueker, 2005).

Similarly, Wolff et al. (2005) identified four potential mantle sources for volcanic rocks in the Jemez Mountains volcanic field but concluded that only two sources are likely important: 1) Proterozoic oceanic lithosphere enriched by basaltic melt and 2) convecting asthenosphere. Modification of the mantle by subduction of Proterozoic oceanic crust associated with complex, piecemeal accretion of island arcs against the North American continent could be the source of the array of volcanic rock types preserved along the JL (Dueker et al., 2001; Wolff et al., 2005). In a later study, Rowe et al. (2015) examined spatial and temporal variations in water, chlorine, fluorine, and sulfur in basaltic magmas in the RGR and on either end of the JL and found an east to west decrease in volatile enrichment that is likely explained by a combination of varying mantle sources and early removal of metasomatized lithospheric mantle.

Volcano Spacing and Ancient Plumes

If the subduction suture theory can be entertained, then possibly the spacing between JL volcanic centers may reflect inherited conduits, plumes, or vertical zones of weakness caused by upward magma migration in a chain of a previous arc system. Several researchers have commented on "regular spacing" in subduction zone (arc) volcanoes (i.e., Marsh, 1979; Tatsumi and Kogiso, 2003). Marsh (1979) proposed that arc centers result from gravitational instabilities (i.e., Rayleigh-Taylor instabilities) in developing magma(s) at the approximate boundary of a downward plunging slab and overlying asthenosphere. Shimozuru and Kubo (1983) published an average volcano spacing of 58±24 km (1σ) for currently active subduction zones. These authors also noted that single chain arcs generally indicate high-angle dip and faster subduction rate of the subducted slab, whereas broad or multi-chain arcs, perhaps reflected in the broad width of the JL, signified lower dip angle and slower rates of convergence. On the other hand, de Bremond d'Ars et al. (1995) measured volcano distributions at 16 arcs containing 479 volcanic systems and concluded that volcanoes are randomly distributed at convergent margins. In spite of these contradictions, we measured the spacing between the approximate centers of the 10 volcanic fields along the JL and the average value is 94±24 km (1σ). Whether or not JL volcanic centers reveal a "regular" or random spacing reflective of past subduction in the Proterozoic, current intraplate volcanism (the last 20 my) is not compositionally similar to "andesitic" volcanism typical of convergent margins.

Thermal and Structural Connections to the Colorado Plateau

The western JL is closely aligned with the southeastern margin of the Colorado Plateau. Several researchers (e.g., Chamberlin, 2007; Crow et al., 2011) have noted a robust pattern of inboard sweep of volcanism through time attributed to thermal erosion along the western and southern margins of the Plateau, but that pattern is not as clear along the southeastern margin. Aldrich and Laughlin (1984) found that extension directions in the Colorado Plateau are southwest-northeast, whereas extension directions are east-west in the RGR, and that the difference in orientation is accommodated in the JL on the west side of the RGR. The accommodating structures, which are oriented north-northeast, disrupted the thermal erosion pattern and focused volcanism into voluminous centers like Mount Taylor and the Jemez Mountains volcanic fields.

East versus West

Chapin et al. (1978) defined the JL to include the aligned volcanic centers toward the northeast across the RGR onto the High Plains with a dogleg, but Aldrich et al. (1981) restricted the extent of the JL to the section west of the RGR. Both the eastern and western segments share many similarities. The compositional ranges and general timing of volcanism (mostly less than 15 Ma) along each belt are similar. The entire JL is underlain by upper mantle with low P- and S-wave speeds (e.g., V_s<4.2; Shen and Ritzwoller, 2016) and is characterized by elevated heat flow. However, there are significant differences, particularly in the stress orientations and distribution of modern seismicity. Aldrich et al. (1981) determined that the least principal stresses, derived from the orientations of faults and dikes that are less than 5 Ma, are northwest-southeast in the western JL and northeast-southwest in the eastern JL. Vent alignments west of the RGR trend northeast and have more

east-southeast to easterly striking trends to the east, especially in the Raton–Clayton field (Fig. 4). Seismicity levels are concentrated perpendicular to sigma 3 in the western JL. In contrast, few earthquakes occur in the eastern JL and the diffuse events generally trend northeast (Fig. 4).

Nakai et al. (2017) offer two explanations for the essentially aseismic nature of the eastern JL. First, these authors note that the presence of solidified mafic sills of Cenozoic or Mesoproterozoic age imaged on the reflection line of Magnani et al. (2004, 2005) may have strengthened the crust. Nakai et al. (2017) use the analogy of the seismic parabola around the Snake River Plain in Idaho and Wyoming as a hypothesis to explain the observations in northeastern New Mexico, although the driver for the northeastern New Mexico system is in the lithospheric mantle. Alternatively, the low-velocity zone in the mid-crust found by Lin et al. (2014) and Fu and Li (2015) may indicate elevated temperature in the crust, which could cause aseismic ductile deformation in the eastern JL that is surrounded by brittle failure induced by differential thermal stresses.

We reiterate that the center of the Jemez Mountains occupied by the Valles caldera and the underlying magma chamber is also aseismic, presumably because molten rock attenuates seismic waves. This seismic characteristic was first recognized by Suhr (1981; see also Goff et al., 1989, p. 395-396) but has been discussed most recently by Sanford et al. (1991) and House and Roberts (2019).

CONCLUSIONS

Surface and subsurface characteristics of volcanic fields along the JL have been extensively studied since the 1970s, resulting in many factual observations. Geophysical and geochemical measurements and data support the idea that the Paleoproterozoic ancestry of this feature created fertile mantle lithosphere that resides within the North American plate (Spence and Gross, 1990). Exactly what triggers the seemingly random temporal and spatial pattern of volcanic eruptions along this zone is a bit of a mystery, but subsequent tectonic events, including the hydration of the mantle by subduction of the Farallon Plate during Laramide deformation and younger regional-scale uplift of the Rocky Mountain region (e.g., Nereson et al., 2013), has created rising magmas that erupt at any time along this zone. Recent $^{40}Ar/^{39}Ar$ dating in the Raton–Clayton field (Zimmerer, 2019) suggests eastward migration of volcanism paralleling plate motion. The plate motion signal might constantly be present on timescales <1 Ma, but we do not yet have the resolution in our current sampling strategies to see that pattern in older volcanic rocks of the JL.

ACKNOWLEDGMENTS

The authors appreciate constructive reviews performed by John Wolff (Washington State University) and Brandon Schmandt (University of New Mexico). Additional editorial comments were made by Virginia McLemore and Kate Zeigler.

REFERENCES

Albrecht, M., Goff, F., Gardner, J.N., Kelley, S., WoldeGabriel, G., Dewhurst, W., Sirles, P., and Kaufman, G., 2011, Multi-disciplinary and integrated geothermal exploration at the Pueblo of Jemez, New Mexico: Geothermal Resources Council Transactions, v. 35, 8 p.

Aldrich, M.J., 1986, Tectonics of the Jemez lineament in the Jemez Mountains and the Rio Grande rift: Journal of Geophysical Research, v. 91, p. 1753-1762.

Aldrich, M.J., and Laughlin, A.W., 1984, A model for the tectonic development of the southeastern Colorado Plateau boundary, Journal of Geophysical Research, v. 89, p. 10,207-10,218, doi:10.1029/JB089iB12p10207.

Aldrich, M.J., Jr., Ander, M.E., and Laughlin, A.W., 1981, Geological and geophysical signatures of the Jemez lineament: a reactivated Proterozoic structure: Los Alamos National Laboratory Report LA-YR-82-561, 35 p.

Amarante, J.F.A., Kelley, S.A., Heizler, M.T., Barnes, M.A., Miller, K.C., and Anthony, E.Y., 2005, Characterization and age of the Mesoproterozoic Debaca Sequence in the Tucumcari Basin, New Mexico, *in* Karlstrom, K.E, and Keller, G.R., eds., The Rocky Mountain Region: An Evolving Lithosphere: Washington, D.C., American Geophysical Union Monograph 154, p. 185-199.

Aprea, M., Hildebrande, S., Fehler, M., Steck, L., Baldridge, W., Roberts, P., Thurber, C., and Lutter, W., 2002, Three-dimensional Kirchhoff migration: Imaging of the Jemez volcanic field using teleseismic data: Journal of Geophysical Research, v. 107, p. 2247-2262.

Aubele, J.C., 1978, Geology of Cerros del Rio volcanic field: New Mexico Mines and Mineral Resources, Circular 163, p. 198-201.

Aubele, J.C., and Crumpler, L.S., 2001, Raton–Clayton and Ocate volcanic fields: New Mexico Geological Society, Guidebook 52, p. 59-76.

Baldridge, W.S., Perry, F.V., and Shafiqullah, M., 1987, Late Cenozoic volcanism of the southeastern Colorado Plateau: I. Volcanic geology of the Lucero area, New Mexico: Geological Society of America Bulletin, v. 99, p. 463-470.

Baldridge, W.S., Perry, F.V., Vaniman, D.T., Neeley, L.D., Leavy, B.D., Laughlin, A.W., Kyle, P., Bartov, Y., Steinitz, G., and Gladney, E.S., 1989, Excursion 8A: Magmatism associated with lithospheric extension: Middle to late Cenozoic magmatism of the southeastern Colorado Plateau and central Rio Grande rift, New Mexico and Arizona: New Mexico Mines and Mineral Resources, Memoir 46, p. 187-230.

Blackwell, D., Richards, M., Frone, Z., Batir, J., Ruzo, A., Dingwall, R., and Williams M., 2011, Temperature at depth maps for the conterminous US and geothermal resource estimates: GRC Transactions, v. 35, GRC1029452.

Blomgren, V., Williams, W., Crossey, L., Karlstrom, K., and Goff, F., 2016, Identifying the sources of CO_2 in carbonic springs in the Albuquerque-Belen Basin: New Mexico Geological Society, Guidebook 67, p. 419-427.

Brennan, S.T., 2017, Chemical and isotopic evidence for CO_2 charge and migration within Bravo Dome and potential CO_2 leakage to the southwest: Energy Procedia, v. 114, p. 2996-3005.

Broadhead, R.F., 1990, Bravo Dome carbon dioxide gas field, *in* Beaumont, E.A., and Foster, N.H., eds., Structural Traps I: Tectonic Fold Traps: Tulsa, American Association of Petroleum Geologists, Treatise of Petroleum Geology, Atlas of Oil and Gas Fields, p. 213-232.

Broadhead, R.F., 2019, Carbon dioxide in the subsurface of northeastern New Mexico: New Mexico Geological Society, Guidebook 70, p. 101-108.

Chapin, C.E., Chamberlain, R.M., Osburn, C.R., White, D.U., and Sanford, A.R., 1978, Exploration framework of the Socorro geothermal area, New Mexico: New Mexico Bureau of Mines and Mineral Resources, Special Publication 7, p. 115-129.

Chamberlin. R.M., 2007, Evolution of the Jemez lineament: Connecting the volcanic dots through Cenozoic time: New Mexico Geological Society, Guidebook 58, p. 80-82.

Channer, M.A., Ricketts, J.W., Zimmerer, M., Heizler, M., and Karlstrom, K.E., 2015, Surface uplift above the Jemez mantle anomaly in the past 4 Ma based on $^{40}Ar/^{39}Ar$ dated paleoprofiles of the Rio San Jose, New Mexico, USA: Geosphere, v. 11, p. 1384-1400.

Condit, C.D., and Connor, C.B., 1996, Recurrence rates of volcanism in basaltic fields; an example from the Springerville volcanic field, Arizona: Geological Society of America Bulletin, v. 108, p. 1225-1241.

Cordell, L., 1978, Regional geophysical setting of the Rio Grande rift: Geolog-

ical Society of America Bulletin, v. 89, p. 1073-1090.
Christiansen, E.H., Burt, D.M., Sheridan, M.F., and Wilson, R.T., 1983, The petrogenesis of topaz rhyolites from the western United States: Contributions to Mineralogy and Petrology, v. 83, p. 16-30.
Crow, R., Karlstrom, K., Asmerom, Y., Schmandt, B., Polyak, V., and DuFrane, S.A., 2011, Shrinking of the Colorado Plateau via lithospheric mantle erosion: Evidence from Nd and Sr isotopes and geochronology of Neogene basalts: Geology, v. 39, p. 27-30, doi: 10 .1130 /G31611 .1.
Crumpler, L.S., 1980a, Alkali basalt through trachyte suite and volcanism, Mesa Chivato, Mount Taylor volcanic field, New Mexico: Geological Society of America Bulletin, v. 91, p. 253-255.
Crumpler, L.S., 1980b, Alkali basalt through trachyte suite and volcanism, Mesa Chivato, Mount Taylor volcanic field, New Mexico: Geological Society of America Bulletin, v. 91, p. 1293-1313.
Crumpler, L.S., 2001, Volcanism in New Mexico: An Overview, *in* Crumpler, L.S., and Lucas S.G., eds., Volcanology in New Mexico: New Mexico Museum of Natural History and Science, Bulletin 18, p. 17-29.
Crumpler, L.S., and Aubele, J.C., 1990, Red Hill volcanic field, New Mexico, *in* Wood, C.A., and Kienle, J., eds., Volcanoes of North America: Cambridge, Cambridge University Press, p. 307-308.
Crumpler, L.S., and Aubele, J.C., 2001, Volcanoes of New Mexico: An abbreviated guide for non-specialists, *in* Crumpler, L.S., and Lucas, S.G., eds., Volcanology in New Mexico: New Mexico Museum of Natural History and Science, Bulletin 18, p. 5-15.
Duffield, W.A., and Sass, J.H., 2003, Geothermal energy – clean power from the Earth's heat: U.S. Geological Survey Circular 1249, 36 p.
de Bremond d'Ars, J., Jaupart, C., and Sparks, R.S.J., 1995, The distribution of volcanoes in active margins: Journal of Geophysical Research, v. 100, p. 20,421-20,432.
Dunbar, N.W., and Phillips, F.M., 2004, Cosmogenic ^{36}Cl ages of lava flows in the Zuni-Bandera volcanic field, north-central New Mexico, U.S.A.: New Mexico Bureau of Geology and Mineral Resources, Bulletin 160, p. 309-317.
Dungan, M.A., 1987, Open-system magmatic evolution of the Taos Plateau volcanic field, northern New Mexico – The genesis of cryptic hybrids: Journal of Petrology, v. 28, p. 955-977.
Dungan, M.A., Thompson, R.A., Stormer, J.S., and O'Neill, J.M., 1989, Excursion 18B: Rio Grande rift volcanism: Northeastern Jemez zone, New Mexico: New Mexico Bureau of Mines and Mineral Resources, Memoir 46, p. 435-486.
Dueker, K., Yuan, H. and Zurek, B., 2001, Thick-structured Proterozoic lithosphere of the Rocky Mountain region: GSA Today, v. 11/12, p. 4-9.
Dunker, K., Wolff, J.A., Harmon, R., Leat, P., Dicken, A., and Thompson, R., 1991, Diverse mantle and crustal components in lavas of the NW Cerros del Rio volcanic field, Rio Grande rift, New Mexico: Contributions to Mineralogy and Petrology, v. 108, p. 331-345.
Edwards, C.L., Reiter, M. A., Shearer, C., and Young, W., 1978, Terrestrial heat flow and crustal radioactivity in northeastern New Mexico and southern Colorado: Geological Society America Bulletin, v. 89, p. 1341-1350.
Eastman, A.D., and Muir, M.P., 2012, Update of a trial of CO_2-based geothermal at the St. Johns Dome: Stanford University, Proceedings of the 37th Workshop on Geothermal Reservoir Engineering, 10 p.
Eggleston, R.E., and Reiter, M., 1984, Terrestrial heat-flow estimates from petroleum bottom-hole temperature data in the Colorado Plateau and the eastern Basin and Range province: Geological Society America Bulletin, v. 95, p. 1027-1034.
Eichelberger, J.C., and Koch, F.G., 1979, Lithic fragments in the Bandelier Tuff, Jemez Mountains, New Mexico: Journal of Volcanology and Geothermal Research, v. 5, p. 115-134.
Feucht, D.W., Bedrosian, P.A., and Sheehan, A.F., 2019, Lithospheric signature of late Cenozoic extension in electrical resistivity structure of the Rio Grande rift, New Mexico, USA: Journal of Geophysical Research, Solid Earth, v. 124, p. 2331-2351, https://doi.org/10.1029/2018JB016242.
Fu, Y.V., and Li, A., 2015, Crustal shear wave velocity and radial anisotropy beneath the Rio Grande Rift from ambient noise tomography: Journal of Geophysical Research Solid Earth, v. 120, p. 1005-1019, doi:10.1002/2014JB011602.
Gao, W., Grand, S. P., Baldridge, W. S., Wilson, D., West, M., Ni, J. F. and Aster, R., 2004, Upper mantle convection beneath the central Rio Grande Rift imaged by P- and S-wave tomography: Journal of Geophysical Research, v. 109, p. B03305, doi:10.1029/2003JB002743.
Gardner, J.N., 1985, Tectonic and petrologic evolution of the Keres Group: Implications for the development of the Jemez volcanic field, New Mexico [Ph.D. dissertation]: Davis, University of California, 293 p.
Gardner, J.N., Goff, F., Garcia, S., and Hagan, R., 1986, Stratigraphic relations and lithologic variations in the Jemez volcanic field, New Mexico: Journal of Geophysical Research, v. 91, p. 1763-1778.
Gardner, J.N., Goff, F., Kelley, S.A., and Jacobs, E., 2010, Rhyolites and associated deposits of the Valles-Toledo caldera complex, New Mexico: New Mexico Geology, v. 32, p. 3-18.
Gilfillan, S.M.V., Ballentine, C.J., Holland, G., Blagburn, D., Lollar, B.S., Stevens, S., Schoell, M., and Cassidy, M., 2008, The noble gas geochemistry of natural CO_2 gas reservoirs from the Colorado Plateau and Rocky Mountain provinces, USA: Geochimica Cosmochimica Acta, v. 72, p. 1174-1198.
Glascock, M.D., Kunselman, R., and Wolfman, D., 1999, Intrasource chemical differentiation of obsidian in the Jemez Mountains and Taos Plateau, New Mexico: Journal of Archeological Science, v. 26, p. 861-868.
Goff, F., 2010, The Valles caldera: New Mexico's supervolcano: New Mexico Earth Matters (winter issue), 4 p.
Goff, F., and Gardner, J.N., 1994, Evolution of a mineralized geothermal system, Valles caldera, New Mexico: Economic Geology, v. 89, p. 1803-1832.
Goff, F., and Goff, C.J., 2015, Hydrogeochemistry and geothermal potential of Montezuma hot springs, New Mexico: New Mexico Geological Society, Guidebook 66, p. 289-302.
Goff, F., and Goff, C.J., 2017, Overview of the Valles caldera (Baca) geothermal system. New Mexico, *in* McLemore, V.T., Timmons, S., and Wilks, M., eds., Energy and Mineral Resources of New Mexico: New Mexico Bureau of Geology and Mineral Resources, Memoir 50F, 65 p.
Goff, F., and Janik, C.J., 2002, Gas geochemistry of the Valles caldera region, New Mexico and comparisons with gases at Yellowstone, Long Valley and other geothermal systems: Journal of Volcanology and Geothermal Research, v. 116, p. 299-323.
Goff, F., Grigsby, C.O., Trujillo, P.E., Jr., Counce, D., and Kron, A., 1981, Geology, water geochemistry and geothermal potential of the Jemez Springs area, Cañon de San Diego, New Mexico: Journal of Volcanology and Geothermal Research, v. 10, p. 227-244.
Goff, F., Gardner, J.N., Baldridge, W.S., Hulen, J.B., Nielson, D.L., Vaniman, D., Heiken, G., Dungan, M.A., and Broxton, D., 1989, Excursions 17B: Volcanic and hydrothermal evolution of Valles caldera and the Jemez volcanic field: New Mexico Bureau of Mines and Mineral Resources, Memoir 46, p. 381-434.
Goff, F., Gardner, J.N., Reneau, S.L., Kelley, S.A., Kempter, K., and Lawrence, J.R., 2011, Geologic map of the Valles caldera, Jemez Mountains, New Mexico: New Mexico Bureau of Geology and Mineral Resources, Geologic Map 79, scale 1:50,000, 30 p. booklet.
Goff, F., Wolff, J.A., McIntosh, W., and Kelley, S.A., 2013, Gabbroic shallow intrusions and lava-hosted xenoliths in the Mount Taylor area, New Mexico: New Mexico Geological Society, Guidebook 64, p. 143-151.
Goff, F., Kelley, S.A., Goff, C.J., McCraw, D.J., Osburn, G.R., Lawrence, J.R., Drakos, P.G., and Skotnicki, S.J., 2019, Geologic map of the Mount Taylor volcano area, New Mexico: New Mexico Bureau of Geology and Mineral Resources, Geologic Map 80, scale 1:36,000, 66 p. booklet.
Goff, F., McIntosh, W., Peters, L., Wolff, J.A., Kelley, S.A., Goff, C.J., and Osburn, G.R., 2020, Volcanic evolution of Mount Taylor Stratovolcano, New Mexico: Facts and misconceptions: New Mexico Geological Society, Guidebook 71, this volume.
Grambling, T.A., Holland, M., Karlstrom, K.E., Gehrels, G.E., and Pecha, M., 2015, Revised location for the Yavapai-Mazatzal crustal province boundary in New Mexico: Hf isotopic data from Proterozoic rocks of the Nacimiento Mountains: New Mexico Geological Society, Guidebook 66, p. 175-184.
Hoard, D., 2007, A brief history of the Cochiti Mining District: New Mexico Geological Society, Guidebook 47, p. 81-82.
Holloway, J.R., and Cross, C., 1978, The San Carlos alkaline rock association: Los Alamos Scientific Laboratory, Open-file Report, p. 171-176.
Holloway, J.R., and Blank, J.G., 1994, Application of experimental results to C-O-H species in natural melts, *in* Carroll, M.R., and Holloway, J.R., eds., Volatiles in Magmas: Washington, D.C., Mineralogical Society of America, Reviews in Mineralogy, v. 30, p. 187-230.
Horning, R.R., Dunbar, N.W., Kyle, P.R., and Baldridge, W.S., 1996, Evolu-

tion of igneous vents intruding basanite at El Porticito, Quemado, New Mexico: New Mexico Geology, v. 18, p. 53.

House, L., and Roberts, P., 2019, Seismicity monitoring in north-central New Mexico by the Los Alamos seismic network: Seismological Research Letters, v. 91, p. 593-600.

Hunt, C.B., 1938, Igneous geology and structure of the Mount Taylor volcanic field, New Mexico: U.S. Geological Survey, Professional Paper 189-B, p. 51-80.

Karlstrom, K.E., and Humphreys, G., 1998, Influence of Proterozoic accretionary boundaries in the tectonic evolution of western North America: Interaction of cratonic grain and mantle modification events: Rocky Mountain Geology, v. 33, no. 2, p. 161-179.

Keating, G.N., and Valentine, G.A., 1998, Proximal stratigraphy and syn-eruptive faulting in rhyolitic Grants Ridge Tuff, New Mexico, USA: Journal of Volcanology and Geothermal Research, v. 81, p. 37-49.

Kelley, S.A., 2015, Geothermal potential of the Raton Basin, New Mexico: New Mexico Geological Society, Guidebook 66, p. 261-274.

Kelley, S., Person, M., Kelley, R., and Pepin, J., 2016, Low-temperature geothermal resources in the Acoma Basin and Lucero Uplift, eastern Cibola and western Valencia counties, New Mexico: New Mexico Geological Society, Guidebook 67, p. 263-274.

Kelley, S.A., McIntosh, W.C., Goff, F., Kempter, K.A., Wolff, J.A., Esser, R., Braschayko, S., Love, D., and Gardner, J.N., 2013, Spatial and temporal trends in pre-caldera Jemez Mountains volcanic and fault activity: Geosphere, v. 9, p. 614-646.

Laughlin, A.W., Brookins, D.G., and Causey, J.D., 1972, Late Cenozoic basalts of the Bandera lava field, New Mexico: Geological Society of America Bulletin, v. 83, p. 1543-1552.

Laughlin, A.W., Aldrich, M.J., Ander, M.E., Heiken, G.H., and Vaniman, D.T., 1982, Tectonic setting and history of late Cenozoic volcanism in west-central New Mexico: New Mexico Geological Society, Guidebook 33, p. 279-284.

Laughlin, A.W., Poths, J., Healey, H.A., Reneau, S., and WoldeGabriel, G., 1994, Dating Quaternary basalts using the cosmogenic ^{3}He and ^{14}C methods with implications for excess Ar: Geology, v. 22, p. 135-138.

Levander, A., Zelt, C.A., and Magnani, M.B., 2005, Crust and upper mantle velocity structure of the Southern Rocky Mountains from the Jemez Lineament to the Cheyenne Belt, *in* Karlstrom, K.E., and Keller, G.R., eds., The Rocky Mountain Region—An Evolving Lithosphere: Washington, D.C., American Geophysical Union, Geophysics Monograph 154, p. 293-308.

Lin, F.C., Tsai, V.C., and Schmandt, B., 2014, 3D crustal structure of the western United States: Application of Rayleigh-wave ellipticity extracted from noise cross-correlations: Geophysical Journal International, v. 198, p. 656-670, doi:10.1093/gji/ggu160.

Lipman, P.W., 1969, Alkali and tholeiitic basaltic volcanism related to the Rio Grande depression southern Colorado and northern New Mexico: Geological Society of America Bulletin, v. 80, p. 1343-1354.

Lipman, P.W., and Mehnert, H.H., 1975, Late Cenozoic basaltic volcanism and development of the Rio Grande depression in the southern Rocky Mountains, *in* Curtis, B.F., ed., Cenozoic History of the Southern Rocky Mountains: Denver, Geological Society of America, Memoir 144, p. 119-154.

Lipman, P.W., and Mehnert, H.H., 1979, The Taos Plateau volcanic field, northern Rio Grande rift, New Mexico, *in* Riecker, R.E., ed., Rio Grande Rift: Tectonics and Magmatism: Washington, D.C., American Geophysical Union, p. 289-311.

Lipman, P.W., and Moench, R.H., 1972, Basalts of the Mount Taylor volcanic field, New Mexico: Geological Society of America Bulletin, v. 83, p. 1335-1344.

Luedke, R., and Smith, R.L., 1978a, Map showing distribution, composition, and age of late Cenozoic volcanic centers in Arizona and New Mexico: U.S. Geological Survey, Miscellaneous Investigations Map I-1091-A, scale 1:1,000,000.

Luedke, R., and Smith, R.L., 1978b, Map showing distribution, composition and age of late Cenozoic volcanic centers in Colorado, Utah and southwestern Wyoming: U.S. Geological Survey, Miscellaneous Investigations Map I-1091-B, scale 1:1,000,000.

Magnani, M.B., Miller, K.C., Levander, A., and Karlstrom, K.E., 2004, The Yavapai-Mazatzal boundary: A long-lived element in the lithosphere of southwestern North America: Geological Society of America Bulletin, v. 116, p. 1137-1142.

Magnani, M.B., Levander, A., Miller, K.C., Eshete, T., and Karlstrom, K. E., 2005, Seismic investigation of the Yavapai-Mazatzal Transition Zone and the Jemez Lineament in northeastern New Mexico, *in* Karlstrom, K.E., and Keller, G.R., eds., The Rocky Mountain Region—An Evolving Lithosphere: Washington, D.C., American Geophysical Union Geophysics Monograph 154, p. 227-238, doi:10.1029/GM154.

Marsh, B.D., 1979, Island arc development: Some observations, experiments, and speculations: Journal of Geology, v. 87, p. 687-713.

Mayo, E.B., 1958, Lineament tectonics and some ore districts of the southwest: Transactions American Institute of Metallurgical Engineers, v. 211, p. 1169-1175.

McIntosh, W.C., 1994, ^{40}Ar/^{39}Ar geochronology of late Miocene to Pleistocene basalts of the Zuni-Bandera, Red Hill-Quemado and Portrillo volcanic fields, New Mexico: New Mexico Geology, v. 16, p. 60-61.

McIntosh, W. C. and Cather, S.M., 1994, 40Ar/39Ar geochronology of basaltic rocks and constraints on late Cenozoic stratigraphy and landscape development in the Red Hill-Quemado area, New Mexico: New Mexico Geological Society, Guidebook 45, p. 209-224.

McLemore, V.T., and Lueth, V.W., 2017, Metallic mineral deposits, *in* McLemore, V.T., Timmons, S., and Wilks, M., eds., Energy and Mineral Resources of New Mexico: New Mexico Bureau of Geology and Mineral Resources, Memoir 50D, 79 p.

McLemore, V.T., and Austin, G.S., 2017, Industrial minerals and rocks, *in* McLemore, V.T., Timmons, S., and Wilks, M., eds., Energy and Mineral Resources of New Mexico: New Mexico Bureau of Geology and Mineral Resources, Memoir 50E, 115 p.

McLemore, V.T. and Chenoweth, W.L., 2017, Uranium resources, *in* McLemore, V.T., Timmons, S., and Wilks, M., eds., Energy and Mineral Resources of New Mexico: New Mexico Bureau of Geology and Mineral Resources, Memoir 50C, 80 p.

Minier, J., 1987, A geothermal study in west-central New Mexico [Ph.D. dissertation]: Socorro, New Mexico Institute of Mining and Technology, 229 p.

Morgan, W.J., and Morgan, J.P., 2007, Plate velocities in the hotspot reference frame, *in* Foulger, G.R., and Jurdy, D.M., eds., Plates, Plumes and Planetary Processes: Boulder, Geological Society of America, Special Paper 430, p. 65-78.

Nakai, J.S., Sheehan, A.F., and Bilek , S.L., 2017, Seismicity of the Rocky Mountains and Rio Grande Rift from the EarthScope Transportable Array and CREST temporary seismic networks, 2008-2010: Journal of Geophysical Research Solid Earth, v. 12, p. 2,173-2,192, doi:10.1002/ 2016JB013389.

Nathenson, M., Guffanti, M., Sass, J.H., and Munroe, R.J., 1982, Regional heat flow and temperature gradients, *in* Reed, M.J., ed., Assessment of low-temperature geothermal resources in the United States – 1982: U.S. Geological Survey Circular 892, p. 9-16.

Nereson, A., Stroud, J., Karlstrom, K., Heizler, M., and McIntosh, W., 2013, Dynamic topography of the western Great Plains: Geomorphic and ^{40}Ar/^{39}Ar evidence for mantle-driven uplift associated with the Jemez lineament of NE New Mexico and SE Colorado: Geosphere, v. 9, p. 521-545, doi: 10 .1130 /GES00837.1.

Nielson, R.L., and Dungan, M.A., 1985, The petrology and geochemistry of the Ocate volcanic field, north-central New Mexico: Geological Society of America Bulletin, v. 96, p. 296-312.

Olmsted, B.W., and McIntosh, W.C., 2004, ^{40}Ar/^{39}Ar Geochronology of the Ocate Volcanic Field, North-Central New Mexico: New Mexico Bureau of Geology and Mineral Resources Bulletin 160, p. 297-308.

O'Neill, J.M., and Mehnert, H.H., 1988, Petrology and physiographic evolution of the Ocate volcanic field, north-central New Mexico: U.S. Geological Survey, Professional Paper 1478-A, 15 p.

Onken, J., and Forman, S., 2017, Terminal Pleistocene to early Holocene volcanic eruptions at Zuni Salt Lake, west-central New Mexico, USA: Bulletin of Volcanology, v. 79, 17 p., https://doi.org/10.1007/s00445-016-1089-1.

Perry, F.V., Baldridge, W.S., DePaolo, D.J., and Shafiqullah, M., 1990, Evolution of a magmatic system during continental extension: The Mount Taylor volcanic field, New Mexico: Journal of Geophysical Research, v. 95, p. 19,327-19,348.

Ramos, F.C., Zimmerer, M.J., Zeigler, K., Pinkerton, S., and Butterfield, N., 2019, Geochemistry of Capulin-phase flows in the Raton–Clayton volcanic field: New Mexico Geological Society, Guidebook 70, p. 139-149.

Rauzi, S.L., 1999, Carbon dioxide in the St. Johns – Springerville area, Apache County, Arizona: Arizona Geological Survey, Open-file Report 99-2, 22 p.

Reiter, M., Edwards, C.L., Hartman, H., and Weidman, C., 1975, Terrestrial heat flow along the Rio Grande rift, New Mexico and Colorado: Geolog-

ical Society America Bulletin, v. 86, p. 811-818.
Rowe, M.C., Wolff, J.A., Gardner, J.N., Ramos, F.C., Teasdale, R., and Heikopp, C.E., 2007, Development of a continental volcanic field: Petrogenesis of pre-caldera intermediate and silicic rocks and origin of the Bandelier magmas, Jemez Mountains (New Mexico, USA): Journal of Petrology, v. 48, p. 2063-2091.
Rowe, M.C., Lassiter, J.C., and Goff, K., 2015, Basalt volatile fluctuations during continental rifting: An example from the Rio Grande Rift, USA: Geochemistry, Geophysics and Geosystems, v. 16, p. 1254-1273.
Rubinstein, J.L., Ellsworth, W.L., McGarr, A., and Benz, H.M., 2014, The 2001–present induced earthquake sequence in the Raton Basin of northern New Mexico and southern Colorado: Bulletin of the Seismological Society of America, v. 104, p. 2162-2181.
Sanford, A.R., Jaksha, L.H., and Cash, D.J., 1991, Seismicity of the Rio Grande rift in New Mexico, *in* Slemmons, D.B., Engdahl, E.R., Zoback, M.D., and Blackwell D.D., eds., Neotectonics of North America: Boulder, Geological Society of America, p. 229-244.
Sanford, A.R., Lin, K., Tsai, I., and Jaksha, L.H., 2002, Earthquake catalogs for New Mexico and bordering areas: 1869–1998: New Mexico Bureau of Geology and Mineral Resources, Circular 210, 15 p.
Sass, J.H., and Morgan, P., 1988, Conductive heat flow in VC-1 and the thermal regime of Valles caldera, Jemez Mountains, New Mexico: Journal of Geophysical Research, v. 93, p. 6027-6039.
Sathaya, K.J., Hesse, M.A., Cassidy, M., and Stockli, D.F., 2014, Constraints on the magnitude and rate of CO2 dissolution at Bravo Dome natural gas field: Proceedings National Academy of Sciences, USA, v. 111, p. 15,332-15,337.
Sathaye, K.J., Smye, A.J., Jordon, J.S., and Hesse, M.A., 2016, Noble gases preserve history of retentive continental crust in the Bravo Dome natural CO_2 field, New Mexico: Earth and Planetary Science Letters, v. 443, p. 32-40.
Schmandt, B., and Humphreys, E., 2010, Complex subduction and small-scale convection revealed by body-wave tomography of the western United States upper mantle: Earth and Planetary Science Letters, v. 297, p. 435-445, doi: 10 .1016 /j .epsl .2010 .06 .047.
Schmandt, B., Jiang, C., and Farrell, J., 2019, Seismic perspectives from the western U.S. on magma reservoirs underlying large silicic calderas: Journal of Volcanology and Geothermal Research, v. 384, p. 158-178.
Self, S., Goff, F., Gardner, J.N., Wright, J., and Kite, J., 1986, Explosive rhyolitic volcanism in the Jemez Mountains, New Mexico: Vent locations, caldera development and relation to regional structure: Journal of Geophysical Research, v. 91, p. 1779-1798.
Shackley, M.S., 1998, Geochemical differentiation and prehistoric procurement of obsidian in the Mount Taylor volcanic field, northwest New Mexico: Journal of Archeological Science, v. 25, p. 1073-1082.
Shackley, M.S., 2005, Obsidian: Geology and Archeology in the North American Southwest: Tucson, University of Arizona Press, 264 p.
Shackley, M.S., and Goff, F., 2016, Geologic origin of the source of Bearhead Rhyolite (Paliza Canyon) obsidian, Jemez Mountains, northern New Mexico: New Mexico Geology, v. 38, p. 52-65.
Shaw, C.A., and Karlstrom, K.E., 1999, The Yavapai-Mazatzal crustal boundary in the southern Rocky Mountains: Rocky Mountain Geology, v. 34, no. 1, p. 37-52.
Shen, W., and Ritzwoller, M.H., 2016, Crustal and uppermost mantle structure beneath the United States: Journal of Geophysical Research Solid Earth, v. 121, p. 4306-4342.
Shimozuru D., and Kubo, N., 1983, Volcano spacing and subduction, *in* Shimozuru D., and Yokoyama, I., eds., Arc Volcanism: Physics and Tectonics: Amsterdam, Springer Netherlands, p. 141-151.
Smith, R.L., and Bailey, R.A., 1968, Resurgent cauldrons: Geological Society of America, Memoir 116, p. 613-662.
Smith, R.L., and Luedke, R.G., 1984, Potentially active volcanic lineaments and loci in western conterminous United States: Washington, D.C., National Academy Press, Studies in Geophysics, Explosive Volcanism: Inception, Evolution and Hazards, p. 47-66.
Smith, R.L., Bailey, R.A., and Ross, C.S., 1970, Geologic map of the Jemez Mountains, New Mexico: U.S. Geological Survey, Miscellaneous Geologic Investigations Map I-571, scale 1:125,000.
Snelson, C.M., Keller, G.R., Miller, K.C., Rumpel, H-M., and Prodehl, C., 2005, Regional crustal structure derived from the CD-ROM 99 seismic refraction/wide-angle reflection profile: The lower crust and upper mantle, *in* Karlstrom K.E., and Keller, G.R., eds., The Rocky Mountain Region—An Evolving Lithosphere: Washington, D.C., American Geophysical Union Monograph Series 154, p. 271-291.
Sosa, A., Thompson, L., Velasco, A.A., Romero, R., and Herrmann, R., 2014, 3-D structure of the Rio Grande rift from 1-D constrained joint inversion of receiver functions and surface wave dispersion: Earth and Planetary Science Letters, v. 402, p. 127-137.
Spence, W., and Gross, R.S., 1990, A tomographic glimpse of the upper mantle source of magmas in the Jemez Lineament, New Mexico: Journal of Geophysical Research, v. 95, p. 10,829-10,849.
Strickland, D., Heizler, M.T., Selverstone, J., Karlstrom, K.E., 2003, Proterozoic evolution of the Zuni Mountains, western New Mexico: Relationship to the Jemez lineament and implications for a complex cooling history: New Mexico Geological Society, Guidebook 54, p. 109-117.
Stone, C., 1979, An overview of the geothermal potential of the Springerville area, Arizona: Arizona Geological Survey, Open-file Report 79-2a, 25 p.
Stormer, J.C., 1972a, Ages and nature of volcanic activity in the southern High Plains, New Mexico and Colorado: Geological Society of America Bulletin, v. 83, p. 2,433-2,448.
Stormer, J.C., 1972b, Mineralogy and petrology of the Raton–Clayton volcanic field, northeastern New Mexico: Geological Society of America Bulletin, v. 83, p. 3,299-3,322.
Stroud, J. R., 1997, The geochronology of the Raton–Clayton volcanic field, with implications for volcanic history and landscape evolution [M.S. thesis]: Socorro, New Mexico Institute of Mining and Technology, 70 p.
Suhr, G., 1981, Seismic crust anomaly under the Valles caldera in New Mexico, USA: Hanover, Unpublished Consulting Report, PRAKLA-SEISMOS, 56 p.
Summers, W.K., 1976, Catalog of thermal waters in New Mexico: New Mexico Bureau of Mines and Mineral Resources, Hydrologic Report 4, 80 p.
Suppe, J., Powell, C., and Berry, R., 1975, Regional topography, seismicity, Quaternary volcanism and present-day tectonics of the western United States: American Journal of Science, v. 275-A, p. 397-436.
Swanberg, C.A., 1979, Chemistry of thermal and nonthermal groundwaters in the Rio Grande rift and adjacent tectonic provinces, *in* Riecker, R.E., ed., Rio Grande Rift: Tectonics and Magmatism: Washington, D.C., American Geophysical Union, p. 279-288.
Takei, Y., 2017. Effects of partial melting on seismic velocity and attenuation: a new insight from experiments: Annual Reviews of Earth and Planetary. Science, v. 45, p. 447-470.
Tatsumi, Y., and Kogiso, T., 2003, The subduction factory: its role in the evolution of the Earth's crust and mantle, *in* Larter, R.D., and Leat, P.T., eds., Tectonic and Magmatic Processes, Intra-Oceanic Subduction Systems: London, Geological Society of London, Special Publication 219, p. 55-80.
Thompson, R.A., Shroba, R.R., Machette, M.N., Fridrich, C.J., Brandt, T.R., and Cosca, M.A., 2015, Geologic map of the Alamosa 30'×60' quadrangle, south-central, Colorado: U.S. Geological Survey Scientific Investigations Map 3342, 23 p., scale 1:100,000.
Vuataz, F.D., Stix, J., Goff, F., and Pearson, C.F., 1984, Low-temperature geothermal potential of the Ojo Caliente warm springs area, northern New Mexico: Los Alamos National Laboratory, Open-file Rept. LA-10106-OBES, 56 p.
West, M., Ni, J., Baldridge, W., Wilson, D., Aster, R., Gao, W., and Grand, S., 2004, Crust and upper mantle shear-wave structure of the southwest United States: Implications for rifting and support for high elevation: Journal of Geophysical Research, v. 109, p. B03309, doi:10.1029/ 2003JB002575.
Whitmeyer, S., and Karlstrom, K.E., 2007, Tectonic model for the Proterozoic growth of North America: Geosphere, v. 3, no. 4, p. 220-259.
Wilson, D., Aster, R., Ni, J., Grand, S., West, M., Gao, W., Baldridge, W.S., and Semken, S., 2005, Imaging the seismic structure of the crust and upper mantle beneath the Great Plains, Rio Grande Rift, and Colorado Plateau using receiver functions: Journal of Geophysical Research., v. 110, p. B05306, doi:10.1029/ 2004JB003492.
Wohletz, K.H., 1978, The eruptive mechanism of the Peridot Mesa vent, San Carlos, Arizona: Los Alamos Scientific Laboratory, Open-file Report, p. 157-171.
WoldeGabriel, G., and Goff, F., 1989, Temporal relationships of volcanism and hydrothermal alteration in two areas of the Jemez volcanic field, New Mexico: Geology, v. 17, p. 986-989.

Wolff, J.A., Brunstad, K.A., and Gardner, J.N., 2011, Reconstruction of the most recent volcanic eruptions from the Valles caldera, New Mexico: Journal of Volcanology and Geothermal Research, v. 199, p. 53-68.

Wolff, J.A., Rowe, M.C., Teasdale, R., Gardner, J.N., Ramos, F.C. and Heikoop, C.E., 2005, Petrogenesis of pre-caldera mafic lavas, Jemez Mountains volcanic field (New Mexico, USA): Journal of Petrology, v. 46, p. 407-439.

Wooden, J.L., and DeWitt, E., 1991, Pb isotope evidence for a major Early Proterozoic crustal boundary in western Arizona, *in* Karlstrom, K.E., ed., Proterozoic Geology and Ore Deposits of Arizona: Arizona Geological Society Digest, v. 19, p. 27-50.

Yuan, H., and Dueker, K., 2005, Upper mantle tomographic V_p and V_s images of the Rocky Mountains in Wyoming, Colorado, and New Mexico: Evidence for a thick heterogeneous chemical lithosphere, *in* Karlstrom K.E., and Keller, G.R., eds., The Rocky Mountain Region — An Evolving Lithosphere: Washington, D.C., American Geophysical Union, Monograph Series 154, p. 329-347.

Zimmerer, M.J., 2019, $^{40}Ar/^{39}Ar$ geochronology, vent migration, and hazard implications of the youngest eruptions in the Raton–Clayton volcanic field: New Mexico Geological Society, Guidebook 70, p. 151-160.

Zimmerer, M.J., Lafferty, J., and Coble, M.A., 2016, The eruptive and magmatic history of the youngest pulse of volcanism at the Valles caldera: Implications for successfully dating late Quaternary eruptions: Journal of Volcanology and Geothermal Research, v. 310, p. 50-57.

Zurek, B., and Dueker, K., 2005, Lithospheric stratigraphy beneath the Southern Rocky Mountains, *in* Karlstrom K.E., and Keller, G.R. eds., The Rocky Mountain Region—An Evolving Lithosphere: Washington, D.C., American Geophysical Union, Monograph Series 154, p. 317-328.

New Mexico Geological Society, Special Publication 14, Geology of the Mount Taylor Area, 2020, p. 17-28.

VOLCANIC EVOLUTION OF MOUNT TAYLOR STRATOVOLCANO, NEW MEXICO: FACTS AND MISCONCEPTIONS

Fraser Goff[1], William McIntosh[1,2], Lisa Peters[2], John A. Wolff[3], Shari A. Kelley[2], Cathy J. Goff[4], and G. Robert Osburn[5]

[1]Department of Earth and Environmental Science, New Mexico Tech, 801 Leroy Place, Socorro, NM 87801; candf@swcp.com
[2]New Mexico Bureau of Geology and Mineral Resources, 801 Leroy Place, Socorro, NM 87801
[3]School of the Environment, Washington State University, Pullman, WA 99164
[4]Independent Consultant, 5515 Quemazon, Los Alamos, NM 87544
[5]Earth and Planetary Science, Washington University, St. Louis, MO 63130

Abstract—Mount Taylor (3445 m elevation) developed from roughly 3.2 to 2.5 Ma and is a composite stratovolcano (Mount Taylor stratovolcano, MTS) composed of coalesced basaltic trachyandesite to rhyolite domes, flows, plugs, dikes, interlayered ash, and comingled debris flows. The main edifice is surrounded by later cones and flows of (mostly) trachybasalt that erupted until 1.27 Ma. Contrary to previous interpretations, the summit trachyandesite flows of MTS (2.75 to 2.72 Ma) are not the youngest eruptions on the edifice. A variety of satellite domes, flows, radial dikes and a central plug of mostly trachydacite were intruded and erupted until 2.52 Ma. Thus, also contrary to previous studies, the youngest eruptions at MTS are not "andesitic." An elongate, eastward-facing Amphitheater about 6.5 km long formed in the approximate center of MTS late in its development. The best explanation for formation of the MTS Amphitheater is erosion by mass wasting and fluvial incision. This feature did not form from large, centralized, late stage explosions, from Mount St. Helens-type lateral blasts with associated fall and ignimbrite, or from Pleistocene glaciation of the edifice, although it may have formed in part from an unrecognizable debris avalanche. Previous studies have speculated that MTS developed a single cone or bulbous dome that once attained a height of 4270 m, but it is more probable that the mixture of small, coalesced vents and domes forming the original summit never rose above 3800 m. Using this maximum elevation, an average diameter of 16 km for the volcano from recent mapping, and the formula for a right circular cone, the estimated volume of MTS is 85 km^3±20%. From this volume and the time span of intense MTS construction (0.76 Ma), the average eruptive (magmatic) flux rate is about 0.11 km^3 per 10^3 years. These values for MTS are small compared to those of Cascades-type subduction zone stratovolcanoes, such as Mount St. Helens.

INTRODUCTION

Mount Taylor is an extinct composite stratovolcano that is part of the greater Mount Taylor–Mesa Chivato volcanic field (Hunt, 1938; Crumpler, 1980a, b), and is one of many volcanic fields that define the northeast-trending Jemez Lineament (JL, Figs. 1, 2; Mayo, 1958; Luedke and Smith, 1978; Goff and Kelley, 2020). Mount Taylor stratovolcano (MTS, 3445 m) forms a conspicuous topographic feature roughly 20 km northeast of Grants and is New Mexico's second largest late Cenozoic volcanic complex after the Valles caldera and Jemez Mountains (Crumpler, 2010). The peak is sacred to the nearby Acoma, Laguna and Zuni pueblos and is known as "Turquoise Mountain," or *Tso Tzil*, to the Diné (Navajo). The present name honors President Zachary Taylor, a major general who became U.S. president in March 1849 and who died prematurely in office in July 1850.

Many researchers have mapped and conducted volcanic and petrologic studies at Mount Taylor starting with Dutton (1885); see Goff et al. (2019) for a comprehensive list. Because of the abundant uranium resources hosted in Jurassic rocks beneath and around the volcano, the New Mexico Bureau of Geology and Mineral Resources produced a series of 7.5-minute geologic quadrangles beginning in 2007 (Goff et al., 2008, 2012, 2014a; McCraw et al., 2009; Osburn et al., 2010; Skotnicki et al., 2012), which resulted in a detailed 1:36,000-scale compilation of the Mount Taylor and southwest Mesa Chivato region (Goff et al., 2019). During this mapping, 107 new $^{40}Ar/^{39}Ar$ dates and 216 new major and trace element chemical analyses were obtained. Toward the end of the mapping campaign, we also employed a portable flux gate magnetometer to acquire magnetic polarities of important volcanic units. The polari-

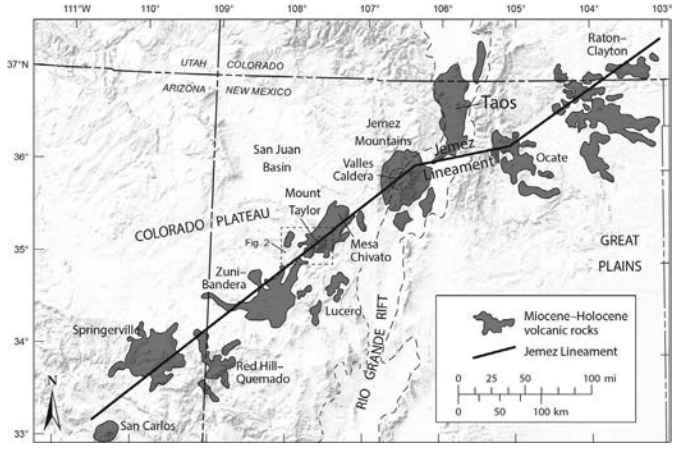

FIGURE 1. Map showing the location of Mount Taylor with respect to other volcanic fields of the Jemez Lineament, to the San Juan Basin, and to basins of the Rio Grande rift. Inset shows location of Figure 2. Modified from Goff et al. (2019).

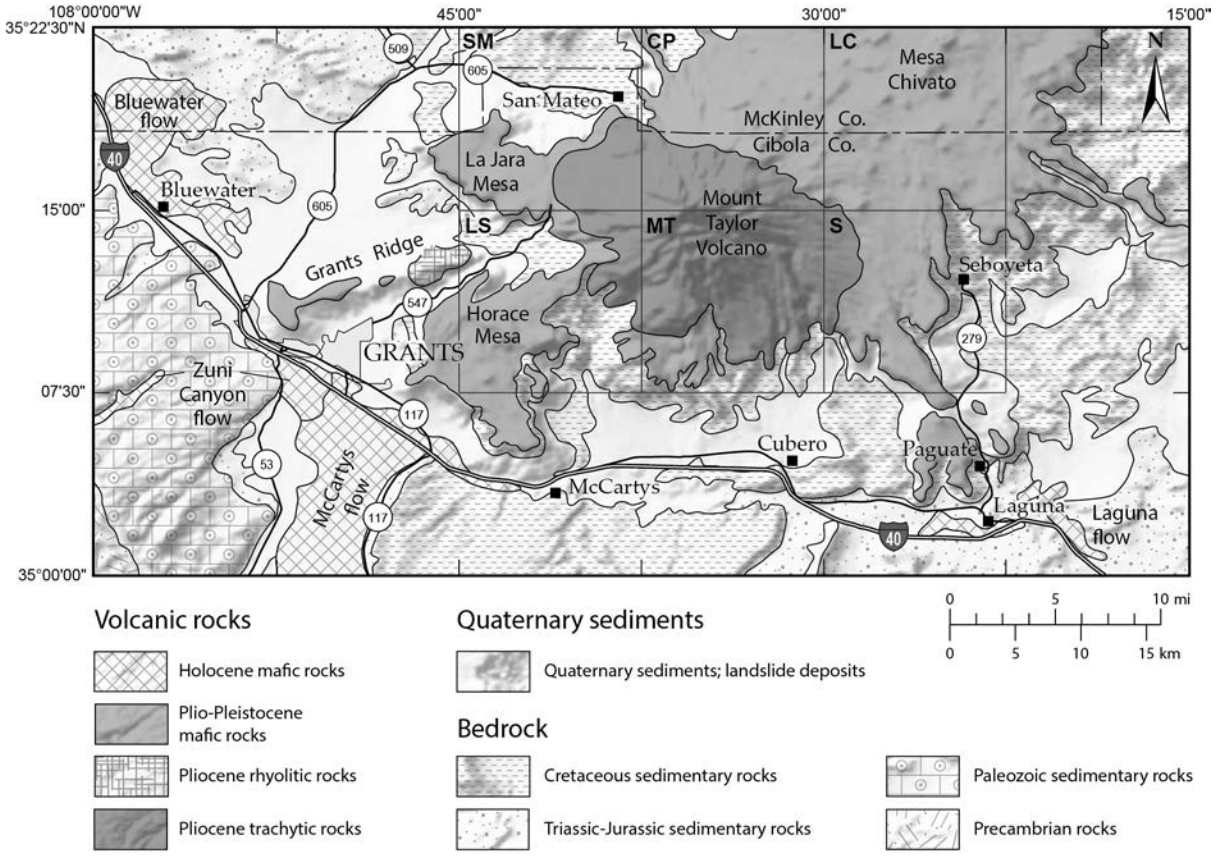

FIGURE 2. Map of Mount Taylor volcano region showing simplified geology and locations of six recently completed 1:24,000 quadrangles: CP = Cerro Pelón, LC= Laguna Cañoneros, LS = Lobo Springs, MT = Mount Taylor, S = Seboyeta, and SM = San Mateo. Modified from Goff et al. (2019).

ties provided an independent check on the dates (see booklet in Goff et al., 2019, for all radiometric and magnetic polarity results). This paper summarizes the geology, dates, chemistry and magnetic polarities of MTS, presents a revised volcanic evolution for its development, and comments on the origin of MTS Amphitheater (Fig. 3). Volcanism on Mesa Chivato and Grants Ridge is not covered herein.

GEOLOGIC BACKGROUND

Jurassic and Cretaceous non-marine and marine sedimentary rocks underlie MTS and Cretaceous strata interfinger with each other around and beneath MTS. The Jurassic Westwater Canyon Member of the Morrison Formation is host to abundant uranium ores that made the Grants district the largest uranium-producing area in the United States from 1951–1980. This district still ranks second in the United States in uranium reserves (Kelley, 1963; McLemore, 2011; McLemore and Chenoweth, 2017). Several hundred boreholes drilled by mining companies through volcanic rocks west and north of MTS traced uranium-bearing Jurassic strata beneath the volcano flanks east of the Mt. Taylor Mine at San Mateo (Goff et al., 2019). The upper Cretaceous section is a transgressive–regressive sequence (Sears et al., 1941; Kelley, 1963; Owen and Owen, 2003) that records a gradual transition from open marine conditions to marginal marine and deltaic settings. Coal production from Upper Cretaceous strata in the map area covered by Goff et al. (2019) was small and limited to the eroded basins south and southwest of MTS (Hoffman, 2017, fig. 10).

MTS overlies the southeast margin of the Laramide San Juan Basin and also lies in a transition zone of extension between the Colorado Plateau to the northwest and the Rio Grande rift (RGR) to the east (Olsen et al., 1979; 1987; Thompson and

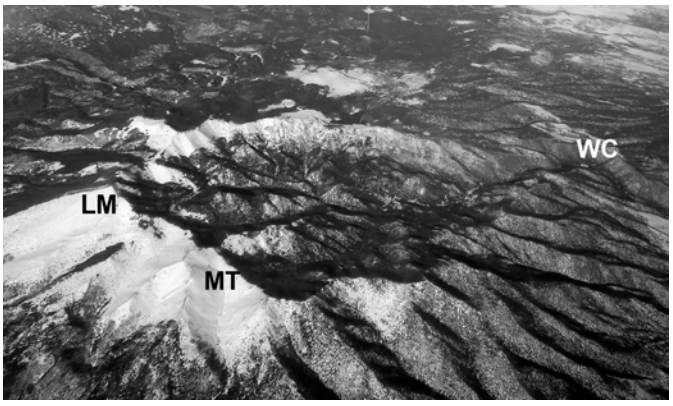

FIGURE 3. Photo taken from an airplane during the winter of 2008 looking northeast across the Amphitheater of MTS toward Mesa Chivato; LM = La Mosca, MT = Mount Taylor; WC = Water Canyon. Photo courtesy of Kirt Kempter.

Zoback, 1979; Aldrich and Laughlin, 1984). Recent interpretation of 3D seismic structure beneath the RGR to a depth of 200 km (Sosa et al., 2014) suggests that the transition zone is a broad low velocity region and that an upwelling sheet or linear bulge of hot mantle material underlies the JL. This upwelling mantle sheet has probably fed the volcanic centers along the JL, including Mount Taylor and Mesa Chivato (Fig. 1).

ANALYTICAL METHODS

Recent mapping of Mount Taylor and surrounding areas was enhanced by petrographic examination of 150 polished thin sections. These observations constrain mineral assemblages and textures in many volcanic units and allow us to assign rock names to units that were not chemically analyzed. Phenocrysts in MTS eruptive products are similar to those in mildly alkalic volcanic terrains erupted in or near some continental rifts (Table 1; Wilson, 1989, fig. 11.12).

In this paper, we highlight 62 of 107 $^{40}Ar/^{39}Ar$ dates (Table 2) obtained during the 2007–2013 quadrangle mapping projects, including only those dates that illustrate the development and evolution of MTS proper. Dates from the Grants Ridge rhyolite center and greater Mesa Chivato are not discussed herein (see Goff et al., 2019, for these results). All dates in Table 2 are calculated using the Fish Canyon Tuff sanidine neutron flux interlaboratory monitor (FC-2) with an assigned age of 28.201 Ma (Kuiper et al., 2008).

To help constrain our geochronology, we measured the magnetic polarity of many samples by handheld (portable) fluxgate magnetometer (all rock types) and Brunton™ compass (basaltic rocks only; Table 2). We used a μMAG™ digital magnetometer built by MEDA, Inc. (Dulles, VA). Many volcanic rocks in the Mount Taylor region were erupted during the magnetic polarity flip from the Gauss Normal Chron to the Matuyama Reverse Chron at 2.581 Ma (Gee and Kent, 2007, table 3). Unfortunately, our magnetic polarity measurements started late in the mapping campaign and many hard-to-access locations were not revisited. Note that this report employs the Plio–Pleistocene boundary of 2.58 Ma in accordance with recent international stratigraphic changes (Cohen et al., 2013).

We also acquired 216 major and trace element chemical analyses of volcanic rocks in the Mount Taylor region using a combination of XRF and ICP-MS methods and analyzed by Washington State University (Fellah, 2011) and ALS Laboratories (Reno, Nevada, see their website for methods). Table 2 lists normalized silica and total alkali contents of 56 dated map units that were key in constraining the evolution of MTS. Complete geochemical data and interpretations will be published at a future time.

VOLCANIC EVOLUTION, MOUNT TAYLOR STRATOVOLCANO

Previous Work

Previous investigations of MTS rocks were conducted by Hunt (1938), Baker and Ridley (1970), Lipman and Moench (1972), Lipman and Mehnert (1979), Crumpler (1982), and Perry et al. (1990). The alkalic (i.e., $Na_2O + K_2O$–rich) chemistry of MTS rocks was noted by all researchers except Baker and Ridley (1970), who mistakenly called the rocks "calc-alkaline." Through the years, rock classification schemes (i.e., "rock names") used by past workers have varied widely, leading to considerable confusion (see Goff et al., 2019, p. 6). Beginning with Hunt (1938), all subsequent studies claimed that the youngest eruptions of the MTS are those that form the high-elevation stack of lavas at the summit (i.e., Mount Taylor proper). Consequently, all previous researchers (e.g., Crumpler, 2010, p. 57) have stated that the youngest MTS summit flows are "andesitic to latitic" in mineralogy and chemistry, post-dating all earlier eruptions of "dacite, quartz latite and rhyolite." As noted below, our investigation revealed a different sequence of eruptions.

Rock Classification from Chemistry

For our Mount Taylor project (Table 1 and Fig. 4), we have used the internationally accepted classification scheme of Le Bas et al. (1986), previously published chemistry, and our own chemical analyses to rename and categorize the volcanic units.

TABLE 1. Phenocryst mineralogy of volcanic rocks, Mount Taylor stratovolcano, New Mexico (Goff et al., 2019).

	Basanite	Basalt	Tbasalt	Tandesite	Trachyte	Tdacite	Rhyolite
Olivine	X	X	X	x		tr	
Analcime	x						
Augite	X	X	X	X	x	X	x
Hypersthene			x	x		x	
Hornblende			x	X	X	X	x
Biotite			tr	x	X	X	X
Plagioclase	X	X	X	X	X	X	x
K-Feldspar				x	x	X	X
Quartz				tr		x	X

X = major, x = minor, tr = trace; Tbasalt = trachybasalt, Tandesite = trachyandesite, Tdacite = trachydacite.

TABLE 2. Summary of $^{40}Ar/^{39}Ar$ dates, magnetic polarities, silica and total alkalis for Mount Taylor stratovolcano.

Site See Fig. 6	Map Unit [1]	Rock Type [2]	Location UTM NAD 27	Ar^{40}/Ar^{39} Lab No.	Phase[3]	Age Analysis[4]	Steps/ Analyses	Age (Ma)[5] ± 2σ	MSWD[6]	Magnetic Polarity[7]	Age Match[8]	Silica[9] (norm)	TAS[9] (norm)
Phase 4: Terminal mafic volcanism													
1	Qyatb	Aphyric tbasalt, Cerro Pelon	026668 390562	59077	Gdm	LTF	6	1.27±0.19	10.78	nd		49.18	6.84
2	Qfqtb	Qtz-bearing tbasalt	0269195 3905411	59754	Gdm	LSH	8	1.54±0.07	1.60	nd		49.51	5.10
3	Qfqtb	Qtz-bearing tbasalt	0258356 3900247	62196	Gdm	LSH	7	1.65±0.04	2.70	R (brun)	yes	48.78	5.20
4	Qyh	Aphyric tbasalt	0264574 3907479	63320	Gdm	BSH	7	1.73±0.02	3.45	confused	lightning	na	na
5	Qyxtb	Xenocrystic tbasalt	025843 390625	58995	Gdm	LSH	9	1.75±0.03	1.80	R (fgate)	yes	48.73	5.82
6	Qatc/Qatb	Aphyric tbasalt	0266761 3908202	59755	Gdm	LSH	8	1.77±0.05	1.18	nd		na	na
7	Qyxtb	Xenocrystic tbasalt	0260840 3917200	58996	Gdm	LSH	8	1.80±0.05	2.80	N (brun)	yes	48.85	5.98
8	Qatd/Qatb	Horace Mesa dike and flow	0257002 3896823	63322	Gdm	BSH	5	1.80±0.01	5.57	N (fgate)	yes	48.38	6.09
9	Qyxtb	Xenocrystic tbasalt	0269287 3904689	59211	Gdm	LSH	10	1.86±0.06	1.93	R(brun)	yes	48.99	5.63
off map N	Qyptb	Gabbro-bearing tbasalt	0267619 3913003	59080	Gdm	LTF	7	2.31±0.13	8.83	R (fgate)	yes	49.09	5.69
10	Qyfpb	Fine-grained tbasalt	0268705 3907280	59213	Gdm	LSH	9	2.38±0.14	3.70	nd		47.60	5.06
Phase 3: Youngest Summit, Amphitheater and Satellite Euptions													
11	Qxgi	Oliv gabbro plug	0267302 3901456	62193	Gdm	LSH	8	1.98±0.05	1.57	nd		47.82	4.90
12	Teta	Enclave tandesite	0261548 3899333	58056	San	LSH	4	2.52±0.07	4.85	R (fgate)	yes	61.38	7.72
13	Tsptd	"Spud Patch" tdacite	0265508 3907887	59081	Gdm	LTF	5	2.55±0.06	3.76	R (fgate)	yes	62.28	9.17
14	Tqtd	Intrusion interior	0264093 3902080	58728	San	LTF	14	2.56±0.02	1.31	R (fgate)	yes	68.61	8.88
15	Tqtd	Intrusion west margin	0263623 3901970	58727	San	LTF	8	2.60±0.02	1.83	R (fgate)	yes	71.11	9.52
Phase 3: Amphitheater Dikes													
16	Thbi	Tdacite, east Amph	0267629 3900865	59112	Bio	LSH	6	2.66±0.06	2.60	N(fgate)	yes	62.78	9.85
17	Tbi	Tdacite west Amph	0263507 3903038	63722	San	LSH	13	2.66±0.01	1.47	nd		67.98	10.83
18	Thbi	Tdacite west Amph	0263207 3903088	63688	Bio	BSH	16	2.67±0.01	1.07	nd		63.31	9.81
19	Tbhd	Tdacite NW Amph	0264782 3903958	63687	Bio	BSH	16	2.67±0.01	2.07	nd		63.42	9.29
20	Tbi	South Wall Tdacite dike	026632 390015	59003	Bio	LSH	11	2.71±0.03	1.40	nd		64.69	10.27
21	Tbi	Tdacite SE Amph	0265107 3900783	59004	Bio	LSH	9	2.79±0.02	0.60	nd		66.68	10.61
22	Tbi	Tdacite, intrudes rhyolite	0265667 3901451	59072	Plag/San	LSH	13	2.80±0.06	2.60	nd		na	na
Phase 3: Satellite Domes and Plugs													
23	Thta	Hbd tandesite W flank	0257095 3903685	58069	Plag	LSH	10	2.62±0.10	0.90	N (fgate)	yes	60.83	9.04
24	Tbd	Tdacite N Amph rim	0266058 3903990	63360	Gdm	BSH	6	2.66±0.01	5.75	N (fgate)	yes	63.77	9.44
25	Thtd	Hbd tdacite NW flank	0262388 3904802	63364	Hbd	BSH	4	2.66±0.02	1.83	N (fgate)	yes	62.37	9.57
26	Tbhtd	Porphyritic tdacite NW flank	0261430 3905862	63362	Bio	BSH	3	2.66±0.01	1.84	N (fgate)	yes	62.72	9.38
27	Tpota [10]	Oliv tandesite NE Amph rim	0268534 3903124	58999	K-feld	LSH	13	2.69±0.04	1.20	nd		62.04	9.11
off map E	Tpota [10]	Oliv tandesite, flow end	0272753 3901225	61215	Gdm	LSH	8	2.69±0.01	1.97	nd		na	na
28	Tbhtd	Tdacite plug S flank	0260199 3898207	59765	Bio	LSH	9	2.70±0.03	2.27	N (fgate)	yes	64.37	9.50
29	Ttdc	Porphyritic tdacite SE rim	0268263 3900104	59001	K-feld	LSH	9	2.72±0.04	1.90	nd		na	na
Phase 3: Mount Taylor and La Mosca													
30	Thta	Tandesite below MT summit	0262890 3902543	62195	Gdm	LSH	11	2.72±0.02	1.65	N (fgate)	yes	57.91	8.37
31	Tsetd	Porphyritic tdacite NW flank	0262306 3907190	59083	Plag	LSH	6	2.73±0.06	1.61	N (fgate)	yes	62.52	9.43
32	Tpbti/Tpbtd	Tdacite intrusion La Mosca	026369 390413	59089	K-feld	LSH	8	2.73±0.03	1.98	nd		66.28	10.64
33	Thtas	Tandesite MT summit	0262711 3902326	62191	Gdm	LSH	7	2.75±0.01	int age	confused	lightning	59.69	8.85

TABLE 2. Continued.

Site See Fig. 6	Map Unit [1]	Rock Type [2]	Location UTM NAD 27	Ar^{40}/Ar^{39} Lab No.	Phase[3]	Age Analysis[4]	Steps/ Analyses	Age (Ma)[5] ± 2σ	MSWD[6]	Magnetic Polarity[7]	Age Match[8]	Silica[9] (norm)	TAS[9] (norm)
Phase 2: Older lavas and domes													
34	Tpb	Classic plag basalt	0262853 3896155	58741	Gdm	FSH	5	2.78±0.06	2.80	confused		50.64	5.89
35	Tptd	Porphyritic plag tdacite	0263193 3898119	58736	Bio	FSH	11	2.80±0.05	2.03	N (fgate)	yes	62.28	9.24
36	Tpb	Classic plag basalt	026734 390269	58997	Gdm	LSH	5	2.81±0.04	2.30	N (fgate)	yes	51.25	6.13
37	Ttai	Oliv tandesite dike	026011 390771	58998	Gdm	LSH	7	2.81±0.03	1.00	nd		57.57	8.57
38	Ttd	Tdacite Rinconada Can	0259159 3898891	59768	Plag	LSH	11	2.81±0.14	1.59	nd		64.12	9.76
39	Tpetd	Enclave tdacite W flank	0260635 3904813	59002	K-feld		8	2.83±0.04	Isochron	N (fgate)	yes	63.57	9.74
40	Tcpt	Porphyritic trachyte W flank	0260825 3903942	59733	San	LSH	15	2.84±0.08	1.12	nd		67.68	11.54
41	Tbht	Bio-hbd trachyte S flank	0264679 3898779	59217	Plag	LSH	9	2.85±0.04	1.36	nd		65.94	10.92
42	Tplta	Plag tandesite NW flank	026143 391001	58994	Gdm	LSH	7	2.88±0.04	1.30	nd		62.22	9.15
Phase 1 (late) to Phase 3 (early): Pyroclastic rocks													
off map E	Ttdt	Pumice, fall deposit	0277885 3897421	61250	San	LSH	11	2.717±0.002	2.42	nd		69.33	9.85
43	Ttdt	Pumice tdacite ignimbrite	0258260 3901541	58057	Bio	LSH	4	2.73±0.06	1.90	nd		64.79	9.10
44	Twst	Pumice ignimbrite SE flank	0268252 3898323	59069	San	LSH	15	2.76±0.03	2.00	nd		na	na
45	Twst	Pumice in undivided tuffs	0270509 3895944	59068	San	LSH	15	2.78±0.03	1.00	nd		69.59	9.90
46	Ttdt	Pumice tdacite ignimbrite	026219 390893	59006	Plag	LSH	7	2.81±0.09	1.70	nd		62.77	8.71
47	Twst	Pumice in undivided tuffs	0270509 3895944	59067	San	LSH	9	2.85±0.07	3.30	nd		na	na
48	Twst	Pumice in undivided tuffs	0270891 3896290	59071	San	LSH	14	2.89±0.04	2.00	nd		66.55	8.98
off map N	Twst	Pumice, fall despost	026846 391648	59218	Plag	LTF	20	3.06±0.12	2.41	nd		65.35	7.99
49	Trt	Pumice, fall desposit	0259632 3911188	59005	Bio	LSH	5	3.10±0.20	5.90	nd		74.07	9.41
Phase 1: Mount Taylor floor													
50	Tre	East Amph rhyolite	0265885 3902701	59070	San	LSH	12	2.93±0.04	0.80	nd		68.67	11.56
51	Trw	West Amph rhyolite	0263405 3902479			K/Ar date, Perry et al, 1990		3.03±0.11				73.79	8.60
52	Ttr	Trachyte, east Amph	0267973 3901341	62185	Gdm	LSH	7	3.16±0.01	0.9?	nd		61.02	10.85
53 [11]	Toab	Alkali basalt Water Can	0273250 3894422	61226	Gdm	LSH	10	3.18±0.04	3.27	N (fgate)	yes	48.01	4.62
off map N	Totb	Aphyric tbasalt	0263545 3914403	59212	Gdm	LSH	7	3.22±0.06	0.52	R (brun)	yes	47.85	5.41
54	Toab	Alkali basalt plug S flank	0260052 3898385	59756	Gdm	LSH	9	3.23±0.12	1.76	R (fgate)	yes	46.39	4.56
55	Tbaa	Amph basanite	0266680 3902034	62189	Gdm	LSH	4	3.24±0.04	1.32	nd		43.60	5.35
56	Tbhtd	Tdacite, Riconada Canyon	0260986 3898996	58070	WR	LSH	5	3.28±0.20	8.50	N (fgate)	yes	63.88	9.82
57	Tbaw	West basanite, Lobo Can	025805 390129	58073	WR	LSH	6	3.66±0.15	2.60	R (fgate)	yes	44.37	6.95
off map SE	Tbae	East basanite SE flank	0277203 3894190	61227	Gdm	LSH	10	3.74±0.02	1.55	R (fgate)	yes	44.33	5.58

[1]From geologic map of Goff et al. (2019)
[2]Tbasalt = trachybasalt, Tandesite = trachyandesite, Tdacite = trachydacite
[3]Bio = biotite, Gdm = groundmass, Hbd = hornblende, K-Feld = K-feldspar, Plag = plagioclase, San = sanidine, WR = whole rock
[4]LTF = laser total fusion, LSH = laser step heat, FSH = furnace step heat, BSH = bulk step heat
[5]Mean Square Weighted Deviation
[6]All dates use the Fish Canyon Tuff sanidine neutron flux interlaboratory monitor (FC-2) with an assigned age of 28.201 Ma (Kuiper et al., 2008).
[7]N = normal polarity, R = reverse polarity, brun = brunton compass, fgate = flux gate magnetometer, nd = not determined
[8]Polarity and age match within error of the date (see Gee and Kent, 2007, or Goff et al., 2019, table 2).
[9]Silica = SiO_2, normalized wt%, TAS = total alkalis, $Na_2O + K_2O$, normalized wt%, na = not analyzed
[10]Unit Tpota was dated at two different locations several kilometers apart to verify age continuity.
[11]Date site is off map to southeast but unit is exposed in Water Canyon.

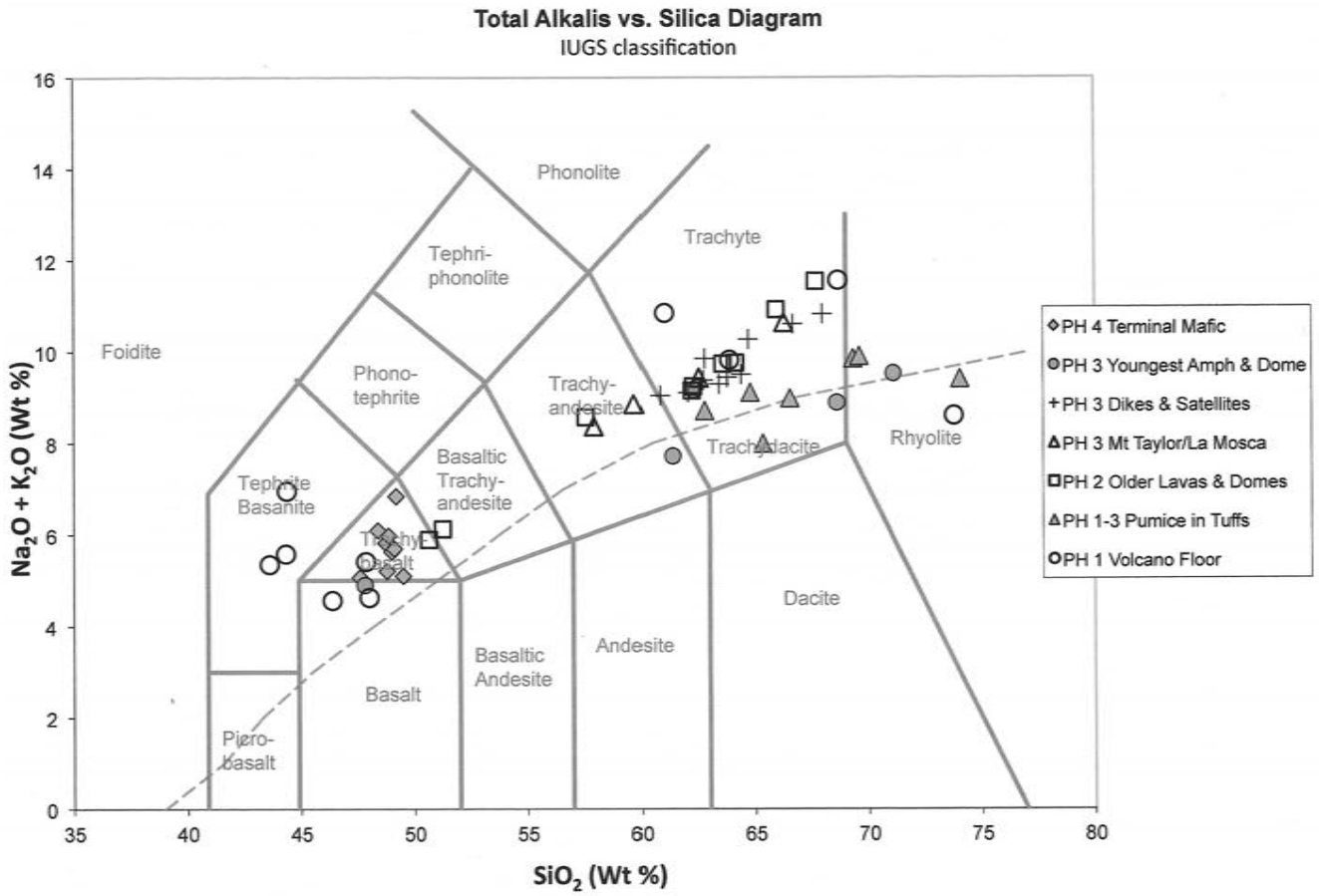

FIGURE 4. Total alkali versus silica plot for MTS rocks listed in Table 2 (Le Bas et al., 1986). Dashed line separates alkaline (top) from calc-alkaline rocks (Irvine and Baragar, 1971). Age ranges: Phase 1, 3.74–2.90 Ma; Phase 2, 2.90–2.75 Ma; Phase 3, 2.75–2.53 Ma; Phase 4, 2.50–1.27 Ma. Amph = Amphitheater.

Thus, most alkali basalts (hawaiites) are now called trachybasalts; basaltic andesites (mugearites) are called basaltic trachyandesites; andesites (latites) are called trachyandesites; and quartz latites are called trachydacites. The only volcanic rocks that we have not renamed are rhyolites and basanites, although we reserve the name trachyte for a few of the most alkali-rich rocks that plot in the trachydacite-trachyte field (Fig. 4).

The total-alkali versus silica plot (Fig. 4) displays the restricted group of dated MTS samples prepared for this paper (Table 2; see Fellah, 2011, fig. 8 or Goff et al., 2019, fig. 8 for comprehensive plots that include Grants Ridge and Mesa Chivato). Figure 4 shows a fairly linear trend between basalt/trachybasalt and trachydacitic end-members. Basanites form a separate group, and there is a separate trend for pyroclastic rocks and rhyolites, with the caveat that such rocks may have lost alkali elements during post-eruptive weathering or alteration. Note that, for the most part, MTS rocks are alkalic, not calc-alkalic as previously stated by Baker and Ridley (1970).

Construction of Mount Taylor Stratovolcano

Our new dates and magnetic polarity measurements indicate that the main edifice and satellite domes of MTS were erupted from about 3.2–2.5 Ma, more or less in agreement with previous researchers, although dissimilar in many details (Lipman and Mehnert, 1979; Perry et al., 1990; Crumpler, 2010). Thus, construction of MTS was essentially complete by the end of the Pliocene at 2.5 Ma, but erosion since that time has decapitated the highest points of the original complex and carved out the Amphitheater (Fig. 3).

MTS is surrounded by and interlayered with mostly mafic lava flows, scoria cones, and a few centers of more silicic composition, which are not discussed further in this paper. Overall, the most common mafic rock is trachybasalt (hawaiite). The few eruptions of basanite and basalt generally occur relatively early in the eruptive history, while trachybasalt is predominant in later eruptions (Figs. 4, 5, 6).

Our dates and those of others show that initial but sporadic volcanism in the Mount Taylor region began at about 4.49±0.08 Ma (Picacho Peak basanite plug and dikes; Hallett et al., 1997) and ended at about 1.27±0.19 Ma (Cerro Pelón trachybasalt cone and flow). Again, this age range generally agrees with the range determined by previous researchers (e.g., Lipman and Mehnert, 1979), but the details are considerably different.

What follows are descriptions of the four phases of eruptions that formed the MTS. Unit name identifiers are from Goff et al. (2019).

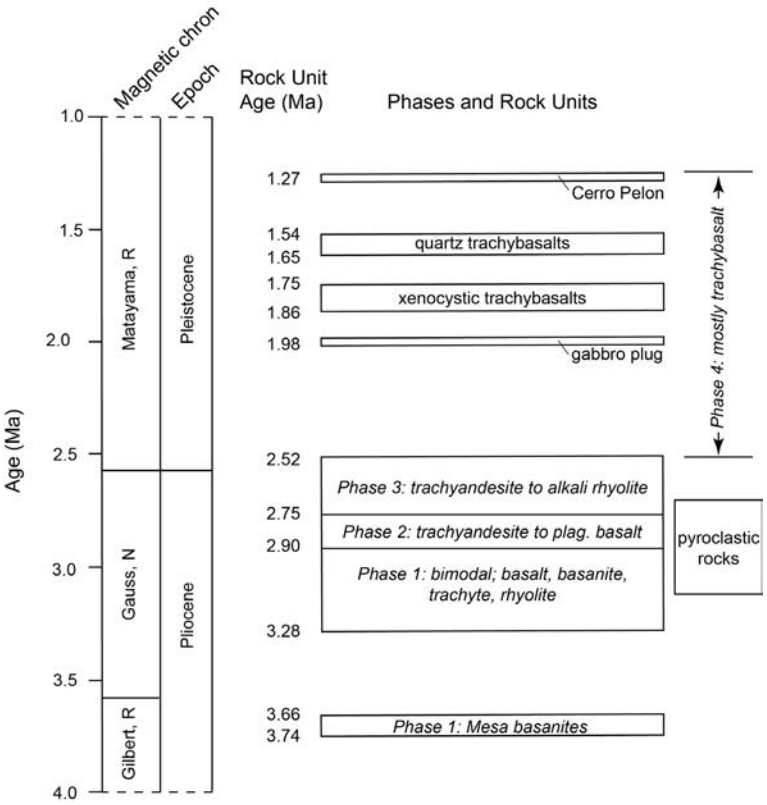

FIGURE 5. Diagram showing the evolution of MTS compared to major magnetic polarity intervals (Chron: see text); ages and rock names from Table 2; plag. = plagioclase.

Phase 1, the volcano floor (3.74–2.93 Ma)

Phase 1 volcanism (Figs. 5, 6) began with the eruption of two widespread flows of basanite that initially formed mesa caps (units Tbae and Tbaw, 3.74–3.66 Ma, Table 2), as documented by previous workers (Lipman and Moench, 1972; Perry et al., 1990). Next came eruption of a trachydacite dome exposed in the bottom of upper Rinconada Canyon (unit Tbhtd). The date for this unit (3.28±0.20 Ma) has a relatively large error, but the magnetic polarity is normal, suggesting an age <3.22 Ma (Table 2). Following emplacement of this dome, another widespread eruption of basanite occurred in the eastern sector of the present Amphitheater (unit Tbaa, 3.24±0.04 Ma), as well as eruptions of alkali basalt (unit Toab, 3.23±0.12 and 3.18±0.04 Ma), now exposed in upper Rinconada Canyon and in the bottom of the central to eastern Amphitheater. Both the later basanite and coeval flows of alkali basalt flowed many kilometers down ravines associated with an earlier Water Canyon (not shown on Fig. 6 for clarity; see Goff et al., 2019). Within what is now the eastern Amphitheater, a small trachyte dome (unit Ttr, 3.16±0.01 Ma) was erupted, followed by emplacement of rhyolite domes and intrusions in the western and central Amphitheater (units Trw and Tre, 3.03±0.11 and 2.93±0.04 Ma, respectively). Small volume rhyolite to trachydacite ignimbrite and fall deposits (units Trt, 3.10±0.20 Ma, and Twst, ranging from 3.04–2.74 Ma) filled early paleocanyons and paleoravines, particularly in the Water and San Mateo canyon areas, and sporadically covered mesa tops around the volcano (Dunbar et al., 2013; Kelley et al., 2013). Products of individual pyroclastic eruptions are <1 km^3 in volume and probably originated during silicic dome eruptions. No large pyroclastic deposits, vents, craters or caldera have been identified at MTS, although thickness trends point to a source or sources in the west-central part of the early edifice.

Phase 2, the stratovolcano grows (2.88–2.78 Ma)

During phase 2, the growing stratovolcano erupted a mixture of trachyandesite, trachydacite, and trachyte lavas and domes, and associated small volume ignimbrites and tuffs (Figs. 4, 5, 6). Two previously unrecognized trachytes (Tbht and Tcpt; Table 2) were dated at 2.85±0.04 and 2.84±0.08 Ma, respectively. The second trachyte is overlain by a thick trachydacite flow (unit Tpetd) dated at 2.83±0.04 Ma, which contains abundant mafic enclaves. Field relations and other dates bracket the early Phase 2 dome eruptions to be between 2.88 and 2.78 Ma. Small volume ignimbrites (e.g., unit Ttdt ranging from 2.81 to 2.73 Ma) continued to fill in preexisting ravines and depressions and are also found in scattered outcrops around the volcano interlayered with trachybasalt and minor basalt lavas, and with early volcaniclastic rocks shed off the developing volcano.

The defining units ending Phase 2 consist of a series of "plagioclase" or "big feldspar" mafic eruptions, often called "plagioclase basalt" (2.81–2.78 Ma). Baker and Ridley (1970) first described these flows. What we call classic plagioclase basalts (Table 2, Figs. 4, 5, 6) are borderline trachybasalt to basaltic trachyandesite in composition. We found that most MTS rocks previously called plagioclase basalt range from basaltic trachyandesite to trachyandesite in composition (Goff et al., 2019). The classic varieties are among the latest eruptions of this group, but these rocks are interlayered within the uppermost intermediate flows making up Phase 2 (e.g., unit Tptd dated at 2.80±0.05 Ma). "Plagioclase basalt" is most common on the central to eastern flanks of MTS, exposed in canyons cutting its southern flank, and on the bluff east of San Mateo Basin.

Phase 3, the final stratovolcano eruptions (2.75–2.52 Ma)

Continued effusion of intermediate composition lavas and domes from 2.75–2.52 Ma characterized volcanic activity for Phase 3. These eruptions originated in part from a composite stock generating radial dikes that developed beneath the central to western Amphitheater (Fig. 6). Our new dates and chemical analyses show that trachyandesite and trachydacite were coeval in time and space. For example, what is now the Mount Taylor summit was built of successive flows of hornblende trachyandesite (units Thta and Thtas, 2.75±0.01 to 2.72±0.02 Ma) erupted from a buried or obliterated vent in the western Amphitheater. "La Mosca" (3,365 m; Fig. 3) is constructed by a small intrusion exposed in the northwest Amphitheater wall (unit Tpbti, 2.73±0.03 Ma) that produced a thick flow of trachydacite (Tpbtd). These are presently the two highest peaks of MTS, but

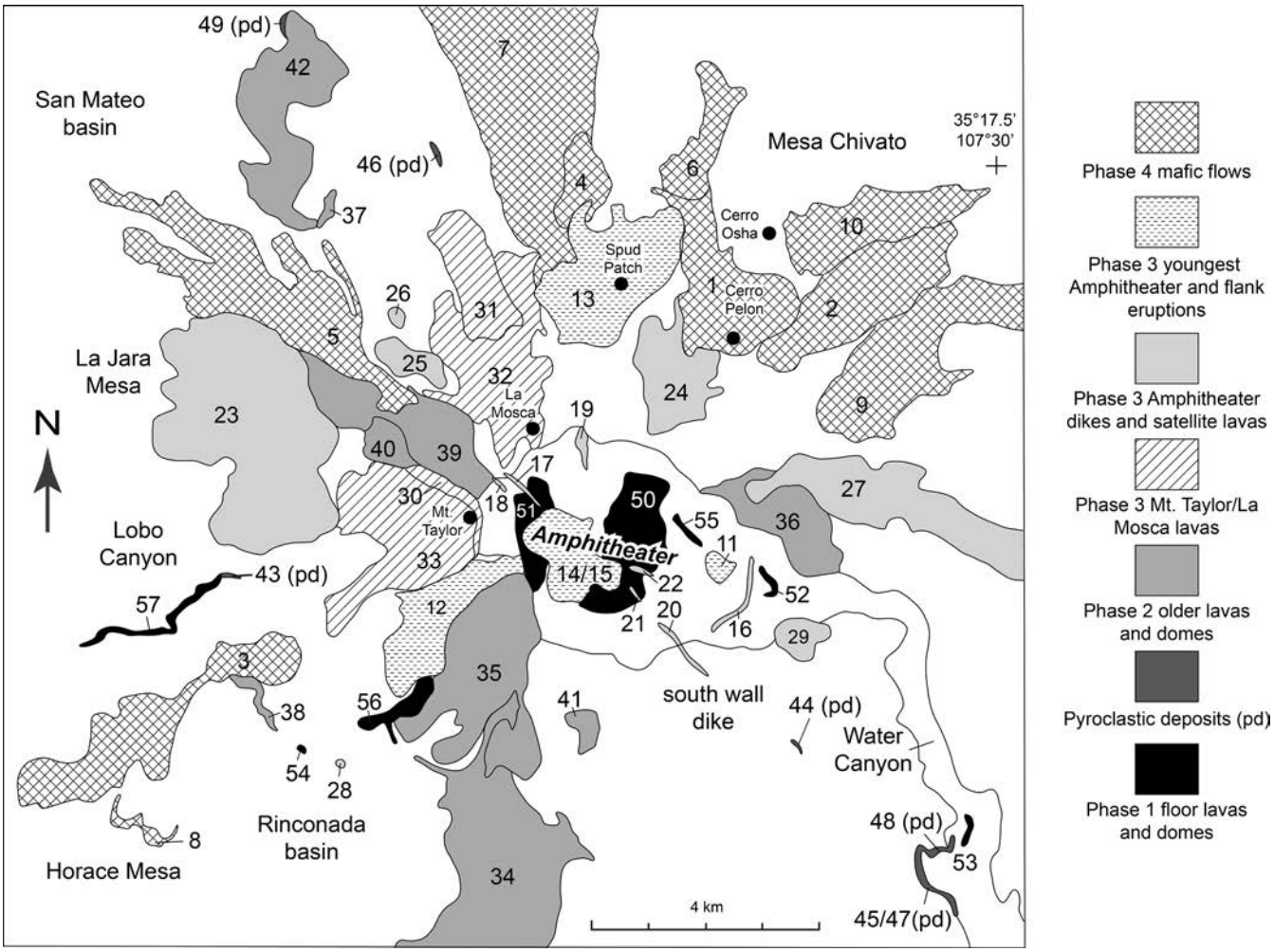

FIGURE 6. Sketch map showing location of MTS rocks according to evolutionary phase of the volcano (Fig. 5). Numbers correspond with location numbers of samples in Table 2, column 1.

due to subsequent erosion, the maximum height of the edifice was higher than now.

During this period, eruptions of ignimbrite and pyroclastic fall deposits virtually ceased. A trachydacite ignimbrite at the head of Lobo Canyon (unit Ttdt) previously identified by Lipman and Mehnert (1979) was dated at 2.73±0.06 Ma. The youngest pyroclastic deposit we found was a relatively thin trachydacite to alkali rhyolite fall deposit east of MTS (e.g., unit Ttdt, 2.717±0.002 Ma). A few dome collapse breccias (glowing avalanche deposits?) are recorded in the larger dome eruptions (i.e., sugary enclave trachydacite, unit Tsetd), but such deposits appear to be a minor component of MTS. In contrast, rapid erosion of the growing volcano formed large aprons and fans of water-transported debris flows and other volcanic sediments interlayered with lava flows. These deposits radiate in all directions away from the volcano, but are thickest to the east and southeast toward the ancestral drainage of the Amphitheater. Possibly, the debris flow sequence contains unrecognizable debris avalanche deposits from Phase 3 domes.

Toward the middle to end of Phase 3 (2.72–2.52 Ma), a series of satellite domes and flows erupted on the margins and flanks of the volcano (e.g., unit Tpota, 2.69±0.02 Ma, average of two dates). These eruptions are mostly trachydacite (Table 2) and match the chemistry and age of several radial dikes exposed within and on the margins of the Amphitheater (2.71 to 2.66 Ma). The last magmatic products emitted from the composite stock are: 1) a trachydacite to alkali rhyolite plug intruded into the western Amphitheater (unit Tqtd, 2.60±0.02 to 2.56±0.02 Ma); 2) the Spud Patch trachydacite satellite dome, erupted on the northern flank of MTS (unit Tsptd, 2.55±0.06 Ma); and 3) an enclave-rich trachyandesite intrusion and flow emplaced on the southwestern margin and flank of MTS (unit Teta, 2.52±0.07 Ma, borderline trachydacite, Figs. 4, 6). The last three magmatic units have reverse magnetic polarity, whereas older Phase 3 rocks have normal polarity. Thus, the youngest magmatism of MTS captures the fundamental change in magnetic polarity at 2.58 Ma (Fig. 5; Gee and Kent, 2007).

Within the eastern Amphitheater floor, a large circular plug of fine-grained olivine gabbro (unit Qxgi, 1.98±0.05 Ma) intruded and uplifted adjacent Cretaceous rocks and caused noticeable hydrothermal alteration of both sandstone and shale (Goff et al., 2019). When viewed from the Amphitheater floor, this columnar-jointed intrusion superficially resembles the famous Devils Tower, Wyoming. It is not clear if this magma

breached the surface to produce a flow. The top of the plug is somewhat vesicular (Hunt, 1938), but any flow that may have erupted from this intrusion has been completely eroded. The gabbro chemically resembles "true" basalt (≤5 wt% alkalis). This is the youngest Phase 3 magmatic event within the Amphitheater and is shown as such on Table 2 and Figure 4 even though it is a mafic intrusion.

Phase 4, terminal mafic volcanism (2.50–1.27 Ma)

Although intermediate to silicic dome and flow eruptions forming MTS ceased at 2.52 Ma, our mapping and dating campaign identified many flank eruptions of mafic flows, cones, and plugs that erupted afterward (Table 2). With few exceptions, these younger eruptions consist of trachybasalt (Fig. 4). A group of peridotite-bearing cones and flows (unit Qyxtb, 1.86–1.75 Ma) erupted from vents northwest, north and northeast of MTS (Goff et al., 2019). Three aphyric trachybasalts erupted on the north and southwest flanks of MTS (units Qyh and Qatb, 1.73, 1.77, and 1.80 Ma). These were followed by a group of distinctive fine-grained quartz-bearing trachybasalts that vented around MTS from 1.65–1.54 Ma (unit Qfqtb). The youngest mafic eruption that we could identify is the cone and flow of Cerro Pelón (unit Qyatb, 1.27±0.19 Ma).

FORMATION OF THE AMPHITHEATER

Controversy still revolves around the origin of MTS Amphitheater (Fig. 3). Four theories have been offered: 1) some form of explosion(s) (Crumpler, 2010, p. 57), 2) a lateral blast or sector collapse (Crumpler, 1982, p. 294; Crumpler, 2010), 3) glaciation (Ellis, 1935; Pierce, 2004), or 4) mass wasting/fluvial erosion (Hunt, 1938; Lipman and Mehnert, 1979; Perry et al., 1990).

First, the Amphitheater did not form from a single large explosion or series of explosions such as occurred at Valles caldera (Smith and Bailey, 1966; Goff et al., 2014b). There are no late, widespread ignimbrite (ash-flow) sheets or other pyroclastic deposits covering the 2.75 to 2.52 million-year-old landscape (i.e., the Phase 3 domes and flows) bordering the Amphitheater, and there are no late-stage circular collapse faults within the inner margins of the Amphitheater. Although non-welded pyroclastic eruptions occurred early in the development of MTS (3.10 to 2.78 Ma; Table 2; Fig. 4), they are volumetrically small (<1 km^3) and mostly restricted to paleocanyons northwest and southeast of the Amphitheater. These early pyroclastic deposits are covered by later Phase 2 dome and flow eruptions forming MTS. In contrast, our very rough estimate of the *original* volume of the Amphitheater, assuming a maximum summit elevation of 3800 m, is 9 km^3 (see below), a volume many times larger than any pyroclastic deposits we observed. This eroded material has been incorporated within the large fan of volcaniclastic sediments that flanks the east and southeast margin of the Amphitheater (see map of Goff et al., 2019).

Second, the Amphitheater did not develop from a Mount St. Helens-type lateral blast deposit (i.e., sector collapse with simultaneous magmatic explosion). Our detailed mapping of MTS identified no late-stage, blast-type pumice deposits or ignimbrites east and southeast of the volcano or elsewhere (e.g., Hoblitt et al., 1981). It is possible that relatively small sector-collapse deposits slid off some of the evolving Phase 2 domes, but we did not observe hummocky landslide or debris avalanche deposits characteristic of catastrophic stratovolcano sector collapse (Voight et al., 1981). Perhaps they are merely hidden in the more voluminous sedimentary debris flow deposits flanking the volcano. Siebert (1984) pointed out that recently formed volcanic amphitheaters formed by debris avalanches have characteristic shapes and breach width approximately equaling the crater width. In contrast, the breach width/crater width of the MTS Amphitheater is about 0.25 (Perry et al., 1990), which could be attributed to significant post-debris avalanche erosion.

Third, the Amphitheater was not carved by Pleistocene glaciation as claimed previously by Ellis (1935) and reiterated more recently by Pierce (2004). Our detailed mapping and early work by Hunt (1938) identified no glacial deposits such as moraines anywhere in or around MTS, nor did we find them above or interlayered in the upper debris flow deposits east and southeast of Water Canyon. The Amphitheater is certainly not U-shaped with a flat floor like classic glacially carved valleys (Fig. 3). More recently, Meyer et al. (2014) tried to find evidence for glaciation (including striated clasts or bedrock) but concluded that glaciation "was unlikely to have occurred for any significant period in the eastern Amphitheater of the mountain where is was previously inferred."

Based on our recent detailed mapping in combination with new dates, we concur with Hunt (1938), Lipman and Mehnert (1979), and Perry et al. (1990) that the Amphitheater most likely developed by simple erosion of the original summit with deposition of the eroded material in the large fan of volcaniclastic sediments east of Water Canyon. Stratovolcanoes with erosional amphitheaters tend to have broad craters with narrow breaches such as observed at MTS (Siebert, 1984; Perry et al., 1990). Doming and fracturing accompanying late-stage injection of radial dikes and the trachydacite-to-alkali rhyolite plug from the composite stock in the west-central part of the volcano probably facilitated erosion. We note that the main trend of 148 radial dikes within MTS is N65°W to N25°W, or approximately parallel to the trend of the Amphitheater (Goff et al., 2019). Magma-induced hydrothermal alteration coinciding with late MTS intrusive activity was observed in many intermediate composition boulders in surrounding debris flows. This alteration likely destabilized the core of the volcano. Emplacement of the late gabbro intrusion beneath the eastern Amphitheater further damaged and weakened the edifice (Goff et al., 2019, p. 17, 29, 32-34). Erosion of the original edifice has created a large eastward-facing basin and has deposited large aprons of volcaniclastic debris around the present MTS.

HOW HIGH WAS PLIOCENE MOUNT TAYLOR

Extrapolation of the exterior morphology of MTS by Crumpler (1982, 2010) suggests the Pliocene summit was once a large bulbous dome, pyroclastic cone or combination thereof, much higher in elevation than now, perhaps as high as 4270

m (14,000 ft) or 825 m higher than today's summit. On the other hand, Perry et al. (1990) observed that present MTS has shallow exterior slope angles of 10 to 12° and contains very minor pyroclastic layers in the summit area, the latter observation verified by our mapping (Goff et al., 2019). The margin of the Amphitheater, including Mount Taylor proper and La Mosca, is composed of many coalesced domes and flows of variable elevation between 3000 and 3443 m. Extrapolation of slope angles from different points around the margin to a hypothetical maximum elevation in the past is somewhat equivocal, but it is our interpretation that MTS never exceeded 3800 m in elevation.

WHAT WAS THE VOLUME OF THE STRATOVOLCANO

Perry et al. (1990) estimated the pre-erosional volume of MTS at 23 km^3 and the volume of eroded material at 3 km^3, mostly from the Amphitheater. The geometric parameters for these calculated estimates are not given in their paper, but, in any event, these estimates seem unrealistically small to us and don't account for a maximum edifice elevation of 3800 m described above. From our recent mapping, the average diameter of MTS, including flanking mafic flows and interlayered debris flow deposits, is about ±16 km. If we assume an average base elevation of 2500 m and a maximum height of 3800 m, the relief of the volcano was once 1300 m. Inserting these values into the formula for a right circular cone, the estimated maximum volume of MTS was more reasonably about 85 km^3 with an estimated error of ±20%. The average slope angle of the original edifice was 9°, essentially equivalent to the Perry et al. (1990) calculation of 10° to 12°, but slope angles near the summit and margins of the Amphitheater are quite variable. For comparison, the estimated original volume of Mount Rainer, Washington, is about 140 km^3 (before erosion), the volume of Mount Adams, Washington, is 290 km^3, and that of Mount Shasta, California, is 350 km^3 (Orr and Orr, 1996).

WHAT WAS THE ERUPTIVE FLUX OF THE STRATOVOLCANO

From the volume of the volcano (85 km^3) and the time span of intense stratovolcano construction (0.76 Ma), we calculate an average eruptive (magmatic) flux rate of 0.11 km^3 per 10^3 years. For comparison, the eruptive flux of the San Francisco volcanic field in Arizona is 0.2 km^3 per 10^3 years (Tanaka et al., 1986), the long-lived Jemez volcanic field is 0.3 to 0.4 km^3 per 10^3 years (Gardner and Goff, 1984), and the incredibly active Mount St. Helens is 4.6 km^3 per 10^3 years (Lipman and Mullineaux, 1981). Thus, the eruptive flux of MTS is much smaller than most Cascades-type subduction zone volcanoes.

CONCLUSIONS

Major conclusions of our recent studies are:

- The summit trachyandesite lavas of MTS erupted 2.75 to 2.72 Ma and are not the youngest eruptions of the volcano. After summit activity waned, volcanism continued for another 200–230 ka around and within the edifice.
- Consequently, the youngest eruptions at MTS did not become progressively "andesitic" with time as previously thought. The summit stack of trachyandesite flows is equivalent in age to the trachydacite flow and intrusion that form La Mosca (2.71 Ma). Our dates and chemistry show that dome, flow and dike eruptions from 2.72 to 2.52 Ma are predominately trachydacite, originating from a composite stock. In fact, one of the youngest igneous events is the emplacement of the trachydacite to alkali rhyolite plug in the western Amphitheater.
- When growth of MTS ceased at 2.52 Ma, the style and chemistry of volcanism transformed to eruptions of primarily trachybasalt cones and flows surrounding the volcano. The youngest eruption anywhere near MTS is Cerro Pelón at 1.27 Ma.
- The elongate, eastward-facing Amphitheater in the approximate center of MTS formed by fluvial and mass-wasting erosional processes in Quaternary time. It did not form from large centralized explosions, from lateral blasts, or from Pleistocene glaciation of the edifice. Injection of late-stage radial dikes and various intrusive bodies and coincidental development of magma-induced hydrothermal alteration weakened the central edifice causing accelerated erosion. An alternative interpretation of precise age data could allow intrusive doming and sector collapse on the east flank to initiate erosion of the MTS amphitheater at about 2.56 Ma.
- It is our contention that the amalgam of small, coalesced flows and domes forming the original summit area of MTS never rose above 3800 m. Our estimated volume of MTS is roughly 85 km^3±20%.
- The volume and eruptive flux (0.11 km^3 per 10^3 years) of MTS was considerably smaller than presently active Cascades-type subduction zone stratovolcanoes.

ACKNOWLEDGMENTS

Geologic mapping and most research were jointly funded by STATEMAP (U.S. Geological Survey and New Mexico Bureau of Geology and Mineral Resources, (NMBGMR). High Mesa Petrographics (White Rock, New Mexico) crafted most of the thin sections. Washington State University and ALS Laboratories in Reno, Nevada, provided most of the chemical analyses. Fraser and Cathy Goff paid for some chemical analyses and thin sections and Kamilla Fellah prepared many of the samples for geochemical analysis. Richard Chamberlin and Matt Zimmerer of NMBGMR provided informative and constructive reviews of the draft manuscript. Additional reviews were obtained from Kate Zeigler (Zeigler Geologic Consulting), Virginia McLemore and Bonnie Frey (NMBGMR).

REFERENCES

Aldrich, M.J., and Laughlin, A.W., 1984, A model for the tectonic development of the southeastern Colorado Plateau boundary: Journal of Geophysical Research, v. 89, p. 10,207-10,218.

Baker, I., and Ridley, W.I., 1970, Field evidence and K, Rb, Sr data bearing on the origin of the Mount Taylor volcanic field, New Mexico, USA: Earth and Planetary Science Letters, v. 10, p. 106-114.

Cohen, K.M., Finney, S.C., Gibbard, P.L., and Fan, J.-X., 2013, The ICS international chronostratigraphic chart: Episodes, v. 36, p. 199-204.

Crumpler, L.S., 1980a, Alkali basalt through trachyte suite and volcanism, Mesa Chivato, Mount Taylor volcanic field, New Mexico: Geological Society of America Bulletin, Part I, v. 91, p. 253-255.

Crumpler, L.S., 1980b, Alkali basalt through trachyte suite and volcanism, Mesa Chivato, Mount Taylor volcanic field, New Mexico: Geological Society of America Bulletin, Part II, v. 91, p. 1293-1313.

Crumpler, L.S., 1982, Volcanism in the Mount Taylor region: New Mexico Geological Society, Guidebook 33, p. 291-298.

Crumpler, L.S., 2010, Mount Taylor, *in* Price, L.G., ed., The Geology of Northern New Mexico's Parks, Monuments, and Public Lands: Socorro, New Mexico Bureau of Geology and Mineral Resources, p. 51-60.

Dunbar, N.W., Kelley, S.A., Goff, F., and McIntosh, W.C., 2013, Rhyolitic pyroclastic deposits at Mount Taylor: Insight into early eruptive processes of a major composite volcano: New Mexico Geological Society, Guidebook 64, p. 72-74.

Dutton, C.E., 1885, Mount Taylor and the Zuni Plateau: U.S. Geological Survey, 6th Annual Report, p. 105-198.

Ellis, R.W., 1935, Glaciation in New Mexico: University of New Mexico Bulletin, Geological Series, v. 5, 31 p.

Fellah, K., 2011, Petrogenesis of the Mount Taylor volcanic field and comparison with the Jemez Mountains volcanic field, New Mexico [M.S. thesis]: Pullman, Washington State University, 92 p.

Gee, J.S., and Kent, D.V., 2007, Source of oceanic magnetic anomalies and the geomagnetic polarity timescale: London, Elsevier, Treatise on Geophysics, v. 5, p. 455-507.

Gardner, J.N., and Goff, F., 1984, Potassium-argon dates from the Jemez volcanic field: Implications for tectonic activity in the north-central Rio Grande rift: New Mexico Geological Society, Guidebook 35, p. 75-81.

Goff, F., and Kelley, S.A., 2020, Facts and hypotheses regarding the Miocene – Holocene Jemez Lineament, New Mexico, Arizona and Colorado: New Mexico Geological Society, Guidebook 71, this volume.

Goff, F., Kelley, S.A., Zeigler, K., Drakos, P., and Goff, C.J., 2008, Preliminary geologic map of the Lobo Springs 7.5-minute quadrangle map, Cibola County, New Mexico: New Mexico Bureau of Geology and Mineral Resources, Open-file Geologic Map 181, 1:24,000, http://geoinfo.nmt.edu/publications/maps/geologic/ofgm/details.cfml?Volume=181.

Goff, F., Kelley, S.A., Lawrence, J.R., and Goff, C.J., 2012, Preliminary geologic map of the Cerro Pelon 7.5 minute quadrangle, Cibola and McKinley counties, New Mexico: New Mexico Bureau of Geology and Mineral Resources, Open-file Geologic Map 202, 1:24,000, http://geoinfo.nmt.edu/publications/maps/geologic/ofgm/details.cfml?Volume=202.

Goff, F., Kelley, S.A., Lawrence, J.R., and Goff, C.J., 2014a, Preliminary geologic map of the Laguna Cañoneros 7.5 minute quadrangle, Cibola and McKinley counties, New Mexico: New Mexico Bureau of Geology and Mineral Resources, Open-file Geologic Map 244, http://geoinfo.nmt.edu/publications/maps/geologic/ofgm/details.cfml?Volume=244.

Goff, F., Warren, R.G., Goff, C.J., and Dunbar, N., 2014b, Eruption of reverse-zoned upper Tshirege Member, Bandelier Tuff from centralized vents within Valles caldera, New Mexico: Journal of Volcanology and Geothermal Research, v. 276, p. 82-104.

Goff, F., Kelley, S.A., Goff, C.J., McCraw, D.J., Osburn, G.R., Lawrence, J.R., Drakos, P.G., and Skotnicki, S.J., 2019, Geologic map of the Mount Taylor volcano area, New Mexico: New Mexico Bureau of Geology and Mineral Resources, Geologic Map 80, 1:36,000 scale (color) w/ 57 page booklet.

Hallett, R.B., Kyle, P.R. and McIntosh, W.C., 1997, Paleomagnetic and $^{40}Ar/^{39}Ar$ age constraints on the chronologic evolution of the Rio Puerco volcanic necks and Mesa Prieta, west-central New Mexico: Implications for transition zone magmatism: Geological Society of America Bulletin, v. 109, p. 95-106.

Hoblitt, R.P., Miller, D.C., and Vallance, J.W., 1981, Origin and stratigraphy of the deposit produced by the May 18 directed blast, *in* Lipman, P.W., and Mullineaux, D.R., eds., The 1980 eruptions of Mount St. Helens, Washington: U.S. Geological Survey, Professional Paper 1250, p. 401-419.

Hoffman, G.K., 2017, Coal Resources, *in* McLemore, V.T., Timmons, S., and Wilks, M., eds., Energy and Mineral Resources of New Mexico: New Mexico Bureau of Geology and Mineral Resources, Memoir 50B, 65 p.

Hunt, C.B., 1938, Igneous geology and structure of the Mount Taylor volcanic field, New Mexico: U.S. Geological Survey, Professional Paper 189-B, p. 51-80.

Irvine, T.N., and Baragar, W.R.A., 1971, A guide to the chemical classification of the common volcanic rocks: Canadian Journal of Earth Science, v. 8, p. 523-548.

Kelley, V.C., 1963, Geology and technology of the Grants uranium region: New Mexico Bureau of Mines and Mineral Resources, Memoir 15, 277 p.

Kelley, S., Dunbar, N., McIntosh, W., and Goff, F., 2013, Third day road log: trip 2 – tuffs of San Mateo Canyon: New Mexico Geological Society, Guidebook 64, p. 70-72.

Kuiper, K.F., Deino, A., Hilgen, H.J., Krijgsman, W., Renne, P.R., and Wijbrans, J.R., 2008, Synchronizing rock clocks of earth history: Science, v. 320, p. 500-504.

Le Bas, M.J., Le Maitre, R.W., Streckeisen, A., and Zanettin, B., 1986, A chemical classification of volcanic rocks based on the total alkali-silica diagram: Journal of Petrology, v. 27, p. 745-750.

Lipman, P.W., and Mehnert, H.H., 1979, Potassium-argon ages from the Mount Taylor volcanic field, New Mexico: U.S. Geological Survey, Professional Paper 1124-B, 8 p.

Lipman, P.W., and Moench, R.H., 1972, Basalts of the Mt. Taylor volcanic field, New Mexico: Geological Society of America Bulletin, v. 83, p. 1335-1344.

Lipman, P.W., and Mullineaux, D.R., 1981, The 1980 eruptions of Mount St. Helens, Washington: U.S. Geological Survey, Professional Paper 1250, 844 p.

Luedke, R.G., and Smith, R.L., 1978, Map showing distribution, composition, and age of late Cenozoic volcanic centers in Arizona and New Mexico: U.S. Geological Survey, Miscellaneous Investigations Series Map I-1091-A.

Mayo, E.B., 1958, Lineament tectonics and some ore districts of the southwest: Transactions American Institute of Metallurgical Engineers, v. 211, p. 1169-1175.

McCraw, D.J., Read, A.S., Lawrence, J.R., Goff, F., and Goff, C.J., 2009, Preliminary geologic Map of the San Mateo 7.5 minute quadrangle, McKinley and Cibola counties, New Mexico: New Mexico Bureau of Geology and Mineral Resources Open-file Geologic Map 194, http://geoinfo.nmt.edu/publications/maps/geologic/ofgm/details.cfml?Volume=194.

McLemore, V.T., 2011, The Grants uranium district: Update on source, deposition, and exploration: The Mountain Geologist, v. 48, p. 23-44.

McLemore, V.T., and Chenoweth, W.L., 2017, Uranium Resources, *in* McLemore, V.T., Timmons, S., and Wilks, M., eds., Energy and Mineral Resources of New Mexico: New Mexico Bureau of Geology and Mineral Resources, Memoir 50C, 67 p.

Meyer, G.A., Muir Watt, P., and Wilder, M., 2014, Was Mount Taylor glaciated in the late Pleistocene? An analysis based on field evidence and regional equilibrium line altitudes: New Mexico Geology, v. 36, p. 32-39.

Olsen, K.H., Keller, G.H., and Stewart, J.N., 1979, Crustal structure along the Rio Grande rift from seismic refraction profiles, *in* Riecker, R.E., ed., Rio Grande Rift: Tectonics and Magmatism: Washington, D.C., American Geophysical Union, p. 127-143.

Olsen, K.H., Baldridge, W.S., and Callender, J.F., 1987, Rio Grande rift: An overview: Tectonophysics, v. 143, p. 119-139.

Orr, E.L., and Orr, W.N., 1996, Geology of the Pacific Northwest: New York, McGraw Hill, 115 p.

Osburn, G.R., Kelley, S.A., and Goff, F., 2010. Preliminary geologic map of the Mount Taylor 7.5- minute quadrangle, Cibola County, New Mexico: New Mexico Bureau of Geology and Mineral Resources Open-file Geologic Map 186, scale 1:24,000, http://geoinfo.nmt.edu/publications/maps/geologic/ofgm/details.cfml?Volume=186.

Owen, D.E., and Owen, D.E., Jr., 2003, Stratigraphy of the Dakota Sandstone and intertongued Mancos Shale along the southern flank of the San Juan

Basin, west-central New Mexico: New Mexico Geological Society, Guidebook 54, p. 325-330.

Perry, F. V., Baldridge, W. S., DePaolo, D. J., and Shafiqullah, M., 1990, Evolution of a magmatic system during continental extension: The Mount Taylor volcanic field, New Mexico: Journal of Geophysical Research, v. 95, p. 19,327-19,348.

Pierce, K.L., 2004, Pleistocene glaciations of the Rocky Mountains, *in* Gillespie, A.R., Porter, S.C., and Atwater, B.F., eds., The Quaternary Period in the United States: Amsterdam, Elsevier, Developments in Quaternary Science 1, p. 63-76.

Sears, J.D., Hunt, C.B., and Hendricks, T.A., 1941, Transgressive and regressive Cretaceous deposits in southern San Juan Basin, New Mexico. U.S. Geological Survey, Professional Paper 193-F, p., 101-121.

Siebert, L., 1984, Large volcanic debris avalanches: Characteristics of source areas, deposits and associated eruptions: Journal of Volcanology and Geothermal Research, v. 22, p. 163-197.

Skotnicki, S.J., Drakos, P.G., Goff, F., Goff, C.J., and Riesterer, J., 2012, Preliminary geologic map of the Seboyeta 7.5-minute quadrangle, Cibola County, New Mexico: New Mexico Bureau of Geology and Mineral Resources, Open-file Geologic Map 226, scale 1:24,000, http://geoinfo.nmt.edu/publications/maps/geologic/ofgm/details.cfml?Volume=226.

Smith, R.L., and Bailey, R.A., 1966, The Bandelier Tuff: A study of ash-flow eruption cycles from zoned magma chambers: Bulletin of Volcanology, v. 29, p. 83-104.

Sosa, A., Thompson, L., Velasco, A.A., Romero, R., and Herrmann, R., 2014, 3-D structure of the Rio Grande rift from 1-D constrained joint inversion of receiver functions and surface wave dispersion: Earth and Planetary Science Letters, v. 402, p. 127-137.

Tanaka, K.L, Shoemaker, E.M., Ulrich, G.E., and Wolfe, E.W., 1986, Migration of volcanism in the San Francisco volcanic field: Geological Society of America Bulletin, v. 97, p. 129-141.

Thompson, G.A., and Zoback, M.L., 1979, Regional geophysics of the Colorado Plateau: Tectonophysics, v. 61, p. 149-181.

Voight, B., Glicken, H, Janda, R.J., and Douglass, P.M., 1981, Catastrophic rock slide avalanche of May 18, *in* Lipman, P.W., and Mullineaux, D.R., eds., The 1980 eruptions of Mount St. Helens, Washington: U.S. Geological Survey, Professional Paper 1250, p. 347-377.

Wilson, M., 1989, Igneous Petrogenesis: London, Unwin Hyman, 466 p.

New Mexico Geological Society, Special Publication 14, Geology of the Mount Taylor Area, 2020, p. 29-35.

EPISYENITES IN THE ZUNI MOUNTAINS, CIBOLA COUNTY, NEW MEXICO — NEW INTERPRETATIONS

Virginia T. McLemore

New Mexico Bureau of Geology and Mineral Resources, New Mexico Institute of Mining and Technology, Socorro, NM, 87801; virginia.mclemore@nmt.edu

Abstract—Brick-red, K-feldspar-rich episyenites (altered rocks that were desilicated and metasomatized by alkali-rich solutions) are found in Proterozoic-age rocks in the Zuni Mountains in central New Mexico. The Zuni episyenites are high in K_2O and depleted in SiO_2 and Na_2O, with slightly enriched heavy REE patterns. The Zuni episyenites are similar in composition to episyenites found in the Caballo and Burro mountains, the Sevilleta National Wildlife Refuge, and at Lobo Hill, but the Zuni episyenites are lower in REE. The Zuni episyenites are younger than ~1000 Ma. Similar episyenites are found elsewhere in New Mexico and southern Colorado and are thought to be part of a Cambrian-Ordovician magmatic event that is documented throughout this region. Unlike episyenites in the Caballo and Burro mountains, which contain moderate to high concentrations of rare earth elements (REE), uranium, and thorium, the episyenites in the Zuni Mountains have little or no economic potential.

INTRODUCTION

Rare earth elements (REE) are considered critical minerals and are becoming more important in our technological society, especially in many of our electronic devices. REE include the 15 lanthanide elements (atomic numbers 57-71), yttrium (Y, atomic number 39), and scandium (Sc, atomic number 21), and are commonly divided into two chemical groups, the light REE (La through Eu) and the heavy REE (Gd through Lu, plus Sc and Y). REE are lithophile elements (or elements enriched in the crust) that have similar physical and chemical properties, and, therefore, occur together in nature. REE deposits have been reported from New Mexico (McLemore et al., 1988a, 1988b; Long et al., 2010; McLemore, 2015, 2018), but were not considered important exploration targets until recently, because the demand in past years has been met by other deposits in the world. However, with the projected increase in demand and potential lack of available production from Chinese deposits, areas in New Mexico are being re-examined for their REE potential (McLemore, 2015, 2018). One type of deposit in New Mexico containing REE is episyenite (Fig. 1; or metasomatite according to the International Atomic Energy Agency, 2018). The purpose of this paper is to update previous work (McLemore and McKee, 1989; McLemore, 2013) by describing the episyenite deposits in the Zuni Mountains, New Mexico, including presenting new geochemical analyses and evaluating their economic potential.

The Zuni Mountains are west and southwest of Grants in Cibola County, New Mexico (Fig. 1). Before 1983, the Zuni Mountains were in Valencia County; Cibola County was created from the western portion of Valencia County in 1983. The major types of mineral deposits in the Zuni Mountains include 1) veins and replacements in Proterozoic rocks, 2) stratabound, sedimentary-copper deposits, 3) fluorite veins, 4) episyenites REE-Th-U metasomatic bodies, 5) high-calcium limestone,

FIGURE 1. Cambrian-Ordovician carbonatites, alkaline and mafic intrusive igneous rocks, and episyenites in New Mexico and Colorado.

6) volcanic cinders (scoria), and 7) iron deposits (McLemore, 2001, 2013). Base and precious metals were found in the Zuni Mountains mining district circa 1900 and at least one metal mill was built in the district.

Episyenites have been known in the Zuni Mountains since the 1980s, but these rocks were generally called igneous syenites (Lambert, 1983; McLemore and McKee, 1989). McLemore and McKee (1989) briefly described and mapped the known occurrences of brick red, K-feldspar-rich, slightly radioactive (2-4 times background) deposits in the Zuni Mountains. Because some of these unusual rocks are known for potential economic deposits of REE, uranium (U), thorium (Th), niobium (Nb), zirconium (Zr), hafnium (Hf), gallium (Ga), and other elements (Long et al., 2010; McLemore, 2015; McLemore et al., 2018), the author remapped and sampled these episyenites to evaluate their mineral-resource potential, and to compare with new results of chemical analyses from episyenites elsewhere in New Mexico. Additional goals were to better understand their tectonic setting and origin. Similar episyenites found elsewhere in New Mexico and southern Colorado are thought to be part of a Cambrian-Ordovician magmatic event that is documented in this region (Fig. 1; McMillan and McLemore, 2004; Riggins et al., 2014). This Cambrian-Ordovician magmatic event is characterized by the intrusion of carbonatites, syenites, monzonites, alkaline granites, and mafic dikes, and is associated with K-metasomatism (i.e. fenites and episyenites) and REE-Th-U mineral deposition.

DEFINITION OF EPISYENITES

The term *episyenite* is used to describe altered rocks that were desilicified and metasomatized by alkali-rich fluids (Leroy, 1978; Recio et al., 1997; Suikkanen and Rämö, 2019). These deposits are also known for their elevated uranium content and are called metasomatite deposits by the International Atomic Energy Agency (2018). Brick-red outcrops in several areas in New Mexico, including the Caballo, Burro, and Zuni mountains and Lobo Hill, were erroneously identified as magmatic syenites and alkali granites (McMillan and McLemore, 2004), but these rocks are actually metasomatic rocks (McLemore, 2013; Riggins, 2014; Riggins et al., 2014). Elsewhere in the world, alkali-rich metasomatic rocks are associated with U and Th deposits (Costi et al., 2002; Condomines et al., 2007; Cuney et al., 2012; International Atomic Energy Agency, 2018; Suikkanen and Rämö, 2019), gold deposits (López-Moro et al., 2013) and tin-tungsten deposits (Charoy and Pollard, 1989; Costi et al., 2002; Borges et al., 2009), but unmineralized episyenites are found as well (Petersson and Eliasson, 1997; Recio et al., 1997; Hecht et al., 1999; Suikkanen and Rämö, 2019). Episyenites are similar to altered rocks formed by fenitization and would be called fenites by some geologists. Fenitization is the alkali-metasomatism associated with carbonatites or alkaline igneous activity (LeBas, 2008). However, we are reluctant to use the term fenite for the rocks studied here because there is no definitive spatial and temporal association with carbonatite or alkaline igneous rocks in the vicinity of the episyenites.

PREVIOUS WORK

This work is part of ongoing studies of mineral deposits in New Mexico conducted by the NMBGMR. The Zuni Mountains were mapped by Goddard (1966) and Lambert (1983). Investigations of the mineral deposits and plutonic rocks in the Zuni Mountains by this author began in 1983 in order to assess their U potential (McLemore, 1983, 1989; McLemore and McKee, 1989). Continued investigations occurred in 1985-1986, as part of the evaluation of mineral resources of Cibola County (McLemore et al., 1986). During 2011-2012, investigations continued in the area in order to evaluate the REE mineral-resource potential (McLemore, 2013). The episyenites were examined in more detail during 2013 and 2018-2019. This report presents new chemical analyses and interpretations that differ from, and update, earlier preliminary reports by McLemore and McKee (1989) and McLemore (2013).

METHODOLOGY

A detailed geologic map was compiled in ArcMap using USGS topographic maps as the map base and by detailed field mapping at a scale of approximately 1:6000 (Fig. 2). A handheld GPS unit was used with the current topography loaded in the unit to more accurately map the episyenites. Locations of samples, whole-rock geochemical analyses, QA/QC (quality assurance and quality control), specific methods of analysis for each element, and detection limits are in Appendix 1.

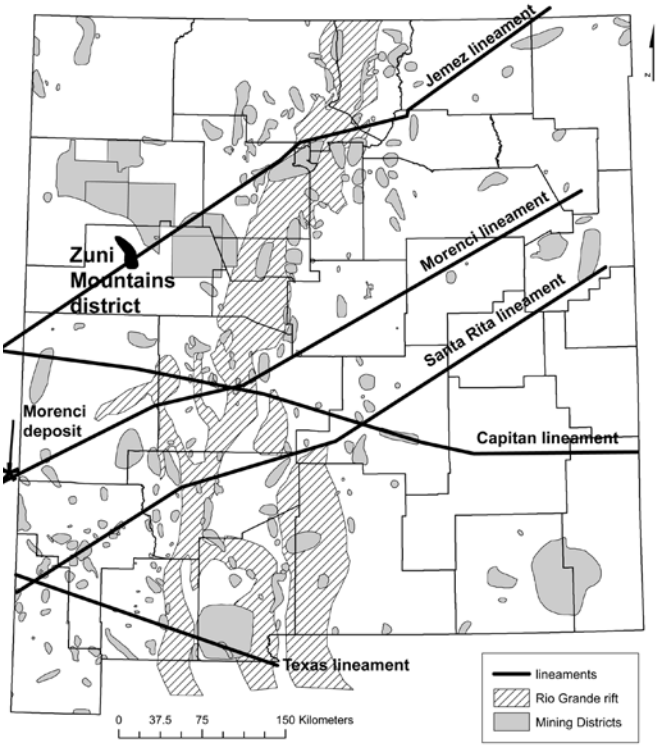

FIGURE 2. Lineaments and mining districts in New Mexico (from McLemore, 2013 as modified from Chapin et al., 1978, 2004; McLemore, 2001; Sims et al., 2002). The Zuni Mountains lie along the Jemez Lineament.

Selected samples of the Proterozoic host rocks and episyenites were collected and analyzed by X-ray fluorescence (XRF) spectroscopy and inductively coupled plasma spectroscopy (ICP-OES and ICP-MS) by Activation Laboratories in 2012 and 2015, methods for which can be found at https://cdn.actlabs.com/wp-content/uploads/2019/10/Actlabs-Schedule-of-Services-Canada-2019-07-22.pd and https://actlabs.com/geochemistry/lithogeochemistry-and-whole-rock-analysis/ and summarized here. The entire sample is crushed to <2 mm, mechanically split to obtain a representative sample and then pulverized to at least 95% <105 microns (μm). All of the steel mills are mild steel and do not introduce Cr or Ni contamination. The method of sample analysis is by lithochemistry research analyses, which employs the most aggressive fusion technique (a lithium metaborate/tetraborate fusion). Fusion is performed by a robot at Actlabs, which provides a fast fusion of the highest quality in the industry. The resulting molten bead is rapidly digested in a weak nitric acid solution. The fusion ensures that the entire sample is dissolved. Then the sample is analyzed by XRF for major elements and ICP-MS for trace elements. Uncertainty of analyses is generally <5%, and duplicate samples and standards were analyzed (Appendix 1).

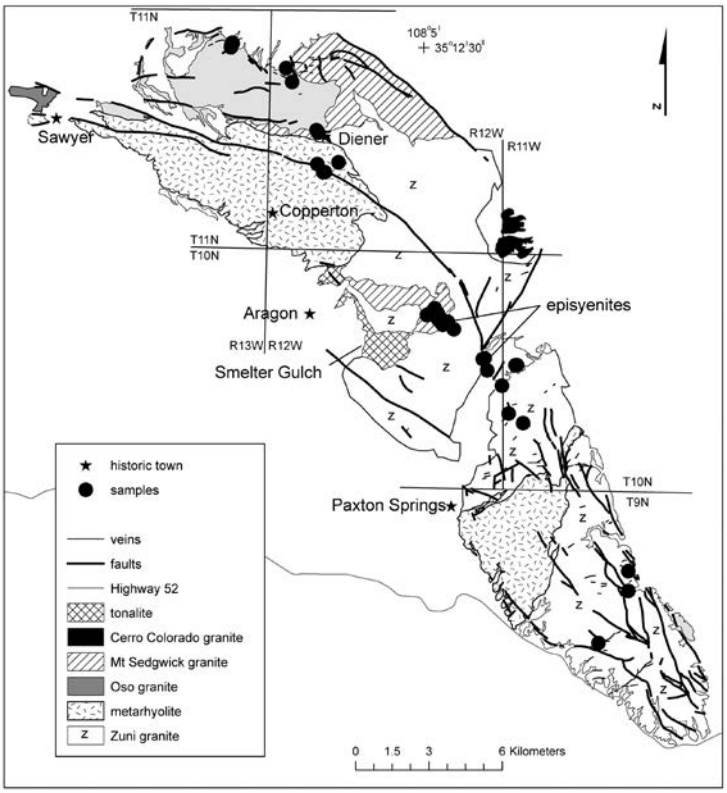

FIGURE 3. Simplified geologic map of the Zuni Mountains (modified by the author from field reconnaissance; from Goddard, 1966 and McLemore, 2013) showing sample locations (McLemore, 2013; Appendix 1). Zuni granite includes metamorphic rocks and aplite.

GEOLOGIC SETTING

The Zuni Mountains lie along the Jemez Lineament, which is defined by northeast-trending alignment of late Cenozoic volcanic fields that extend from the San Carlos field in Arizona to the Raton-Clayton field in northeastern New Mexico and Colorado (Fig. 2; Chapin et al., 1978; Aldrich et al., 1986; Goff and Kelley, this volume). A mafic intrusion of late Cenozoic age likely underlies the Zuni uplift as indicated by geophysical data (Ander and Huestis, 1982) and the presence of a Quaternary basaltic vent in the core of the range (Maxwell, 1986). Proterozoic granite and metamorphic rocks form the core of the Zuni Mountains (Fig. 3) and are unconformably overlain by sedimentary deposits of Permian age (Abo, Yeso and San Andres formations; Goddard, 1966). Episyenites are found only in Proterozoic rocks. The youngest volcanic formations in the area are Quaternary basalt flows and scoria cones of the Zuni-Bandera volcanic field.

DESCRIPTION OF PROTEROZOIC ROCKS AND EPISYENITES IN THE ZUNI MOUNTAINS

Proterozoic granite and metamorphic rocks

The oldest rocks in the area are hornblendite and serpentinized peridotite (1630.2±2 Ma, $^{40}Ar/^{39}Ar$, Strickland et al., 2003), and a metarhyolite with an U/Pb age of about 1655 Ma (Bowring and Condie, 1982). Other rock types in the Zuni Mountains Proterozoic terrain include gneiss, schist, amphibolite, syenite, pegmatites, and diabase dikes (Goddard, 1966; Fitzsimmons, 1967; Lambert, 1983; Mawer and Bauer, 1989; Strickland et al., 2003). The diabase dikes are 1130±20 Ma ($^{40}Ar/^{39}Ar$, Strickland et al., 2003).

Existing data suggest four geographically and geochemically distinct granites are present in the Zuni Mountains (Fig. 2; Condie, 1978; McLemore, 2013): Mt. Sedgwick granite (high calcium), Zuni granite (high silica), Cerro Colorado gneissic aplite (high silica), and Oso granite (high potassium). A fifth unnamed pluton in the northern Zuni Mountains has not been sampled. The megacrystic granite, the Mt. Sedgwick granite, has a $^{40}Ar/^{39}Ar$ age of 1432±2 Ma (Strickland et al., 2003). The metarhyolite is similar geochemically to the Oso granite and the Zuni and Cerro Colorado granites are geochemically similar to each other. The Zuni Mountain granites are calcic to calc-alkaline and peraluminous granites. Condie (1978) suggested that the high-calcium granites were formed by partial melting of siliceous granulite in the lower crust and the high-silica and high-potassium granites formed by fractional crystallization of shallow high-calcium magmas.

Episyenites

Several radioactive, pink to red, small stock-like to flat-lying tabular bodies (<300 m long), near-vertical pipes (<30 m in diameter), and dike-like bodies (<2 m wide, 400 m long) of episyenites are mapped (Fig. 3). Outcrops are prominent (Fig. 4) and the contacts between the episyenite bodies and the host rocks vary from location to location, from very sharp to distinctly gradational crosscutting the foliation of the host rock.

Zones of vuggy breccia are found in some of the episyenites (Fig. 5), suggesting fluid migration. The episyenites vary in texture from fine-grained to coarse-grained, and are similar in texture to the host granite or metarhyolite.

The episyenites contain 20-80% alkali-feldspar, 20-40% plagioclase, 0-10% quartz, 1-5% opaque minerals (predominantly iron oxides), trace-5% biotite (partially to completely altered to chlorite), and trace amounts of apatite, sericite, and calcite. Some alkali-feldspar crystals are more than a centimeter long. Plagioclase is commonly altered to carbonate, hematite, and clay. Iron oxides occur as fine-grained red-brown disseminations within the feldspars, and as small red cubes and octahedrons that were probably once magnetite. The rocks are almost devoid of ferromagnesian minerals. Chlorite, commonly vermicular, fills cavities and fractures, and replaces primary magmatic phases.

FIGURE 5. Episyenite with zones of vuggy breccia.

WHOLE-ROCK GEOCHEMISTRY

Selected samples of granite and episyenites in the Zuni Mountains were analyzed for major and trace elements (Appendix 1). Most Zuni episyenites are high in K_2O (as high as 15.7%) and are depleted in SiO_2 and Na_2O (Fig. 6, 7), with slightly enriched heavy REE patterns (Fig. 8). Generally, the episyenites contain higher concentrations of K_2O, Al_2O_3, Rb, and Ba and lower concentrations of Na_2O and Sr than the granites and metarhyolites in the Zuni Mountains (Fig. 6; Appendix 1). The episyenites have similar chondrite-normalized REE patterns as the host granites and metarhyolites (Fig. 8; Appendix 1). Note that the concentrations of TiO_2, P_2O_5, and Y are similar in concentration to the granites (Appendix 1). The episyenites in the Zuni Mountains contain <16 ppm Th, <4 ppm U, <14 ppm Nb, <147 ppm Y, and <200 ppm total REE (Appendix 1), which are uneconomic concentrations. The Zuni episyenites are similar in composition to episyenites found in the Caballo and Burro Mountains, Sevilleta National Wildlife Refuge, and at Lobo Hill, but the Zuni episyenites are lower in REE (Fig. 8; McLemore, 1986, 2016; McLemore and McKee,

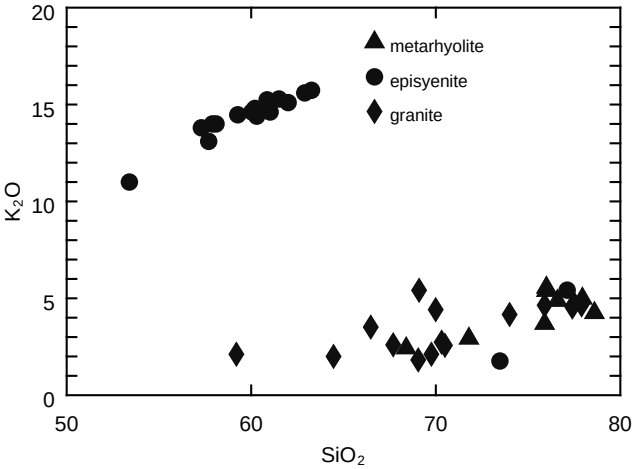

FIGURE 6. SiO_2 verses K_2O plot of the Zuni granites and episyenites. Chemical analyses are in Appendix 1 (including QA/QC). Uncertainty of analyses is generally <5% (Appendix 1).

FIGURE 4. Rugged outcrops of brick red episyenite (upper center).

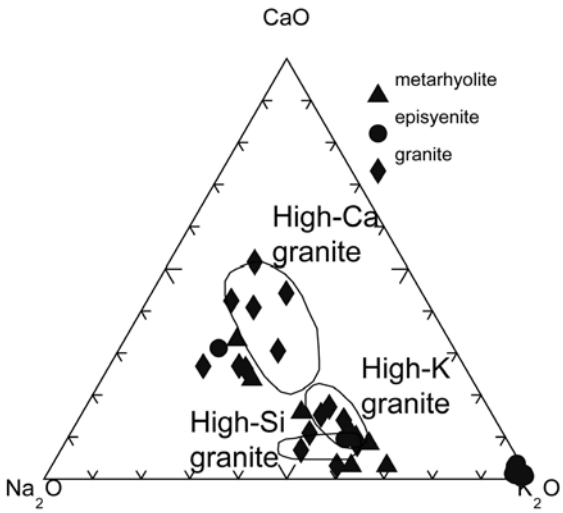

FIGURE 7. Na_2O-CaO-K_2O plot of the Zuni granites and episyenites. Geochemical fields shown after Condie (1978). Chemical analyses are in Appendix 1 (including QA/QC). Uncertainty of analyses is generally <5% (Appendix 1).

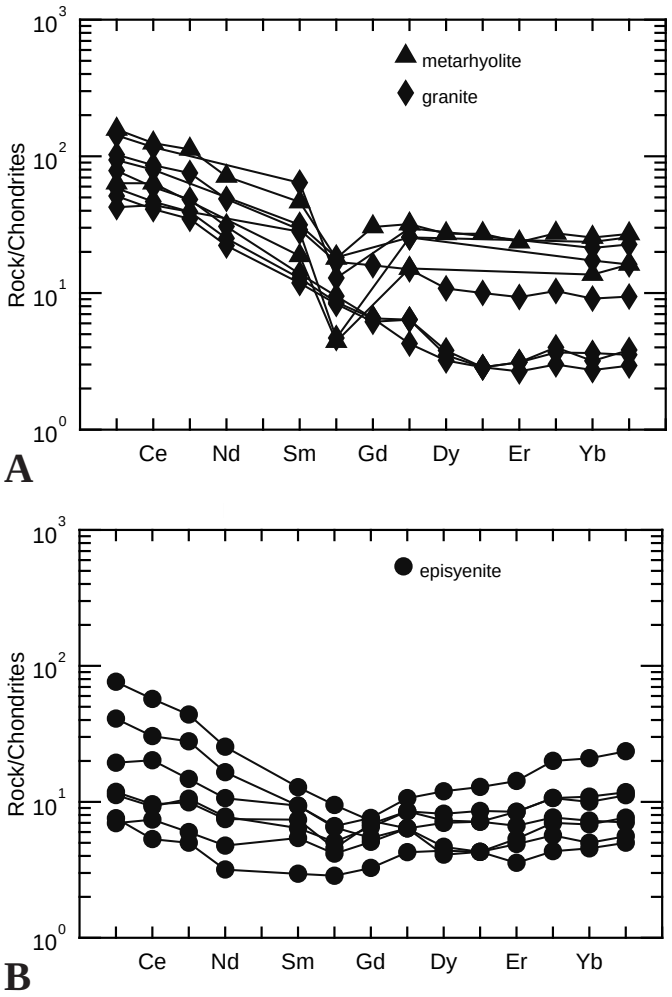

FIGURE 8. Similar sample/chondrite normalized REE patterns for the Zuni episyenites (**A**) and granites and metarhyolites (**B**). Chondrite values from Nakamura (1974). Chemical analyses are in Appendix 1 (including QA/QC). Uncertainty of analyses is generally <5% (Appendix 1).

1988, 1989; McLemore et al., 1999, 2018; McMillan and McLemore, 2004; Riggins, 2014; Riggins et al., 2014; Smith, 2018).

DISCUSSION AND CONCLUSIONS

Origin of episyenites

Replacement textures, high K-feldspar contents, and high K_2O concentrations support a metasomatic origin of the Zuni episyenites. The field and mineralogical observations suggest that the Zuni episyenites were formed by interaction of a K-rich fluid with granitic host rocks, possibly along faults, fractures, and shear zones. The most altered rocks contain more than 15 wt.% K_2O, which is close to the composition of end-member orthoclase (15.6 wt% K_2O; Deer et al., 1992; Riggins, 2014; Riggins et al., 2014), suggesting the most altered rocks are composed almost completely of newly formed secondary K-feldspar. The K-rich fluid that caused metasomatism was likely silica undersaturated, resulting in dissolution and/or alteration of primary quartz, biotite and other accessory silicate phases (Cathelineau, 1986), and precipitation of secondary K-feldspar with iron-oxide inclusions. Similar characteristics are observed in the episyenites found in the Caballo and Burro mountains (Riggins, 2014; Riggins et al., 2014; Smith, 2018; McLemore et al., 2018).

Episyenite texture, mineralogy and mineral chemistry from the Caballo, Burro, and Zuni mountains suggest that processes that formed the episyenites was K-metasomatism, with the original fluids possibly derived from carbonatites or alkaline melts, then possibly altered again by younger fluids (Riggins, 2014; Riggins et al., 2014; Smith, 2018; McLemore et al., 2018). Carbonatites and alkaline intrusive rocks are commonly enriched in sodium, potassium and REE, due to magmatic processes such as crystal fractionation and late magmatic hydrothermal activity (Sheard et al., 2012; Gysi and Williams-Jones, 2013; Walters et al., 2013). Primitive carbonatitic melts contain significant amounts of sodium and potassium that are incompatible in the crystallizing assemblage, and are fractionated into the residual melt, which can then be lost to late-stage metasomatic fluids (LeBas, 2008). However, some researchers suggest that granitic intrusions could provide the heat necessary for meteoric fluid circulation resulting in the formation of episyenites (Leroy, 1978; Cuney et al., 2012; Petersson et al., 2014; Suikkanen and Rämö, 2019); whereas others suggest that hydrothermal fluids formed by regional thermal anomalies within post-orogenic crust during extension, provide the fluids and heat to form episyenites (Boulvais et al., 2007; Jaques et al., 2016; Smith, 2018). Additional study is needed to identify the source of the original fluids that formed episyenites.

Age of episyenites

The episyenites are metasomatized Proterozoic granite and metarhyolite. Strickland et al. (2003) dated an episyenite as <700 to 1000 Ma ($^{40}Ar/^{39}Ar$), but the age spectra is disturbed and does not provide an accurate age. Most episyenites dated ($^{40}Ar/^{39}Ar$) from the Caballo Mountains also exhibit disturbed spectra and do not provide accurate ages (Riggins, 2014; Smith, 2018). Fluids of varying ages are suspected to have reset the feldspar ages (Smith, 2018; McLemore et al., 2018; Suikkanen and Rämö, 2019). Fluids have migrated along the Jemez Lineament since Proterozoic times, as evidenced by varying ages of igneous intrusions and mineral deposits in the Zuni Mountains (Chapin et al., 1978, 2004; Aldrich et al., 1986; McLemore, 2013). Thus the age of the episyenites is still uncertain but is probably Proterozoic (700-1000 Ma) or Cambrian-Ordovician (~500 Ma). The metasomatic hydrothermal alteration is not related to late Cenozoic volcanism of the Zuni-Bandera volcanic field.

Outlook for mineral resource potential in the future

Unlike episyenites in the Caballo and Burro mountains, the episyenites in the Zuni Mountains have little to no economic potential, except perhaps as red decorative stone. Episyenites at Lobo Hill, near Moriarty have been mined for decorative stone and are at least 30 m thick. A few Zuni episyenites are

radioactive, but all Zuni samples are low in U, Th, yttrium, niobium and REE (Appendix 1; Fig. 8). It is possible that the Zuni episyenites could be enriched in U, Th, yttrium, niobium and REE at depth, but drilling is required to investigate their subsurface potential. Future research could include mineral chemistry (identification of REE, uranium, and thorium minerals) and more precise dating of these rocks, especially in the Lobo Hill area where the episyenites have been exposed by quarrying.

ACKNOWLEDGMENTS

This paper and related studies are part of an on-going study of the mineral resources of New Mexico at NMBGMR, Dr. Nelia Dunbar, Director and State Geologist, and were partially funded by USGS Mineral Resources External Research Program (award number G12AP20051). Miles Silberman and Nelia Dunbar reviewed an earlier version of this manuscript and their comments are greatly appreciated. Additional reviews were provided by Shari Kelley (NMBGMR) and Fraser Goff (NM Tech).

REFERENCES

Aldrich, M.J., Laughlin, A.W., Meade, J.S., and Peirce, H.W., 1986, The Jemez lineament: structural boundaries and control on sedimentary facies, tectonism and mineralization: Proceedings of the 6th International Conference on Basement Tectonics, p. 104-113.

Ander, M.E. and Huestis, S.P., 1982, Mafic intrusion beneath the Zuni-Bandera volcanic field, New Mexico: Geological Society of America Bulletin, v. 93, p. 1142-1150.

Borges, R.M.K., Villas, R.N.N., Fuzikawa, K., Dall'Agnol, R., and Pimenta, M.A., 2009, Phase separation, fluid mixing, and origin of the greisens and potassic episyenite associated with the Água Boa pluton, Pitinga tin province, Amazonian craton, Brazil: Journal of South American Earth Science, v. 27, p. 161-183.

Boulvais, P., Ruffet, G., Cornichet, J., and Mermet, M., 2007, Cretaceous albitization and dequartzification of Hercynian peraluminous granite in the Salvezines Massif (French Pyrénées): Lithos, v. 93, p. 89-106.

Bowring, S.A. and Condie, K.C., 1982, U-Pb zircon ages from northern and central New Mexico: Geological Society of America, Abstracts with Programs, v. 14, p. 304.

Cathelineau, M., 1986, The hydrothermal alkali metasomatism effects on granitic rocks: quartz dissolution and related subsolidus changes: Journal of Petrology, v. 27, p. 945-965.

Chapin, C.E., Chamberlin, R.M., Osburn, G.R., White, D.W., and Sanford, A.R., 1978, Exploration framework of the Socorro geothermal area, New Mexico: New Mexico Geological Society, Special Publication 7, p. 115-129.

Chapin, C.E., McIntosh, W.C., and Chamberlin, R.M., 2004, The Late Eocene-Oligocene peak of Cenozoic volcanism in southwestern New Mexico, *in* Mack, G.H. and Giles, K.A., eds., The Geology of New Mexico, a geologic history: New Mexico Geological Society, Special Publication 11, p. 271-293.

Charoy, B. and Pollard, P.J., 1989, Albite-rich, silica-depleted metasomatic rocks at Emuford, northeast Queensland: mineralogical, geochemical, and fluid inclusion constraints on hydrothermal evolution and tin mineralization: Economic Geology, v. 84, p. 1850-1874.

Condie, K.C., 1978, Geochemistry of Proterozoic granitic plutons from New Mexico, U.S.A.: Chemical Geology, v. 21, p. 131-149.

Condomines, M., Loubeau, O., and Patrier, P., 2007, Recent mobilization of U-series radionuclides in the Bernardan U deposit (French massif central): Chemical Geology, v. 244, p. 304-315.

Costi, H.T., Dall'Agnol, R., Borges, R.M.K., Minuzzi, O.R.R., and Teixeira, J.T., 2002, Tin-bearing sodic episyenites associated with the Proterozoic, A-type Água Boa Granite, Pitinga mine, Amazonian craton, Brazil: Gondwana Research, v. 5, p.435-451.

Cuney, M., Emetz, A., Mercadier, J., Mykchaylov, V., Shunko, W., and Yuslenko, A., 2012, Uranium deposits associated with Na-metasomatism from central Ukraine: A review of some of the major deposits and genetic constraints: Ore Geology Reviews, v. 44, p. 82-106.

Deer, W.A., Howie, R.A., and Zussman, J., 1992, An Introduction to the Rock-forming Minerals: Hong Kong, Longman Scientific & Technical, v. 2, 696 p.

Fitzsimmons, J.P., 1967, Precambrian rocks of the Zuni Mountains: New Mexico Geological Society, Guidebook 18, p. 119-121.

Goddard, E. N., 1966, Geologic map and sections of the Zuni Mountains fluorspar district, Valencia County, New Mexico: U. S. Geological Survey, Miscellaneous Geologic Investigations Map I-454, scale 1:31,680.

Goff, F., and Kelley, S.A., 2020, Facts and hypotheses regarding the Miocene – Holocene Jemez Lineament, New Mexico, Arizona, and Colorado: New Mexico Geological Society, Guidebook 71, this volume.

Gysi, A.P., and Williams-Jones, A.E., 2013, Hydrothermal mobilization of pegmatite-hosted REE and Zr at Strange Lake, Canada: A reaction path model: Geochimica et Cosmochimica Acta, v. 122, p. 324-352.

Hecht, L., Thuro, K., Plinninger, R., and Cuney, M., 1999, Mineralogical and geochemical characteristics of hydrothermal alteration and episyenitization in the Königshain granites, northern Bohemian massif, Germany: International Journal of Earth Sciences, v. 88, p. 236-252.

International Atomic Energy Agency, 2018, Geological classification of uranium deposits and selected examples: IAEA-TECDOC-1842, 430 p., https://www-pub.iaea.org/MTCD/Publications/PDF/TE1842_web.pdf.

Jaques, L., Noronha, F., Liewig, N., and Bobos, I., 2016, Paleofluids circulation associated with the Gerês late-orogenic granitic massif, northern Portugal: Chem Erde Geochem, v. 76, p. 659-676.

Lambert, E.E., 1983, Geology and petrochemistry of ultramafic and orbicular rocks, Zuni Mountains, Cibola County, New Mexico [M.S. thesis]: Albuquerque, University New Mexico, 166 p.

LeBas, M.J., 2008, Fenites associated with carbonatites: Canadian Mineralogist, v. 46, p. 915-932.

Leroy, J., 1978, The Margnac and Fanay uranium deposits of the La Crouzille district (western Massif Central, France): Geologic and fluid inclusion studies: Economic Geology, v. 73, p. 1611-1634.

Long, K.R., van Gosen, B.S., Foley, N.K. and Cordier, D., 2010, The principle rare earth element deposits of the United States—A summary of domestic deposits and a global perspective: U.S. Geological Survey, Scientific Investigations Report 2010-5220, 104 p., http://pubs.usgs.gov/sir/2010/5220/.

López-Moro, F.J., Moro, M.C., Timón, S.M., Cembranos, M.L., and Cóar, J., 2013, Constraints regarding gold deposition in episyenites: the Permian episyenites associated with the Villacampo shear zone, central western Spain: International Journal of Earth Sciences (Geol Rundsch), v. 102, p. 721-744.

Mawer, C.K. and Bauer, P.W., 1989, Precambrian rocks of the Zuni uplift: A summary with new data on ductile shearing: New Mexico Geological Society, Guidebook 40, p. 13-147.

Maxwell, C.H., 1986, Geologic map of El Malpais lava field and surrounding areas, Cibola County, New Mexico: U.S. Geological Survey, IMAP 1595, scale 1:62,500.

McLemore, V.T., 1983, Carbonatites in the Lemitar and Chupadera Mountains, Socorro County, New Mexico: New Mexico Geological Society, Guidebook 34, p. 235-240.

McLemore, V.T., 1986, Geology, geochemistry, and mineralization of syenites in the Red Hills, southern Caballo Mountains, Sierra County, New Mexico: New Mexico Geological Society, Guidebook 37, p. 151-159.

McLemore, V.T., 1989, Base and precious metal deposits in the Zuni Mountains, Cibola County, New Mexico: New Mexico Geological Society, Guidebook 40, p. 317-319.

McLemore, V. T., 2001, Silver and gold resources in New Mexico: New Mexico Bureau of Mines and Mineral Resources, Resource Map 21, 60 p.

McLemore, V.T., 2013, Geology and mineral resources in the Zuni Mountains mining district, Cibola County, New Mexico: Revisited: New Mexico Geological Society, Guidebook 64, p. 131-142.

McLemore, V.T., 2015, Rare Earth Elements (REE) Deposits in New Mexico: Update: New Mexico Geology, v. 37, p. 59-69, http://geoinfo.nmt.edu/publications/periodicals/nmg/current/home.cfml.

McLemore, V.T., 2016, Episyenites in the Sevilleta National Wildlife Refuge, Socorro County, New Mexico—preliminary results: New Mexico Geo-

logical Society, Guidebook 67, p. 255-262.

McLemore, V.T., 2018, Rare earth elements (REE) deposits associated with Great Plain margin deposits (alkaline-related), southwestern United States and eastern Mexico: *Resources*, v. *7*(1), 8; 44 p., doi:10.3390/resources7010008; http://www.mdpi.com/2079-9276/7/1/8.

McLemore, V.T., and McKee, C., 1988, Geochemistry of Burro Mountains syenites and adjacent Proterozoic granite and gneiss and the relationship of a Cambrian–Ordovician magmatic event in New Mexico and southern Colorado: New Mexico Geological Society, Guidebook 39, p. 89-98.

McLemore, V.T. and McKee, C, 1989, Geology and geochemistry of syenites and adjacent Proterozoic granitic and metamorphic rocks in the Zuni Mountains, Cibola County, New Mexico: New Mexico Geological Society, Guidebook 40, p. 149-155.

McLemore, V.T., Broadhead, R.F., Barker, J.M., Austin, G.S., Klein, K., Brown, K.B., Murray, D., Bowie, M.R., and Hingtgen, J.S., 1986, A preliminary mineral-resource potential of Cibola County, northwestern New Mexico: New Mexico Bureau of Mines and Mineral Resources, Open-file Report OF-230, 403 p.

McLemore, V.T., McMillan, N.J., Heizler, M., and McKee, C., 1999, Cambrian alkaline rocks at Lobo Hill, Torrance County, New Mexico: More evidence for a Cambrian-Ordovician aulacogen: New Mexico Geological Society, Guidebook 50, p. 247-253.

McLemore, V.T., North, R.M., and Leppert, S., 1988a, Rare-earth elements (REE), niobium and thorium districts and occurrences in New Mexico: New Mexico Bureau of Mines and Mineral Resources, OF-324, 28 p.

McLemore, V.T., North, R.M., and Leppert, S., 1988b, Rare-earth elements (REE) in New Mexico: New Mexico Geology, v. 10, p. 33-38.

McLemore, V.T., Smith, A., Riggins, A.M., Dunbar, N., Frempong, K.B., and Heizler, M.T., 2018, Characterization and origin of episyenites in the southern Caballo Mountains, Sierra County, New Mexico: New Mexico Geological Society, Guidebook 69, p. 207-216.

McMillan, N.J. and McLemore, V.T., 2004, Cambrian-Ordovician magmatism and extension in New Mexico and Colorado: New Mexico Bureau of Mines and Geology Resources, Bulletin 160, 12 p., http://geoinfo.nmt.edu/publications/bulletins/160/downloads/01mcmill.pdf (accessed 8/22/11).

Nakamura, N., 1974, Determination of REE, Ba, Fe, Mg, Na, and K in carbonaceous and ordinary chondrites: Geochimica et Cosmochimica Acta, v. 38, p. 757-775.

Petersson, J. and Eliasson, T., 1997, Mineral evolution and element mobility during episynitization (dequartzification) and albitization in the post-kinematic Bohus granite, southwest Sweden: Lithos, v. 42, p. 123-146.

Petersson, J., Fallick, A.E., Broman, C., Eliasson, T., 2014, Imprints of multiple fluid regimes on episyenites in the Bohus granite, Sweden. Lithos v. 196-197, p. 99-114.

Recio, C., Fallick, A.E., Ugidos, J.M., and Stephens, W.E., 1997, Characterization of multiple fluid-granite interaction processes in the episyneites of Avila-Béjar, central Iberian massif, Spain: Chemical Geology, v. 143, p. 127-144.

Riggins, A.M., 2014, Origin of the REE-bearing episyenites in the Caballo and Burro Mountains, New Mexico [M.S. thesis]: Socorro, New Mexico Institute of Mining and Technology, 348 p.

Riggins, A.M., Dunbar, N., McLemore, V.T., Heizler, M., McIntosh, W. and Frempong, K., 2014, Mineralogy, geochemistry, and chronology of the Caballo and Burro Mountains REE-bearing episyenites (abs.): Society of Economic Geology*: Building Exploration Capability for the 21st Century, Program. (poster)*, http://geoinfo.nmt.edu/staff/mclemore/projects/documents/Riggins_SEG.pdf, *accessed 2/3/16.*

Sheard, E.R., Williams-Jones. A.E., Heiligmann, M., Pederson, C., and Trueman, D.L., 2012, Controls on the concentration of zirconium, niobium, and the rare earth elements in the Thor Lake rare metal deposit, Northwest Territories, Canada: Economic Geology, v. 107, p. 81-104.

Sims, P.K., Stein, H.J., and Finn, C.A., 2002, New Mexico structural zone—an analog of the Colorado mineral belt: Ore Geology Reviews, v. 21, p. 211-225.

Smith, A.E., 2018, Multi-stage processes for generation of REE-enriched episyenites and fenites in New Mexico and Colorado: the role of magmatic and diagenetic fluids based on $^{40}Ar/^{39}Ar$ geochronology, whole rock geochemistry and radiogenic isotopes [M.S. thesis]: Socorro, New Mexico Institute of Mining and Technology, 352 p.

Strickland, D., Heizler, M.T., Selverstone, J., and Karlstrom, K.E., 2003, Proterozoic evolution of the Zuni Mountains, western New Mexico: Relationship to the Jemez lineament and implications for a complex cooling history: New Mexico Geological Society, Guidebook 54, p. 109-117.

Suikkanen, E. and Rämö, O.T., 2019, Episyenites—charactristics, genetic constraints and mineral potential: Mining, Metallurgy, and Exploration, v. 36, p. 861-878.

Walters, A.S., Goodenough, K.M., Hughes H.S.R., Roberts, A.G., Gunn, A.G., Rushton, J., and Lacinska, A., 2013, Enrichment of rare earth elements during magmatic and post-magmatic processes; a case study for the Loch Loyal syenite complex, northern Scotland: Contributions to Mineralogy and Petrology, v. 166, p. 1177-1202.

Appendices can be found at http://nmgs.nmt.edu/repository/index.cfml?rid=2020001

New Mexico Geological Society, Special Publication 14, Geology of the Mount Taylor Area, 2020, p. 37-40.

TALL 'HORNITO-STYLE' LAVA STALAGMITES AND LAVA COLUMN IN LAVA COLUMN CAVE, EL MALPAIS NATIONAL MONUMENT

Victor J. Polyak[1] and Paula P. Provencio[2]

[1]Senior Research Scientist, Earth and Planetary Sciences, University of New Mexico, Albuquerque, New Mexico 87131; polyak@unm.edu

[2]Research Specialist, Institute of Meteoritics, Earth and Planetary Sciences, University of New Mexico, Albuquerque, New Mexico 87131

Abstract—New Mexico hosts spectacular lava tube caves that exhibit remarkable lava features. Most of these caves are in El Malpais National Monument. Two types of lava features, lava columns and lava stalagmites, are named for their resemblance to columns and stalagmites common to limestone caves. Lava Column Cave, in El Malpais National Monument, exhibits rare large examples of a lava column and two lava stalagmites. We measured one of the lava stalagmites and the lava column heights to be 3.17 meters (10.4 feet) and 4.45 meters (14.6 feet), respectively, making them among the largest thus far reported in El Malpais National Monument. We also observed that these lava features have central conduits. We suggest they formed the same way that hornitos and squeeze-ups form on lava flow surfaces, by lava extruding from the floor of the cave, rather than from accumulation of dribbles and blobs of lava falling from the ceiling. Our interpretation for the origin of these lava features differs from the origin of the more typical lava stalagmites and columns.

INTRODUCTION

Many lava features within lava tube caves resemble speleothems, and accordingly speleothem types have been borrowed to describe lava tube cave features, especially for lava stalagmites, stalactites, and helictites (Hill and Forti, 1997; Palmer, 2007). Wentworth and Macdonald (1953) described the origin of lava stalagmites and two types of lava stalactites in Hawaii caves. Lava stalagmites were noted by Waters et al. (1990) in California caves. A detailed description of features such as lava stalagmites and columns in lava tube caves is provided by (Larson, 1991, 1993). These features are well-represented in caves of El Malpais National Monument, New Mexico.

Lava stalagmites are defined as mounds of agglutinated droplets of lava (Wentworth and Macdonald, 1953), which describes the more typical occurrence of lava stalagmites, or as vertically oriented accumulation and accretion of droplets and dribbles of semi-solid and solid lava (Larson, 1991, 1993). Lava stalagmites and columns that could form from extrusion of lava from the floor do not quite fit these definitions, even though a vertical accumulation occurs. This type of lava stalagmite or column having the source of lava from the floor, we suggest, would fit the description of a squeeze-up or a hornito, which usually forms on the lava flow surface above lava tubes, and not in the caves. Hornitos are also known as driplet spires or cones that retain a central conduit (Larson, 1991, 1993; Wentworth and Macdonald, 1953) and sometimes occur on a lava tube floor (Larson, 1991, 1993). Squeeze-ups and hornitos on lava flow surfaces (not in the caves) can have the appearance of lava stalagmites (Fig. 1). Three very wide and tall lava features in Lava Column Cave, El Malpais National Monument, form as a lava column and two lava stalagmites, but exhibit central conduits, like hornitos. Here, we describe these features in Lava Column Cave as lava stalagmites and a lava column and include the physical description of the two lava features. The smaller lava stalagmite, while large, had fallen over and was not included in this study.

LAVA FEATURES OF INTEREST

There are important lava tube caves in New Mexico (Goar and Mosch, 1992), and specifically in El Malpais National Monument, where lava features typical of lava tube caves are well-exhibited. Most common are lava stalagmites, lava soda-straw stalactites, and lava helictites. These features are spectacular but are usually very small and hard to see, particularly the lava features on cave floors. As such, they are especially vulnerable to damage by visitation (Polyak and Provencio, 2006). With the exception of the Lava Column Cave lava column and stalagmites, the vast majority of lava stalactites, columns, and stalagmites in El Malpais National Monument caves are interpreted to have formed by accretion of dripping lava during lava tube system activity. The lava column and lava stalagmites described herein are much larger than other lava features noted in El Malpais National Monument, which makes them extraordinary.

Lava Column Cave is located in the Bandera flow, and therefore the cave and its lava features formed about 11,000 years ago (Dunbar and Phillips, 2004; Laughlin et al., 1994). The cave is relatively small with only ~50 meters of passage that is 8 to 10 meters wide and 3 to 6 meters high (Fig. 2A). Overall, the cave is nearly devoid of distinct lava features, and the only ones of interest are located at the back of the cave. The intact lava stalagmite is adjacent to the lava column (Fig. 2B). The overall appearance of the lava column gives the impression that lava was injected from the ceiling rather than the floor of the cave. Closer examination shows the presence of central conduits in both the lava column and nearby upright

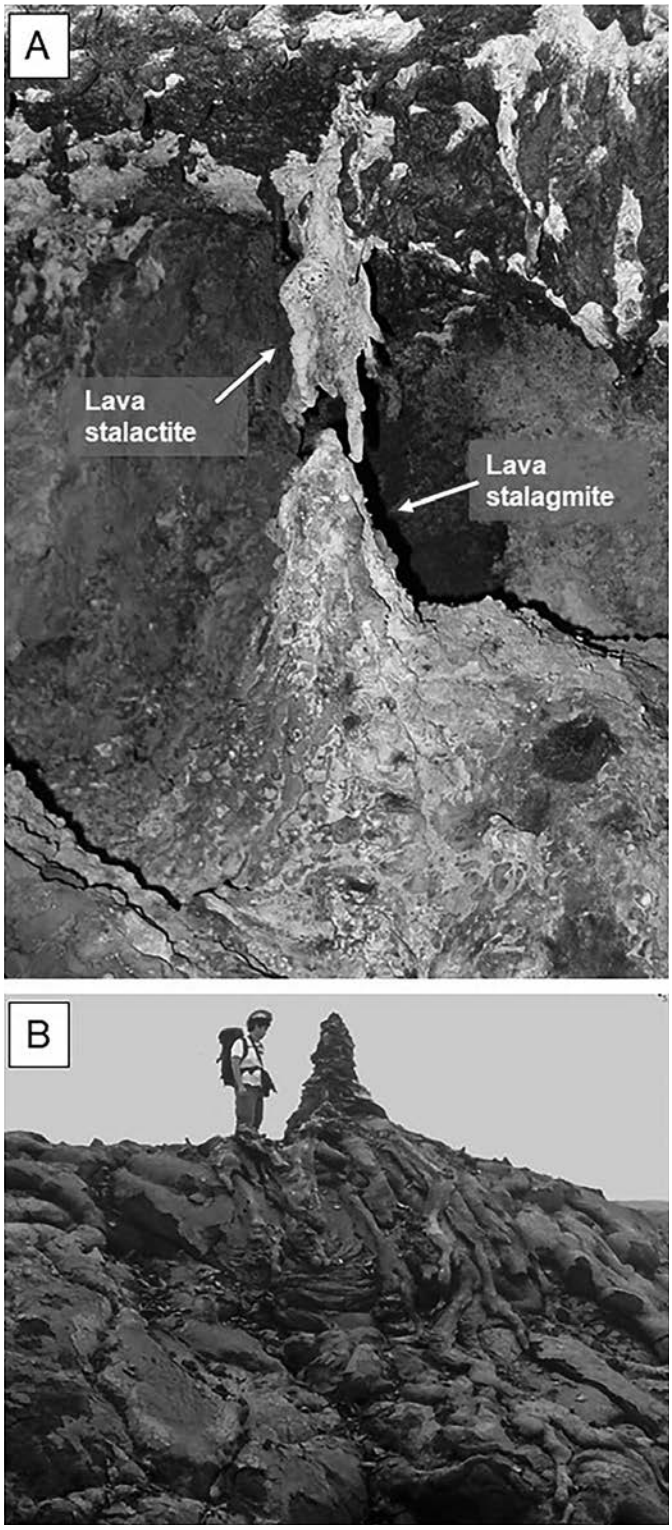

FIGURE 1. **A**) Photograph of a typical lava stalagmite. Note the presence of a lava stalactite immediately above the lava stalagmite. If these had connected, then they would have formed a lava column. **B**) Photograph showing a stalagmite-shaped squeeze-up on a tumulus on the surface of the 1919 Kilauea lava flow (courtesy of Dr. William R. Halliday). Squeeze-ups and hornitos on lava flow surfaces can resemble cave stalagmites.

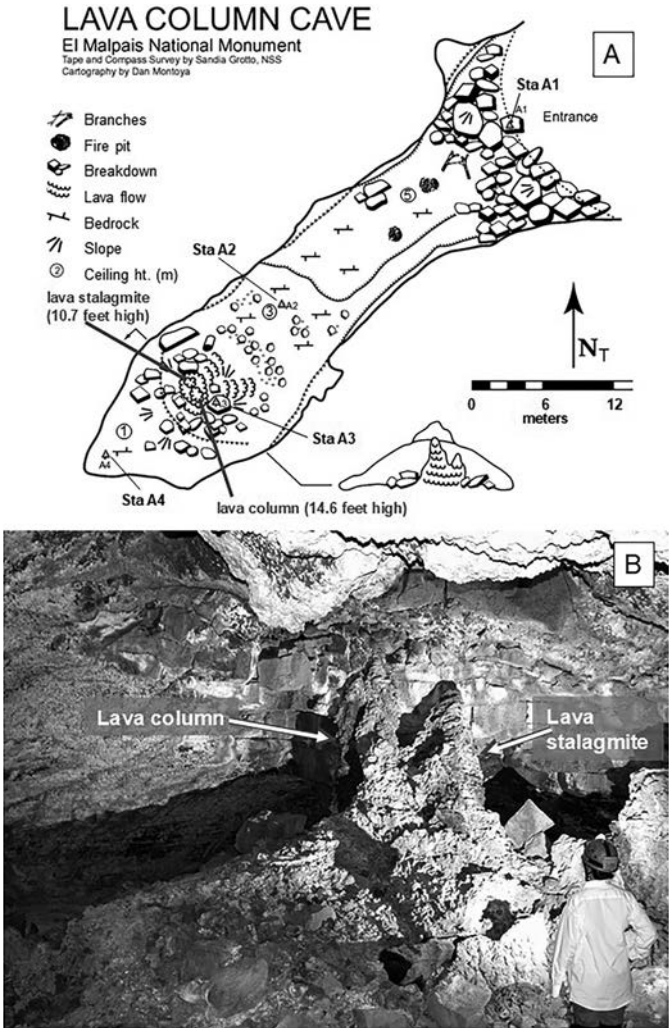

FIGURE 2. **A**) Map of Lava Column Cave indicating the location of a large lava stalagmite and lava column. The map was generated by the Sandia Grotto of the National Speleological Society for El Malpais National Monument. **B**) Photograph showing the lava column and lava stalagmite.

lava stalagmite, which indicates an origin like that described for hornitos or spatter cones, features that form on the surface of lava flows.

Examination of the central conduits of the lava stalagmite and column indicate that the conduit diameter is ~0.15 meters and the depth of the conduit descends to near the same level as the cave floor (Fig. 3). There was no distinct indication of a point of injection of lava at the base of the conduits. The heights of the hornito-style lava stalagmite and column above the cave floor are 3.17 meters (10.4 feet) and 4.45 meters (14.6 feet), respectively, making these exceptionally large lava features. The interior of the conduits (at the top) are lined with lava coralloids that slightly point downward. The exterior of the stalagmite and column are stacked lobes of lava, and a lava toe extrudes from the lava column.

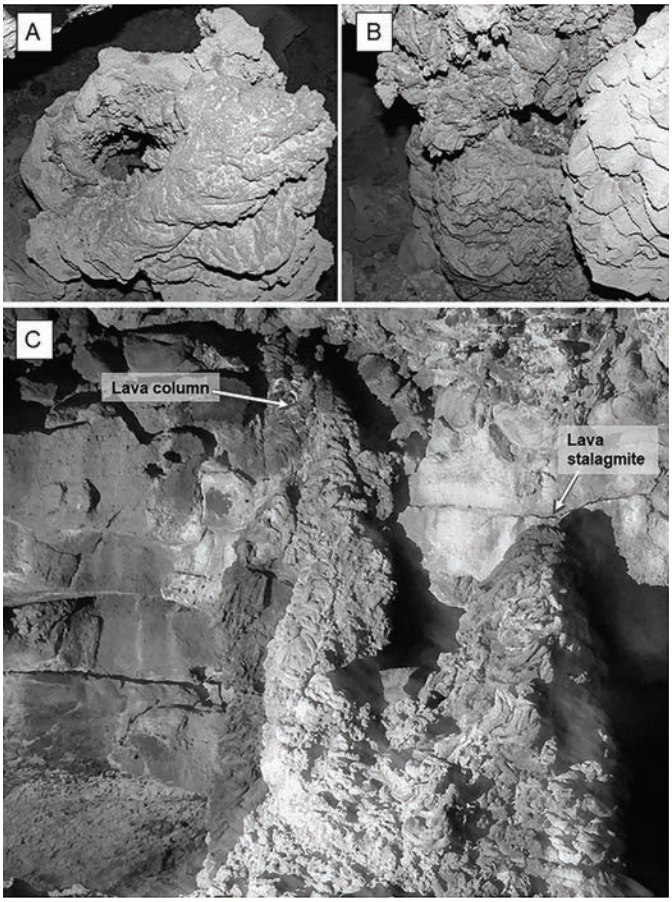

FIGURE 3. This figure shows the central conduit of the lava stalagmite (**A**) and the lava column (**B**). Note that the bottom photograph (**C**) shows the top half of the lava stalagmite and lava column, and that the source of lava to form the column (and the stalagmite) is from the floor, not from the ceiling as it appears.

DISCUSSION

We suggest that these squeeze-up hornito-type lava features that formed in a lava tube cave should be formally described as a lava column and two lava stalagmites even though we interpret them to have different origins than typical lava columns and stalagmites. Given that the Lava Column Cave lava stalagmite and column formed like a hornito, then the material that accreted to form these features was injected into the cave from the floor, not from the ceiling. There are no distinct lava features above the stalagmite or column that would indicate spattering, which suggests that the squeezing up of lava was relatively slow and steady, and not violent. The lava column accreted high enough to connect with the ceiling, and issue lava up into a depression in the ceiling, making it look as though the lava that formed the lava column was sourced from the ceiling (Fig. 3C). Final subsidence of lava in the central conduits must have been fluid enough to spread out evenly with the floor of the cave. Considering that hornitos are commonly formed over lava tubes, the presence of these features suggests that there was another lava tube level below the tube that formed Lava Column Cave. While somewhat rare, multi-level tubes are observed in some of the caves in these lava flows.

Other than the lava features in Lava Column Cave, the tallest lava stalagmites and lava columns in El Malpais National Monument caves are less than one meter in length. To our knowledge the world's tallest lava column measured is 7.8 meters from Majanggul (Manjang) Cave, Korea (Dell'Amore, 2012; Jeon and Woo, 2018; Okada et al., 1991). Lava stalagmites that exceed 3 meters in height in Mathaioni Cave (Kenya) are reported as possibly the largest lava stalagmites in the world (Forti et al., 2003). These heights are similar to but slightly higher than those of Lava Column Cave lava stalagmite and column. However, there appears to be a lack of information regarding descriptions, including heights of these types of lava features. Lava Column Cave has what might be considered among the highest and largest lava stalagmites and lava column in the world.

ACKNOWLEDGMENTS

We thank William R. Halliday, M.D., for communication regarding the squeeze-up, hornito-like origin of the Lava Column Cave stalagmites and column upon seeing our presentation of these features several years ago. Members of the Sandia Grotto of the National Speleological Society helped with surveys and measurements of these lava features. Trips to the cave were permitted by El Malpais National Monument. Reviews of this paper were kindly provided by Bogdan P. Onac (University of South Florida), Arthur N. Palmer (Emeritus at State University of New York at Oneonta), Shari Kelley (NM Bureau of Geology and Mineral Resources), and Fraser Goff (NM Institute of Mining and Technology).

REFERENCES

Dell'Amore, C., 2012, Exploring Asia's Longest Lava Tube, National Geographic News: https://blog.nationalgeographic.org/2012/09/13/exploring-asias-longest-lava-tube/.

Dunbar, N.W., and Phillips, F.M., 2004, Cosmogenic ^{36}Cl ages of lava flows in the Zuni-Bandera volcanic field, north-central New Mexico, USA, *in* Cather, S.M., McIntosh, W.C., and Kelley, S.A., eds., Tectonics, geochronology, and volcanism in the southern Rocky Mountains and Rio Grande rift: NM Bureau of Geology and Mineral Resources, Bulletin, v. 160, p. 309-317.

Forti, P., Galli, E., and Rossi, A., 2003, Minerogenesis of volcanic caves of Kenya: International Journal of Speleology, v. 32, n. 1, p. 3-18.

Goar, M., and Mosch, C.J., 1992, Lava caving areas in New Mexico, *in* Proceedings 6th International Symposium on Volcanospeleology: Huntsville, National Speleological Society, p. 50-57.

Hill, C.A., and Forti, P., 1997, Cave Minerals of the World: Huntsville, National Speleological Society, 463 p.

Jeon, Y., and Woo, K.S., 2018, 25. Geotourism in Jeju Island UNESCO Global Geopark, South Korea, *in Dowling, R., and Newsome, D., eds.*, Handbook of Geotourism: Northampton, Edward Elgar Publishing, p. 329.

Larson, C.V., Nomenclature of lava tube features, *in* Proceedings 6th International Symposium on Volcanospeleology: Huntsville, National Speleological Society, p. 231-248.

Larson, C.V., 1993, An Illustrated Glossary of Lava Tube Features: Western Speleological Survey, 56 p.

Laughlin, A.W., Poths, J., Healey, H.A., Reneau, S., and WoldeGabriel, G., 1994, Dating of Quaternary basalts using the cosmogenic ^{3}He and ^{14}C methods with implications for excess ^{40}Ar: Geology, v. 22, p. 135-138.

Okada, T., Itaya, T., Sawa, I., and Hong, S.-H., 1991, K-Ar age determination of a lava stalagmite in Manjang gul, Jeju island, Korea: Journal of Southeast Asian Earth Sciences, v. 6, p. 127-130.

Palmer, A. N., 2007, Cave Geology: Dayton, Cave Books, 454 p.
Polyak, V.J., and Provencio, P.P., 2006, Protecting lava tube caves, *in* Hildreth-Weker, V., and Werker, J. C., eds., Cave Conservation and Restoration: Huntsville, National Speleological Society, p. 133-140.
Waters, A.C., Donnelly-Nolan, J.M., and Rogers, B.W., 1990, Selected caves and lava-tube systems in and near Lava Beds National Monument, California: U.S. Geological Survey, Bulletin 1673, 102 p.
Wentworth, C.K., and Macdonald, G.A., 1953, Structures and forms of basaltic rocks in Hawaii: U.S. Geological Survey, Bulletin 994, 98 p.

New Mexico Geological Society, Special Publication 14, Geology of the Mount Taylor Area, 2020, p. 41-46.

HUMATE IN THE UPPER CRETACEOUS FRUITLAND FORMATION IN NORTHWESTERN NEW MEXICO

Robert W. Newcomer[1], John P. Nybo[2], and Jakob R. Newcomer[3]

[1]Toltec Mesa Resources LLC, 7823 Quintana Drive N.E., Albuquerque, New Mexico 87109
[2] NyBoCo Geoscience, 12070 N. Highway 14, Cedar Crest, New Mexico 87008
[3] New Mexico Museum of Natural History, 1801 Mountain Road N.W., Albuquerque, New Mexico 87104

Abstract—Humate is a naturally occurring, high humic acid content material. It is associated with weathered coal and humate-rich mudstones and shales in the Upper Cretaceous Fruitland Formation in northwestern New Mexico. These humate-bearing deposits have been mined primarily to produce humic substances used as soil amendments. Mining of humate in New Mexico started in the 1970s, and nearly 60,000 metric tons were mined by six operators in 2016. Humic substances are water soluble and are beneficial to soils and plants. They are high molecular weight molecules (generally between 5,000 to 50,000 g/mol), with complex structures, large surface areas and cation-exchange capacities, and multiple functional groups. These properties facilitate molecular binding to salts, metals, and hydrophobic compounds in soils and water. Humic substances may play a key role in controlling the aqueous concentrations, mobility, bioavailability and toxicity of contaminants in the environment.

INTRODUCTION

Mining and the production of humate resources in northwestern New Mexico has been growing steadily since the 1970s. Mineable humate deposits are associated with weathered coal and organic-rich Upper Cretaceous sedimentary rocks in the San Juan Basin. This paper focuses on the humate associated with the Upper Cretaceous Fruitland Formation in the Star Lake Coal Field, about 48 km west of Cuba, New Mexico (Fig. 1). Humate and humic substances are formed from the decay of plants and the weathering of the coal deposits. Humic substances are complex compounds of polymeric organics with molecular weights ranging from a few hundred to several hundred thousand or even a few million grams per mole. Humic substances are used primarily as soil amendments but also have or have had applications in pharmaceuticals, wood finishing, water treatment, hydrocarbon remediation, and as drilling fluid additives. There may also be future applications in mine-waste remediation.

Shomaker and Hiss (1974) provided an overview of humate mining in northwestern New Mexico in the 1970s. At that time, humate and humic substances were recognized largely as soil amendments with agricultural applications. Roybal and Barker (1987) described the state of the industry in 1980s and the growing use of humic materials in other applications. This paper provides an update and outlines the growing humate mining and production industry in New Mexico.

WHAT IS HUMATE?

Humate terminology can be confusing, particularly as it relates to its use in scientific, mining and business terms (Hoffman et al., 1994; Table 1). The weathering and decay of organic matter and coal produces dark-colored humate. Humate contains humic substances, which are naturally occurring het-

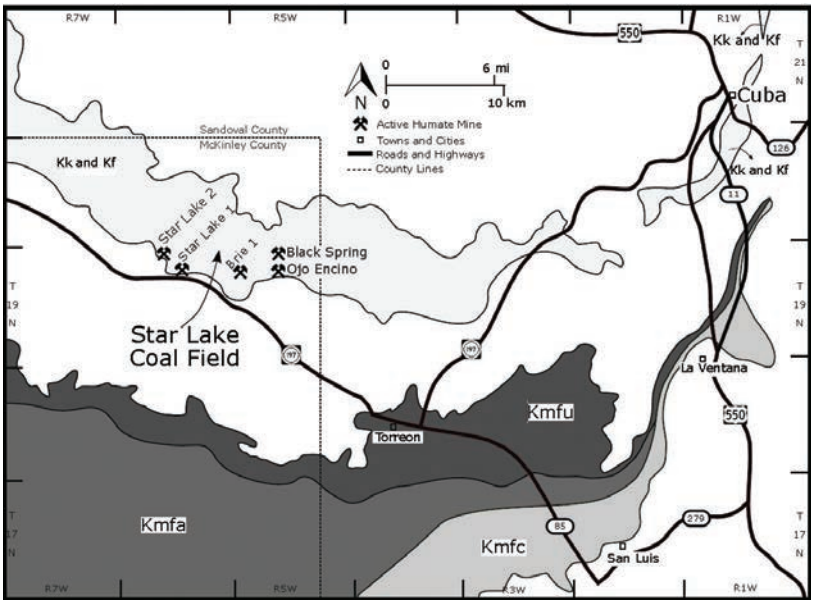

FIGURE 1. Map of Star Lake Coal Field area showing active humate mines in northwest New Mexico. Kk = Kirtland Formation; Kf = Fruitland Formation; Kmfu = Menefee Formation, upper coal bed; Kmfa = Menefee Formation, Allison Member; Kmfc = Menefee Formation, Cleary Coal Member. Geology modified after Hoffman et al., 1992. Locations of active humate mines as listed with the New Mexico Mining and Minerals Division as of 2019.

TABLE 1. Terms and definitions for humic acid-rich and associated materials (modified after Roybal and Barker, 1987).

Terminology	Definition
Carbonaceous Mudstone/Shale	Called humate by geologists if it contains base-soluble humic acids
Fulvate	Salt of fulvic acid
Fulvic Acid	Base-soluble and acid-soluble fraction of humate; fraction of humic substances soluble in water under all pH conditions
Humalite	A soft, brown coal-like material, which has many similarities to leondardite (an informal term, used in Alberta, Canada) that occurs as a weathering product of sub-bituminous coal and carbonaceous shales
Humate (singular)	Geologically a weathered coal (brown coal), carbonaceous claystone/mudstone/shale rich in humic matter
Humates (plural)	Chemically, salts of humic acids
Humic Acid (singular)	Base-soluble organic material; fraction of humic substances not soluble in water under acidic conditions (below pH of 2), but soluble at higher pH
Humic Acids (plural)	Humic, fulvic and ulmic acids; hydrogen ion in exchange sites; Base soluble organic material insoluble in acid
Humic Substances (Matter, Substances, Deposits)	A general category of naturally occurring, biogenic, heterogeneous organic substances that have a high molecular weight and are refractory; completely decomposed organic matter containing humic acid
Humin(s)	Chemically an alkali-insoluble fraction of humate; fraction of humic substances not soluble in water at any pH value
Humus	Chemically an alkali-soluble fraction of humate; lithologically a carbonaceous mudstone or shale; oxidized (weathered) lignite or coal, rich in organic matter; dark, organic, well decomposed soil material consisting of plant, and animal residues and various inorganic elements
Leondardite	Oxidized (weathered lignite); sometimes includes weathered sub-bituminous coal, but this is not the preferred term for weathered coal
Ulmate	Salt of ulmic acid
Ulmic Acid	Base-soluble organic material that is acid insoluble then alcohol soluble
Weathered Coal	Oxidized coal that contains humic acids due to the weathering process

erogeneous mixtures of organic materials. Humification is the process of forming these substances as a product of the decomposition of organic material during weathering and degradation of plant material (Tan, 2014). Humus is the alkali-soluble fraction of humate. Even though humic acid was first extracted from humus in 1786, it wasn't until the 1970s that the technology was available to assess the chemical structure of the molecule in some detail (Susic, 2001).

The humic substance molecule has a high molecular weight (generally between 5,000 to 50,000 g/mol). These molecules are partly colloidal and weakly acidic due to their humic acid and fulvic acid contents (Roybal and Barker, 1987). Humic substances are not pure materials, which has resulted in ambiguous use by geologists, chemists, soil scientists, agronomists and producers. For instance, the weathered coal that is mined for its humic acid content is an extremely variable mixture of base-soluble humic, fulvic and ulvic acids, as well other organics and their salts.

The use of the term "humic acid" varies between geology and chemistry with geological humic acid including additional smaller molecules and having a greater acidity than chemical humic acid derived in the laboratory (Roybal and Barker, 1987). Humic acids are structurally complex molecules and are amorphous with poorly defined x-ray patterns. Molecular structural models for humic substances can be broadly divided into two main types, the "macromolecular" and "supramolecular mixture" (Billingham, 2012). Billingham (2012) provides a summary of the various molecular structural theories and the history of research associated with them.

Humic substances have large cation-exchange capacities (CEC) ranging from 200 to 500 milliequivalents per 100 grams at a pH of 7. The wide range in CEC can be explained by the variations in acidity between humic acid and humate (chemical), because a molecule with hydrogen-filled exchange sites yields humic acid with lower pH than a molecule with sites filled with other cations that yield chemical humate. Therefore, the determination of various forms of humate in the laboratory and for classification purposes is generally operationally defined (Hoffman et al., 1992).

Soil humic substances are known to be beneficial for soils and plants (Billingham, 2012; Tan, 2014). As a conditioner of soils, humate generally increases soil aggregation, water-holding capacity and improves soil aeration and permeability. Chemically, it increases the CEC and provides a stronger buffering capacity to resist chemical changes in the soils. Although some of the literature regarding humate benefits is promotional and the effectiveness and value of humic substances is not always clear, there are many published studies showing the direct and indirect benefits to plant growth when tested under controlled conditions (Tan, 2014; Wright and Lenssen, 2013; Billingham, 2012; Hartwigsen, and Evans, 2000; Lee and Bartlett, 1976; Lyons and Genc, 2016).

Chemists consider humate to be a salt of humic acid, a comparatively restricted usage. The term humate is used lithologically, in geology and mining, for mud rocks rich in organic acids, for weathered coal and humic-acid containing organics found in the pore spaces in sandstones. The later usage is applied throughout the rest of this paper.

GEOLOGY AND COAL ASSOCIATION

This paper focuses on one author's experience with mining operations and the development of humate resources at Menefee Mining Company's Black Spring Mine. At the Black Spring Mine, humate is mined from open cuts in weathered coal beds in the uppermost part of the Cretaceous Fruitland Formation (Dames and Moore, Inc., 1979; Schneider and Kirschbaum, 1981; Fig. 2). The Black Spring Mine is in the eastern part of the Star Lake Coal Field, which is described in Shomaker et al. (1971). Humate deposits also occur in some of the older Cretaceous sedimentary rocks that underlie the Fruitland Formation in the San Juan Basin. These humate deposits include the weathered coal and organic-rich shales in the Menefee and Crevasse Canyon Formations (Mesaverde Group) east and south of the Black Spring Mine (Roybal and Barker, 1987).

The Star Lake Coal Field is in the southeasternmost part of the San Juan Basin. The San Juan Basin is an asymmetric structural depression in northwestern New Mexico that also extends into a small part of northeastern Arizona, southern Utah and southern Colorado. According to Fassett and Hinds (1971), the depression contains sedimentary rocks of Cambrian, Devonian, Mississippian, Pennsylvanian, Permian, Triassic, Jurassic, Late Cretaceous, Tertiary and Quaternary age. The maximum known thickness of sedimentary rocks is at least 4300 m in the deepest part of the basin. Late Cretaceous rocks, of which the Fruitland Formation is part, are more than 1800 m thick. These rocks, which contain coal and humate deposits, consist largely of intertonguing marine and non-marine units that represent three basin-wide transgressive-regressive cycles of deposition (Fassett and Hinds, 1971).

The final regression of the Cretaceous seaway resulted in deposition of the marine Pictured Cliffs Sandstone (a point-bar sand deposit, with the sea on the northeast side and swampy areas on the south side between the bar and the land). The Pictured Cliffs Sandstone is overlain by and intertongues with the Fruitland Formation. The Fruitland Formation is overlain by the Kirtland Formation. With the withdrawal of the seaway, uplift within the southern Rocky Mountains, and structural deformation to the San Juan Basin, terrestrial sediments were deposited over the Kirtland strata. These later units included the Upper Cretaceous to Paleogene Ojo Alamo Sandstone and Paleogene to early Eocene Nacimiento Formation and San Jose Formation. In the Star Lake Coal Field, this deposition occurred episodically adjacent to the active Nacimiento uplift (Smith, 1992). Late Cretaceous and Paleogene terrestrial strata record the local disruption and partitioning of the Cretaceous foreland basin and retreat of the seaway by Laramide time (~65 million years ago).

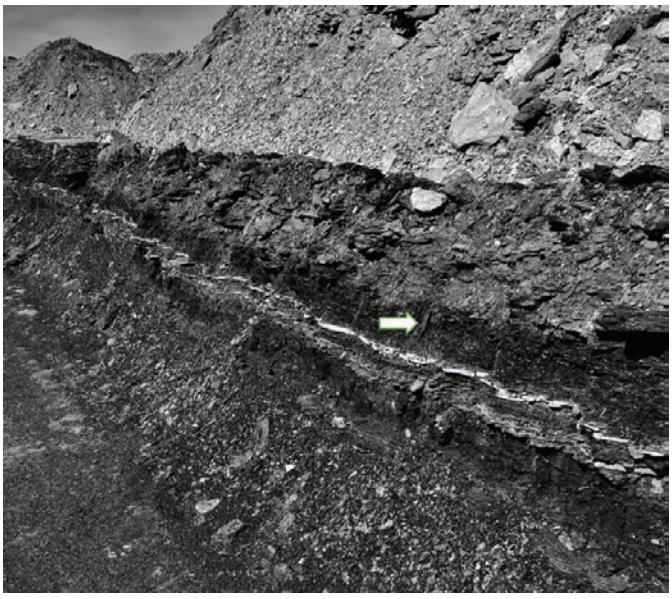

FIGURE 2. Humate deposit in Cretaceous Fruitland Formation at the Black Spring Mine. Note pen in right center of photograph for scale (see arrow).

The Fruitland Formation thickness in the San Juan Basin ranges between 61 and 91 m. In the Star Lake field area, the Fruitland Formation is thinner, ranging from 15 to 30 m due to depositional thinning in the eastern part of the San Juan Basin and erosion prior to deposition of the Ojo Alamo Sandstone.

Since the Fruitland Formation grades upwards into the Kirtland Formation, it is somewhat arbitrarily mapped as it varies spatially. Smith (1992) provided a summary of the stratigraphy of these rocks in the southeastern part of the San Juan Basin and indicated that the top of the Fruitland Formation should be mapped at the top of the highest coal bed or carbonaceous shale bed (or a correlative thin shale) above the last coal (Ayers et al., 1990; Hoffman et al., 1992).

The Fruitland Formation, in the Star Lake Coal Field, dips generally from one to five degrees to the north-northwest (Hoffman et al., 1992). In the Black Spring Mine area, the Fruitland and associated coal/humate beds occur approximately parallel to the depositional strike (essentially parallel to the shoreline of the Cretaceous seaway). The terrestrial direction was south-southwest, and the sea was to the north-northeast.

The Fruitland Formation contains an abundant record of biota that lived along part of the western shore of North America in the Late Cretaceous (Lucas and Mateer, 1983). Fruitland strata are also the major coal-bearing unit in Upper Cretaceous rocks, and it reflects depositional environments associated with extensive marshy habitats (Hunt and Lucas, 1992). Detailed sedimentology indicates the Fruitland Formation was deposited as mixed terrestrial-marine facies along a shoreline locally influenced by deltaic complexes that developed along river systems and extended into the sea. Surface drainages associated with these river systems flowed to the northeast at approximate right angles to the Cretaceous seaway coastline. The overlying Kirtland Formation sediments are largely fluvial in nature and formed as the land advanced to the northeast and the seaway retreated in that direction. These fluvial systems were believed to be low-sinuosity meandering and braided streams with well-drained floodplains. With the migration of the seaway northeastward, no more coal was formed. Fruitland Formation depositional environments represent a transitional phase between completely marine and completely continental deposits during shoreline regression. Periods when the rate of retreat of the shoreline was slow, relatively stable swamp areas developed,

which resulted in thicker coal deposits in the lower part of the Fruitland (e.g., the Carbonero bed, with a thickness of up to 24 m of coal and partings).

HUMATE MINING IN NEW MEXICO

The mining of humate appears to have started in New Mexico in the early 1970s. There were two operators mining humate, and one deposit in development in 1974 (Shomaker and Hiss, 1974). Roybal and Barker (1987) reported a production of 12,293 m^3 (an estimated 12,270 metric tons, assuming a dry bulk density of 1 g/cm^3) of humate in 1983. The growth of humate production since the early 1980s has been relatively steady, and the totals since 1989 are shown in Table 2. Production from 1989 to 2016 has reflected a nearly 10-fold increase, and in 2018 there were five operators working various properties within New Mexico and four operators in the Star Lake Coal Field (Fig. 1).

Weathered coals of the Upper Cretaceous of northwestern New Mexico contain many millions, and possibly billions, of tons of humate (Shomaker and Hiss, 1974). Most of the mining of humate has focused on the thicker, near-surface, deposits that are close to processing facilities in Cuba, New Mexico.

The Black Spring Mine is permitted as a Minimal Impact Mine Project under the New Mexico Mining Act and began operations in 2011. The humate is mined from shallow cuts, and, as mining is advanced into new areas, the old cuts are concurrently reclaimed. Using loaders, the run-of-mine material is transported by truck to a production plant in Cuba, New Mexico. The material is stockpiled at the plant, crushed and screened to uniform particle-size fractions, and bagged for sale (granular products; Earthgreen Products Inc., 2020). The finest size fraction is dissolved in water and then dried to form a concentrated water-soluble powder (powdered products). This material is packaged in drums for sale.

TABLE 2. Humate production in New Mexico between 1989 and 2018 (from New Mexico Energy, Minerals and Natural Resources Department records; this does not include production from tribal lands and reservations, as one operator produced from trust lands, and there has been additional production from the Navajo Coal Mine).

Year	Number of Operating Mines	Production (metric tons)
1989	2	6418
1990	0-1	not reported
1991	3	9084
1992	3	7737
1993	2	1401
1994	2	6897
1995	0-1	not reported
1996	0-1	not reported
1997	0-1	not reported
1998	2	10,891
1999	3	9575
2000	2	10,254
2001	4	17,536
2002	3	18,397
2003	5	15,645
2004	5	17,848
2005	5	21,534
2006	4	25,093
2007	5	25,307
2008	5	31,405
2009	5	28,420
2010	4	30,654
2011	3	36,928
2012	5	52,768
2013	6	52,234
2014	5	50,402
2015	5	45,691
2016	6	59,074
2017	6	51,569
2018	5	53,914

CURRENT USES OF HUMIC SUBSTANCES

There are generally two types of products produced from mined humate in New Mexico, powdered and granular forms. Today, the primary applications from these products are in agriculture, with additional uses in industrial, animal feed and pharmaceuticals (Billingham, 2012). Hoffman and Austin (2006) described the use of humic substances primarily as soil amendments and discussed other end uses, such as a dispersants to control viscosity in drilling fluids, as stabilizers for ion-exchange resins in water treatment, as stains in wood finishing, and as binders for briquets made from lignite char. Humate and humic substances have also been examined to determine their suitability in the remediation of hydrocarbon-, metal- and salt-contaminated soils and groundwater (Mosley, 1998; Bezuglova and Shestopalov, 2005).

HUMATE GEOCHEMISTRY

Essington (2004) defines humate as very complex, amorphous mixtures of highly heterogeneous chemically reactive, yet refractory molecules. They are produced by the early diagenesis and decay of biomatter and form ubiquitously in the environment via processes involving chemical reactions. During decomposition and humification, plant material or other biomatter undergoes diverse modifications (Tan, 2014; Rashid, 1985). These modifications depend primarily on the nature, amount and types of organic matter. The number and nature of microbial populations and the physiochemical conditions associated with the humification (amount of oxygen, rate

of burial, effects of clay minerals) are believed to influence the formation of the humic substances (Susic 2001; Rashid, 1985).

The amount of oxygen in the system is important as it affects the rate of degradation of plant organics. Rashid (1985) notes that the chemical characteristics of humic compounds vary with the degree of oxidation. The humic acid contents tend to be higher in sediments where oxidation is occurring. The total acidity of the humic compounds is also noted to be considerably lower in anoxic sediments than in oxic sediments.

The higher quantities of humic and other organic compounds are more often found in sediments enriched in clay minerals, relative to those with poor clay content (Rashid, 1985). Clays appear to have a catalytic effect on the decomposition of organic matter and on the process of humification. The clays and other aluminosilicate minerals may also accelerate the variety of organic reactions and transformations that occur as part of the humification process. Humic substances can also attach themselves to clay minerals and can solubilize nearly 10 times their own molecular weight in clay particles (Susic, 2001). This can create some of the very large humic particles with very large apparent molecular weights.

According to Essington (2004), several mechanisms and two categories of pathways have been used to describe the genesis of humic substances: 1) those that are purely biological and involve enzymatic decomposition of biopolymers and the enzymatic recombination of the microbiological byproducts; and 2) those that involve the biotic decomposition of biopolymers and the abiotic assemblage of macromolecular structures or aggregates. Much of the understanding of the specific mechanisms and pathways for humic substance formation are theoretical (Billingham, 2012; Susic, 2001). It is likely that the formation of humic substances involves elements of both pathways in the formation of a given humate deposit.

Ultimately, the humic substances become exceedingly complex macromolecules and/or supramolecular mixtures held together by weak chemical bonding forces, hydrogen bonding, or both. Unfortunately, irrespective of the specific mechanism(s) of formation or structural characteristics, humate is usually studied in detail only after the humic substances have been isolated and purified chemically (Susic, 2001). The focus of the many studies of humic substances has been on their elemental composition, their functional groups, and their interactions with other ions and chemicals in the environment. Essington (2004) notes that humic substances are formed through random polymerization or aggregation of a diverse array of compounds from a pool comprised of the microbial degradates of biopolymers. Therefore, the probability of finding two humic molecules that are exactly alike is small, particularly among the larger humic molecules. He also notes that even though the humic substances are refractory (resistant to change), they can evolve and degrade, further enhancing their random character. The macrostructural and supramolecular characteristics of humic substances, especially *in situ*, remain poorly understood.

If humic substances are produced with early diagenesis of buried organic matter, the process of humate formation could begin shortly after (in geologic time), provided there is enough oxygen available. Diagenesis typically involves changes to the buried sediments due to interactions with pore waters (connate and groundwater), minerals, organic material and gases as the sediments experience increases in temperature and pressure with burial. In the case of the Fruitland coals, another period of humate formation would have been expected when the coals were uplifted to the surface, reacted with oxygenated groundwater and were exposed to weathering processes.

HUMATE AND URANIUM

There is a natural association of uranium with humate in Cretaceous and Jurassic sedimentary rocks in the Grants Mining District in New Mexico (Leventhal, 1980; Turner-Peterson, 1985). Some of the humate ores consist of trace uranium minerals and dark humate in organic-rich sandstones (Fig. 3). The relationship between uranium and plant detritus as well as humic substances has been known on a worldwide scale (Leventhal, 1980). Humic substances are effective cation exchangers and are capable of concentrating uranium and other metals from dilute solutions. They appear to be important in the formation of the uranium deposits in the Grants mining district.

In addition to the interest in the relationship between humate and uranium in the formation of the deposits, there has been recent interest in their interrelationships relative to the fate and transport of uranium and other metals released from the uranium mine waste (Velasco et al., 2019). Recent work with uranium-bearing humic substances (described as natural organic material [NOM]) has been conducted to better understand the occurrence of and chemical reactions between the organic matter and the uranium. Organic matter and the associated humate strongly affect the redox, complexation and precipitation chemistry of uranium. Organic matter also appears to influence the mobility of the dissolved and particulate forms of uranium (+4) and uranium (+6) (Velasco et al., 2019). The unique characteristics of humic substances (i.e., their solubility

FIGURE 3. Uranium minerals with dark humate in Jurassic sandstone from Grants Mining District (1 cm cube for scale).

in water, large molecular size, surface areas and CEC) may be effective in mitigating uranium and other metals released from mine wastes. Additional work is needed to better understand these relationships.

CONCLUSIONS

The mining and production of humate and the processing to recover humic substances is expected to be a growth industry in New Mexico well into the future. This is largely due to demand for agricultural amendments to increase crop yield and improve soil conditions. Ongoing research for other uses of humate and humic substances is moving forward on many fronts, and there are likely to be other beneficial uses developed that will further increase demand for the humate resources in the marketplace.

ACKNOWLEDGMENTS

The authors sincerely appreciate Gretchen Hoffman and John Shomaker for the helpful manuscript reviews and input. We also wish to acknowledge the support of Tyler Lown-Vandenburg and John Lown with Menefee Mining Corp. for access to the humate exposures at the Black Spring Mine and for the thoughtful discussions regarding the benefits and value of humic substances.

REFERENCES

Ayers, W.B., Jr., Kaiser, W.R., Ambrose, W.A., Swartz, T.E., Laubach, S.E., Tremain, C.M., and Whitehead, N.H., III., 1990, Geologic evaluation of critical production parameters for coalbed methane resources, Part 1 - San Juan Basin: Gas Research Institute, Contract No. 5087-214-1544, Annual Report, 175 p.

Bezuglova, O., and Shestopalov, A., 2005, The use of humates for the detoxification of soils contaminated with heavy metals, *in* Perminova, I.V., Hatfield, K., and Hertkorn N., eds., Use of Humic Substances to Remediate Polluted Environments: From Theory to Practice: Dordrecht, Springer, NATO Science Series (Series IV: Earth and Environmental Series), v. 52, p. 185-200.

Billingham, K., 2012, Humic products – Potential or presumption for agriculture: New South Wales Government, Department of Primary Industries, JN 11159, 106 p.

Dames and Moore, Inc., 1979, Coal resource occurrence maps and coal development potential maps of the Star Lake Quadrangle, McKinley and Sandoval Counties, New Mexico: U.S. Geological Survey, Open-File Report 79-115, 27 p., 16 plates.

Earthgreen Products Inc., 2020, <http://www.earthgreen.com/>, (accessed February 19, 2020).

Essington, M.E., 2004, Soil and Water Chemistry – An Integrative Approach: Boca Raton, CRC Press LLC, 534 p.

Fassett, J.E., and Hinds, J.S., 1971, Geology and Fuel Resources of the Fruitland Formation and Kirtland Shale of the San Juan Basin, New Mexico and Colorado: U.S. Geological Survey, Professional Paper 676, 76 p.

Hartwigsen, J.A., and Evans, M.R., 2000, Humic acid seed and substrate treatment promote seedling root development: HortScience, v. 35, n. 7, p. 1231-1233.

Hoffman, G.K., and Austin, G.S., 2006, Soil Amendments, *in* Kogel, J.E., Triveldi, N.C., Barker, J.M., and Krukowski, S.T., eds., Industrial Minerals and Rocks (7th ed.): Littleton, Society for Mining, Metallurgy and Exploration, Inc., p. 1161-1172.

Hoffman, G.K., Beaumont, E.C., and Bellis, D., 1992, Environmental controls related to coal quality variations in the Fruitland Formation, San Juan Basin, New Mexico: Geological Society of America, Special Paper 267, p. 37-55.

Hoffman, G.K., Verploegh, J., and Barker, J.M., 1994, Geology and chemistry of humate deposits in the southern San Juan Basin, New Mexico: Society of Mining Engineers. Presentation at SME Annual Meeting Albuquerque, NM, February 14-17, 1994, Preprint 94-142.

Hunt, A.P., and Lucas, S.G., 1992, Stratigraphy, paleontology and age of the Fruitland and Kirtland Formations (Upper Cretaceous), San Juan Basin, New Mexico: New Mexico Geological Society, Guidebook 43, p. 217-239.

Lee, Y.S., and Bartlett, R.J., 1976, Stimulation of plant growth by humic substances: Soil Science Society of America Journal, v. 40, p. 876-879.

Leventhal, J.S., 1980, Organic geochemistry and uranium in Grants Mineral Belt, Rautman, C.A., ed., *in* Geology and mineral technology of the Grants uranium region 1979: New Mexico Bureau of Mines and Mineral Resources, Memoir 38, p. 75-85.

Lucas, S.G., and Mateer, N.J., 1983, Vertebrate paleoecology of the Late Campanian (Cretaceous) Fruitland Formation, San Juan Basin, New Mexico (USA): Second Symposium on Mesozoic Terrestrial Ecosystems, Jadwisin, Poland, v. 28, n. 1-2, p. 195-204.

Lyons, G., and Genc, Y., 2016, Commercial humates in agriculture: real substance or smoke and mirrors? – Review: Agronomy, v. 6, n. 50, 8 p.

Mosley, R., 1998, The effects of humates on remediation of hydrocarbon and salt contaminated soils: Proceedings 5th International Petroleum Environmental Conference, Albuquerque, New Mexico, October 20-23, 1998, 15 p.

Rashid, M.A., 1985, Geochemistry of Marine Humic Compounds: New York, Springer-Verlag, 300 p.

Roybal, G.H., and Barker, J.M., 1987, Geology and production of humate and weathered coal in New Mexico: Society of Mining Engineers, Transactions, v. 280, p. 2105.

Schneider, G.B., and Kirschbaum, M.A., 1981, Coal resources of the Fruitland Formation, Ojo Encino EMRIA study site, McKinley County, New Mexico: U.S. Geological Survey, Open-File Report 81-783, 23 p.

Shomaker, J.W., Beaumont, E.C., and Kottlowski, F.E., eds., 1971, Strippable low-sulfur coal resources of the San Juan Basin in New Mexico and Colorado: New Mexico Bureau of Mines and Mineral Resources, Memoir 25, p. 15-30.

Shomaker, J.W., and Hiss, W.L., 1974, Humate mining in northwestern New Mexico: New Mexico Geological Society, Guidebook 25, p. 333-336.

Smith, L.N., 1992, Stratigraphy, sediment dispersal and paleogeography of the Lower Eocene San Jose Formation, San Juan Basin, New Mexico and Colorado: New Mexico Geological Society, Guidebook 43, p. 297-309.

Susic, M., 2001, A history of humic acid research, more than two centuries of humic acid research-why so long? <https://humicacid.wordpress.com/a-history-of-humic-acid-research> (accessed on February 1, 2020)

Tan, K.H., 2014, Humic Matter in Soil and the Environment – Principles and Controversies (2nd ed.):, Boca Raton, CRC Press LLC, 463 p.

Turner-Peterson, C.E., 1985, Lacustrine-humate model for primary uranium ore deposits, Grants uranium region, New Mexico: American Association of Petroleum Geologist Bulletin, v. 69, p. 1990-2020.

Velasco, C.A., Artyushkova, K., Abdul-Mehdi, S.A., Osburn, C.L., Gonzalez-Estrella, J., Lezama-Pacheco, J.S., Cabaniss, S.E., and Cerrato, J.M., 2019, Organic functional group chemistry in mineralized deposits containing U(IV) and U(VI) from the Jackpile mine in New Mexico: Environmental Science and Technology, v. 53, p. 5758-5767.

Wright, D., and Lenssen, A.W., 2013, Humic and fulvic acids and their potential in crop production: Agriculture and Environmental Extension Publication, v. 187, 3 p.

New Mexico Geological Society, Special Publication 14, Geology of the Mount Taylor Area, 2020, p. 47-53.

NEW MEXICO URANIUM MINERALS

Virgil W. Lueth

New Mexico Bureau of Geology and Mineral Resources, New Mexico Tech, 801 Leroy Place, Socorro, NM 87801;
Virgil.Lueth@nmt.edu

PRIMARY URANIUM MINERALS AND MINERALS FREQUENTLY CONTAINING U AS IMPURITIES* FROM NEW MEXICO

(as defined on page 306 by Lauf, R.J., 2016, Mineralogy of Uranium and Thorium: Atglen, Schiffer Publishing, 352 p.)

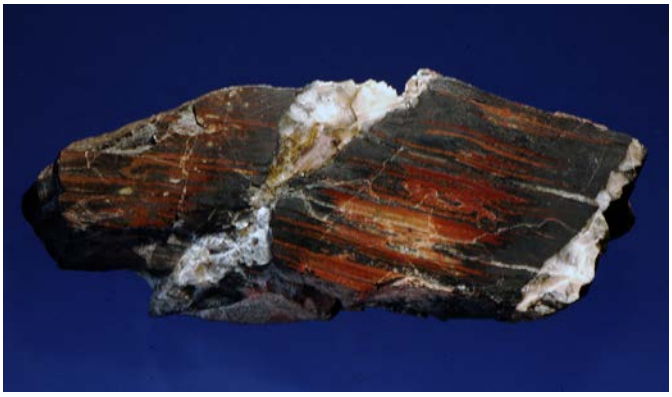

Uraninite, UO_2, with hematite and calcite.
Specimen is 15 cm across.
NMBGMR Museum No. 13133, Section 25 Mine, Ambrosia Lake District, McKinley County, NM. Gift of William Bergloff.

Coffinite, $U(SiO_4)\cdot nH_2O$, in sandstone.
Specimen is 12 cm across.
NMBGMR Museum No. 15808, Section 23 Mine, Ambrosia Lake District, McKinley County, NM. Gift of Nick Ferris.

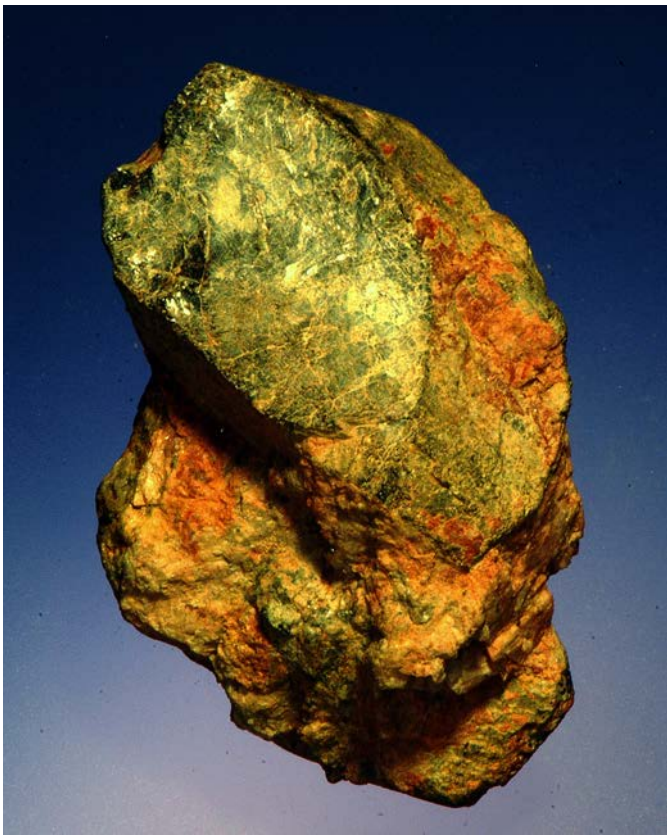

Samarskite, $YFe^{3+}Nb_2O_8$.
Specimen is 5 cm tall.
NMBGMR Museum No. 6011, Petaca District, Rio Arriba Co., NM.

Xenotime, $Y(PO_4)$.
Specimen is 3 cm tall.
NMBGMR Museum No. 12715, Truchas Mine, Nambe District, Santa Fe County, NM.

Polycrase, $Y(Ti,Nb)_2(O,OH)_6$.
Crystal is 3 cm across.
Mary Mine, Petaca district, Rio Arriba Co., NM. On loan from Mel Stairs.

Euxenite, $(Y,Ca,Ce,U,Th)(Nb,Ta,Ti)_2O_6$,.
Specimen is 5 cm across.
NMBGMR No. 18309, White Signal District, Grant County, NM.

Microlite, $U_{2-m}Ta_2O_{6-w}OH_{-n}$, with quartz and microcline.
Crystal is 0.8 cm across.
NMBGMR Museum No. 15592, Harding Mine, Picuris District, Taos County, NM. Gift of Dave Bunk.

Pyrochlore, $U_2Nb_2O_6(OH,F)$, on orthoclase.
Crystal is 1.5 cm across.
NMBGMR Museum No. 13483, Rociada District, Mora County, NM. Gift of Al and Betty Tlush.

Allanite, $\{Ca^{2+},Sr^{2+}REE^{3+}\}_2\{Al,Fe,Mn^{3+},Fe,Mg^{2+}\}_3(Si_2O_7)(SiO_4)(OH)$.
Center crystal is 1 cm across.
NMBGMR Museum No. 10021, Mina Terra Estrella, Lincoln County, NM. Gift of Mac Canby and Peter Evatt.

Monazite, $Ce(PO_4)$.
Crystal is 5 cm across.
NMBGMR Museum No. 12683, Cow Camp, San Miguel County, NM.

Columbite-Tantalite, $(Fe,Mn)Nb_2O_6$.
Crystal is 3.5 cm across.
NMBGMR Museum No. 18327, Petaca District, Rio Arriba County, NM.

SECONDARY URANIUM MINERALS

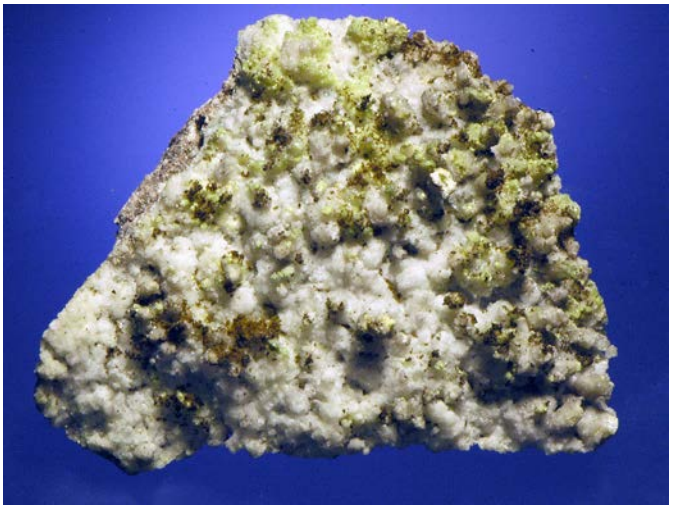

Andersonite, $Na_2Ca(UO_2)(CO_3)_3 \cdot 6H_2O$, with gypsum and calcite on sandstone.
Specimen is 10 cm across.
NMBGMR Museum No. 18960.

Cuprosklodowskite, $Cu(UO_2)_2(SiO_3OH]_2 \cdot 6H_2O$.
Specimen is 11 cm tall.
NMBGMR Museum No. 13172, Iron Mountain No. 2 District, Sierra County, NM. Gift of Robert Weber.

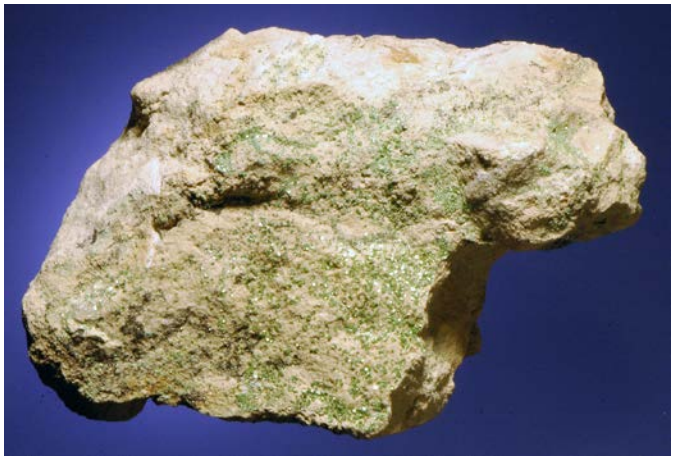

Metatorbernite, $Cu(UO_2)_2(PO_4)2 \cdot 8H_2O$, on sandstone.
Specimen is 8 cm across.
NMBGMR Museum No. 13169, Jeter Mine, Ladrone District, Socorro County, NM. Gift of Robert Weber.

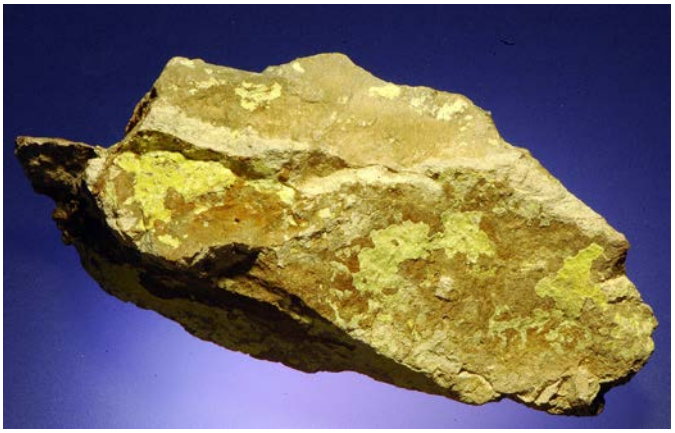

Autunite, $Ca(UO_2)2(PO_4)_2 \cdot 10\text{-}12H_2O$, on sandstone.
Specimen is 9 cm across.
NMBGMR Museum No. 16180, Jeter Mine, Ladrone District, Socorro County, NM. Gift of Robert H. Weber.

Carnotite, $K_2(UO_2)_2V_2O_8 \cdot 3H_2O$, on sandstone.
Specimen is 6 cm long.
NMBGMR Museum No. 12690, Carrizo Mountain, San Juan County, NM.

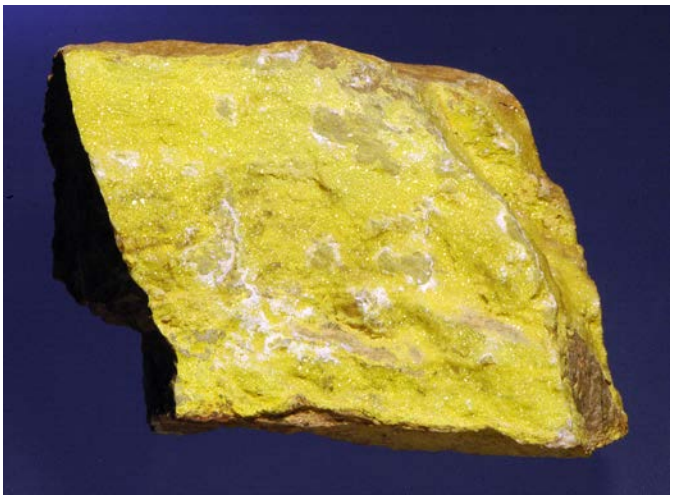

Tyuyamunite, $Ca(UO_2)_2(VO_4)_2 \cdot 5\text{-}8H_2O$ on limestone.
Specimen is 9 cm across.
NMBGMR Museum No. 7606, Section 9 Mine, Ambrosia Lake District, McKinley County, NM.

Bayleyite, $Mg_2(UO_2)(CO_3)_3 \cdot 18H_2O$ on sandstone.
Specimen is 7 cm across.
NMBGMR Museum No. 12998, Poison Canyon, Ambrosia Lake District, McKinley County, NM.

Metatyuyamunite, $Ca(UO_2)_2(VO_4)_2 \cdot 3H_2O$ on limestone.
Specimen is 8 cm across.
NMBGMR Museum No. 16310, Ambrosia Lake District, Cibola County, NM.
Gift of Hilja K. Herfurth.

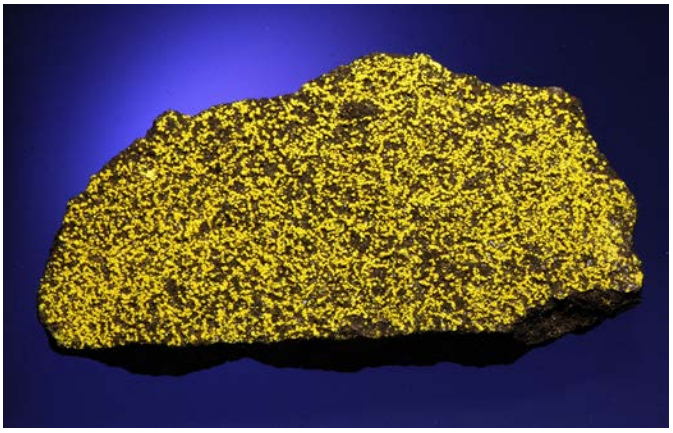

Zippeite, $K_3(UO_2)_4(SO_4)_2O_3(OH)\cdot 3H_2O$, on coffinite and sandstone.
Specimen is 17 cm across.
NMBGMR No. 18498, Grants District, Cibola County, NM. Gift of Gary and Priscilla Young.

Liebigite, $Ca_2(UO_2)(CO_3)_3\cdot 11H_2O$, on calcite and sandstone.
Crystals are approximately 4 cm long.
NMBGMR No. 17769, Section 23 Mine, Ambrosia Lake District, McKinley County, NM. Gift of the Sanchez Collection.

Uranophane, $Ca(UO_2)_2(SiO_3OH)_2\cdot 5H_2O$, on calcite.
Crystals are about 1-2 cm long.
NMBGMR Museum No. 13134, Section 25 Mine, Ambrosia Lake District, McKinley County, NM. Gift of William R. Berglof. Photograph by Jeff Scovil.

Kasolite, $Pb(UO_2)(SiO_4)\cdot H_2O$, on granite.
Photomicrograph is 2 mm across.
NMBGMR Museum No. 19056, Red Hills, Sierra County, NM. Specimen and photomicrograph a gift of Jerry Cone.

New Mexico Geological Society, Special Publication 14, Geology of the Mount Taylor Area, 2020, p. 53-63.

URANIUM DEPOSITS IN THE POISON CANYON TREND, AMBROSIA LAKE SUBDISTRICT, GRANTS URANIUM DISTRICT, MCKINLEY AND CIBOLA COUNTIES, NEW MEXICO

VIRGINIA T. MCLEMORE

New Mexico Bureau of Geology and Mineral Resources, 801 Leroy Place, Socorro, NM, 87801; virginia.mclemore@nmt.edu

ABSTRACT—The Poison Canyon uranium discovery was an important economic event in the Grants Uranium District, New Mexico. Not only was it the first sandstone-hosted uranium deposit discovered and mined that ultimately led to the larger Ambrosia Lake Trend, but the main types of uranium deposits, primary and redistributed, were first recognized in the Poison Canyon Trend. More than 10 million lbs of U_3O_8 were produced from mines in the Poison Canyon Trend and additional historic resources remain. The Poison Canyon Trend is south of the Ambrosia Lake Trend, north of Grants and Milan in the southern San Juan Basin. The uranium deposits are hosted by the Poison Canyon sandstone, an informal name (economic usage) of one of the uranium-bearing sandstone units at the top of the Westwater Canyon Member or the lower part of the overlying Brushy Basin Member of the Jurassic Morrison Formation. Many of the uranium deposits in the Poison Canyon Trend have been mined out and what uranium remained at these older mines is probably uneconomic to recover, especially in the western portion of the area. The mineral-resource potential for uranium in the unmined portions of the Poison Canyon Trend is high, especially in the eastern portion of the trend. However, it is unlikely that any of these deposits will be mined in the near future because of economic conditions and numerous challenges to mine uranium in New Mexico.

INTRODUCTION

Most of the economic uranium deposits in New Mexico are hosted by sandstones, and most of the uranium production in New Mexico has come from the Westwater Canyon and Brushy Basin members of the Jurassic Morrison Formation in the Grants Uranium District in McKinley and Cibola (formerly Valencia) Counties (Hilpert, 1969; McLemore, 1983; McLemore and Chenoweth, 1989, 1991, 2017). The Grants District represents one large area in the southern San Juan Basin, extending from east of Laguna to west of Gallup and consists of eight subdistricts (Fig. 1; McLemore and Chenoweth, 1989, 2017). During a period of nearly three decades (1951–1980), the Grants District yielded nearly 347 million lbs of U_3O_8, almost all of New Mexico's production, and more uranium than any other district in the United States (McLemore and Chenoweth, 1989, 2017). Although there are no operating mines in the Grants District today, numerous companies have acquired uranium properties and plan to explore and develop deposits in the district in the future.

The first economic discovery of uranium in sandstone in the Grants District was made on January 4, 1951, east of Haystack Butte in the southern Ambrosia Lake Subdistrict of the Grants District (Fig. 2). The area was named Poison Canyon for the abundance of locoweed, a poisonous plant. The host rock is either a tongue of the Westwater Canyon Member or the lower part of the overlying Brushy Basin Member of the Morrison Formation (Hilpert, 1969). This unit would later be called the Poison Canyon sandstone, an informal name of economic usage.

Many published and unpublished reports have been released before 1990 describing the uranium deposits in the Grants Dis-

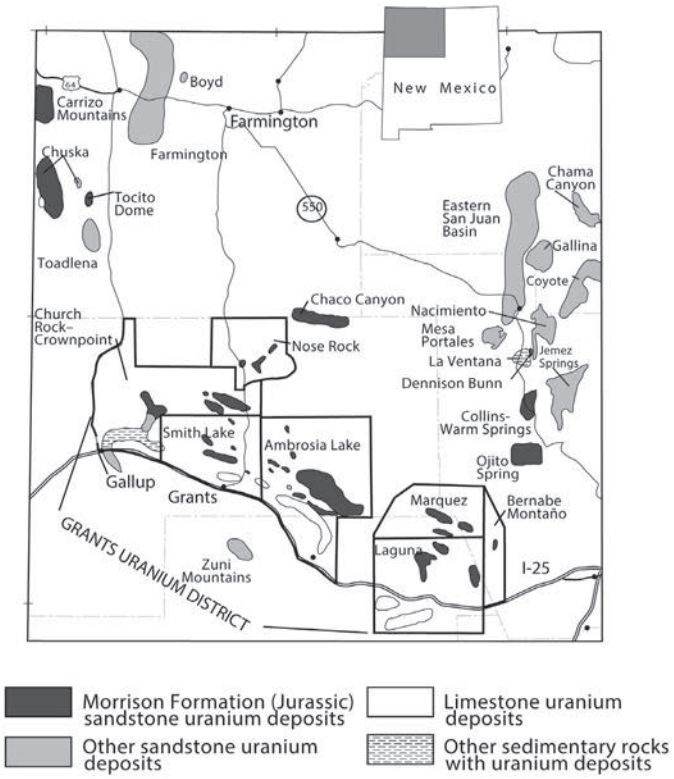

FIGURE 1. Subdistricts in the Grants Uranium District in the San Juan Basin, New Mexico (McLemore and Chenoweth, 1989, 1991). Polygons outline approximate areas of known uranium deposits.

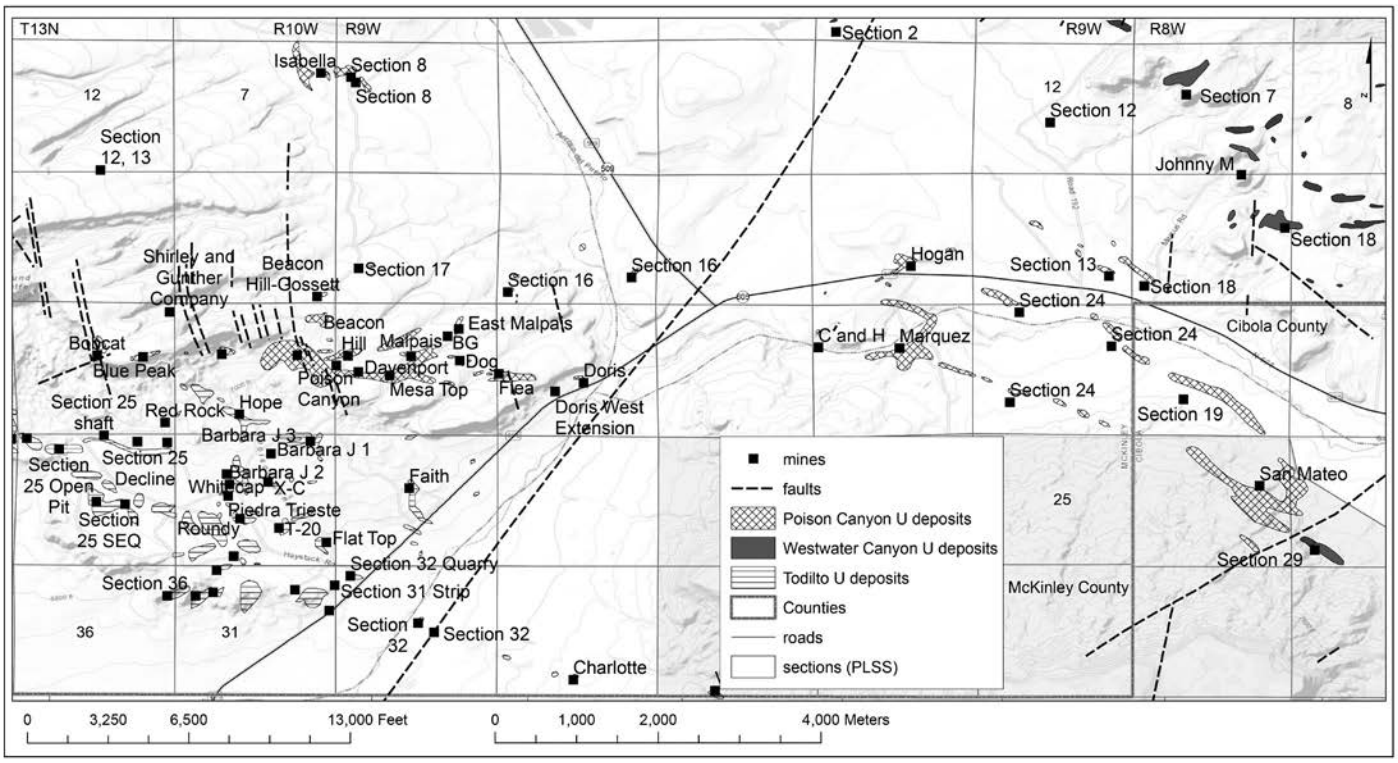

FIGURE 2. Uranium deposits in the Poison Canyon Trend, Ambrosia Lake Subdistrict (revised from Chapman, Wood and Griswold, Inc., 1979; McLemore and Chenoweth, 1991). A color version is in the color plates section of this guidebook and in supplemental material. PLSS=Public Land Survey System

trict (cited in McLemore, 1983; McLemore and Chenoweth, 1989, 2017), but few reports have updated the status of the deposits in the Poison Canyon area (McLemore et al., 2013). The Poison Canyon uranium discovery was an important economic event in the Grants District. Not only was it the first sandstone-hosted uranium deposit discovered and mined that ultimately led to the larger Ambrosia Lake Trend, but the main types of uranium ore deposits in the Grants District, primary and redistributed, were first recognized in the Poison Canyon Trend. More than 10 million lbs of U_3O_8 were produced from mines in the Poison Canyon Trend, and additional historic resources remain that could be mined in the future (Tables 1, 2). Most of the recent studies on the Grants District have focused on reclamation, while only a few recent reports have discussed the uranium geology and future economic potential of these deposits.

The purpose of this report is to summarize the history, stratigraphy, and mineralized deposits in the Poison Canyon Trend (including uranium production), as well as provide some insights into the age, source and future mineral-resource potential of the uranium deposits in the Poison Canyon Trend. Most of the mines in the Poison Canyon Trend have been or are being reclaimed, and studies on their reclamation are discussed elsewhere. The Poison Canyon Trend, as defined in this report, is from the Section 14 prospect near the Bobcat and Blue Peak mines (southeast of Mesa Montanosa) southeastward to the San Mateo Mine, which is west of the village of San Mateo (Fig. 2; Rapaport, 1963).

METHODOLOGY

All known uranium mines, mills, deposits, and occurrences are entered into the New Mexico Mines Database (McLemore et al., 2002). Since its creation in 1927, the New Mexico Bureau of Geology and Mineral Resources (NMBGMR) has collected published and unpublished data on the districts, mines, deposits, occurrences, and mills, including uranium mines, and is slowly converting these data into a relational database, the New Mexico Mines Database, using Microsoft Access. The New Mexico Mines Database provides data available on mines and districts in New Mexico. The available data for this database is from a variety of published and unpublished reports (including theses and dissertations) and miscellaneous unpublished files in the NMBGMR mining archive, and includes information on location, production, reserves, resource potential, significant deposits, geology, geochemistry (rock, water, etc.), well data, mining methods, maps, ownership, and other data, if available. The New Mexico Mines Database provides detailed information on the mineralogy, host rock lithology, and metal association of each mine or mining district. The database also includes limited geochemical data of both solid (host rock, ore, mine wastes, tailings, stream sediments, etc.) and water (surface, ground, pit lakes, etc.) samples. New information is continuously becoming available and is incorporated into the database regularly. See McLemore et al. (2002) for a more detailed description of the database. Much of the information in this paper is summarized from the database, and includes information from field investigations, published papers

TABLE 1. Production from uranium mines in the Poison Canyon Trend 1951-1971 (revised from U.S. Atomic Energy Commission, production records; McLemore, 1983).

Mine ID	Mine Name	Ore (short tons)	Uranium (pounds)	Grade (%U_3O_8)	Vanadium (pounds)	Years
NMMK0012	Beacon Hill-Gossett	41,650	161,045	0.19	22,671	1956-1963, 1966-1967
NMMK0013	BG	30,033	128,644	0.22		1969-1971
NMMK0018	Blue Peak	12,051	44,020	0.19	18,707	1951-1961, 1964
NMMK0019	Bobcat	117	186	0.06	71	1956
NMMK0045	Davenport	7517	28,829	0.17		1957-1968
NMMK0048	Dog	244,177	906,235	0.19		1957-1975, 1978-1980
NMMK0049	Doris	33,487	122,872	0.18		1958-1961, 1979-1980
NMMK0050	Doris West Extension					1979-1981
NMMK0054	East Malpais	30,333	139,818	0.23		1958-1960
NMMK0082	Hogan	129,551	678,510	0.26		1959-1962
NMMK0086	Isabella	76,749	237,061	0.15		1959-1962, 1980
NMMK0099	Malpais	42,070	198,492	0.24		1958-1961
NMMK0105	Marquez	717,031	3,759,653	0.26		1958-1966
NMMK0107	Mesa Top	108,261	512,965	0.24	144,610	1954-1961, 1967-1968
NMMK0133	Poison Canyon	217,066	1,004,594	0.23	338,094	1952-1980
NMMK0172	Section 8	47,808	165,319	0.17		1958-1966, 1970, 1978-1980
NMMK0210	Section 24 (Chill Wills)	10,950	37,693	0.17		1960-1963
NMCI0053	San Mateo	842,463	2,863,024	0.17		1959-1971
Total		***2,591,314***	***10,988,960***		***524,153***	

TABLE 2. Estimates of the remaining uranium resources in the Poison Canyon Trend (revised from McLemore et al., 2013; Wilton, 2018). Some uranium resources remain at the Marquez mine. The resource and reserve data presented are historical and are provided for information purposes only. They do not conform to Canadian National Instrument NI 43-101 or U.S. Securities and Exchange Commission requirements.

Mine ID	Mine Name	Remaining Resource (short tons)	Grade (U_3O_8%)	Uranium (pounds)	Depth (m)	Year of resource
NMMK0210, NMMK0211, NMMK0212	Section 24 (Treeline)	1,500,000	0.13	593,448	137-183	1978
NMMK0727	Section 13	?	0.039-0.216	855,313	246-267	2008
Total		***>1,500,000***		***1,448,761***		

(Rapaport, 1963; Holmquist, 1970; McLemore, 1983), and NMBGMR file data.

A detailed mineral deposit map of the Poison Canyon Trend was compiled in ArcMap using USGS topographic maps as the map base at a scale of approximately 1:12,000, the New Mexico Mines Database, as well as digitized outlines of mineralized deposits from NMBMGMR file data, published reports, and unpublished company data (Fig. 2; color version is in the color plates section of this guidebook and in supplemental material). Most of the outlines of the ore deposits were obtained from the mining companies in the mid-1980s (Rapaport, 1963; Chapman, Wood and Griswold, Inc., 1979; McLemore and Chenoweth, 1989, 1991) and updated by recent reports.

The production and resources figures in Tables 1 and 2 are the most recent data available and were obtained from published and unpublished sources (NMBGMR file data). Production and resources figures are subject to change as new data are obtained. The resource and reserve data presented in Table 2 are historical and are provided for information purposes only, and do not conform to Canadian National Instrument NI 43-101 or U.S. Securities and Exchange Commission requirements.

GEOLOGIC SETTING

The Morrison Formation is Late Jurassic (Kimmeridgian-Tithonian) and extends throughout much of western United States (Hilpert, 1969; Dunagan and Turner, 2004; Dickinson, 2018). Sedimentary units within the formation were deposited in a variety of environments, including alluvial plain, eolian, lacustrine, and nearshore marine. The formation is divided

into the Salt Wash (oldest), Recapture, Westwater Canyon, and Brushy Basin (youngest) members; overlies the Jurassic Bluff Sandstone and Summerville Formation; and is overlain by the Cretaceous Dakota Formation (see stratigraphic chart, back cover). The Salt Wash Member is not found in the Ambrosia Lake Subdistrict. The Ambrosia Lake Subdistrict is one of the most faulted areas of the Grants District where high-angle normal faults either trend north to northeast, northeast to east, or northwest. Most of the faults are younger than the Dakota Formation and have displacements of 15 to 30 m.

The Poison Canyon sandstone is an informal name (economic usage) of one of the uranium-bearing sandstone units in the Morrison Formation (Fig. 3; Zitting et al., 1957; Hilpert and Corey, 1956; Hilpert and Freeman, 1956; Hilpert, 1969). There has been a controversy among economic geologists as to whether the Poison Canyon sandstone is the uppermost sandstone unit at the top of the Westwater Canyon Member (Santos, 1963; Tessendorf, 1980; Condon, 1989) or the lowermost sandstone at the base of the Brushy Basin Member (Hilpert, 1963; Turner-Peterson et al., 1980; Turner-Peterson, 1985; Bell, 1986; Dahlkamp, 2010). Furthermore, other economic geologists (Hoskins, 1963) use this name to designate any persistent sandstone in the Brushy Basin Member in the Ambrosia Lake and Smith Lake subdistricts. The relationship between the Westwater Canyon and Brushy Basin contact is a stratigraphic difficulty inherent with interfingering fluvial units, and picking the contact between the two units can be difficult and arbitrary. However, for the purposes of this report, the Poison Canyon sandstone refers to the specific sandstone found in the Poison Canyon Trend that is separated from lower Westwater Canyon sandstones by a regional, 4.6- to 7.6-m thick, greenish shale, often called the K shale (Fig. 3). Stratigraphic relationships can be confusing because the Poison Canyon sandstone is a braided-stream deposit formed at the top of the Westwater Canyon wet alluvial fan system (Galloway, 1980) prior to the deposition of the predominantly shale units of the Brushy Basin Member that has local persistent streams cutting through the shale sequences (Fig. 3). These stratigraphic naming problems are in part, a result of the depositional nature of the units and some geologists use geophysical logs and cuttings in addition to outcrops and measured sections to determine the stratigraphic relationships, whereas other geologists use only outcrops and measured sections.

The Poison Canyon sandstone generally consists of three units: a lower sandstone, middle shale, and upper sandstone. The sandstone is yellow to gray, fine- to coarse-grained, poorly sorted, cross-bedded arkosic sandstone approximately 15 m thick at the Poison Canyon Mine, and varies from 10 to 25 m thick elsewhere. Volcanic rock fragments are common along with clay balls and lenses. It extends to the east and north from the mine and vertically grades upwards into the Brushy Basin Member. Most of the uranium deposits are near the base of the sandstone, and most of the deposits are found where the Poison Canyon sandstone is greater than 15 m thick (Hilpert, 1969). Paleocurrent studies of the Poison Canyon sandstone indicate predominantly east to northeast current directions, whereas the older upper Westwater Canyon sandstones indicate predominantly east to southeast current directions (Turner-Peterson et al., 1980; Turner-Peterson, 1985). The lower Westwater Canyon sandstones flowed east-southeast (Turner-Peterson et al., 1980; Turner-Peterson, 1985).

The regional presence of extensive zeolites in the Brushy Basin Member was previously interpreted to represent deposition in a shallow alkaline lake (Lake T'oo'dichi'; Turner-Peterson, 1980, 1985; Turner-Peterson and Fishman, 1991; Demko et al., 2004; Turner, 2010a,b), but re-evaluation of the geochemistry and sedimentology has led to a revised interpretation. Revised interpretations have redefined Lake T'oo'dichi' as widespread, discontinuous wetlands of isolated ponds and marshes (Anderson and Lucas, 1997; Turner, 2004) fed by groundwater from a regional aquifer (Dunagan and Turner, 2004; Turner, 2010a,b; Dickinson, 2018). The Poison Canyon sandstone is interpreted as a local fluvial sandstone flowing into or across the Lake T'oo'dichi'. The gray smectite mudstones were deposited marginally to the lake.

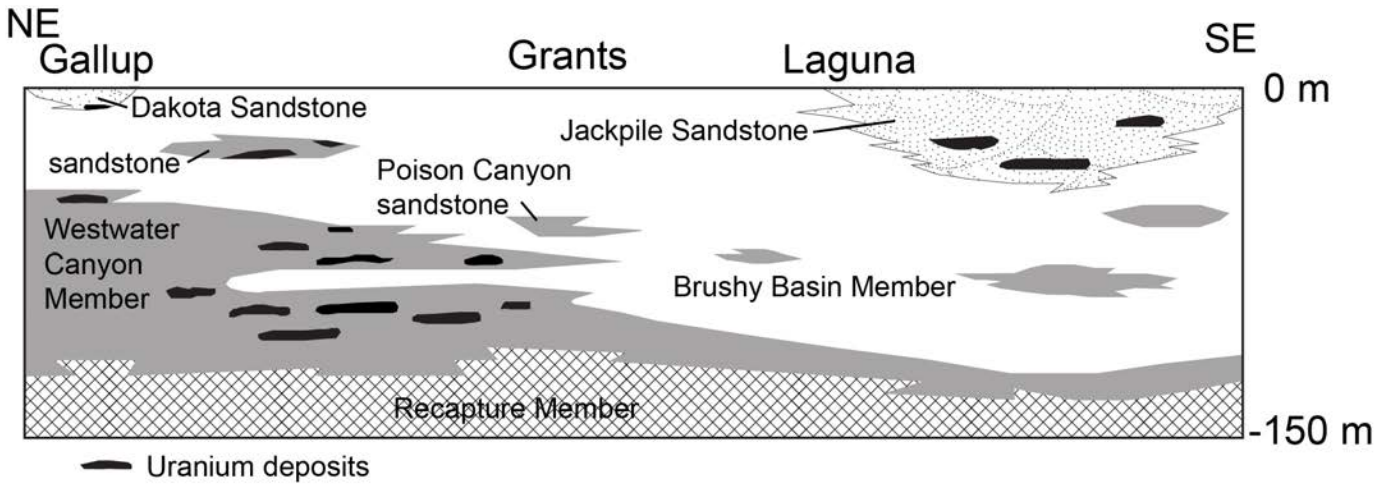

FIGURE 3. Schematic cross-section from Gallup to east of Laguna showing relationship of the Poison Canyon sandstone to the Westwater Canyon and Brushy Basin Members of the Morrison Formation (modified from Hilpert, 1969).

Three types of uranium deposits are found in the Morrison Formation (including the Westwater Canyon Member, Poison Canyon sandstone, Brushy Basin Member, Jackpile Sandstone, and extending into the Cretaceous Dakota Formation in the Church Rock-Crownpoint Ssubdistrict): 1) primary, tabular (also called trend or blanket), 2) redistributed (also called roll-type or stack), and 3) remnant-primary sandstone uranium deposits (Hilpert, 1969; Saucier, 1981; Adams and Saucier, 1981; McLemore and Chenoweth, 1989, 2017). A fourth type of uranium deposit, tabular sandstone uranium-vanadium deposits are found in the Salt Wash and Recapture members of the Morrison Formation in the western San Juan Basin (McLemore and Chenoweth, 1989, 2017). It is important to note that the older Jurassic Todilto Limestone is mineralized south of the Poison Canyon Trend (Berglof and McLemore, 2003; McLemore, 2020). The descriptions of the economic geology and uranium deposits are found in numerous reports, many cited in McLemore (1983), Hilpert (1969), McLemore and Chenoweth (1989, 1991, 2017), McLemore et al. (2013), and Dahlkamp (2010).

DESCRIPTION OF SELECTED URANIUM DEPOSITS

Sandstone uranium deposits in the Poison Canyon Trend are a cluster of similar ore bodies that are spatially close together, that formed by similar geologic processes, and that could have been mined as one to three large mine operations (Holen and Finch, 1982). But the ownership of the Poison Canyon Trend deposits was complicated with various sections owned by private owners, state of New Mexico, Navajo Indian allotments, and federal lands (referred to as checkerboard ownership), resulting in the numerous underground operations (albeit no longer operating). Therefore, the entire Poison Canyon Tend could be considered one large uranium deposit (similar to a mine producing multiple ore shoots along one vein) that was operated by different mining companies.

Appendix 1 is a summary of the location and other data of the uranium mines, prospects, and unmined deposits in the Poison Canyon Trend. Production from the uranium mines in the Poison Canyon Trend is in Table 1, and estimates of the remaining uranium resources are in Table 2. Figure 2 shows the trend of the uranium deposits (a color version of this figure is in the color plates portion of this volume). Figure 4 shows grade-tonnage relationships of uranium deposits, comparing the Grants uranium deposits with other world-class uranium deposits. Descriptions and mining history of selected Poison Canyon Trend mines are below.

Blue Peak Mines

In 1951, yellow uranium minerals (predominantly carnotite, tyuyamunite, autunite, schroeckingerite; Dodd, 1955; Rapaport, 1963) were found associated with black carbonaceous material (humates) in limonitic sandstone outcrops, just above the K shale layer. Blue Peak Mining Co. began operating the Blue Peak mines in March 1951 from seven adits and stripping along the rim (Holmquist, 1970). The Blue Peak mines were the first sandstone operations in the Ambrosia Lake Subdistrict

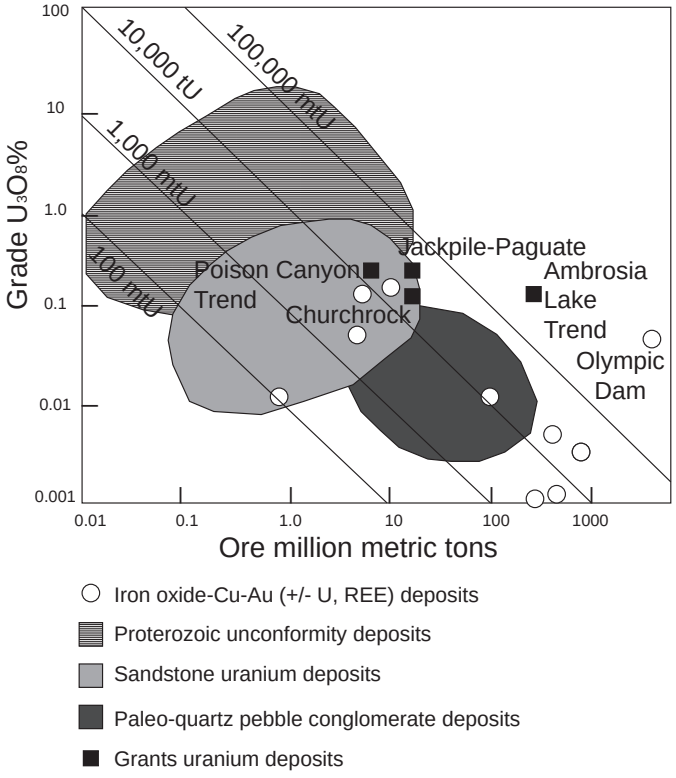

FIGURE 4. Grade-tonnage of major uranium deposits, showing major Grants uranium deposits. Fields are modified from Hitzman and Valenta (2005) and Thakur et al. (2018) with specific deposit data from Holen and Finch (1982), McLemore (1983), Chenoweth (1989), and McLemore et al. (2013).

(Rapaport, 1963; McLemore, 1983). Several different operators developed and mined the deposits (Table 3; Holmquist, 1970). Total production amounted to 12,051 short tons of ore yielding 44,020 lbs U_3O_8 (grade 0.19%) and 18,707 lbs of V_2O_5 from 1951 to 1964 (Table 1, 3). Most of the uranium deposits were mined, but small isolated mineralized bodies remained that would be difficult and uneconomic to recover (U.S. Atomic Energy Commission files).

The entire mined deposit was approximately 213 m long and 10-30 m wide. Mineralized stopes exhibited 10 to 100 fractures per hundred linear meters, whereas barren and low-grade stopes exhibited 1.5 to 3 fractures per hundred linear meters. This correlation between fractures and mineralization provided a definitive guide to locating uranium deposits in the Poison Canyon Trend (Rapaport, 1963).

Poison Canyon Mine

Open-pit mining began at the Poison Canyon Mine in December 1951, and the first ore shipped in early 1952 (U.S. Atomic Energy Commission production records). A series of north-trending faults slightly offset the ore bodies and subsequently redistributed the uranium along the faults (Fig. 2; Mathewson, 1953; Konigsmark, 1958; Rapaport, 1963; Tessendorf, 1980). Uranium grade and thickness increase adjacent to the faults (Dodd, 1955). The primary uranium deposits were 3.6 m thick, and coffinite, tyuyamunite, and autunite were

TABLE 3. Uranium production from the Blue Peak Mine, 1951-1964 (from U. S. Atomic Energy Commission, production records; McLemore, 1983).

Year	Shipper	Ore (short tons)	Uranium (pounds)	Grade (%U_3O_8)	Grade (%V_2O_5)
1951	Blue Peak Mining Co.	766	5488	0.36	0.15
1952	Blue Peak Mining Co.	3998	12,474	0.16	0.08
1953	Shattuck Denn Corp.	1039	3826	0.18	0.09
1955	Blue Peak Mining Co., San Michaels College Foundation	148	867	0.29	0.08
1956	Colohoma Uranium, Inc.	347	2180	0.31	0.13
1957	Three Jacks Mining	549	2676	0.25	
1958	Three Jacks Mining	219	861	0.20	
1959	Farris Mining Co.	3751	11,146	0.15	
1960	Farris Mining Co., Lloyd O. Sutton	726	3113	0.21	
1961	Lloyd O. Sutton	417	1234	0.15	
1964	Lee Garcia	91	155	0.09	
Total 1951-1964		***12,051***	***44,020***	***0.19***	

the primary uranium minerals (Konigsmark, 1958); pascoite, a vanadium mineral, and ilsemannite, a molybdenum mineral, also are reported (Tessendorf, 1980). Some of the redistributed uranium was vertically distributed or stacked along the fault and was up to 12 m thick. The uranium bodies were 3-15 m to 137 m wide in the shear zone. Underground mining started in 1955 (Holmquist, 1970), and Farris Brothers continued operations in 1960. Subsequently, Reserve Oil and Minerals Corp. located additional uranium deposits in 1976 and mined underground at the mine through 1980 (Tessendorf, 1980). Total production from all companies amounted to 217,066 short tons of ore yielding 1,004,594 lbs U_3O_8 (0.23% U_3O_8) and 338,094 lbs V_2O_5 from 1952 to 1980 (Table 1). Not all production was reported between 1970 and 1980, although most of the uranium deposits were mined out.

Hogan Mine

The Hogan Mine, discovered by drilling in 1957, operated between 1959 and 1979 through a 103.6 m shaft in a thick portion of the Poison Canyon sandstone (24 m thick). Three redistributed, vertical uranium deposits (designated basal, intermediate, and upper zones) in the Hogan Mine were found along an anticlinal fold that is parallel to the San Mateo fault (Rapaport, 1963). The deposit was developed by underground methods typical of the times (Mining World, 1959), and total production amounted to 129,551 short tons of ore containing 678,510 lbs U_3O_8 at a grade of 0.26% U_3O_8 from 1959 to 1962; an unknown amount of uranium was produced from 1963-1979. Most, if not all of the uranium deposits were mined out.

Marquez Mine

The Marquez (Marcus) Mine, discovered by drilling in 1955, operated through a 571.5-m incline (Weege, 1963) from 1958 to 1966 and was the largest deposit in the Poison Canyon Trend (Rapaport, 1963) with a production of 717,031short tons of ore containing 3,759,653 lbs U_3O_8 at a grade of 0.26% U_3O_8 (Table 4). The deposit consisted of northeast-trending, narrow, elongated ore bodies, more than 1.6 km long, mostly at the base of the Poison Canyon sandstone. Uranium is associated with organic matter that consists of humates, coal fragments, and silicified wood fragments within the 7.6-m-thick, upper, medium- to fine-grained, arkosic sandstone. Uranium is associated with humates. During retreat mining and recovery of pillars, the workings started to cave, and some uranium was lost (Johnston, 1963; Holmquist, 1970). Although, some uranium probably remains, it will be difficult and dangerous to mine by conventional techniques.

Mesa Top Mine

The Mesa Top Mine, discovered by drilling in 1954, operated between 1959 and 1968 through a 45.7 m shaft. The Mesa Top shaft closed in 1959, and the ore was hoisted through the nearby Malpais shaft. The mine yielded 108,261 short tons of ore containing 512,965 lbs U_3O_8 (grade of 0.24% U_3O_8) and 144,610 lbs V_2O_5 from 1954 to 1961 (Table 1); an unknown amount of uranium was produced from 1967 to 1968. Most, if not all of the uranium deposits were mined.

San Mateo Mine

The San Mateo deposit is the easternmost deposit in the Poison Canyon Trend and was discovered in 1957 with more than 83,820 m of drilling in 250 holes in 1957-1958 (Holmquist, 1970). The 337-m three-compartment shaft was sunk in 1958 by Centennial Dev. Co. and operated by Rare Metals Co. Water was encountered at 213 m (Holmquist, 1970). Total production from 1959 to 1971 amounted to 842,463 short tons of ore containing 2,863,024 lbs U_3O_8 (Table 5). In 1964, United Nuclear acquired the property, and in 1981, Homestake obtained ownership of the property. There could be additional, unmined uranium deposits in the area.

TABLE 4. Uranium production from the Marquez Mine, 1959-1966 (from U. S. Atomic Energy Commission, production records; McLemore, 1983). There may have been additional, unreported production in 1971.

Year	Shipper	Ore (short tons)	Uranium (pounds)	Grade (%U_3O_8)
1958	Calumet and Hecla	75,393	402,968	0.27
1959	Calumet and Hecla	139,958	786,122	0.28
1960	Calumet and Hecla	132,467	657,674	0.25
1961	Calumet and Hecla	103,435	609,362	0.28
1962	Calumet and Hecla	106,933	555,840	0.26
1963	Calumet and Hecla	104,984	529,468	0.25
1964	Calumet and Hecla	16,558	92,997	0.28
1965	United Nuclear	5145	18,268	0.18
1966	United Nuclear	32,158	106,954	0.17
Total 1958-1966		***717,031***	***3,759,653***	***0.26***

Section 24 (Chill Wills, Treeline) Deposits

Several, small uranium deposits were discovered in the Poison Canyon sandstone in Section 24 by drilling in the late 1970s. The Section 24 (also known as Chill Wills) Mine yielded 10,950 short tons of ore containing 37,693 lbs of U_3O_8 (0.17% U_3O_8) from 1960 to 1963. In 1978, Conoco identified an historic resource of 593,448 short tons of ore grading 0.13% U_3O_8 elsewhere in Section 24 (also known as Treeline; Table 2; Fig. 2). Currently, enCore Energy Corp. owns the property and is examining it for potential in situ recovery (*https://www.encoreenergycorp.com/uranium-assets/isr-projects/treeline/*, accessed 1/18/20).

AGE AND SOURCE OF URANIUM MINERALIZATION

The age of the uranium deposits in the Grants District is constrained by numerous isotopic studies (Table 6, Fig. 5; McLemore, 2011) and supports a potential Jurassic volcanic arc as a source of uranium (Christiansen et al., 2015). Jurassic volcanism, intra-arc sedimentation and plutonism are well documented throughout the Jurassic volcanic arc west and southwest of the San Juan Basin (Fig. 6; Saleeby and Busby-Spera, 1992; Miller and Busby, 1995; Blakey and Parnell, 1995; Lawton and McMillan, 1999; Kowallis et al., 2001; du Bray, 2007). Uranium and vanadium concentrations show a decrease in the volcanic ash beds, consistent with uranium and vanadium being derived from volcanic ash from the Jurassic arc (Christiansen et al., 2015). Zircon ages from the Brushy Basin and Westwater Canyon members are consistent with the Jurassic volcanic arc as a source, as well as Proterozoic basement rocks (Dickinson and Gehrels, 2008). The uranium also could be from groundwater derived from a volcanic highland to the southwest (Sanford, 1982, 1992).

$^{40}Ar/^{39}Ar$ ages of plagioclase and alkali feldspar from the younger Brushy Basin Member of the Morrison Formation range from 145 to 153 Ma (Kowallis et al., 1991, 1999). Rb/Sr isochrons of clay minerals from the Poison Canyon sandstone indicated minimum ages of 105 Ma and 130 Ma (Brookins, 1980, 1989), but the isochrons are disturbed because of alteration. Primary, tabular uranium deposits in the older Westwater Canyon Member of the Ambrosia Lake and Smith Lake subdistricts are 130-140 Ma (references in Table 6; Fig. 5). The primary, tabular uranium deposits in the Poison Canyon Trend are likely of similar age. Younger, redistributed uranium deposits in the Ambrosia Lake Subdistrict are much younger, 3-12 Ma in age (references in Table 6; Fig. 5).

TABLE 5. Uranium production from the San Mateo Mine, 1959-1971 (from U. S. Atomic Energy Commission, production records; McLemore, 1983). There may have been additional, unreported production in 1971.

Year	Shipper	Ore (short tons)	Uranium (pounds)	Grade (%U_3O_8)
1959	Rare Metals Corp.	5532	19,248	0.17
1960	Rare Metals Corp.	4077	12,865	0.16
1961	Rare Metals Corp.	74,662	234,570	0.16
1962	Rare Metals Corp., El Paso Natural Gas Co.	85,798	334,288	0.19
1963	El Paso Natural Gas Co.	100,811	409,609	0.20
1964	El Paso Natural Gas Co., United Nuclear Corp.	42,220	173,357	0.21
1965	United Nuclear Corp.	48,508	199,000	0.21
1966	United Nuclear Corp.	73,934	294,025	0.20
1967	United Nuclear Corp.	144,102	484,206	0.17
1968	United Nuclear Corp.	86,345	239,707	0.14
1969	United Nuclear Corp.	118,989	296,096	0.12
1970	United Nuclear Corp. (Reserve Oil and Minerals Corp.)	52,134	152,828	0.15
1971	United Nuclear Corp.	5351	13,225	0.17
Total 1959-1971		***842,463***	***2,863,024***	***0.17***

ORIGIN OF URANIUM MINERALIZATION

There is no consensus on the origin of the primary, tabular sandstone uranium deposits (Sanford, 1992; McLemore and Chenoweth, 2017). The majority of the proposed models for formation of the Ambrosia Lake sandstone uranium deposits suggest that deposition occurred at a groundwater interface between two fluids of different chemical compositions and/or oxidation-reduction states.

Subsequent models, such as the lacustrine-humate and brine-interface models, have refined or incorporated portions of these early theories. In the lacustrine-humate model, groundwater was expelled by compaction from lacustrine muds formed by a large playa lake (Turner-Peterson, 1985; Turner-Peterson and Fishman, 1986). The ground-

TABLE 6. Sequence of uranium deposition in the Grants Uranium District (from youngest to oldest; modified from McLemore, 2011). The age of the mineralizing event is from isotopic dating (Fig. 5) or is estimated by the author based upon stratigraphic position.

Depositional Event	Age	Reference
Secondary Todilto limestone deposits	Tertiary, 3-7 Ma	Berglof (1989)
Redistributed uranium deposits (Cretaceous Dakota Sandstone, Jurassic Brushy Basin and Westwater Canyon Sandstone members)	Tertiary, 3-12 Ma	Miller and Kulp (1963), Nash and Kerr (1966), Nash (1968), Brookins et al. (1977), Brookins (1980), Ludwig et al. (1982), Hooper (1983)
Redistributed uranium deposits (Cretaceous Dakota Sandstone, Jurassic Brushy Basin and Westwater Canyon Sandstone members)	Cretaceous, 80-106 Ma	Smith, R., and McLemore, V.T. (unpublished)
Uranium in the Jackpile sandstone	110-115 Ma	Lee (1976)
Uranium in the Brushy Basin Sandstone Member	Unknown, estimated 130-115 Ma	
Uranium in the Poison Canyon sandstone	Unknown, estimated 140-115 Ma	
Uranium in the Westwater Canyon Sandstone Member	148-130 Ma	Miller and Kulp (1963), Nash and Kerr (1966), Nash (1968), Brookins et al. (1977), Brookins (1980), Ludwig et al. (1982), Hooper (1983)
Deposition of the Morrison Formation units	Unknown, estimated before 130 Ma	
Todilto limestone uranium deposits	155-150 Ma	Berglof (1970, 1989)
Deposition of the Todilto limestone	Before 155 Ma	

water was expelled into the underlying fluvial sandstones where humate or secondary organic material precipitated as a result of flocculation into tabular bodies within sandstone hosts. During or after precipitation of the humate bodies, uranium was precipitated from groundwater (Turner-Peterson, 1985; Turner-Peterson and Fishman, 1986). This model proposes the humate bodies were formed prior to uranium deposition.

In the brine-interface model, uranium and humate were deposited during diagenesis by reduction at the interface of meteoric fresh water and groundwater brines (Granger and Santos, 1986). In another variation of the brine-interface model, groundwater flow is driven by gravity, not compaction (Sanford, 1982, 1992). Groundwater flowed down dip and discharged in the vicinity of the uranium deposits. Uranium

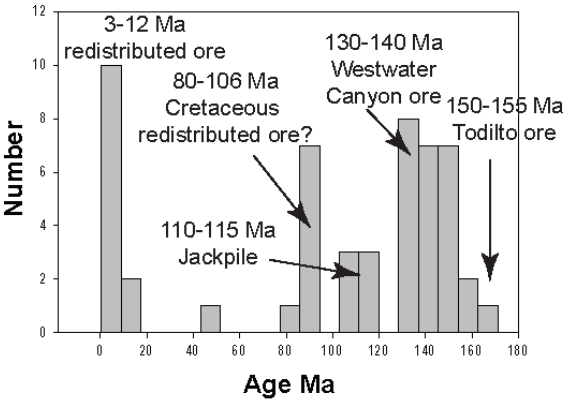

FIGURE 5. Age determinations of Grants District mineralization (from McLemore, 2011). Includes Pb/U, K/Ar, Rb/Sr, and fission track dates from Miller and Kulp (1963), Nash and Kerr (1966), Nash (1968), Berglof (1970, 1989), Brookins et al. (1977), Brookins (1980), Ludwig et al. (1982), Hooper (1983) and is summarized by Wilks and Chapin (1997). The Brushy Basin Member is 153 to 145 Ma (Kowallis et al., 1991, 1999) and the uranium ore ranges from 130 Ma to 105 Ma (Brookins, 1980).

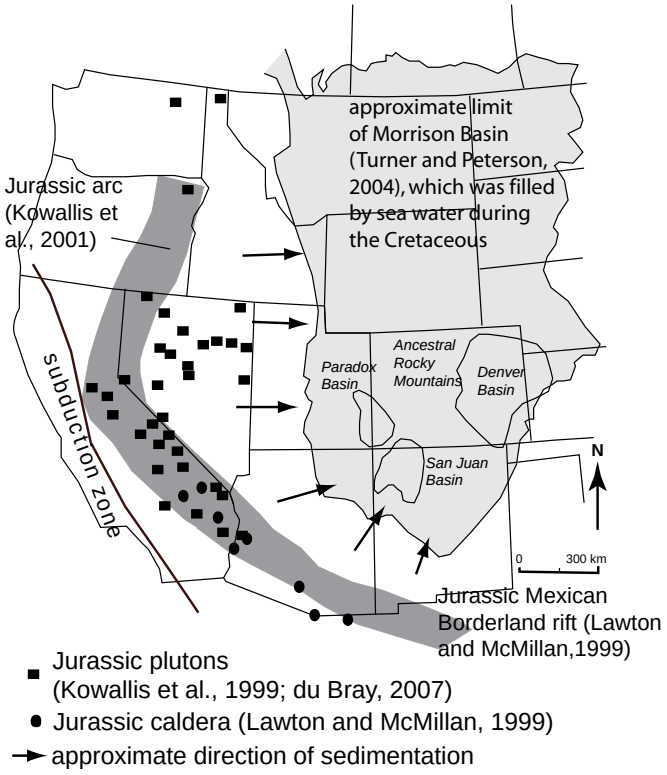

FIGURE 6. Approximate location of the Jurassic arc in relation to the Morrison Basin (from McLemore, 2011; McLemore and Chenoweth, 2017). The gray polygon represents the chain of volcanoes formed during the Jurassic Period, with the Morrison Basin in beige. Three subbasins also are delineated, including the Grants District in the southern San Juan Basin. From Kowallis et al. (1999), du Bray (2007), and Lawton and McMillan (1999).

precipitated in the presence of humates at a gravitationally stable interface between relatively dilute, shallow meteoric water and saline brines that migrated up dip from deeper in the basin (Sanford, 1982, 1992). Modeling of the regional groundwater flow in the Colorado Plateau during Late Jurassic and Early Cretaceous times supports the brine-interface model (Sanford, 1982). The groundwater flow was impeded by up-thrown blocks of Proterozoic crust and forced upwards. These zones of upwelling are closely associated with uranium-vanadium deposits throughout the Colorado Plateau (Sanford, 1982).

Uranium leached from the altered volcanic ash and from erosion of the Proterozoic granitic highland could have been carried by groundwater and surface waters into the Morrison Formation, forming the uranium deposits found in the Ambrosia Lake Subdistrict. The presence of organic material caused the precipitation of the uranium in the deposits. After formation of the primary, tabular sandstone uranium deposits during Tertiary time, oxidizing groundwater migrated through the uranium deposits and remobilized some of the primary, tabular sandstone uranium deposits (Saucier, 1981). Uranium was reprecipitated ahead of the oxidizing waters forming redistributed sandstone uranium deposits. Where the sandstone host surrounding the primary deposits was impermeable and the oxidizing waters could not dissolve the deposit, remnant-primary sandstone uranium deposits remain.

MINERAL-RESOURCE POTENTIAL

Many of the uranium deposits in the Poison Canyon Trend have been mined out and what uranium mineralization remained at these mines is probably uneconomic to recover, especially in the western portion of the Poison Canyon Trend. Historic resources were determined in a few deposits that were never mined (Table 2; McLemore et al., 1986, 2013, this report). The mineral-resource potential for uranium in the unmined portions of the eastern portion of the Poison Canyon Trend is high (Table 2). However, it is unlikely that any of these deposits will be mined in the near future because of economic conditions and numerous challenges to mine uranium in New Mexico, as summarized by McLemore et al. (2013).

SUMMARY

The Poison Canyon Trend is from the Section 14 prospect near the Bobcat and Blue Peak mines (southeast of Mesa Montanosa) southeastward to the San Mateo Mine, which is west of the village of San Mateo. The first economic discovery of uranium in sandstone in the Grants District was made in the Poison Canyon Trend of the Ambrosia Lake Subdistrict. Not only was it the first sandstone-hosted uranium deposit discovered and mined that ultimately led to the larger Ambrosia Lake Trend, but the main types of uranium ore deposits in the Grants District, primary and redistributed, were first recognized in the Poison Canyon Trend. More than 10 million lbs of U_3O_8 were produced from mines in the Poison Canyon Trend, and additional historic resources remain that could be mined in the future. The primary, tabular uranium deposits in the Poison Canyon Trend are likely 130-140 Ma. Younger, redistributed uranium deposits in the Poison Canyon and Ambrosia Lake Trends are much younger, 3-12 Ma in age. There is no consensus on the origin of the primary, tabular sandstone uranium deposits; however, the majority of the proposed models for formation of the Ambrosia Lake sandstone uranium deposits suggest that deposition occurred at a groundwater interface between two fluids of different chemical compositions and/or oxidation-reduction states. The mineral-resource potential for uranium in the unmined portions of the eastern portion of the Poison Canyon Trend is high, but, it is unlikely that any of these deposits will be mined in the near future because of economic conditions and numerous challenges to mine uranium in New Mexico.

ACKNOWLEDGMENTS

This paper is part of an on-going study of the mineral resources of New Mexico at NMBGMR, Dr. Nelia Dunbar, Director and State Geologist. This report benefited from many past discussions with William Chenoweth, Bob Smith, Ted Wilton, James Bonner, Bill Bergloff, David Fitch, and many others; thanks to all of you. Steve Cather and David Fitch provided some insight into the stratigraphic position of the Poison Canyon sandstone. Ted Wilton and Alva Saucier reviewed an earlier version of this manuscript, and their comments are appreciated.

REFERENCES

Adams, S.S., and Saucier, A.E., 1981, Geology and recognition criteria for uraniferous humate deposits, Grants uranium region, New Mexico—final report: United States Department of Energy, Report GJBX-2(81), 225 p.

Anderson, O.J., and Lucas, S.G., 1997, Lake T'oo'dichi' and the Brushy Basin Member of the Morrison Formation: New Mexico Geological Society, Guidebook 48, p. 2.

Bell, T.E., 1986, Deposition and diagenesis of the Brushy Basin Member and upper part of the Westwater Canyon Member of the Morrison Formation, *in* Turner-Peterson, C.E., Santos, E.S., and Fishman, N.S., eds., A Basin Analysis Case Study—the Morrison Formation, Grants Uranium Region, New Mexico: Tulsa, American Association of Petroleum Geologists, Studies in Geology 22, p. 77-91.

Berglof, W.R., 1970, Absolute relationships in selected Colorado Plateau uranium ores [Ph.D. dissertation]: New York, Columbia University, 140 p.

Berglof, W.R., 1989, Isotopic ages of uranium deposits in the Todilto Limestone, Grants district, and their relationship to the ages of other Colorado Plateau deposits: New Mexico Geological Society, Guidebook 43, p. 351-358.

Berglof, W.R., and McLemore, V.T., 2003, Economic geology of the Todilto Formation: New Mexico Geological Society, Guidebook 43, p. 179-189.

Blakey, R.C., and Parnell, R.A., Jr., 1995, Middle Jurassic volcanism: The volcanic record in the eolian Page Sandstone and related Carmel Formation, Colorado Plateau, *in* Miller, D.M., and Busby, C., eds., Jurassic Magmatism and Tectonics of the North American Cordillera: Boulder, Geological Society of America, Special Paper 299, p. 393-411.

Brookins, D.G., 1980, Geochronologic studies in the Grants mineral belt, *in* Rautman, C.A., *compiler,* Geology and mineral technology of the Grants uranium region 1979*:* New Mexico Bureau of Mines and Mineral Resources, Memoir 38, p. 52–58.

Brookins, D.G., 1989, Spurious Rb-Sr systematics of clay minerals from the Poison Canyon Sandstone, Grants mineral belt, New Mexico: Isochron/West – Bulletin of Isotopic Geochronology, v. 54, p. 13-14.

Brookins, D.G., Lee, M.J., and Shafiqullah, M., 1977, K-Ar ages for clay-size and silt-size fractions for uranium ore from the Grants uranium belt, New Mexico: Isochron/West – Bulletin of Isotopic Geochronology, v. 18, p. 17–19.

Chapman, Wood, and Griswold, Inc., 1979, Geologic map of the Grants uranium region, New Mexico: New Mexico Bureau of Mines and Mineral Resources, Geologic Map 31, scale 1:126,720.

Chenoweth, W.L., 1989, Ambrosia Lake, New Mexico—A giant uranium district: New Mexico Geological Society, Guidebook 40, p. 297-302.

Christiansen, E.H., Kowallis, B.J., Dorais, M.J., Hart, G.L., Mills, C.N., Pickard, M., and Parks, E., 2015, The record of volcanism in the Brushy Basin Member of the Morrison Formation: Implications for the Late Jurassic of western North America: Geological Society of America, Special Paper 513, 42 p.

Condon, S.M., 1989, Revisions of Middle Jurassic nomenclature in southeastern San Juan Basin, New Mexico: U.S. Geological Survey Bulletin, 1808-E, p. 1–21.

Dalkamp, F.J., 2010, Uranium Deposits of the World—USA and Latin America; Berlin, Springer-Verlag, 516 p.

Demko, T.M., Currie, B.S., and Nicoll, K.A., 2004, Regional paleoclimatic and stratigraphic implications of paleosols and fluvial/overbank architecture in the Morrison Formation (Upper Jurassic), western interior, USA: Sedimentary Geology, v. 167, p. 115–135.

Dickinson, W.R., 2018, Tectonosedimentary Relations of Pennsylvanian to Jurassic Strata on the Colorado Plateau: Boulder, Geological Society of America, Special Paper 533, 184 p.

Dickinson, W.R., and Gehrels, G.E., 2008, Sediment delivery to the Cordilleran foreland basin: Insights from U-Pb ages of detrital zircons in upper Jurassic and Cretaceous strata of the Colorado Plateau: American Journal of Science, v. 308, p. 1041-1082.

Dodd, P.H., 1955, Examples of uranium deposits in the Upper Jurassic Morrison Formation of the Colorado Plateau, *in* Contributions to the geology of uranium and thorium by the U.S. Geological Survey and Atomic Energy Commission for the United Nations International Conference on Peaceful Uses of Atomic Energy, Geneva, Switzerland, 1955: U.S. Geological Survey, Professional Paper 300, p. 243-262.

du Bray, E., 2007, Time, space, and composition relations among northern Nevada intrusive rocks and their metallogenic implications: Geosphere, v. 3, p. 381-405.

Dunagan, S.P., and Turner, C.E., 2004, Regional paleohydrologic and paleoclimatic settings of wetland/lacustrine depositional systems in the Morrison Formation (Upper Jurassic), western interior, USA: Sedimentary Geology, v. 167, p. 269-296.

Galloway, W.E., 1980, Deposition and early hydrologic evolution of Westwater Canyon wet alluvial-fan system, *in* Rautman, C.A., compiler, Geology and technology of the Grants uranium region: New Mexico Bureau of Mines and Mineral Resources, Memoir 38, p. 59-69.

Granger, H.C., and Santos, E.S., 1986, Geology and ore deposits of the Section 23 mine, Ambrosia Lake district, New Mexico, *in* Turner-Peterson, C.E., Santos, E.S., and Fishman, N.S., eds., A Basin Analysis Case Study: The Morrison Formation, Grants Uranium Region, New Mexico: Tulsa, American Association of Petroleum Geologists, Studies in Geology 22, p. 185–210.

Hilpert, L.S., 1963, Regional and local stratigraphy of uranium-bearing rocks, *in* Kelley, V.C., compiler, Geology and technology of the Grants uranium region: New Mexico Bureau of Mines and Mineral Resources, Memoir 15, p. 6-18.

Hilpert, L.S., 1969, Uranium resources of northwestern New Mexico: U.S. Geological Survey, Professional Paper 603, 166 p.

Hilpert, L.S., and Corey, A.F., 1957, Northwest New Mexico, *in* Geologic investigations of radioactive deposits—semiannual progress report, December I, 1956 to May 31, 1957: U.S. Geological Survey, Trace Element Inv. TEI-690, p. 366-381.

Hilpert, L.S., and Freeman, V.L., 1956, Guides to uranium deposits in the Morrison Formation, Gallup-Laguna area, New Mexico, *in* Page, L.R., Stocking, H.E., and Smith, H.B., eds., Contributions to the geology of uranium and thorium by the U.S. Geological Survey and Atomic Energy Commission for the United Nations International Conference on peaceful uses of atomic energy, Geneva, Switzerland, 1955: U.S. Geological Survey, Professional Paper 300, p. 299-302.

Hitzman, M., and Valenta, R.K., 2005, Uranium in Iron Oxide-Copper-Gold (IOCG) systems: Economic Geology, v. 100, p. 1657–1661.

Holen, H.K., and Finch, W.I., 1982, World's largest giant uranium deposit in New Mexico? U.S. Geological Survey, Open-file Report 82-539, 6 p.

Holmquist, R.J., 1970, The discovery and development of uranium in the Grants mineral belt, New Mexico: U.S. Atomic Energy Commission, Report RME-172, 122 p.

Hooper, R.L., 1983, Fission-track dating of the Mariano Lake uranium deposit, Grants mineral belt, New Mexico [Ph.D. dissertation]: St. Louis, Washington University, 148 p.

Hoskins, W.G., 1963, Geology of the Black Jack No. 2 mine, Smith Lake area, *in* Kelley, V.C., compiler, Geology and technology of the Grants uranium region: New Mexico Bureau of Mines and Minerals Resources, Memoir 15, p. 49-52.

Johnston, G.C., 1963, Subsidence and pillar recovery in the west area of the Marquez mine, *in* Kelley, V.C., compiler, Geology and technology of the Grants uranium region: New Mexico Bureau Mines and Mineral Resources, Memoir 15, p. 256-263.

Konigsmark, T.A., 1958, Uranium deposits in the Morrison Formation on the northeast flank of the Zuni uplift exclusive of Ambrosia Lake, New Mexico: U.S. Atomic Energy Commission, RME-115, 34 p.

Kowallis, B.J., Christiansen, E.H., and Deino, A.L., 1991, Age of the Brushy Basin Member of the Morrison Formation, Colorado Plateau, western USA: Cretaceous Research, v. 12, p. 483-493.

Kowallis, B.J., Christiansen, E.H., Deino, A.L., Peterson, F., Turner, C.E., Kunk, M.J., and Obradovich, J.D., 1999, Age of the Morrison Formation: Modern Geology, v. 22, p. 235-260.

Kowallis, B.J., Christiansen, E.H., Deino, A.L., Zhang, C. and Everett, B.H., 2001, The record of Middle Jurassic arc volcanism in the Carmel and Temple Cap formations of southwestern Utah: Geological Society of America Bulletin, v. 113, p. 373-387.

Lawton, T.F., and McMillan, N.J., 1999, Arc abandonment as a cause for passive continental rifting: Comparison of the Jurassic Mexican Borderland rift and the Cenozoic Rio Grande rift: Geology, v. 27, p. 779–782.

Lee, M.J., 1976, Geochemistry of the sedimentary uranium deposits of the Grants mineral belt, southern San Juan Basin, New Mexico [Ph.D. dissertation]: Ithaca, New York, Cornell University, 241 p.

Ludwig, K.R., Rubin, B., Fishman, N.S., and Reynolds, R.L., 1982, U-Pb ages of uranium ores in the Church Rock uranium district, New Mexico: Economic Geology, v. 77, p. 1942-1945.

Mathewson, D.E., 1953, Geology of the Poison Canyon mine, Valencia County, section 19, T13N, R9W, near Grants, New Mexico: U.S. Atomic Energy Commission, Technical Memo, TM-24, 7 p.

McLemore, V.T., 1983, Uranium and thorium occurrences in New Mexico: distribution, geology, production, and resources; with selected bibliography: New Mexico Bureau of Mines and Mineral Resources, Open-file Report OF-182, 950 p., also U.S. Department of Energy, Report GJBX-11(83).

McLemore, V.T., 2011, The Grants uranium district: Update on source, deposition, and exploration: The Mountain Geologist, v, 48, p. 23–44.

McLemore, V.T., 2020, Economic importance of the Jurassic Todilto Formation and origin of the ore-controlling intraformational folds: New Mexico Geological Society, Guidebook 71, this volume.

McLemore, V.T., and Chenoweth, W.C., 1989, Uranium resources in New Mexico: New Mexico Bureau of Mines and Mineral Resources, Resource Map 18, 37 p.

McLemore, V.T. and Chenoweth, W.C., 1991, Uranium mines and deposits in the Grants district, Cibola and McKinley Counties, New Mexico: New Mexico Bureau of Mines and Mineral Resources, Open File Report 353, 22 p.

McLemore, V.T. and Chenoweth, W.C., 2017, Uranium resources, *in* McLemore, V.T., Timmons, S., and Wilks, M., eds., Energy and Mineral Deposits in New Mexico: New Mexico Bureau of Geology and Mineral Resources Memoir 50 and New Mexico Geological Society Special Publication 13, 80 p.

McLemore, V.T., Broadhead, R.F., Barker, J.M., Austin, G.S., Klein, K., Brown, K.B., Murray, D., Bowie, M.R., and Hingtgen, J.S., 1986, A preliminary mineral-resource potential of Cibola County, northwestern New Mexico: New Mexico Bureau of Mines and Mineral Resources, Open-file Report 230, 403 p.

McLemore, V.T., Donahue, K., Krueger, C.B., Rowe, A., Ulbricht, L., Jackson, M.J., Breese, M.R., Jones, G., and Wilks, M., 2002, Database of the uranium mines, prospects, occurrences, and mills in New Mexico: New Mexico Bureau of Geology and Mineral Resources, Open file Report 461, CD-ROM.

McLemore, V.T., Hill, B., Khalsa, N., and Lucas Kamat, S.A., 2013, Uranium

resources in the Grants uranium district, New Mexico: An update: New Mexico Geological Society, Guidebook 64, p. 117–126.

Miller, D.M., and Busby, C., 1995, Preface, *in* Miller, D.M. and Busby, C., eds., Jurassic Magmatism and Tectonics of the North American Cordillera: Boulder, Geological Society of America, Special Paper 299, p. v-vi.

Miller, D.S., and Kulp, J.L., 1963, Isotopic evidence on the origin of the Colorado Plateau uranium ores: Geological Society of America Bulletin, v. 74, p. 609-630.

Mining World, 1959, Successful small mine in big uranium district: Mining World, v. 59, p. 46-49.

Nash, J.T., 1968, Uranium deposits in the Jackpile sandstone, New Mexico: Economic Geology, v. 63, p. 737-750.

Nash, J.T., and Kerr, P.F., 1966, Geologic limitations on the age of uranium deposits in the Jackpile Sandstone, New Mexico: Economic Geology, v. 61, p. 1283-1287.

Rapaport, I.J., 1963, Uranium deposits of the Poison Canyon ore trend, Grants district, *in* Kelley, V.C., compiler, Geology and technology of the Grants uranium region: New Mexico Bureau of Mines and Minerals Resources, Memoir 15, p. 122-135.

Saleeby, J.B., and Busby-Spera, C., 1992, Early Mesozoic tectonic evolution of the western US Cordillera, *in* Burchfield, B.C., Lipman, P.W., and Zoback, M.L., eds., The Cordilleran Orogen: Conterminous US: Geological Society of America, The Geology of North America, v. G-3, p. 107-168.

Sanford, R.F., 1982, Preliminary model of regional Mesozoic groundwater flow and uranium deposition in the Colorado Plateau: Geology, v. 10, p. 348–352.

Sanford, R.F., 1992, A new model for tabular-type uranium deposits: Economic Geology, v. 87, p. 2041-2055.

Santos, E.S., 1963, Relation of ore deposits to the stratigraphy of host rocks in the Ambrosia Lake area, *in* Kelley, V.C., compiler, Geology and mineral technology of the Grants uranium region: New Mexico Bureau of Mines and Mineral Resources, Memoir 15, p. 53-59.

Saucier, A.E., 1981, Tertiary oxidation in Westwater Canyon Member of the Morrison Formation, *in* Rautman, C.A., compiler, Geology and mineral technology of the Grants uranium region, 1979: New Mexico Bureau of Mines and Mineral Resources, Memoir 38, p. 116-121.

Tessendorf, T.N., 1980, Redistributed orebodies of Poison Canyon, sec. 18 and 19, T.13N., R.9W., McKinley County, New Mexico, *in* Rautman, C.A., compiler, Geology and mineral technology of the Grants uranium region 1979: New Mexico Bureau of Mines and Mineral Resources, Memoir 38, p. 226-229.

Thakur, S., Chudasama, B., and Porwal, A., 2018, Global Grade-and-Tonnage modeling of uranium deposits, *in* Quantitative and Spatial Evaluations of Undiscovered Uranium Resources: International Atomic Energy Agency, IAEA-TECDOC-1861, p. 226-272,

Turner, C.E., 2004, Reconstruction of the Upper Jurassic Morrison Formation extinct ecosystem—A synthesis: Sedimentary Geology, v. 167, p. 309–355.

Turner, C.E., 2010a, Brushy Basin Member—Lake T'oo'dichi': New Mexico Geological Society, Guidebook 61, p. 23-24.

Turner, C.E., 2010b, Montezuma Creek: Brushy Basin and Lake T'oo'dichi': New Mexico Geological Society, Guidebook 61, p. 31-32.

Turner-Peterson, C.E., 1980, Tabular uranium ore in Poison Canyon area, Morrison Formation, San Juan Basin, and application of lacustrine-humate model: American Association Petroleum Geologists Bulletin, v. 64, p. 795.

Turner-Peterson, C.E., 1985, Lacustrine-humate model for primary uranium ore deposits, Grants uranium region, New Mexico: American Association of Petroleum Geologists Bulletin, v. 69, p. 1999–2020.

Turner-Peterson, C.E., and Fishman, N.S., 1986, Geologic synthesis and genetic models for uranium mineralization in the Morrison Formation, Grants uranium region, New Mexico, *in* Turner-Peterson, C.E., Santos, E.S., and Fishman, N.S., eds., A Basin Analysis Case Study – The Morrison Formation, Grants Uranium Region, New Mexico: Tulsa, American Association Petroleum Geologists, Studies in Geology 22, p. 357-388.

Turner-Peterson, C.E., and Fishman, N.S., 1991, Jurassic Lake T'oo'dichi': a large alkaline saline lake, Morrison formation, eastern Colorado Plateau: Geological Society of America, Bulletin v. 103, p. 538-558.

Turner-Peterson, C.E., Gundersen, L.C., Francis, D.S., and Aubrey, W.M., 1980, Fluvial-lacustrine sequences in the Upper Jurassic Morrison Formation and the relationship of facies to tabular uranium ore deposits in the Poison Canyon area, Grants mineral belt, New Mexico, *in* Turner-Peterson, C.E., ed., Uranium in Sedimentary Rocks—Application of the Facies Concept to Exploration: Society Economic Paleontologists and Mineralogists, Rocky Mountain Section Publication, p. 177-211.

Weege, R.J., 1963, Geology of the Marquez mine, Ambrosia Lake area, *in* V.C. Kelley, compiler, Geology and technology of the Grants uranium region: New Mexico Bureau Mines and Mineral Resources, Memoir 15, p. 117-121.

Wilks, M., and Chapin, C.E., 1997, The New Mexico Geochronological Database: New Mexico Bureau of Mines and Mineral Resources Digital Data Series-Databases, NMDDS-B1, CD.

Wilton, D.T., 2018, Technical report on the Ambrosia Lake uranium project, McKinley County, New Mexico, USA: Westwater Resources, Incorporated, 82 p.

Zitting, R.T., Webb, M.D., and Groth, F.A., 1957, Geology of the Ambrosia Lake area uranium deposits, McKinley County, New Mexico: Mines Magazine, v. 4, p. 53-58.

Appendices can be found at http://nmgs.nmt.edu/repository/index.cfml?rid=2020002

New Mexico Geological Society, Special Publication 14, Geology of the Mount Taylor Area, 2020, p. 67-75.

SANDSTONE-HOSTED URANIUM DEPOSITS AT THE CEBOLLETA LAND GRANT, CIBOLA COUNTY, NEW MEXICO

Ted Wilton[1], William X. Chávez, Jr.[2], and Samantha Caldwell[3]

[1]Westwater Resources, Inc., 3536 Desert Fox Drive, Sparks, Nevada 89436; twilton@radiumtrail.us
[2]New Mexico Tech, 801 Leroy Place, Socorro, New Mexico 87801
[3]Freeport McMoRan, Inc., Bagdad, Arizona 86321

Abstract—The Cebolleta Land Grant of west-central New Mexico is the site of five sandstone-hosted uranium deposits that represent the northeastern extension of the prolific Jackpile–Paguate uranium mineralized zone and the northern part of the Laguna mining district. The uranium mineralization at Cebolleta, which is hosted in the Jackpile Sandstone Member of the Upper Jurassic Morrison Formation, has been extensively delineated by more than 1,000 drill holes, two open pit mines, and three underground mines. The mineralization occurs as a series of generally tabular-shaped bodies that were deposited within various lenses of the Jackpile Sandstone. Individual uranium deposits at the land grant exhibit many of the characteristics of *primary*, *redistributed*, and *remnant* types of uranium deposits that are hosted in the Westwater Canyon Member of the Morrison Formation elsewhere within the Grants Mineral Belt. Coffinite and minor uraninite are the principal primary uranium minerals in the deposits. Secondary uranium minerals, which are the result of post-mining oxidation of the primary coffinite and uraninite-rich zones, are exposed in the two former St. Anthony open pits. Significant unmined uranium mineralization is present in the area of the former mines, between and adjoining the now inactive St. Anthony and JJ#1 mines, and extending to the northeast of the former mines.

INTRODUCTION

The Cebolleta Land Grant (La Merced del Pueblo de Cebolleta) is a former Spanish land grant that is located in northeastern Cibola County, New Mexico, 45 mi (72 km) west of the city of Albuquerque and 10 mi (16 km) north of the Pueblo of Laguna (Fig. 1). Situated southeast of Mount Taylor, the land grant lies in an area of mesas and valleys along the southeastern margin of the San Juan Basin.

The land grant, which hosts five significant sandstone-hosted uranium deposits (St. Anthony, Area I, Area II, Area III and Area V) in the northern part of the Laguna mining district (Fig. 2), is positioned near the southeastern end of the prolific Grants Mineral Belt, one of the largest concentrations of sandstone-hosted uranium deposits in the world, and has been the single largest source of uranium production for the United States (Turner-Peterson et al., 1986; Dahlkamp, 1993; Cuney and Kyser, 2008). The mineral belt encompasses five uranium mining districts in the southern part of the San Juan Basin, from the Laguna area, near its southeastern end, northwesterly for a distance of nearly 100 mi (160 km) to the vicinity of the town of Gallup. Collectively, mines in the mineral belt have produced in excess of 340 million pounds of U_3O_8 (McLemore, 2010) between 1948 and 2002. Readers will note that our use of the term "Grants Mineral Belt" (i.e., Brookins, 1975, 1979; Fitch, 1979; Saucier, 1976) to describe the regional concentration of sandstone-hosted uranium deposits in the area between Gallup on the northwest and Laguna on the southeast is not universally applied. Various other researchers have utilized the terms "Grants Uranium Region" (i.e., Kelley, 1963; Rautman, 1979; Dahlkamp, 2010) or

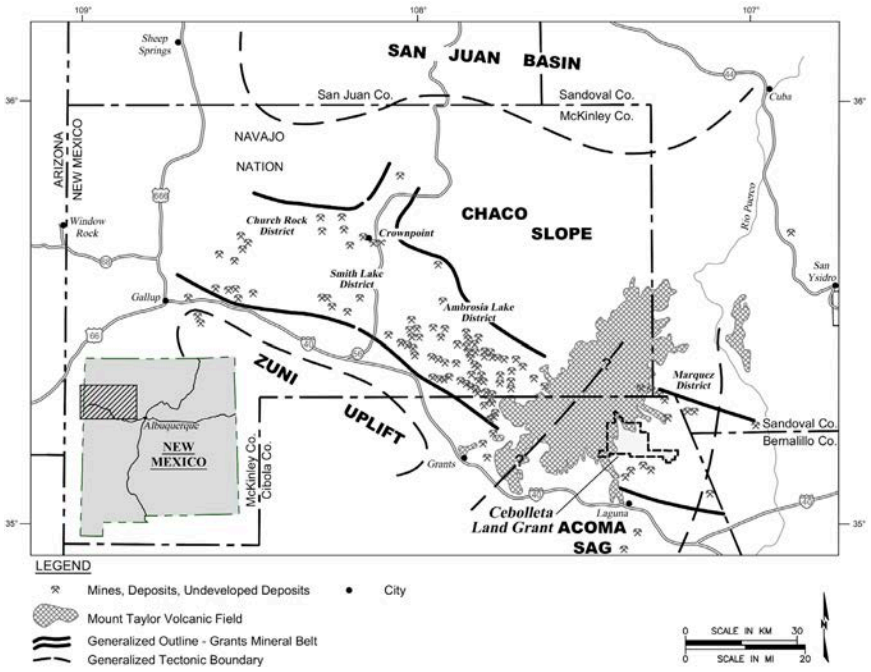

FIGURE 1. West-central New Mexico map. Cebolleta Land Grant situated at the southeast end of the Grants Mineral Belt. Map depicts tectonic features of the region. See section about geologic setting for more details.

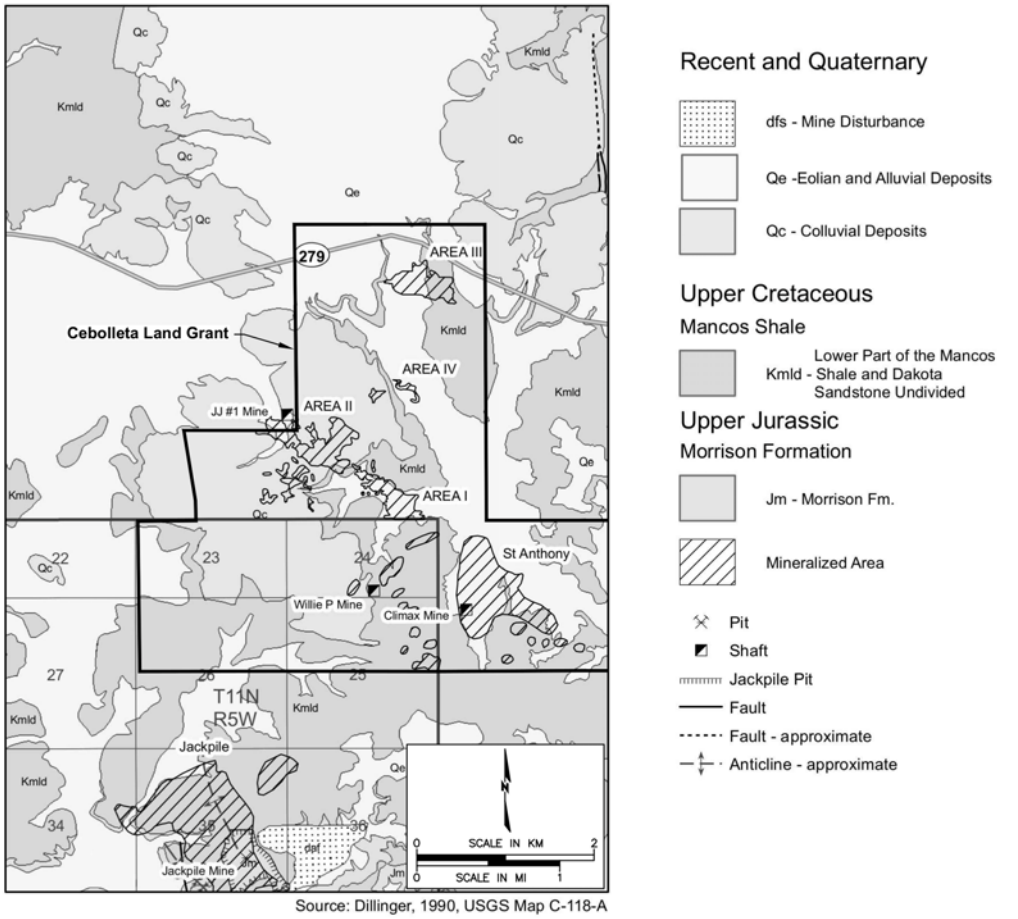

FIGURE 2. Generalized geologic map of the Cebolleta Grant and adjoining part of the Laguna Mining District. Uranium deposits outlined in hachures (geology modified from Dillinger, 1990b).

"Grants Uranium District" (i.e., McLemore, 2010; McLemore and Chenoweth, 1991; McLemore, et al., 2013) to describe this mineralized region. The same holds true for the more localized concentrations of uranium deposits within the Grants Mineral Belt, such as the Laguna Mining District, where the term "mining district" has been used by many authors (i.e., Moench and Schlee, 1967; Adams et al., 1978; Baird et al., 1979; Jacobsen, 1979), while others have applied the term "subdistrict" for the more localized concentrations of uranium deposits (i.e., McLemore, 2010; McLemore and Chenoweth, 1991). We use the term "Grants Mineral Belt" to delineate the regional concentration of uranium deposits in the southern part of the San Juan Basin.

Uranium mineralization at the Cebolleta Land Grant occurs as a series of tabular bodies hosted within the Jackpile Sandstone Member of the Upper Jurassic Morrison Formation. Historical uranium production from the land grant was derived from three underground and two open-pit mines, and significant uranium resources remain in the area.

MINING HISTORY

Exploration for uranium deposits in the Laguna mining district, which includes a portion of the Cebolleta Land Grant, commenced in 1951, when surface exposures of high-grade uranium mineralization were discovered by the Anaconda Copper Co. (Beck et al., 1980) on a portion of the Laguna Pueblo lands contiguous with the southern boundary of the Cebolleta Land Grant. Anaconda's identification of mineralized outcrops led to the discovery of the Jackpile and Paguate uranium deposits, which were subsequently developed into the largest uranium mine complex in the United States. Concurrent with the development of the Jackpile open pit mine, Anaconda conducted a regional exploration drilling program on the nearby Evans Ranch, 3 mi (5 km) northeast of the Jackpile deposit, culminating in the initial discovery of uranium mineralization in the Jackpile Sandstone that was to ultimately become the L-Bar uranium project. The Anaconda exploration program included more than 350 drill holes on the Evans Ranch, but did not advance beyond the exploration stage (Geo-Management, unpubl. report for Sohio Western Mining Co., 1972). In the late 1990s, ownership of the western part of the Evans Ranch (also known as the L-Bar Ranch) was conveyed to its former traditional property owners, the Cebolleta Land Grant.

There has been considerable uranium exploration and production on the Cebolleta Land Grant immediately northeast of the Jackpile–Paguate Mine. The first recorded commercial production of uranium on the Cebolleta Land grant was in 1951 by Hanosh Mines, Inc., who extracted 167 short tons (151 tonnes) of material that averaged 0.09% U_3O_8 (W.L. Chenoweth, pers. commun., 2016) from a small underground mine. Drilling by the Climax Uranium Co. from 1954 to 1956 resulted in the discovery of an important deposit in Section 30, T11N, R4W. Production from the resulting M-6 Mine began in July 1957 and continued until October 1960, yielding 78,555 tons (71,264 tonnes) that averaged 0.20% U_3O_8 and contained 320,647 lbs (145,443 kg) of U_3O_8 (Chenoweth, pers. commun., 2016).

In the 1970s, the United Nuclear Corp. (UNC) and its subsidiary Teton Exploration Drilling Co. carried out an extensive exploration program in the vicinity of the former Climax Mine and discovered significant and widespread uranium mineralization in the Jackpile Sandstone on lands leased from the Cebolleta Land Grant. UNC developed two small open pits and one

underground mine, known as the St. Anthony Mine Complex (Baird et al., 1980). Mining was completed at St. Anthony in late 1979, and the milling of stockpiled material continued into 1980. Total production from the St. Anthony Mines amounted to approximately 1.6 million lbs (725,747 kg) of U_3O_8 for the period 1975 through 1980 (Moran and Daviess, 2014).

Reserve Oil and Minerals acquired the adjoining Evans/L-Bar Ranch in 1968 and formed a joint venture with Sohio Western Mining. Sohio operated the joint venture and re-discovered extensive uranium mineralization on the property that was initially discovered by Anaconda in the early 1950s, leading to the development of the large-scale JJ #1 Underground Mine and a uranium mill (L-Bar project), which operated from late 1976 to mid-1981. During the life of the L-Bar project, the JJ #1 Mine produced approximately 898,600 short tons (815,000 tonnes) of material averaging 0.123% U_3O_8, yielding 2,218,800 lbs (1,006,492 kg) of U_3O_8 (Boyd et al., 1984, unpubl. report for Sohio Western Mining Co.).

Collectively, approximately 3.8 million lbs (1,723,649 kg) of U_3O_8 have been produced from uranium deposits on the Cebolleta Land Grant. Although uranium mining and processing ceased on the land grant in 1981, considerable uranium resources remain on land grant properties. Westwater Resources, Inc., currently holds a mining lease from the Cebolleta Land Grant on the lands that encompass the former St. Anthony and L-Bar mines.

GEOLOGIC SETTING

The Cebolleta Land Grant is situated near the southeastern end of the Grants Mineral Belt, a northwest-southeast oriented zone of uranium deposits that are primarily hosted in various members of the Upper Jurassic Morrison Formation. The mineral belt, which is approximately 100 mi (160 km) long and up to approximately 25 mi (40 km) wide, is positioned on the Chaco Slope (Kelley, 1955) between the southern part of the San Juan Basin and the northeastern flank of the Zuni uplift and within the adjoining Acoma Sag (Fig. 1). Sedimentary rocks exposed along the trend of the mineral belt range in age from Upper Triassic through Late Cretaceous (Dillinger, 1990a, b). Jurassic sedimentary rocks of continental origin, including the economically important Morrison Formation, are exposed in a narrow band that generally parallels the northwest-trending axis of the Zuni Uplift. Cretaceous rocks, principally shales and sandstones, are exposed in the northeasterly portion of the mineral belt and unconformably overlie the Morrison Formation. Pliocene-Pleistocene volcanic rocks of the Mt. Taylor volcanic field obscure a portion of the southeastern part of the mineral belt, immediately to the west of the Cebolleta Land Grant (Moench and Schlee, 1967; Goff et al., 2015, Dillinger, 2009 b).

The Grants Mineral Belt encompasses five major mining districts (listed from southeast to northwest): Laguna, Marquez (which lies to the north of the Laguna district and contains uranium deposits hosted only in the Westwater Canyon Member of the Morrison Formation), Ambrosia Lake, Smith Lake, and Church Rock. The Grants Mineral Belt has produced more than 340 million lbs (154,221,280 kg) of U_3O_8, ranking it as one of the largest uranium-producing regions in the world (McLemore et al., 2013) and arguably the world's largest concentration of sandstone-hosted uranium deposits (Dahlkamp, 1993).

Uranium deposits of the Grants Mineral Belt are hosted principally in the Westwater Canyon Member (Jmw), the Poison Canyon sandstone (an informal unit of economic usage), the Brushy Basin Member (Jmb) and the Jackpile Sandstone Member (Jmj) of the Morrison Formation. Additional uranium deposits, with less significant production, are hosted on limestones of the Middle Jurassic Todilto Formation.

STRATIGRAPHY

Sedimentary rocks exposed within the Cebolleta Land Grant (Fig. 2) range in age from Late Jurassic through Late Cretaceous (Baird et al., 1980; Jacobsen, 1980; Moench and Schlee, 1967; Schlee and Moench, 1967). The Upper Jurassic Morrison Formation (Jm), is the principal host formation for uranium deposits throughout the Grants Mineral Belt. The Morrison Formation overlies rocks of the Jurassic San Rafael Group and is, in turn, unconformably overlain by the Cretaceous Dakota Sandstone (Kd), which in turn interfingers with and is overlain by the Mancos Shale (Km). The stratigraphic relationships of the various members of the Morrison Formation and underlying San Rafael Group have evolved as studies of Jurassic stratigraphic units throughout the Colorado Plateau region continue to be studied (e.g., Lucas and Anderson, 1997; Dickinson and Gehrels, 2010; Cather, et al., 2013). The stratigraphic nomenclature in general use by mine geologists working in the Laguna district and at the Cebolleta Land Grant uranium deposits is depicted in Figure 3 and is the convention used in this paper.

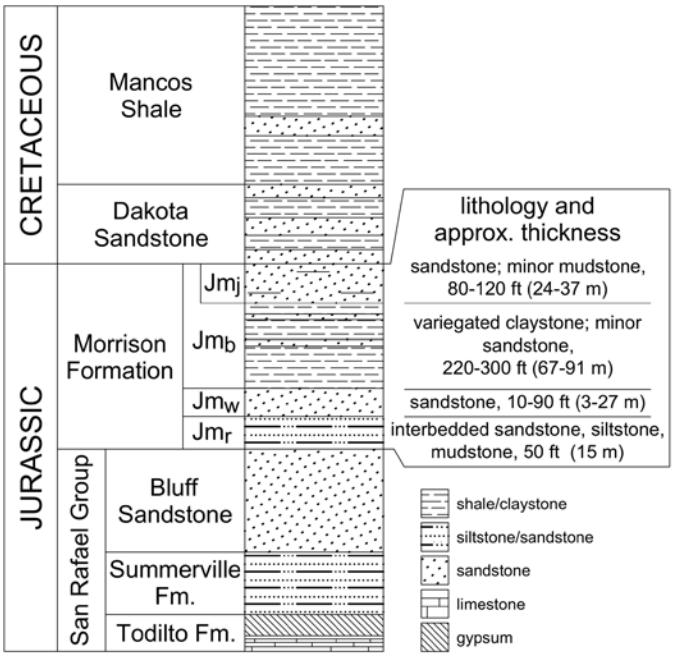

FIGURE 3. Stratigraphic column for the Cebolleta Land Grant with Morrison Formation nomenclature used in this paper (modified from Rautman, 1980).

The Morrison Formation is comprised of four distinct members in the area of the Cebolleta Land Grant (in ascending order): Recapture (Jmr), Westwater Canyon (Jmw), Brushy Basin (Jmb) and Jackpile Sandstone Members (Jmj). The basal unit of the Morrison Formation is the Recapture Member, which is approximately 50 ft (15 m) in thickness in the Laguna area (Moench and Schlee, 1967). Moench and Schlee (1967) describe it as a sequence of interbedded mudstone, siltstone, sandstone and minor limestone, grayish-red on weathered exposures, while fresh exposures of the various lithologies are gray (limestone), grayish-green (mudstone), and grayish-yellow (sandstone). The Recapture Member is not exposed on the Cebolleta Land Grant.

Overlying the Recapture member is the Westwater Canyon Member, which is the principal host for sandstone-hosted uranium deposits throughout much of the Grants Mineral Belt. In the area of the Cebolleta Land Grant, it ranges in thickness from 10 to 90 ft (3 to 27 m) and is comprised principally of grayish-yellow to pale orange sandstones, with a thin (3 ft) interval of greyish-red siltstone dividing it into upper and lower units. The Westwater Canyon sandstones are generally poorly sorted, range from fine to coarse grained, and are sub-arkosic to arkosic in composition (Moench and Schlee, 1967).

Overlying the Westwater Canyon is the Brushy Basin Member, which ranges in thickness from 220 to approximately 300 ft (67 to 91 m). The Brushy Basin is a visually distinctive unit comprised dominantly of variegated mudstone, claystone and shale, with lesser sandstone beds near the base that are hosts for uranium mineralization in the Ambrosia Lake, Smith Lake and Church Rock mining districts.

Overlying the Brushy Basin is the uppermost member of the Morrison, the Jackpile Sandstone Member (Owen et al., 1984; Aubrey, 1992). The Jackpile Sandstone is a light gray to white sandstone that forms vertical exposures. Within the Cebolleta Land Grant, exposures of the Jackpile Sandstone are limited to narrow bands along the base of Gavilan Mesa, south of the St. Anthony Mine, and in Arroyo Pedro Padilla, east of the St. Anthony Mines. It is a visually distinctive sandstone unit that is the host for the major uranium deposits at the former Jackpile–Paguate, Woodrow, St. Anthony, and L-Bar mines. Overall, the thickness of the Jackpile Sandstone ranges from approximately 80 to 120 ft (24 to 37 m) as determined from exploration drill holes and from exposures in the Willie P Underground Mine (Baird et al., 1980) and the JJ#1 Mine (Jacobsen, 1980).

The contact between the Brushy Basin and the Jackpile members is gradational to scoured in some locations (Owen et al., 1984). The Jackpile Sandstone interfingers with the uppermost part of the Brushy Basin Member in the Willie P Mine (Baird et al., 1980) and at the head of Oak Canyon (SW1/4 sec.10, T10N, R5W), about 2 mi southeast of the village of Paguate (Schlee and Moench, 1963b). The areal extent of the Jackpile is limited to the southeastern-most end of the Grants Mineral Belt and the southeastern part of the San Juan Basin and the Chama Basin (Owen et al., 1984).

At the Cebolleta Land Grant, the Jackpile Sandstone ranges from subarkosic to arkosic in composition (Moench and Schlee, 1967, Owen et al., 1984), with minor lenses of quartzose sandstone in the upper portion of the unit in the St. Anthony south pit (Caldwell, 2019). Individual sandstone lenses are generally dominated by fine- to medium-grained, pervasively cross-bedded, sub-arkosic sands, with local lenses of coarse-grained sands. Correlation of individual sandstone lenses throughout the Jackpile Sandstone is difficult, due to abundant channel features that routinely cut into underlying sandstones or lateral sandstone lenses. As such, the Jackpile Sandstone displays a high degree of variability, both laterally and vertically, as demonstrated in the former JJ #1 Mine and the St. Anthony south pit. In the JJ#1 Mine, the Jackpile has been subdivided into upper and lower units (FitzGerald et al., unpubl. report for Sohio Western Mining Co., 1979), with the upper unit comprised primarily of quartzose sandstone with essentially no mudstone lenses, and the lower unit comprised of subarkosic to arkosic sandstone interbedded with numerous green mudstone lenses. In contrast, where exposed in the walls of the two open pits at St. Anthony, the Jackpile is dominantly sandstone with few mudstone lenses. The Jackpile Sandstone was deposited in a braided-stream environment (Owen et al., 1984).

Overall, the Jackpile is a white to light gray/light tan sandstone, locally exhibiting a pinkish hue where feldspar content is relatively high. The white to light gray coloration is a distinctive characteristic of Jackpile Sandstone exposures throughout the Laguna district, including exposures in the St. Anthony north pit. In contrast, exposures in the St. Anthony south pit, which is approximately 2500 ft (760 m) southeast of the north pit, are tan to light gray to pale orange in color, due to post-depositional oxidation. Minor zones of hematite and limonite staining impart slight red to orange casts in the vicinities of some mineralized zones in both open pits.

Individual sandstone lenses are cemented primarily with kaolinitic clay in the middle and upper parts of the unit, and to a lesser extent by quartz and calcite, primarily in the lowermost part of the unit (Moench and Schlee, 1967). Alteration of the sandstones is manifested primarily by the partial conversion of feldspar to kaolinite. Accessory minerals include trace amounts of pyrite (Baird et al., 1980; Caldwell, 2019), zircon, tourmaline, garnet, and rutile. Nash (1968) noted, from exposures at the Jackpile Mine, that biotite, amphibole, magnetite and pyroxene are generally absent.

Baird et al. (1980) discuss two types of carbonaceous material within the Jackpile Sandstone in the Willie P Underground Mine. They reported the presence of carbonaceous material "coalified *in-situ*" and as "sand-sized material" interstratified in cross-beds. They also reported the presence of humate, occurring primarily as pore fillings between sand grains. Carbonaceous material (humate) is present in limited exposures along the south wall of the St Anthony north pit and locally in the south pit, primarily in proximity to zones of uranium mineralization. This material occurs as small (2 to 6 in, 51 to 152 mm), sparse, poorly developed, sub-vertical rod-shaped features, as amorphous masses, and as local accumulations of carbonaceous detritus on bedding planes near the bases of individual sandstone lenses. An anonymous report (1977) describes lithologies intersected by an exploration shaft at the St. Anthony north pit as similar vertical "carbon rods" in one mineral-

ized zone. The overall content of carbonaceous material in the open pit mines, either in the form of plant debris or as humate, is very low when compared to descriptions from the Willie P and JJ#1 mines, thereby providing support that the uranium mineralization in these areas is remnant in nature (south pit) and redistributed (north pit). In the JJ#1 Mine, carbonaceous material is present as plant detritus and humate accumulations. In contrast, Jacobsen (1980) reported that for the trend-type deposit at the JJ#1 Mine no significant uranium mineralization occurred where carbonaceous material was absent.

The Cretaceous Dakota Sandstone unconformably overlies the Jackpile Sandstone and is a light grey to pale tan quartzose sandstone with lenses of black carbonaceous shale. Exposures of the Dakota in the north and south pits range from 6 to about 10 ft (1.8 to 3 m) in thickness.

STRUCTURE

The Cebolleta Land Grant and the adjoining Jackpile–Paguate Mine lie within the Acoma Sag (Kelley, 1955; Nash, 1968), near the southeastern end of the Chaco Shelf. The Acoma Sag is a regional syncline that is bounded on the west by the southeastern end of the Zuni uplift and on the east by the Lucero uplift (Kelley, 1955). Structure within the sag is relatively simple, with rocks displaying shallow dips and small folds that generally trend to the northwest (Woodward, 1982).

Rocks on the Cebolleta Land Grant dip gently to the north and northwest toward the San Juan Basin, at less than 2 degrees. Faults with significant offset have not been recognized in the project area, although several small-scale, high-angle faults were observed in the workings of the former JJ #1 Underground Mine (Jacobsen, 1980) and minor north-trending normal faults were mapped in the Lobo Mountain area (Schlee and Moench, 1963 b). The faults observed in the JJ#1 Mine do not appear to have offset uranium mineralization, nor do they appear to have influenced the localization of mineralization (Jacobsen, 1980).

A very small fold, or structural dome, was identified in the southern part of the Willie P Underground Mine. A second, larger northeasterly-trending fold is present in the area of the Lobo Camp 3 mi (4.8 km) northeast of St. Anthony (Schlee and Moench, 1963 a). Overall, however, there is little in the way of deformation of rocks of the Laguna district (Moench and Schlee, 1967).

URANIUM MINERALIZATION

Nearly all of the uranium deposits in the Grants Mineral Belt (which includes the Cebolleta Land Grant) occur as sandstone-hosted deposits in fluvial clastic rocks of the Upper Jurassic-age Morrison Formation. Three general types of sandstone-hosted deposits have been recognized by workers in the mineral belt (Kittel et al., 1967; Granger and Santos, 1986):

- Primary deposits, which have also been described as trend or pre-fault deposits. They are broad, undulatory layers of uranium mineralization controlled primarily by the texture or fabric of the host sandstones. Mineralization in primary deposits is localized around accumulations of humate and carbonaceous plant debris that served as reductants to precipitate dissolved uranium from ground water;
- Redistributed deposits, which are also referred to as post-fault, stack, or secondary deposits, are irregularly shaped bodies of mineralization that were controlled by both the stratigraphic characteristics of the host rocks and faults, fractures and/or joints. Redistributed deposits result from oxidation and remobilization of uranium derived from primary deposits. Redistributed deposits have little or no humate associated with the mineralization; and
- Remnant deposits are, as the name implies, remnants of primary deposits that have been partially to nearly totally mobilized and redistributed. Remnant deposits tend to be discrete bodies of mineralization entirely enclosed within otherwise oxidized host rocks. Mineralization is often localized by small accumulations of carbonaceous material.

While this classification of sandstone-hosted deposits is based on the characteristics of uranium mineralization in the Westwater Canyon Member of the Morrison Formation, it applies to Jackpile Sandstone-hosted deposits with two important caveats: 1) the geometry of primary deposits in the Jackpile Sandstone do not necessarily reflect the overall geometry or architecture of individual Jackpile Sandstone channel sands or individual lenses, whereas 2) primary deposits hosted in the Westwater Canyon commonly reflect the overall orientation

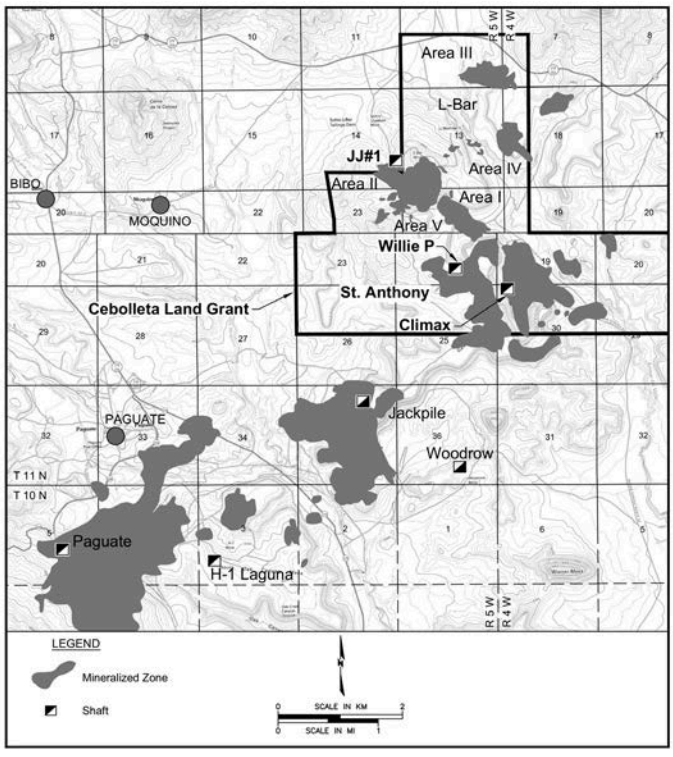

FIGURE 4. Uranium deposits of the Cebolleta Land Grant and adjoining areas of the Laguna Mining District. Areas depicted in gray are uranium deposits.

of the sandstone bodies (Jacobsen, 1980; Wilton, 2017). In addition, redistributed deposits in the Jackpile Sandstone at the Cebolleta Land Grant area are not localized along faults or fractures as is the case with Westwater Canyon-hosted redistributed deposits.

Uranium deposits in the Jackpile Sandstone range from moderate to large size, as demonstrated by the Jackpile and Paguate deposits, which are contiguous with the south boundary of the Cebolleta Land Grant (Fig. 4). The Jackpile deposit is more than 10,000 ft (3 km) long and averages 2000 ft (609 m) wide. Individual mineralized lenses rarely exceed 15 ft (4.5 m) in thickness, but the aggregate thickness of several "stacked" layers range up to 50 ft (15 m). Moench (1963) described the Jackpile Mine uranium deposits as "composed of one or more semi-tabular layers." In plan view, individual mineralized lenses range from nearly equant to strongly elongate. Viewed in vertical section, the mineralized intervals are suspended within sandstone intervals; only locally do they extend to stratigraphic discontinuities such as prominent mudstone beds, diastems, or formational contacts. The overall characteristics of mineralized zones in the St. Anthony and L-Bar deposits on the Cebolleta Land Grant are similar to the Jackpile and Paguate deposits, although the sizes of individual deposits are less, ranging from 500 to 1000 ft (152 to 305m) in width and from 2000 to 3000 ft (610 to 910 m) in length.

While Dahlkamp (2010) attributes the source of uranium in the Laguna mining district and Cebolleta Land Grant to the mobilization of uranium from either granitic rocks of the ancestral Mogollon highlands (southwest of the Cebolleta Land Grant) or from the devitrification of tuffaceous rocks contained in the host sandstones and particularly in the Brushy Basin Member, it is our opinion that deriving uranium from the underlying Brushy Basin Member is unlikely. However, there has been long-lived debate among uranium geologists as to the source(s) of uranium in sandstone-hosted deposits, and definitive proof of the source of the metal has yet to be established. Ultimately, uranium minerals were deposited in the host sandstones, where chemical reactions (reduction) associated with humic acids derived from plant material caused precipitation of dissolved uranium from the groundwater (Adams and Saucier, 1981).

As currently defined, there are five significant uranium deposits at the Cebolleta Land Grant (Fig. 4):

1. Area I and its southeastern extension,
2. Area II and V (including the former JJ#1 L-Bar Mine),
3. Area III,
4. St. Anthony north and south pits, and
5. Willie P (St. Anthony underground).

The uranium deposits on the Cebolleta Land Grant share a common set of geological characteristics:

- Economically significant mineralization is hosted by the Jackpile Sandstone, although minor mineralization is hosted in sandstones of the Brushy Basin Member and the Dakota Sandstone;
- Most of the mineralization is hosted in medium- to coarse-grained sandstones that exhibit large-scale tabular cross-stratification (Baird et al., 1980);
- Near the margins of the deposits, the mineralization thins appreciably, although halos of low-grade mineralization may surround deposits;
- Higher grade mineralization usually occurs in the centers of the mineralized zones;
- Although mineralization is present throughout the entire stratigraphic sequence of the Jackpile Sandstone, the strongest mineralization is concentrated in the lower part of the unit (Jacobsen, 1980; Wilton, 2017);
- Individual deposits do not show an overall preferred orientation or trend and do not reflect the regional northeasterly orientation of the main Jackpile Sandstone channel trend; and
- The primary deposits are associated with amorphous carbonaceous material and humate (Nash, 1966; Piette, 1970; Baird et al., 1980; Jacobsen, 1980; Caldwell, 2019). At the JJ#1 Mine, no meaningful concentrations of uranium mineralization occur without associated carbonaceous material (Jacobsen, 1980). It should be noted, however, that the remnant and redistributed deposits, as exposed in the two St. Anthony open pits, do not have appreciable amounts of carbonaceous material associated with them.

The mineralization in the St. Anthony south pit appears to be a remnant deposit that has been partially depleted of uranium, which was redeposited in the nearby (down-dip) north pit. Mineralization in the north pit is more pervasive in individual sandstone lenses, is associated with minor concentrations of humate and other carbonaceous plant debris and is redistributed mineralization. In the JJ#1 Mine and Area I and Area III, trend-type uranium deposits occur as tabular bodies that may be more than 1,000 ft (305 m) in length and attain thicknesses of 6 to 12 ft (1.8 to 3.7 m). The upper and lower boundaries of these mineralized bodies are generally abrupt. There is a tendency for individual deposits to develop in clusters. Locally, these clusters are related to the coalescence of separate channel sandstone bodies. In this instance, mineralization is often thicker and of higher grade than adjoining areas.

Extensive chemical and radiometric analyses on core samples by former mine operators (Geo-Management, unpubl. report for Sohio Western Mining Company, 1972; Olsen and Kopp, unpubl. report for Sohio Western Mining Company, 1982) demonstrate that radiometric and chemical assay methods generally yield comparable results (Wilton, 2017). Evaluation of samples from 47 core holes at St. Anthony, however, indicated that chemical analyses yielded somewhat higher grades than radiometric assays indicate. As such, the mineralization at the Cebolleta Land Grant is considered to be in radiometric to chemical equilibrium.

Exploration drilling north of the St. Anthony Mines delimited four substantial uranium deposits, the Area I, Area II and V, and Area III deposits. Mining by Sohio was restricted to parts of the II and V deposits (JJ #1 Mine). The Area I deposit, located in the southern end of the L-Bar complex, extends south into the northern St. Anthony area, and additional uranium mineralization is present adjacent to the St. Anthony open pits and the Willie P Underground Mine. Two of the former Sohio (L-Bar) uranium deposits, the Area I and Area III deposits, which host

substantial mineral resources and are excellent examples of trend-type mineralization are described below.

Area I Deposit

At the Area I deposit, grade, thickness, and GT (grade times thickness) contour maps were prepared for each of the mineralized horizons. Uranium grades were calculated from gamma-ray logs (down-hole geophysical logging) with grades denoted as weight percent "eU_3O_8" (where "e" denotes "equivalent" U_3O_8 as determined from radiometric assays rather than chemical assaying methods). Four distinct and separate mineralized horizons were identified in the Area I deposit – "upper", "middle", "lower", and "basal" zones.

Mineralization in the middle zone is a broad, southeast-northwest trending body that is 600 to 800 ft (183 to 244 m) wide and approximately 900 ft (274 m) long. Drill-hole intersections of mineralized zones, using a GT cut-off value of 0.5, indicate that the horizon averages 10.2 ft (3.1 m) thick with an average grade of 0.12% eU_3O_8. Mineralization in the lower zone occurs as a sinuous, lenticular, southeast-northwest trending body that is 150 to 400 ft (46 to 122 m) wide and approximately 2400 ft (731 m) long. This mineralized interval at a 0.5 GT cut-off averages 9.8 ft (2.98 m) thick with an average grade of 0.153% eU_3O_8.

The mineralized zones appear continuous throughout the Area I deposit. As well, the Area I deposit has a higher frequency of thin, less continuous mineralized horizons than are observed at other deposits. The higher average grades and more laterally continuous uranium mineralization are hosted in the middle and lower zones at the Area I deposit.

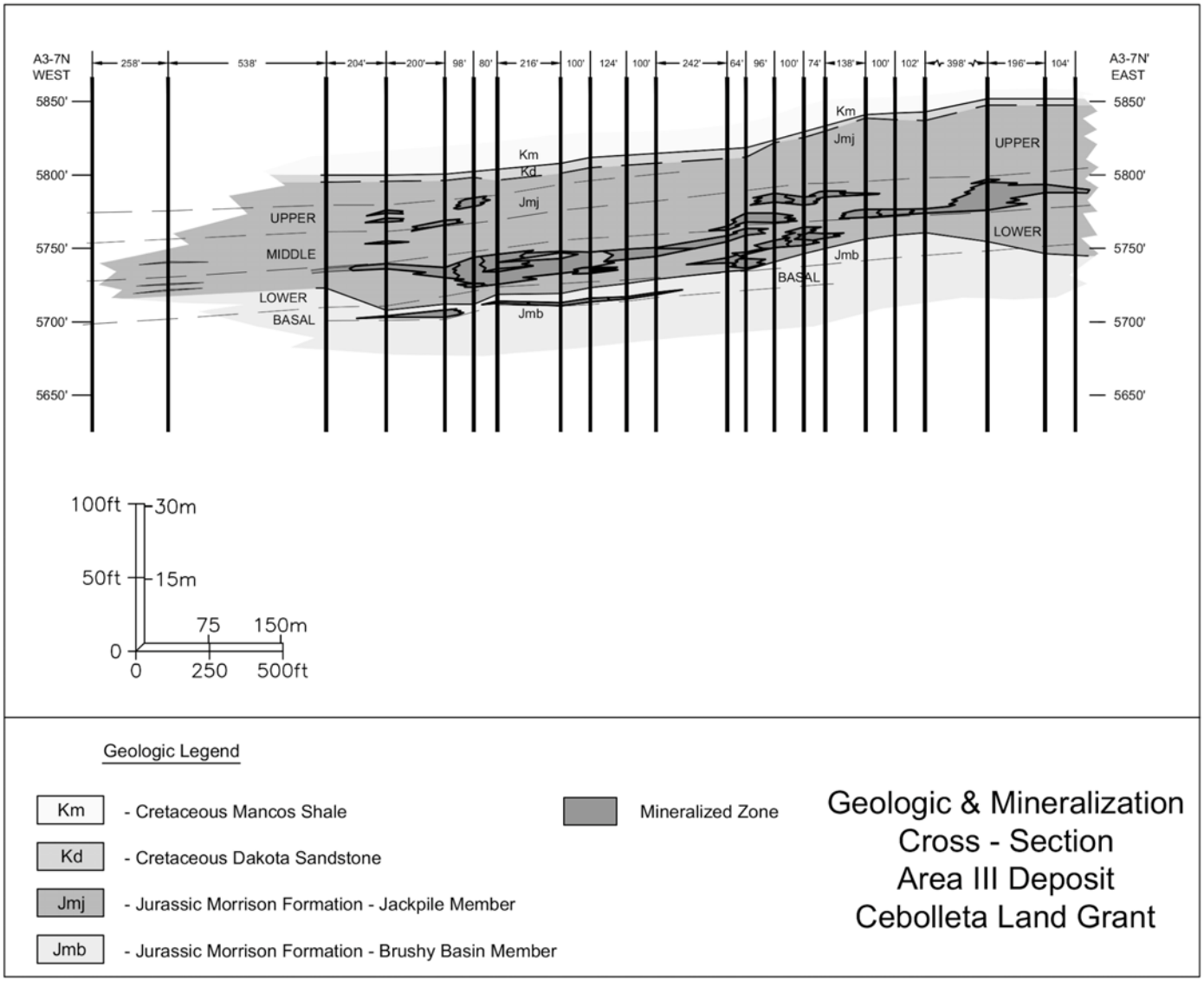

FIGURE 5. East-west cross section (looking north) of the Area III Uranium Deposit. Geologic units and mineralized intervals identified from drill-hole gamma-ray/self-potential and resistivity logs. The "lower" mineralized zone demonstrates lateral continuity over a distance of more than 1,300 ft (396 m) at grades of 0.10% eU_3O_8 or greater (The "e" in eU_3O_8 denotes "equivalent" U_3O_8 as determined from radiometric assays rather than chemical assaying methods).

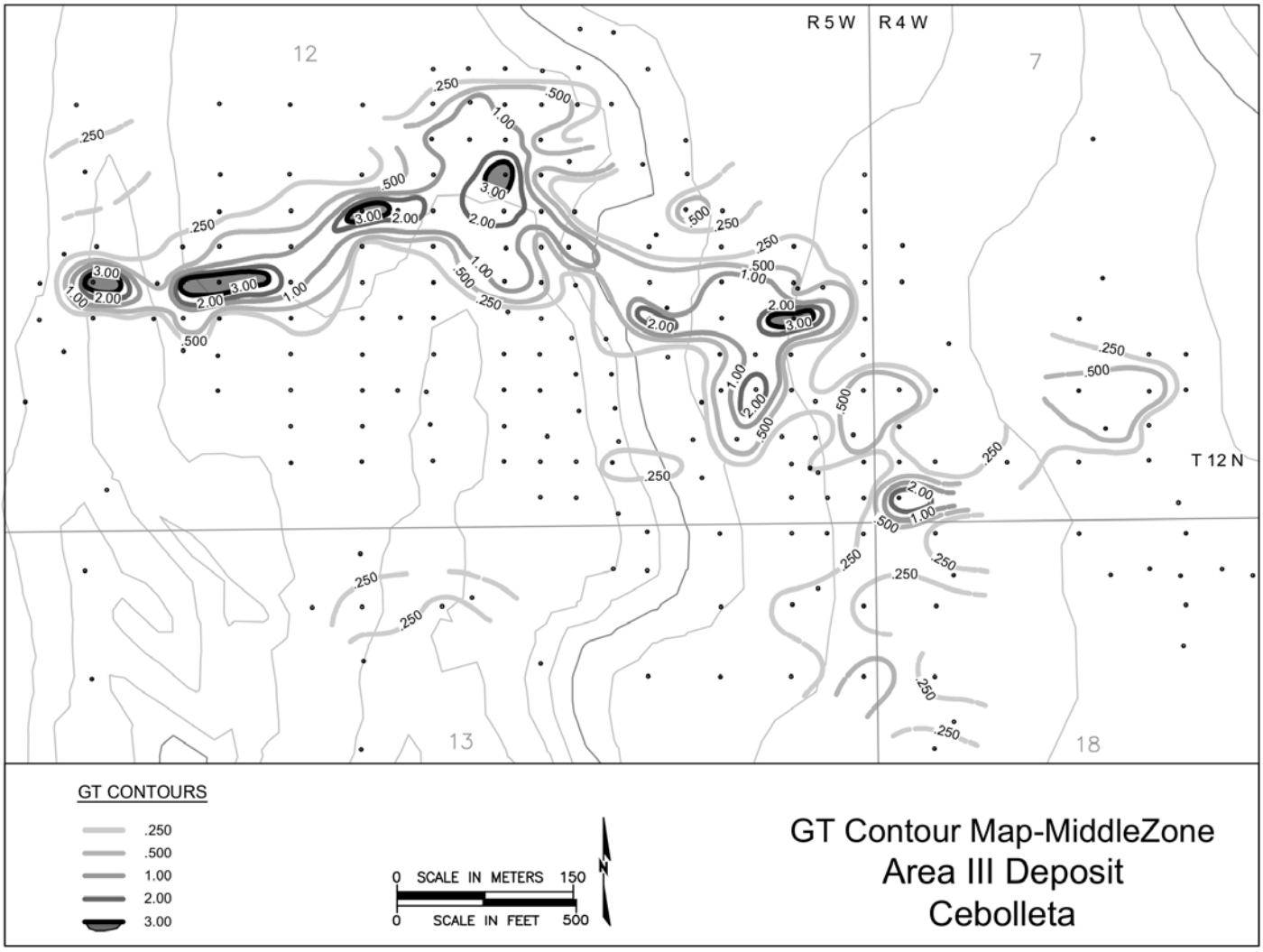

FIGURE 6. Grade times thickness (GT) contour map of the "middle" mineralized zone, Area III deposit. The "middle zone" at Area III demonstrates good lateral continuity of mineralization in a general east-west direction at a GT cut-off of 0.50 (ft-% eU_3O_8).

Area III Deposit

Geologic and mineralization sections were constructed across the Area III deposit utilizing the mineral intercept data from the Sohio drill-hole maps and individual gamma-ray geophysical logs (Fig. 5). Mineralization is continuous in tabular or lenticular bodies 2 ft (0.6 m) to more than 30 ft (9 m) in thickness. Grades greater than 0.10 % eU_3O_8 are commonly present, with numerous intercepts of 0.20% eU_3O_8 or greater. This mineralization occurs throughout the entirety of the Jackpile Sandstone, which is 80 to 100 ft (24 to 30 m) thick.

Area III mineralization, as at Area I, was assigned to four intervals, again designated as the upper, middle, lower, and basal zones (Fig. 5). The better and more laterally continuous mineralized bodies are in the middle and lower zones in the Jackpile Sandstone. Mineralization is also present in the Brushy Basin Member at and immediately beneath the lower contact of the Jackpile Sandstone, in the basal zone.

Mineralization in the middle zone (Fig. 6) occurs in an arcuate, east-west trending, elongate body that is 200 to 500 ft (61 to 152 m) wide and approximately 2100 ft (640 m) long (Fig. 6). A composite of mineral intercepts at a 0.5 GT cut off averages 8.3 ft (2.5 m) in thickness at an average grade of 0.183% eU_3O_8. Mineralization in the lower zone is represented by a continuous, lenticular, east-west trending body that is 300 to 500 ft (91 to 152 m) wide and approximately 2,200 ft (670 m) long. A composite of mineral intercepts at a 0.5 GT cut off averages 10.2 ft (3.1 m) thick with an average grade of 0.172% eU_3O_8.

The Area I and Area III deposits display certain similar geologic characteristics, including four mineralized horizons and similar lengths, widths and thicknesses. Grade variations between the middle zone in the two deposits is appreciable, as is the sinuous nature of the lower mineralized zone in the Area I deposit. The continuity of mineralization the lower zone of the Area III deposit is in marked contrast to that of the Area I deposit and the mineralization in the St. Anthony area. As such, it is an excellent example of the mode of occurrence of trend-type mineralization in the Cebolleta area.

Controls on Mineralization

Principal controls on uranium mineralization on the Cebolleta Land Grant are primary sedimentary structures, including channel fills, bars and cross-bedding in the Jackpile Sandstone (Jacobsen, 1980; Baird et al., 1980). In the primary deposits, concentrations of carbonaceous material (humate and/or carbonaceous plant debris) served as reductants that precipitated uranium from circulating ground water. The distribution of carbonaceous material tends to be localized, as observed in the former JJ#1 Mine (Jacobsen, 1980) and in the pit walls of the two St. Anthony open pits. Jacobsen (1980) notes that there are no significant accumulations of uranium without carbonaceous material; the same relation has been noted by UNC geologists (Baird et al., 1980) in the former Willie P Mine. However, this relationship is not well developed in low grade (0.03% to 0.06% U_3O_8) mineralized areas currently exposed in the St. Anthony north and south pits. This reflects the remnant nature of mineralization in the south pit and the redistributed nature of mineralization in the north pit. As such, the uranium-precipitating mechanism for this part of the Cebolleta Land Grant remains to be determined.

Baird et al. (1980) noted the distinct association of substantial zones of uranium mineralization with medium- to coarse-grained sandstones that exhibit large-scale tabular cross-bedding in the Willie P Mine. Similar relationships between uranium mineralization and sedimentary features have been noted in the south high wall of the St. Anthony north pit.

While there is a strong northeasterly trend to the thickness contours of the Jackpile sandstone in the Laguna district (which includes the Cebolleta Land Grant), there is no similar trend to individual uranium deposits. Baird et al. (1980) state that there is an apparent northwest trend with respect to mineralization in the St. Anthony area. This northwest trend, which was not observed by Sohio geologists at the former JJ #1 Mine (Jacobsen, 1980), may have resulted from the erosional retreat of the Jackpile Sandstone outcrop (Baird et al., 1980) and the subsequent oxidation and redistribution of uranium mineralization closer to the outcrop. Additional analyses of drill-hole data and contouring of grade-thickness products for the un-mined uranium deposits in the L-Bar portion of the Cebolleta Land Grant do not indicate any discernable regional trend to mineralization, but deposit-scale trends were observed from this work.

MINERALOGY

Coffinite [$U(SiO_4)_{1-x}(OH_{4x})$] and uraninite (UO_2) are the principal uranium minerals in the primary and redistributed mineralized zones at the St. Anthony deposits (Moench and Schlee, 1978; Robertson and Associates, unpubl. report for Sohio Western Mining Company, 1978; Adams et al., 1978). Organo-uranium complexes have also been reported from St. Anthony (Baird et al., 1980), although these mineralized zones may also contain weakly crystalline coffinite as the principal uranium mineral. Several samples collected from the St. Anthony north and south pits, including a high-grade pod of remnant mineralization in the north highwall of the south pit, yielded samples containing fine-grained and weakly crystalline coffinite as the principal uranium mineral, with minor uraninite overgrowths (Caldwell, 2019), as identified by polished section and XRD analysis (Caldwell, 2019).

Post-Mine Stability of Uranium Minerals

Assessment of uranium minerals hosted in Jurassic-age continental arkosic sandstones of the Jackpile Sandstone Member, exposed in former open-pit mine subcrops of the St. Anthony north and south pits, shows that post-mine, weathering-derived replacement of reduced uranium minerals has locally modified such minerals to a series of variably-hydrated, highly-oxidized derivatives (Caldwell, 2019).

Because uranium minerals, especially carbonates and sulfates, are soluble under weakly- to low-pH conditions (Brugger et al., 2015), the development of such minerals identified in this study and that of Caldwell (2019) at St. Anthony, following open pit mining, indicates that hydrated sulfate and carbonate minerals were engendered through reaction of reduced uranium minerals with oxidizing, near-neutral pH regional groundwaters. The presence of kaolinite and illite suggest that these minerals are likely part of the original uranium-mineralization suite, as each of these minerals represent at least weakly-acidic solution compositions (e.g., Anderson, 1982).

Reduced Uranium Minerals

X-Ray diffraction analyses of surface and near-surface mineralized samples (see next paragraph) indicate that "coffinite" [generally $U(SiO_4)_{1-x}(OH)_{4x}$] and poorly-crystalline "uraninite" are present locally as geochemically residual reduced uranium minerals. Pyrite is identified in trace amounts, and only locally. These reduced minerals are considered to represent original uranium distribution at St. Anthony in our assessment of post-mining geochemical reactions.

St. Anthony Post-Mining Uranium Minerals

To assess the effects of post-mining oxidation on the reduced and partially oxidized ore minerals in the St. Anthony mine, surface and very near-surface samples were collected from former open pit mine exposures; samples generally comprised crusty to efflorescent patches of gaudy cream-yellow to greenish-amber minerals that displayed anomalous radioactive signatures. Some grey, interstitial mineralization was also sampled so as to represent likely reduced uranium occurrence. No woody or obviously organic material was observed in our sample traverses at St. Anthony.

Although it is acknowledged that uranium dissolution and mobility is enhanced in groundwaters characterized by near-neutral pH and elevated carbonate activity (e.g., see Eröss, et al., 2018; uranium mobile as UO_2^{++}(aq); vanadium mobile as vanadate oxyanionVO_4^{+3}(aq) (e.g., see Gustaffson, 2019)), St. Anthony mineral assemblages, which include patchy to interstitial gypsum (Caldwell, 2019), suggest that Ca^{++}(aq) activity was likely too great to permit spatially-significant uranium mi-

gration; instead, we suggest that reduced and partially-oxidized uranium minerals were oxidized and variably hydrated *in-situ* with nominal lateral uranium transport. We also acknowledge that this apparent lack of lateral migration may be a function of time such that geographically-significant post-mining uranium re-distribution is not as yet evident.

Post-mining uranium minerals comprise sulfates and carbonates, with scant phosphates. The most volumetrically-important St. Anthony post-mining uranium minerals as determined by Caldwell (2019) are the sulfates zippeite [$K_3(UO_2)_4(SO_4)_2O_3(OH)\cdot 3H_2O$] and natrozippeite [$Na_5(UO_2)_8(SO_4)_4O_5(OH)_3\cdot 12H_2O$], with minor jachymovite [$(UO_2)_8(SO_4)(OH)_{14}\cdot 13(H_2O)$]; these sulfates are associated with ubiquitous gypsum. The St. Anthony Mine host rocks, via weathering-related oxidative destruction of widespread but volumetrically minor pyrite, apparently provided the locally-derived, weakly-acidic solutions (Garrels and Christ, 1968) necessary for the development of these sulfate minerals. The occurrence of Na-zippeite, and associated uranyl Na-carbonate minerals noted below, indicates that groundwaters are characterized by high $aNa^+(aq)$ and, as indicated by widespread gypsum, high $aCa^{++}(aq)$.

Carbonate-hosted uranium minerals comprise andersonite [$Na_2Ca(UO_2)(CO_3)\cdot 6H_2O$], cejkaite [$Na_4(UO_2)(CO_3)_3$], and trace oswaldpeetersite [$(UO_2)_2(CO_3)(OH)_2\cdot 4H_2O$] as efflorescent coatings and crusts on fractures along mine highwalls. Scant but widespread calcite is observed with these carbonate minerals. The occurrence of these uranyl carbonates represent the modification of reduced uranium minerals by high $aNa^+(aq)$, near-neutral pH groundwaters (e.g., see figure 1 in Xie et al., 2019; Garrels and Christ, 1968); this observation is consistent with andersonite occurrences in the Ambrosia Lake district (Section 31 Mine, Wiesenburger and Chávez, 1979) and supports the assessment that the recent groundwater modification of Cebolleta Land Grant uranium ores was provoked by near-neutral, oxidizing solutions.

Phosphate-hosted uranium comprises a series of local and volumetrically scant minerals consisting of sabugalite [$HAl(UO_2)_4(PO_4)_4\cdot 16(H_2O)$], autunite [$Ca(UO_2)_2(PO_4)_2\cdot 10\text{-}12H_2O$], meta-autunite [$Ca(UO_2)_2(PO_4)_2\cdot 2\text{-}6(H_2O)$], and trace chernikovite [$(H_3O)_2(UO_2)_2(PO_4)_2\cdot 6(H_2O)$] (Caldwell, 2019). Uranium phosphate minerals display generally limited solubility (Munasinghe et al., 2020) and represent moderately- to weakly-acidic pH weathering environments; their presence therefore suggests that locally lower-pH conditions existed during St. Anthony Mine phosphate-mineral genesis. Given the generally arkosic nature of the Jurassic-age host rocks, it is likely that St. Anthony Mine phosphate is sourced from the weathering of residual apatite.

We conclude that recent, weakly-acidic to near-neutral groundwaters characterized by geochemically high activities of $Na^+(aq)$ and $Ca^{++}(aq)$ are responsible for post-mining modification of reduced uranium ore minerals of the St. Anthony mine. Local low-pH environments were likely engendered by oxidative destruction of pyrite, permitting the development of uranyl phosphate minerals and serving as a source of sulfate. The apparent limited spatial mobility of the observed post-mining sulfate, carbonate, and phosphate uranium minerals is a function of the general but time-dependent stability of these minerals in the current oxidizing open pit mine environment and the limited time since these minerals were developed upon cessation of mining.

SUMMARY

Sandstone-hosted uranium deposits on the Cebolleta Land Grant are present as *trend, redistributed, and remnant* type deposits throughout the 80 to 120 ft (24 to 27 m) thickness of the Jackpile Sandstone. *Trend*-type mineralization displays a strong affinity to carbonaceous material, in particular humate, while carbonaceous material is generally absent in *redistributed* and *remnant* mineralization. Coffinite and uraninite are the principal uranium minerals (Caldwell, 2019) in the deposits, whereas post-mining oxidation of mineralization has resulted on the formation of uranium-bearing sulfate and carbonate minerals.

ACKNOWLEDGMENTS

We extend our appreciation to Allan V. Moran and Jeffrey D. Phinisey for their thoughtful and constructive reviews of this paper. We thank Westwater Resources, Inc., and Christopher M. Jones for providing access to historical data on the uranium deposits at St. Anthony and L-Bar, and for support for preparation of illustrations. The senior author thanks his former colleagues at Neutron Energy, in particular Michael W. Coleman and David Hertzke, both of whom contributed greatly to the understanding of the geology of the uranium deposits on the Cebolleta Land Grant, and their individual and collective efforts are hereby acknowledged. Samantha Caldwell's work was funded by New Mexico EPSCoR (funded by the National Science Foundation, NSF, award #IIA-1301346) and in part by Westwater Resources, Inc.

REFERENCES

Adams, S.S., Curtis, H.S., Hafen, P.L., and Salek-Nejad, H., 1978, Interpretations of Postdepositional Processes Related to the Formation and Destruction of the Jackpile-Paguate Uranium Deposit, Northwest New Mexico: Economic Geology, v. 73, p. 1635-1654.

Adams, S.S., and Saucier, A.E., 1981, Geology and recognition criteria for uraniferous humate deposits, Grants uranium region, New Mexico, final report: U.S. Department of Energy, Open-file Report GJBX-2(81), 225 p.

Aubrey, W.M., 1992, New interpretations of the stratigraphy and sedimentology of uppermost Jurassic to lowermost Cretaceous strata in the San Juan Basin of northwestern New Mexico: U.S. Geological Survey, Bulletin 1808-J, 17 p.

Baird, C.W., Martin, K.W, and Lowery, R.M., 1980, Comparison of braided-stream depositional environment and uranium deposits at Saint Anthony underground mine: New Mexico Bureau of Mines and Mineral Resources, Memoir 38, p. 292-298.

Beck, R.G., Cherrywell, C.H., Earnest, D.F., and Fern, W.C., 1980, Jackpile-Paguate deposit – a review: New Mexico Bureau of Mines and Mineral Resources, Memoir 38, p. 269-275.

Brookins, D.G., 1975, Uranium Deposits of the Grants, New Mexico, Mineral Belt: U.S. Energy Research and Development Administration Final Report GJBX-16(76), 153 p.

Brookins, D.G., 1979, Uranium Deposits of the Grants, New Mexico Mineral Belt (II): U.S. Department of Energy Open-file Report GJBX-141(79),

411 p.
Brugger, J., Burns, P., and Meisser, N., 2003, Contribution to the mineralogy of acid drainage of uranium minerals: Marecottite and the zippeite-group: American Mineralogist, v. 88, no. 4, p. 676-685.
Caldwell, S., 2018, Paragenesis of uranium minerals in the Grants Mineral Belt, New Mexico, applied geochemistry and the development of oxidized uranium mineralization [M.S. thesis]: Socorro, New Mexico Institute of Mining and Technology, 178 p.
Cather, S.M., Zeigler, K.E., Mack, G.H., and Kelley, S.A., 2013, Toward standardization of Phanerozoic stratigraphic nomenclature in New Mexico: Rocky Mountain Geology, v. 48, no. 2, p. 101-124.
Cuney, M., and Kyser, K., 2008, Recent and not-so-recent developments in uranium deposits and implications for exploration: Mineralogical Association of Canada, Short Course 39, 257 p.
Dahlkamp, F.J., 1993, Uranium Ore Deposits: Berlin, Springer-Verlag, 460 p.
Dahlkamp, F.J., 2010, Uranium Deposits of the World, USA and Latin America: Berlin, Springer-Verlag, 516 p.
Dickinson, W.R., and Gehrels, G.E., 2010, Implications of U-Pb ages of detrital zircons in Mesozoic strata of the Four Corners region for provenance relations in time and space: New Mexico Geological Society, Guidebook 61, p. 135-146.
Dillinger, J.K., 1990a, Geologic and Structure Contour Maps of the Gallup 30' by 60' Quadrangle, McKinley County, New Mexico: U.S. Geological Survey Miscellaneous Investigations Series Map I-2009, scale 1:100,000.
Dillinger, J.K., 1990b, Geologic map of the Grants 30' by 60' quadrangle, west-central New Mexico: U.S. Geological Survey, Coal Investigations Map C-118-A, scale 1:100,000.
Erőss, A., Csondor, K., Izsák, B., Vargha, M., Horváth, Á., and Pándics, T., 2018, Uranium in Groundwater – The Importance of hydraulic regime and groundwater flow system's understanding: Journal Environmental Radioactivity, v. 195, p. 90-96.
Fitch, D.C., 1980, Exploration for uranium deposits, Grants mineral belt: New Mexico Bureau of Mines and Mineral Resources, Memoir 38, p. 40-51.
Garrels, R.M., and Christ, C.L., 1965, Solutions, Minerals, and Equilibria: New York, Harper and Row, 450 p.
Goff, F., Kelly, S.A., Goff, C.J, McCraw, D.J., Osborn, G.R., Lawrence, J.R., Drakos, P.G., and Skotnicki, S.J., 2015, Geologic map of Mount Taylor, Cibola and McKinley Counties, New Mexico: New Mexico Bureau of Geology and Mineral Resources, Open-file Report OFR-571, scale 1:36,000.
Granger, H.C., and Santos. E.S., 1986, Geology and ore deposits of the section 23 mine, Ambrosia Lake district, New Mexico: American Association of Petroleum Geologists, Studies in Geology 22, p. 185-210.
Gustaffson, J.P., 2019, Vanadium Geochemistry in the Biogeosphere – Speciation, Solid-Solution Interactions, and Ecotoxicity: Applied Geochemistry, v. 102, p. 1-25.
Hatchell, W.O., and Wentz, C., 1981, Uranium Resources and Technology, A Review of the New Mexico Uranium Industry 1980: Santa Fe, New Mexico Energy and Minerals Department, 226 p.
Jacobsen, L.C., 1980, Sedimentary controls on uranium ore at L-Bar deposits, Laguna district, New Mexico: New Mexico Bureau of Mines and Mineral Resources, Memoir 38, p. 284-291.
Kelley, V.C., 1955, Regional Tectonics of the Colorado Plateau and Relationship to the Origin and Distribution of Uranium: University of New Mexico Publications in Geology No. 5, 120 p.
Kittel, D.F., Kelley, V.C., and Melancon, P.E., 1967, Uranium deposits of the Grants region: New Mexico Geological Society, Guidebook 18, p. 173-183.
Lucas, S.G., and Anderson, O.J., 1997, The Jurassic San Rafael Group, Four Corners region: New Mexico Geological Society, Guidebook 48, p. 115-155.
McLemore, V.T., 2010, The Grants Uranium District, New Mexico: Update on source, deposition, and exploration: The Mountain Geologist, v. 48, no. 1, p. 23-44.
McLemore, V.T., and Chenoweth, W.L., 1991, Uranium mines and deposits in the Grants district, Cibola and McKinley counties, New Mexico: New Mexico Bureau of Mines and Mineral Resources, Open-file Report 353, 10 p.
McLemore, V.T., Hill, B., Khalsa, N., and Lucas Kamat, S.A., 2013, Uranium resources in the Grants uranium district, New Mexico: An Update: New Mexico Geological Society, Guidebook 64, p. 117-126.
Moench, R.H., 1963, Geologic limitations of the age of uranium deposits in the Laguna district: New Mexico Bureau of Mines and Mineral Resources, Memoir 15, p. 156-166.
Moench, R.H., and Schlee, J.S., 1967, Geology and Uranium deposits of the Laguna district, New Mexico: U.S. Geological Survey, Professional Paper 519, 117 p.
Moran, A.V., and Daviess, F., 2014, NI 43-101 Technical report on resources, Cebolleta uranium project Cibola County, New Mexico, USA: Uranium Resources, Inc., 122 p. http://www.uraniumresources.com/docs/default-source/Technical-Reports/ni-43-101-technical-report-on-resources-cebolleta-uranium-project-cibola-county-new-mexico-usa---april-1-2014.pdf?sfvrsn=0 (accessed January 23, 2020).
Munasinghe, P.S., Elwood Madden, M., Books, S., Elwood Madden, A., 2020, Dynamic interplay between uranyl phosphate precipitation, sorption, and phase evolution: Applied Geochemistry (in-review).
Nash, J.T., 1968, Uranium deposits in the Jackpile Sandstone, New Mexico: Economic Geology, v. 63, p. 737-750.
Owen, D., Walters, L.J., and Beck, R.G., 1984, The Jackpile Sandstone Member of the Morrison Formation in west-central New Mexico – a formal definition: New Mexico Geology, v. 6, p. 45-52.
Rautman, C.J. (compiler), 1980, Geology and mineral technology of the Grants uranium region 1979: New Mexico Bureau of Mines and Mineral Resources, Memoir 38, 400 p.
Schlee, J.S., and Moench, R.H., 1963a; Geologic Map of the Moquino Quadrangle, New Mexico: U.S. Geological Survey, Geologic Map GQ-209, scale 1:24,000.
Schlee, J.S. and Moench, R.H., 1963b, Geologic Map of the Mesita Quadrangle, New Mexico: U.S. Geological Survey, Geologic Map GQ-210, scale 1:24,000.
Wilton, T., 2017, Uranium deposits at the Cebolleta project, Laguna mining district, Cibola County, New Mexico: New Mexico Geology, v. 39, no. 1, p. 1-10.
Woodward, L.A., 1982, Tectonic framework of Albuquerque country: New Mexico Geological Society, Guidebook 33, p. 141-145.
Xie, Y., Chen, C., Ren, X., Wang, X., Wang, H., and Wang, X., 2019, Emerging natural and tailored materials for uranium-contaminated water treatment and environmental remediation: Progress in Materials Science, v. 103, p. 180-234.

New Mexico Geological Society, Special Publication 14, Geology of the Mount Taylor Area, 2020, p. 77-88.

THE JACKPILE-PAGUATE URANIUM MINE, GRANTS URANIUM DISTRICT: CHANGES IN PERSPECTIVES FROM PRODUCTION TO SUPERFUND SITE

Virginia McLemore[1], Bonnie A. Frey[1], Eliane El Hayek[2], Eshani Hettiarachchi[3], Reid Brown[4], Olivia Chavez[5], Shaylene Paul[6], and Milton Das[3]

[1]New Mexico Bureau of Geology and Mineral Resources, New Mexico Institute of Mining and Technology, 801 Leroy Place, Socorro, New Mexico 87801, virginia.mclemore@nmt.edu;
[2] University of New Mexico, Department of Civil, Construction and Environmental Engineering, University of New Mexico, Albuquerque, New Mexico 87131;
[3]Department of Chemistry & Biochemistry, University of California San Diego, Gilman Drive, La Jolla, Ca, 92093;
[4]Wyoming Department of Environmental Quality, Cheyenne, Wyoming 82001;
[5]Boston University, Department of Physiology and Biophysics, Boston, Massachusetts 02118; and
[6]Navajo Technical University, Crownpoint, New Mexico 87313

Abstract—Production from the Jackpile-Paguate deposit ceased in 1982, ending one of the world's largest uranium open-pit mines of the era. Jurassic Morrison Formation fluvial deposits provided suitable hosts for humate-bearing primary, redistributed and remnant sandstone uranium deposits in the area. Mining from uranium deposits in the northern Laguna Pueblo yielded more than 95.8 million lbs of U_3O_8, making it a world class uranium deposit. However, perspectives at the mine and throughout the Grants Uranium District, once the "uranium capital of the world", have changed with time from production and economic benefits for companies, miners, businessmen, and nearby communities, like the Pueblo of Laguna, to the modern focus on remediation, understanding the mobility of uranium, and mitigating the health effects for uranium mine workers and nearby residents. Thousands of miners lived and worked in the Grants District, and although health effects were beginning to be studied at that time, the long-term environmental and health effects are only now being recognized. Today, the mine's history remains relevant, as concerns about the release of elevated uranium concentrations in groundwater from the remediated area led to the Superfund designation of the site in 2013. Coincidentally, a research effort to examine the mobility, legacy and source of uranium began that same year by a team from New Mexico Institute of Mining and Technology and the University of New Mexico. Many research efforts were concentrated on the area in and around the Jackpile-Paguate Mine, resulting in numerous relevant reports that not only identify important mobility pathways for uranium, but also define biological, chemical and physical processes between uranium, workers, nearby residents and the ecosystem.

INTRODUCTION

Jackpile-Paguate Mine, located in the Laguna Subdistrict in the eastern portion of the Grants Uranium District in Cibola County (Fig. 1), developed one of the largest sandstone-hosted uranium deposits in the world (Holen and Finch, 1982; Dalkamp, 2010; McLemore, 2020a**)**. Uranium was originally used in nuclear weapons for the Cold War between the United States and Russia, but by the mid-1960's, uranium was used mostly to fuel commercial nuclear power electric plants. During uranium mining at the Jackpile-Paguate Mine, Grants was known as "the uranium capital of the world," and uranium production and exploration in the area resulted in economic benefits for nearby communities, including the Pueblo of Laguna, Grants, Gallup and other communities. Thousands of miners lived and worked in the Grants District, and health ef-

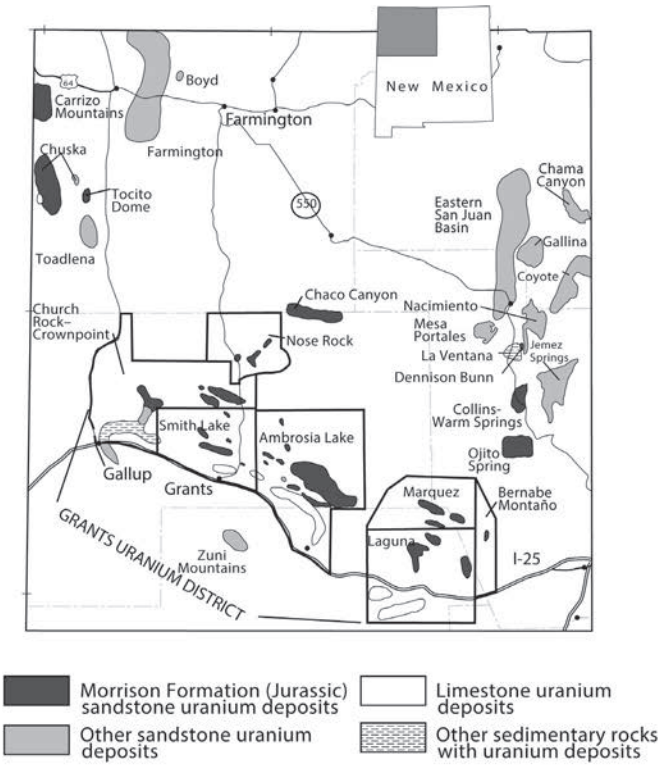

FIGURE 1. Subdistricts in the Grants Uranium District and other districts in the San Juan Basin, New Mexico with uranium deposits (McLemore and Chenoweth, 1989, 1991). Polygons outline approximate areas of known uranium deposits.

fects were beginning to be studied at that time. Since closure in 1982, the Jackpile-Paguate Mine has been plagued with expensive environmental cleanup and serious health issues in the former workers and local population. The mine was designated a Superfund site in 2013. Today, Laguna is a Pueblo nation comprised of six villages with a population of approximately 7700, and the area has been occupied since about A.D. 1300.

The Jackpile-Paguate deposit is one of many sandstone-hosted deposits in northwestern New Mexico. Most of the economic uranium deposits in New Mexico are hosted by sandstones, and most of the uranium production in New Mexico has come from the Westwater Canyon Member of the Jurassic Morrison Formation and the Jackpile Sandstone in the Grants Uranium District in McKinley and Cibola (formerly Valencia) counties (McLemore, 1983; McLemore and Chenoweth, 1989, 1991, 2017). The Grants District represents one large area in the southern San Juan Basin, extending from east of Laguna to west of Gallup, and consists of eight subdistricts (Fig. 1; McLemore and Chenoweth, 1989, 2017). During a period of nearly three decades (1951-1980), the Grants District yielded nearly 347 million lbs of U_3O_8, almost all of New Mexico's production, and more uranium than any other district in the United States (McLemore and Chenoweth, 1989, 2017). Although there are no operating mines in the Grants District today, numerous companies have acquired uranium properties and plan to explore and develop deposits in the district in the future (McLemore et al., 2013). Meanwhile, the Jackpile-Paguate Mine is undergoing additional reclamation. The purpose of this paper is to summarize the mining/reclamation history, the geology, the mineralized deposits, and environmental studies related to this large uranium deposit.

MINING HISTORY

Uranium exploration and production in New Mexico occurred in five periods: 1) radium boom, 1918–1923; 2) vanadium production, 1926–1940's; 3) post WWII, 1948–1970; 4) uranium boom, 1970–1982; and 5) a present uranium exploration and reclamation boom, 2008–present (McLemore and Chenoweth, 2017).

The Jackpile-Paguate Mine was discovered in 1951, during the 3rd period, and production continued into the 4th period. Exploration did not resume on the Pueblo of Laguna during the 5th period; activity during this time focused on reclamation and numerous studies on environmental effects of uranium mining. Potential uranium deposits north of the Jackpile-Paguate Mine have been recently examined for future development, but no permits have been issued at the time of this publication (McLemore et al., 2013; Wilton et al., 2020).

In 1951, the Anaconda Minerals Company obtained a permit from the Pueblo of Laguna to search for uranium on Laguna lands. In November 1951, an exploration team from Anaconda investigated an airborne radioactive anomaly on a mesa informally known as "Jack's Pile" on the Laguna lands (Hough, 1955). Subsequent field investigation and drilling led to the discovery of one of the world's largest sandstone-hosted uranium deposits, the Jackpile-Paguate Mine. Anaconda obtained a mining lease from the Pueblo of Laguna in May 1952. The lease was renegotiated in 1963 and 1976 to add additional land to the mine complex.

Anaconda signed a contract with the Atomic Energy Commission (AEC) on December 27, 1951, for the production of uranium concentrate by a mill to be built near Bluewater, approximately 64 km west of Laguna that would process ores from the Jackpile-Paguate and other mines in the Grants-Laguna area. This was the first of nine mills to be built in New Mexico (Albrethsen and McGinley, 1982; McLemore, 2020b).

In June 1956, exploration drilling by Anaconda made another major discovery in the area west of the Jackpile open pit mine (Kittel, 1963). This would be developed into the Paguate open pit. The Jackpile-Paguate Mine actually consists of three open pits: Jackpile (475 acres), North (140 acres) and South Paguate (400 acres) pits (Fig. 2). At the end of mining, there were 32 waste dumps and 23 low-grade ore stockpiles that were ultimately regraded, covered, and seeded (U.S. Department of the Interior, 1985). Underground mining began in 1971 with the opening of the Alpine Test. Anaconda opened nine underground adits with more than 1076 m of underground workings (Table 1). An adit is a horizontal or near horizontal entrance to underground workings to extract ore. The mine complex was within 305 m of the village of Paguate and included part of the perennial Rio Paguate. The Rio Moquino flows into the Rio Paguate, which flows south of the Jackpile-Paguate Mine into the Rio San Jose.

Approximately 800 people worked in the mine, and most were members of the Pueblo of Laguna. Although the mine solved unemployment in the Pueblo for the 29 years that mine was in operation, once the mine closed, unemployment dramatically rose again in the Pueblo. Subsequently, many former miners experienced serious health effects (respiratory diseases, cirrhosis of the liver, and lung cancer; Boice et al., 2008; Schubauer-Berigan et al., 2009).

The Woodrow Mine (Fig. 2; Table 2), near the Jackpile-Paguate Mine, was discovered by an airborne anomaly in 1954 and was named after the pilot of the plane that discovered the anomaly (Holmquist, 1970). A drill hole was enlarged to a two-compartment, 70 m shaft with two levels that intersected the mineralized circular breccia pipe (7 to 10 m diameter).

The first attempts of *in situ* uranium recovery in the Grants District was by Anaconda at the Windwhip deposit (Fig. 2), near the Jackpile-Paguate Mine, in April 1970 (Hunkin, 1971; Holen and Hatchell, 1986; McLemore et al., 2016). During *in situ* uranium recovery, a fluid is pumped into a uranium deposit that dissolves the uranium in place. That uranium-bearing fluid is then pumped back to the surface and processed to recover the uranium. The Windwhip deposit was below the groundwater level in the lower Jackpile Sandstone at a depth of 61-73 m. A kaolinitic clay in the Dakota Formation overlies the Jackpile Sandstone at this site and shales of the Brushy Basin Member underlie the deposit, forming an ideal geologic seal for *in situ* uranium recovery. Two injection wells and 29 production wells were utilized in two separate well fields to mine the deposit. The uranium-bearing fluids, called pregnant liquor, were pumped to a surge tank then resin tanks at the

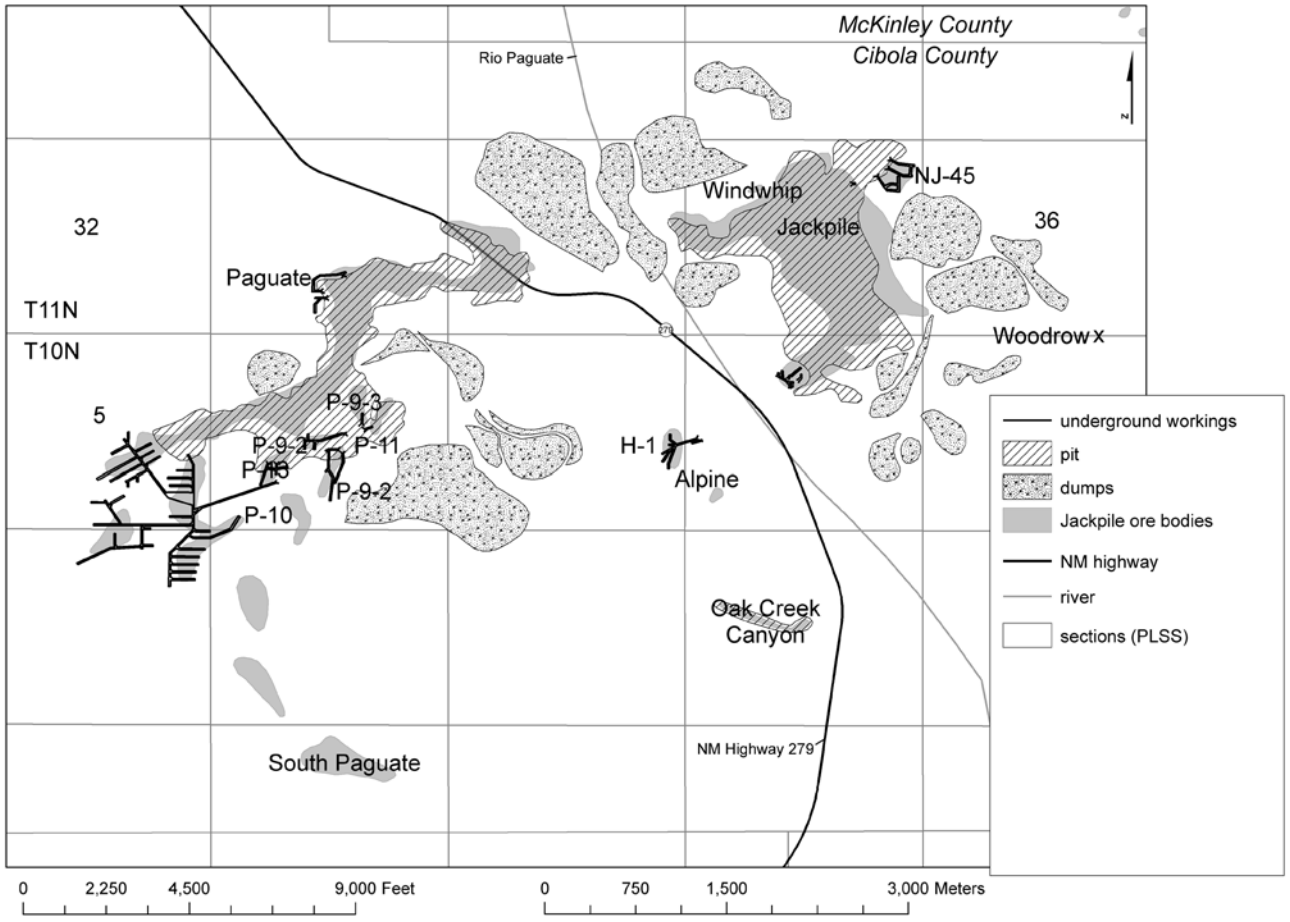

FIGURE 2. Mine map of the Jackpile-Paguate Mine, showing outlines of ore bodies and mine workings in 1982 (revised from McLemore and Chenoweth, 1991). PLSS= Public Land Survey System

TABLE 1. Summary of individual mine features (R.D. Lynn, written communication, March 13, 1982; U.S. Department of the Interior, 1985). Mine ID refers to the number of the mine feature in the New Mexico Mines Database (McLemore et al., 2005).

Mine Id	Mine	Start date	End date	Length	Depth	Comments
NMCI0018	Jackpile	5/1952	1982			pit
NMCI0035	North Paguate	6/1956				pit
NMCI0280	South Paguate					pit
NMCI0002	Alpine	9/1971	4/1973	110	70	Small operation, 2 adits, plugged
NMCI0015	H-1	7/1973	4/1975	475	140-200	Small operation, 2 adits, plugged, 3 vent holes, plugged
NMCI0030	P-9-2	3/1974	11/1976	100	140-160	Large operation, 5 adits, accessed from South Paguate pit
NMCI0031	P-9-3	11/1975	2/1976	310		
NMCI0033	P-11	11/1975	2/1976	170		
NMCI0037	PW 2/3	2/1978	8/1980	65	40-140	Small operation, 2 adits, accessed from North Paguate pit, back-filled
NMCI0034	P-13	6/1981	1/1982	150	200-600	Small operation, 2 adits, accessed from South Paguate pit, ore remains, workings flooded
NMCI0028	NJ-45	6/1981	2/1982	50	10	Small operation beneath Gavilan Mesa accessed from Jackpile pit, 3 adits, covered, only 1/3 of ore recovered
NMCI0032	P-7/10	1/1974	11/1981	2100	200-600	Large operation, workings filled with water, 2000 ft decline, covered
NMCI0281	P15/17					Operation approved but never developed, approximately 1.2 million short tons of ore remains (0.094-0.3 % U_3O_8)
NMCI0106	Woodrow	1953	1956	230		230 ft vertical shaft, backfilled
NMCI0105	Windwhip	1970	1970			Pit, *in situ* leach test

TABLE 2. Production from the Woodrow Mine (from U.S. Atomic Energy Commission, production records, NMBGMR file data; McLemore, 1983).

Year	Tons ore	Pounds U_3O_8	% U_3O_8	%V_2O_5
1953	47	1137	1.21	0.03
1954	3521	98,253	1.40	0.05
1955	553	5419	0.49	0.03
1956	1205	7712	0.32	0.03
Total	***5326***	***112,521***		

site. The uranium-bearing resin was shipped to the Anaconda Bluewater mill (Holen and Hatchell, 1986). It is unclear if the test was successful, but Anaconda did not use *in situ* recovery technology anywhere else in the Grants District.

From the initial production in 1953 to the final shipment in 1982, an estimated 26.6 million short tons of ore was produced from the Jackpile-Paguate open-pit mine, yielding 95,832,350 lbs of U_3O_8 (grade 0.39% U_3O_8; Table 3; New Mexico Bureau of Geology and Mineral Resources (NMBGMR) files; Grants Beacon, 1982; McLemore, 1983; McLemore et al., 2013, appendix 1). At the end of mining, approximately 23 million short tons of uranium material remained at the Jackpile-Paguate Mine in stock piles (21 million short tons at 0.02-0.059% U_3O_8) and known unmined resources (2 million short tons at 0.094-0.3 % U_3O_8; U.S. Department of the Interior, 1985). The total Jackpile-Paguate deposit, including production, remaining reserves, and ore estimated to have been removed by erosion, was approximately 165 million pounds of U_3O_8 (Holen and Finch, 1982). More than 400 million short tons of rock, waste rock and soil were removed from the area. The mine closed because of the depressed uranium market due to cancellations of new electric power plants, and the remaining lower grade material was not economic to mine at the time.

A Record of Decision (ROD) for the Jackpile-Paguate Uranium Mine Reclamation Project was signed between the Bureau of Land Management (BLM) and Bureau of Indian Affairs (BIA) in December 1986, and reclamation of the Jackpile-Paguate Mine began in 1989 (Olsen and Bone, 1991). Negotiations between Anaconda (now Atlantic Richfield Corporation, ARCO), BLM, BIA and Pueblo of Laguna resulted in Anaconda paying the Pueblo $45 million to reclaim the mine. The Pueblo formed the Laguna Construction Company to perform the work. The Jackpile-Paguate Mine would be the first uranium mine in the United States to be reclaimed, and there were no existing reclamation examples, guidance, laws or regulations to aid the Pueblo in the reclamation efforts (Olson and Bone, 1991). The Laguna Construction Company backfilled

TABLE 3. Uranium and vanadium production from the Jackpile-Paguate Mine, Laguna Subdistrict, Grants Uranium District. Vanadium production is unknown from 1971 to 1982. The production figures are the best data available and were obtained from published and unpublished sources (NMBGMR file data; McLemore, 1983; McLemore et al., 2013, appendix 1). Production figures are subject to change as new data are obtained.

Year of production	Quantity U_3O_8 lbs	Quantity V_2O_5 lbs
1952-1970	46,194,350	5,315,237
1971	3,822,000	
1972	4,390,000	
1973	4,650,000	
1974	4,588,000	
1975	3,880,000	
1976	5,366,000	
1977	4,860,000	
1978	6,196,000	
1979	4,290,000	
1980	3,600,000	
1981	3,328,000	
1982	668,000	
Total	***95,832,350***	***5,315,237***

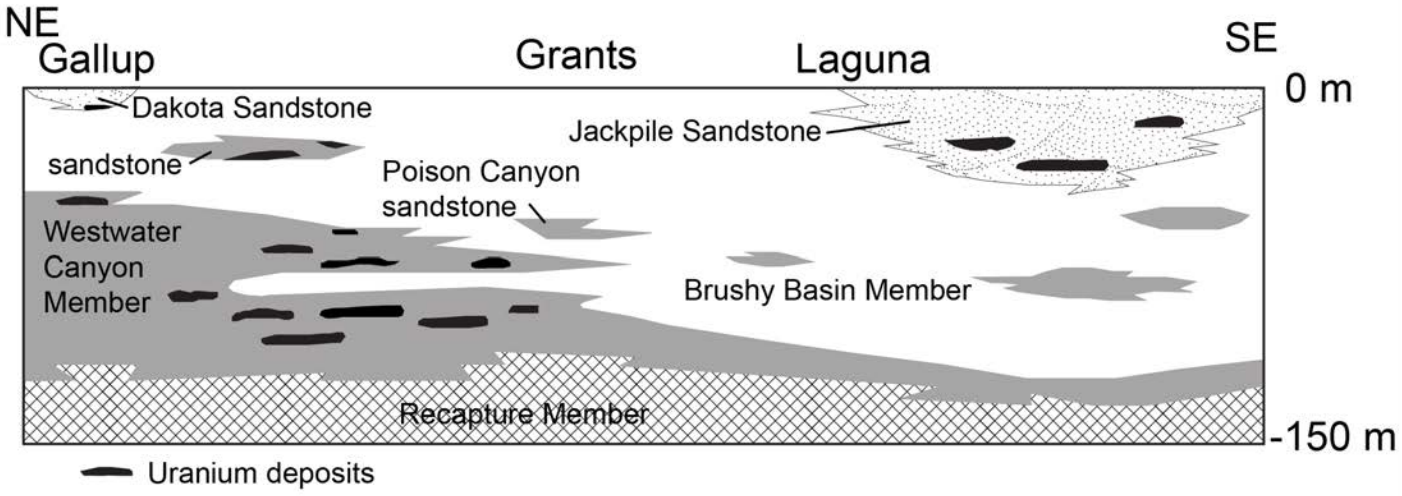

FIGURE 3. Schematic cross-section from Gallup to east of Laguna showing the relationship of the Jackpile Sandstone to the Westwater Canyon and Brushy Basin members of the Morrison Formation (modified from Hilpert, 1969).

the mines, removed uranium-bearing material near Rio Paguate, contoured and covered the remaining mine waste rock piles, and seeded the area with grasses and other plants. Reclamation was completed in 1995, and a 15-year monitoring study began. In September 2007, a ROD Compliance Assessment for the Jackpile-Paguate Mine was performed, and the results of that assessment determined that the post-reclamation was incomplete and had not met the requirements of the original ROD and Environmental Impact Statement. In response to many studies of environmental and health issues, results of monitoring studies, and local requests, the Jackpile-Paguate Mine was designated a Superfund site in 2013 and is in the Remedial Investigation and Feasibility stage (https://cumulis.epa.gov/supercpad/SiteProfiles/index.cfm?fuseaction=second.Cleanup&id=0607033#bkground, accessed 7/27/2020). In 2017, EPA required that ARCO conduct the Remedial Investigation and Feasibility Study (USEPA, 2013, 2018).

GEOLOGY

Stratigraphy

The Jurassic Morrison Formation consists of three members in the Grants District (oldest to youngest): the Recapture, Westwater Canyon, and Brushy Basin members. The ore-bearing Salt Wash Member of the Morrison Formation found in the Carrizo Mountains and the Shiprock District in western New Mexico is absent in the Laguna area. The Recapture Member hosts small uranium deposits locally but was not a significant source of production in the Grants District. The Westwater Canyon Member is the predominant host for uranium in much of the Grants District, especially in the Ambrosia Lake Subdistrict, and consists of 15 to 91 m of reddish-brown or gray arkosic sandstones with interbedded gray and green to greenish-gray shales (Nash, 1968; Hilpert, 1969). The Westwater Sandstone Member is thinner in the Laguna area compared to the Ambrosia Lake area (Hilpert, 1969). Westwater Canyon sandstones exhibit features typical of a fluvial environment, whereas the siltstones and shales are typical of overbank and lacustrine environments (Turner-Peterson, 1980). Shales of the Brushy Basin Member locally interfinger with the Westwater Canyon Member. The Brushy Basin Member is 30 to 152 m thick and consists of light greenish-gray shales and mudstones and a few interbedded sandstone lenses. The Brushy Basin Member is thicker in the Laguna area compared to the Ambrosia Lake area.

Although, the Westwater Canyon Member hosts several small uranium deposits in the Laguna Subdistrict, the larger more economic deposits are in the Jackpile Sandstone (Nash, 1968; Hilpert, 1969; McLemore, 1983). The Jackpile Sandstone overlies the Brushy Basin Member (Fig. 3) and is found only in the Laguna area. The Jackpile Sandstone is truncated by a basal Cretaceous unconformity and is overlain by the Cretaceous Dakota Formation. It consists of as much as 70 m of white kaolinitic sandstone with minor interbeds or lenses of pale green shale and mudstone, and features typical of a braided-stream environment are common (Baird et al., 1980; Jacobsen, 1980; Moench and Schlee, 1967). South of Laguna, the Jackpile Sandstone is truncated due to erosion, whereas north of Laguna the sandstone splits into two or more sandstones. There is a controversy as to the age and stratigraphic position of the Jackpile Sandstone. Many geologists included the Jackpile Sandstone in the Brushy Basin Member since geologic mapping shows the Jackpile Sandstone interfingering with the upper Brushy Basin Member (Moench and Schlee, 1967; Hilpert, 1969; Baird et al., 1980). However, Aubrey (1992) was one of the first geologists to suggest that the Jackpile Sandstone is equivalent to the Lower Cretaceous Burro Canyon Formation and should not be part of the Brushy Basin Member. Recent detrital-zircon ages from the Jackpile Sandstone further support a Cretaceous age and designation as a lateral equivalent to part of the Cretaceous Burro Canyon Formation (Dickinson and Gehrels, 2010; Dickinson, 2018).

Description of the uranium deposits

The Jackpile ore body was an elongate, primary tabular deposit approximately 2.4 km long and 0.8 km wide, and the Paguate ore body was more than 3.2 km long and several hundred m wide. Individual ore deposits were up to 4.6 m thick, and stacked ore deposits were up to 15 m thick and found mostly in the lower Jackpile Sandstone (Moench, 1963). Uranium is found as replacements of detrital grains, grain coatings, pore fillings, concentrations around clay galls, irregular and diffuse masses of uranium and humates, and thin, discontinuous coal-like lenses. Detrital uranium grains were reported by Jacobsen (1980) and Baird et al. (1980). Uranium commonly was found at sandstone-shale interfaces (Moench and Schlee, 1967; Beck et al., 1980). The ore minerals were coffinite and uraninite, with minor secondary uranium and vanadium minerals that were associated with humate and other organic material. Uranium ore grades were as high as 0.9% U_3O_8 (McLemore, 1983). Fossil logs are common in the Jackpile Sandstone, but unlike the highly uranium mineralized logs in the Ambrosia Lake Subdistrict, most of the Jackpile logs do not contain uranium minerals (Moench and Schlee, 1967; Hilpert, 1969). Although trace amounts of molybdenum and selenium were found associated with Jackpile ore, concentrations were less than those found associated with Westwater Canyon ore in the Ambrosia Lake Subdistrict and Brushy Basin ore in the Smith Lake Subdistrict (McLemore, 1983). The age of the Jackpile uranium deposits is 110-115 Ma, younger than primary uranium deposits elsewhere in the Grants District (Nash and Kerr, 1966; Lee, 1976; Brookins, 1980; McLemore, 2020a).

ENVIRONMENTAL AND URANIUM TRANSPORT STUDIES

There have been numerous environmental and health studies centered around the Jackpile-Paguate Mine and the Grants District. Early studies focused mostly on water availability (Risser et al., 1984) and quality (West, 1972; Kaufmann et al., 1976; Longmire and Brookins, 1982; Popp et al., 1984; Zehner, 1985), vegetation (Kelley, 1979), and health of workers (Schubauer-Berigan et al., 2009), nearby residents, and animals (Momeni et al., 1983; Lapham et al., 1989; Gilliland et

al., 2000). More recent studies are more inclusive of the entire ecosystem affected by uranium mining, defining the processes involved. These include a wide range of topics:

- concentrations of uranium in groundwater and surface water (Blake et al., 2017),
- uranium in vegetation and soils (Gorospe, 2013; El Hayek et al., 2018),
- bioaccumulation (El Hayek et al., 2018, 2019),
- the role of dust (Brown, 2017),
- uranium mineralogy (Moench, 1962; Caldwell, 2018, Hettiarachchi et al., 2019),
- uranium mobility (De Vore, 2015; Avasarala, 2018; Velasco et al., 2019),
- and microbial communities (Chavez, 2016).

From 2013 to 2018, a joint National Science Foundation-funded team of researchers from the New Mexico Institute of Mining and Technology (NMIMT) and the University of New Mexico (UNM) investigated uranium mobility, uranium sources and environmental studies in and around the Jackpile-Paguate Mine. The purpose of these studies (part of a New Mexico EPSCoR program called Energize New Mexico, https://www.nmepscor.org/who-we-are/timeline, accessed 7/27/2020) was to generate new research on uranium mining and legacy issues using modern techniques that were not available during the mining boom. The results of this work will aid decisions regarding uranium extraction and remediation, as well as aid environmental, community and individual health near areas affected by uranium deposits and resulting mining activities. What follows is a brief description of some of these studies; some are described elsewhere in this volume in more detail (Brown and Cadol, 2020; Pearce, 2020; Wilton et al., 2020).

Uranium mobility and accumulation

The interaction between mine wastes, stream sediments, and surface water of the Rio Paguate was evaluated in a study by Blake et al. (2017) to understand uranium mobility and accumulation adjacent to the Jackpile-Paguate Mine. The mineral coffinite ($U(SiO_4)\cdot nH_2O$) was identified in this study by X-Ray diffraction analyses from mine waste solids even after exposure to oxidizing conditions (i.e., weathering) for several decades (Blake et al., 2017; Caldwell, 2018). Uranium concentrations in these solids range from 320 to 9200 mg/kg, whereas uranium concentrations in the stream bed and stream bank sediments of the Rio Paguate range from 1 to 5 mg/kg. Higher uranium concentrations (2 to 21 mg/kg) were measured in sediments from a wetland area 4.5 km downstream from the mine. These observations may be explained by the elevated organic matter in wetland sediments and uranium's affinity for sorption to organic matter. Coffinite was not observed in the stream or wetland sediments.

Surface water samples, collected and analyzed between September 2014 and August 2016, revealed higher concentrations of uranium in surface water adjacent to the mine (35.3 to 772 µg/L) compared to water from the wetland (5.77 to 110 µg/L). Uranium concentrations from water samples from the hyporheic zone below the streambed are 20 to 30 times higher than the surface water concentrations from the same location at the same time. This could be due to the proximity of the hyporheic zone samples to the mine site and depositional processes at this location. The uranium concentrations in the Rio Paguate vary with season and appear to be affected by hydrogeological and geochemical processes at different times of the year. Snowmelt from nearby mountain peaks, monsoonal rains, or dry seasons could affect the mobility of uranium in the ecosystem by means of dissolution, dilution, adsorption, chemical precipitation or other geochemical processes.

Uranium distribution among particle-size fractions

Uranium partitioning by particle-size fractions in waste rock piles from within uranium waste materials can have a significant impact on the transport of uranium to the surrounding environment. The distribution of minerals and major and trace elements in different particle size fractions is an important factor in understanding the availability of minerals for dissolution and oxidation during weathering and the mobility of the resulting mineral constituents. Unpublished results of an ongoing project to understand the geochemical distribution within different particle size fractions are summarized here (McLemore, 2012; McLemore et al., 2018).

In most geologic materials, the composition of the different size fractions is a result of the composition of the parent material and the geologic, geochemical, and pedological processes responsible for the formation of the geologic materials, as well as post-mining blasting, hauling, dumping, and emplacement into the waste rock pile (McLemore et al., 2018). The composition of various size fractions provides an insight into what chemical changes can be expected as geological materials break down to smaller particles. Weathering of minerals involves mostly surface reactions, and the rates of these reactions depend upon the available reactive surface area of the mineral. Mineral surface area is dependent upon the mineralogy, irregularities in the mineral structure (such as fractures, element impurities, and crystal structure), the extent to which the mineral is liberated from the rock matrix, particle size (especially mineral grain size), particle shape, and the surface morphology (i.e., roughness of the mineral surface). Furthermore, when mineral surfaces are covered with coatings, such as iron oxyhydroxides or humates, oxidation and dissolution of the mineral can be inhibited. Thus, particles of different sizes expose different proportions of the surfaces for chemical reaction, which plays an important role in weathering and mobility of uranium in the environment.

Samples were collected in the field from waste rock piles at the St. Anthony open pits, located north of the Jackpile-Paguate Mine and analyzed in the laboratory. The samples from the St. Anthony pits are from the Jackpile Sandstone and are similar to material mined from the Jackpile-Paguate Mine. Waste material at the Jackpile-Paguate Mine is covered with topsoil and not available for sampling. A composite sample (generally 15-20 subsamples) of rock or other material was collected using picks, shovels and hand trowels at each site, homogenized, and stored in 5-gallon buckets. Each size fraction (bulk

or not sieved, 12.5-4.76, 4.76-2, 2-0.5, 0.5-0.125, and <0.125 mm) for chemical analyses was separated using stainless steel sieves and sent to ALS laboratories in Reno, Nevada, for analyses. Laboratory methods included whole-rock geochemistry, petrographic analysis, paste pH and conductivity, particle-size analysis, acid base accounting and net acid generation.

Numerous studies of waste rock piles from base and precious metal mines have shown that the smallest size fractions (<0.125 mm) contained the largest concentrations of metals (see Morkeh and McLemore, 2012; McLemore, 2012). However, the distribution of uranium in different particle size fractions of waste rock piles from uranium mines is more complex and currently under study. The amount of uranium increased with increasing particle size or was concentrated in the middle sizes (two fractions, 4.76 to 2 mm and 2 to 0.5 mm) in the St. Anthony samples, whereas arsenic and carbon had complex variations with change in grain size (McLemore et al., 2018). Uranium and vanadium show a strong correlation, indicating that these elements are associated with each other in these deposits. The samples are heterogeneous and range in concentration from 24 to 11,050 ppm uranium. Chemical analyses indicate that uranium is correlated (R>0.6) with vanadium, carbon, zirconium, yttrium, lead, arsenic, selenium, and heavy rare earth elements (Eu, Gd, Tb, Dy, Ho, Er, Tm, Yb, Lu). These results suggest that weathering of uranium deposits maybe more complex than weathering of metal deposits. More work is recommended to confirm and understand these complexities.

Dust Transport

In arid regions, dust transport and deposition are important processes of soil formation (Reheis et al., 1995). Natural and anthropogenic sources generate dust, which can impact soils downwind. Mining is of particular interest because a large amount of earth is moved, exposing erodible surfaces that contain ore as well as co-occurring gangue (non-economic minerals associated with the ore minerals) minerals, which can release contaminants into the surrounding area. Dust generation from active mine sites can be an important mechanism for contaminant movement. Understanding the mechanisms of dust generation as well as contaminant concentrations within the air column may be important in mine management strategies, such as where to locate exposed ore/waste rock stockpiles and how to develop remediation plans.

At the Jackpile-Paguate Mine site, dust movement and its transport of associated metals (uranium, vanadium, cobalt, chromium, manganese, and lead) were investigated (Brown, 2017). Dust samples were collected at 15 sites across the Jackpile-Paguate Mine site (Fig. 4) at 0.25 m, 0.5 m, 1.0 m and 1.5 m above the land surface. Dust collected at greater heights (1.0 and 1.5 m compared to 0.25 m) contained higher metal concentrations. Additionally, dust contained higher manganese, lead and chromium values than mine-site average soil concentration. Uranium concentrations in dust were highest at the 1.5 m collection height and were significantly elevated above average soil concentrations.

In contrast, mass flux (grams per day per meter squared) decreased with increasing sample collection height. The inverse relationship between concentration and mass flux is likely due to a positive feedback between particle-size fractionation, which occurs in the air column based on dust particle mass, and the increasing surface area of smaller dust particles. Results show that, by mass, the bulk of the sediment transport occurs in the first 25 cm above the land surface, which is consistent with results found in literature (Bagnold, 1936; Butterfield, 1999; Dong et al., 2004). However, natural processes concentrate contaminants of concern in the finer fractions of dust, which allow for suspension of contaminants and transport down wind.

Several processes were found to be important in controlling dust transport at the Jackpile-Paguate Mine site: vegetation, location (exposure to wind) and soil moisture (see Brown and Cadol, 2020). Location was the most important factor in determining dust flux. More exposed areas of the site were associated with higher dust flux, suggesting that location of waste and ore stockpiles should be based on minimizing exposure to wind.

Seasonal effects were also considered. New Mexico typically experiences a windy season in the spring and early summer. The results showed that dust flux was the greatest in the spring as expected. Unexpectedly, dust flux in the winter showed a marked decrease compared to the other three seasons despite having the highest two recorded wind gusts and a similar sustained winds profile compared to spring. The combination of elevated soil moisture and intermittent snow cover likely contributed to the observed reduction in dust flux during the winter. These results suggest that seasonal weather patterns should be incorporated into strategies that mitigate dust generation.

Bioaccumulation

Understanding the accumulation of uranium in plants is important to evaluate the transport and fate of uranium in biotic systems and to assess potential risk to humans, livestock and other organisms. A recent study at the Jackpile-Paguate Mine

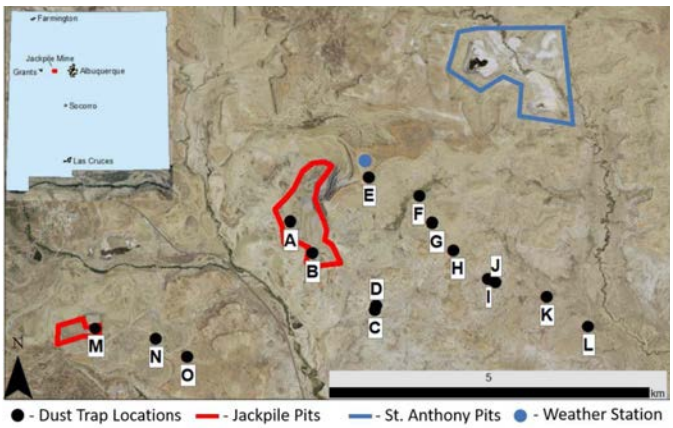

FIGURE 4. Site map of dust sampling at the Jackpile-Paguate Mine (modified from Brown, 2017). The black points represent dust trap locations. Solid lines indicate the extent of the pits. St. Anthony Mine is outlined by a dashed line. The star indicates the location of the weather station, which collects data on daily weather conditions.

measured uranium bioaccumulation in plant samples (shoots and roots) collected from the stream banks of the Rio Paguate near and within the wetland area up to 5 km downstream of the mine (El Hayek et al., 2018). Regional and abundant plants were collected (grass, willow [*Salix*], and cattail [*Typha latifolia L.*]) to assess potential human exposure at the site. The co-located sediments in the rhizosphere (the soil zone that surrounds plant roots) contained uranium concentrations up to twice the local uranium background, with the highest concentration measured in sediments collected from the rhizosphere of the wetland area (7-20 mg/kg; Blake et al., 2017). The rhizosphere of plants at these sites may also be exposed to the contaminated water of the Rio Paguate, with seasonal uranium concentrations ranging from 35 to 772 µg/L (Blake et al., 2017). Results indicated that grass roots accumulated uranium in concentrations 2 to 18 times higher (3.1-21.3 mg/kg) than willow and cattail roots. The highest uranium accumulation was detected in grass roots (21.3 mg/kg) at the wetland site, where sediment uranium concentrations were highest. The water chemistry at Rio Paguate (pH, calcium, uranium, and carbonate) suggests that aqueous ternary uranyl-carbonate complexes (Ca-U-CO_3) play an important role in uranium interaction with sediments and plant roots in the rhizosphere (Blake et al., 2017; El Hayek et al., 2018).

This research continued under lab conditions where hydroponic experiments were performed to examine the effect of calcium (0, 12 and 240 mg/L) and uranium (30, 100, 300 and 700 µg/L) concentrations in carbonate solutions at pH 7.5 (El Hayek et al., 2018, 2019). Indian mustard plant (*Brassica juncea*), a known uranium hyper-accumulator, was selected as the model organism. Scanning transmission electron microscopy and electron microprobe analyses showed that, in water free of calcium, uranium accumulated only in the cell walls at the surface of the root. No detectable accumulation of uranium was obtained at high calcium concentrations. The outcomes of these studies highlight the effect of initial uranium concentration and other co-occurring elements (such as calcium) on uranium speciation and bioavailability.

Microbiological Study at the Jackpile-Paguate Mine

Microbes can play an important role in the precipitation and dissolution of mineral components. A 2016 study aimed to characterize the microbial communities in the soil in relation to uranium concentrations and the effects of mining (Chavez, 2016). Six soil samples from areas close to the mine were taken aseptically (Fig. 4, sites A, C, D, I, K, L), and DNA was extracted and high-throughput metagenomic sequencing was performed at the National Center for Genome Resources in Santa Fe, New Mexico. The results showed a wide range of typical arid soil microbes and a strong representation from metal reducers (e.g., *Geobacter* spp.). There was also evidence that the relative abundances of some genera, including *Rhodopseudomonas*, *Bradyrhizobium* and *Rubrobacter*, are affected by concentrations of nickel, selenium and zinc. Uranium and background radiation did not appear to drive functional gene or phylogenetic differences among the soils sampled.

Uranium dissolution in lung fluids

Uranium is a naturally occurring element of which labile concentrations can increase due to human activities such as mining (Asic et al., 2017). This fairly abundant heavy metal is chemically toxic (LD_{50} = 14 mg/kg per body mass of an individual; LD_{50} is the lethal dose of uranium for 50% of an administered population) and can present radiological-toxicity depending on its isotopic composition and exposure route (Asic et al., 2017; Briner, 2010). During exposure to uranium, uranyl cations (UO_2^{2+}) bind to DNA in mammalian cells, combining to form a single molecular product (chemically known as a uranium-DNA adduct) that could cause mutations. The mutations trigger a range of protein synthesis errors, some of which may lead to various cancers, decrease in the antioxidative potential of lung tissues, and cause death of macrophages, the white blood cells important to the immune system (Stearns et al., 2005; Schneider et al., 2007; Periyakaruppan et al., 2007; Hsieh and Yamane, 2008; Pereira et al., 2012; Orona and Tasat, 2012). Cardiovascular and metabolic disease rates remain high among Navajo Nation residents near abandoned uranium mines in the southwestern United States.

Human exposure to uranium occurs via two major routes: 1) oral exposure via drinking water and food, and 2) inhalation of uranium-contaminated dust. Studies suggest both exposure routes play a vital role in the cardiovascular and metabolic disease rates (Harmon et al., 2017). Dust particles that are smaller than 10 µm can enter human respiratory systems and particles much smaller in size (less than 5 µm) can reach the alveolar region of human lungs, where the blood-gas exchange occurs. Particles that are not taken into the lungs continue to the gastro-intestinal tract (Kastury et al., 2017). The dust particles that reach the alveolar region of the lungs can interact with lung fluids thereby changing their chemical composition. Similarly, particles that continue to the gastro-intestinal tract can ultimately reach the stomach and interact with gastric fluids.

In the first phase of our studies (Hettiarachchi et al., 2019), dust samples collected from four different locations around the Jackpile-Paguate Mine (Fig. 4, sites A,C, E and G) and a sediment sample from St. Anthony Mine, which is five kilometers to the northeast, were investigated for their interactions in two simulated lung fluids (SLFs): 1) Artificial Lysosomal Fluid (ALF), which simulates the acidic fluid conditions inside macrophages, the white blood cells that eliminate dust particles from the alveolar region of the lungs (Stine and Brown, 1996); and 2) Gamble's Solution (GS), which simulates the pH neutral extracellular environment in the interstitium of the lungs (Guney et al., 2017; Kastury et al., 2017). The collected dust was treated with these SLFs in custom-built glass reactors for 24 hours. The system kept oxygen purged and at 37°C. The SLFs were then analyzed for their total dissolved uranium. In brief, the results show that the solid uranium in the dust dissolves in the lung fluids producing primarily UO_2^{2+} as confirmed by colorimetric measurements of uranyl-curcumin-triton-X system. The geochemical modeling studies conducted with PHREEQC 3.3.8 combined with experimental data further confirmed that the solubility of dust-uranium is controlled by the mineralogy

of the dust particles. The uranium dissolutions, modeled introducing one mineral at a time, suggested that autunite, carnotite, tyuyamunite, and uraninite were more soluble in GS than in ALF, with total dissolved uranium in GS/ALF ratios of 1.58, 16.1, 17.8, and 1.01, respectively. The uranium-bearing minerals schoepite, torbernite, coffinite, and uranophane were more soluble in ALF than in GS, with total dissolved uranium in GS/ALF ratios of 0.58, 0.26, 0.95, and 0.26, respectively. This suggests that understanding the behavior of inhaled uranium-containing dust in these mining areas, with the specific focus on site mineralogy, is vitally important in evaluating the chemical toxicity of uranium, independent of radiation studies.

In the second phase of the research, the researchers examined the fate of uranium particles in the gastro-intestinal tract. Dust was collected from three sites near Jackpile-Paguate Mine (Sites K, L and M in Fig. 4) and sediment from near St. Anthony Mine and a sample of mine waste rock from St. Anthony Mine was used. Here, the particles interacted with solutions that mimic the highly acidic gastric fluid of stomach and the slightly acidic fluid of the lower intestinal tract. The studies conducted with simulated gastro-intestinal fluids have shown higher uranium solubility compared to respiratory system simulations, also dependent on the various mineralogical components in the dust.

SUMMARY

The life cycle of the Jackpile-Paguate Mine has played an important role in U.S. and local history, supplying what has been considered a critical defense and energy material to the nation (Federal Register notice, 2018) and presenting a hazard to local communities and the environment. Today most of the high-grade uranium deposits in the Jackpile-Paguate area have been mined out. Three low-grade ore piles remain at the site and were regraded, contoured, covered, and seeded. Additional uranium resources remain in the Jackpile-Paguate area, especially in the St. Anthony Mine area (Wilton et al., 2020), but it is unknown how much uranium remains or if remaining uranium will ever be economic to recover. Additional mineral-resource studies are required before any future mining of uranium occurs. The Laguna Pueblo must agree to any further mining of uranium on Pueblo lands. Therefore, it is unlikely that any of the deposits at the Jackpile-Paguate Mine will be mined in the near future because of poor economic conditions, safety and public health concerns, community and cultural concerns, and other challenges common to uranium mining in New Mexico, as summarized by McLemore et al. (2013).

The recent hydrologic, biologic and chemical research by UNM and NMIMT workers has identified several pathways that contaminants can enter the environment, the community, and human physiology through water, soil, dust and plants. The results may help guide extraction, remediation and health care considerations for generations. Among the conclusions:

- Coffinite, a silicate with reduced uranium species, can remain in the ecosystem after several decades of exposure to oxidizing conditions.
- Seasonal variations have considerable impact on the mobilization of uranium, whether by water or wind.
- Rock and sediment grain size play an important role in the mobility of metals. Continued research will help identify the size fractions that concentrate uranium in mine sites like the Jackpile-Paguate Mine.
- Wind patterns should be considered when placing mine waste piles and other mine features.
- Uranium accumulation in plants can be affected by the water chemistry in a system (e.g., calcium in carbonate water can prevent uranium from accumulating in plants when uranium concentrations $\leq$700 µg/L).
- The soil microbes in the former mine site represent genera that are known to chemically reduce metal species.
- Mineralogy of dust particles and pH of lung and gastric fluids influence if and where uranium dissolves from inhaled dust in the body.

Although the mining of resources for weapons-grade uranium and uranium fuel at Laguna Pueblo has ceased and is unlikely to resume, the legacy of mining activities continues to provide challenges for local communities, ARCO, federal and local governments, and researchers. Perspectives toward this subject will likely continue to evolve as new remediation, energy, extraction and analytical technologies are developed.

ACKNOWLEDGMENTS

This paper is part of an on-going body of research conducted by workers at NMIMT and UNM, including long-term New Mexico mineral resource studies at the NMBGMR. Dr. Nelia Dunbar, Director and State Geologist, supported this research. Ted Wilton, Dan Cadol, and Johanna Blake reviewed an earlier version of this manuscript and their comments are appreciated. Funding of student and post-doctoral research summarized in this paper was by New Mexico EPSCoR (NSF award #IIA-1301346), the NMBGMR, the Mineral Engineering Department of NMIMT, the Society for Mining, Metallurgy and Exploration, the New Mexico Geological Society, the U.S. Geological Survey, National Institute of General Medical Sciences Grant 8P20GM103451-12, Institutional Development Award (IDeA) from the National Institute of General Medical Sciences of the National Institutes of Health (Grant #: P20GM103451), and the NCGR New Mexico IDeA Networks of Biomedical Research Excellence Sequencing and Bioinformatics Pilot Project (Award #: NMINBRE_T.Kieft_Oct_2014). José Cerrato, Sumant Avasarala, Bruce Thompson, Ted Wilton, and Johanna Blake provided many lively discussions and assistance throughout this project. Additional technical support by Marcus Silva, Alexandra Pearce, John Asafo-Akowuah and Samantha Caldwell is appreciated. We also wish to express our gratitude to the many individuals at NMIMT, UNM, and New Mexico EPSCoR for their time and dedication to the recent projects described in this paper.

REFERENCES

Albrethsen, H., Jr., and McGinley, F.E., 1982, Summary history of domestic uranium procurement under US Atomic Energy Commission contracts—final report: United States Department of Energy, Report GJBX-220 (82), 161 p.

Asic, A., Kurtovic-Kozaric, A., Besic, L., Mehinovic, L., Hasic, A., Kozaric, M., Hukic, M., Marjanovic, D., 2017, Chemical toxicity and radioactivity of depleted uranium: The evidence from in vivo and in vitro studies: Environmental Research, v. 156, p. 665–673. https://doi.org/10.1016/j.envres.2017.04.032.

Aubrey, W.M., 1992, New interpretations of the stratigraphy and sedimentology of uppermost Jurassic to lowermost Upper Cretaceous strata in the San Juan Basin of northwestern New Mexico: U.S. Geological Survey, Bulletin 1808-J, p. 1–17.

Avasarala, S., 2018, Physical and chemical interactions affecting U and V transport from mine wastes [PhD. Dissertation]: Albuquerque, University of New Mexico, 172 p.

Bagnold, R.A., 1936, The movement of desert sand: Proceedings of the Royal Society of London, v. 157, Issue 892, p. 594-620.

Baird, C.W., Martin, K.W, and Lowery, R.M., 1980, Comparison of braided-stream depositional environment and uranium deposits at Saint Anthony underground mine: New Mexico Bureau of Mines and Mineral Resources, Memoir 38, p. 292-298.

Beck, R.G., Cherrywell, C.H., Earnest, D.F., and Fern, W.C., 1980, Jackpile-Paguate deposit – a review: New Mexico Bureau of Mines and Mineral Resources, Memoir 38, p. 269-275.

Blake, J.M., De Vore, C.L., Avasarala, S., Ali, A.M., Roldan, C., Bowers, F., Spilde, M.N., Artyushkova, K., Kirk, M.F., Peterson, E., 2017, Uranium mobility and accumulation along the Rio Paguate, Jackpile mine in Laguna Pueblo, New Mexico: Environmental Science: Processes and Impacts, v. 19, p. 605–621

Boice, J.D., Cohen, S.S., Mumma, M.T., Chadda, B., and Blot, W.J., 2008, A cohort study of uranium millers and miners of Grants, New Mexico, 1979-2005: Journal of Radiological Protection, v. 28, no. 3, p. 303-326

Briner, W., 2010, The toxicity of depleted uranium: International Journal of Environmental Research and Public Health, vol. 7, p. 303–313. https://doi.org/10.3390/ijerph7010303.

Brookins, D.G., 1980, Geochronologic studies in the Grants mineral belt, *in* Rautman, C.A., ed., Geology and mineral technology of the Grants uranium region 1979: New Mexico Bureau of Mines and Mineral Resources, Memoir 38, p. 52-58.

Brown, R.D., 2017, Geochemistry and Transport of Uranium-Bearing Dust at Jackpile mine, Laguna, New Mexico [M.S. Thesis]: Socorro, New Mexico Institute of Mining and Technology, 89 p.

Brown, R., and Cadol, D., 2020, Vegetation density and vapor pressure deficit: Potential controls on dust flux at the Jackpile uranium mine, Laguna Pueblo, New Mexico: New Mexico Geological Society, Guidebook 71, this volume.

Butterfield, G.R., 1999, Near-bed mass flux profiles in aeolian sand transport: High-resolution measurements in a wind tunnel: Earth Surface Processes and Landforms, v. 24, no. 5, p. 393–412.

Caldwell, S., 2018, Paragenesis of uranium minerals in the Grants Mineral Belt, New Mexico, applied geochemistry and the development of oxidized uranium mineralization [M.S. Thesis]: Socorro, New Mexico Institute of Mining and Technology, 178 p.

Chavez, O.R., 2016, Microbiology of a reclaimed uranium mine, Laguna Pueblo, NM [M.S. Thesis]: Socorro, New Mexico Institute of Mining and Technology, 40 p.

Dalkamp, F.J., 2010, Uranium deposits of the World—USA and Latin America; Berlin, Springer-Verlag, 516 p.

De Vore, C.L., 2015, Chemical interactions and mobility of uranium near abandoned mine wastes at Rio Paguate, Laguna, New Mexico: Technical Report, https://digitalrepository.unm.edu/wr_sp/17 (accessed 5/14/2020).

Dickinson, W.R., 2018, Tectonosedimentary relations of Pennsylvanian to Jurassic strata on the Colorado Plateau: Geological Society of America, Special Publication 533, 184 p.

Dickinson, W.R., and Gehrels, G.E., 2010, Implications of U-Pb ages of detrital zircons in Mesozoic strata of the Four Corners region for provenance relations in space and time: New Mexico Geological Society, Guidebook 61, p. 135–146.

Dong, Z., Wang, H., Liu, X., and Wang, X., 2004, The blown sand flux over a sandy surface: a wind tunnel investigation on the fetch effect: Geomorphology, v. 57, Issues 1-2, p. 117-127.

El Hayek, E., Torres, C., Rodriguez-Freire, L., Blake, J.M., De Vore, C.L., Brearley, A.J., Spilde, M.N., Cabaniss, S., Ali, A.M.S., Cerrato, J.M., 2018, Effect of calcium on the bioavailability of dissolved uranium (VI) in plant roots under circumneutral pH: Environmental Science and Technology, v. 52, p. 13,089–13,098.

El Hayek, E., Brearley, A.J., Howard, T., Hudson, P., Torres, C., Spilde, M.N., Cabaniss, S., Ali, A.M.S., Cerrato, J.M., 2019, Calcium in carbonate water facilitates the transport of U(VI) in *Brassica juncea* roots and enables root-to-shoot translocation: ACS Earth and Space Chemistry, v. 3, no. 10, p. 2190-2196.

Federal Register notice, 2018 Final list of critical minerals 2018: Office of the Secretary, Interior Department, https://www.govinfo.gov/content/pkg/FR-2018-05-18/pdf/2018-10667.pdf (accessed June 15, 2020).

Grants Beacon, 1982, Jackpile ships last load of ore: Newspaper, 2/12/82.

Gorospe, M., 2013, Uranium mobility in vegetation, soils and water below the Jackpile uranium mine, New Mexico [M.S. thesis]: Socorro, New Mexico Institute of Mining and Technology, 135 p.

Gilliland, F.D., Hunt, W.C., Pardilla, M., and Key, C.R., 2000, Uranium mining and lung cancer among Navajo men in New Mexico and Arizona, 1969 to 1993: Journal of Occupational and Environmental Medicine, v. 42, no. 3, p. 278-83.

Guney, M., Bourges, C.M.J., Chapuis, R.P., and Zagury, G.J., 2017, Lung bioaccessibility of As, Cu, Fe, Mn, Ni, Pb, and Zn in fine fraction (< 20 μm) from contaminated soils and mine tailings: Science of the Total Environment, v. 579, p. 378–386. https://doi.org/10.1016/j.scitotenv.2016.11.086.

Harmon, M.E., Lewis, J., Miller, C., Hoover, J., Ali, A.-M.S., Shuey, C., Cajero, M., Lucas, S., Zychowski, K., Pacheco, B., Erdei, E., Ramone, S., Nez, T., Gonzales, M., and Campen, M.J., 2017, Residential proximity to abandoned uranium mines and serum inflammatory potential in chronically exposed Navajo communities: Journal of Exposure Science and Environmental Epidemiology, v. 27, p. 365–371. https://doi.org/10.1038/jes.2016.79.

Hettiarachchi, E., Paul, S., Cadol, D., Frey, B., Rubasinghege, G., 2019, Mineralogy controlled dissolution of uranium from airborne dust in simulated lung fluids (SLFs) and possible health implications: Environmental Science and Technology Letters, v. 6, no. 2, p. 62-67.

Hilpert, L.S., 1969, Uranium resources of northwestern New Mexico: U.S. Geological Survey, Professional Paper 603, 166 p.

Holen, H.K., and Finch, W.I., 1982, World's largest giant uranium deposit in New Mexico?: U.S. Geological Survey, Open-file Report 82-539, 6 p.

Holen, H.K., and Hatchell, W.O., 1986, Geological characterization of New Mexico uranium deposits for extraction by *in situ* leach recovery: New Mexico Bureau of Mines and Mineral Resources, Open-file Report 251, 93 p.

Holmquist, R.J., 1970, The discovery and development of uranium in the Grants mineral belt, New Mexico: U.S. Atomic Energy Commission, Report RME-172, 122 p.

Hough, H.W., 1955, The team that found the Jackpile mine: Uranium Magazine, February, p. 6-11.

Hsieh, P., and Yamane, K., 2008, DNA mismatch repair: Molecular mechanism, cancer, and ageing: Mechanisms of Ageing and Development, v. 129, p. 391–407. https://doi.org/10.1016/j.mad.2008.02.012.

Hunkin, G.C., 1971, A review of *in situ* leaching: Proceedings American Institute of Mining and Engineering, annual meeting, AIME reprint 71-AS-88, 28 p.

Jacobsen, L.C., 1980, Sedimentary controls on uranium ore at L-Bar deposits, Laguna district, New Mexico: New Mexico Bureau of Mines and Mineral Resources, Memoir 38, p. 284-291.

Kastury, F., Smith, E., and Juhasz, A.L., 2017, A critical review of approaches and limitations of inhalation bioavailability and bioaccessibility of metal(loid)s from ambient particulate matter or dust: Science of the Total Environment, v. 574, p. 1054–1074. https://doi.org/10.1016/j.scitotenv.2016.09.056.

Kaufmann, R.F., Eadie, G.G., and Russell, C.R., 1976, Effects of uranium mining and milling on ground water in the Grants mineral belt, New Mexico: Groundwater, v. 14, p. 296-308.

Kelley, N.E., 1979, Vegetational stabilization of uranium spoil areas, Grants,

New Mexico: Los Alamos Scientific Laboratory Report LA-7624-T, 95 p.
Kittel, D.F., 1963, Geology of the Jackpile mine area, *in* Kelley, V.C., ed., Geology and technology of the Grants uranium region: New Mexico Bureau of Mines and Mineral Resources, Memoir 13, p. 167–176.
Lapham, S.C., Millard, J.B., and Samet, J.M., 1989, Health implications of radionuclide levels in cattle raised near U mining and milling facilities in Ambrosia Lake, New Mexico: Health Physics, v. 56. no. 3, p. 327-340.
Lee, M.J., 1976, Geochemistry of the sedimentary uranium deposits of the Grants mineral belt, southern San Juan Basin, New Mexico [Ph.D. dissertation]: Ithaca, Cornell University, 241 p.
Longmire, P.A., and Brookins, D.G., 1982, Geochemical studies of discharge water from a uranium acid-leach process: New Mexico Geological Society, Guidebook 33, p. 367-370.
McLemore, V.T., 1983, Uranium and thorium occurrences in New Mexico—distribution, geology, production, and resources, with selected bibliography: New Mexico Bureau of Mines and Mineral Resources, Open-file Report 183, 1541 p.
McLemore, V.T., 2012, Geologic processes affecting the chemistry, mineralogy, and acid potential on particle size fractions: Examples from waste rock piles in New Mexico, USA: Proceedings 9th ICARD, Ottawa, Canada, May 20-26, 2012, 12 p., https://geoinfo.nmt.edu/staff/mclemore/projects/environment/documents/0115-McLemore.pdf (accessed 5/14/2020).
McLemore, V.T., 2020a, Uranium deposits in the Poison Canyon Trend, Ambrosia Lake subdistrict, Grants uranium district, McKinley and Cibola Counties, New Mexico: New Mexico Geological Society, Guidebook 71, this volume.
McLemore, V.T., 2020b, Uranium mills in New Mexico: New Mexico Geological Society, Guidebook 71, this volume.
McLemore, V.T., and Chenoweth, W.L., 1989, Uranium resources in New Mexico: New Mexico Bureau of Mines and Mineral Resources, Resource Map 18, 36 p.
McLemore, V.T. and Chenoweth, W.L., 1991, Uranium mines and deposits in the Grants district, Cibola and McKinley Counties, New Mexico: New Mexico Bureau of Mines and Mineral Resources, Open File Report OF-353, 22 p.
McLemore, V.T., and Chenoweth, W.C., 2017, Uranium resources, *in* McLemore, V.T., Timmons, S., and Wilks, M., eds., Energy and mineral deposits in New Mexico: New Mexico Bureau of Geology and Mineral Resources Memoir 50 and New Mexico Geological Society Special Publication 13, 80 p.
McLemore, V.T., Hoffman, G., Smith, M, Mansell, M., and Wilks, M., 2005, Mining districts of New Mexico: New Mexico Bureau of Geology and Mineral Resources, Open-file Report 494, http://geoinfo.nmt.edu/publications/openfile/details.cfml?Volume=494 (accessed 5/14/2020)
McLemore, V.T., Hill, B., Khalsa, N., and Lucas Kamat, S.A., 2013, Uranium resources in the Grants uranium district, New Mexico: An update: New Mexico Geological Society, Guidebook 64, p. 117–126.
McLemore, V.T., Silva, M., Asafo-Akowuah, J., and Frey, B., 2018, Chemical variations among particle size fractions: examples from uranium deposits in New Mexico, USA (abstr.): Geological Society of America Annual Meeting, Indianapolis, Indiana, Geological Society of America Abstracts with Programs. Vol. 50, No. 6, ISSN 0016-7592, https://gsa.confex.com/gsa/2018AM/meetingapp.cgi/Paper/321564 (accessed 5/14/2020).
McLemore, V.T., Wilton, T., and Pelizza, M.S., 2016, *In situ* recovery of sandstone-hosted uranium deposits in New Mexico: past, present, and future issues and potential; Investigation of *in situ* leach (ISL) mining of uranium in New Mexico and post-mining reclamation: New Mexico Geology, v. 38, no. 4, p. 68-85.
Moench, R.H., 1962, Properties and paragenesis of coffinite from the Woodrow mine, New Mexico: American Mineralogist, v. 47, p. 26-33.
Moench, R.H., 1963, Geologic limitations of the age of uranium deposits in the Laguna district: New Mexico Bureau of Mines and Mineral Resources, Memoir 15, p. 156-166.
Moench, R.H., and Schlee, J.S., 1967, Geology and uranium deposits of the Laguna district, New Mexico: U.S. Geological Survey, Professional Paper 519, 117 p.
Momeni, M.H., Tsai, S.Y.H., Yang, J.Y., Gureghian, A.B., and Dungey, C.E., 1983, Radiological impacts of Jackpile-Paguate uranium mines: An analysis of alternatives of decommissioning: U.S. Bureau of Land Management, Report ANL/ES—131, DE83 010687, 232 p.
Morkeh, J., and McLemore, V.T., 2012, The effect of particle size fractions on chemistry, mineralogy, and acid potential of the Questa rock piles, Taos County, New Mexico: New Mexico Bureau of Mines and Mineral Resources, Open-file Report, 96 p.
Nash, J.T., 1968, Uranium deposits in the Jackpile Sandstone, New Mexico: Economic Geology, v. 63, no. 7, p. 737–750.
Nash, J.T., and Kerr, P.F., 1966, Geologic limitations on the age of uranium deposits in the Jackpile Sandstone, New Mexico: Economic Geology, v. 61, p. 1283–1287.
Olsen, J.H., Jr. and Bone, M.J., 1991, Regulatory and reclamation design process update: Jackpile uranium mine reclamation project: American Society of Mining and Reclamation, Proceedings, p. 3-8, https://www.asmr.us/Portals/0/Documents/Conference-Proceedings/1991/0003-Olsen.pdf (accessed 5/8/2020).
Orona, N.S., and Tasat, D.R., 2012, Uranyl nitrate-exposed rat alveolar macrophages cell death: Influence of superoxide anion and TNF α mediators: Toxicology and Applied Pharmacology, v. 261, p. 309–316. https://doi.org/10.1016/j.taap.2012.04.022 (accessed 5/8/2020).
Pearce, A.R., 2020, Environmental geochemistry of St. Anthony mine uranium ores: New Mexico Geological Society, Guidebook 71, this volume.
Pereira, S., Camilleri, V., Floriani, M., Cavalié, I., Garnier-Laplace, J., and Adam-Guillermin, C., 2012, Genotoxicity of uranium contamination in embryonic zebrafish cells: Aquatic Toxicology, v. 109, p. 11–16. https://doi.org/10.1016/j.aquatox.2011.11.011 (accessed 5/8/2020).
Periyakaruppan, A., Kumar, F., Sarkar, S., Sharma, C.S., and Ramesh, G.T., 2007, Uranium induces oxidative stress in lung epithelial cells: Archives of Toxicology, v. 81, p. 389–395, https://doi.org/10.1007/s00204-006-0167-0 (accessed 5/8/2020).
Popp, C.J., Love, D.W., Hawley, J.W., and Novo-Gradc, K., 1984, Radionuclide and heavy metal distribution in 20th century sediments of major streams in the eastern part of the Grants uranium region, New Mexico, *in* Stone, W.L., ed., Selected papers on water quality and pollution in New Mexico: New Mexico Bureau of Mines and Mineral Resources, Hydrologic Report 7, p. 34-48
Reheis, M.C., Goodmacher, J.C., Harden, J.W., McFadden, L.D., Thomas, K.R., Shroba, R.R., Sowers, J.M., and Taylor, E.M., 1995, Quaternary soils and dust deposition in southern Nevada and California Quaternary soils and dust deposition in southern Nevada and California: GSA Bulletin, v. 107, no. 9, p. 1003–1022.
Risser, D.W., Davis, P.A., Baldwin, J.A., and McAda, D.P., 1984, Aquifer testes at the Jackpile-Paguate uranium mine, Pueblo of Laguna, west-central New Mexico: U.S. Geological Survey, Water Resources Investigations Report 84-4255, 26 p.
Schneider, J., Phillips, M., Yamini, P., Dork, T., and Woitowitz, H.-J., 2007, ATM gene mutations in former uranium miners of SDAG Wismut: A pilot study: Oncology Reports, v. 17, p. 477– 482.
Schubauer-Berigan, M.K., Daniels, R.D., and Pinkerton, L.E., 2009, Radon exposure and mortality among white and American Indian uranium miners: an update of the Colorado Plateau cohort: American Journal of Epidemiology, v. 169, no. 6, p. 718-730.
Stearns, D.M., Yazzie, M., Bradley, A.S., Coryell, V.H., Shelley, J.T., Ashby, A., Asplund, C.S., and Lantz, R.C., 2005, Uranyl acetate induces hprt mutations and uranium-DNA adducts in Chinese hamster ovary EM9 cells: Mutagenesis, v. 20, p. 417–423. https://doi.org/10.1093/mutage/gei056.
Stine, K.E., and Brown, T.M., 1996, Principles of Toxicology (1st ed.): New York, CRC Lewis, 272 p.
Turner-Peterson, C.E., 1980, Tabular uranium ore in Poison Canyon area, Morrison Formation, San Juan Basin, and application of lacustrine-humate model: American Association Petroleum Geologists Bulletin, v. 64, no. 5, 795 p.
U.S. Department of the Interior, 1985, Jackpile-Paguate uranium mine reclamation project: Environmental Impact Statement, 260 p.
USEPA, 2013, National Priorities List: Jackpile-Paguate uranium mine: U.S. Environmental Protection Agency, https://semspub.epa.gov/work/06/300064.pdf (accessed 5/14/2020).
USEPA, 2018, Site Status Summary for Jackpile Paguate uranium mine: U.S. Environmental Protection Agency, https://semspub.epa.gov/work/06/100011388.pdf (accessed 4/20/2020).
Velasco, C.A., Artyushkova, K., Ali, A.S., Osburn, C.L., Gonzalez-Estrella, J., Lezama-Pacheco, J.S., Cabaniss, S.E., and Cerrato, J.M., 2019, Organic functional group chemistry in mineralized deposits containing

U(IV) and U(VI) from the Jackpile mine in New Mexico: Environmental Science and Technology, v. 53, p. 5758-5767.

West, S.W., 1972, Disposal of uranium-mill effluent by well injection in the Grants area, Valencia County, New Mexico: U.S. Geological Survey, Professional Paper 386D, 27 p.

Wilton, T., Chávez, W.X., Jr., and Caldwell, S., 2020, Sandstone-hosted uranium deposits at the Cebolleta Land Grant, Cibola County, New Mexico: New Mexico Geological Society, Guidebook 71, this volume.

Zehner, H.H., 1985, Hydrology and water-quality monitoring considerations, Jackpile uranium mine, northwestern New Mexico: U.S. Geological Survey, Water Resources Investigations Report 85-4226, 61 p.

New Mexico Geological Society, Special Publication 14, Geology of the Mount Taylor Area, 2020, p. 89-96.

THE ENVIRONMENTAL LEGACY OF URANIUM MINING AND MILLING IN NEW MEXICO

Bruce Thomson

Center for Water & the Environment, Department of Civil, Construction & Environmental Engineering, University of New Mexico, Albuquerque, NM 87131; bthomson@unm.edu

Abstract—Between 1951 and 1989, the Grants mining district of northwestern New Mexico produced more uranium than any other district in the United States. Almost 250 mines were located in New Mexico, consisting of both open pit and underground mines. Open pit mines, especially the large Jackpile–Paguate Mine on the eastern flank of Mt. Taylor, left a large area of open pits and exposed strata that remains largely unremediated. The Jackpile–Paguate Mine is now a Superfund site. Underground mines had a large impact on regional aquifers, but groundwater levels have largely recovered after closure. Eight mills were built to process uranium ore at one time or another in the state using either the acid leach (seven mills) or alkaline leach process. The Bokum Mill was built but never operated. Tailings were disposed as a slurry in unlined tailings piles. Tailings wastewater was of very poor quality characterized by either low pH (acid leach mills) or high pH (alkaline leach mill), high total dissolved solids, and high concentrations of metals and radionuclides. Most mills were located in remote locations and present little threat to health or the environment, but the Homestake Mill near Milan, NM was declared a Superfund site in 1983 and remediation is continuing. Though no mining or milling has occurred for over 20 years, it is important to understand the legacy of uranium production to develop effective remediation strategies and minimize risks to health and the environment if production resumes in the future.

INTRODUCTION

Uranium was discovered in 1789 by the German chemist Martin Heinrich Klaproth in the mineral pitchblende, which contains a mixture of uraninite ($UO_{2(s)}$) and smaller amounts of schoepite ($U_3O_{8(s)}$; LANL, 2013). Originally, it had limited use as a coloring agent in glass and ceramic glazes. Nuclear fission, the splitting of a heavy atom into two smaller atoms by bombarding it with neutrons, was discovered in December 1938 by Germans Otto Hahn and his assistant Fritz Strassmann, and a theoretical understanding of the process was proposed a month later by Lise Meitner and her nephew Otto Robert Frisch (Rhodes, 1986). The enormous amount of energy released by fission reactions was immediately recognized along with its potential as a source of power and as the basis for a powerful weapon. This led to the Manhattan Project, which began in 1942. Less than six years after the discovery of fission, an entirely new industry involving the production of nuclear power and the manufacturing of nuclear weapons was created.

Much of the research on the bomb, as well as its construction, was done in Los Alamos, New Mexico. Most of the uranium used for the Manhattan Project came from the Shinkolobwe mine in the Belgian Congo (now the Democratic Republic of the Congo), an incredibly rich pitchblende deposit containing up to 65% U_3O_8 (Nichols, 1987), although a small fraction came from tailings from vanadium mills in Colorado and Utah (Hewlett and Anderson, 1990). Therefore, it is ironic that shortly after the war, world class uranium deposits were discovered less than 150 miles from Los Alamos.

In less than seven years, the demand for uranium grew explosively, and U.S. production went from near zero in 1950 to 35 million lbs/yr of uranium concentrate (represented as U_3O_8) by 1956 (EIA, 2019). Uranium mining occurred at numerous locations throughout the country, especially in the western states (EIA, 2018). The DOE (2014a) identified 4225 mines that produced uranium for U.S. defense programs. Of these, 247 mines were located in New Mexico and produced 47% of total ore mined domestically. Sixty-five mines were on Navajo lands located in the Grants mining district (also often referred to as the Grants mineral district or the Grants uranium district; EPA et al., 2007). McLemore et al. (2013) described the major uranium ore deposits in the Grants district, including their locations and estimated reserves. Thomson (in press) provides a broader discussion of environmental contamination from uranium mining and milling in the western U.S. and its relevance to health impacts. It includes a summary of waste stabilization and remediation technologies.

LEGACY EFFECTS OF URANIUM MINING

Early production of uranium ore in New Mexico came from small surface mines, while underground mining became more prevalent as companies chased ever deeper ore bodies. However, Anaconda moved about 400 million tons of ore, subore, rock, waste material, and overburden between 1952 and 1982 at the Jackpile–Paguate open pit mine complex on the Laguna Pueblo near the southeastern flank of Mt. Taylor (EPA, 2020a). The mine produced about 25 million tons of ore. The complex covered almost 7900 acres and was 625 ft deep at its deepest point. A 1982 photo of one of the pits at this mine is presented in Figure 1. Note the presence of a small pit lake.

Underground uranium mines had minor surface impact and typically consisted of a building for the mine hoist and changing facilities, a pad for waste rock and low grade ore storage, and ponds for treating mine water. Figure 2 is a photo of an underground mine that shows these features. While most large

FIGURE 1. Air photo of one of the pits of the Jackpile mine showing a small pit lake at the bottom (photo by author, 1982).

FIGURE 2. Air photo of the Kerr-McGee Section 36 mine (photo by author, 1981).

mines (ore production >100,000 tons) have been remediated, remediation of many small mines has not been addressed or the mine status is unknown (DOE, 2014a). Remediation generally consisted of blocking mine openings to prevent access and, at some sites, regrading waste rock piles to limit erosion and airborne dust transport. Potential long-term environmental impacts are unknown.

While the surface impact of underground mining was minor, the impact on groundwater resources was substantial as ever deeper mines became located below regional aquifers. These mines required pumping large volumes of water, up to 3,000 gal/min, to keep the mines dewatered. Lyford et al. (1980) estimated that the total amount of mine dewatering was 10,000 acre-ft/yr ($12x10^6$ m^3/yr) in 1979, and predicted regional groundwater declines of 1,000 ft or more by 2000 in the Grants district. Mine closure following collapse of the industry in the 1980s prevented this occurrence, and aquifer drawdowns have largely recovered.

No open pit or underground uranium mining is currently practiced in the United States. All domestic uranium mining is produced from *in-situ* recovery (ISR) mines (see Thomson and Heggen, 1983 for a summary of ISR technology) located in Wyoming (four mines) and Nebraska (one mine; EIA, 2019). Several small scale and pilot ISR uranium mining projects were conducted in New Mexico between 1970 and 1980 with limited success (McLemore et al., 2016). One of the most notable projects was a large field scale pilot test of ISR technology that was done near Crownpoint, NM (Vogt et al., 1984). The Crownpoint project consisted of a series of injection and extraction wells located on 100-ft centers, each drilled to a depth of about 2,000 ft. An oxidizing solution of $NaHCO_3$ was circulated through the ore body to oxidize and extract uranium, which was then recovered by ion exchange (IX) at the surface. The pilot mine test began in 1979 and concluded in 1980, and was followed by six years of intermittent aquifer restoration efforts, which demonstrated that groundwater quality could be restored to below groundwater standards (Hydro Resources, Inc., 1997).

The principal contaminants in wastewater from underground mines were sediments, uranium and radium. The industry developed a very simple treatment process, illustrated in Figure 3 (Thomson and Heggen, 1983). Solids were removed in settling ponds. Uranium was removed by IX. Finally, barium chloride ($BaCl_2$) was added to precipitate radium as a Ba-Ra-SO_4 co-precipitate, which was also removed by settling. An example of a mine water treatment system is shown in Figure 2. In this system, mine water passed through two settling ponds to remove suspended solids, then into an IX facility to recover uranium (the building near the left margin of Fig. 2). Barium chloride ($BaCl_2$) was added at this point and the Ba-Ra-SO_4 co-precipitate settled in the third pond. Treated water then flowed through a polishing wetland and into a dry arroyo. IX recovery of uranium was profitable, and the Phillips/United Nuclear Corporation and Kerr McGee Mills continued to recover uranium from mine water from closed mines until 1982 (DOE, 2018) and 2002 (McLemore and Chenoweth, 2017), respectively.

Unquestionably the biggest impact of underground uranium mining on human health was due to radon inhalation (Brugge and Buchner, 2011). The radon isotope radon-222 is an intermediate product in the decay chain of uranium-238 and decays by alpha emission with a half-life of 3.8 d. Because it is an inert gas, radon is non-reactive. However, radon and its daughter products can be adsorbed onto particles of smoke and dust that are subsequently trapped in the lungs where high energy alpha decay particles damage lung tissues. This greatly increases the risk of cancer and other pulmonary diseases. The Centers for Disease Control and Prevention (CDC, 2017) summarized the health risks of underground uranium mining and reported a six-fold increase in lung cancer for white miners and a three-

fold increase for non-white miners. The difference in risk was explained by a lower incidence of smoking among non-white miners, especially Navajos. The high incidence of cancer in underground miners led the Navajo Nation to pass the Diné Natural Resources Protection Act in 2005 that banned uranium mining on the reservation (Navajo Nation Council, 2005).

LEGACY EFFECTS OF URANIUM MILLING

Eight mills were built to process uranium ore in New Mexico (EPA, 2011), however, the Bokum Mill near Marquez, NM, never operated. Milling consisted of grinding the ore to fine particles, leaching the ore with an acid or base solution, and then extracting the dissolved uranium from solution using either solvent extraction or IX. A generic process flow diagram is presented in Figure 4. All of the New Mexico uranium mills used the acid-leach process except the United Nuclear–Homestake Partners Mill near Milan, NM, which was an alkaline leach mill. The barren tailings were piped as a slurry to a nearby tailings pile, which was retained behind a dam or berm constructed with sand from the tailings. The quality of water in the tailings slurry was poor with very high concentrations of total dissolved solids, uranium, radionuclides, and other constituents (Table 1).

None of the tailings piles constructed before 1980 were lined, hence, infiltration of contaminants into underlying

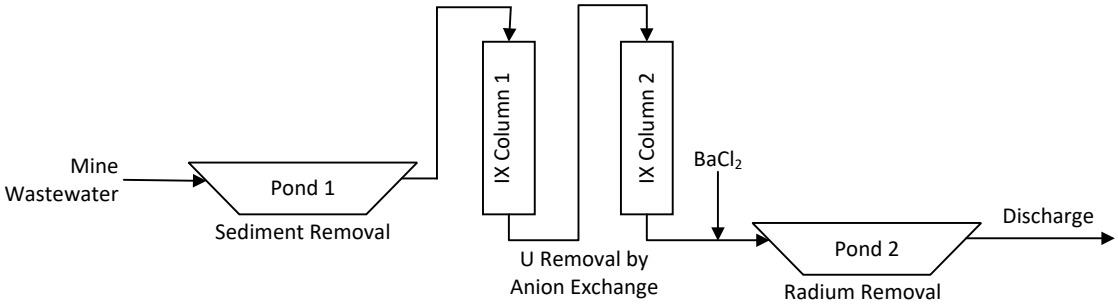

FIGURE 3. Diagram of typical mine water treatment process used by New Mexico uranium mines.

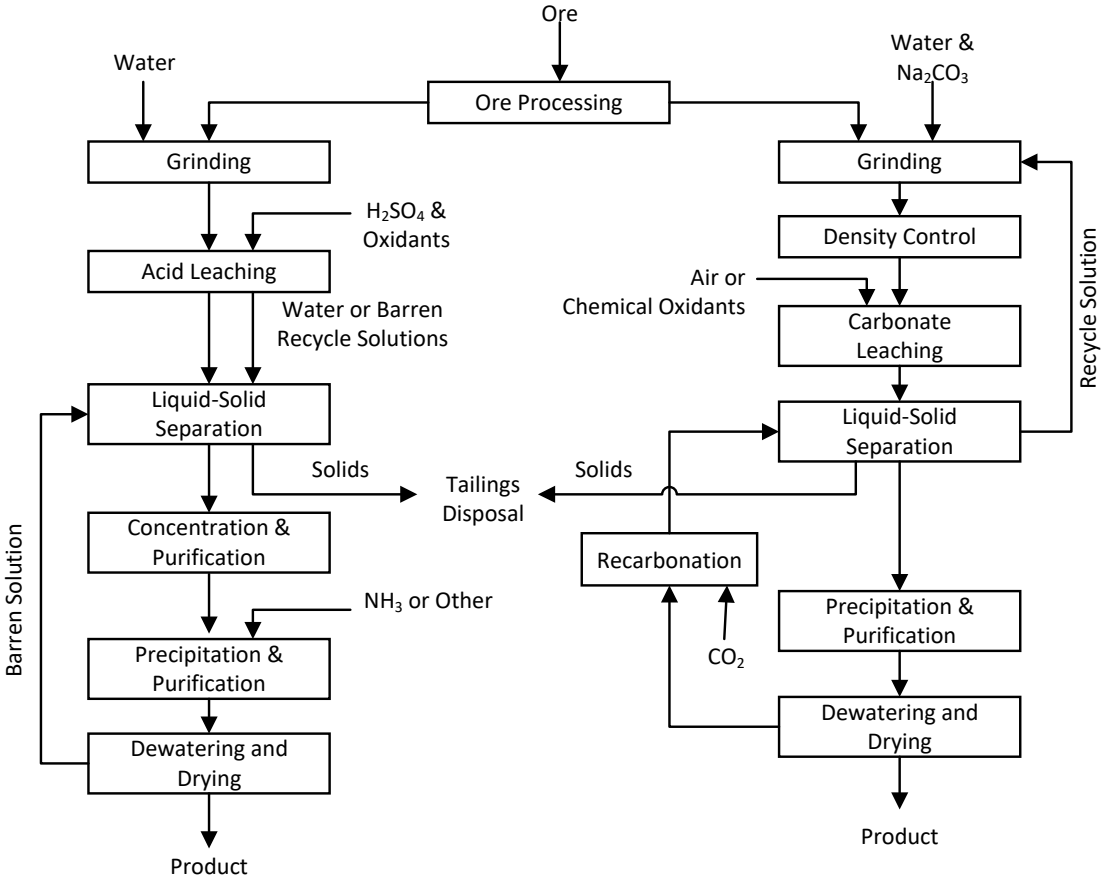

FIGURE 4. General process diagram of the acid-leach and alkaline-leach processes for milling uranium ore (adapted from Merritt, 1971).

TABLE 1. Water quality data from acid-leach and alkaline-leach uranium mines in New Mexico (Thomson et al., 1982). All concentrations in mg/L except as noted.

	Four Acid Leach Mills (average of 14 samples)			*One Alkaline Leach Mill (average of five samples)*		
Constituent	*Minimum*	*Median*	*Maximum*	*Minimum*	*Median*	*Maximum*
Arsenic	0.18	1.3	5.6	2.1	5.0	7.2
Nitrate (as N)	3.3	400	3960	1.1	16	335
Molybdenum	0.2	0.9	29.5	72	98	105
Selenium	0.006	0.21	6.97	22.1	29.5	51.2
Sulfate	300	29,700	56,000	550	8400	16,700
Uranium	1.1	15	69	4.2	53	70
Vanadium	39	74	107	1.2	14	16
pH (pH units)	0.3	1.05	2.15	9.9	10.1	10.3
Ra-226 (pCi/L)	15	70	1800	56	58	90
Gross a Rad. (pCi/L)	3200	38,000	73,000	3400	6700	10,000

groundwater occurred. Because most of the mills were at remote locations, threats to human health were negligible. However, the Anaconda Bluewater and United Nuclear–Homestake Partners Mills were located close to subdivisions near Milan, NM, and caused regional groundwater contamination that impacted domestic wells. In 1985, Homestake paid to connect residents to the Milan public water system to provide them with safe drinking water. Groundwater near the Homestake and Anaconda Bluewater tailings piles contains elevated concentrations of uranium, selenium and other constituents from natural sources. In addition, the hydraulic gradient in this area is very flat and has changed as a result of pumping from the aquifers by domestic, agricultural and industrial users, infiltration from the tailings piles, infiltration from San Mateo Creek, and groundwater remediation activities. Thus, determination of groundwater hydrology and background water quality is one of the objectives of EPA's current field investigations (EPA, 2016).

Generally, the objective of groundwater remediation programs is to clean the water to meet groundwater standards, not necessarily to drinking water standards or background water quality conditions. At mill sites, the standards are established by the Nuclear Regulatory Commission (NRC), while state groundwater standards apply outside of the property boundary. Alternative abatement standards (AAS) may be established if cleanup to NRC or state standards is not feasible by the maximum use of commercially accepted abatement technology (NMAC 20.6.2.4103). Alternative abatement standards have been established for groundwater quality beneath a number of sites, including the Anaconda Bluewater Mill, the L-Bar disposal site, the Ambrosia Lake disposal site, and the Rio Algom Mill, and an application for AAS has been made for the Homestake Mill site (EPA, 2015).

Other uranium mill tailings sites in New Mexico have been remediated by consolidating wastes from near the site into a single pile and covering them with an engineered cap. The principal objectives of stabilizing the piles include: 1) isolate and stabilize the tailings to prevents their mobilization by wind or erosion, 2) prevent rain and snow melt from seeping through the pile and contaminating underlying groundwater, and 3) prevent radon gas from diffusing up through the cover to the atmosphere.

REGULATORY PROGRAMS DEALING WITH LEGACY URANIUM PRODUCTION

There are three major federal programs that provide regulatory authority over legacy wastes from U production, including a program administered by DOE under the Uranium Mill Tailings Radiation Control Act (UMTRCA), and a program administered by the EPA for remediation of sites under the Comprehensive Environmental Response, Compensation and Liability Control Act (CERCLA), also known as Superfund. Finally, a large financial settlement with successors of a former uranium mining and milling company, referred to as the Tronox settlement, has provided funds for investigation and remediation of sites on and near the Navajo Nation. These are discussed below.

UMTRCA

UMTRCA was passed in 1978 and gave DOE responsibility to ensure safe disposal, stabilization, and long-term monitoring of tailings from uranium milling (DOE, 2014b). Two categories of sites were identified: Title I sites that were inactive when the legislation was passed and Title II sites that were still active or had corporate owners still active in uranium production. DOE assumed responsibility for the Title I sites, and the site owners were given responsibility for waste stabilization and closure of the Title II sites. Twenty four sites across the country were identified as Title I sites, though the list was later reduced to 22 sites. Two Title I sites were in NM, one in Shiprock and another in Ambrosia Lake. Once a site has been closed, title to the property is transferred to the DOE, which provides long-term custody, monitoring, and care under its Legacy Management Program (DOE, 2020). Table 2 gives the location and summary information about uranium mill tailings piles in New Mexico. Note that three of the tailings piles have not

TABLE 2. Summary of uranium mill tailings piles in New Mexico.

Site Name	Company	Title I or II*	Years Operated	Year Closed	Mass of Tailings (M tons)	Reference
Ambrosia Lake	Phillips Petroleum/United Nuclear Corp.	I	1958-1963	1995	2.5	DOE, 2020
Bluewater, NM Disposal Site	Anaconda Copper/ARCO	II	1953-1982	1995	24	DOE, 2020
Homestake	United Nuclear/Homestake Partners	N/A	1958-1990	-	22	NRC,2018a
L-Bar Mill	SOHIO	II	1977-1981	2000	2.1	DOE, 2020
Rio Algom	Kerr McGee/Quivara/Rio Algom	N/A	1958-2002	-	33	NRC, 2018b
Shiprock	Kerr McGee/Vanadium Corporation of America	I	1954-1963	1985	2.5	DOE, 2020
Church Rock	United Nuclear Corp.	N/A	1977-1982	-	3.5	NRC, 2019

*N/A are sites not currently in DOE Legacy Management program.

been completely closed, and therefore their titles have not been transferred to DOE for ownership and long-term management.

Superfund

The second federal program that continues to play an important role in mine waste and mill tailings management is the Superfund program. Three sites in New Mexico are being addressed by the Superfund program: the Homestake Mill site near Milan and the United Nuclear Church Rock site which were both listed in 1983, and the Jackpile–Paguate Uranium Mine on the Laguna Pueblo which was listed in 2013 (EPA, 2016).

The Homestake tailings pile was declared a Superfund site in 1983 primarily due to concerns about radon emanation from the pile. However, the pile, like other tailings piles in New Mexico, was unlined, which resulted in extensive contamination of shallow groundwater principally by nitrate, selenium, and uranium (Weaver and Hoffman, 2019). A small failure of the tailings dam occurred in 1977, but no off-site release of contaminants occurred (IAEA, 2004). Cleaning up groundwater to background water quality has been the principal focus of remediation activities at this site in recent decades. Remediation consists of pumping contaminated groundwater to a treatment plant where it is treated by IX and reverse osmosis (RO), then reinjected down-gradient from the plume to force the flow of contaminated groundwater flow back towards the collection wells. Waste brine from the RO process is disposed of in evaporation ponds. Figure 5 taken in 1981 shows the proximity of the Homestake tailings pile to residences and the large amount of water present on top of the pile. A photo of the site taken in 2020 (Fig. 6) shows the partly stabilized pile and the RO concentrate evaporation ponds, which use fountains to spray water into the air to increase the rate of evaporation.

The Jackpile–Paguate Mine site was mined from 1952 to 1982. The health concerns at the site include exposure to airborne dust and radionuclides and contaminated surface water. Partial reclamation of the mine was conducted between 1982 and 1994 and mainly consisted of stabilization of waste-rock piles. However, continuing concerns about health risks to nearby residents led to the site being declared a Superfund site

FIGURE 5. Photograph of the Homestake uranium mill tailings pile in 1981.

FIGURE 6. Photograph of the Homestake uranium mill tailings pile in 2020.

in 2013 (EPA, 2020a). Current work at the site is limited to air monitoring and planning for future remediation.

The United Nuclear Corporation opened a uranium mine near the Church Rock Chapter of the Navajo Nation, 17 miles northeast of Gallup, NM in 1968. The company subsequently built an acid leach mill that operated from 1977 to 1982. Tailings were disposed in a pond created by a dam built using the sand fraction of the tailings. On the morning of July 16, 1979, the tailings dam failed and released a slurry containing 1,100 short tons of mill tailings and 94 million gallons of very acidic water (pH ~1.2) to the Puerco River (also known as Rio Puerco; Brugge et al., 2007; U.S. House of Representatives, 1979). The Puerco River flows south and west through the town of Gallup and then westward onto the Navajo Nation. Contaminated water flowed approximately 80 miles down the dry river bed, but did not reach any perennial streams. The region is sparsely populated and though the river is not a source of potable supply, it is used by grazing animals.

An analysis of the failure suggested that differential settling within the dam occurred prior to failure, which resulted in formation of cracks (Nelson and Kane, 1980). Sand was placed next to the dam to form a sand "beach," which was expected to fill these cracks. However, the water level in the pile rose above the top of the sand beach and saturated the sand of the tailings pile dam, which decreased its strength and caused instability with subsequent failure. The very low pH of the tailings fluid was likely a contributing factor, as it caused dispersal of clays and other materials in the dam, further decreasing soil strength.

Van Metre and Gray (1992) reported that the total amount of U (1,500 kg) and gross-alpha radioactivity (46 Ci) released by the spill was small fraction of the cumulative amounts of U and gross-alpha radioactivity released by mine dewatering between 1960 and 1979 of 560,00 kg and 230 Ci, respectively. They concluded that most of the U was immobilized on alluvial sediments and therefore migration through groundwater was limited.

The failure of the tailings dam was a public relations disaster for the U.S. uranium industry as it brought national attention to its poor waste management practices and the potential risks associated with these wastes. Remediation activities under the Superfund program consist of consolidating and stabilizing the mine and mill wastes and cleaning up groundwater in the alluvium and upper portions of the Cretaceous Gallup Sandstone (EPA, 2020b).

Estimates of up to 16.4 million lbs of U_3O_8 in undeveloped uranium ore remain near the Church Rock site (McLemore et al., 2013).

Tronox Settlement

For almost three decades, there has been little federal attention paid to the environmental legacy of uranium development in the Grants mining district; however, a large source of funds became available beginning in 2015, due to a legal settlement with successors to Kerr McGee. Tronox was a chemical company that mainly produced titanium dioxide. It was divested from Kerr-McGee in 2006, which among other things, ceded all of Kerr-McGee's uranium properties to Tronox. Kerr-McGee was subsequently purchased by Anadarko Petroleum Corporation, also in 2006. In 2009, Tronox filed for bankruptcy and also filed suit against Kerr-McGee, Anadarko and others claiming that the uranium properties were transferred without revealing the environmental liabilities that were associated with them. Based on the magnitude of the environmental damages, the U.S. intervened in the case to recover environmental response costs. The case was settled in 2015 with Anadarko agreeing to pay $5.15 billion to fund remediation activities at 17 sites, the "largest recovery relating to governmental environmental claims and liabilities" (EPA, 2016). The Tronox settlement provided approximately $1 billion for remediation of U mining and milling problems on and near the Navajo Nation.

Funds from the Tronox settlement are being used to address approximately 101 mines on and near Navajo lands. A map of the mines on and near the Navajo Nation, that also identifies those mines that will be remediated with funds from the Tronox settlement, is presented in Figure 7. Abandoned mines near Mt. Taylor are referred to by EPA as the Eastern Abandoned Uranium Mine (AUM) Region that extends westward from the community of San Mateo, NM to Church Rock, NM.

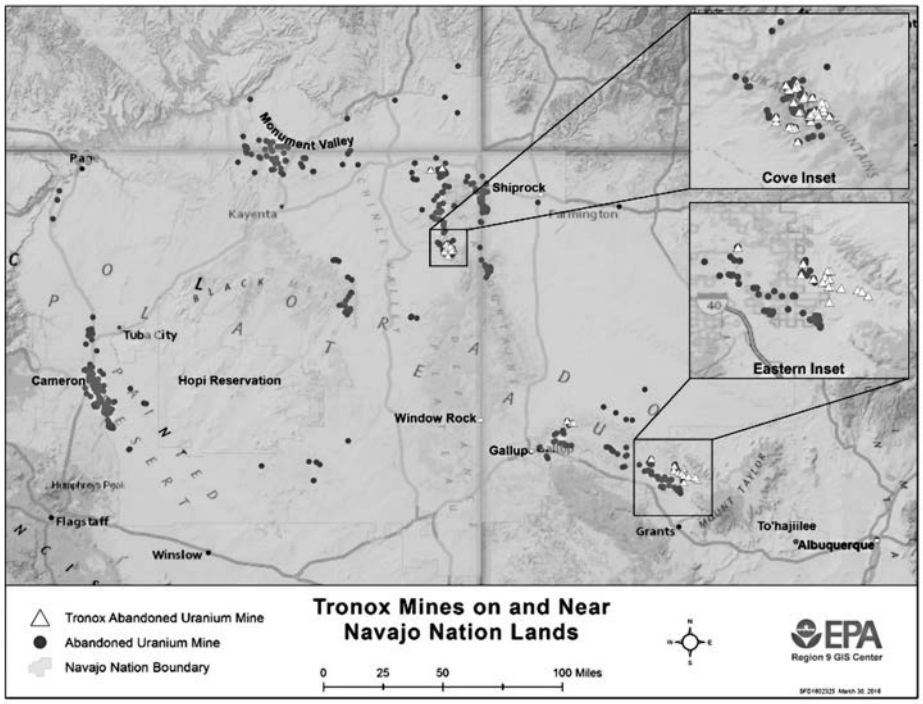

FIGURE 7. Map of uranium mines on and near the Navajo Nation and identification of those which will be remediated with funds from the Tronox settlement (EPA, 2019).

About 15 of these mines will be remediated with Tronox funds (EPA, 2019). As part of the investigation, EPA and the state of New Mexico have used Tronox funds to describe the nature and extent of groundwater contamination in the San Mateo Creek watershed from near Milan, NM up to its headwaters near San Mateo, NM.

Other Federal, State, and Tribal Agencies Involvement in Remediation of Legacy Impacts from Uranium Mining and Milling

Most activities to address legacy impacts from uranium development in the Grants mining district are being led by either the DOE, which is mainly focused on mill sites, and the EPA, which has responsibility for remediation of Superfund sites and abandoned mines. Other agencies with significant responsibility for addressing legacy issues include (EPA, 2011; EPA, 2016):

- U.S. Bureau of Land Management – Identify and cleanup abandoned mines on BLM property. Participate in permitting of proposed mines on BLM property.
- U.S. Forest Service – Identify and cleanup abandoned mines on USFS property. Participate in permitting of proposed mines on USFS property.
- NM Environment Department – Protect ground and surface water supplies by participating in field investigations and establishing appropriate water quality standards.
- NM Energy, Minerals and Natural Resources Department – Maintain a database of mine sites, oversee mine closure and reclamation of mines. Permits new mines.
- NM Department of Health – Conduct public health surveillance to assess exposure to uranium
- Pueblo Governments – Participate in public outreach, field investigations and remediation activities.
- Navajo Nation – Because of its size and the large number of abandoned mines and mills present, the Navajo Nation has its own Abandoned Mine Lands Department that conducts its own investigations and reclamation in collaboration with EPA Region IX and the DOE (Navajo AML Department, 2020).

CONCLUSIONS

Since the discovery of major uranium reserves in New Mexico after 1950, uranium production has played a major role in the economy and culture of New Mexico. In 1979, there were 38 producing mines supplying ore to six operating mills, and the industry employed 7,000 people (SJBRUS, 1980). In 2020, the only activity is associated with remediation of legacy sites, along with minor exploration and permitting for possible future development.

However, New Mexico is estimated to have 179 million lbs of U_3O_8 at $50/lb, second in total reserves only to Wyoming, and additional resources are available (McLemore and Chenoweth, 2017). A number of mine projects have been proposed (McLemore et al., 2013). Three notable projects in the advanced permitting stage are the Roca Honda underground mine (near Jesus Mesa on the northwest flank of Mt. Taylor), and two projects under development by Laramide Resources (an underground mine near Church Rock, NM and an *in-situ* recovery (ISR) mine near Crownpoint, NM; Laramide Resources, 2020).

Whether uranium production resumes in New Mexico is uncertain. Nevertheless, it is vital that the environmental impacts of past uranium development be recognized and understood to address mistakes from the past and allow careful development with appropriate protections of human health and the environment should uranium development occur in the future.

ACKNOWLEDGMENTS

The comments and suggestions of two reviewers, Dr. Virginia McLemore of the NM Bureau of Geology and Mineral Resources, and Anchor Holm, P.E., of the NM State Land Office, greatly improved the accuracy and quality of this paper. The paper also benefitted from critical comments and suggestions provided by the editors, Bonnie Frey and Dr. Dana Ulmer-Scholle. Their assistance is gratefully acknowledged.

REFERENCES

Brugge, D., and Buchner, V., 2011, Health Effects of Uranium: New Research Findings: Reviews on Environmental Health, v. 26, n. 4, p. 231–249, https://doi.org/10.1515/REVEH.2011.032.

Brugge, D., Yazzie-Lewis, E., and Benally, T.H., eds., 2007, The Navajo People and Uranium Mining: Albuquerque, University of New Mexico Press, 232 p.

CDC, 2017, Uranium Miners (1) – NIOSH Study Summary, Worker Health Study Summaries: Research on Long Term Exposure, Uranium Miners: web site Center for Disease Control and Prevention, Atlanta, https://www.cdc.gov/niosh/pgms/worknotify/uranium.html (accessed on 2/10/20).

DOE, 2014a, Defense-Related Uranium Mines Location and Status Topic Report, LMS/S-10693: Grand Junction, Office of Legacy Management, US Department of Energy, 252 p., https://www.energy.gov/sites/prod/files/2017/07/f35/S10693_LocStatus.pdf.

DOE, 2014b, UMTRCA Title I & II: Uranium Mill Tailings Radiation Control Act Sites [Fact Sheet]: Grand Junction, Office of Legacy Management, U.S. Department of Energy, 2 p., https://www.energy.gov/sites/prod/files/2014/10/f19/UMTRCA.pdf.

DOE, 2018, Ambrosia Lake, New Mexico, Disposal Site: Fact Sheet: Grand Junction, Office of Legacy Management, U.S. Department of Energy, 2 p., https://www.energy.gov/sites/prod/files/2019/12/f69/Ambrosia%20Lake%2C%20New%20Mexico%2C%20Disposal%20Site%20Fact%20Sheet.pdf.

DOE, 2020, DOE Office of Legacy Management: https://www.energy.gov/lm/sites/lm-sites (DOE website accessed 3/31/20).

EIA, 2018, U.S. uranium imports continue as domestic production remains at historical lows, Energy Information Administration website, https://www.eia.gov/todayinenergy/detail.php?id=37192 (accessed on 12/20/19).

EIA, 2019, 2018 Domestic Uranium Production Report: Washington, D.C., U.S. Energy Information Administration, 24 p., https://www.eia.gov/uranium/production/annual/pdf/dupr.pdf.

EPA, USACE, and TerraSpectra Geomatics, 2007, Abandoned Uranium Mines and the Navajo Nation: Navajo Nation AUM Screening Assessment Report and Atlas with Geospatial Data: San Francisco, U.S. Environmental Protection Agency, U.S. Army Corps of Engineers, TerraSpectra Geomatics, 198 p., https://www.epa.gov/sites/production/files/2017-01/documents/navajo_nation_aum_screening_assess_report_atlas_geospatial_data-2007-08.pdf.

EPA, 2011, The legacy of abandoned uranium mines in the Grants Mineral

Belt, New Mexico, Region 6: Dallas, U.S. Environmental Protection Agency, 6 p., https://www.epa.gov/sites/production/files/2015-08/documents/uranium-mine-brochure.pdf.

EPA, 2015, Grants Mining District, New Mexico, 2015-2020 Five-Year Plan to Assess and Address Health and Environmental Impacts of Uranium Mining and Milling, DRAFT: Dallas, U.S. Environmental Protection Agency, Region VI, 45 p., https://www.epa.gov/sites/production/files/2015-10/documents/draft_2015_five-year_plan_grants_mining_district_10_9_15.pdf.

EPA, 2016, Grants Mining District, New Mexico 2015 – 2020 Five-Year Plan to Assess and Address Health and Environmental Impacts of Uranium Mining and Milling, Region 6: Dallas, U.S. Environmental Protection Agency, 24 p., https://www.epa.gov/sites/production/files/2016-06/documents/gmd_2015_2020_five-year_plan_29mar16.pdf.

EPA, 2019, Navajo Nation: Cleaning Up Abandoned Uranium Mines: U.S. Environmental Protection Agency website, https://www.epa.gov/navajo-nation-uranium-cleanup/tronox-abandoned-uranium-mines (accessed 6/30/19).

EPA, 2020a, Jackpile-Paguate Uranium Mine, Laguna Pueblo, NM: U.S. Environmental Protection Agency Superfund Site website, https://cumulis.epa.gov/supercpad/cursites/csitinfo.cfm?id=0607033 (accessed 2/10/20).

EPA, 2020b, Superfund Site: United Nuclear Corp. Church Rock, NM: U.S. Environmental Protection Agency Superfund website, https://cumulis.epa.gov/supercpad/cursites/csitinfo.cfm?id=0600819 (accessed 3/31/20).

Hewlett, R.G., and Anderson, O.E.J., 1990, The New World: A History of the United States Atomic Energy Commission, Volume I, 1939–1946, *in* California Studies in the History of Science (Book 2): Berkeley, University of California Press, 781 p., ISBN 978-0-520-07186-5.

Hydro Resources, Inc., 1997, Final environmental impact statement to construct and operate the Crownpoint Uranium Solution Mine, Crownpoint, NM, Docket No. 40-8968. NUREG-1508, BLM NM-01-93-02, BIA EIS-92-001: Washington, D.C., U.S. Nuclear Regulatory Commission, 452 p., https://www.nrc.gov/docs/ML0821/ML082170248.pdf.

IAEA, 2004, Long term stabilization of uranium mill tailings (Final Report of a Co-Ordinated Research Project 2000–2004, IAEA-TECDOC-1403: Vienna, International Atomic Energy Agency, 309 p., https://www-pub.iaea.org/MTCD/Publications/PDF/te_1403_web.pdf

LANL, 2013, Periodic table of the elements: LANL: Los Alamos National Laboratory, https://periodic.lanl.gov/92.shtml (accessed on February 10, 2020).

Laramide Resources, 2018, Churchrock Project and ISR Division Overview. Laramide Resources, https://laramide.com/projects/church-rock-and-isr-projects/ (accessed 3/13/20).

Lyford, F.P., Frenzel, P.F., and Stone, W.J., 1980, Preliminary estimates of effects of uranium-mine dewatering on water levels, San Juan Basin: New Mexico Bureau of Mines and Mineral Resources, Memoir 38, p. 320-333.

McLemore, V.T., and Chenoweth, W.L., 2017, Uranium Resources, *in* McLemore, V.T., Timmons, S., Wilks, M., eds., Energy and Mineral Resources of New Mexico: Volume C, Memoir 50C, New Mexico Bureau of Geology and Mineral Resources, Socorro, NM, 67 p., https://geoinfo.nmt.edu/staff/mclemore/projects/uranium/documents/50C_URANIUM_inprog_013ginger.pdf.

McLemore, V.T., Wilton, T., and Pelizza, M.S., 2016, *In situ* recovery of sandstone-hosted uranium deposits in New Mexico: Past, present, and future issues and potential: New Mexico Geology, v. 38, p. 68–76, https://geoinfo.nmt.edu/publications/periodicals/nmg/38/n4/nmg_v38_n4_p68.pdf.

McLemore, V.T., Hill, B., Khalsa, N., Lucas Kamat, S.A., 2013, Uranium resources in the Grants Uranium District, New Mexico: An update: New Mexico Geological Society, Guidebook 64, p. 117–126.

Merritt, R.C., 1971, The Extractive Metallurgy of Uranium: Golden, Colorado School of Mines Research Institute, 576 p.

Navajo Nation Council, 2005, Diné Natural Resources Protection Act of 2005, Resolution of the Navajo Nation Council, Window Rock, AZ: Navajo Nation Council, https://www.grandcanyontrust.org/sites/default/files/gc_uranium_navajoCouncilResolution.pdf.

Navajo AML Department, 2020, Navajo Nation Abandoned Mine Lands Reclamation Department: Window Rock, Navajo Nation, https://www.aml.navajo-nsn.gov/ (accessed April 3, 2020).

Nelson, J.D., and Kane, J.D., 1980, Failure of the Church Rock Tailings Dam: Ft. Collins, Symposium on Uranium Mill Tailings Management, Colorado State University, p. 505-510, https://en.wikisource.org/wiki/The_Failure_of_the_Church_Rock_Tailings_Dam.

Nichols, K.D., 1987, The Road to Trinity: New York, William Morrow & Co., 401 p., ISBN 0-688-06910-X.

Nuclear Regulatory Commission, 2018a, Homestake-Grants Uranium Recovery Facility: U.S. Nuclear Regulatory Commission website, https://www.nrc.gov/info-finder/decommissioning/uranium/is-homestake.pdf (accessed 2/10/20).

Nuclear Regulatory Commission, 2018b, Rio Algom - Ambrosia Lake Uranium Recovery Facility: U.S. Nuclear Regulatory Commission website, https://www.nrc.gov/info-finder/decommissioning/uranium/rio-algom-ambrosia-lake.html (accessed 2/10/20).

Nuclear Regulatory Commission, 2019, United Nuclear Corporation Church Rock Mill Site: U.S. Nuclear Regulatory Commission website, https://www.nrc.gov/info-finder/decommissioning/uranium/united-nuclear-corporation-unc-html (accessed 2/10/20).

Rhodes, R., 1986, The Making of the Atomic Bomb: New York, Simon & Schuster, 896 p., ISBN 1-4516-7761-8.

SJBRUS, 1980, Uranium development in the San Juan Basin region: A report on environmental issues; San Juan Basin Regional Uranium Study: Albuquerque, U.S. Department of the Interior, 547 p.

Thomson, B.M., Longmire, P.A., and Gallaher, B.M., 1982, The hydrologic environment and uranium production in New Mexico, *in* Water & Energy: Technical and Policy Issues: American Society of Civil Engineers, p. 525-531.

Thomson, B.M., and Heggen, R.J., 1983, Uranium and Water: Managing Common Resources: Chemtech, v. 13, n. 5, p. 294–99.

Thomson, B.M., in press, Environmental Contamination from Uranium Mining and Milling in the Western U.S., *in* Siegel, M., Selinus, O., and Finkelman, R.B., eds., Practical Applications of Medical Geology: New York, Springer International Publishing.

U.S. House of Representatives, 1979, Mill tailings dam break at Church Rock, New Mexico: Washington, D.C., Oversight Hearing before the Subcommittee on Energy and the Environment, Serial No. 96-25, Committee on Interior and Insular Affairs, 232 p.

Van Metre, P.C., and Gray, J.R., 1992, Effects of uranium mining discharges on water quality in the Puerco River Basin, Arizona and New Mexico: Hydrological Sciences Journal, v. 37, p. 463–80, https://doi.org/10.1080/02626669209492612.

Vogt, T.C., Strom, E.T., Venuto, P.B., Winget, J.E., and Scoggins, M.W., 1984, *In-Situ* Leaching of Crownpoint, New Mexico, Uranium Ore: Part 6 - Section 9 Pilot Test: Journal of Petroleum Technology, v. 36, n. 12, p. 2243–54.

Weaver, B., and Hoffman, G.L., 2019, Annual monitoring report/performance review for Homestake's Grants Project pursuant to NRC License SUA-1471 and Discharge Plan DP-300 2018, NRC Accession Number ML 19101A375, Grants, NM: Homestake Mining Company and Hydro-Engineering, LLC, 877 p., https://adamswebsearch2.nrc.gov/webSearch2/main.jsp?AccessionNumber=ML19101A375.

New Mexico Geological Society, Special Publication 14, Geology of the Mount Taylor Area, 2020, p. 97-104.

VEGETATION DENSITY AND VAPOR PRESSURE DEFICIT: POTENTIAL CONTROLS ON DUST FLUX AT THE JACKPILE URANIUM MINE, LAGUNA PUEBLO, NEW MEXICO

Reid Brown[1] and Daniel Cadol[2]

[1]Uranium Recovery Program, Wyoming Department of Environmental Quality, Cheyenne, WY, 82001; reiddbrown@gmail.com
[2]New Mexico Institute of Mining and Technology, Socorro, NM, 87801; Daniel.Cadol@nmt.edu

Abstract—A recent study investigated various processes that control dust transport at a former uranium mine in Laguna Pueblo, New Mexico. Two processes were found to be important in controlling dust transport at the Jackpile mine site: vegetation and soil moisture content inferred from the vapor pressure deficit (VPD). To determine the importance of vegetation, two dominant species were considered: juniper and grass. Dense juniper stands had higher soil uranium concentrations compared to other vegetation types and densities. Moderate and sparse stands had median soil uranium concentrations equal to or less than grass-dominated systems. This suggests that there is a critical stand density that reduces wind speed between individual plants, reducing scour. Designing dust mitigation strategies to maintain stands at this critical density could be important for future site remediation. Seasonal effects on wind speed and soil moisture were also considered. The results showed that dust flux was the greatest in the spring. Unexpectedly, dust flux in the winter showed a marked decrease compared to the other three seasons despite having the highest two recorded wind gusts and a similar sustained winds profile compared to spring. Weather data collected on site was used to calculate the VPD to use as a proxy for soil moisture. The winter experienced the lowest VPD. A low VPD indicates there is more moisture in the air reducing the gradient driving soil moisture evaporation. Based on the positive relationship with dust flux, calculated VPD was able to reproduce seasonal trends of soil moisture reliably and is a good proxy for soil moisture when that data is unavailable.

INTRODUCTION

For nearly a century, factors controlling dust generation and transport have been a major topic of interest in the global scientific research community. These studies have covered wind-tunnel studies to field research, ranging from the pebble scale up to the landscape and even global scale (Bagnold, 1936; Lyles and Schmeidler, 1974; Gibbens et al., 1983; Gillette and Stockton, 1989; Dong et al., 2004; Ajmone-Marsan et al., 2008; Ben-Ami et al., 2012). All this effort has been focused on dust generation, transport, and deposition, because these are important processes that span multiple disciplines from soil formation to contaminant transport to human and environmental health. There are a myriad of sources and factors, both natural and anthropogenic, that influence dust generation and transport. One anthropogenic source of dust that is of particular interest to New Mexico is dust generation caused by mining activities. New Mexico has a long history of mining activities throughout the state, with operations both large and small. The size of the mine, topography, vegetation and climate all influence the amount of dust that can be produced during a mine's life. Both active and improperly reclaimed mines can increase dust generation compared to natural systems (Gillette, 1980; Silvester, 2009) and transport contaminants, degrading local air quality as well as being integrated into the soil where the dust is deposited (Reheis, 1995). Here, we investigate the processes controlling the mobilization and deposition of mine-sourced dust from the Jackpile Mine, a former uranium mine located in northwestern New Mexico that is currently being reclaimed. The Jackpile Mine is located within the Laguna Pueblo, New Mexico, approximately 50 km west of Albuquerque (Fig. 1).

Dust generation has been shown to be significantly less in vegetated plots compared to bare plots of land (Merino-Martín et al., 2014). Vegetation, or lack thereof, at a site impacts the roughness of a surface, which is an important factor in both dust generation and deposition. Surface roughness is a first-order control on resistance to the movement of wind. This increased resistance from surface characteristics increases the displacement height, below which there is limited turbulence and wind velocity, promoting gravitational settling of suspended particles. For example, at the Jackpile Mine site, there are several scales of surface roughness. There is topographic relief, which can range on the order of 10-100 meters, and vegetation variation, which can range in heights from 0.3 m to 2.0 m. Taller surface obstructions vertically displace the wind column due to an increase in the height at which the wind velocity is equal to zero (zero-plane of displacement – Z_d) (Fig. 2). Surface roughness of a vegetated area is determined by vegetation height with the Z_d typically estimated at 0.7 times the vegetation height (Z_{veg}) (Dingman, 2008). Slower wind velocities have a reduced vertical component of turbulence and thus reduce the particle sizes that can remain suspended. If the surface roughness elements are tall or dense enough, the near-ground wind speed can decay to zero (Stearns, 1970). Vegetation cover has been shown to reduce dust flux (Van de Ven et al., 1989; Breshears et al., 2009; Merino-Martín et al., 2014) and promote deposition by physically trapping sediment

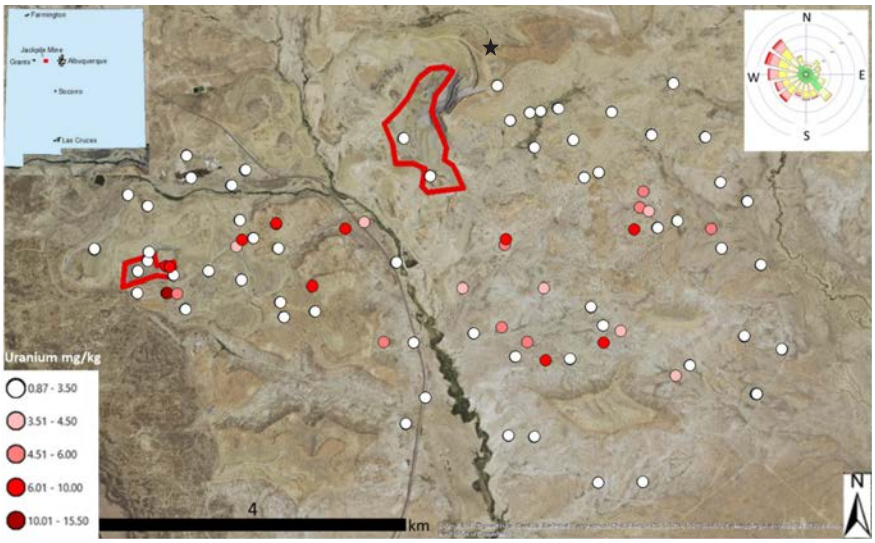

FIGURE 1. The lightest circles are soil samples with a soil uranium concentration at or below site background level as determined by NURE data (Smith, 1997). Remaining soil samples above site background levels with uranium centration increasing with shade of gray. The darker the shade of gray the higher the soil uranium concentration. The pits are outlined in gray. Windscale in upper right; see Figure 3 for more detail. Weather station location denoted by the black star.

particles (Van de Ven et al., 1989). For arid environments, even sparse vegetation is important for reducing soil loss since vegetation height is more important than vegetation density in reducing erosion (Van de Ven et al., 1989).

In addition to vegetation cover, soil moisture is an important factor in the erodibility of a soil. A completely dry soil is much more erodible compared to a damp soil (Elmore et al., 2008). Increased soil moisture content can cause small friable soil particles to form larger aggregates, which are more difficult to mobilize by wind. Not every weather station has the ability to measure soil moisture, and for those that do, the probes can fail. We wanted to come up with a proxy for soil moisture that could be widely applied to weather stations and data sets lacking soil moisture data. We settled on the vapor pressure deficit (VPD), which is a measure of the difference between saturation pressure and the actual vapor pressure. This difference is a key component in evaporation and represents the gradient that drives vapor transport away from the evaporating surface. During the winter, grass is dead and juniper transpiration is depressed. Large weather systems could bring in moist air but would likely be associated with precipitation events or at least reduce the evaporation of moisture from the soil. There are no large water bodies near the mine site, thus the largest source for the moisture is the soil.

The Jackpile Mine site, which is located in an arid setting, is an ideal location to test both vegetation density and VPD as controls on dust transport. The disturbed landscape combined with sparse rainfall and windy conditions should produce source areas of dust across the site. According to the U.S. EPA National Priority Listing (USEPA, 2012), the metals of concern at the site are uranium, chromium, manganese, cobalt, vanadium and zinc Site remediation efforts were carried out in 1995, consisting of covering waste rock piles and re-contouring unstable pit walls and waste piles (U.S. Department of the Interior, 1986). Vegetation was planted to reduce erosion. In 2007, a compliance assessment was conducted and failed (U.S. Department of the Interior, 1986). The mine site was proposed to the National Priorities List in 2012 and became a Superfund designated site in 2013.

Dust traps were installed across the mine site, in areas with different vegetation types and densities, to collect windblown sediment. In addition to the mass of sediment collected, the mass of known contaminants bound to the dust will also be informative. Soil concentrations of the contaminants of concern listed above were analyzed for a representative range of vegetation types. Pairing climate data with dust flux collected concurrently helped refine our knowledge on the relationship between local climate, vegetation and dust transport.

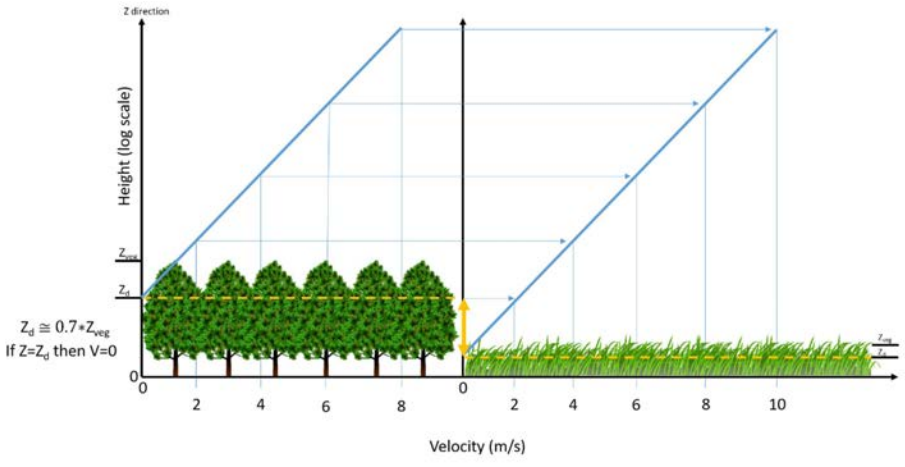

FIGURE 2. The impact of changing vegetation height (Zveg) on the zero-plane of displacement (Zd) and the wind velocity profile. Height (Z) is given in log-scale (after Dingman, 2008 and Bagnold, 1941).

MINING HISTORY, GEOLOGY, AND CLIMATE

The Jackpile ore body is a tabular, sandstone-hosted deposit. The Jackpile Sandstone is located in a 21-km by 56-km depression in the Brushy Basin Member of the Morrison Formation, which is Jurassic in age (Schlee and Moench, 1961). Its thickness ranges from 0-61 m and is generally treated as the upper member of the Morrison Formation in its locale (Nash, 1968).

The Jackpile Sandstone is arkosic and was derived from granitic, volcanic and sedimentary rocks (Nash, 1968). The study site is predominantly composed of mesa tops overlying Cretaceous sedimentary rocks and Quaternary valley fill. There are rocks of Jurassic age exposed, but these are less extensive in the area compared to Cretaceous rocks and Quaternary sediments and are primarily limited to mesa slopes (Moench and Schlee 1961; Nash 1986). Jackpile Mine was leased and operated by Anaconda Minerals Company, a division of Atlantic Richfield Company, from 1951–1983. During that time 400 million tons of rock were moved and 25 million tons of ore were removed. The ore grade averaged 0.1-1.3% U_3O_8 (U.S. EPA, 2012). Rock material was considered waste if the uranium grade was less than 0.06%.

The climate is semiarid, with the site receiving most of its annual rainfall during the monsoon season from July to August. The rest of the year is generally dry with occasional snow in the winter. The spring windy season is dominated by winds from the west and northwest. Throughout the year winds from these directions consistently average the highest wind speeds as well as have the highest gust speeds. Though winds come from all directions, the majority of the aeolian transport is expected to be toward the southeast of the main pit.

EXPERIMENTAL DESIGN

Site selection for dust traps was primarily based on two factors: (1) distance from the main Jackpile pit and (2) vegetation type, enabling analysis of the effect of these two variables on dust flux. The two prominent types of vegetation in the area are a 30- to 40-cm tall grass and 2+-m tall juniper woodlands. Vegetation density ranged from bare ground to sparse (gap between individual plants >5x vegetation height), moderate (5x height > gap > 1x height), and dense (1x height > gap). Sites were assigned to each vegetation density class. The class assignments were not quantitatively measured but were estimated by inspection. More emphasis was placed on vegetation type than soil type. Soil analysis was not carried out as part of the project but should be considered in future work.

Fifteen vertical sets (stems) of Big Spring Number Eight (BSNE) dust flux traps were installed across the study site. The dust traps consist of a round metal post with four dust traps attached at heights of 0.25, 0.5, 1.0 and 1.5 m above the ground surface. The traps have a tail fin and are designed to pivot around the central post like a wind vane and always point into the wind. Dust samples were collected roughly every two months to allow enough sample to be collected to process and yet still test seasonal impacts on dust transport. Dust flux was calculated by dividing the measured mass of a dust sample by its collection time and by the area of the trap opening. Because of the remote location we were unable to capture individual wind events. However, the traps are designed to prevent collected dust from being blown out even if multiple wind events are sampled during a collection period.

Sample locations for a broader soil survey were selected using a random sampling scheme. The study area was divided into four zones: Mesa Woodland, Mesa Grass, Valley Woodland, Valley Grass Sample points were randomly generated within each zone. A total of 120 sample locations were generated, with a minimum distance between points of 300 m. This helped cover a larger area with a small sample size to reduce bias for collecting several samples close to each other. The pre-mining background levels of uranium in the soil were estimated using a subset of the National Uranium Resource Evaluation (NURE) data collected in the immediate vicinity of the mine site in the 1970s (Smith, 1997). Unfortunately, the NURE survey did not include Laguna Pueblo lands and the author was unable to find site specific data for background soil uranium levels in U.S. EPA reports or from the mine operator.

Sediment samples were processed using the EPA 3052b digestion method. In many cases, dust samples were digested in entirety due to small sample size. During sample preparation, soil samples were sieved to remove gravel larger than 2.0 mm. Soil samples were ground with a ring and puck for homogenization and to aid digestion. Dissolved samples were diluted as needed and analyzed on an Agilent 7900 ICP-MS. Dust samples typically had too little mass and were not diluted. Doing so would have yielded heavy metal concentrations in dust below the minimum detection limit of the ICP-MS.

A weather station was installed on top of Gavilan Mesa at the northern end of the study area to get site specific meteorological data. This location was chosen because it was far from the edges of the mesa, and there were no nearby vegetation obstructions. The area had a large unobstructed fetch in all directions, and, as the high point in the study area, it likely received the maximum wind speed. We did not install soil moisture probes on site, but the weather station collected relative humidity and temperature hourly. From these parameters, we were able to calculate the VPD.

We chose to use permutation tests to compare mean values of dust flux between seasons as well as the concentration of uranium on sediment samples. This was done to address non-normality in our datasets associated with a few important but extreme wind events and right skewed soil uranium concentrations. The result of the permutation test is a p-value that indicates the likelihood that the two datasets were randomly drawn from the same population and could generate the observed means (Helsel and Hirsch, 2002). We chose a threshold of significance to be α=0.05; this is the typical significance threshold used in the scientific community, yet the authors acknowledge it is also somewhat arbitrary. If the p-value ≤ 0.05, then the means are deemed to be different, implying the samples are from different populations.

RESULTS AND DISCUSSION

Dust transport was observed throughout the year, primarily driven by the strongest winds coming from the west-northwest. Annual and seasonal data all showed similar trends (Fig. 3). Dust flux varied seasonally, likely due to seasonal variations in average wind speed as well as seasonal weather patterns that control soil moisture. Both vegetation and topography during active mining and subsequent reworking impacted the wind profile, influencing deposition of uranium-bearing dust

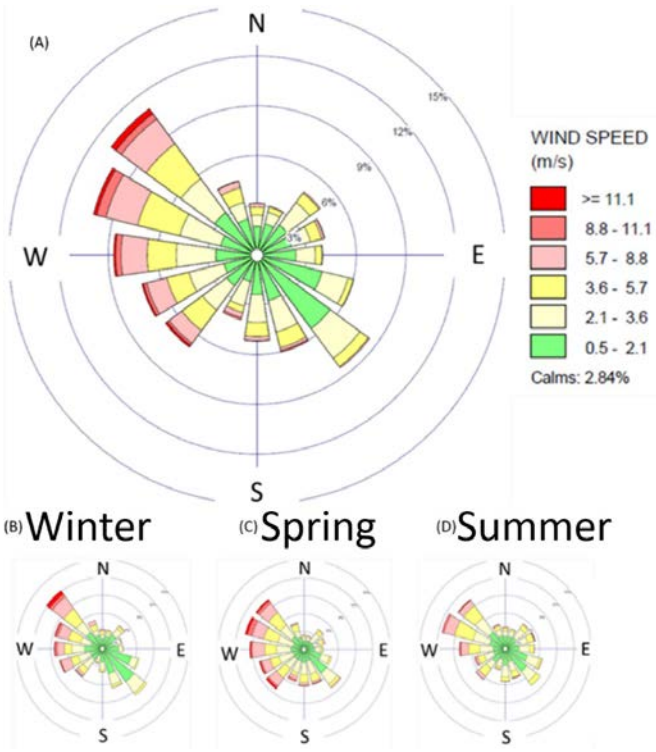

FIGURE 3. **A)** Each wedge corresponds to a direction the wind originates from with the length of the wedge corresponding to the percent of time coming from that direction. The colors correspond to the wind speed, closest to center are the lowest wind speeds. The darkest shade of gray corresponds to the highest wind speeds and is also the outermost bin. **B-D**) are the seasonal data. Standard season dates were used to split the data into each season.

and leading to higher uranium concentrations in valleys relative to mesa tops and in dense juniper stands relative to other vegetation communities. The concentration of uranium in dust collected at 1.0 m and 1.5 m was significantly higher than in bulk soils ($p=0.046$). There was no difference between dust collected at 1.0 m and 1.5 m or in the finest soil fraction with a grain diameter less than 0.063 mm ($p=0.92$). The similarity in uranium concentration of the fine soil fraction and the dust indicates that aeolian transport preferentially mobilizes the finest soil fraction, which also has the highest heavy metal concentration (see discussion in Brown (2017) for more details about why small size fractions absorb metals).

Wind speed and direction were critical to this study. At the study site, the most frequent wind direction we recorded was out of the northwest (Fig. 3), likely due to the topography of the area, particularly Mt. Taylor, rising to the west of Jackpile Mine. Wind speed and direction impacted all aspects of this study, from the amount of sediment transported to the direction the dust travels to how much is deposited and where. Over the course of the study the wind patterns were remarkably consistent. Our results agree with Anaconda Mineral Company's continuous environmental monitoring program that spanned from 1977 to 1983 (U.S. Department of the Interior, 1986). This consistency suggests that our wind data are representative of long-term local trends and were similar to the conditions present throughout the life of the mine.

Soils ranged from coarse to fine across the study site. However, by mass most of the sediment particles fell in the 0.25 mm and 0.125 mm size classes for ever soil. The particle-size distribution in soils is important because soil is the erodible material that is the source of the dust. While particle shape and packing are important, on average larger particles are more difficult to mobilize (Bagnold, 1936). Between 60 and 90% (by mass) of the top 5 cm of most soils we measured consisted of particles smaller than 0.25 mm in diameter. Bagnold (1936) reported a threshold wind speed value of 0.2 m/s to transport dune sand with 0.25 mm diameter. Threshold wind speed values for transport are predicted to increase for particles smaller than 0.1 mm in diameter due to particle surface charges and due to position within the laminar sub-layer; however, the thresholds of transport for the particles observed in this study are all well within wind speeds recorded on site.

The largest mass flux for the 0.25, 0.5, and 1.0 m heights occurred during the spring sample collection (Fig. 4), an intuitive result stemming from the larger sediment particles that can be mobilized in stronger winds. Larger particles will substantially increase the mass flux since more mass is transported per grain of sediment. Our results showed little seasonal variation in the mass flux at the higher collection heights (1.0 and 1.5 m) relative to the variation at lower heights. This may indicate more seasonal consistency for the more moderate winds necessary to maintain the very fine particles in suspension that dominated flux at these heights. While the larger sand grains may not have been mobilized as often in the fall, summer, or winter, the fine particles were still being transported. This result could suggest that regional sources and wind patterns may be more important than local conditions as height above the

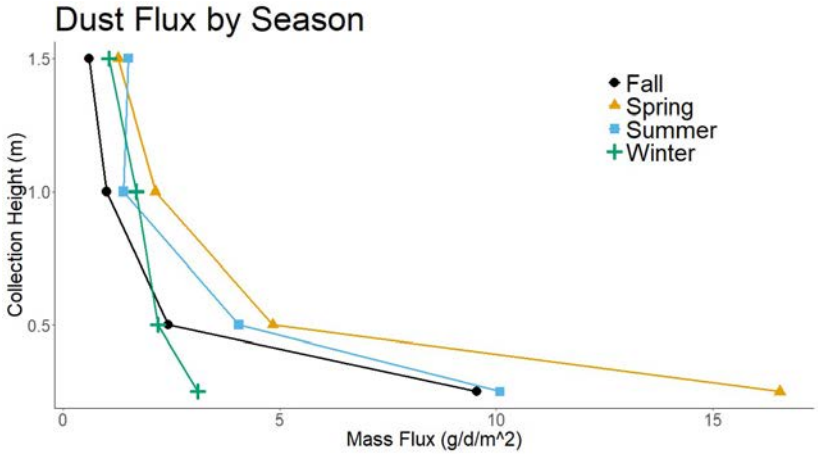

FIGURE 4. Dust flux (x-axis) plotted as a function of collection height (y-axis) and season (point shapes). Data collected in spring, summer, fall and winter are represented by triangle, square, circle, and cross dots respectively. The lines are illustrative only and not meant to be an interpolation between points.

surface increases. This would imply that managing air quality with respect to dust for communities and the environment downwind of should include management plans for both local point source and regional sources of dust.

Similar wind patterns were observed during the winter and spring sampling seasons, however these similarities were not reflected in dust flux. The two largest individual wind speeds occurred during the winter sampling period (Fig. 5). Additionally, wind blew from the west for a significant amount of time during spring and winter (46% to 38%, respectively). During both spring and winter, the wind gusted to the highest windspeed class for about 1.5% of the time. As expected the spring recorded the greatest dust mass flux. Winter sampling period mass flux was depressed for the lowest collection height (Fig. 4). A likely cause for the reduction in dust flux during the winter is increased soil moisture due to snowfall, colder temperatures, and higher relative humidity. The time period of the winter sampling coincided with the lowest VPD measured during the study as well as the lowest mass flux collected (Figs. 4, 5).

While VPD is not a direct measure of soil moisture, we argue that it is a reasonable proxy, since it is a primary control on the rate at which water evaporates from a soil. A lower VPD reduces the potential rate at which soil loses moisture to the atmosphere. The VPD does not describe absolute soil moisture content, nor do our calculations account for wind increasing evaporation. However, we contend that while VPD may be a poor measure of soil moisture on a daily scale, it could be a representative on the month or seasonal scale where many days in a row of below annual average VPD in the winter could indicate a soil with more moisture compared to average or above average spring and summer seasons (Fig. 6). When the data is analyzed on a seasonal scale, winter is found to be statistically lower on average than spring or summer ($p < 2x10^{-16}$, $p < 2x10^{-16}$ respectively). Fall VPD was found to be statistically lower than Winter VPD ($p= 8.11x10^{-8}$), however only the last 12 days of fall were included in our data collection and likely do not represent the entire season. These results show that VPD significantly varies by season and that the low VPD coincides with the least dust flux, suggesting that VPD is a reasonable approximation for soil moisture content at the season scale.

Dust flux is not continuous throughout the collection period. Dust flux generally comes in short bursts associated with larger wind events (Brookfield, 1970). Ash and Wasson (1983) defined a measure for sand movement frequency as the number of days with recorded wind speeds above 8 m/s. For this study we adopted this convention to analyze seasonal relationships of wind speed and dust flux. Spring and fall had both a similar proportion of days with maximum wind speed exceeding 8 m/s and similar collection period length. Despite this, spring had four times the amount of dust flux at the 0.25 m collection height and double the dust flux at the 0.5 m collection height (Fig. 4). The spring season had an increasing trend of maximum daily VPD (Fig. 7), which leads to the intuitive conclusion that drying soil and frequent elevated wind speeds generates the most dust flux. Further emphasizing the relationship between VPD and wind speed can be seen in a comparison of winter and summer. The summer collection period was 32 days shorter

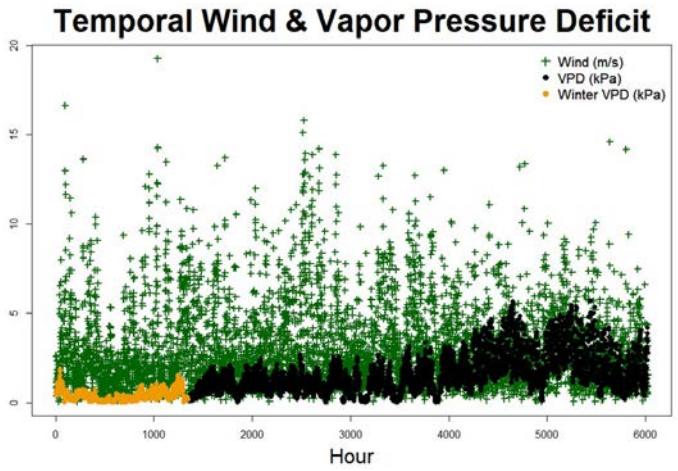

FIGURE 5. Vapor pressure deficit (VPD) in kPa and wind speed in m/s as a function of time in hours. All variables are plotted relative to the same generic y-axis scale. Both wind in m/s and VPD in kPa can use the same scale. Individual hourly wind measurements are crosses. VPD measured during the winter are light gray circles. VPD was calculated hourly.

and recorded days with winds above 8 m/s less often, yet, compared to winter, the transport of dust at the 0.25 m collection height was nearly triple and the dust flux at the 0.5 m collection height doubled (Fig. 4). Within less time the summer season was able to transport more dust, meaning that the increase in maximum daily VPD during the summer was able to overcome reduced high wind frequency (Figs. 6, 7). When the reduced length of the summer collection period is considered, it further emphasizes the importance of soil moisture as a control on dust flux and that VPD can detect these important seasonal soil moisture trends.

Variations in soil uranium concentrations were confounding. While the pattern of soil uranium concentration is consistent with southeastward dust transport (Fig. 2), many of the soil samples were located in areas that had been disturbed by

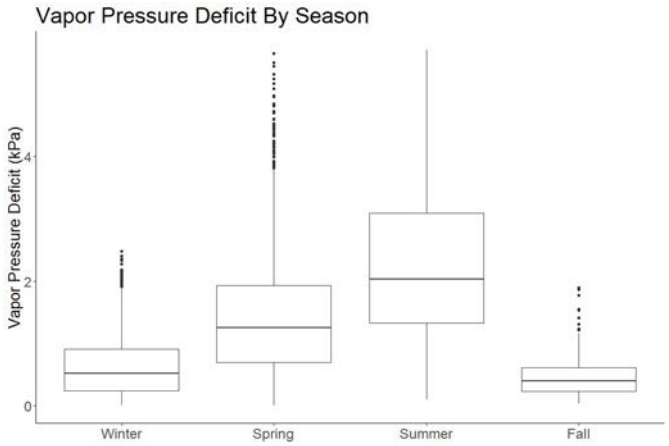

FIGURE 6. Vapor Pressure Deficit (VPD) by season. Average winter VPD is less than spring and summer VPD ($p < 2x10-16$). Fall VPD is less than winter VPD ($p=8.11x10-8$).

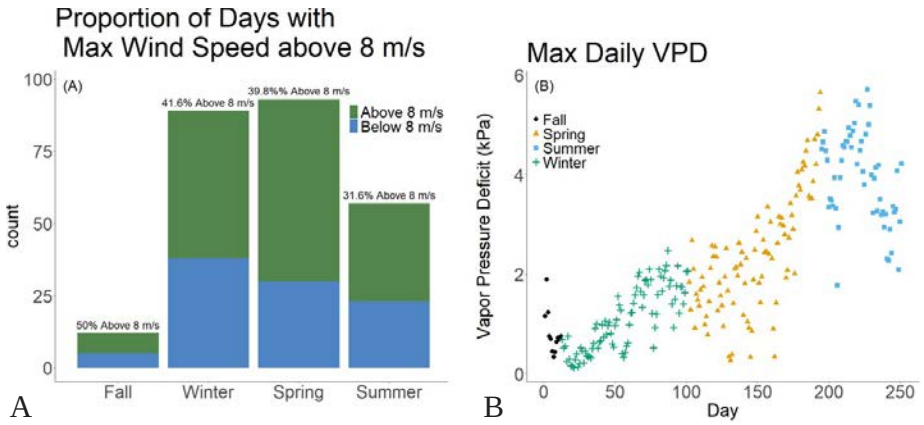

FIGURE 7. Comparison of days with maximum wind speed above 8 m/s by season. Proportions: Fall – 50.0%, Winter – 41.6%, Spring – 39.8%, Summer – 31.6% (**A**). Maximum daily vapor pressure deficit VPD by season represented by different points (**B**).

mining activities and were located in Quaternary sediments potentially eroded from Jackpile sandstone outcrops; this prohibits confidently determining the source of elevated uranium in many of the samples without additional data. That said, it is worth noting that uranium concentrations increased with dust collection height ($p<0.05$), and sample concentrations from the highest dust traps were nearly statistically elevated above site-wide soil uranium concentrations ($p = 0.052$). This suggests that dust deposition is one of several potential mechanisms that contribute to the observed increases in soil uranium concentration southeast of the mine.

Erodible sediments have different threshold wind velocities depending on their composition. The threshold velocity can be lowered by both anthropogenic and natural processes that disturb the sediment surface (Gillette et al., 1980). There were many anthropogenic sources of disturbance that would have increased the erodibility of soil. During mine operations, sources of dust included the exposed pit, rock crushers, uncovered waste rock piles, and onsite ore stock piles. Blasting and heavy machinery generate large amounts of dust, which then could be carried down wind of the source area (Silvester et al., 2009). During mine operation the waste rock piles were left uncovered, and, though less concentrated than ore, the waste and overburden contained up to 0.06% U_3O_8 (U.S. Department of the Interior, 1986). Observed wind events on site, both past and present, have been strong enough to mobilize sediment. Ore and waste rock piles exposed to these events in the past could potentially be a source of uranium-bearing dust. We were unable to conclusively source the origin of the uranium in the soil downwind of the mine; however, our results, combined with previous and concurrent research, suggest that when Jackpile mine was active, dust transport may have been a more important mechanism in altering soils downwind of the mine compared to present day.

Restoring natural vegetative cover is a critical component of the remediation process and has widely been used as one metric of restoration success. One major reason for this is that vegetation has been shown to affect wind velocity, with greater wind resistance in denser vegetation (Breshears et al., 2009; Wolfe and Nickling, 1993). Qualitative data on vegetation density was collected at each site in the soil survey. Both vegetation types were classified as dense, moderate or sparse (Fig. 8). If no juniper was present then the site was automatically considered a grassland, and thus only grasslands were classified as bare. Grasslands have a slight increase in the soil uranium concentration with increasing density. Juniper woodlands have a large increase in median soil uranium concentration for the densest stand (Fig. 8).

While there was no difference between dust flux in valley woodlands and valley grasslands, the median soil uranium concentration was higher in woodlands compared to grasslands (Brown, 2017). The bulk of the increase came from the densest stands of juniper (Fig. 8). Unfortunately, the densest stands were included only in the soil survey, and no dust traps were installed in dense juniper stands. Not knowing the magnitude of the dust flux moving through dense stands limits further discussion to speculation. However, it does reinforce the difficulty in establishing a link between horizontal dust flux and deposition rates. There are potential mechanisms that could enhance the deposition of fines even with large flux moving through the woodlands. For example, the increased surface area of the juniper and its fine, dense foliage could trap dust particles until they are washed to the ground in the next rain. Additionally, the dense stand would reduce near surface wind velocity reducing resuspension and dust flux out of the stand of vegetation.

No attempt was made to control for stand size in this study. It is very possible that continuous stand size is a critical factor in the ability of taller vegetation to promote dust deposition especially at lower stand densities. Wolfe and Nickling

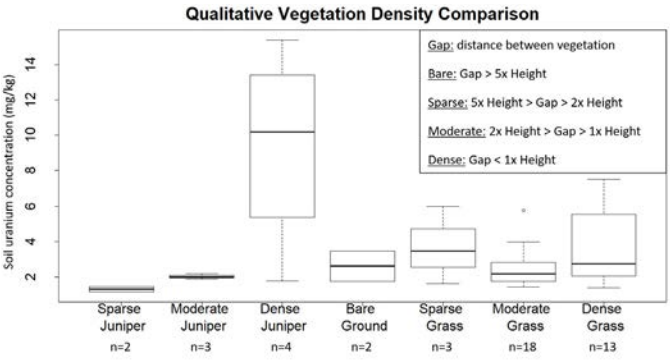

FIGURE 8. Soil uranium concentration grouped by the seven vegetation density classifications. Gap refers to the distance between the vegetation. Bare is considered areas where grass clumps were more than five times grass height apart. Sparse is vegetation that had gaps between five times and two times vegetation height. Moderate is vegetation that had gaps between two times and one times vegetation height. Dense was vegetation that has gaps less than the vegetation height.

(1993) showed that stands of vegetation below a critical density can actually contribute to scour of soil between the individual plants. The critical stand density promotes skimming flow over and around the stand of vegetation so that little to no wind can penetrate the stand itself. This process could be the reason for the relatively small difference in soil uranium concentration between sparse and moderate stands of juniper compared to dense stands. In fact, median soil uranium concentrations in sparse and moderately dense stands of juniper appear to be similar to and potentially lower than median soil uranium concentrations in bare and grass-dominated systems (Fig. 8), suggesting that scour may be occurring around sparse larger vegetation. This may be due to the stand of vegetation not being dense enough to vertically displace the wind column and instead channelizes the wind between the individual plants. However, caution should be taken with this conclusion given the limited number of soil samples from sparse and moderate juniper stands. Future work, particularly in arid environments, should look at stand densities that are realistically achievable and can maintain themselves long-term after remediation has ended. If these stand densities and the stand area do not promote skimming flow of wind then other vegetative cover should be considered to protect the land surface. This is particularly important when considering the vegetative cover to place on surfaces susceptible to erosion, such as on slopes, covered waste rock piles or tailings impoundments.

CONCLUSIONS

Climate and environment are both important factors controlling the generation of dust in both disturbed and natural landscapes. Wind and VPD combine to produce seasonal variations in dust flux at the Jackpile mine site. What makes VPD a particularly attractive parameter is that it only requires two common probes used in many weather station setups: temperature and relative humidity. Many mine operators and municipalities could begin tracking VPD as a proxy for soil moisture without purchasing new equipment. The seasonal effect was primarily observed at lower collection heights suggesting that regional sources of dust generation may be more important than sources on site when local soil moisture content is elevated or at times of depressed wind speeds. Meteorological data and soil uranium concentrations are consistent with southeasterly transport of uranium from Jackpile mine pits, but the relative contribution of uranium-bearing dust from mining activities to the soil is unsettled due to unknown pre-mining conditions. Though sample size was small, vegetation stand density may be an important factor controlling the erodibility of the soil in the vegetation stand's immediate vicinity. Sparse and moderate stands were similar in soil uranium concentration to grassland systems suggesting there may be a critical stand density that needs to be achieved before significant dust deposition occurs in juniper stands. This relationship could have important implications in future remediation efforts when deciding what species to plant and where to plant them to control erosion and dust generation.

ACKNOWLEDGMENTS

There were many individuals and groups that came together to make this project possible. New Mexico EPSCoR funded the bulk of the project through the National Science Foundation award #IIA-1301346. Additional funds came from a 2015 NMGS grant in aid. None of the samples would have been analyzed without the hard work of Bonnie Frey and the New Mexico Bureau of Geology Geochemistry Lab. Reviewers Drs. Gayan Rubasinghege and Jeffrey Pepin provided great comments, without which, this paper wouldn't have reached its full potential. The authors would also like to thank students Olivia Chaves and Kyle Stark who provided field assistance. Lastly, site access would have been dangerous to impossible without the guidance and accompaniment of the Pueblo of Laguna Environmental and Natural Resources Department (ENRD) staff. Staff from Laguna ENRD additionally provided significant site details as well as rich historical context.

REFERENCES

Ajmone-Marsan, F., Biasioli, M., Kralj, T., Grčman, H., Davidson, C.M., Hursthouse, A.S., Madrid, L., and Rodrigues, S., 2008, Metals in particle-size fractions of the soils of five European cities: Environmental Pollution, v. 152, p. 73-81.

Ash, J.E., and Wasson, R.J., 1983, Vegetation and sand mobility in the Australian desert dunefield: Zeitschrift fur Geomorphologie, Supplementband, v. 45, p. 7-25.

Bagnold, R.A., 1936, The movement of desert sand: Proceedings of the Royal Society of London, Series A-Mathematical and Physical Sciences, v. 157, no. 892, p. 594-620.

Bagnold, R.A., 1941, The Physics of Wind Blown Sand and Desert Dunes: New York, William Morrow and Co., 336 p.

Ben-Ami, Y., Koren, I., Altaratz, O., Kostinski, A.B., and Lehahn, Y., 2012, Discernible rhythm in the spatio/temporal distributions of transatlantic dust: Atmospheric Chemistry and Physics, v. 12, p. 2253-2262.

Breshears, D.D., Whicker, J.J., Zou, C.B., Field, J.P., and Allen, C.D., 2009, A conceptual framework for dryland aeolian sediment transport along the grassland–forest continuum: effects of woody plant canopy cover and disturbance: Geomorphology, v. 105, no. 1-2, p. 28-38.

Brookfield, M., 1970, Dune trends and wind regime in central Australia: Zeitschrift fuer Geomorphologie, v. 10, p. 121-153.

Brown, R.D., 2017, Geochemistry and transport of uranium-bearing dust at Jackpile Mine, Laguna, New Mexico [Master's Thesis]: Socorro, New Mexico Institute of Mining and Technology, 89 p., <https://geoinfo.nmt.edu/geoscience/research/home.cfml?ID=83> (accessed March 7, 2020).

Dingman, S.L., 2008, Physical Hydrology, (reissued): Long Grove, Waveland Press Inc., 656 p.

Dong, Z., Wang, H., Liu, X., and Wang, X., 2004, The blown sand flux over a sandy surface: a wind tunnel investigation on the fetch effect: Geomorphology, v. 57, no. 1-2, p. 117-127.

Elmore, A.J., Kaste, J.M., Okin, G.S., and Fantle, M.S., 2008, Groundwater influences on atmospheric dust generation in deserts: Journal of Arid Environments, v. 72, p. 1753-1765.

Gibbens, R.P., Tromble, J.M., Hennessy, J.T., and Cardenas, M., 1983, Soil movement in mesquite dunelands and former grasslands of southern New Mexico from 1933 to 1980 Prosopis glandulosa, erosion rates: Rangeland Ecology and Management/Journal of Range Management Archives, v. 36, p. 145-148.

Gillette, D.A., Adams, J., Endo, A., Smith, D., and Kihl, R., 1980, Threshold velocities for input of soil particles into the air by desert soils: Journal of Geophysical Research: Oceans, v. 85, no. C10, p. 5621-5630.

Gillette, D.A., and Stockton, P. H., 1989, The effect of nonerodible particles on wind erosion of erodible surfaces: Journal of Geophysical Research: Atmospheres, v. 94, no. D10, p. 12,885-12,893.

Helsel, D.R., and Hirsch, R.M., 2002, Statistical methods in water resources,

in Reston, VA, U.S. Geological Survey, Hydrologic Analysis and Interpretation, Book 4: Techniques of Water-Resources Investigations 04-A3, 522 p.

Lyles, L., Schrandt, R.L., and Schmeidler, N.F., 1974, How aerodynamic roughness elements control sand movement: Transactions of the ASAE, v. 17, no.1, p. 134-0139.

Merino-Martín, L., Field, J.P., Villegas, J.C., Whicker, J.J., Breshears, D.D., Law, D.J., and Urgeghe, A.M., 2014, Aeolian sediment and dust fluxes during predominant "background" wind conditions for unburned and burned semiarid grassland: Interplay between particle size and temporal scale: Aeolian Research, v. 14, p. 97-103.

Nash, J.T., 1968, Uranium deposits in the Jackpile sandstone, New Mexico: Economic Geology, v. 63, no. 7, p. 737-750.

Reheis, M.C., Goodmacher, J.C., Harden, J.W., McFadden, L.D., Rockwell, T.K., Shroba, R.R., Sowers, J.M., and Taylor, E.M., 1995, Quaternary soils and dust deposition in southern Nevada and California: Geological Society of America Bulletin, v. 107, p. 1003-1022.

Schlee, J.S., and Moench, R.H., 1961, Properties and Genesis of "Jackpile" Sandstone, Laguna, New Mexico, in Peterson, J.A. and Osmond, J.C., Geometry of Sandstone Bodies: Tulsa, AAPG Special Volume 22, p. 134-150.

Silvester, S.A., Lowndes, I.S., and Hargreaves, D.M., 2009, A computational study of particulate emissions from an open pit quarry under neutral atmospheric conditions: Atmospheric Environment, v. 43, p. 6415-6424.

Smith, S.M., 1997, National Geochemical Database reformatted data from the National Uranium Resource Evaluation (NURE) hydrogeochemical and stream sediment reconnaissance (HSSR) program: U.S. Geological Survey, Open-File Report 97-492 (accessed 14 April, 2017).

Stearns, C.R., 1970, Determining surface roughness and displacement height: Boundary-Layer Meteorology, v. 1, no. 1, p. 102-111.

U.S. Department of the Interior, 1986, Final environmental impact statement for the Jackpile-Paguate Uranium Mine Reclamation Project: Laguna Indian Reservation, Cibola County, New Mexico: Albuquerque, U.S. Department of the Interior, Bureau of Land Management. Rio Puerco Resource Area., U.S. Bureau of Indian Affairs, Albuquerque Area Office, 304 p.

USEPA, 2012, Jackpile Mine: Site Listing Narrative, https://semspub.epa.gov/work/06/300064.pdf (accessed 15 January, 2020).

Van de Ven, T.A.M., Fryrear, D.W., and Spaan, W.P., 1989, Vegetation characteristics and soil loss by wind: Journal of Soil and Water Conservation, v. 44, p. 347-349.

Wolfe, S. A., and Nickling, W.G., 1993, The protective role of sparse vegetation in wind erosion: Progress in Physical Geography, v. 17, p. 50-68.

New Mexico Geological Society, Special Publication 14, Geology of the Mount Taylor Area, 2020, p. 105-110.

ENVIRONMENTAL GEOCHEMISTRY OF ST. ANTHONY MINE URANIUM ORES

Alexandra R. Pearce

New Mexico Institute of Mining and Technology, Earth and Environmental Science Department, 801 Leroy Place, Socorro NM 87801

Abstract—The St. Anthony Mine, in the Laguna mining subdistrict of the Grants uranium district, is slated for remediation. Its "Large Pit" has been accumulating uraniferous runoff and infiltrated groundwater since active mining ended in 1979. The site's responsible party, United Nuclear Corporation, has successfully petitioned for alternative abatement standards of regulated parameters, including uranium, as a result of geochemical modeling (using uranophane) and environmental impact assessments, which predicted unavoidably high levels of dissolved uranium post-reclamation. This study examined the geochemistry and leachability of ore samples to evaluate the potential for uranium, vanadium and arsenic release into groundwater under industrial leaching and post-closure conditions. The uranium ore of St. Anthony Mine is characterized by uraniferous organic matter — where uranium is part of an amorphous, organic-carbon rich matrix, which permeates the sandstone, and a minor secondary, oxidized mineral component. This study did not identify the mineral uranophane. Batch leaching tests showed that significant uranium, vanadium and arsenic are released under oxidizing, alkaline conditions. Groundwater leaching experiments showed appreciable release of uranium and vanadium, but not arsenic. Higher levels of organic carbon in ore material slows leaching rates.

INTRODUCTION

Although active mining at the St. Anthony Mine (Fig. 1) ceased in 1979 (Wilton, 2017), it is still awaiting remediation. Uranium concentrations in groundwater are high enough that an alternative abatement standard has been set for the site: 12.4 mg/L, 400 times the drinking water limit (U.S. Environmental Protection Agency, 2001). As the location is naturally host to large ore bodies permeated by groundwater, it is technically infeasible to lower uranium concentrations to the regulatory limits. The reclamation plan for St. Anthony includes partially backfilling the mine's "Large Pit" to mitigate issues of it acting as a hydraulic sink. Groundwater, discharging into the pit and pooling at the bottom, is highly contaminated with uranium due to evapo-concentration and weathering of exposed ores in pit walls (State of New Mexico, 2017). However, once the pit is filled and a pre-mining hydraulic gradient is reestablished, through-flowing groundwater may slowly carry dissolved uranium away from it. Despite this possibility, the host member where contamination is confined, the Jackpile Sandstone, is not currently and is unlikely to ever be used as a drinking water source (State of New Mexico, 2017).

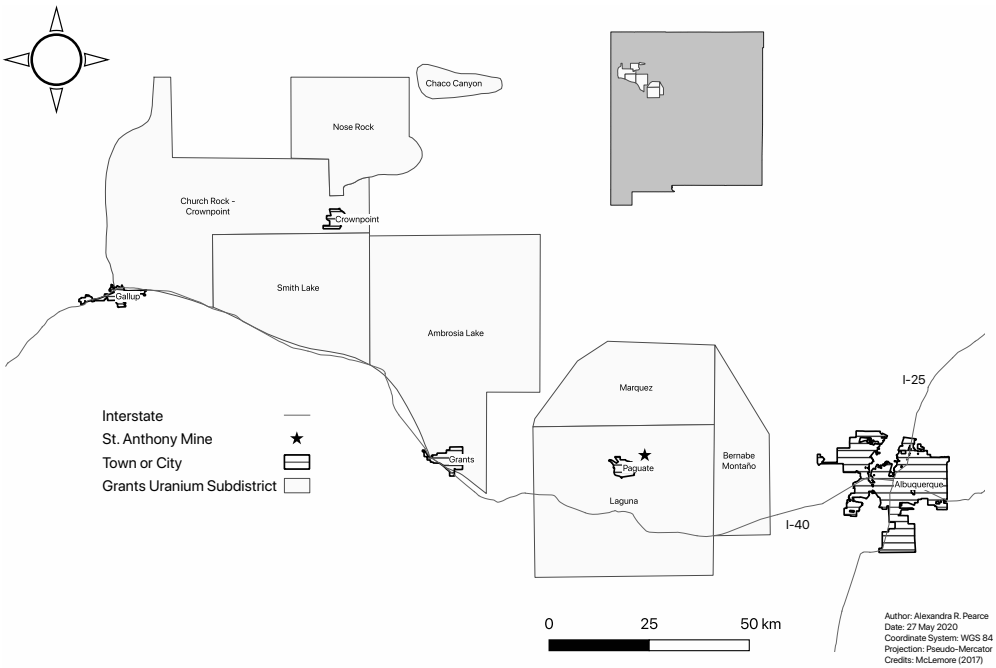

FIGURE 1. Map of the St. Anthony Mine's location (black star) within the Grants uranium district (subdistricts labeled, modified from McLemore, 2017).

The tabular uranium ore bodies of northwestern New Mexico, including those at the St. Anthony mine, formed at the focus of a 400,000 km^2 watershed encompassing the San Juan Basin. The paleo-hydrologic regime was such that saline, regional groundwater discharged into topographic depressions and mixed with fresher local waters laden with humic acids. Humic acids scavenged dissolved uranium and flocculated as humates, thus fixing uranium within a jellylike mass of organic matter that permeated the Jackpile Sandstone (Sanford, 1994). These deposits sustained several mines in the area, known

collectively as the Cebolleta project (Wilton, 2017), which yielded 3.8 million lbs of U_3O_8 by 1981. Of this, St. Anthony produced some 1.6 million lbs. Despite the large amounts of uranium extracted, extensive mineralogical characterization was not performed on ore material beyond the identification of tetravalent uranium minerals uraninite (UO_2) and coffinite ($USiO_4$), "organo-uranium complexes", and "unidentified, oxidized uranium complexes" (Wilton, 2017).

The contamination issues at St. Anthony arise from the mobility of uranium in an oxidizing environment. Once weathered from ores, its hexavalent form (U^{6+}) has a strong affinity for just about any organic acid or oxyanion it may encounter in groundwater, and uranyl (UO_2^{2+}) -carbonate, -sulfate, and -phosphate complexes may carry uranium long distances through an aquifer before precipitating out of solution. Uranyl carbonates are the most common groundwater species, encountered in carbonate-enriched systems at higher pH levels. Uranium carbonate minerals (e.g., cejkaite, $Na_4(UO_2)(CO_3)_3$) form in response to evaporation or increased carbon dioxide concentration. Uranyl sulfate complexes are present in waters at lower pH levels and will form minerals such as zippeite ($K_3(UO_2)_4(SO_4)_2O_3(OH)\cdot 3H_2O$) if groundwater evaporates (Hazen et al., 2009). Phosphate will complex with uranium where there are insufficient carbonate species (Cumberland et al., 2016). Uranyl phosphate minerals form under highly oxidizing conditions (e.g., autunite ($(UO_2)_2(PO_4)_2\cdot 11H_2O$)). Uranyl ions can also precipitate with vanadium to form relatively insoluble minerals such as tyuyamunite ($Ca(UO_2)(V_2O_8)\cdot 9H_2O$; Hazen et al., 2009). Cejkaite, zippeite, and uranium vanadates may be encountered as efflorescent growths on pit walls at St. Anthony (Caldwell, 2018).

The site's responsible party, United Nuclear Corporation, used the uranyl silicate mineral uranophane ($Ca(UO_2)_2(SiO_3\,OH)_2\cdot 5H_2O$) and silica saturation in a geochemical model to predict post-closure uranium levels (State of New Mexico, 2017). The alternative standard of 12.4 mg/L is the upper limit of uranium concentration of their model, Uranophane is one of the most common oxidized uranium minerals (Hazen et al., 2009) and was likely a convenient proxy for the more than two hundred U^{6+} minerals that may form under oxidizing, circumneutral conditions (Bowell et al., 2011).

Uranium poses great risk to human health (Hund et al., 2015), but its dissolution may also be associated with that of other toxic metals such as arsenic (Bowell et al., 2011), as well as vanadium. Arsenic may be present in Jackpile Sandstone ores within pyrite (Moench and Schlee, 1967), or as a component of organic matter (Liu et al., 2011). The availability of potentially harmful aqueous species and the extent to which groundwater may be impacted is controlled by the deposit mineralogy and water chemistry. This study characterized ore samples from the St. Anthony Mine to determine the ore's potential to release heavy metals into the environment when exposed to an industry standard alkaline lixiviant, as might be used in in-situ recovery efforts (Vogt et al., 1982), and native groundwater. This work is part of a broader study examining the leachability of ores found in the Grants uranium district.

METHODS

Two samples (SA2, SA4) were taken from an exposed ore face in the St. Anthony Mine (Fig. 2). Polished thin sections were made from epoxy-impregnated billets and were examined with an electron probe microanalyzer (EPMA) at the University of New Mexico's Institute of Meteoritics. Bulk geochemical analyses for metals, carbon and sulfur forms were performed by ALS Ltd. Geochemistry Lab (Vancouver, Canada) on ground subsamples. Batch-leaching experiments on disaggregated ores (500–74 µm size fractions) were carried out to determine potential metal loading under active mining and post-closure conditions, represented by a calculated pseudo-first-order rate constant (k), defined as follows:

$$k = 1/t\ (\ln Co - \ln C),$$

where t: time (48 hours), Co: initial concentration of the metal in the ore; C: post-leaching metal concentration

Briefly, disaggregated ore replicates were exposed to an alkaline lixiviant solution (1.98g/L H_2O_2 + 2g/L $NaHCO_3$, pH 8.2) and unaugmented groundwater (SA4 ore only) sourced from a Westwater Canyon Formation aquifer (pH 7.4). Leach-

FIGURE 2. Satellite image of St. Anthony Mine's unreclaimed pits and pit lake. The black star represents this study's sampling location.

ate was analyzed via inductively coupled plasma mass spectrometry (ICP-MS) for metals. Uncertainty values for analytical methods are listed in Appendix 1.

RESULTS

Ore Characterization

St. Anthony ores are arkosic, low-porosity (<4%) sandstones that have been enriched by an amorphous and nonstoichiometric uranium phase (Fig. 3A) associated with organic carbon. The samples are relatively high in bulk arsenic, uranium and vanadium (Table 1). Though the samples were collected from the same ore pocket, sample SA4 has higher levels of carbon and sulfur forms, arsenic, phosphorus and uranium. Sample SA2 contains more vanadium.

Figures 3 and 4 show examples of the major uranium phases encountered in both SA2 and SA4. Through high-resolution EPMA mapping, it is evident that organic matter is multiphase (Fig. 3). The organic matter is characterized by successions of barren and uraniferous types fixed in the sandstone. Figure 3 shows the association of barren and uraniferous organic matter. Figure 4 shows a region where the sandstone matrix is barren organic matter. EPMA point analyses (Table 2) show that the uraniferous organic matter is non-mineral (containing 10.80% carbon and 15.53% uranium). A secondary uranium-phosphorus phase also occurs, filling fractures (Fig. 3) and pores (Fig. 4). It is much higher in uranium (59.62%).

Leaching Behavior

Table 3 lists the reaction rate constants and metals leached for each experimental replicate. The leaching kinetics of the St. Anthony ores imply metal loading under both alkaline lixiviant and groundwater leaching conditions, although arsenic does not enter solution in appreciable amounts when exposed to groundwater. Metal solubility (inferred from k values) is, expectedly, an order of magnitude lower under groundwater leaching conditions. After 48 hours, approximately 11% of SA4's total uranium is leached when exposed to an oxidizing alkaline lixiviant, whereas, only 3% is released into groundwater. Sample SA4 contains approximately two times more uranium than SA2 (Table 1), yet it released, on average, about 15% less uranium than SA2 into the alkaline solution. Conversely, SA4 released 30% more vanadium than SA2 under alkaline leaching conditions, although SA2 contains 25% more vanadium. SA4, which has 2.4 times more arsenic than SA2, released 2.8 times more arsenic into the alkaline solution. In terms of reaction rates (Table 3), SA2 leached uranium 1.6 times faster, vanadium 1.7 times slower, and arsenic at similar rates compared to SA4.

DISCUSSION

The processes that emplaced the tabular ore bodies at St. Anthony fixed uranium with organic matter, reflected by the predominant phase identified by this study: amorphous, nonstoichiometric, and intimately associated with organic carbon

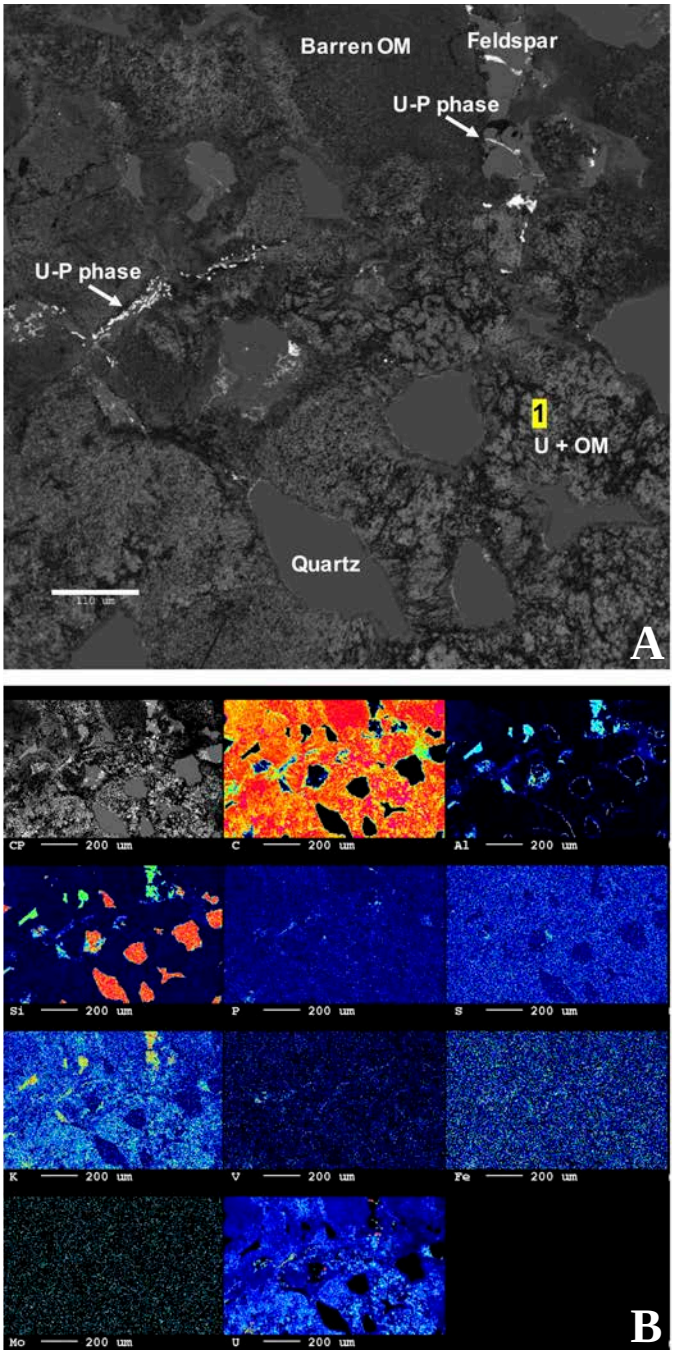

FIGURE 3. Backscattered electron image (**A**) and corresponding element map (**B**) of sample SA2. These images show the association between uranium (U) and organic matter (OM), as well as the secondary uranium-phosphorus (U-P) phase precipitated along fractures in feldspar grains. Warmer colors in B indicate a higher associated intensity of an element (e.g., carbon).

(Fig. 3). The organic matter is multi-phase: one characterized by higher potassium and uranium, the other devoid of the two elements. The latter "barren" organic matter is seen as large blebs in the upper half of Figure 3 images and as the matrix of Figure 4.

A minor uranium-phosphorus phase component was also identified in the samples, as seen in elevated uranium and phosphorus areas in backscatter images (Figs. 3, 4). It fills pore

TABLE 1. Bulk geochemistry of St. Anthony ores.

	SA2	SA4
C (%)	2.89	6.95
Organic C (%)	2.14	3.5
Carbonate C (%)	0.83	1.96
S (%)	0.24	0.33
Sulfide S (%)	0.12	0.15
Sulfate S (%)	0.12	0.18
As (ppm)	30.5	74
P (ppm)	300	660
U (%)	0.52	1.02
V (ppm)	2610	1960

space (Fig. 4) and cracks in feldspar grains (Fig. 3). Based on its texture and distribution, it is deduced to be a secondary mineral, an alteration product of the "primary" carbonaceous ore. This phase was identified as the mineral meta-autunite, Ca(UO2)2(PO4)2•2-6(H2O), which contains 54.21–59.06% uranium. EPMA point analysis in SA4 (Table 2, point 2) shows a uranium weight percent in this range. Though point analyses for phosphorus were not performed, it is strongly congruent with uranium in the element map (Fig. 3B). Meta-autunite contains 7.05–7.36% phosphorus, which would bring the total weight percent shown for SA4 in Table 2 (90.97%) to close to 100% (~ 98%).

Previous work characterizing the hexavalent uranium minerals on the pit wall faces at St. Anthony (Caldwell, 2018) identified uranyl carbonates, sulfates, phosphates and vanadates via X-ray powder diffraction analysis. Uranophane, though used in the site's post-closure model, was not a component of the examined St. Anthony ores, in this or Caldwell's (2018) study. It appears that hexavalent uranium minerals are, volumetrically, a minor component of the site's uraniferous material. Therefore, the leaching kinetics and attendant environmental impact of St. Anthony's wastes and ores will be controlled by the major reservoir of uranium: uraniferous organic matter. This is a phase that does not have well-constrained leachability or thermodynamic data. Furthermore, uraniferous organic matter may have undergone significant reworking and radiation damage since it was precipitated (Hansley and Spirakis, 1992).

Batch tests, which provide an excess of leachate, are used to approximate the ultimate recovery of a particular element

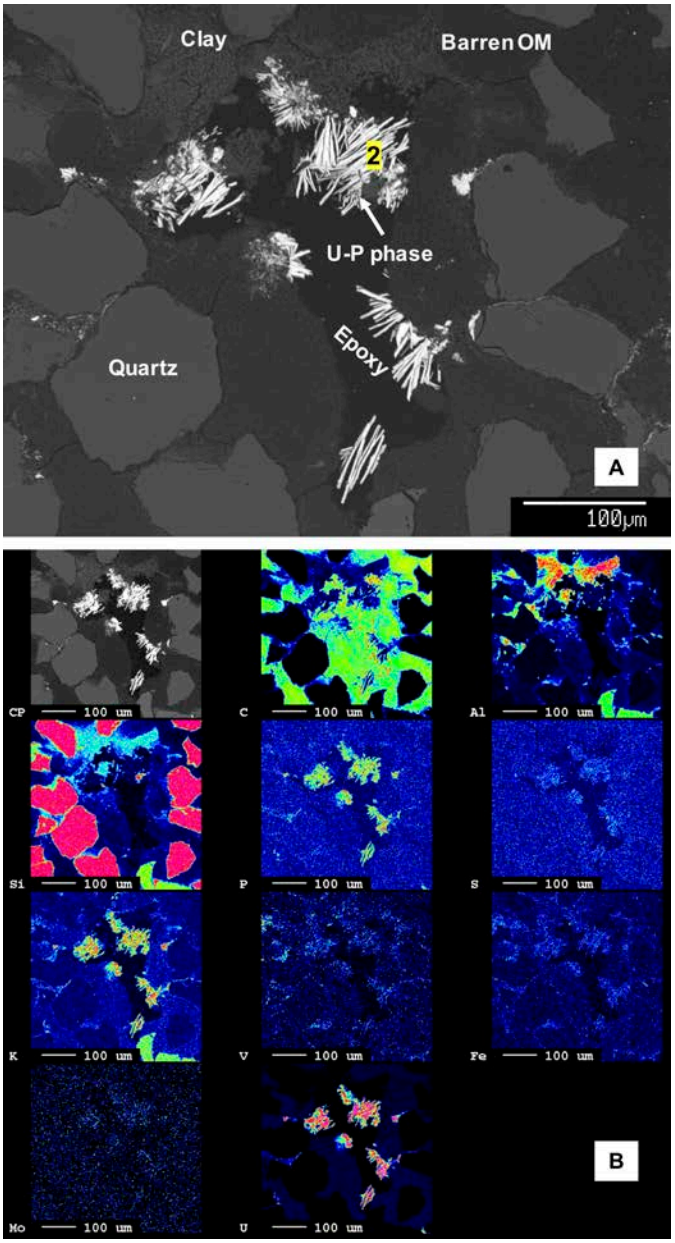

FIGURE 4. Backscattered electron image (**A**) and corresponding element map (**B**) of a zone in sample SA4, hosting crystals of a uranium-phosphorus (U-P) phase, likely meta-autunite. Note this phase is surrounded by barren organic matter (OM). Warmer colors in B indicate a higher associated intensity of an element.

TABLE 2. EPMA point analyses of elemental weight percent for labelled points in Figures 3 and 4. LOD: Limit of detection.

		Weight Percent (%)													
Point	*Sample*	**C**	**Si**	**S**	**Pb**	**U**	**K**	**Ca**	**As**	**Al**	**Ti**	**V**	**Fe**	**O**	**Total**
1	***SA2***	10.8	3.68	0.44	0.09	15.53	0.64	0.33	<LOD	23.83	0.02	0.1	0.98	30.56	87
2	***SA4***	2.33	0.04	0.01	<LOD	59.62	0.21	3.55	0.07	<LOD	0.03	<LOD	<LOD	25.1	90.97

TABLE 3. Reaction rates and proportions of metals leached from ore samples under alkaline lixiviant and groundwater leaching experimental conditions. -r: Experimental replicate, *k*: reaction rate constant.

	k (hr^{-1}) × 10^{-3}			% Leached		
Alkaline Leaching	***U***	***V***	***As***	***U***	***V***	***As***
SA2	2.6	0.4	0.5	11.8	1.7	2.5
SA2-r	2.4	0.3	0.4	10.9	1.6	1.7
SA4	1.5	0.6	0.4	7.2	2.8	2.1
SA4-r	1.6	0.6	0.6	7.6	2.9	2.7
Groundwater Leaching						
SA4	0.7	0.005	-	3.2	0.83	-
SA4-r	0.6	0.004	-	2.9	0.72	-

(Vogt et al., 1982). The leaching data reported here (Table 3) show that milled ores, characterized by uraniferous organic matter, readily release uranium, vanadium and arsenic under alkaline leaching conditions, and also release uranium and vanadium when exposed to ambient groundwater. However, in material that is in-place or left piled on the surface as whole rock, barren organic matter may armor uraniferous clots from dissolution, whether as a physical barrier to flow or by maintaining locally reducing conditions. Dissolved uranium could be re-mineralized by organic material into a more refractory form, thus preventing its future dissolution into oxidized waters. For example, mobile uranium may be reduced and fixed as coffinite by organic material (Deditius et al., 2008) or, providing there is enough vanadium and calcium present (e.g., a vanadiferous lignite and calcic groundwaters), as tyuyamunite (Stewart et al., 1999). The former process has been found by Deditus et al. (2008) to have occurred continuously over the last 30 million years in deposits associated with the Mount Taylor Mine, which is on the northwest side of Mount Taylor.

The biggest difference between SA2 and SA4 lies in their carbon, uranium and phosphorus contents—SA4 contains two times more of each component than SA2. On average, sample SA4 released less of its total uranium, and at a slower rate, than SA2 did under alkaline leaching conditions. It is feasible that the higher organic content of SA4 inhibited uranium dissolution, whether by maintaining reducing micro-environments, or by consuming the oxidant (H_2O_2). It could be hypothesized that under the highly oxidizing alkaline leach conditions, uranium-phosphate minerals/mineraloids may have precipitated out of solution after uranium and phosphorus were dissolved from SA4. However, given that the leaching solution was extremely high in carbonate (2g/L $NaHCO_3$), carbonate would have out-competed phosphate to complex with uranium.

Sample SA4 released more vanadium into solution than SA2 did, despite having a lower whole-rock percentage of this element. Vanadium in these systems may be associated with organic matter, vanadium-micas (roscoelite), and vandiferous clays (Spirakis, 1996). It is therefore possible that more vanadium was in a soluble form (e.g., sorbed to clays) in SA4 than in SA2. Arsenic release from the samples was proportional to their bulk concentrations, implying a similar mineral reservoir within these samples.

The Jackpile Sandstone has been so thoroughly impregnated by organic matter, uraniferous or otherwise, that the original porosity has been much reduced, meaning significant fluid flow through the remaining ore zones is limited. Upon burial, there will no longer be evaporation-induced concentration of uranium in an open pit or aerial exposure of ores at the pit walls. Uranium dissolution may be slowed.

CONCLUSIONS

The major reservoir of uranium within St. Anthony ores is associated with organic matter. Post-closure interactions between ore material and oxidized groundwater may release uranium and vanadium, but not arsenic. A highly oxidizing alkaline leaching agent could be used to extract uranium, but the leachate could also contain significant amounts of vanadium and arsenic. Future work should take the complex organic hosts of uranium into consideration to better evaluate if uranophane is an appropriate modeling parameter for St. Anthony Mine. Future groundwater quality trends, once the Large Pit has been backfilled, will be of great scientific interest, not least to see if they match the modeled predictions (which informed the alternative abatement standards). St. Anthony's long-awaited reclamation is one step of many needed to address the legacy of uranium mining in the state of New Mexico.

ACKNOWLEDGMENTS

This study was funded by grants from NM Established Program to Stimulate Competitive Research (National Science Foundation Award # IIA-1301346), New Mexico Geological Society, and New Mexico Water Resources Research Institute. Thanks are due to Dr. Kierran Maher for his help with the direction of this study; Ted Wilton (Westwater Resources Inc.) for access to the St. Anthony Mine and its materials; Marcus Silva for his positive presence in the lab and field; Michael Spilde at University of New Mexico for facilitating the analysis of these unusual samples on the EPMA; and Bonnie Frey for use of the New Mexico Bureau of Geology and Mineral Resource's Analytical Laboratory. This paper benefitted greatly from input by reviewers Drs. Dana Ulmer-Scholle and Virgil Lueth.

REFERENCES

Bowell, R.J., Grogan, J., Hutton-Ashkenny, M., Brough, C., Penman, K., and Sapsford, D.J., 2011, Geometallurgy of uranium deposits: Minerals Engineering, v. 24, p. 1305–1313, doi: 10.1016/j.mineng.2011.05.005.

Caldwell, S.E., 2018, Paragenesis of uranium minerals in the Grants Mineral Belt, New Mexico: Applied geochemistry and the development of oxidized uranium mineralization [MS thesis]: Socorro, New Mexico Institute of Mining and Technology, 185 p.

Cumberland, S.A., Douglas, G., Grice, K., and Moreau, J.W., 2016, Uranium mobility in organic matter-rich sediments: A review of geological and geochemical processes: Earth-Science Reviews, v. 159, p. 160–185, doi: 10.1016/j.earscirev.2016.05.010.

Deditius, A.P., Utsunomiya, S., and Ewing, R.C., 2008, The chemical stability of coffinite, USiO4·nH2O; 0 < n < 2, associated with organic matter: A case study from Grants uranium region, New Mexico, USA: Chemical Geology, v. 251, p. 33–49, doi: 10.1016/j.chemgeo.2008.02.009.

Hansley, P.L., and Spirakis, C.S., 1992, Organic matter diagenesis as the key to a unifying theory for the genesis of tabular uranium-vanadium deposits in the Morrison Formation, Colorado Plateau: Economic Geology, v. 87, p. 352–365, doi: 10.2113/gsecongeo.87.2.352.

Hazen, R.M., Ewing, R.C., and Sverjensky, D.A., 2009, Evolution of uranium and thorium minerals: American Mineralogist, v. 94, p. 1293–1311, doi: 10.2138/am.2009.3208.

Hund, L., Bedrick, E.J., Miller, C., Huerta, G., Nez, T., Ramone, S., Shuey, C., Cajero, M., and Lewis, J., 2015, A Bayesian framework for estimating disease risk due to exposure to uranium mine and mill waste on the Navajo Nation: Journal of the Royal Statistical Society. Series A: Statistics in Society, v. 178, p. 1069–1091, doi: 10.1111/rssa.12099.

Liu, G., Fernandez, A., and Cai, Y., 2011, Complexation of Arsenite with Humic Acid in the Presence of Ferric Iron: Environmental Science & Technology, v. 45, p. 3210–3216, doi: 10.1021/es102931p.

Mclemore, V.T., 2017, Mining districts and prospect areas in New Mexico: New Mexico Bureau of Geology and Mineral Resources, Resource Map 24, scale 1:1,000,000.

Moench, R.H., and Schlee, J.S., 1967, Geology and Uranium Deposits of the Laguna District, New Mexico: U.S. Geological Survey Professional Paper 519, p. 122.

Sanford, R.F., 1994, A quantitative model of ground-water flow during formation of tabular sandstone uranium deposits: Economic Geology, v. 89, p. 341–360, doi: 10.2113/gsecongeo.89.2.341.

Spirakis, C.S., 1996, The roles of organic matter in the formation of uranium deposits in sedimentary rocks: Ore Geology Reviews, v. 11, p. 53–69, doi: 10.1016/0169-1368(95)00015-1.

State of New Mexico, 2017, In the matter of: the petition for alternative abatement standards for the former St. Anthony Mine, Cibola County in the state of New Mexico: New Mexico Water Quality Control Commission. http://www.emnrd.state.nm.us/MMD/MARP/documents/2017-09-29AASH_FinalOrder.pdf. Accessed 10 March 2020.

Stewart, C.L., Reimann, L.J., and Swapp, S.M., 1999, Mineralogic considerations for uranium in-situ leach mining: A preliminary study of uranium and associated mineralogy of roll-front uranium deposits in Wyoming and Nebraska: Wyoming Geological Association 50th Annual Field Conference Guidebook, p. 155–165.

U.S. Environmental Protection Agency, 2001, Radionuclides Rule: A Quick Reference Guide: https://nepis.epa.gov/Exe/ZyPDF.cgi?Dockey=30006644.txt (accessed March 2020).

Vogt, T.C., Dixon, S.A., Strom, E.T., Johnson, W.F., and Venuto, P.B., 1982, In-situ leaching of Crownpoint, New Mexico uranium ore: Part 2 - laboratory study of a mild leaching system: Society of Petroleum Engineers Journal, p. 1013–1022.

Wilton, T., 2017, Uranium deposits at the Cebolleta project, Laguna mining district, Cibola County, New Mexico: New Mexico Geology, v. 39, p. 1–10.

Appendices can be found at http://nmgs.nmt.edu/repository/index.cfml?rid=2020003

New Mexico Geological Society, Special Publication 14, Geology of the Mount Taylor Area, 2020, p. 111-122.

A COMPARISON OF SANDSTONE MODAL COMPOSITION TRENDS FROM EARLY PERMIAN (WOLFCAMPIAN) STRATA OF THE ABO FORMATION IN THE ZUNI AND MANZANO MOUNTAINS WITH AGE-EQUIVALENT STRATA THROUGHOUT NEW MEXICO

Alicia L. Bonar[1], Brian A. Hampton[2], and Greg H. Mack[2]

[1]School of Geosciences, University of Oklahoma, Norman, OK 73019; alicia.bonar@ou.edu
[2]Department of Geological Sciences, New Mexico State University, Las Cruces, NM 88003

Abstract—Early Permian (Wolfcampian) nonmarine siliciclastic strata of the Abo Formation and age-equivalent units record exhumation, erosion, and sedimentation associated with the final orogenic phase of the Ancestral Rocky Mountains throughout New Mexico. Sandstone modal composition data and documentation of secondary feldspar alteration (albitization) from these strata are presented here to provide first-order constraint on the provenance and diagenetic changes that occurred during and after these strata were deposited. Overall, compositional trends from this study exhibit elevated occurrences of quartz and feldspar grains with minor lithic fragments (Q–56%, F–42%, L–2%) and are interpreted to have been derived from Precambrian continental-block/basement sources that consisted of the Yavapai, Mazatzal, and Granite-Rhyolite provinces and recycled strata of the Grenville foreland basin (i.e., DeBaca Group of southeastern New Mexico). Strata contain elevated occurrences of plagioclase and K-feldspar grains (Qm–52%, P–35%, K–13%) with isolated sedimentary, volcanic, and metamorphic fragments (Ls–41%, Lv–32%, Lm–27%). There is a noticeable change in the relative abundance of plagioclase and K-feldspar as well as lithic fragments when comparing data from the Zuni and Manzano mountains with samples collected further north with field localities in southern part of the state. Strata in the northernmost field locality exhibit the highest overall percentages of K-feldspar (Qm–48%, P–29%, K–23%) compared with strata in the Zuni and Manzano Mountains (Qm–47%, P–44%, K–9%) and southernmost New Mexico (Qm–63%, P–36%, K–1%). The relative decrease in K-feldspar occurrences from north to south accompanies an increase in the amount and degree of observed K-feldspar albitization. Nearly all K-feldspar grains are partially to completely albitized in all field localities south of the Zuni and Manzano Mountains. Although secondary feldspar alteration trends presented here warrant a more detailed and comprehensive study, K-feldspar replacement and albitization appears to be most pervasive in localities that have the thickest successions of evaporite-rich overburden (i.e., regions south of the Zuni and Manzano Mountains). Evaporative concentrations of salts in these basins could have provided sodium-rich brines that reacted with K-feldspar to produce albite. Albitization may have also occurred due to high heat flow associated with regional-scale tectonic subsidence events (e.g., Sevier and Laramide foreland subsidence, and/or Rio Grande rift subsidence) that buried strata to depths and temperatures that initiated K-feldspar albitization (i.e., ~2000–2500 m and ~60–70°C), or high heat flow associated with igneous activity related to the Rio Grande rift.

INTRODUCTION

The Ancestral Rocky Mountains were marked by thick-skinned, basement-involved, block uplifts that affected much of the south-central and southwestern continental United States during latest Mississippian–Early Permian time (Fig. 1A; e.g., Kluth and Coney, 1981; Ross and Ross, 1985; Kluth, 1986; Algeo et al., 1992; Soreghan, 1992; Devaney and Ingersoll, 1993; Ye et al., 1996; Hoy and Ridgeway, 2002; Barbeau, 2003; Dickinson and Lawton, 2003; Soreghan et al., 2012; Lawton et al., 2017; Leary et al., 2017). By the Early Permian, at least eight basement-cored block uplifts throughout New Mexico were thought to be exposed and possibly still tectonically active (Fig. 1A). Exhumation during this time resulted in some of the largest volume and coarsest fraction of nonmarine siliciclastic sediment associated with the Ancestral Rocky Mountains with strata reaching >1000 m thick in some localities (Kluth and Coney, 1981; Kottlowski, 1960a; Kues and Giles, 2004). It is thought that much of the Early Permian nonmarine strata throughout New Mexico were sourced primarily from the Uncompahgre uplift in southwestern Colorado and northern New Mexico and were transported southward to the Early Permian paleoshoreline (Fig. 1A; e.g., Mack and James, 1986; Mack et al., 2003a; Kues and Giles, 2004). The Pedernal and Sierra Grande uplifts may have also contributed detritus to nonmarine systems during this time (Fig. 1A; Kluth and Coney, 1981; Kues and Giles, 2004).

By the end of the Early Permian, clastic and carbonate strata onlapped and covered nearly all basement uplifts in New Mexico with the exception of parts of the Pedernal uplift (Kelley, 1971; Kottlowski, 1985; Kluth, 1986; Mack, 2003b). Ancestral Rocky Mountain orogenesis in New Mexico is thought to have terminated by Leonardian time, and the stratigraphic record of this transition is preserved primarily by marginal marine-dominated strata of the gypsum-rich Yeso Formation, wind-blown eolian sandstone of the Glorieta Formation, and limestone and gypsum-rich strata of the San Andres Formation (e.g., Kottlowski, 1985; Mack and Dinterman, 2002; Mack et al., 2003b).

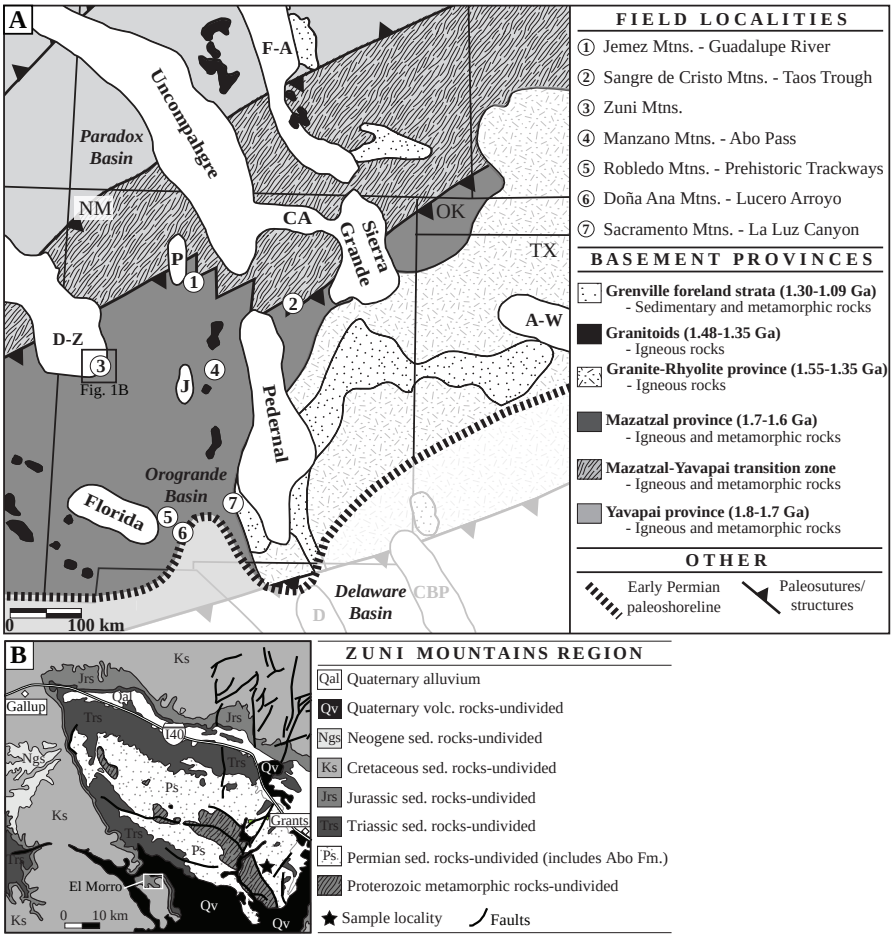

FIGURE 1. **A**) Early Permian (Wolfcampian) paleogeography and Precambrian province map of the southwestern U.S. with emphasis on late Paleozoic Ancestral Rocky Mountain (ARM) basement uplifts and adjacent basins in New Mexico and Colorado. Basement provinces and ages are from Karlstrom et al. (2004),Whitmeyer and Karlstrom (2007), and Mulder et al. (2017). Approximate location of ARM basement uplifts (gray pattern) from Kluth and Coney (1981), Ross and Ross (1985), Ye et al. (1996), Baltz and Myers (1999), Soreghan et al. (2012), and Leary et al. (2017). Abbreviated ARM basement uplifts include Peñasco (P), Joyita (J), Cimarron Arch (CA), Diablo (D), Central Basin Platform (CBP), and Amarillo-Wichita (A-W) uplifts. White circles denote project field localities for this study in northern, central, and southern New Mexico. **B**) Generalized geologic map of the Zuni Mountains region near Grants, New Mexico. Star denotes sample locality just east of El Morro National Monument. Modified from the New Mexico Bureau of Geology and Mineral Resources (NMBGMR) (2003) database and Kelley (2003).

The focus of this study is the provenance and secondary feldspar alteration trends of Early Permian (Wolfcampian), the coarse- to fine-grained, nonmarine, synorogenic strata of the Abo Formation in the Zuni and Manzano Mountains and age-equivalent nonmarine strata that crop out throughout New Mexico to the north and south. Presented here are new sandstone modal composition data and documentation of minor to extensive occurrences of secondary feldspar albitization from seven field localities from throughout New Mexico (Figs. 1A, 2). New provenance data and albitization trends from these strata provide first-order constraints on bedrock source areas that contributed detritus to Early Permian sedimentary basins and also provide insight into post-depositional diagenetic alteration that took place after erosion and sedimentation associated with the Ancestral Rocky Mountains.

FIELD LOCALITIES AND STRATIGRAPHY OF INTEREST

A total of seven field localities from across New Mexico were selected for this study and include sites in the Zuni and Manzano Mountains where nonmarine channel strata are exposed (Figs. 1A, 2). A summary of each field locality can be found in the online Data Repository (http://nmgs.nmt.edu/repository). The following text provides a general stratigraphic overview at each field locality and is presented in geographic order from north to south in New Mexico to provide a proximal-to-distal, source-to-sink context for south-flowing Early Permian (Wolfcampian) fluvial systems.

Northern New Mexico – Jemez and Sangre de Cristo Mountains

Early Permian (Wolfcampian) nonmarine strata of interest in north-central and northeastern New Mexico include (1) the Abo Formation in the Guadalupe River valley of the southwestern Jemez Mountains (Figs. 1A, 2) and (2) the Sangre de Cristo Formation in the Taos Trough of the southern Sangre de Cristo Mountains (Figs. 1A, 2). The Abo Formation in the Guadalupe River region ranges from 150–190 m thick (Lucas et al., 2013) and consists primarily of interbedded fine- to medium-grained massive and cross-stratified sandstone and massive and laminated siltstone (Figs. 2, 3A). Age-equivalent strata of the Sangre de Cristo Formation in the Taos Trough are characterized by interbedded clast-supported conglomerate, fine- to coarse-grained cross-stratified sandstone, and massive to laminated mudstone (Figs. 2, 3B) with an overall thickness that ranges considerably from 55–900 m (e.g., Soegaard and Caldwell, 1990; Baltz and Myers, 1999).

Central New Mexico – Zuni and Manzano Mountains

Two field localities in central and west-central New Mexico include the southeastern margin of the Zuni Mountains southwest of Grants (and due east of El Morro National Monument; Figs. 1B, 2) and the Abo Pass field locality in the southern Manzano Mountains (Figs. 1A, 2). In both localities, the Abo Formation consists primarily of interbedded fine- to medium-grained, massive and cross-stratified sandstone and massive and laminated mudstone (Figs. 2, 3C, D). In the Zuni Mountains, the Abo Formation ranges from 180–215 m

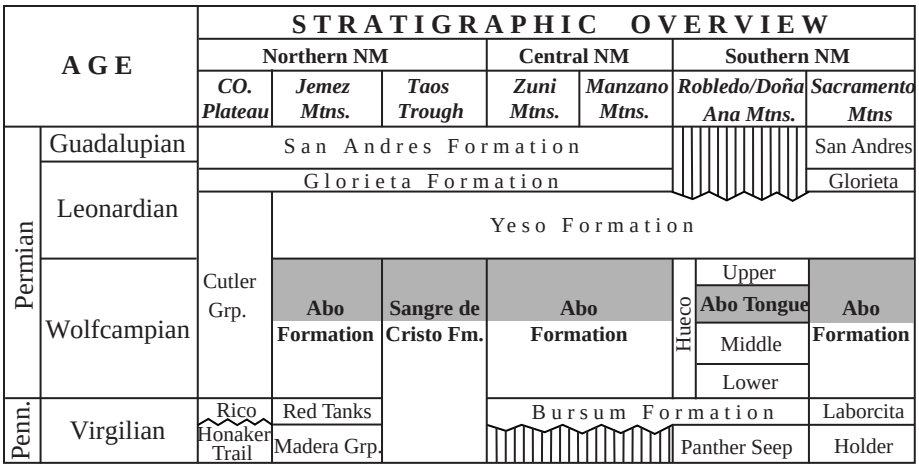

FIGURE 2. Generalized summary of Late Pennsylvanian and Early Permian stratigraphy throughout New Mexico. Stratigraphic interval of interest (shaded gray) includes the upper Abo and Sangre de Cristo Formations as well as the Abo Tongue of the Hueco Formation. Stratigraphy from Seager et al., (1976), Mack and James (1986), Mack et al. (1998), Kues and Giles (2004), Lucas et al. (2005) and Lucas et al. (2013).

thick and directly overlies Precambrian basement of the Defiance-Zuni uplift (Fig.1; Mack et al., 1998). The Abo in the Manzano Mountains is approximately 300 m thick (Lucas et al., 2013).

Southern New Mexico – Robledo, Doña Ana, and Sacramento Mountains

Early Permian (Wolfcampian) nonmarine strata of interest in south-central New Mexico include (1) siliciclastic portions of the Hueco Formation (Abo Tongue) near the Prehistoric Trackways National Monument along the eastern margin of the Robledo Mountains and in Lucero Arroyo along the western margin of the Doña Ana Mountains (Figs. 1A, 2), as well as (2) the Abo Formation near La Luz Canyon along the southwestern margin of the Sacramento Mountains (Figs. 1A, 2). Note that we use combined stratigraphic nomenclature from Kottlowski (1960a, 1960b, 1963) and Jordan (1971, 1975) when referencing Hueco-equivalent strata in the Robledo and Doña Ana Mountains (Fig. 2) and nomenclature from Pray (1961) for Wolfcampian strata in the southwestern Sacramento Mountains (i.e., Abo Formation; Fig. 2).

The coarsest nonmarine portions of the Abo Tongue in the Robledo and Doña Ana Mountains consist primarily of massive, laminated, ripple- and trough-cross stratified sandy siltstone and claystone (Figs. 2, 3E). In both the Robledo and Doña Ana Mountains, the Abo ranges from 120–300 m thick, and thins southward to 60–150 m where it is interbedded with Wolfcampian marine limestone units of the Hueco Formation (Needham and Bates, 1943; Mack et al., 1998, 2003b; Lucas et al., 2013). The coarsest parts of the Abo Formation in the Sacramento Mountains are characterized by interbedded, clast-supported conglomerate and medium- to coarse-grained cross-stratified sandstone (Figs. 2, 3F). Individual clasts consist primarily of quartzite and granite (Pray, 1961; Malone et al., 2017), and the thickness of the Abo in the Sacramento Mountains ranges from 80–335 m thick (Otte, 1959; Pray, 1961).

SANDSTONE MODAL COMPOSITION

Petrographic and compositional data were obtained from 16 sandstone samples (n=6400 grain counts) collected from Early Permian (Wolfcampian) nonmarine strata from seven field localities (Figs. 1A, 2). Samples were collected from the coarsest sand-size fraction preserved in fluvial-channel architectural elements at each field locality. Standard petrographic thin sections were cut and stained for plagioclase and potassium feldspar (K-feldspar). Thin sections were analyzed according to the modified Gazzi-Dickinson point-counting methods (Dickinson, 1970; Ingersoll et al., 1984). Modal composition was determined by identifying 400 grains from each thin section. Table 1 provides a summary of parameters used for sandstone point counts. A summary of all raw and recalculated point-count data collected from this study can be found in the online Data Repository (http://nmgs.nmt.edu/repository). Recalculated data are based on procedures defined by Ingersoll et al. (1984) and Dickinson (1985).

Overall, the modal composition of Early Permian (Wolfcampian) strata from throughout New Mexico is characterized by

Table 1. Summary of grain parameters for sandstone point counts.

Quartz (Q) = Qm + Qp + chert
- Monocrystalline quartz (Qm)
- Polycrystalline quartz (Qp)
- Chert (C)
Feldspar (F) = P + K
- Plagioclase (P)
- Potassium feldspar (K)
Lithic fragments (L) = Ls + Lm + Lv
- Lithic sedimentary (Ls)
- *Mudstone (Lsm)*
- *Sandstone (Lss)*
- *Limestone - micrite (Lslm)*
- *Limestone - non-micrite (Lsl)*
- Lithic metamorphic (Lm)
- *Phyllite (Lmp)*
- *Schist (Lms)*
- *Quartzite (Lmq)*
- *Gneiss (Lmg)*
- Lithic volcanic (Lv)
Lt = Ls + Lm + Lv + Qp + chert

*Grains of calcite, mica, and dense minerals also included in point-count totals

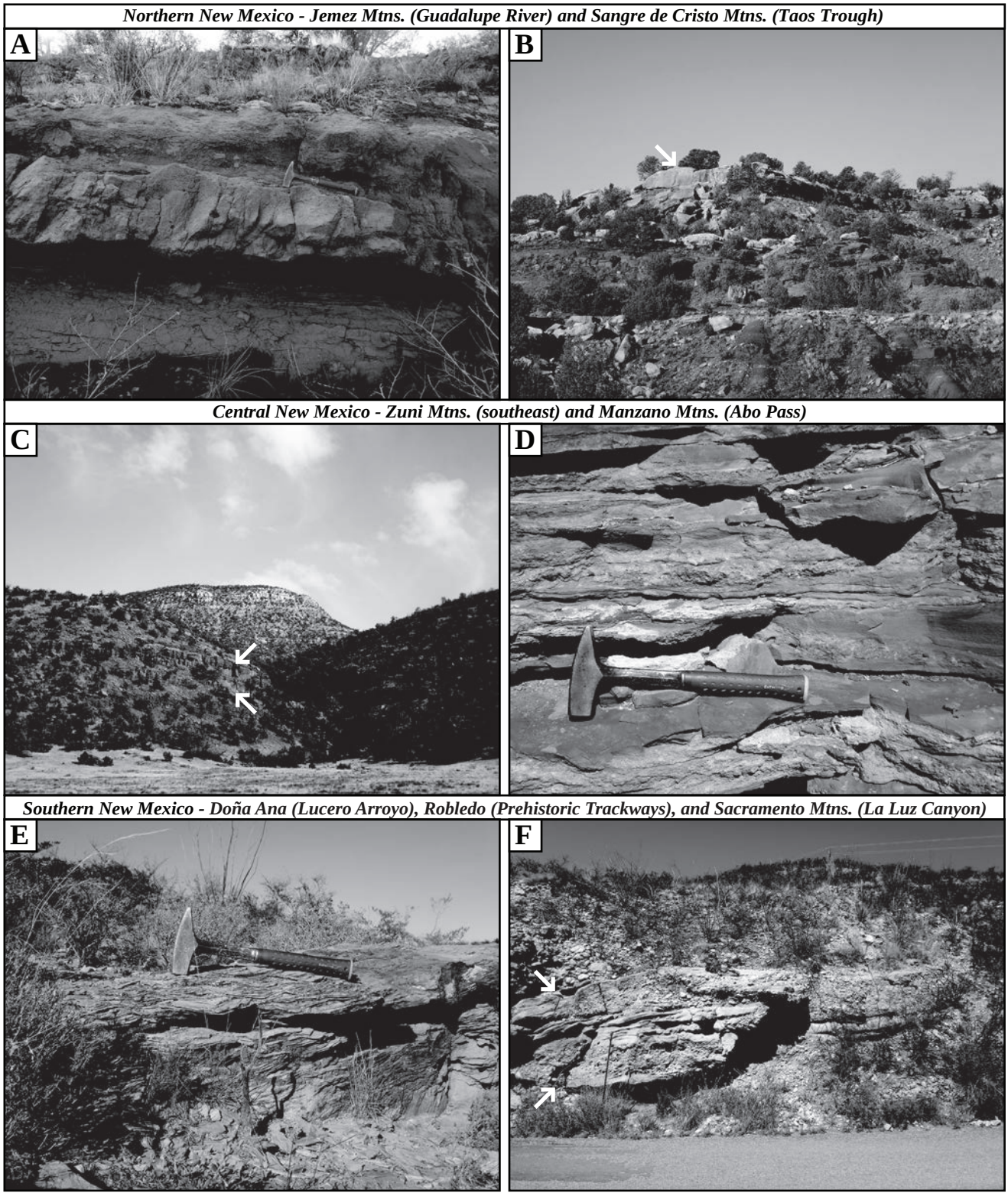

FIGURE 3. Field outcrop photos of nonmarine portions of the Abo, Hueco, and Sangre de Cristo Formations. **A**) Interbedded sandstone and siltstone of the Abo Formation in the southwestern Jemez Mountains (Guadalupe River region). Rock hammer for scale. **B**) Tabular and lenticular sandstone and mudstone deposits of the Sangre de Cristo Formation in the southern Sangre de Cristo Mountains (Taos Trough). White arrow denotes a channel sandstone unit that is 2–3 m thick. **C**) View to the north of the Abo Formation and gypsum-rich beds of the overlying Yeso Formation in the Zuni Mountains of west-central New Mexico. White arrows show base and top of a 2.5-m-thick sandstone. **D**) Thin, tabular beds of siltstone and fine-grained sandstone that make up the Abo Formation near Abo Pass in the Manzano Mountains (rock hammer for scale). **E**) Ripple-cross stratified siltstone and very fine-grained nonmarine sandstone of the Hueco Formation at Lucero Arroyo in the Doña Ana Mountains of southern New Mexico (rock hammer for scale). **F**) Lenticular bed made up primarily of clast-supported cobble-conglomerate in the southern Sacramento Mountains. White arrows show base and top of a~2.5-m-thick channel conglomerate.

predominantly quartz and feldspar with minor occurrences of lithic fragments (Q–56%, F–42%, L–2%; Figs. 4, 5, 6). Quartz grains consist of monocrystalline quartz (Qm) and polycrystalline quartz (Qp) with monocrystalline quartz being the most common constituent (Fig. 4). The feldspar population is made up largely of plagioclase (P) but does have a significant amount of K-feldspar (K; Qm–52%, P–35%, K–13%; Figs. 5A, B, 6). Lithic grains, in order of decreasing occurrences, consist of lithic sedimentary (Ls), lithic volcanic (Lv) and lithic metamorphic (Lm; Ls–41%, Lv–32%, Lm–27%; Figs. 4A, C, 5B, 6). Lithic sedimentary fragments consist of sandstone, mudstone (Fig. 4A), and limestone (micrite) grains. Lithic volcanic grains consist primarily of fragments with microphenocrysts of quartz and feldspar (Fig. 4B). The most common lithic metamorphic fragments are gneiss with subordinate occurrences of quartzite, schist, and phyllite (Fig. 4C). Calcite makes up ~3% of total grains counted whereas mica and dense mineral fragments make up ~1% of all grains counted.

Based on Q-F-L percentages, nearly all samples plot in the arkose field of Folk (1968) with the exception of southern samples from the Abo Formation in the Sacramento Mountains plotting in the subarkose field and a second southern sample from the Hueco Formation plotting in the quartzarenite field (Fig. 6). Similarly, all samples plot either in the Transitional-Continental or Basement-Uplift province of Dickinson et al. (1983) except for two samples from the Jemez Mountains of northern New Mexico and the two previously mentioned southern samples. These samples plot in the Craton (Q-F-L) or Quartzose Recycled (Qm-F-Lt) province fields of Dickinson et al. (1983), near the end of the path of increasing maturity from the Continental Block province (Qm-F-Lt). The following text provides a summary comparison of modal composition trends from Early Permian (Wolfcampian) strata from field localities in northern, central, and southern New Mexico.

Northern New Mexico – Abo Formation and Sangre de Cristo Formation

The Abo Formation in the Guadalupe River valley of the southwestern Jemez Mountains is characterized by elevated occurrences of quartz and feldspar (Fig. 6; Q–56%, F–43%, L–1%) with K-feldspar and monocrystalline quartz making up the highest percentage of total feldspar and quartz grains (Fig. 6; Qm–49%, P–22%, K–29%). Lithic fragments are dominated by metamorphic and volcanic grains (Fig. 6; Lv–48%, Lm–52%, Ls–0%). Calcite and mica grains make up ~9% and ~0.5% of total occurrences, respectively. To the east, the Sangre de Cristo Formation in the Taos Trough of the southern Sangre de Cristo Mountains is also dominated by occurrences of feldspar and quartz (Fig. 6; Q–48%, F–51%, L–1%) with monocrystalline quartz and plagioclase making up the highest quartz and feldspar percentages (Fig. 6; Qm–47%, P–44%, K–9%). Here, lithic grains consist largely of volcanic and sedimentary fragments (entirely micrite) and subordinate metamorphic fragments (Fig. 6; Lv–46%, Lm–17%, Ls–37%). Calcite and mica grains make up ~0.1% and ~0.5% of total grain occurrences, respectively.

Average relative feldspar percentages from the Abo Formation in the Guadalupe River valley of the southwestern Jemez Mountains total 51% with K-feldspar making up 29% (Fig. 6; Qm–49%, P–22%, K–29%). Samples from this field locality have the highest relative percentage of K-feldspar in this study and there is no evidence of any secondary textures or albitization of feldspar. The Sangre de Cristo Formation in the Taos Trough has an average relative feldspar of 44% with K-feldspar making up 9% (Fig. 6; Qm–47%, P–44%, K–9%). Worm-like vermicules (i.e., myrmekitic textures) are rare but do occur in isolated plagioclase grains and appear as irregular intergrowths of quartz in a single grain of plagioclase (Fig. 7A). Some plagioclase and K-feldspar from these samples show textural signs of partial to complete albitization with minor occurrence of red-brown Fe-oxide typical of albite alteration (Figs. 4C, 7B).

Central New Mexico – Abo Formation

The Abo Formation which crops out along the southeastern margin of the Zuni Mountains is made up primarily of feldspar and quartz (Fig. 6; Q–48%, F–50%, L–2%) with plagioclase and monocrystalline quartz making up the highest percentages of overall feldspar and quartz grains (Fig. 6; Qm–45% P–43% K–12%). Lithic grains consist entirely of metamorphic and volcanic fragments (Fig. 6; Lv–37%, Lm–63%, Ls–0%). There are no occurrences of calcite grains in these samples and mica makes up ~3% of total occurrences. To the east, the Abo Formation in the Abo Pass field locality of the southern Manzano Mountains is dominated by quartz and feldspar (Fig. 6; Q–53%, F–43%, L–4%) with monocrystalline quartz and plagioclase making up the highest percentages of total quartz and feldspar (Fig. 6; Qm–54%, P–46%, K–0%). Lithic fragments consist entirely of lithic sedimentary grains of micrite (Fig. 6; Lv–0%, Lm–0%, Ls–100%). Calcite and mica grains make up ~2% and ~0.25% of total grain occurrences, respectively.

Relative total feldspar from the Abo Formation in the Zuni Mountains is 55% with K-feldspar making up 12% (Fig. 6; Qm–45%, P–43%, K–12%). No granophyric or myrmekitic textures were observed in feldspars from these samples, but there is textural evidence on both plagioclase and K-feldspar grains of minor secondary albite alteration. Relative feldspar percentages from the Abo Formation in the Abo Pass field locality of the southern Manzano Mountains total 46% with plagioclase making up 100% of all feldspar grains (Fig. 6; Qm–54%, P–46%, K–0%). Feldspars exhibit minor secondary albitization, but no granophyric or myrmekitic textures were observed.

Southern New Mexico – Hueco Formation (Abo Tongue) and Abo Formation

Nonmarine portions of the Hueco Formation (“Abo Tongue”), which crops out along the eastern margin of the Robledo Mountains and in Lucero Arroyo along the western margin of the Doña Ana Mountains, consists primarily of quartz, subordinate feldspar, and rare lithic fragments (Fig. 6; Q–76%,

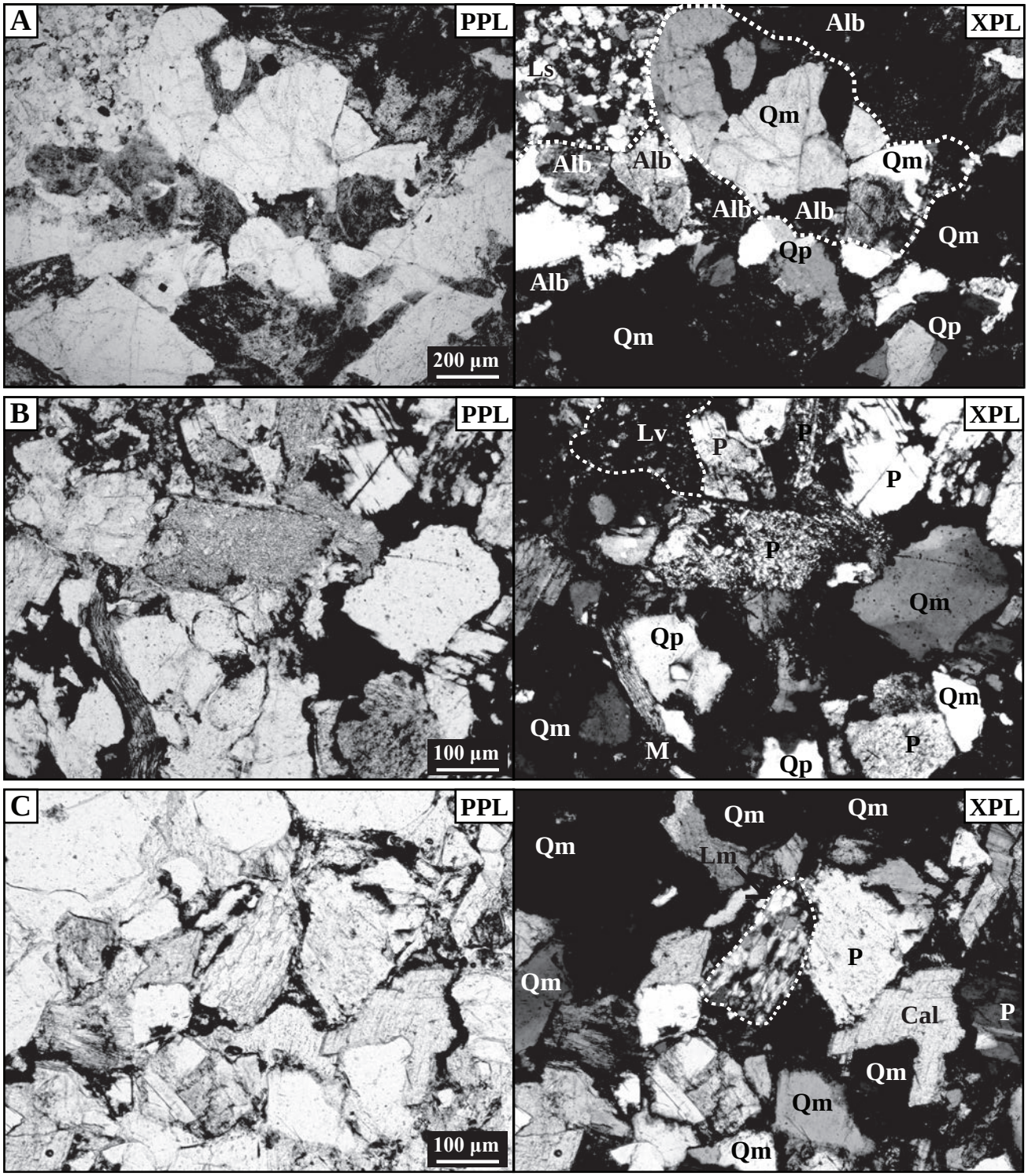

FIGURE 4. Photomicrographs of Early Permian, nonmarine sandstone with plane-polarized light (PPL) view on the left and identical polarized (XPL) view on the right. Dashed lines depict grain boundaries. **A**) Monocrystalline quartz (Qm), polycrystalline quartz (Qp), lithic sedimentary fragments (Ls), and albitized feldspar (Alb) from southern New Mexico. **B**) Monocrystalline quartz (Qm), polycrystalline quartz (Qp), lithic volcanic fragments (Lv), plagioclase (P), and biotite mica (M) from northern New Mexico. **C**) Monocrystalline quartz (Qm), metamorphic fragments (Lm), plagioclase (P), and calcite grains (Cal.) from northern New Mexico.

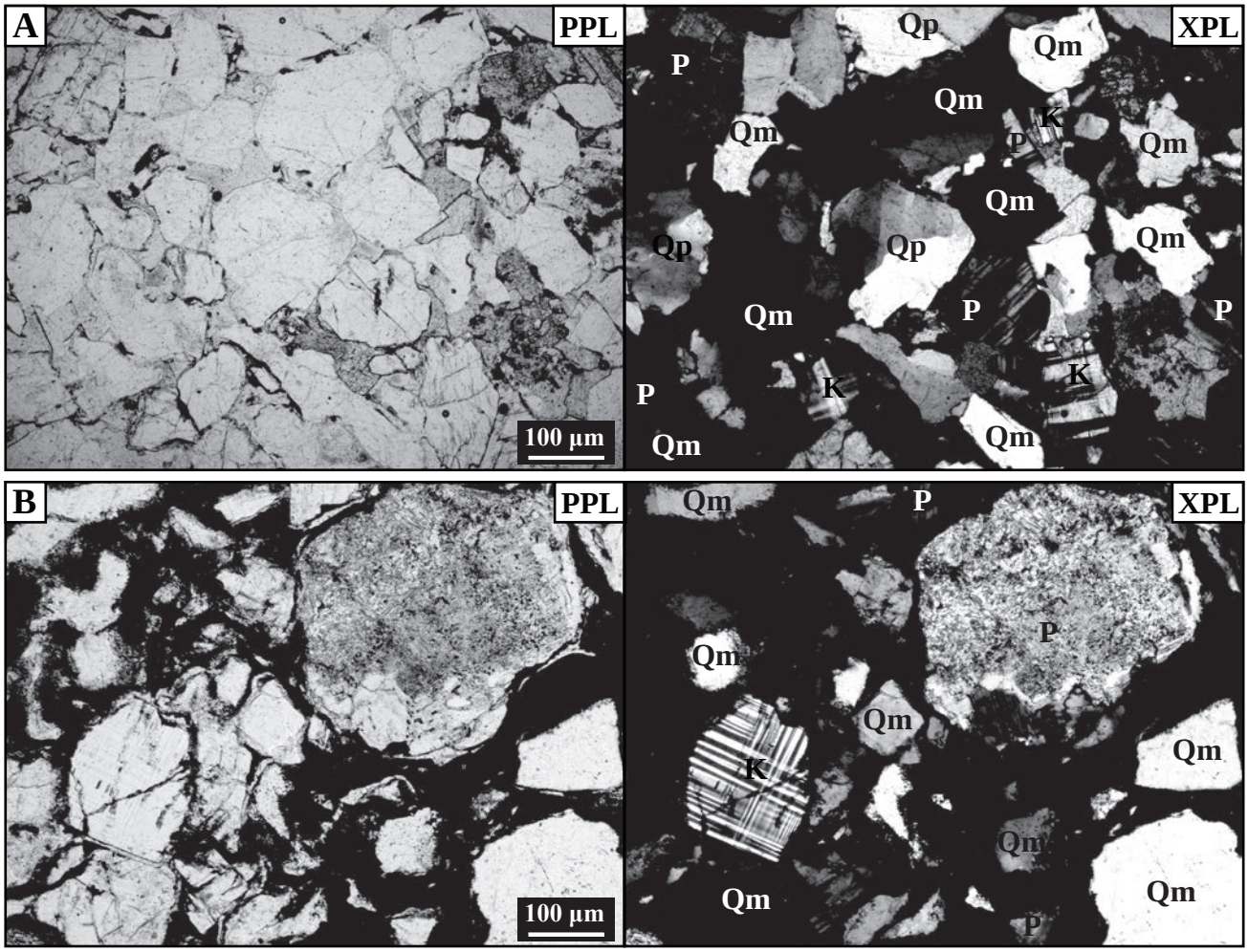

FIGURE 5. Photomicrographs of Early Permian, nonmarine sandstone from northern New Mexico with plane-polarized light view on the left and identical cross-polarized view on the right. **A**) Monocrystalline quartz (Qm), plagioclase (P), and K-feldspar (K) from northern New Mexico. **B**) Monocrystalline quartz (Qm), plagioclase (P), and microcline K-feldspar (K) from northern New Mexico.

F–23%, L–1%). Monocrystalline quartz makes up the majority of quartz grains and plagioclase makes up all feldspar grains (Fig. 6; Qm–76%, P–24%, K–0%). Lithic fragments consist of sedimentary and volcanic grains (Fig. 6; Lv–33%, Lm–0%, Ls–67%) with sandstone and siltstone making up ~63% of total lithic sedimentary fragments and micrite making up the other ~37%. Calcite and mica grains make up ~1% and just over 0.5% of total grain occurrences, respectively. The Abo Formation near La Luz Canyon along the southwestern margin of the Sacramento Mountains is characterized by elevated occurrences of quartz and feldspar and subordinate lithic fragments (Fig. 6; Q–57%, F–38%, L–5%) with monocrystalline quartz and plagioclase making up the majority of quartz and feldspar percentages (Fig. 6; Qm–54%, P–45%, K–1%). Lithic fragments are dominated by lithic sedimentary grains (Fig. 6; Lv–10%, Lm–2%, Ls–88%), of which sandstone and siltstone make up ~70% of total lithic sedimentary fragments and micrite makes up the other ~30%. Calcite makes up ~0.5% of total grain occurrences and there are no documented occurrences of mica.

Average relative feldspar percentages from nonmarine portions of the Hueco Formation in the Robledo Mountains and Doña Ana Mountains are the lowest in this study at 24% with plagioclase making up all feldspar grains (Fig. 6; Qm–76%, P–24%, K–0%). No granophyric or myrmekitic textures were observed in feldspars, but albite alteration is common and pervasive throughout these samples. Total relative feldspar percentages from the Abo Formation near La Luz Canyon along the southwestern margin of the Sacramento Mountains are 46% with K-feldspar only making up 1% (Fig. 6; Qm–54%, P–45%, K–1%). Nearly all plagioclase and K-feldspar grains from these samples exhibit albite-replacement textures with occurrences of Fe-oxide, and in some cases, albite overgrowths and cementation (Fig. 7B). Myrmekitic textures as well as fine-grained granophyric intergrowths of quartz on isolated feldspar grains (Fig. 7C) do occur but are rare.

DISCUSSION AND CONCLUSIONS

Spatial trends in sandstone modal composition and feldspar alteration from Early Permian (Wolfcampian) nonmarine strata of the Abo Formation in the Zuni and Manzano Mountains and age-equivalent strata from around New Mexico provide an op-

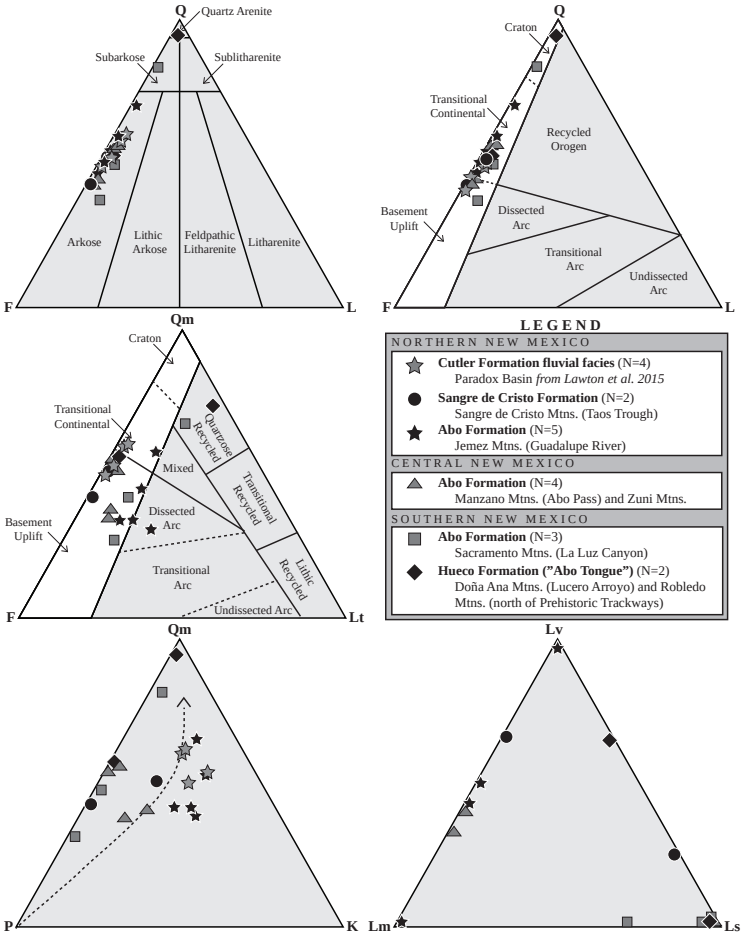

FIGURE 6. Q-F-L, Qm-F-Lt, Qm-P-K, and Lv-Lm-Ls ternary diagram plots for Early Permian, nonmarine strata from throughout New Mexico. Sandstone fields from Folk (1968) and provenance fields after Dickinson et al. (1983). Dashed line on Qm-P-K diagram reflects path of increasing sandstone maturity.

portunity to better constrain primary, original source provinces that shed detritus during the final phase of the Ancestral Rocky Mountain orogenesis in New Mexico, as well as diagenetic changes that took place after sedimentation. New data from this study support an interpretation wherein these strata were derived largely from a combination of basement-uplift, transitional-continental, and cratonic provinces (Fig. 6; Dickinson et al., 1983).

Elevated occurrences of feldspar, lithic volcanic and lithic metamorphic fragments, and mica in the Zuni Mountains and throughout central and northern New Mexico are interpreted to reflect detrital contributions from igneous and metamorphic basement rocks derived from the southern margin of the Uncompahgre basement uplift, and likely a combination of the Uncompahgre, Sierra Grande, and northern Pedernal uplift (e.g., Yavapai, Mazatzal, and Granite-Rhyolite provinces; Fig. 1A). Similar compositional trends have been reported from the Cutler Formation (Abo Formation equivalent; Fig. 2) of the Paradox basin in southwestern Colorado where the Cutler crops out proximal to rocks of the Uncompahgre uplift (Figs. 1A, 2, 6; Lawton et al., 2015). he Defiance-Zuni uplift was apparently not a major contributor of detritus given the fine-grained nature of the Abo directly adjacent to this uplift in the Zuni Mountains, rather than coarser, less texturally mature sediments expected closer to the source (Fig. 1B).

The Abo Formation and equivalent nonmarine strata in southern New Mexico contain variable proportions of feldspar and predominantly lithic sedimentary fragments consisting of mudstone, sandstone, and micrite with pedogenic floodplain origins. Isolated, fine-grained stratigraphic intervals with low occurrences of feldspar and elevated occurrences of quartz in the Robledo Mountains are interpreted to represent the distal-most fluvial systems that originated from the southern margin of the Uncompahgre and possibly the western margin of the Pedernal uplift (e.g., Yavapai, Mazatzal, Granite-Rhyolite, and Grenville foreland provinces; Fig. 1A). Strata in the Doña Ana and Sacramento Mountains were likely derived primarily from the western margin of the Pedernal uplift (e.g., Mazatzal, Granite-Rhyolite, and overlying, younger strata of the Grenville foreland provinces – DeBaca Group of southeastern New Mexico) and possibly the southern margin of the Uncompahgre and Sierra Grande basement uplifts (e.g., Yavapai, Mazatzal, and Granite-Rhyolite provinces; Fig. 1A).

Secondary alteration textures observed in this study include partial seritization reflecting normal breakdown of feldspar and widespread partial to complete secondary albitization of K-feldspar grains (Fig. 7B). Albitization increases considerably (at the expense of K-feldspar percentages) from north to south with the most extreme examples occurring in the southernmost field localities. Myrmekitic and granophyric textures observed in this study (Figs. 7A, C) are interpreted to reflect primary, original textures in basement source areas that formed prior to erosion and sedimentation. Although secondary albitization of K-feldspar grains does affect sandstone modal composition trends when comparing percentages of plagioclase and K-feldspar grains, it does not change the overall interpretation of these strata being derived from cratonic, transitional-continental, and basement-uplift source areas. It does, however, shed light on potential secondary processes that affected these strata after deposition. Although interpreting the exact timing and mechanisms responsible for secondary albitization in Early Permian nonmarine clastic strata throughout New Mexico is beyond the scope of this study, we do offer a brief review of potential drivers that could have played a role in influencing feldspar occurrence and albitization.

Secondary albitization is common during diagenesis of felsic, arkosic sedimentary strata (e.g., Boles, 1982; Walker, 1984; Gold, 1987; Saigal et al., 1988; Aagaard et al., 1990; Morad et al., 1990; Ramseyer et al., 1992; Parsons et al., 2005) and often involves the process of sodium metasomatism. Where felsic sedimentary strata react with available saline fluids, silt- and sand-size K-feldspar and plagioclase are partially to completely replaced by albite at a range of basin depth and temperature conditions (e.g., Land and Milliken, 1981; Boles, 1982; Walker, 1984; Land, 1984; Land and Fisher, 1987; Saigal et

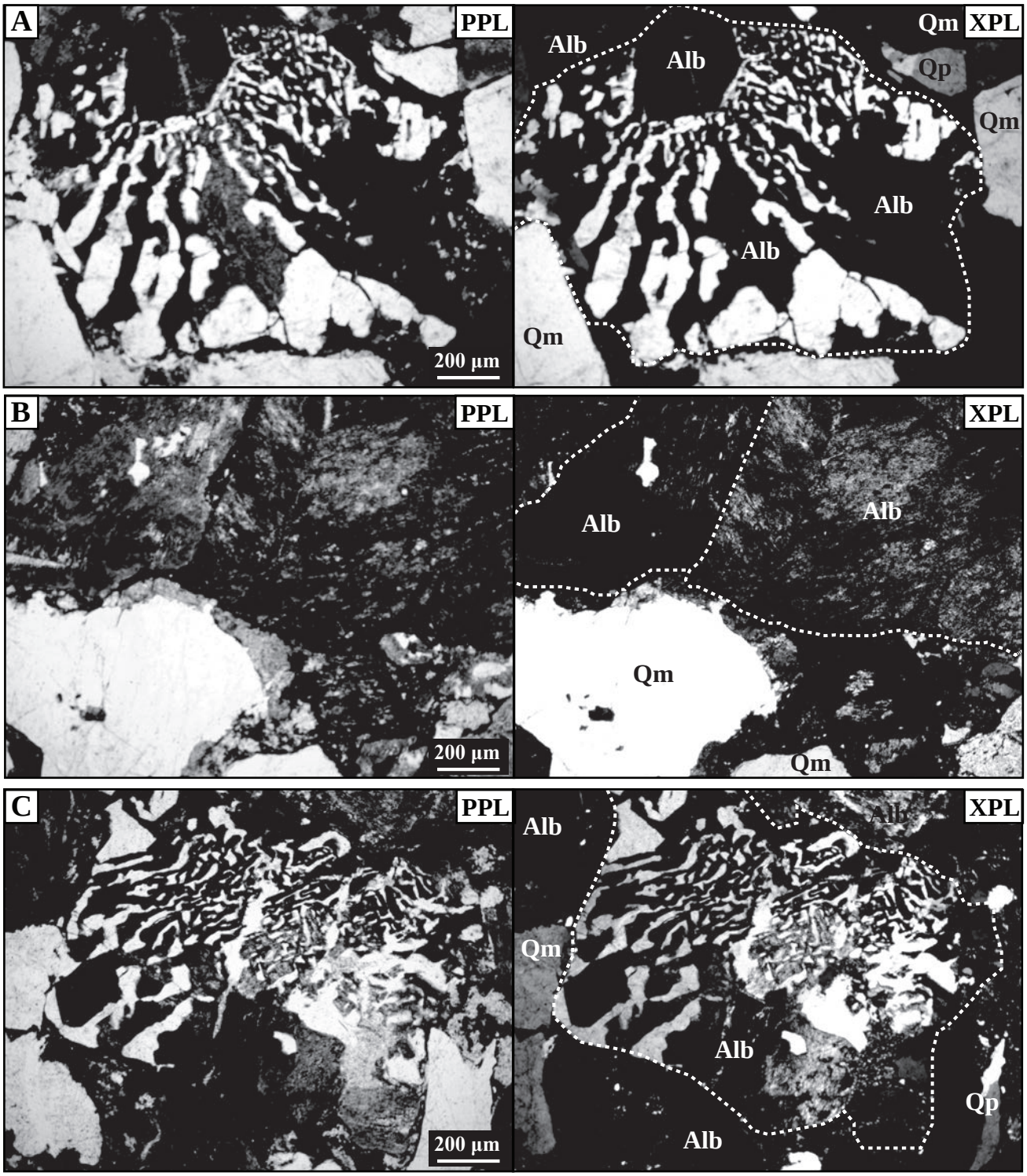

FIGURE 7. Photomicrographs of Early Permian, nonmarine sandstone from southern New Mexico with plane-polarized light view on the left and identical cross-polarized view on the right. Dashed lines depict grain boundaries. **A**) Rare, worm-like vermicules (i.e., myrmekitic textures) on quartz and albitized feldspar grains (Alb). **B**) Pervasive albite-replacement textures including albite overgrowths and cementation. **C**) Rare granophyric textures on quartz and albitized feldspar.

al., 1988; Gold, 1987). At the surface and at shallower basin depths, evaporative concentration of salts in the groundwater of a closed basin will yield Na-rich brines that can react with detrital silicates to develop authigenic albite. At depth, the onset of albitization of K-feldspar occurs around 60–70°C (near depths of ~2500 m) when formation waters transition out of the stability field of K-feldspar and begin to approach the stability field of albite (Aagaard et al., 1990).

During early-middle Leonardian–early Guadalupian time, much of southern, east-central, and northeastern New Mexico

experienced a marine transgression that is recorded by shelf and marginal marine, sandy-sabkha, and lagoon-evaporite strata of the lower to middle Yeso Formation and equivalent units, (e.g., Mack and Dinterman, 2002), nonmarine, eolian strata of the Glorieta Formation, and shelf carbonate strata of the interfingering and mostly overlying San Andres Formation (e.g., Kelley and Wood, 1946; Baltz, 1965; Kottlowski, 1969; Johnson 1973; Broadhead and King, 1988; Colpitts, 1989; Fig. 2). With the exception of the northernmost Jemez locality (Guadalupe River field site), which was marked by fluvial and eolian sedimentation (Baars, 1962; Stanesco, 1991; Huffman and Condon, 1993; Mack and Dinterman, 2002), all other field localities in this study experienced shelf-carbonate sedimentation with much of central and eastern New Mexico recording gypsum-, and anhydrite-dominated facies of the San Andres Formation. The occurrence and deposition of gypsum- and anhydrite-rich facies above the Abo Formation … corresponds to areas where increased degrees of albitization and lower percentages of K-feldspar are observed, thus pointing to a shallow basin environment during diagenesis.

In addition to the availability of large volumes of Late Permian, marginal-marine overburden and associated shallow, sodium-rich brines, it is worth noting the regional subsidence history throughout New Mexico since the Early Permian as tectonic burial events may have been partially responsible for generating moderate to deep basin depths and elevated heat flow. Much of New Mexico experienced long-wavelength flexure and subsidence during the Late Cretaceous associated with eastward propagation of the Sevier foreland basin (e.g., DeCelles, 2004). However, subsidence from the Sevier alone does not seem to account for the north-south variability observed in feldspar occurrence and alteration. Late Cretaceous–early Eocene subsidence associated with short-wavelength, "wedge-top" like basins that formed ahead of thick-skinned, basement-involved Laramide uplifts may also be partially responsible but also do not alone adequately account for feldspar trends in these strata. We also consider basin subsidence that developed as a result of the late Eocene–Present Rio Grande rift. Except for one sample area located just off-axis of the rift along the eastern margin of the Colorado Plateau (Zuni Mountains), all other field localities are within the rift axis. It is possible secondary alteration that occurred both within the rift axis and off rift axis was driven in part by elevated heat flow associated with early-to late rift volcanism (e.g., Zuni-Bandera volcanic field just east of the Zuni Mountains).

ACKNOWLEDGMENTS

This project was supported in part from student grant awards (to A. Bonar) from the New Mexico Geological Society (NMGS), Albuquerque Gem and Mineral Society, Geological Society of America (GSA), SEPM, Rocky Mountain SEPM, as well as from the Southern Rift Institute (SRI) at New Mexico State University. We are thankful to the U.S. Bureau of Land Management for facilitating access and sampling in the Robledo and Doña Ana Mountains. This manuscript was improved by helpful and informative reviews from Evey Ganaway Dalton and Richard Langford and editorial comments by Shari Kelley and Kate Zeigler. We also thank Bruce Allen for providing comments on an earlier draft of this manuscript.

REFERENCES

Aagaard, P., Egeberg, P.K., Saigal, G.C., Morad, S., Bjorlykke, K., 1990, Diagenetic albitization of detrital K-feldspar in Jurassic, Lower Cretaceous, and Tertiary clastic reservoir rocks from offshore Norway, II. Formation water chemistry and kinetic considerations: Journal of Sedimentary Petrology, v. 60, p. 575–581.

Algeo, T.J., 1992, Continental-scale wrenching of south-western Laurussia during the Ouachita-Marathon orogeny and tectonic escape of the Llano block: West Texas Geological Society, Guidebook, 92-92, p. 115-131.

Baars, D.L., 1962, Permian system of Colorado Plateau: American Association of Petroleum Geologists Bulletin, v. 46, p. 149-218.

Baltz, E.H., 1965, Stratigraphy and history ofRaton Basin and notes on San Luis Basin, Colorado-New Mexico: American Association of Petroleum Geologists Bulletin, v. 49, p. 2041–2075.

Baltz, E.H. and Myers, D.A., 1999, Stratigraphic framework of upper Paleozoic rocks, southeastern Sangre de Cristo Mountains, New Mexico with a section on speculations and implications for regional interpretation of Ancestral Rocky Mountains paleotectonics: New Mexico Bureau of Mines and Mineral Resources, Memoir 48, 269 p.

Barbeau, D.L., 2003, A flexural model for the Paradox Basin: implications for the tectonics of the Ancestral Rocky Mountains: Basin Research, v. 15, p. 97-115.

Boles, J.R., 1982, Active albitization of plagioclase, Gulf Coast, Tertiary: American Journal of Sciences, v. 282, p. 165–180.

Broadhead, R.F., and King, W.E., 1988, Petroleum geology of Pennsylvanian and lower Permian strata, Tucumcari Basin, east-central New Mexico: New Mexico Bureau of Mines and Mineral Resources, Bulletin 119, 75 p.

Colpitts, R.M., 1989, Permian reference section for southeastern Zuni Mountains, Cibola County, New Mexico: New Mexico Geological Society, Guidebook 40, p. 177–180.

DeCelles, P.G., 2004, Late Jurassic to Eocene evolution of the Cordilleran thrust belt and foreland basin system, western USA: American Journal of Science, v. 304, p. 105–168.

Devaney, K.A., and Ingersoll, R.V., 1993, Provenance evolution of Upper Paleozoic sandstones of north-central New Mexico, *in* Johnson, M.J., and Basu, A., eds., Processes Controlling the Composition of Clastic Sediments: Denver, Geological Society of America, Special Paper 284, 91 p.

Dickinson, W.R. 1970, Interpreting provenance relations from detrital modes of greywacke and arkose: Journal of Petrology, v. 40, p. 695–707.

Dickinson, W.R., 1985, Interpreting the provenance relations from detrital modes of sandstones, *in* Zuffa, G.G., ed., Provenance of Arenites: Dordrecht, D. Reidel Publishing Co., p. 333-361.

Dickinson, W.R., Beard, S.L., Brackenridge, G.R., Erjavec, J.L., Ferguson, R.C., Inman, K.F., Knepp, R.A., Linberg, F.A., and Ryber, P.T., 1983, Provenance of North American Phanerozoic sandstones in relation to tectonic setting: Geological Society of America Bulletin, v. 94, p. 222-235.

Dickinson, W.R., and Lawton, T.F., 2003, Sequential inter-continental suturing as the ultimate control for the Pennsylvanian Ancestral Rocky Mountains deformation: Geology, v. 31, p. 609-612.

Folk, R.L., 1968, Petrology of Sedimentary Rocks: Austin, Hemphill's, 182 p.

Gold, P.B., 1987, Textures and geochemistry of authigenic albite from Miocene sandstones, Louisiana Gulf Coast: Journal of Petrology, v. 57, p. 353–362.

Hoy, R.G., and Ridgeway, K.D., 2002, Syndepositional thrust-related deformation and sedimentation in an Ancestral Rocky Mountains basin, Central Colorado trough, Colorado, USA: Geological Society of America Bulletin, v. 114, p. 804-828.

Huffman, A.C., Jr., and Condon, S.M., 1993, Stratigraphy, structure, and paleogeography of Pennsylvanian and Permian rocks, San Juan Basin and adjacent areas, Utah, Colorado, Arizona, and New Mexico: U.S. Geological Survey Bulletin 1808-O, 44 p.

Ingersoll, R.V., Bullard, T.F., Ford, R.L., Grimm, J.P., Pickle, J.D., Sares, S.W., 1984, The effect of grain size on detrital modes: a test of the Gazzi-

Dickinson point-counting method: Journal of Sedimentary Petrology, v. 54, p. 103–116.

Johnson, R.B., 1973, Geologic map of the Pecos quadrangle, San Miguel and Santa Fe Counties, New Mexico: U.S. Geological Survey, Geologic Quadrangle Map GQ-1110, scale 1:24,000.

Jordan, C. F., 1971, Lower Permian stratigraphy of southern New Mexico and West Texas [Ph.D. dissertation]: Houston, Rice University, 140 p.

Jordan, C.F., 1975, Lower Permian (Wolfcampian) sedimentation in the Orogrande basin, New Mexico: New Mexico Geological Society, Guidebook 26, p. 109-117.

Karlstrom, K.E., Amato, J.M., Williams, M.L., Heizler, M., Shaw, C.A., Read, A.S. and Bauer, P., 2004, Proterozoic tectonic evolution of the New Mexico region: a synthesis, *in* Mack, G. H. and Giles, K. A., eds., The Geology of New Mexico: A Geologic History: New Mexico Geological Society, Special Publication 11, p. 1–34.

Kelley, S.A., 2003, Laramide exhumation history of the Zuni Mountains, west-central New Mexico: Geological Society of America, Abstracts with Programs, v. 35, p. 295.

Kelley, V.C., and Wood, G.H., 1946, Geology of the Lucero uplift, Valencia, Socorro, and Bernalillo Counties, New Mexico: U.S. Geological Survey, Oil and Gas Investigations Preliminary Map 47, scale 1:63,360.

Kelley, V.C., 1971, Geology of the Pecos country, southeastern New Mexico: New Mexico Bureau of Mines and Mineral Resources, Memoir 24, 75 p.

Kluth, C.F., 1986, Plate tectonics of the Ancestral Rocky Mountains, *in* Peterson, J.A., ed., Paleotectonics and sedimentation in the Rocky Mountain region, United States: Tulsa, American Association of Petroleum Geologists, Memoir 41, p. 353-369.

Kluth, C.F., and Coney, P.J., 1981, Plate tectonics of the Ancestral Rocky Mountains: Geology, v. 9, p. 10-15.

Kottlowski, F.E., 1960a, Summary of the Pennsylvanian sections in southwestern New Mexico and southeastern Arizona: New Mexico Bureau of Mines and Mineral Resources, Bulletin 66, 187 p.

Kottlowski, F.E., 1960b, Reconnaissance geologic map of Las Cruces thirty-minute quadrangle: New Mexico Bureau of Mines and Mineral Resources, Geologic Map 14, Scale 1:126,720.

Kottlowski, F.E., 1963, Paleozoic and Mesozoic strata of southwestern and south-central New Mexico: New Mexico Bureau of Mines and Mineral Resources, Bulletin 79, p. 100.

Kottlowski, F.E., 1969, San Andres Limestone west of the Sacramentos: New Mexico Geological Society, Special Publication 3, p. 5–11.

Kottlowski, F.E., 1985, Shoreline facies of the Yeso Formation in the northern Pedernal Hills: New Mexico Geological Society, Guidebook 36, p. 167-169.

Kues, B.S., and Giles, K.A., 2004, The late Paleozoic Ancestral Rocky Mountains system in New Mexico, *in* Mack, G.H., and Giles, K.A., eds., The Geology of New Mexico, A Geologic History: New Mexico Geological Society, Special Publication 11, p. 95-136.

Land, L.S., 1984, Frio sandstone diagenesis, Texas Gulf Coast: A regional isotopic study, *in* McDonald, D.A., and Surdam, R.C., eds., Clastic Diagenesis: Tulsa, American Association of Petroleum Geologists, Memoir 37, p. 47–62.

Land, L.S, and Fisher, R.S., 1987, Wilcox sandstone diagenesis, Texas Gulf Coast: A regional isotopic comparison with the Frio Formation: London, Geological Society, Special Publications, v. 36, p. 219–235.

Land, L.S., and Milliken, K.L, 1981, Feldspar diagenesis in the Frio Formation, Brazoria Country, Texas: Geology, v. 9, p. 314–318.

Lawton, T.F., Buller, C.D., and Parr, T.R., 2015, Provenance of a Permian erg on the western margin of Pangea: Depositional system of the Kungurian (late Leonardian) Castle Valley and White Rim sandstones and subjacent Cutler Group, Paradox Basin, Utah, USA: Geosphere v. 11, n. 5, p. 1475–1506.

Lawton, T.F., Cashman, P.H., Trexler, J.H. Jr., and Taylor, W.J., 2017, The Late Paleozoic southwestern Laurentian borderland: Geology, v. 45, n. 8, p. 675-678.

Leary, R.J., Umhoefer, P.J., Smith, M.E., Riggs, N.R., 2017, A three-sided orogen: a new tectonic model for Ancestral Rocky Mountain uplift and basin development: Geology, v. 45, n. 8, p. 735-738.

Lucas, S.G., Krainer, K. and Colpitts, R.M., Jr., 2005, Abo-Yeso (Lower Permian) stratigraphy in central New Mexico: New Mexico Museum of Natural History and Science, Bulletin 31, p. 101-117.

Lucas, S.G., Krainer, K., Chaney, D.S., DiMichele, W.A., Voigt, S., Berman, D.S., and Henrici, A.C., 2013, The Lower Permian Abo Formation in central New Mexico: New Mexico Museum of Natural History and Science, Bulletin 59, p. 161–179.

Mack, G.H., 2003, Lower Permian paleoclimatic indicators in New Mexico and their comparison to the paleoclimate model: New Mexico Geological Society, Guidebook 54, p. 231-240.

Mack, G.H. and James, W.C., 1986, Cyclic sedimentation in the mixed siliciclastic-carbonate Abo-Hueco transitional zone (Lower Permian), southwestern New Mexico: Journal of Sedimentary Petrology, v. 56, p. 635-647.

Mack, G.H., Kottlowski, F.E., and Seager, W.R., 1998, The stratigraphy of south-central New Mexico: New Mexico Geological Society, Guidebook 49, p. 135-154.

Mack, G.H. and Dinterman, P.A., 2002, Depositional environments and paleogeography of the Lower Permian (Leonardian) Yeso and correlative formations in New Mexico: The Mountain Geologist, v. 39, p. 75-88.

Mack, G.H., Leeder, M., Perez-Arlucea, M., and Bailey, B.D.J., 2003a, Early Permian silt-bed fluvial sedimentation in the Orogrande basin of the Ancestral Rocky Mountains, New Mexico, USA: Sedimentary Geology, p. 159-178.

Mack, G. H., Leeder, M., Perez-Arlucea, M., and Bailey, B. D. J., 2003b, Sedimentology, paleontology, and sequence stratigraphy of Early Permian estuarine deposits, south-central New Mexico, USA: Palaios, v. 18, p. 403–420.

Malone, D.H., Craddock, J.P., Deck, E.A., Banik, T.J, and Hampton, B.A., 2017, Detrital zircon geochronology of quartzite clasts in the Permian Abo Formation, Sacramento Mountains, New Mexico, USA: The Mountain Geologist, v. 54, n. 2, p. 53–68.

Morad, S., Bergan, M., Knarud, R., Nystuen, J.P., 1990, Albitization of detrital plagioclase in Triassic Reservoir sandstones from the Snorre Field, Norwegian North Sea: Journal of Sedimentary Petrology, v. 60, n. 3, p. 411–425.

Mulder, J.A., Karlstrom, K.E., Fletcher, K., Heizler, M.T., Timmons, J.M., Crossey, L.J., Gehrels, G.E., and Pecha, M., 2017, The syn-orogenic sedimentary record of the Grenville Orogeny in southwest Laurentia: Precambrian Research, v. 294, p. 33–52.

Needham, C.E. and Bates, R.L., 1943, Permian type sections in central New Mexico: Geological Society of America Bulletin, v. 54, n. 11, p. 1653-1668.

New Mexico Bureau of Geology and Mineral Resources, 2003, Geologic Map of New Mexico, scale 1:500,000.

Otte, C., Jr., 1959, Late Pennsylvanian and Early Permian stratigraphy of the northern Sacramento Mountains, Otero County, New Mexico: New Mexico Bureau of Mines and Mineral Resources, Bulletin 50, 111 p.

Parsons, I., Thompson, P., Lee, M.R., and Cayzer, N., 2005, Alkali feldspar microtextures as provenance indicators in siliciclastic rocks and their role in feldspar dissolution during transport and diagenesis: Journal of Sedimentary Research, v. 75, p. 921–942.

Pray, L.C., 1961, Geology of the Sacramento Mountains escarpment, Otero County, New Mexico: New Mexico Bureau of Mines and Mineral Resources, Bulletin 35, 144 p.

Ramseyer K., Aldahan, A.A., Collini, B., and Landstrom, O., 1992, Petrological modifications in granitic rocks from the Siljan impact structure: Evidence from cathodoluminescence: Tectonophysics, v. 216, p. 195–204.

Ross, C.A. and Ross, J.R.P., 1985, Paleozoic tectonics and sedimentation in West Texas, southern New Mexico, and southern Arizona: West Texas Geological Society, Publication 85–81, p. 221–230.

Saigal, G.C., Morad, S., Bjorlykke, K., Egeberg, P.K., and Aagaard, P., 1988, Diagenetic albitization of detrital K-feldspar in Jurassic, Lower Cretaceous, and Tertiary clastic reservoir rocks from offshore Norway, I. Textures and Origin: Journal of Sedimentary Petrology, v. 58, no. 6, p. 1003-1013.

Seager, W. R., Kottlowski, F. E., and Hawley, J. W., 1976, Geology of Doña Ana Mountains, New Mexico: New Mexico Bureau of Mines and Mineral Resources, Circular 147, 36 p.

Soegaard, K., and Caldwell, K.R., 1990, Depositional history and tectonics significance of alluvial sedimentation in the Permo-Pennsylvanian Sangre de Cristo Formation, Taos Trough, New Mexico: New Mexico Geological Society, Guidebook 41, p. 277-289.

Soreghan, G.S., 1992, Preservation and paleoclimatic significance of eolian dust in the Ancestral Rocky Mountains Province: Geology, v. 20, p.

1111–1114.

Soreghan, G.S., Keller, G.R., Gilbert, M.C., Chase, C.G., and Sweet, D.E., 2012, Load-induced subsidence of the Ancestral Rocky Mountains recorded by preservation of Permian landscapes: Geosphere, v. 8, p. 654-668.

Stanesco, J.D., 1991, Sedimentology and depositional environments of the Lower Permian Yeso Formation, northwestern New Mexico: U.S. Geological Survey, Bulletin 1808-M, 12 p.

Walker, T.R., 1984, Diagenetic albitization of potassium feldspar in arkosic sandstones: Journal of Sedimentary Research, v. 54, p. 3-16.

Whitmeyer, S.J., and Karlstrom, K.E., 2007, Tectonic model for the Proterozoic growth of North America: Geosphere, v. 3, no. 4, p. 220-259.

Ye, H., Royden, L., Burchfiel, C., and Schueplach, M., 1996, Late Paleozoic deformation of western North America: the greater Ancestral Rocky Mountains: American Association of Petroleum Geologists Bulletin, v. 80, p. 1397-1432.

Appendices can be found at http://nmgs.nmt.edu/repository/index.cfml?rid=2020004

New Mexico Geological Society, Special Publication 14, Geology of the Mount Taylor Area, 2020, p. 123-133.

TRIASSIC STRATIGRAPHY OF THE SOUTHEASTERN COLORADO PLATEAU, WEST-CENTRAL NEW MEXICO

SPENCER G. LUCAS

New Mexico Museum of Natural History, Albuquerque, New Mexico 87104; spencer.lucas@state.nm.us

Abstract—Triassic strata are well exposed along the southeastern Colorado Plateau and in adjacent areas in west-central New Mexico (McKinley, Catron, Cibola and parts of Valencia and Socorro counties). The oldest Triassic strata are assigned to the Anton Chico Member of the Moenkopi Formation, which disconformably overlies Permian strata and is disconformably overlain by the Upper Triassic Chinle Group. The Moenkopi Formation in west-central New Mexico is as much as 68 m thick, and consists of mostly grayish-red and reddish-brown sandstone, mudstone siltstone and conglomerate. Overlying Triassic strata in west-central New Mexico are assigned to seven formations of the Chinle Group (in ascending order) – the Shinarump /Zuni Mountains formations, the Bluewater Creek/San Pedro Arroyo formations, the Petrified Forest Formation (including Blue Mesa, Sonsela and Painted Desert members), the Owl Rock Formation and the Rock Point Formation – and to the Wingate Sandstone. As much as 24 m of silica-pebble conglomerate/sandstone and pedogenically-modified and color-mottled siltstone, mudstone and sandstone of the Shinarump and Zuni Mountains formations, which are lateral equivalents, are at the base of the Chinle Group. The 50-60 m of Bluewater Creek Formation are dominated by red sandstones and mudstones and are laterally equivalent to the southeast to the color-mottled San Pedro Arroyo Formation. The Petrified Forest Formation is up to 441 m thick and is divided into the (ascending) Blue Mesa, Sonsela and Painted Desert members. The Blue Mesa Member is 21-45 m thick and mostly purplish and greenish bentonitic mudstone with calcrete nodules and a white tuffaceous sandstone locally present at the base. The Sonsela Member is 15-61 m thick and mostly yellowish-gray, cross-bedded sandstone and siliceous conglomerate with fossil logs. The Painted Desert Member is up to 325 m thick and is mostly reddish brown mudstone and siltstone. It includes some relatively thin, but laterally persistent sandstone units, the Perea and Correo beds. The Owl Rock Formation is up to 35 m thick and characterized by reddish siltstone and beds of white limestone. The Rock Point Formation is up to 70 m thick and consists of repetitively-bedded, reddish-brown sandstone and siltstone. The Wingate Sandstone is the stratigraphically-highest Triassic (?) unit in west-central New Mexico. The Moenkopi Formation is Anisian in age, whereas the Chinle Group ranges from middle Carnian to Rhaetian in age. The base of the Moenkopi Formation is a regional unconformity (Tr-0/Tr-2 unconformities), and the base of the Chinle Group is the regional Tr-3 unconformity. There are two within-Chinle regional unconformities, Tr-4 at the Sonsela base and Tr-5 (=J-0) at the Rock Point base. The Middle Jurassic Entrada Sandstone overlies Triassic strata across west-central New Mexico at the J-2 unconformity.

INTRODUCTION

Triassic strata in west-central New Mexico (Fig. 1) are assigned to the Moenkopi Formation and overlying Chinle Group (Fig. 2). Since Marcou (1858) first identified Triassic rocks in this part of the state (and in some other areas in New Mexico), a variety of lithostratigraphic relationships and names have been proposed. Triassic strata in west-central New Mexico are exposed over four outcrop belts: (1) the Triassic outcrop belt along the northern and western flanks of the Zuni Mountains, mostly between Gallup and Grants; (2) the Triassic outcrops located primarily on the Zuni Indian Reservation in western Cibola County and southwestern McKinley County: (3) Triassic outcrops in the upper drainage of Largo Creek and its tributaries, far western Catron County; and (4) Triassic strata that crop out in and around the Lucero uplift of eastern Cibola, western Valencia and northwestern Socorro counties (Fig. 1). Here, I review Triassic lithostratigraphy, chronostratigraphy and unconformities in these four outcrop belts.

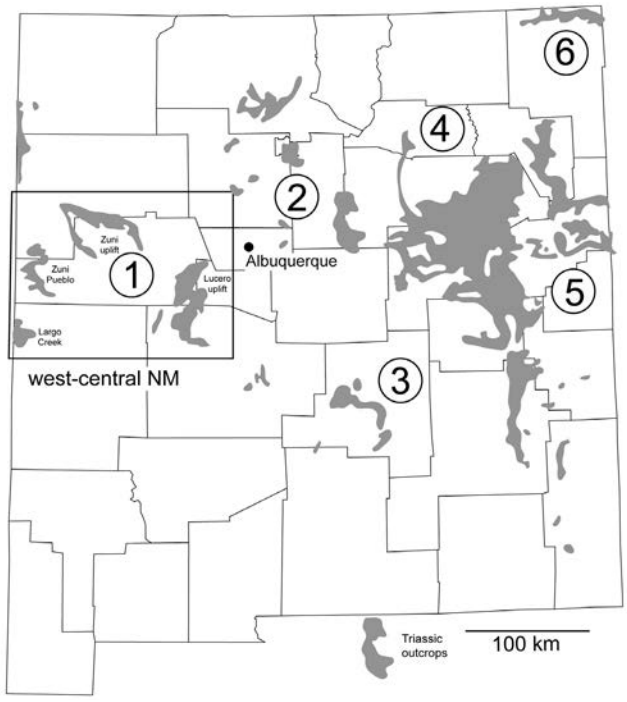

FIGURE 1. Distribution of Triassic outcrops in New Mexico showing location of west-central New Mexico outcrops. The numbers refer to the columns in Figure 12.

SOME HISTORY

Stewart et al. (1972a), Lucas and Hayden (1989) and Heckert and Lucas (2002, 2003) provided detailed reviews of the

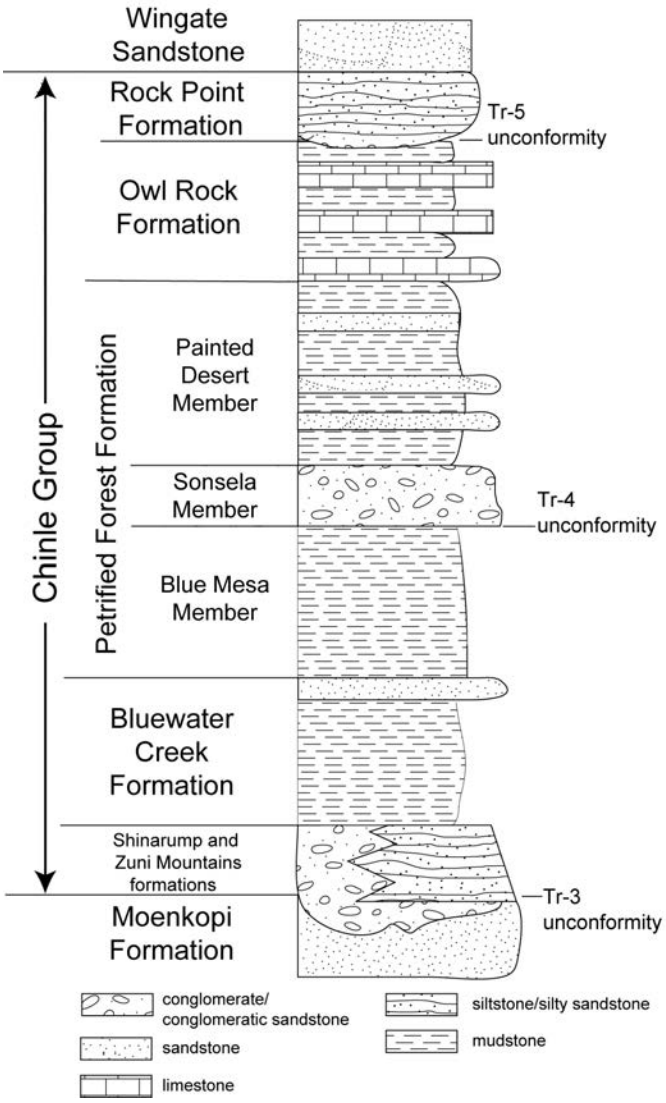

FIGURE 2. Generalized lithologic column of Triassic strata in west-central New Mexico.

development of the lithostratigraphic nomenclature of Triassic strata in west-central New Mexico, so I present only a brief review. Ten significant works represent turning points or syntheses of our understanding of Triassic stratigraphy in west-central New Mexico (Fig. 3).

Marcou (1858) identified Triassic strata in west-central New Mexico as "Trias" or "'New Red Sandstone." Newberry (1876) applied the informal name "Salt Group" to Permian and Triassic strata up to and including what is now termed the Sonsela Member, and he referred overlying Triassic and Jurassic strata to his "Marl Series." Working in the Zuni Mountains-Mount Taylor area, Dutton (1885) first applied formal stratigraphic names to Triassic strata in west-central New Mexico. He coined the name Wingate Sandstones for strata later assigned to the Entrada Sandstone and used Gilbert's (1875) term Shinarump Conglomerate for strata now termed Sonsela.

Darton (1910, p. 44-53) reviewed in detail the Triassic strata exposed throughout west-central New Mexico. Below Dutton's (1885) Wingate Sandstones, Darton equated Dutton's Lower Trias with Ward's (1901) Leroux Formation, at the base of which he identified the Shinarump Conglomerate. Below his Shinarump, Darton termed the Triassic strata Moencopie (?) formation (= Moencopie beds of Ward, 1901) above Pennsylvanian strata he considered correlative to the Aubrey Group of northern Arizona.

Darton (1928) followed the then current USGS practice in abandoning Ward's (l901) term Leroux in favor of Gregory's (1915) name Chinle. However, Darton (1910, 1928) erred in correlating what is now known to be the Sonsela Member in west-central New Mexico with the Shinarump Conglomerate in Arizona. Consequently, he assigned underlying Upper Triassic strata to the Lower-Middle Triassic Moenkopi Formation.

Bates (1942) first recommended abandoning Darton's use of Moenkopi in west-central New Mexico. Thus, when Kelley and Wood (1946) mapped a Triassic stratigraphy specific to the Lucero uplift, they did not assign any strata to the Moenkopi (although some later workers did, e.g., Momper, 1957). They identified the lower, grayish-red, sand-dominated portion of the Triassic section as Shinarump Conglomerate overlain by "shale"-dominated Chinle Formation capped by a prominent sandstone at Mesa Gigante that they named the Correo Sandstone Member of the Chinle (Fig. 3).

Smith (1954, 1957), working in the Zuni uplift, followed McKee (1954), who argued that both the Moenkopi and the Shinarump are not present in west-central New Mexico. Smith thus used an informal subdivision of the Triassic strata in this area, all of which he assigned to the Chinle Formation (Fig. 3). Smith's lower and upper Chinle members were mudrock dominated and split by the sandstone-dominated middle member. Smith also assigned to the Correo Sandstone Member the upper Chinle sandstones west of Mesa Gigante that were stratigraphically much lower in the Chinle-mudrock section.

Cooley's (1957) detailed study of Triassic stratigraphy in the drainage of the Little Colorado River was published by Akers et al. (1958), Cooley (1958, 1959a, b) and Cooley et al. (1969). At the base of the Triassic section, Cooley tentatively identified "upper Moenkopi (?)" above Permian strata. At the base of the overlying Chinle Formation, he identified scattered channel-type deposits as Shinarump, and he named a lower member the Mesa Redondo Member. A "lower red member" rested on the Shinarump and was capped by the thick, mudrock-dominated Petrified Forest Member split by the Sonsela Sandstone Bed. According to Cooley (1957), the youngest Triassic rock-stratigraphic unit in west-central New Mexico, the Owl Rock Member of the Chinle Formation, only extends as far east as Thoreau. He also noted that the underlying upper Petrified Forest Member contains a number of laterally persistent sandstone beds, including the Correo Sandstone Bed.

Stewart et al. (1972b, c) followed the nomenclature of Cooley with few significant changes. The only addition was their recognition of the "mottled strata" at the base of the Chinle in west-central New Mexico. Lucas and Hayden (1989) named the Bluewater Creek Member but otherwise used the same lithostratigraphy. Subsequent extensive stratigraphic work by Heckert (1997) and by the author in collaboration with Heckert, Ander-

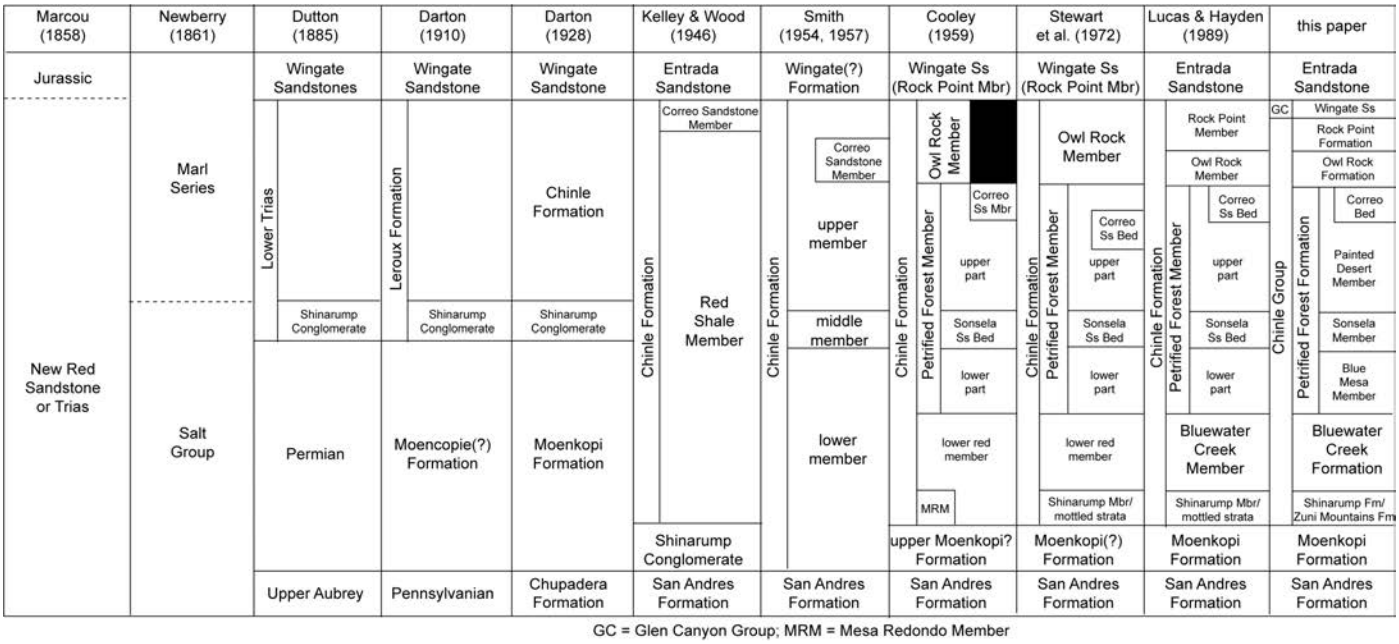

FIGURE 3. Historical development of lithostratigraphic nomenclature of Triassic strata in west-central New Mexico.

son, Hunt and Tanner produced the lithostratigraphy advocated here and briefly summarized below (Lucas, 1995, 2004).

MOENKOPI FORMATION

The oldest Triassic strata in west-central New Mexico are assigned to the Anton Chico Member of the Moenkopi Formation of Lucas and Hunt (1987). The Moenkopi Formation is as much as 25 m thick and consists primarily of sandstone (lithic arenites and lithic wackes), siltstone and minor conglomerate and mudstone (e.g., Lucas and Hayden, 1989). Moenkopi strata are mostly grayish red, but some beds are reddish purple, pale green or orange brown. Sandstone beds are trough cross-bedded or laminar. The conglomerate clasts are mostly intraformational calcrete and mudrock rip ups, but locally chert and limestone clasts are present, likely derived from the underlying Permian San Andres Formation.

In west-central New Mexico, the Middle Triassic (see below) Anton Chico Member of the Moenkopi Formation rests with profound unconformity on the lower Permian San Andres Formation or, locally, on the lower Permian Glorieta Sandstone. One striking aspect of this unconformity is paleotopography of the Moenkopi-San Andres contact that includes a karst topography developed in the top of the San Andres Formation in the Zuni uplift (Fig. 4). The Moenkopi Formation in west-central New Mexico is disconformably overlain by the Shinarump or Zuni Mountains formations at the base of the Upper Triassic Chinle Group (Figs. 5, 6).

CHINLE GROUP

Lucas (1993) raised the Chinle to group rank, although some workers continue to recognize it as a formation (e.g., Cather et al., 2013). I recognize seven formations of the Chinle Group in west-central New Mexico (in ascending order): Shinarump/ Zuni Mountains formations, Bluewater Creek/San Pedro Arroyo formations, Petrified Forest Formation, Owl Rock Formation and Rock Point Formation (Figs. 2, 3, 6).

Shinarump and Zuni Mountains formations

As just noted, the base of the Chinle Group is a profound disconformity on the Moenkopi Formation across west-central New Mexico. This disconformity is locally marked by beds of

FIGURE 4. Paleokarst feature developed in the top of the Permian San Andres Formation with collapse debris of Moenkopi Formation in Sixmile Canyon in the northern Zuni Mountains (NE1/4 T14N, R16W, McKinley County).

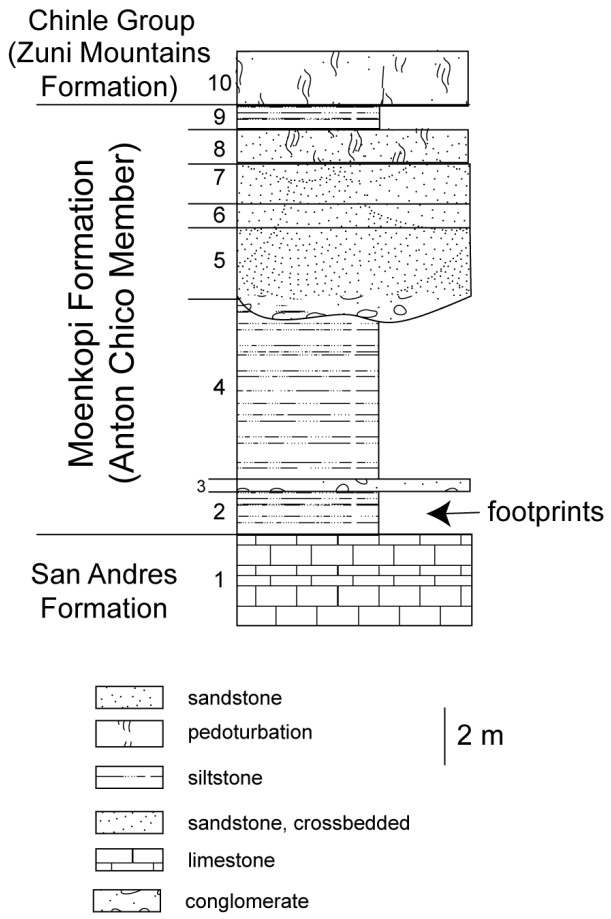

FIGURE 5. Characteristic stratigraphic section of Moenkopi Formation in west-central New Mexico at Bluewater Creek in the northern Zuni Mountains (NE 1/4 T12N, R12W, Cibola County).

silica-pebble conglomerate and quartzose sandstone that represent some of the easternmost outcrops of the Shinarump Formation. Laterally equivalent are pedogenically modified siltstones, mudstones and sandstones that Stewart et al. (1972b) termed the "mottled strata" and that Heckert and Lucas (2003) named the Zuni Mountains Formation.

The Zuni Mountains Formation consists of pedoturbated sandstone and siltstone that are color-mottled shades of purple, red, yellow, white, blue and gray. The most extensive exposures of the Zuni Mountains Formation in west-central New Mexico are south of Fort Wingate (Lucas and Hayden, 1989), where about 25 m of Zuni Mountains strata are exposed between the Moenkopi Formation and Bluewater Creek Formation of the Chinle, mapped by Anderson et al. (2003). These strata host abundant vertical, tubular sandstone casts (Fig. 7) originally interpreted as lungfish burrows (Dubiel et al., 1987; McAllister, 1988), later as crayfish burrows (Hasiotis and Dubiel, 1993; Hasiotis et al., 1993), but best identified as rhizoliths (Lucas and Hayden, 1989; Tanner and Lucas, 2007).

Up to 7 m thick, the Shinarump Formation in west-central New Mexico is generally too thin and laterally discontinuous to be mappable at a scale of 1:24,000. Shinarump strata are yellowish gray to light brown, trough cross-bedded conglomeratic sandstone, conglomerate and quartzose sandstone. Conglomerate clasts are almost all siliceous (chert and quartzite), and pieces of silicified wood up to 0.5 m in diameter are locally present. The name Agua Zarca Member (or Formation) has been applied to similar deposits in north-central New Mexico (Cather et al., 2013).

Bluewater Creek Formation

Diverse workers long identified the presence of a lower, red, sandy interval of the Chinle Formation between the Shinarump Member/mottled strata and the lower part of the Petrified Forest Member on the southeastern Colorado Plateau (Cooley, 1957, 1959a; Repenning et al., 1969; Stewart et al., 1972b). Lucas and Hayden (1989) named this interval in west-central New Mexico the Bluewater Creek Member of the Chinle Formation, and Lucas (1993) raised it to formation rank.

The Bluewater Creek Formation rests conformably on the Zuni Mountains Formation and is conformably overlain by the Blue Mesa Member of the Petrified Forest Formation. In west-central New Mexico, the Bluewater Creek Formation is consistently 50-60 m thick and can be divided into three lithofacies (see Heckert and Lucas, 2002, 2003): (1) a relatively thin interval (5-10 m thick) of greenish gray bentonitic mudstone and carbonaceous shale that is only locally present at the base of the member (Fig. 6), including the "Ciniza Lake Beds" of Ash (1978); (2) beds of mudstone and minor siltstone, some with horizons of calcrete nodules, that are brightly variegated reddish brown, bluish gray and grayish purple, that form colorful badlands and are the bulk of the formation's outcrops (Fig. 8); and (3) sandstone beds, generally 4-6 m thick but locally up to 20 m thick, that are fine- to medium-grained micaceous sublitharenite and litharenite and are ripple-laminar, laminar or tabular bedded.

Locally, the sandstone beds have conglomerate lenses of calcrete-pebble rip ups. A persistent and relatively thick sandstone interval in the upper part of the Bluewater Creek Formation is the McGaffey Member of Anderson and Lucas (1993). The Bluewater Creek Formation is present throughout the Zuni uplift and present in the subsurface in the Zuni Pueblo area where it interfingers with Cooley's (1958) Mesa Redondo Member (Repenning et al., 1969). In the Lucero uplift, the Bluewater Creek Formation grades southeastward into the San Pedro Arroyo Formation (Lucas and Heckert, 1994).

Petrified Forest Formation

The majority of the Chinle Group in west-central New Mexico is assigned to the Petrified Forest Formation, which is up to 441 m thick. The threefold division of the Petrified Forest Formation recognized in east-central Arizona can be identified in west-central New Mexico (Lucas, 1993; Heckert and Lucas, 2002, 2003). Thus, the lower part of the Petrified Forest Formation is the Blue Mesa Member (mostly bluish and purple, bentonitic mudstones) overlain by the Sonsela Member (mostly sandstone and conglomerate) below the reddish, mudstone- and siltstone-dominated Painted Desert Member (Figs. 2, 6).

The most extensive outcrops of the Petrified Forest Formation in west-central New Mexico are along the northern dip slope of the Zuni uplift.

Blue Mesa Member

The Blue Mesa Member in west-central New Mexico forms a slope between the Bluewater Creek Formation and overlying Sonsela Member (Fig. 8). It is 21-45 m thick and mostly purplish and greenish, highly bentonitic mudstone with numerous calcrete nodules. The base of the member at most outcrops in west-central New Mexico is a white tuffaceous sandstone (Figs. 6, 8). The Blue Mesa Member thins from west to east due to erosion at the base of the overlying Sonsela Member (Heckert and Lucas, 1996; Fig. 6). Indeed, the Blue Mesa Member is absent in the Lucero uplift where the Sonsela rests directly on the Bluewater Creek Formation and laterally equivalent strata of the San Pedro Arroyo Formation (Lucas and Heckert, 1994).

Sonsela Member

The Sonsela Member in west-central New Mexico is a cuesta- and cliff-forming unit of two sandstone intervals, each 8-12 m thick, split by a mudrock interval that is 4-10 m thick (Figs. 6, 9). The Sonsela forms the prominent hogback between Fort Wingate and I–40 and the top of the northern dip-slope of the Zuni Mountains from Thoreau to Prewitt just south of I–40. The thickness of the Sonsela Member in west-central New Mexico ranges from 15-61 m (Cooley, 1957, 1959a; Repenning et al., 1969; Heckert and Lucas, 2002, 2003).

The sandstone intervals of the Sonsela Member consist of light-gray to yellowish-brown, fine-grained to conglomeratic, cross-bedded sandstone (sublitharenites and subarkoses) with thin lenses of bluish-gray to grayish-purple mudstone and siltstone. Conglomeratic sandstone and some beds of conglomerate are usually present, and clasts are siliceous – mostly chert and quartzite – but include some mudstone and calcrete rip ups. Particularly characteristic of the Sonsela Member in west-central New Mexico are silicified fossil logs up to 1 m in diameter.

Painted Desert Member

The Painted Desert Member is poorly exposed in west-central New Mexico. The most extensive outcrops are those near Thoreau in the northern half of Tl4N, R12W, R13W and R14W. As much as 335 m thick near Thoreau (Repenning et al., 1969), the Painted Desert Member is mostly variegated brownish-red, grayish-red, pale reddish-brown and pale reddish-purple mudstone, siltstone and sandy siltstone beds. Sandstone beds in this thick, mudrock-dominated unit are micaceous and cross-bedded. A few thin conglomerate beds have clasts that are mudstone and calcrete-pebble rip ups.

Near Thoreau, there are several prominent sandstone beds in the Petrified Forest Member. These beds are composed of pale-red and grayish-red, very fine- to medium-grained, planar cross-bedded sandstone. Cooley (1957) applied formal names (Chambers, Taaiylone, Zuni River and Perea) to beds like these in eastern Arizona and west-central New Mexico, and Lucas et al. (1997a) formalized the name Perea Bed for a sandstone unit low in the Painted Desert Member in the Fort Wingate-Perea area (Fig. 10).

The Correo Bed of Kelley and Wood (1949) is a prominent sandstone interval in the upper part of the Painted Desert Member named for outcrops at Mesa Gigante in the northern Lucero uplift (Stewart et al., 1972b; Lucas et al., 1987, 1997b; Lucas, 1993). It has been recognized as far east as the Hagan basin of Sandoval County (Lucas, 1991a), in the southeastern San Juan Basin (Lucas and Heckert, 1996), and possibly as far west as R12W just east of Thoreau (Lucas and Hayden, 1989).

San Pedro Arroyo Formation

Along the southern and eastern edges of the Lucero uplift most of the strata of the lower part of the Chinle Group belong to the San Pedro Arroyo Formation of Lucas (1991b; also see Spielmann and Lucas, 2009). The San Pedro Arroyo Formation in the Lucero uplift is as much as 90 m thick and consists of grayish-red-purple mudstones with minor sandstone, conglomerate, siltstone and calcrete laterally equivalent to muddier strata of the Bluewater Creek Formation to the north and west (Lucas and Heckert, 1994).

At Carrizo Spring in the eastern Lucero uplift, the lower part of the San Pedro Arroyo Formation contains a limestone interval that is the Ojo Huelos Member of Lucas (1991a). This limestone is micrite and pisolitic rudstone that is color-mottled medium gray, grayish-orange, pale-reddish brown and dusky purple, and some beds contain chert or are silicified (Lucas et al., 2004; Tanner and Lucas, 2012). It represents pedogenic calcrete and palustrine deposits (Tanner and Lucas, 2012).

OWL ROCK FORMATION

The Owl Rock Formation conformably overlies the Painted Desert Member of the Petrified Forest Formation and is present, but very poorly exposed, in the Zuni Pueblo area north of the Zuni River (Cooley, 1957, 1959a; Repenning et al., 1969). The best exposures of the Owl Rock Formation in west-central New Mexico are on the northern dip slope of the Zuni Mountains between Red Rocks north of Fort Wingate (NE ¼, Tl5N, R 17W) and in the Mount Powell-Thoreau area (NE ¼, Tl4N, Rl4W, and N ½, Tl4N, Rl3W).

In west-central New Mexico, the Owl Rock Formation is as much as 35 m thick and contains laterally persistent beds of pale-red and pale-reddish-brown, calcareous siltstone, thin-bedded sandy siltstone and light-greenish-gray limestone and nodular limestone. The limestone beds (Fig. 11) are characteristic of the unit. They are up to 4 m thick, well indurated and have rhizoliths and other evidence of pedogenesis. They are pedogenic calcrete and palustrine-lacustrine limestones (Tanner, 2000, 2003). Across west-central New Mexico, the Owl Rock Formation is overlain disconformably by the Entrada Sandstone, the Rock Point Formation of the Chinle Group, or the Wingate Sandstone (Stewart et al., 1972b; Maxwell, 1982, 1988a, b; Lucas and Heckert, 1996, 2003).

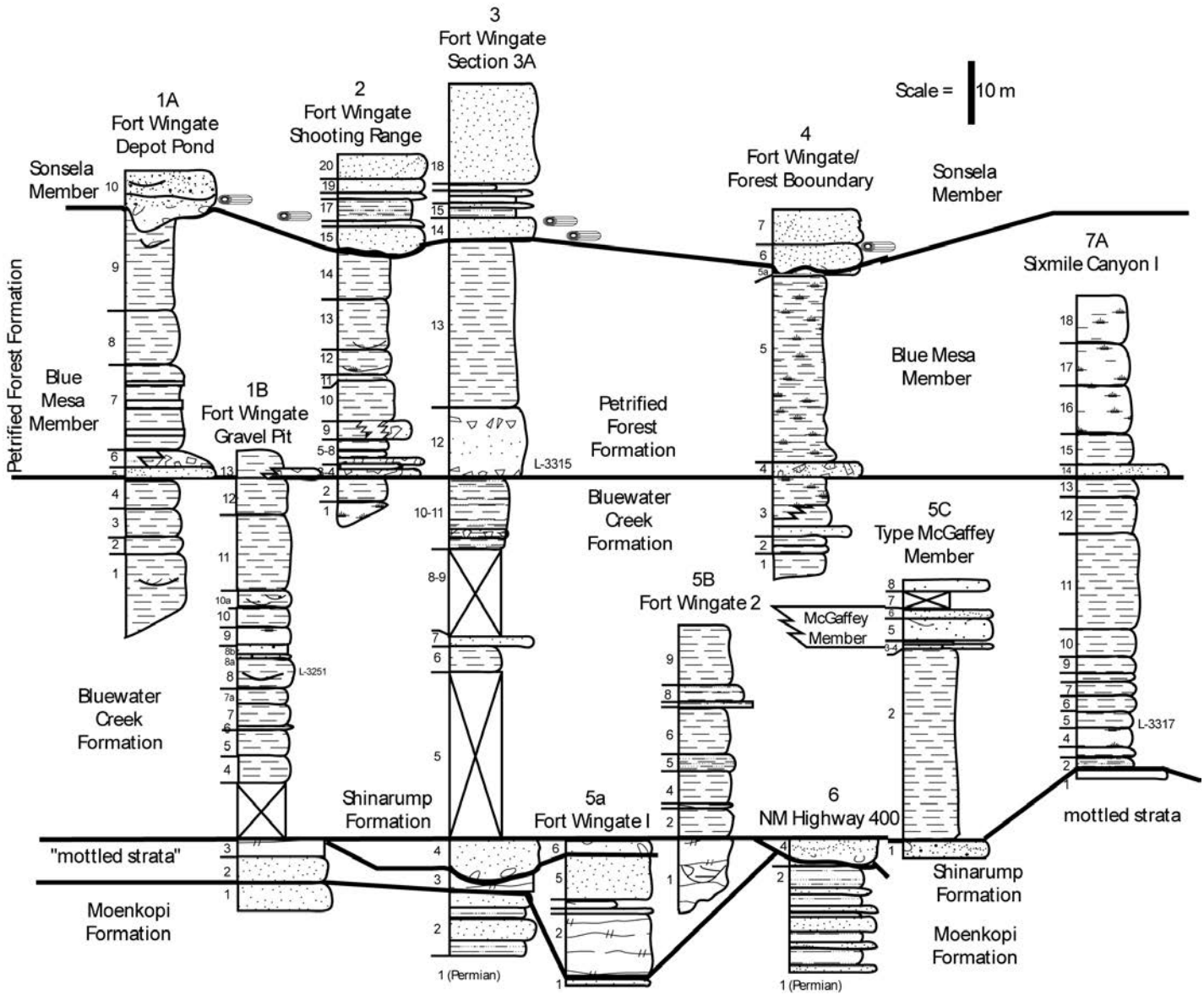

FIGURE 6. Stratigraphy of lower part of Chinle Group in the Zuni Mountains (after Heckert and Lucas, 2002). See Heckert and Lucas (2002) for precise locations of stratigraphic sections.

Rock Point Formation

Across west-central New Mexico, the Rock Point Formation is repetitively bedded, reddish-brown beds of sandy siltstone and silty sandstone. The siltstone beds are massive, whereas the sandstone beds are laminar, ripple laminar or massive. The sandstones are micaceous quartzarenite. In west-central New Mexico, the Rock Point Formation is best exposed in the Zuni Pueblo area in the Zuni Buttes-Dowa Yalanne area (T10N, R19W and R20W). Here, it is 37 m or more of pale- to moderate-reddish brown, intercalated beds of fine-grained sandstone, sandy siltstone and silty mudstone that is flaggy to slabby bedded. The Rock Point Formation is not present to the south in Catron County, where strata of the Painted Desert Member of the Petrified Forest Formation are at the top of the Triassic section. However, it is present in the Zuni uplift, where it is disconformably overlain by the Wingate Sandstone (to the west) and the Dewey Bridge Member (to the east) of the Entrada Sandstone (e.g., Maxwell, 1982).

Uppermost Chinle strata in the Lucero uplift have long been assigned to the Rock Point Formation. Here, Maxwell (1988a, b) identified the Rock Point Member as isolated outcrops of as much as 50 m of pale-red, moderate-red and reddish-purple, shaley siltstone and mudstone with a few sandstone beds. The

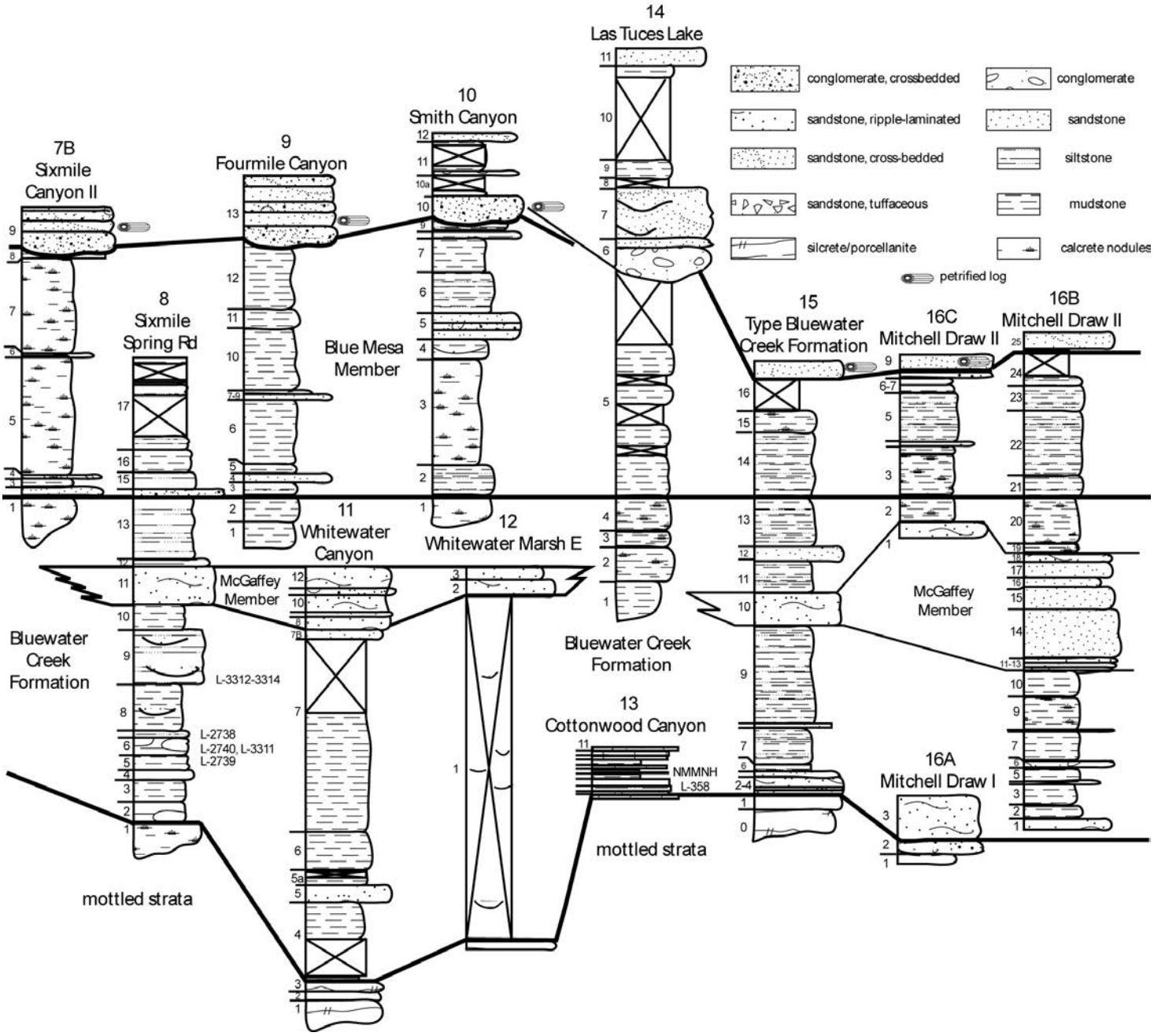

FIGURE 6. Continued.

maximum Rock Point Formation thickness is 70 m in the Petaca Pinta area in the SW1/4, T6N, R6W, and the SE1/4, T6N, R7W (Lucas and Heckert, 1994).

WINGATE SANDSTONE

The unit called the Wingate Sandstone in west-central New Mexico has a long and complicated nomenclatural history reviewed in detail by Lucas and Heckert (2003). I accept the conclusion that this unit is correlative to the unit Harshbarger et al. (1957) named the Lukachukai Member of the Wingate Sandstone in the Four Corners region, which is now the Wingate Sandstone of regional usage. The Wingate Sandstone in the Four Corners region encompasses the Triassic-Jurassic boundary (e.g., Lucas and Tanner, 2007), so it is possible the strata of the Wingate Sandstone in west-central New Mexico are of Early Jurassic age.

CHRONOSTRATIGRAPHY AND REGIONAL UNCONFORMITIES

The ages of Triassic stratigraphic units in west-central New Mexico are based primarily on biostratigraphy supplemented by limited magnetostratigraphic data and radioisotopic ages from across the Triassic outcrop belts in the western United States (see Lucas, 1993, 1997, 2013, 2018; Lucas et al., 2012;

FIGURE 7. Outcrop of Zuni Mountains Formation at Fort Wingate, showing color mottling due to pedogenesis and prominent, vertical, tubular rhizoliths (NE ¼ T14N, R16W, McKinley County).

FIGURE 8. Part of the type section of the Bluewater Creek Formation at Bluewater Creek (NE ¼ T12N, R12W, McKinley County).

FIGURE 9. Characteristic outcrop of Sonsela Member of the Petrified Forest Formation along Sixmile Canyon in the northern Zuni Mountains (NE ¼ T14N, R16W, McKinley County). Note overturned cross-beds in the middle of the photograph.

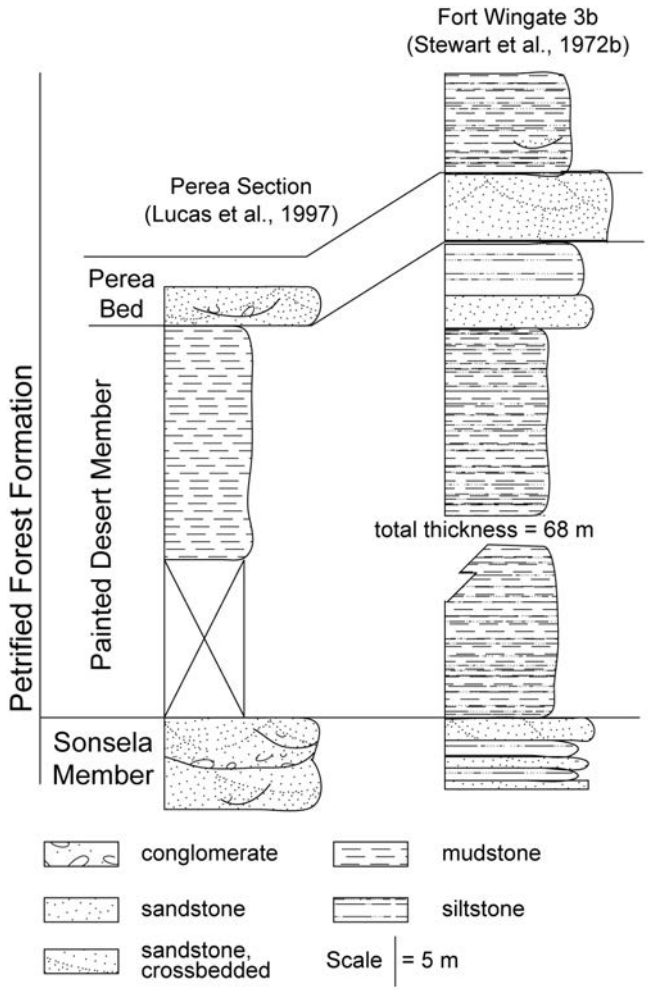

FIGURE 10. Some representative stratigraphic sections of part of the Painted Desert Member of the Petrified Forest Formation near Fort Wingate.

FIGURE 11. Characteristic outcrop of part of Owl Rock Formation, on the frontage road of I–40 near Red Rocks (NE ¼ T15N, R17W, McKinley County). Note prominent, thick limestone interval in lower part of outcrop. Measuring stick is 1.5 m long.

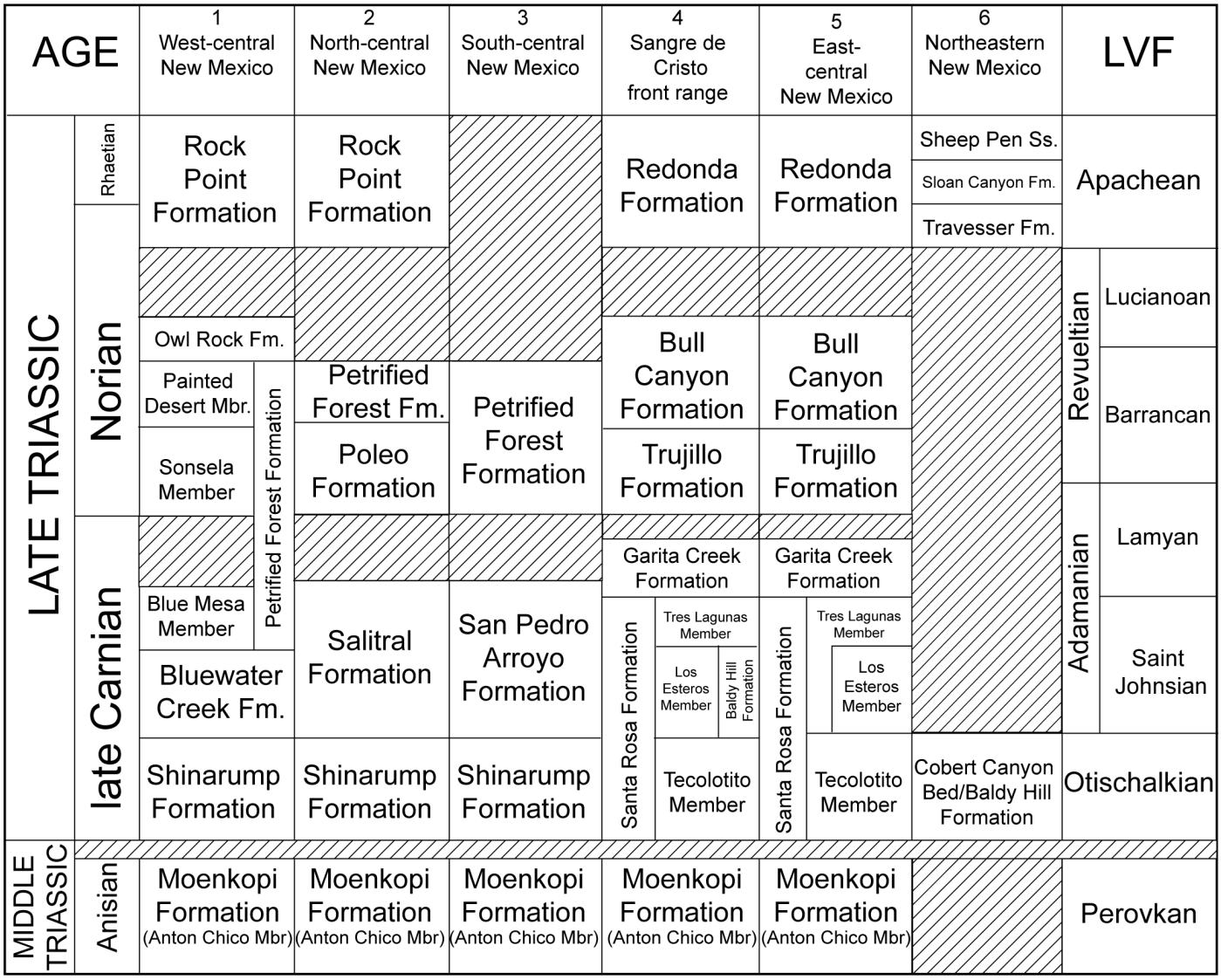

FIGURE 12. Correlation of Triassic stratigraphic units in New Mexico (after Lucas, 2004). The column numbers refer to numbers on the map in Figure 1. LVF = land-vertebrate faunachrons.

Heckert and Lucas, 2015; and Lucas and Tanner, 2018, for summaries). Biostratigraphy and magnetostratigraphy indicate that the Anton Chico Member of the Moenkopi Formation is of early Anisian (Bithynian) age (e.g., Lucas and Schoch, 2002). Chinle Group strata are of Late Triassic age (middle Carnian to Rhaetian) based on all available age data (i.e., biostratigraphy, some radioisotopic ages and magnetostratigraphy).

As noted above, the base of the Moenkopi Formation is an unconformity, a compounding of the Tr-0 through Tr-2 unconformities of Pipiringos and O'Sullivan (1978), a hiatus of about 30 Ma. The base of the Chinle Group is the Tr-3 regional unconformity of Pipiringos and O'Sullivan (1978), a hiatus of at least 15 Ma. The stratigraphic correlation and chronology of the Chinle Group advocated here (Fig. 12) and elsewhere identify two intra-Chinle Group unconformities and thus delineate three depositional sequences (Fig. 2). Lucas (1993) labeled these two unconformities Tr-4 and Tr-5 (= J-0), following the scheme of Pipiringos and O'Sullivan (1978).

Evidence for the widespread intra-Chinle Group unconformities is fourfold: (1) Correlative rocks immediately above each unconformity overlie rocks of different ages in different areas. This probably reflects differential erosion associated with each unconformity; (2) There is a major lithologic change associated with each unconformity. Rocks of the upper part of the Shinarump-Blue Mesa sequence are smectitic mudstones, siltstones and pedogenic silcretes/calcretes overlain by sandstones and conglomerates at the base of the Sonsela-Owl Rock sequence. Smectitic mudstones and pisolitic calcretes of the upper part of the Sonsela-Owl Rock sequence are directly overlain by non-smectitic siltstones and mudstones and fine-grained, laterally persistent sandstones of the Rock Point sequence; (3) At the Tr-4 unconformity, channeling into and reworking of underlying sediment is evident in many areas (e.g., Heckert and Lucas, 1996). At the Tr-5 unconformity, there is evidence of extensive subaerial weathering (pedogenesis) of sediments immediately beneath

the unconformity; and (4) Each unconformity corresponds to a significant reorganization of the biota. Few genera of tetrapods cross an unconformity, so that many tetrapod taxa are unique to each of the three depositional sequences (Lucas, 2018). This is also generally true of palynomorphs, megafossil plants, ostracods and fishes. A temporal hiatus associated with each unconformity best explains this pattern. The Middle Jurassic Entrada Sandstone rests with unconformity (compound J1/J2 unconformity) on Triassic strata across west-central New Mexico.

ACKNOWLEDGMENTS

This paper reports field research that began in the 1980s. I owe much to my collaborators in that research, Orin Anderson, the late Steve Hayden, Andy Heckert, Adrian Hunt and Larry Tanner. I also thank many people and organizations for making this paper possible, particularly the U.S. Forest Service for permitting fieldwork. Some of the line figures were drawn, in part, by A. Heckert. Adrian Hunt and Larry Tanner provided helpful reviews of the manuscript.

REFERENCES

Akers, J.P., Cooley, M.E., and Repenning, C.A., 1958, Moenkopi and Chinle formations of Black Mesa and adjacent areas: New Mexico Geological Society, Guidebook 9, p. 88-94.

Anderson, O.J., and Lucas, S.G., 1993, McGaffey Member of Upper Triassic Bluewater Creek Formation, west-central New Mexico: New Mexico Museum of Natural History and Science, Bulletin 3, p. G30.

Anderson, O.J., Lucas, S.G., and Maxwell, C.H., 2003, Geologic map of the Fort Wingate 7.5-minute quadrangle: New Mexico Bureau of Mines and Mineral Resources, Geologic Quadrangle Map, Open-file Report 473, scale 1:24,000.

Ash, S.R., ed., 1978, Geology, paleontology, and paleoecology of a Late Triassic lake, western New Mexico: Brigham Young University, Geology Studies, v. 25, no. 2, 95 p.

Bates, R.L., 1942, The oil and gas resources of New Mexico: New Mexico Bureau of Mines and Mineral Resources, Bulletin 18, p. 83-140.

Cather, S.M., Zeigler, K.A., Mack, G.H., and Kelley, S.A., 2013, Toward standardization of Phanerozoic stratigraphic nomenclature in New Mexico: Rocky Mountain Geology, v. 48, p. 101-124.

Cooley, M.E., 1957, Geology of the Chinle Formation in the upper Little Colorado drainage area. Arizona and New Mexico [M.S. thesis]: Tucson, University of Arizona, 317 p.

Cooley, M.E., 1958, The Mesa Redondo Member of the Chinle Formation, Apache and Navajo counties, Arizona: Plateau, v. 31, p. 7-15.

Cooley, M.E., 1959a, Triassic stratigraphy in the state line region of west central New Mexico and east-central Arizona: New Mexico Geological Society, Guidebook 10, p. 66-73.

Cooley, M.E., 1959b, Ancient cave deposit near Thoreau, New Mexico: Plateau, v. 3, p. 89.

Cooley, M.E., Harshbarger, J.W., Akers, J.P., and Hardt, W.F., 1969, Regional hydrogeology of the Navajo and Hopi Indian Reservations, Arizona, New Mexico, and Utah: U.S. Geological Survey, Professional Paper 521A, 61 p.

Darton, N.H., 1910, A reconnaissance of parts of northwestern New Mexico and northern Arizona: U. S. Geological Survey, Bulletin 435, 88 p.

Darton, N.H., 1928, "Red beds" and associated formations in New Mexico: U.S. Geological Survey, Bulletin 794, 356 p.

Dubiel, R.F., Blodgett, R.H., and Bown, T.M., 1987, Lungfish burrows in the Upper Triassic Chinle and Dolores formations, Colorado Plateau: Journal of Sedimentary Petrology, v. 57, p. 512-521.

Dutton, C.E., 1885, Mount Taylor and the Zuni Plateau: U.S. Geological Survey, Sixth Annual Report. p. 105-198.

Gilbert. G.K., 1875, Report upon the geology of portions of Nevada, Utah, California, and Arizona: U.S. Geological and Geographical Surveys West of the 100th Meridian [Wheeler], v. 3. p. 17-187.

Gregory, H.E., 1915, The igneous origin of the "glacial deposits" on the Navajo Reservation: American Journal of Science, v. 40. p. 97-115.

Harshbarger. J.W., Repenning, C.A., and Irwin. J.H., 1957, Stratigraphy of the uppermost Triassic and the Jurassic rocks of the Navajo country: U.S. Geological Survey, Professional Paper 291, 74 p.

Hasiotis, S.T., and Dubiel, R.F., 1993, Crayfish burrows and their paleohydrologic significance – Upper Triassic Chinle Formation, Fort Wingate, New Mexico: New Mexico Museum of Natural History and Science, Bulletin 3, p. G24-G26.

Hasiotis S.T., Mitchell, C.E., and Dubiel, R.F., 1993, Application of morphologic burrow interpretations to discern continental burrow architects: lungfish or crayfish?: Ichnos, v. 2, p. 315-333.

Heckert, A.B., 1997, Litho- and biostratigraphy of the lower Chinle Group, east-central Arizona and west-central New Mexico, with a description of a new theropod (Dinosauria: Theropoda) from the Bluewater Creek Formation [M. S. thesis]: Albuquerque, University of New Mexico, 278 p.

Heckert, A.B., and Lucas, S.G., 1996, Stratigraphic description of the Tr-4 unconformity, west-central New Mexico and eastern Arizona: New Mexico Geology, v. 18, p. 61-70.

Heckert, A.B., and Lucas, S.G., 2002, Lower Chinle Group (Upper Triassic: Carnian) stratigraphy in the Zuni Mountains, west-central New Mexico: New Mexico Museum of Natural History and Science, Bulletin 21, 51-72.

Heckert, A.B., and Lucas, S.G., 2003, Triassic stratigraphy in the Zuni Mountains, west-central New Mexico: New Mexico Geological Society, Guidebook 54, p. 245–262.

Heckert, A.B., and Lucas, S.G., 2015, Triassic vertebrate paleontology in New: New Mexico Museum of Natural History and Science, Bulletin 68, p. 77-95.

Kelley, V.C., and Wood, G.H., 1946, Lucero uplift, Valencia, Socorro, and Bernalillo counties, New Mexico: U.S. Geological Survey, Oil and Gas Investigations Preliminary Map OM-47.

Lucas, S.G., 1991a, Correlation of Triassic strata of the Colorado Plateau and southern High Plains, New Mexico: New Mexico Bureau of Mines and Mineral Resources, Bulletin 137, p. 47-56.

Lucas, S.G., 1991b, Triassic stratigraphy, paleontology and correlation, south-central New Mexico: New Mexico Geological Society, Guidebook 42, p. 243-259.

Lucas, S.G., 1993, The Chinle Group: revised stratigraphy and chronology of Upper Triassic nonmarine strata in the western United States: Museum of Northern Arizona, Bulletin 59, p. 27-50.

Lucas, S.G., 1995, Triassic stratigraphy and chronology in New Mexico: New Mexico Geology, v. 17, p. 8-13.

Lucas, S.G., 1997, Upper Triassic Chinle Group, western United States: A nonmarine standard for Late Triassic time, *in* Dickins, J.M., Yang, Z., Yin, H., Lucas, S.G. and Acharyya, S.K., eds., Late Palaeozoic and Early Mesozoic Circum-Pacific Events and Their Global Correlation: Cambridge, Cambridge University Press, p. 209-228.

Lucas, S.G., 2004, The Triassic and Jurassic systems in New Mexico, *in* Mack, G.H., and Giles, K.A., eds., The Geology of New Mexico: A Geologic History: Socorro, New Mexico Geological Society Special Publication 11, p. 137-152.

Lucas, S.G., 2013. Plant megafossil biostratigraphy and biochronology, Upper Triassic Chinle Group, western USA: New Mexico Museum of Natural History and Science, Bulletin 61, p. 354-365.

Lucas, S.G., 2018, Late Triassic terrestrial tetrapods: Biostratigraphy, biochronology and biotic events, *in* Tanner, L.H., ed., The Late Triassic World: Springer, Topics in Geobiology 46, p. 351-405.

Lucas, S.G., and Hayden, S.N., 1989, Triassic stratigraphy of west-central New Mexico: New Mexico Geological Society, Guidebook 40, p. 191–211.

Lucas, S.G., and Heckert, A.P., 1994, Triassic stratigraphy in the Lucero uplift, Cibola, Valencia and Socorro Counties, New Mexico: New Mexico Geological Society, Guidebook 45, p. 241-254.

Lucas, S.G., and Heckert, A.B., 1996, Stratigraphy and correlation of Triassic strata around the Nacimiento and Jemez uplifts, northern New Mexico: New Mexico Geological Society, Guidebook 47, p. 199-204.

Lucas, S.G., and Heckert, A.B., 2003, Jurassic stratigraphy in west-central; New Mexico: New Mexico Geological Society, Guidebook 54, p. 289-301.

Lucas, S.G., and Hunt, A.P., 1987, Stratigraphy of the Anton Chico and Santa

Rosa formations, Triassic of east-central New Mexico: Journal of the Arizona-Nevada Academy of Science, v. 22, p. 21-33.

Lucas, S.G., and Schoch, R.R., 2002, Triassic temnospondyl biostratigraphy, biochronology and correlation of the German Buntsandstein and North American Moenkopi Formation: Lethaia, v. 35, p. 97-106.

Lucas, S.G., and Tanner, L.H., 2007, Tetrapod biostratigraphy and biochronology of the Triassic-Jurassic transition on the southern Colorado Plateau, USA: Palaeogeography, Palaeoclimatology, Palaeoecology, v. 244, p. 242-256.

Lucas, S.G., and Tanner, L.H., 2018, Record of the Carnian wet episode in strata of the Chinle Group, western USA: Journal of the Geological Society, v. 175, p. 1004-1011.

Lucas, S.G., Allen, B.D. and Hayden, S.N., 1987, Type section of the Triassic Correo Sandstone Bed, Chinle Formation, Cibola County, New Mexico: New Mexico Journal of Science, v. 27, p. 87-93.

Lucas, S.G., Heckert, A.B., and Anderson, O.J., 1997a, Triassic stratigraphy and paleontology on the Fort Wingate quadrangle, west-central New Mexico: New Mexico Geology, v. 19, p. 33-42.

Lucas, S.G., Heckert, A.B., and Hunt, A.P., 2004, Triassic strata at Carrizo Arroyo, Lucero uplift, central New Mexico: New Mexico Museum of Natural History and Science Bulletin 25, p. 83-87.

Lucas, S.G., Heckert, A.B., Estep, J.W., and Anderson, O.J., 1997b, Stratigraphy of the Upper Triassic Chinle Group, Four Corners region: New Mexico Geological Society, Guidebook 48, p. 81-108.

Lucas, S.G., Tanner, L.H., Kozur, H.W., Weems, R.E., and Heckert, A.B., 2012, The Late Triassic timescale: Age and correlation of the Carnian-Norian boundary: Earth-Science Reviews, v. 114, p. 1-18.

Marcou, J., 1858, Geology of North America, with two reports on the prairies of Arkansas and Texas, the Rocky Mountains of New Mexico, and the Sierra Nevada of California, originally made for the United States Government: Zurich, Zurcher and Furrer, 144 p.

Maxwell, C.H., 1982, Mesozoic stratigraphy of the Laguna-Grants region: New Mexico Geological Society, Guidebook 33, p. 261-266.

Maxwell, C.H., 1988a, Geologic map of the Cerro del Oro quadrangle, Cibola County, New Mexico: U.S. Geological Survey, Miscellaneous Field Studies Map MF-2033, scale 1:24,000.

Maxwell, C.H., 1988b, Geologic map of the Marmon Ranch quadrangle, Cibola County, New Mexico: U.S. Geological Survey, Miscellaneous Field Studies, Map MF-2049, scale 1:24,000.

McAllister, J.A., 1988, Lungfish burrows in the Upper Triassic Chinle and Dolores formations, Colorado Plateau—comments on the recognition criteria of fossil lungfish burrows: Journal of Sedimentary Petrology, v. 58, p. 365-369.

McKee, E.D., 1954, Stratigraphy and history of the Moenkopi Formation of Triassic age: Geological Society of America, Memoir 61, 133 p.

Momper, J. A., 1957, Pre-Morrison stratigraphy of the southern and western San Juan Basin: Four Comers Geological Society, Guidebook 2, p. 85-94.

Newberry, J.S., 1876, Geological report, in Macomb, J.N., ed., Report of the exploring expedition from Santa Fe, New Mexico, to the junction of the Grand and Green Rivers of the Great Colorado River of the West, in 1859, under the command of Capt. J. N. Macomb: U.S. Army. Engineer Department, p. 101-109.

Pipiringos, G.N., and O'Sullivan, R.B., 1978, Principal unconformities in Triassic and Jurassic rocks, Western Interior United States—a preliminary survey: U.S. Geological Survey, Professional Paper 1035A, p. 1-29.

Repenning. C.A., Cooley. M.F., and Akers, J.P., 1969, Stratigraphy of the Chinle and Moenkopi formations, Navajo and Hopi Indian reservations Arizona, New Mexico, and Utah: U.S. Geological Survey, Professional Paper 521-8, 34 p.

Smith, C.T., 1954, Geology of the Thoreau quadrangle, McKinley and Valencia counties, New Mexico: New Mexico Bureau of Mines and Mineral Resources, Bulletin 3, 36 p.

Smith, C.T., 1957, Geology of the Zuni Mountains, Valencia and McKinley counties, New Mexico: Four Corners Geological Society, Guidebook 2, p. 53-61.

Spielmann, J.A., and Lucas, S.G., 2009, Triassic stratigraphy and biostratigraphy in Socorro County, New Mexico: New Mexico Geological Society, Guidebook 60, p. 213-226.

Stewart, J.H., Poole, F.G., and Wilson. R.F., 1972a, Changes in nomenclature of the Chinle Formation on the southern pan of the Colorado Plateau: 1850s-1950s: Museum of Northern Arizona, Bulletin 47, p. 75-103.

Stewart, J.H., Poole, F.G., and Wilson, R.F., 1972b, Stratigraphy and origin of the Chinle Formation and related Upper Triassic strata in the Colorado Plateau region: U.S. Geological Survey, Professional Paper 690, 336 p.

Stewart, J.H., Poole, F.G., and Wilson, R.F., 1972c, Stratigraphy and origin of the Triassic Moenkopi Formation and related strata in the Colorado Plateau region: U.S. Geological Survey, Professional Paper 691, 195 p.

Tanner, L.H., 2000, Palustrine-lacustrine and alluvial facies of the (Norian) Owl Rock Formation (Chinle Group), Four Corners Region, southwestern U.S.A.: implications for Late Triassic paleoclimate: Journal of Sedimentary Research, v. 70, p. 1280-1289.

Tanner, L.H., 2003, Pedogenic features of the Chinle Group, Four Corners region: Evidence of Late Triassic aridification: New Mexico Geological Society, Guidebook 54, 269-280.

Tanner, L.H., and Lucas, S.G., 2007, Origin of sandstone casts in the Upper Triassic Zuni Mountains Formation, Chinle Group, Fort Wingate, New Mexico: New Mexico Museum of Natural History and Science, Bulletin 40, p. 209-214.

Tanner, L.H., and Lucas, S.G., 2012, Carbonate facies of the Upper Triassic Ojo Huelos Member, San Pedro Arroyo Formation (Chinle Group), southern New Mexico: Paleoclimatic implications. Sedimentary Geology, v. 273-274, p. 73-90.

Ward, L.F., 1901, Geology of the Little Colorado Valley: American Journal of Science, v. 12, p. 401-413.

New Mexico Geological Society, Special Publication 14, Geology of the Mount Taylor Area, 2020, p. 135-144.

JURASSIC STRATIGRAPHY OF THE SOUTHEASTERN COLORADO PLATEAU, WEST-CENTRAL NEW MEXICO: 2020 SYNTHESIS

Spencer G. Lucas

New Mexico Museum of Natural History, Albuquerque, New Mexico 87104; spencer.lucas@state.nm.us

Abstract—Jurassic strata exposed on the southeastern Colorado Plateau in west-central New Mexico encompass part of the southern edge of the Jurassic outcrop belt in the Western Interior. The water-deposited Jurassic stratigraphic units pinch out or are truncated southward in west-central New Mexico, so that in the southernmost reaches of the Jurassic outcrop belt the entire Jurassic section is merged eolian sandstones. These merged eolian sandstones are assigned to the Zuni Sandstone, and to the north and northeast the Jurassic section is assigned to (in ascending order) the Entrada Sandstone (Dewey Bridge and Slick Rock members), the Todilto Formation (Luciano Mesa and Tonque Arroyo members), the Summerville Formation, the Bluff Formation (main body and Recapture Member), the Acoma Tongue of the Zuni Sandstone (all in the San Rafael Group) and the Morrison Formation (Salt Wash, Brushy Basin and Jackpile members). The ages of Jurassic lithostratigraphic units in west-central New Mexico range from Callovian to Tithonian based on regional stratigraphic relationships and on radioisotopic ages and biostratigraphic data, mostly from Utah and Colorado. The lithostratigraphy advocated for Jurassic strata in west-central New Mexico provides the basis for a Jurassic sequence stratigraphy in west-central New Mexico that recognizes four regional unconformities: J-2 (base of the Entrada and Zuni sandstones), J-3 (base of the Todilto Formation), J-5 (base of the Salt Wash Member of the Morrison Formation) and K-0 (base of the Cretaceous Dakota Formation).

INTRODUCTION

Jurassic strata are well exposed on the southeastern Colorado Plateau in west-central New Mexico (Fig. 1). These strata have yielded uranium, groundwater and building stone that have long made them a major focus of geologic studies, especially in the latter half of the 20th century (e.g., Condon and Peterson, 1986; Lucas and Heckert, 2003). Extensive stratigraphic analyses and mapping were an integral part of these studies and have led to a stratigraphic nomenclature that has both evolved through time and been a major source of debate (Fig. 2). Here, I present a brief review of the Jurassic stratigraphy of west-central New Mexico that employs a Jurassic stratigraphic nomenclature that embodies sound application of stratigraphic principles, reflects regional lithostratigraphic architecture and has a firm basis in defensible correlations. This review is an update of Lucas and Heckert (2003) and incorporates much information, including some of the illustrations, published in that earlier review.

SOME HISTORY

Several articles have reviewed previous studies of the Jurassic stratigraphy of west-central New Mexico (e.g., Baker et al., 1936; Condon and Peterson, 1986; Lucas and Anderson, 1998; Lucas and Heckert, 2003; Cather et al., 2013), obviating the need for a detailed review here. Instead, I briefly trace the development of Jurassic stratigraphic concepts and nomenclature, emphasizing the key works of Dutton (1885), Darton (1928a, b), Baker et al. (1936, 1947), Dane and Bachman (1965), Condon and Peterson (1986) and Lucas and Anderson (1998; Fig. 2).

Marcou (1858) "guessed" a Jurassic age for some of the strata exposed in west-central New Mexico (because they overlie red beds he considered Triassic), and Dutton (1885) followed suit, lacking any compelling evidence to assign any of the strata to the Jurassic (Lucas, 2001, 2003). Dutton (1885) coined the names Wingate Sandstones (considered by him to be

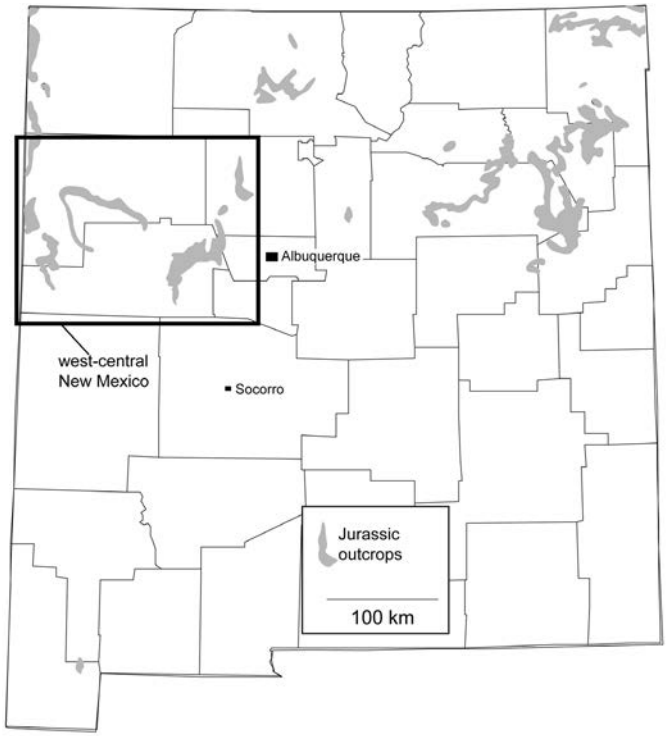

FIGURE 1. Location of outcrops of Jurassic strata in New Mexico with the area of west-central New Mexico indicated (after Dane and Bachman, 1965, and Lucas and Heckert, 2003).

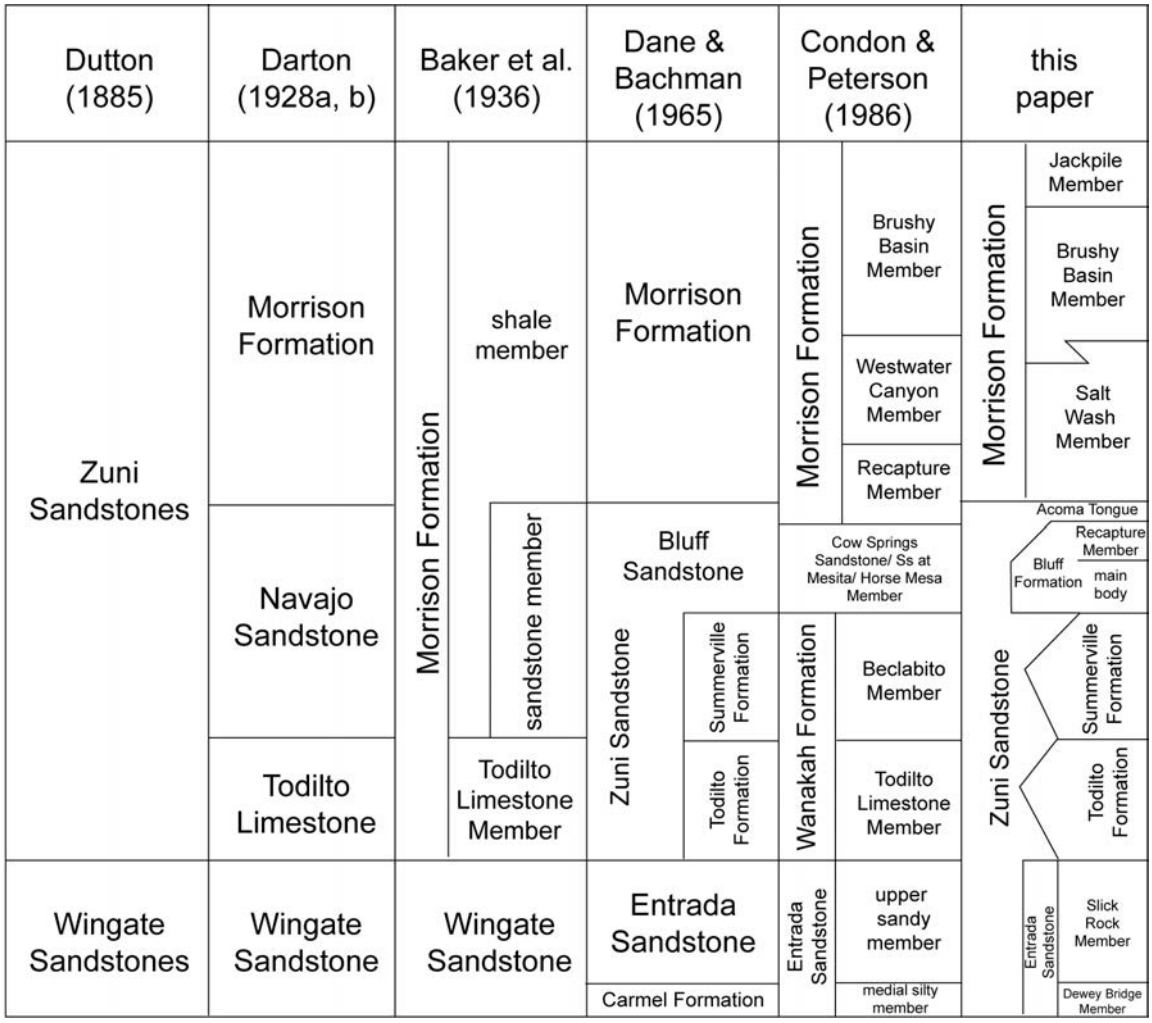

FIGURE 2. Development of Jurassic stratigraphic nomenclature in west-central New Mexico (modified from Lucas and Heckert, 2003).

Triassic) and Zuni Sandstones for Jurassic strata in west-central New Mexico (Lucas, 2003; Fig. 2).

Darton's (1928a, b) view of the Jurassic stratigraphy of west-central New Mexico (Fig. 2) was based primarily on the work of Gregory (1917), including the erroneous placement of the Todilto Formation beneath the Navajo Sandstone. Darton (1928a) recognized the Wingate Sandstone *sensu* Dutton but did not use the term Zuni Sandstone. Instead, he assigned most of the Jurassic section to the Todilto, Navajo and Morrison formations, the latter considered by Darton to be most likely of Cretaceous age (Fig. 2).

The classic monograph by Baker et al. (1936) represented the first explicit attempt to assemble a synthetic Jurassic stratigraphy of much of the Colorado Plateau. It corrected some earlier mistakes; for example, the Navajo Sandstone was correlated correctly so that the Todilto Formation was placed much higher in the section (Fig. 2). The Morrison base was moved down to include the Todilto Formation and all overlying Jurassic strata (Fig. 2).

Baker et al. (1936) also made a significant error in concluding that the San Rafael Group of Utah (Carmel, Entrada and Summerville formations of Gilluly and Reeside, 1928) pinched out between the Morrison and Wingate in the Four Corners, north of Red Rock, Arizona (Baker et al., 1936, pl. 2 and fig. 7). Therefore, they indicated that Dutton's Wingate Sandstone in west-central New Mexico is much older than (stratigraphically lower than) the San Rafael Group of Utah.

This and other errors were corrected by Baker et al. (1947) in a five-page published note that repudiated the principal conclusions of their 1936 monograph. Thus, they removed the Todilto and Summerville from the Morrison, and, at least in Colorado and New Mexico, considered them members of Burbank's (1930) Wanakah Formation. They also concluded that the Red Rock cliffs at Fort Wingate, type section of Dutton's Wingate Sandstone, were correlative to Gilluly and Reeside's Entrada Sandstone. The simplest solution would have obeyed priority and replaced the name Entrada with Wingate and given a new name to the lower eolianite of the Glen Canyon Group that had erroneously been called Wingate. Instead, Baker et al. (1947, p. 1667) argued that "through use in numerous publications, they [Wingate and Entrada *sensu* Baker et al., 1936] are firmly entrenched in geologic literature and are well known to many geologists….the abandonment of this nomenclature through the application of the principles of priority would be unfortunate

and confusing." Therefore, Baker et al. (1947) continued usage of Wingate Sandstone for the lower eolianite of the Glen Canyon Group, abandoned Dutton's type Wingate locality, and called the type Wingate strata Entrada. Nevertheless, this actually did much violence to usage, at least in New Mexico, where Wingate Sandstone *sensu* Dutton (1885) was well entrenched in the geologic literature (e.g., Darton, 1928a; Heaton, 1939; Dobrovolny et al., 1946) and had even been embodied in Darton's (1928b) geologic map of New Mexico.

Dane and Bachman (1965), in their state geologic map of New Mexico, well reflected the 1960s consensus on Jurassic stratigraphy in west-central New Mexico (Fig. 2). This was the official U.S. Geological Survey (USGS) stratigraphy, and it was that of Gilluly and Reeside (1928) and the corrected regional correlations of Baker et al. (1947), with some of the gaps in their coverage filled by Harshbarger et al. (1957). Dane and Bachman (1965) thus recognized a Jurassic section of Carmel, Entrada, Todilto, Summerville, Bluff and Morrison formations laterally equivalent in part to eolian sandstones they called Zuni Sandstone (Fig. 2).

In the 1980s, a new USGS lithostratigraphy of the southern Colorado Plateau (Fig. 2) was agreed on, well summarized by Condon and Peterson (1986). The Jurassic stratigraphy in west-central New Mexico advocated here (Fig. 2) is that of Anderson and Lucas, published in a series of articles: Anderson and Lucas (1992, 1994, 1995, 1996, 1997, 1998), and Lucas and Anderson (1996, 1997, 1998), and elaborated by Lucas and Woodward (2001), Lucas et al. (1995, 1999, 2001, 2005, 2014) and Lucas (2004, 2014, 2018). This is also the Jurassic stratigraphy used on the current geological map of New Mexico (NMBGMR, 2003). Indeed, the present article is largely a summary of the Anderson-Lucas Jurassic stratigraphy in west-central New Mexico, and more extensive discussion and justification of it can be found in the articles just cited.

Some Lithostratigraphic Conventions

The lithostratigraphic nomenclature advocated here recognizes most of the units of the USGS stratigraphers (e.g., Condon and Peterson, 1986) but applies different names to some of them. The differences in names largely reflect disagreements over regional correlations. Thus, because almost all of the names used for Jurassic lithostratigraphic units in west-central New Mexico are based on type sections in Utah and Colorado, the correlation of those names from their type sections is critical to the nomenclature used. The Anderson-Lucas Jurassic stratigraphy developed in the 1990s was based in large part on restudy of all the type sections of Jurassic units recognized on the Colorado Plateau and their regional correlation based on fieldwork.

Lithostratigraphy is a taxonomy of lithostratigraphic units based on their lithology and stratigraphic architecture. Like any good taxonomy, a good lithostratigraphy contains the maximum amount of information by conveying an accurate stratigraphic architecture and correlations. Sound lithostratigraphy is also parsimonious. It uses a minimum of names — only those necessary to denominate mappable lithologic units (formations) and their unambiguous subdivisions (members and beds). Formations are mappable at a scale of 1:24,000. Only a single name is needed for each lithosome. Formation (and group) boundaries are at surfaces of lithologic contrast, and chronostratigraphic (time) boundaries are not confused with lithostratigraphic boundaries. Physical stratigraphic evidence (e.g., lithologic changes, stratal geometry, and/or presence or absence of subjacent strata) is used to identify unconformities, and they are assigned a time value based on chronostratigraphy.

The lithostratigraphy of Jurassic strata in west-central New Mexico advocated here is just such a parsimonious lithostratigraphy. However, the stratigraphy employed by the USGS (see Condon and Peterson, 1986) did not follow these practices, nor do the relatively recent recommendations of Cather et al. (2013), which do little more than recommend we continue to use the USGS lithostratigraphic nomenclature of Jurassic units in west-central New Mexico.

LITHOSTRATIGRAPHY

Jurassic strata in west-central New Mexico (Fig. 1) crop out in four distinct outcrop belts: (1) in the southeastern San Juan Basin along the western flank of the Nacimiento uplift and in the northern portion of the Rio Puerco fault zone near San Ysidro in Sandoval County; (2) on the northern part of the Lucero uplift north of the point where the Cretaceous Dakota Formation rests on Upper Triassic strata of the Chinle Group; (3) on the northern dipslope of the Zuni Mountains and along its monoclinally-controlled western edge; and (4) along the New Mexico-Arizona state line, which is in part along the eastern edge of the Defiance uplift. The lithostratigraphy, of course, varies somewhat across these outcrop belts, but a fairly uniform lithostratigraphic nomenclature can be applied to most of the Jurassic strata across west-central New Mexico (Fig. 3).

West-central New Mexico encompasses part of the southern edge of the Jurassic outcrop belt in the Western Interior (e.g., Silver, 1948; McKee et al., 1956). Thus, some of the Jurassic stratigraphic units pinch out or are truncated southward in west-central New Mexico, so that in the southernmost reaches of the Jurassic outcrop belt the entire Jurassic section is merged eolian sandstones (a succession of the eolian sandstone units, missing the intercalated non-eolian strata, as is best seen at Zuni Pueblo: Figs. 4-5). Lucas and Heckert (2003) referred to these as the water-deposited and the eolian lithofacies belts (Fig. 4). Therefore, a dual lithostratigraphic nomenclature needs to be used for some of the Jurassic section in west-central New Mexico, one that reflects this merger of lithostratigraphic units (Fig. 2).

In west-central New Mexico, the water-deposited lithofacies belt begins at about I–40 and extends northward into the San Juan Basin. This lithofacies belt includes several water-deposited Jurassic units, the Todilto, Summerville and Morrison formations, not found to the south in the eolian lithofacies belt. These water-deposited units are intercalated with eolian units, so that the water-deposited lithofacies belt consists of a section of Middle and Upper Jurassic eolian and water-deposited strata (Fig. 4).

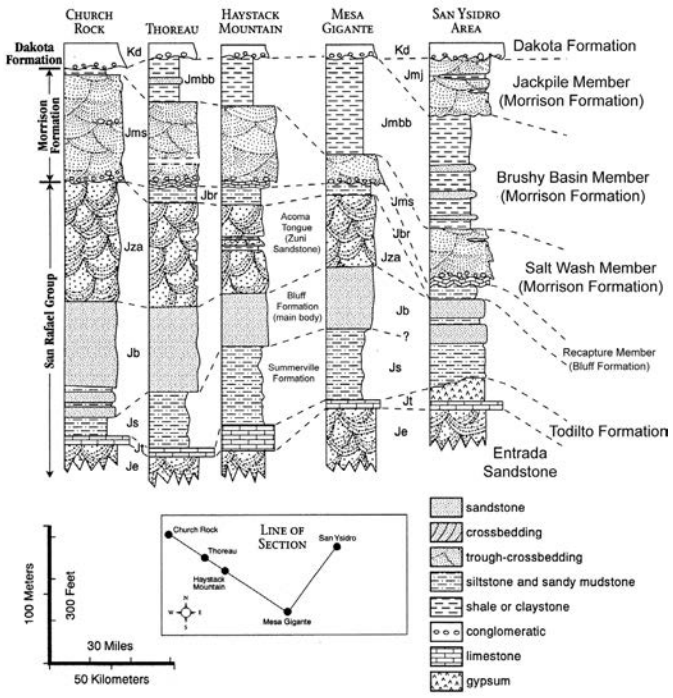

FIGURE 3. Regional correlation of Jurassic strata in west-central New Mexico (after Anderson and Lucas, 1996). Kd = Dakota Formation. Morrison Formation members are: Jmj = Jackpile, Jmbb = Brushy Basin, Jms = Salt Wash. San Rafael Group formations are: Jza = Zuni Sandstone (Acoma Tongue), Jb = Bluff Formation (Jbr = Recapture Member), Js = Summerville Formation, Jt = Todilto Formation, and Je = Entrada Sandstone.

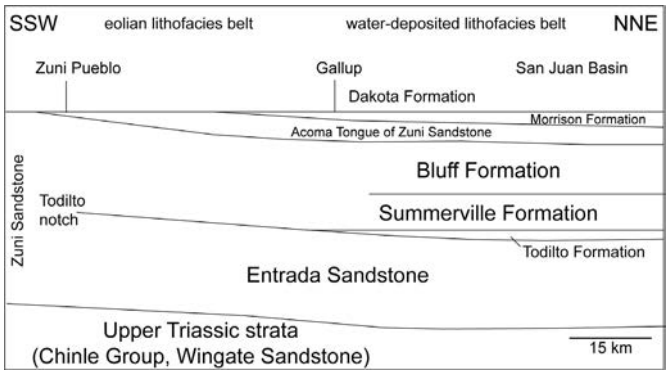

FIGURE 4. Jurassic stratigraphic relationships between the water-deposited and eolian lithofacies belts in west-central New Mexico (after Anderson and Lucas, 1994).

Zuni Sandstone

South of I–40, and best displayed at Zuni Pueblo, the Todilto, Summerville and Morrison formations thin and disappear (either pinchout or are truncated, or a combination of both), and the Jurassic section becomes a succession of eolianites about 150 m thick (Figs. 4-5). I refer to this succession as the Zuni Sandstone, following Anderson (1993), Anderson and Lucas (1994), Lucas and Anderson (1997), and Lucas and Heckert (2003).

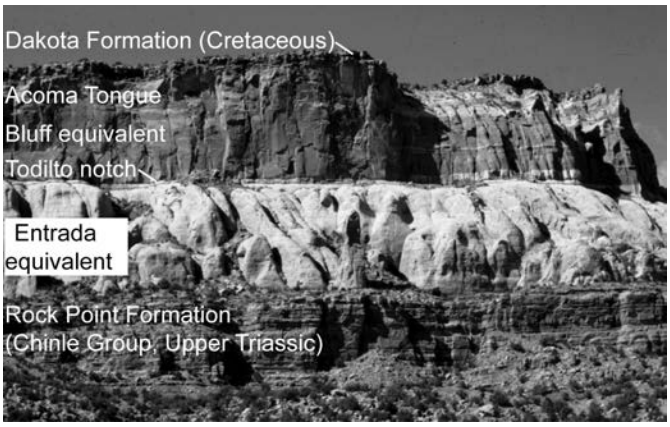

FIGURE 5. Type section of the Zuni Sandstone at Dowa Yalaane near Zuni Pueblo (SE 1/4 T10N, R19W, McKinley County), showing the correlation of units advocated here (see Fig. 4).

At Dowa Yalaane (Taaiyalone), the sacred mesa of the Zuni People near Zuni Pueblo, which is the type section of the Zuni Sandstone (Dutton, 1885; Anderson, 1983, 1993; Lucas and Heckert, 2003), the formation can be divided into three units (Fig. 5). The lower ~80 m is eolian sandstone that, based on stratigraphic position and lithology, I correlate to the Entrada Sandstone to the north. A prominent notch (break) in the sandstone above that interval is the unconformity surface that marks the pinchout/truncation of the Todilto Formation and the Summerville Formation. The eolian sandstone above the notch, about 60 m thick, is here equated to the main body of the Bluff Formation based on its stratigraphic position and lithology. The surface above the Bluff interval represents the pinchout/truncation of the Recapture Member of the Bluff Formation (Note that this guidebook's roadlogs follow Gregory (1938) and Condon and Peterson (1986), among others, in placing the Recapture Member in the Morrison Formation; see discussion of the Bluff and Morrison formations below). The eolian sandstone above that is the Acoma Tongue of the Zuni Sandstone of Anderson (1993). The surface above the Acoma Tongue is the pinchout/truncation of the Morrison Formation and is overlain by the Cretaceous Dakota Formation. However, I stress that these purely lithostratigraphic correlations of the Zuni Sandstone to units to the north and northeast merit further study and verification from other data.

Entrada Sandstone

The dominantly eolian Entrada Sandstone is at the base of the Jurassic section across much of west-central New Mexico. Still, the stratigraphic relationships and nomenclature at the base of the Jurassic section in west-central New Mexico have long been a contentious problem. As noted above, Dutton (1885) applied the name Wingate Sandstones to the oldest "Jurassic" strata near Fort Wingate in McKinley County, New Mexico. More than 40 years later, in Utah, Gilluly and Reeside (1928) named the same lithostratigraphic unit the Entrada Sandstone. As noted above, Baker et al. (1936) miscorrelated

Dutton's type Wingate and Gilluly and Reeside's type Entrada to such an extent that Wingate came to be applied to a much older eolian sandstone interval (in the Glen Canyon Group) on the southern Colorado Plateau, and Dutton's type Wingate came to be called Entrada.

Condon and Peterson (1986) well summarized the current thinking of the USGS on Entrada stratigraphy (Fig. 2). They followed Green (1974) and recognized a tripartite Entrada Sandstone in west-central New Mexico — 1) his lower "Iyanbito Member," 2) a medial silty member, and 3) an upper sandy member — that has been mapped by several workers, including Cooley et al. (1969). Robertson and O'Sullivan (2001) named the "medial silty member" the Rehoboth Member of the Entrada Sandstone and indicated correlation of the upper sandy member with the Slick Rock Member (Wright et al., 1962) of the Four Corners (also see O'Sullivan, 2003).

In contrast, Lucas and Heckert (2003; also see Heckert and Lucas, 1998; Lucas and Anderson, 1998; Lucas et al., 2001) excluded the "Iyanbito Member" from the Entrada. As Harshbarger et al. (1957) and Cooley et al. (1969) well demonstrated, it is the equivalent of the "Lukachukai Member" of the Wingate Sandstone (sensu Harshbarger et al., 1957) and therefore a unit of likely Late Triassic age beneath the J-2 unconformity. The "medial silty member" of the Entrada in west-central New Mexico is equivalent to the Dewey Bridge Member of Wright et al. (1962), and the upper sandy member is equivalent to their Slick Rock Member. Therefore, the Rehoboth Member of Robertson and O'Sullivan (2001) is an unnecessary junior synonym of the Dewey Bridge Member (Lucas et al., 2001). To support these conclusions, which are consistent with the stratigraphy and the mapping of Harshbarger et al. (1957) and Cooley et al. (1969), Lucas and Heckert (2003, fig. 3) correlated numerous stratigraphic sections of the Entrada and Wingate sandstones with the type sections of the Dewey Bridge (southeastern Utah) and Slick Rock (southwestern Colorado) members through the Four Corners southward along the Chuska Mountains and across west-central New Mexico.

The Entrada Sandstone in west-central New Mexico thus consists of two members, Dewey Bridge and Slick Rock, though the Wingate Sandstone is usually too thin in cliff exposures to be mapped separately from the Entrada (Fig. 6). The Dewey Bridge Member is up to 18 m thick and consists of moderate reddish brown to moderate reddish orange, laminar and ripple laminar silty sandstone and siltstone. Some small scale cross-beds are present locally. The overlying Slick Rock Member forms bold cliffs in west-central New Mexico up to 122 m thick. It is pinkish-gray, yellowish-gray and moderate reddish-orange sandstone that is very fine to medium grained and mostly cross-bedded, though some tabular bedding is present.

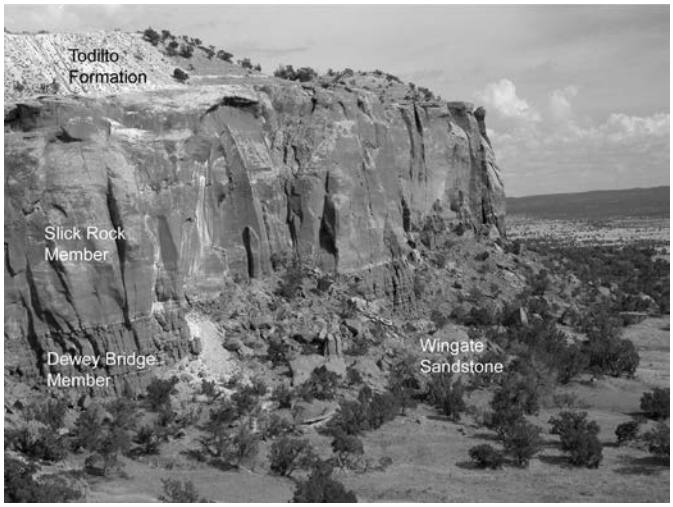

FIGURE 6. Outcrop of Entrada Sandstone just north of Thoreau (NW 1/4 T14N, R12W). Note thin and massive Wingate Sandstone at base of cliff, overlain by thick-bedded Dewey Bridge Member of Entrada Sandstone.

Todilto Formation

The Todilto Formation is one of the most distinctive lithostratigraphic units in the Jurassic section of west-central New Mexico—a striking interval of limestone and/or gypsum in a section dominated by sandstone, siltstone and mudstone (Fig. 7). The unit is found across much of west-central New Mexico as a relatively thin interval of dark gray, kerogenic limestone, the Luciano Mesa Member of Anderson and Lucas (1996). However, in the eastern part of west-central New Mexico, north and east of Grants, near Mesita and Mesa Gigante, the upper, gypsum member of the Todilto Formation (Tonque Arroyo Member of Anderson and Lucas, 1996) is also present above the Luciano Mesa Member and beneath the Summerville Formation (Fig. 7). This gypsum member represents a smaller, evaporitic basin that developed after the larger salina basin in which the limestone member was deposited (Lucas et al., 1985; Armstrong, 1995; Kirkland et al., 1995; Fig. 8).

The Luciano Mesa Member is up to 9 m thick and is light- to medium-gray, mostly microlaminated, kerogenic micrite. Anderson and Kirkland (1960) suggested that the microlaminae form varved couplets, and they counted these couplets to estimate a deposition duration of about 14,000 years for the Luciano Mesa Member. Folding in the limestones of the Luciano Mesa Member ranges in scale from millimeters to meters, and many of the large folds are the loci of uranium

FIGURE 7. Outcrop of Todilto Formation at the mesa just north of Mesita (NW 1/4 T9N, R11W, Cibola County).

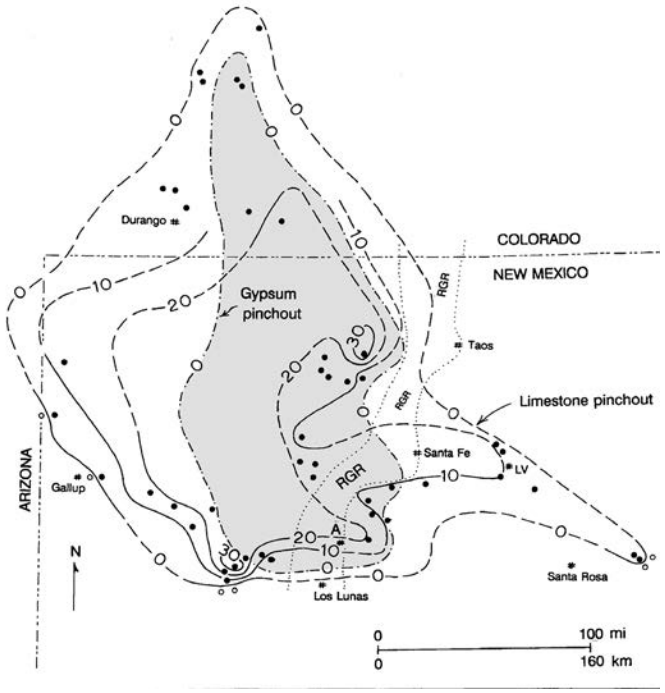

FIGURE 8. Approximate depositional limits of the Jurassic Todilto limestone member (Luciano Mesa Member) and the overlying Todilto gypsum member (Tonque Arroyo Member) (modified from Kirkland et al., 1995). The dotted outline is the Rio Grande rift (RGR). A = Albuquerque, LV = Las Vegas. The isopach contours for the Todilto limestone member are in feet. From Lucas and Woodward (2001).

mineralization. Lucas et al. (2014) examined the Todilto folds to conclude that they have resulted from varied processes that produced dome-like stromatolitic mounds, tepee-like structures, small-scale enterolithic folds and large-scale folds of likely diagenetic origin.

In west-central New Mexico, the upper, gypsum member of the Todilto Formation (Tonque Arroyo Member) is as much as 37 m thick and mostly light-gray to white gypsum (Fig. 7). The gypsum is massive, with chicken-wire texture, or laminated, and grades into anhydrite in the subsurface. Locally, the gypsum beds are contorted due to dissolution and differential expansion and contraction associated with volume changes during conversion of anhydrite to gypsum and vice versa.

Summerville Formation

In west-central New Mexico, the Summerville Formation forms horizontally bedded cliffs or steep slopes between the Todilto Formation and Entrada Sandstone below and the Bluff Formation above (Fig. 7). The Summerville Formation mostly consists of moderate reddish brown, dark reddish brown and grayish red beds of silty sandstone, siltstone and mudstone that are interbedded in a repetitive fashion. Some beds are white or pinkish gray. The sandstone mostly is laminar or ripple laminar, though locally small-scale cross-beds may be present. Some beds are gypsiferous, and some thin beds of gypsum and limestone are present locally. As much as 49 m thick in west-central New Mexico, the Summerville Formation overlies the Todilto Formation and is overlain by the Bluff Formation. The two members of the Summerville – the Beclabito and the Tidwell that are recognized in eastern Utah and adjacent areas (Lucas and Anderson, 1997) – cannot be distinguished in west-central New Mexico. This is because the Tidwell Member is laterally equivalent to the Bluff Sandstone in Utah (Lucas, 2014), so the entire Summerville Formation in west-central New Mexico is the unit named Beclabito Member of the Wanakah Formation by Condon and Huffman (1985).

Summerville strata are present across much of northern New Mexico and southern Colorado and have been assigned various names, including Wanakah, Bell Ranch and Ralston Creek. One name is sufficient for one mappable lithostratigraphic unit of consistent lithotype, so I continue to advocate use of the term Summerville Formation across its entire outcrop belt (also see Anderson and Lucas, 1992, 1994, 1996; Lucas and Anderson, 1997, 1998; Lucas et al., 1999; Lucas and Woodward, 2001; Lucas and Heckert, 2003; Lucas et al., 2005; Lucas, 2014, 2018).

Bluff Formation

In west-central New Mexico, the Bluff Formation gradationally overlies the Summerville Formation and consists of two distinct members. The lower, sandstone-dominated member is the equivalent of the type Bluff Sandstone near Bluff, Utah (Gregory, 1938). In west-central New Mexico, it is as much as 70 m of grayish-yellow, grayish-green, pale-red and moderate-orange, laminated and trough cross-bedded, fine- to medium-grained sandstone (Figs. 9-10). This unit is the main body of the Bluff Formation (Lucas and Anderson, 1997), which is mostly of eolian origin. However, unlike the Slick Rock Member of the Entrada Sandstone, the Bluff in west-central New Mexico generally lacks thick sets of high-angle cross-beds with truncated upper boundaries (reactivation surfaces). Instead, it is dominated by horizontal bedforms (commonly 0.5-5.0 m thick) and indistinctly cross-bedded facies.

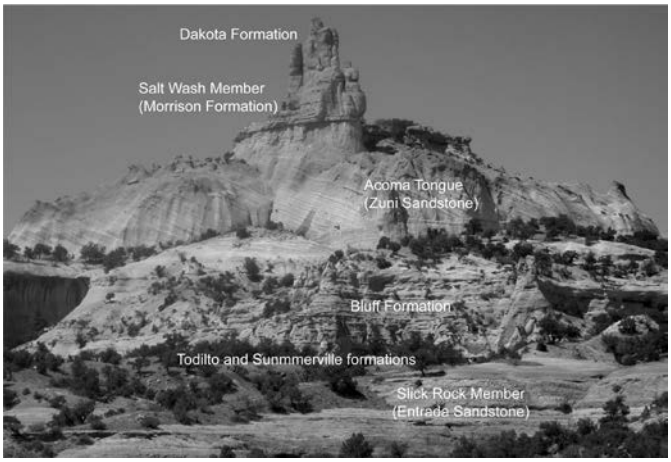

FIGURE 9. The Jurassic section at Church Rock (NE 1/4 T15N, R17W, McKinley County). Note the very thin (less than 5 m thick) interval of the Todilto and Summerville formations near their pinchout.

FIGURE 10. Outcrop of the Morrison Formation north of Milan (NE 1/4 T13N, R10W, McKinley County).

Above the main body of the Bluff Formation in west-central New Mexico is a thicker (up to 113 m thick) and complex lithosome called the Recapture Member by all workers (Fig. 10). USGS workers recognize the Recapture as the basal member of the Morrison (e.g., Condon and Peterson, 1986), whereas I assign it to the Bluff Formation based primarily on the work of Lucas and Anderson (1997, 1998) and Lucas (2014), which demonstrates the integrity of a Bluff lithesome that includes the Recapture Member. The Recapture is pale reddish-brown, light-brown, dark reddish-brown and greenish-gray beds of fine- to medium-grained sandstone intercalated with some mudstone beds. The sandstones are either massive or tabular or display large scale cross-beds indicative of eolian deposition. Thus, Recapture facies are of both fluvial and eolian origin (e.g., Condon and Peterson, 1986).

The main body of the Bluff Formation has multiple names used by workers of the USGS who do not recognize a single, sandstone-dominated lithosome between the Summerville Formation and Morrison Formation. Thus, the Bluff in west-central New Mexico has been termed "Cow Springs Sandstone," "Horse Mesa Member of Wanakah Formation" and "Sandstone at Mesita" (e.g., Harshbarger et al., 1957; Condon and Peterson, 1986; Condon, 1989), all unnecessary synonyms of Bluff Formation. Bluff strata are also included in the "Recapture Member of the Morrison Formation" by many USGS workers (e.g., Condon and Peterson, 1986). Indeed, inclusion in the Morrison Formation of eolian beds of the Bluff or Acoma Tongue of the Zuni Sandstone has led to the idea that eolianites are part of the lower Morrison Formation (e.g., Condon and Peterson, 1986). There are no eolianites in the Morrison Formation as that unit is used here.

Acoma Tongue of the Zuni Sandstone

Locally, the sandstone interval above the Bluff Sandstone and below the Salt Wash Member of the Morrison Formation is as much as 70 m thick and is a boldly cross-bedded eolian sandstone with easterly dipping foresets (Fig. 9). This is the Acoma Tongue of the Zuni Sandstone of Anderson (1993), and it is present at various outcrops in west-central New Mexico from near Mesita to Church Rock to Zuni Pueblo (Figs. 3, 4, 5, 9). The striking cross-beds distinguish it from the more flat-bedded Bluff eolian sandstones below (cf. Fig. 9). The Acoma Tongue is the stratigraphically highest eolianite in the Jurassic section and is the top of the San Rafael Group.

Morrison Formation

For many years, the USGS recognized three principal Morrison Formation members in west-central New Mexico (in ascending order): Recapture, Westwater Canyon and Brushy Basin (Fig. 2). A fourth, uppermost Jackpile Member was later recognized after Owen et al. (1984) formalized the name.

Detailed work by Anderson and Lucas (1994, 1995, 1997, 1998) in southeastern Utah demonstrated that, based on lithology and stratigraphic architecture (particularly its relationship to the Bluff main body), the type Recapture Member of the Morrison Formation of Gregory (1938) is best reassigned to the San Rafael Group as the upper member of the Bluff Formation. Furthermore, as demonstrated by Anderson and Lucas (1994), Gregory's (1938) Westwater Canyon Member of the Morrison Formation is the same unit Lupton (1914) had earlier named Salt Wash Member. In light of these conclusions, the Morrison Formation in west-central New Mexico consists of three members (in ascending order): Salt Wash, Brushy Basin and Jackpile members (Fig. 10).

The Salt Wash Member is the sandstone-dominated lower part of the Morrison Formation, as much as 135 m thick in west-central New Mexico. Its sandstone beds are yellowish gray, reddish gray or red, and fine to coarse grained, locally conglomeratic and are mostly cross-bedded or tabular bedded. Intercalated mudstone and siltstone beds are reddish brown to greenish gray. The Salt Wash Member rests with distinct unconformity on either the Acoma Tongue of the Zuni Sandstone, the Recapture Member or the main body of the Bluff Formation. The absence of the Acoma Tongue and/or the Recapture Member at some sections is *prima facie* evidence of the unconformity, as is the scour-and-fill and substantial change in grain size and lithotypes at the base of the Salt Wash Member (e.g., Anderson and Lucas, 1994, 1997).

The Salt Wash Member grades upward into (and interfingers with) the mudstone-dominated Brushy Basin Member, which is as much as 107 m thick in west-central New Mexico (Fig. 10). Brushy Basin lithologies are mostly mudstone and claystone with intercalated minor beds of sandstone. These mudrock beds are variegated green-reddish brown and grayish purple and are characteristically bentonitic. The sandstone beds are brown and yellowish gray and are fine to medium grained, locally conglomeratic and generally feldspathic. They are either cross-bedded or laminar bedded.

The overlying Jackpile Member (Fig. 10) is as much as 91 m of mostly white, kaolinitic, fine- to medium-grained, cross-bedded sandstone and silica-pebble conglomerate. Minor interbeds of pale green mudstone and siltstone are present. The Cretaceous Dakota Formation rests with evident uncon-

formity on the Jackpile Member across much of west-central New Mexico

CHRONOSTRATIGRAPHY

Most of the data to determine the ages of Jurassic lithostratigraphic units in west-central New Mexico comes from outside of New Mexico, particularly 1) regional stratigraphic correlations of some units to marine units deposited in Idaho and northern Utah, 2) radioisotopic ages from Jurassic strata in Utah and Colorado and 3) available biostratigraphy of these units, also mostly from fossils found in Utah, Colorado and Wyoming (Fig. 11). To summarize briefly:

1. The age of at least the lower part of the Entrada Sandstone is Bathonian-early Callovian based on its stratigraphic relationship to the Carmel Formation, which has yield radioisotopic ages of ~166-167 Ma and contains marine invertebrate fossils (Imlay, 1980).

2. The Todilto Formation is homotaxial with the marine Curtis Formation of Utah. Wilcox (2007) and Wilcox and Currie (2008) recently presented new biostratigraphic data that indicate the lower part of the Curtis Formation is of Oxfordian age. So, this is the age of the Todilto Formation, which had yielded only a temporally long-ranging fish taxon and other endemic taxa that provided no precise biostratigraphic constraints on its age.

3. The Summerville Formation has yielded radioisotopic ages from its upper, Tidwell Member in Utah that indicate it is of Oxfordian age (Trujillo and Kowallis, 2015).

4. The Bluff Formation is bracketed by Late Jurassic units that indicate it is early Late Jurassic in age. However, it has not yielded data by which to determine its age directly.

5. The Salt Wash and Brushy Basin members of the Morrison Formation yield dinosaur and other fossils generally considered to be of Late Jurassic age (e.g., Lucas, 2009). Radioisotopic ages from the Morrison Formation in Utah and Colorado (upper Salt Wash Member, Brushy Basin Member) indicate an age span of about 152-149 Ma and thus indicate a primarily Tithonian age (Trujillo and Kowallis, 2015; Galli et al., 2018; Maidment and Muxworthy, 2019).

6. The possibility that the Jackpile Member of the Morrison Formation is a Lower Cretaceous unit equivalent to the "Burro Canyon" (=Cedar Mountain) Formation to the north merits further investigation (cf. Aubrey, 1986). Indeed, detrital zircon data support that correlation (Dickinson and Gehrels, 2010; Dickinson, 2018) but are not the most robust data for age determinations. Here, the Jackpile Member remains tentatively of Late Jurassic age.

REGIONAL UNCONFORMITIES

Pipiringos and O'Sullivan (1978) proposed a succession of Jurassic unconformities that delimit sequences throughout part or all of the Jurassic Western Interior basin. Four of these

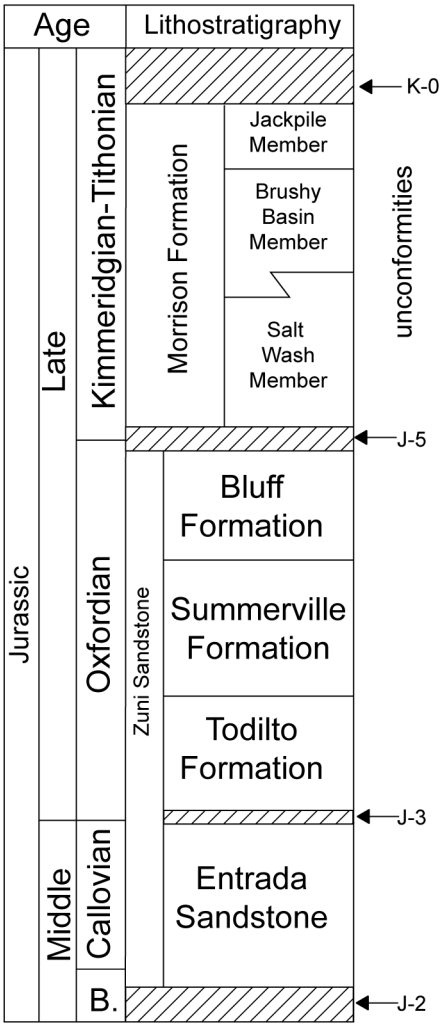

FIGURE 11. Jurassic sequence stratigraphy in west-central New Mexico. B. = Bathonian.

regional unconformities can be identified in west-central New Mexico's Jurassic section (Fig. 11).

The J-2 unconformity separates Middle Jurassic strata of the Entrada Sandstone from underlying Upper Triassic strata of the Wingate Sandstone and Chinle Group. This striking unconformity was unambiguously identified across all of the Jurassic outcrop belt in west-central New Mexico by Pipiringos and O'Sullivan (1978). Because the Middle Jurassic Entrada Sandstone rests on Triassic strata, the J-2 unconformity is actually a compound unconformity that includes the J-1 unconformity of Pipiringos and O'Sullivan (1978).

The J-3 unconformity of Pipiringos and O'Sullivan (1978) is the basal transgressive unconformity that separates the Entrada Sandstone from the overlying Curtis Formation (also see Wilcox and Currie, 2008). I correlate the Curtis with the Todilto, which suggests that the Todilto base is the J-3 unconformity. Indeed, local stratigraphic relief, rip-up clasts and floating pebbles, as well as sharp lithologic contrast—kerogenic limestone on eolianite sandstone—suggest the base of the Todilto Formation is an unconformity. Thus, there are good reasons to equate the Todilto base to the J-3 unconformity at the base

of the Curtis (Lucas and Anderson, 1996, 1997). Identification of catastrophic flooding at the onset of Todilto deposition (Ahmed Benan and Kocurek, 2000) is consistent with equating the Todilto base to the J-3 surface.

The J-4 unconformity is not evident in west-central New Mexico. The base of the Morrison Formation was identified by Pipiringos and O'Sullivan (1978) as the J-5 unconformity. I recognize this unconformity at the base of the Salt Wash Member of the Morrison Formation across west-central New Mexico, but note that USGS workers have long placed that unconformity stratigraphically lower, in the Bluff or Summerville intervals (e.g., Condon and Peterson, 1986). The J-5 unconformity is a tectonosequence boundary that represents a significant tectonic reorganization of Jurassic depositional systems in the Western Interior. This is the change from the depositional basin of the San Rafael Group, which had a paleoslope down to the northwest, to the depositional basin of the Morrison Formation, which had a paleoslope down to the east (Anderson and Lucas, 1997; Lucas and Anderson, 1997).

The K-0 unconformity of Pipiringos and O'Sullivan (1978) separates Cretaceous strata (Burro Canyon and Dakota formations, possibly the Jackpile Member of the Morrison Formation) from underlying Jurassic strata across west-central New Mexico. In west-central New Mexico, either the Encinal Canyon Member (Albian?) or Oak Canyon Member (Cenomanian) of the Dakota Formation rest with profound unconformity on the Morrison Formation.

ACKNOWLEDGMENTS

I owe a heavy debt to Orin Anderson, Andrew Heckert and Adrian Hunt for their collaboration in the field on Jurassic lithostratigraphy and related issues. John Foster and Adrian Hunt and the editors provided helpful reviews of the manuscript.

REFERENCES

Ahmed Benan, C.A., and Kocurek, G., 2000, Catastrophic flooding of an aeolian dune field: Jurassic Entrada and Todilto formations, Ghost Ranch, New Mexico, USA: Sedimentology, v. 47, p. 1069-1080.

Anderson, O.J., 1983, Preliminary report on redefinition of Zuni Sandstone, west-central New Mexico: New Mexico Geology, v. 5, p. 56-59.

Anderson, O.J., 1993, Zuni Sandstone and Acoma Tongue defined: New Mexico Geology, v. 15, p. 38-39.

Anderson, O.J., and Lucas, S.G., 1992, The Middle Jurassic Summerville Formation, northern New Mexico: New Mexico Geology, v. 14, p. 79-92.

Anderson, O.J., and Lucas, S.G., 1994, Middle Jurassic stratigraphy, sedimentation and paleogeography in the southern Colorado Plateau and southern High Plains, *in* Caputo, M.V., Peterson, J.A., and Franczyk, K.J., eds., Mesozoic systems of the Rocky Mountain region, USA: Denver, RMS-SEPM, p. 299-314.

Anderson, O.J., and Lucas, S.G., 1995, Base of the Morrison Formation, Jurassic, of northwestern New Mexico and adjacent areas: New Mexico Geology, v. 17, p. 44-53.

Anderson, O.J., and Lucas, S.G., 1996, Stratigraphy and depositional environments of Middle and Upper Jurassic rocks, southeastern San Juan Basin, New Mexico: New Mexico Geological Society, Guidebook 47, p. 205-210.

Anderson, O.J., and Lucas, S.G., 1997, The Upper Jurassic Morrison Formation in the Four Corners region: New Mexico Geological Society, Guidebook 48, p. 139-155.

Anderson, O.J., and Lucas, S.G., 1998, Redefinition of Morrison Formation (Upper Jurassic) and related San Rafael Group strata, southwestern U.S.: Modern Geology, v. 22, p. 39-69.

Anderson, R.Y., and Kirkland, D.W., 1960, Origin, varves and cycles of Jurassic Todilto Formation: American Association of Petroleum Geologists Bulletin, v. 44, p. 37-52.

Armstrong, A.K., 1995, Facies, diagenesis and mineralogy of the Jurassic Todilto Limestone Member, Grants Uranium district, New Mexico: New Mexico Bureau of Mines and Mineral Resources, Bulletin 153, 41 p.

Aubrey, W.M., 1986, The nature of the Dakota-Morrison boundary, southeastern San Juan Basin: AAPG Studies in Geology, no. 22, p. 93-104.

Baker, A.A., Dane, C.H., and Reeside, J.B., Jr., 1936, Correlation of Jurassic formations of parts of Utah, Arizona, New Mexico, and Colorado: U.S. Geological Survey, Professional Paper 183, 66 p.

Baker, A.A., Dane, C.H., and Reeside, J.B., Jr., 1947, Revised correlation of Jurassic formations of parts of Utah, Arizona, New Mexico, and Colorado: American Association of Petroleum Geologists Bulletin, v. 31, p. 1664-1668.

Burbank, W.S., 1930, Revision of geologic structure and stratigraphy in the Ouray district of Colorado and its bearing on ore deposition: Colorado Scientific Society Proceedings, v. 12, no. 6, 231 p.

Cather, S.M., Zeigler, K.A., Mack, G.H., and Kelley, S.A., 2013, Toward standardization of Phanerozoic stratigraphic nomenclature in New Mexico: Rocky Mountain Geology, v. 48, p. 101-124.

Condon, S.M., 1989, Modifications to Middle and Upper Jurassic nomenclature in the southeastern San Juan Basin, New Mexico: New Mexico Geological Society, Guidebook 40, p. 231-238.

Condon, S.M., and Huffman, A.C., Jr., 1985, Revision in nomenclature of the Middle Jurassic Wanakah Formation, northwestern New Mexico and northeastern Arizona: U.S. Geological Survey, Bulletin 1633-A, 12 p.

Condon, S.M., and Peterson, F., 1986, Stratigraphy of Middle and Upper Jurassic rocks of the San Juan Basin: Historical perspective, current ideas, and remaining problems: AAPG Studies in Geology, no. 22, p. 7-26.

Cooley, M.E., Harshbarger, J.W., Akers, J.P., and Hardt, W.F., 1969, Regional hydrogeology of the Navajo and Hopi Indian Reservations, Arizona, New Mexico, and Utah: U.S. Geological Survey, Professional Paper 521-A, 61 p.

Dane, C.H., and Bachman, G.O., 1965, Geologic map of New Mexico: Washington, D.C., U.S. Geological Survey, scale 1:500,000.

Darton, N.H., 1928a, "Red beds" and associated formations in New Mexico, with an outline of the geology of the state: U.S. Geological Survey, Bulletin 794, 356 p.

Darton, N.H., 1928b, Geologic map of New Mexico: Washington, D.C., U.S. Geological Survey, scale 1:500,000.

Dickinson, W.R., and Gehrels, G.E., 2010, Implications of U-Pb ages of detrital zircons in Mesozoic strata of the Four Corners region for provenance relations in space and time: New Mexico Geological Society, Guidebook 61, p. 135–146.

Dickinson, W.R., 2018, Tectonosedimentary relations of Pennsylvanian to Jurassic strata on the Colorado Plateau: Geological Society of America, Special Publication 533, 184 p.

Dobrovolny, E., Summerson, C.H., and Bates, R.L., 1946, Geology of northwestern Quay County, New Mexico: U.S. Geological Survey Oil and Gas Investigations Preliminary Map 62.

Dutton, C.E., 1885, Mount Taylor and the Zuni Plateau: U.S. Geological Survey, 6th Annual Report, p. 105-198.

Galli, K.G., Buchwaldt, R., Lucas S.G., and Tanner, L., 2018, New chemical abrasion thermal ionization mass spectrometry dates from the Brushy Basin Member, Morrison Formation, western Colorado: Implications for dinosaur evolution: Journal of Geology, v. 126, p. 473-486.

Gilluly, J., and Reeside, J.B., Jr., 1928, Sedimentary rocks of the San Rafael Swell and some adjacent areas in eastern Utah: U.S. Geological Survey, Professional Paper 150, p. 61-84.

Green, M.W., 1974, The Iyanbito Member (a new stratigraphic unit) of the Jurassic Entrada Sandstone, Gallup-Grants area, New Mexico: U.S. Geological Survey Bulletin 1395-D, p. D1-D12.

Gregory, H.E., 1917, Geology of the Navajo Country: U.S. Geological Survey, Professional Paper 93, 161 p.

Gregory, H.E., 1938, The San Juan Country: U.S. Geological Survey, Professional Paper 188, 123 p.

Harshbarger, J.W., Repenning, C.A., and Irwin, J.H., 1957, Stratigraphy of the

uppermost Triassic and Jurassic rocks of the Navajo country: U.S. Geological Survey, Professional Paper 291, 74 p.
Heaton, R.L., 1939, Contribution to Jurassic stratigraphy of Rocky Mountain region: American Association of Petroleum Geologists Bulletin, v. 23, p. 1153-1177.
Heckert, A.B., and Lucas, S.G., 1998, The "type" Wingate Sandstone (Upper Triassic-Lower Jurassic) and the homotaxial Entrada Sandstone (Middle Jurassic): Resolving stratigraphic problems on the southern Colorado Plateau: New Mexico Geology, v. 20, p. 54.
Imlay, R.W., 1980, Jurassic paleobiogeography of the conterminous United States in its continental setting: U.S. Geological Survey, Professional Paper 1232, 44 p.
Kirkland, D.W., Denison, R.E., and Evans, R., 1995, Middle Jurassic Todilto Formation of northern New Mexico and southwestern Colorado: marine or nonmarine?: New Mexico Bureau of Mines and Mineral Resources, Bulletin 147, 37 p.
Lucas, S.G., 2001, The first geologic map of New Mexico: New Mexico Geology, v. 23, p. 84-88.
Lucas, S.G., 2003, Clarence Dutton's stratigraphy of west-central New Mexico: New Mexico Geological Society, Guidebook 54, p. 209-218.
Lucas, S.G., 2004, The Triassic and Jurassic systems in New Mexico, *in* Mack, G.H. and Giles, K.A., eds., The Geology of New Mexico: A Geologic History: New Mexico Geological Society Special Publication 11, p. 137-152.
Lucas, S.G., 2009, Global Jurassic tetrapod biochronology: Volumina Jurassica, v. 6, p. 99-108.
Lucas, S.G., 2014, Lithostratigraphy of the Jurassic San Rafael Group from Bluff to the Abajo Mountains, southeastern Utah: Stratigraphic relationships of the Bluff Sandstone: Volumina Jurassica, v. 12, p. 55-68.
Lucas, S.G., 2018, The Upper Jurassic Morrison Formation in north-central New Mexico—linking Colorado Plateau stratigraphy to the stratigraphy of the High Plains: Geology of the Intermountain West, v. 5, p. 117-129.
Lucas, S.G., and Anderson, O.J., 1996, The Middle Jurassic Todilto salina basin, American Southwest: Museum of Northern Arizona, Bulletin 60, p. 479-482.
Lucas, S.G., and Anderson, O.J., 1997, The Jurassic San Rafael Group, Four Corners region: New Mexico Geological Society, Guidebook 48, p. 115-132.
Lucas, S.G., and Anderson, O.J., 1998, Jurassic stratigraphy and correlation in New Mexico: New Mexico Geology, v. 20, p. 97-104.
Lucas, S.G., and Heckert, A.B., 2003, Jurassic stratigraphy in west-central; New Mexico: New Mexico Geological Society, Guidebook 54, p. 289-301.
Lucas, S.G., and Woodward, L.A., 2001, Jurassic strata in east-central New Mexico and their regional significance: New Mexico Geological Society, Guidebook 52, p. 203-212.
Lucas, S.G., Anderson, O.J., and Pigman, C., 1995, Jurassic stratigraphy in the Hagan basin, north-central New Mexico: New Mexico Geological Society, Guidebook 46, p. 247-255.
Lucas, S.G., Estep, J.W., and Anderson, O.J., 1999, Correlation of Jurassic strata from the Colorado Plateau to the High Plains, across the Rio Grande rift, north-central New Mexico: New Mexico Geological Society, Guidebook 50, p. 317-326.
Lucas, S.G., Heckert, A.B., and Anderson, O.J., 2001, The Middle Jurassic Entrada Sandstone near Gallup, New Mexico: Discussion: The Mountain Geologist, v. 38, p. 225-227.
Lucas, S.G., Kietzke, K.K., and Hunt, A.P., 1985, The Jurassic System in east-central New Mexico: New Mexico Geological Society, Guidebook 36, p. 213-243.
Lucas, S.G., Krainer, K., and Berglof, W.A., 2014, Folding in the Middle Jurassic Todilto Formation, New Mexico-Colorado, USA: Volumina Jurassica, v. 12, p. 39-54.
Lupton, C.T., 1914, Oil and gas near Green River, Grand County, Utah: U.S. Geological Survey, Bulletin 541, p. 115-133.
Maidment, S.C.R., and Muxworthy, A., 2019, A chronostratigraphic framework for the Upper Jurassic Morrison Formation, western U.S.A.: Journal of Sedimentary Research, v. 89, p. 1017-1083.
Marcou, J., 1858, Geology of North America, with two reports on the prairies of Arkansas and Texas, the Rocky Mountains of New Mexico, and the Sierra Nevada of California, originally made for the United States government: Zurich, Zürcher and Furrer, 144 p.
McKee, E.D., Oriel, S.S., Swanson, V.E., MacLachlan, M.E., MacLachlan, J.C., Ketner, K.B., Goldsmith, J.W., Bell, R.V., Jameson, D.J., and Imlay, R.W., 1956, Paleotectonic maps of the Jurassic System: U.S. Geological Survey, Miscellaneous Investigations Map I-175, scale 1:5,000,000.
NMBGMR (New Mexico Bureau of Geology and Mineral Resources), 2003, Geological map of New Mexico. Socorro, scale 1:500,000.
O'Sullivan, R.B., 2003, The Middle Jurassic Entrada Sandstone in northeastern Arizona and adjacent areas: New Mexico Geological Society, Guidebook 54, p. 303-308.
Owen, D.E., Walters, L.J., Jr. and Beck, R.G., 1984, The Jackpile Sandstone Member of the Morrison Formation in west-central New Mexico—a formal definition: New Mexico Geology, v. 6, p. 45-52.
Pipiringos, G.N. and O'Sullivan, R.B., 1978, Principal unconformities in Triassic and Jurassic rocks, Western Interior, U.S.: A preliminary survey: U.S. Geological Survey, Professional Paper 1035-A, 29 p.
Robertson, J.F. and O'Sullivan, R.B., 2001, The Middle Jurassic Entrada Sandstone near Gallup, New Mexico: The Mountain Geologist, v. 38, p. 53-69.
Silver, C., 1948, Jurassic overlap in western New Mexico: American Association of Petroleum Geologists Bulletin, v. 32, p. 68-81.
Trujillo, K.C., and Kowallis, B., 2015, Recalibrated legacy $^{40}Ar/^{39}Ar$ ages for the Upper Jurassic Morrison Formation, Western Interior, U.S.A.: Geology of the Intermountain West, v. 2, p. 1-8.
Wilcox, W.T., 2007, Sequence stratigraphy of the Jurassic Curtis, Summerville, and Stump formations, Utah and northwest Colorado [M.S. thesis]: Oxford, Miami University, 108 p.
Wilcox, W.T., and Currie, B.S., 2008, Sequence stratigraphy of the Jurassic Curtis, Summerville, and Stump formations, eastern Utah and northwest Colorado: Rocky Mountain Association of Geologists and Utah Geological Association, Publication 37, p. 9-41.
Wright, J.C., Shawe, D.R., and Lohman, S.W., 1962, Definition of members of Jurassic Entrada Sandstone in east-central Utah and west-central Colorado: American Association of Petroleum Geologists Bulletin, v. 46, p. 2057-2070.

New Mexico Geological Society, Special Publication 14, Geology of the Mount Taylor Area, 2020, p. 145-151.

JURASSIC STRATIGRAPHIC NOMENCLATURE FOR NORTHWESTERN NEW MEXICO

Steven M. Cather

New Mexico Bureau of Geology and Mineral Resources, New Mexico Tech, 801 Leroy Place, Socorro, NM 87801;
steven.cather@nmt.edu

Abstract—Nomenclatural debates concerning Jurassic strata of northwestern New Mexico are long-standing and contentious. I present arguments here that support the following: (1) The term Wanakah Formation has little utility in New Mexico, where its two constituent members are typically mapped as formations. The lower of these two formations is the Todilto Formation. The upper should be termed the Beclabito Formation, as these strata cannot be confidently correlated to the type Summerville Formation of central Utah. (2) The Bluff Sandstone should be a broadly inclusive unit that encompasses all prominent eolianites above the Beclabito and its equivalents, and should be regarded as a formation within the eolianite-bearing San Rafael Group. (3) The Recapture Member should remain part of the Morrison Formation because, despite containing eolianites and sabkha deposits, much of the unit is fluvial. The contact between eolianites and fluvial strata within it is commonly not well enough exposed to be mapped reproducibly. (4) The Westwater Canyon Member of the Morrison Formation is a valid term and should not be renamed the Salt Wash Member. (5) The Jackpile Sandstone Member should be removed from the Morrison Formation and instead should be mapped as the Lower Cretaceous Jackpile Sandstone or as Burro Canyon Formation.

In general, lithologic identity (depositional environment) provides the best basis for nomenclature. Lateral correlation and stratigraphic subdivision using unconformities in the Jurassic section have proven problematic, because many such unconformities are not regional in scope and are likely diachronous.

INTRODUCTION

The evolution of stratigraphic nomenclature for Jurassic beds in northwestern New Mexico has been problematic. Perhaps no other region of the state has generated more nomenclatural debates. Differences in nomenclature have arisen not only from arguments based on priority or the preoccupation of stratigraphic terms, but also from ambiguities in the physical correlation of strata and the significance of unconformities in the Colorado Plateau region. For example, Dickinson (2018) regarded most of the regionally recognized, intra-Jurassic unconformities to represent nothing more than diachronous, time-transgressive surfaces between prograding or laterally migrating depositional systems. As such, he questioned the utility of sequence-stratigraphic models that are based on the concept of synchronous, regional unconformities. The scarcity of paleontologic and radioisotopic age constraints for Jurassic strata has also contributed to correlation uncertainties.

Here, I modify and expand upon a discussion of stratigraphic nomenclature for the Jurassic San Rafael Group and Morrison Formation presented in an earlier paper by Cather et al. (2013), which outlines the current policy for Phanerozoic stratigraphic nomenclature in geologic maps produced by the New Mexico Bureau of Geology and Mineral Resources. The present paper is intended only as a synopsis. For additional discussion, see Condon and Peterson (1986), Condon (1989, 1993), Peterson (1994), Lucas and Anderson (1993, 1997), Anderson and Lucas (1997), Lucas and Heckert (2003), O'Sullivan (2003, 2010a, b), Lucas (2004), Turner and Peterson (2004, 2010), and Dickinson (2018).

ENTRADA SANDSTONE

The basal unit of the Jurassic section in most of northwestern New Mexico was originally termed the Wingate Sandstone by Dutton (1885). These same strata were subsequently renamed the Entrada Sandstone by Gilluly and Reeside (1928). The term Wingate was eventually applied to a stratigraphically lower, Upper Triassic–Lower Jurassic eolianite (see summary in Lucas and Heckert, 2003) present in extreme northwestern New Mexico (Craigg, 2001; Dickinson, 2018).

The Entrada Sandstone *sensu* Gilluly and Reeside unconformably overlies Upper Triassic strata throughout most of northwestern New Mexico. Largely eolian, the Entrada is equivalent to the Exeter Sandstone (Lee, 1902) of northeastern New Mexico. The Entrada is Middle Jurassic and has been variously divided into two or three members (e.g., Lucas and Heckert, 2003; O'Sullivan, 2003; Dickinson, 2018). No consensus has yet emerged concerning the member-rank nomenclature for the Entrada Sandstone.

TODILTO FORMATION VS. TODILTO LIMESTONE MEMBER OF WANAKAH FORMATION

The Entrada Sandstone is overlain by Jurassic water-laid deposits in the San Juan Basin area. These deposits are termed the Todilto and Summerville formations by some workers and the Wanakah Formation by others. Near the Zuni Uplift these water-laid deposits pinch out. The stacked equivalents of the Entrada and Bluff eolianites south of the pinch out have been termed the Zuni Sandstone by Lucas and Heckert (2003). Although the term Zuni Sandstone has been redefined several

times since first introduced by Dutton in 1885, I find the Lucas and Heckert (2003) concept of the term to be useful where the Entrada and Bluff eolianites are not divisible by the presence of the "Todilto notch," which represents an unconformity corresponding to the Todilto/Wanakah pinch out.

The Todilto Formation (Gregory, 1917) is a mappable unit of limestone and gypsum throughout much of northwestern New Mexico and, thus, has long been considered a formation by most geologists in the state. The U.S. Geological Survey (USGS), however, regards the unit as the Todilto Limestone Member of the lower Wanakah Formation. The term Wanakah was first applied to Devonian strata in New York, but was subsequently applied to Middle Jurassic strata the Four Corners area as well (Burbank, 1930; see summaries in Condon, 1993, and O'Sullivan, 2010a). Despite this oft-mentioned duplication of names, there has been long usage of the term Wanakah in the Four Corners region by both the USGS and the Colorado Geological Survey that continues to the present day.

Lucas and Anderson (1993, p. 66) stated that duplication of stratigraphic names, such as Wanakah, "...is a recipe for nomenclatural chaos." There is, in fact, little potential for confusion between the two Wanakah units due to their wide geographic separation and differing ages. I know of no examples, either in print or in conversation, of nomenclatural misunderstanding of the two units. Given the common usage of the term Wanakah Formation in the Four Corners region since 1930, it seems unlikely that further objections to the term based on homonymy will result in its abandonment.

The term Wanakah Formation, however, has not been widely used as a map unit in New Mexico, largely because its constituent members are there mostly regarded as formations, and the utility of a "Wanakah Group" has not been demonstrated. I recommend mapping the Todilto as a formation in northwestern New Mexico, except possibly in the Defiance Uplift region, where it is thin (~1–3 m) and its inclusion as the lower member of the Wanakah Formation is justifiable.

SUMMERVILLE FORMATION VS. BECLABITO MEMBER OF THE WANAKAH FORMATION

The term Summerville Formation was coined for a marginal marine, thin-bedded, dominantly siltstone succession that overlies the marine Curtis Formation in the San Rafael Swell region of south-central Utah (Gilluly and Reeside, 1928). The Summerville consists of tidal flat, supratidal, and sabkha deposits (Wilcox, 2007; Zuchuat et al., 2019). The term Summerville was subsequently exported some 500 km to the southeast to New Mexico (Rapaport et al., 1952), where it was applied to salina-margin and sabkha sandstones and mudstones above the salina deposits of Todilto Formation. The importation of the term Summerville to New Mexico is based partly on the now-disputed correlation of the underlying, physically disjunct Todilto and Curtis Formations (they are divided laterally by the Moab Tongue of the Entrada Sandstone).

Lucas and Heckert (2003, p. 295) stated, "The Todilto Formation in west-central New Mexico occupies the same stratigraphic position as the Curtis Formation in east-central Utah (between the Entrada and Summerville formations). Both units are of Callovian age, but current biostratigraphic data are insufficient to document a precise correlation." They further asserted (p. 295), "The Summerville Formation in west-central New Mexico is *physically continuous* with the Summerville Formation in the type area of southeastern Utah."

In contrast, O'Sullivan (1980) stated, "Work in the area northwest of Moab shows that all of the Summerville is beveled out eastward by an unconformity at the base of the Morrison Formation and is absent in the Moab area." Members of the USGS (e.g., Pipiringos and O'Sullivan, 1978; Condon, 1989; Peterson, 1994; O'Sullivan, 2010a) regard the New Mexico strata as older than, and not laterally continuous with, the Summerville Formation of Utah. They applied the term Beclabito Member of the Wanakah Formation to the New Mexico beds.

Dickinson (2018) preferred use of the term Summerville Formation in New Mexico. He interpreted these strata to be laterally continuous with and "homotaxially equivalent" (i.e., lithologically similar but not necessarily the same age; Dickinson, 2018, p. 11 and 110) to the beds in Utah.

The Entrada Sandstone, Todilto Formation, and Summerville/Beclabito comprise an essentially conformable succession in the San Juan Basin area. None of these units have been directly dated in New Mexico. The Todilto Formation contains the fossil fishes *Hulettia americana* and *Caturus dartoni* that, although not themselves age-diagnostic, are also present in the Bathonian Stockade Beaver Shale Member and Canyon Springs Sandstone Member of the Sundance Formation of South Dakota–Wyoming (Fig. 1; Lucas et al., 1985; Lucas and Anderson, 1997). These fish fossils, together with regional inferences about the age of the underlying Entrada Sandstone, have led to tentative age assignments for the Todilto that range from early to middle Callovian (Schultze and Enciso, 1983; Schaeffer and Patterson, 1984; Lucas et al., 1985; Kirkland et al., 1995; Lucas and Anderson, 1997; Lucas, 2014).

Recent paleontologic dating of the Curtis Formation in Utah, however, indicates it is younger than the widely interpreted Callovian age of the Todilto Formation. Dinoflagellate cysts (*Wanea fimbriata*, *Stephanelytron redcliffense*) and the ammonite *Quenstedtoceras* (*Pavloviceras*), recovered from the lower Curtis Formation in the San Rafael Swell–Uinta Uplift area of Utah, indicate it is lower to middle Oxfordian (Fig. 1; Wilcox and Currie, 2006; Wilcox, 2007). The Summerville Formation of Utah must be Oxfordian as well, based on the presence of ~156.8 Ma ashes (lower Kimmeridgian) in the overlying Morrison Formation (Fig. 1). The age of the Curtis in Utah had previously been inferred to be late middle Callovian, based on lithologic similarities with the Pine Butte Member of the Sundance Formation (Imlay, 1980).

If correlation of the Curtis Formation of Utah with the Todilto Formation of New Mexico is viable, then the New Mexico strata must be significantly younger (Oxfordian) than previously thought. This requires that the Todilto/Sundance fishes ranged in age at least from the Bathonian to the Oxfordian and that the entire Todilto through Bluff succession in New Mexico was deposited in less than about 6 my (see age constraints in Fig. 1).

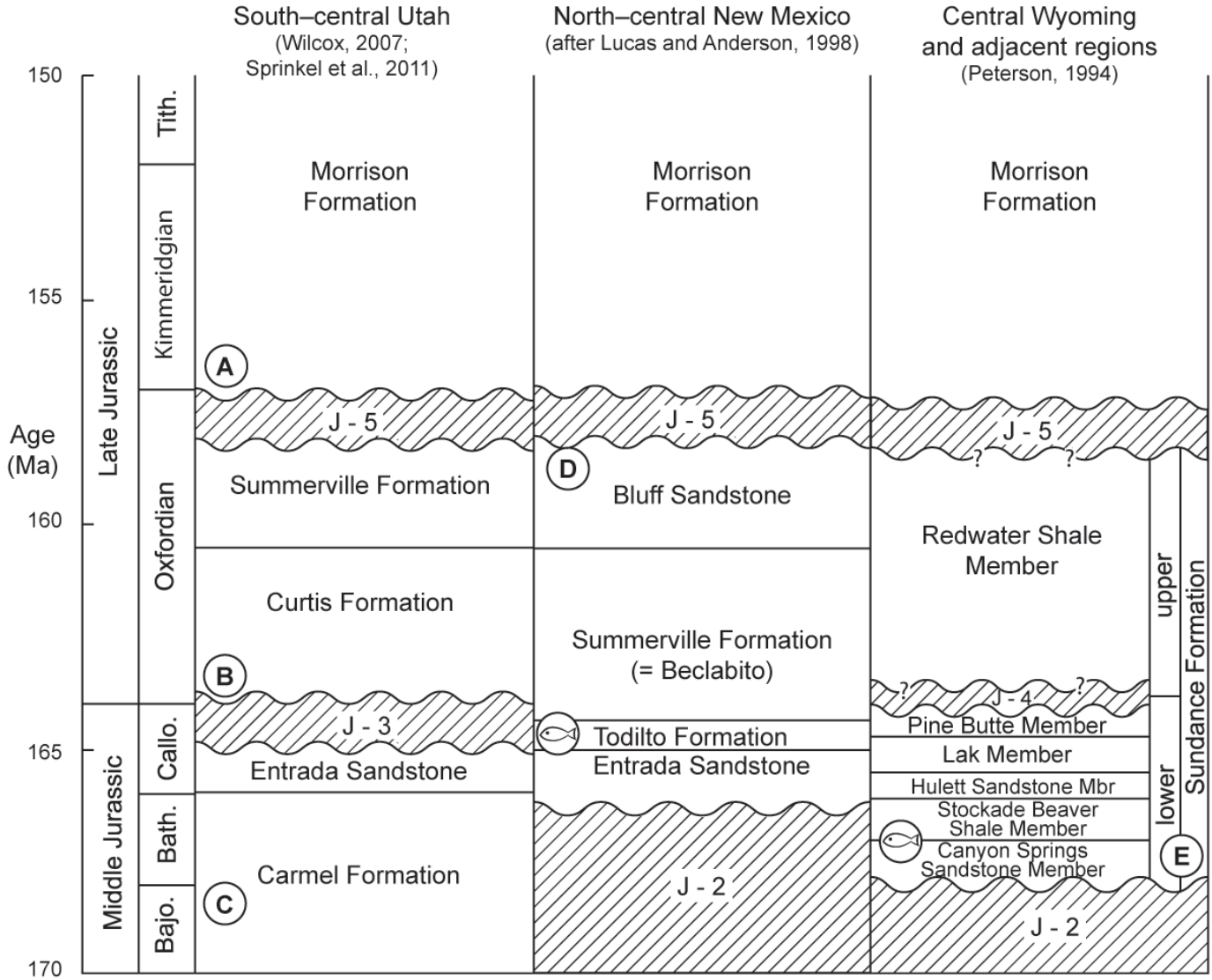

FIGURE 1. Chronostratigraphic correlation chart showing age constraints (circled letters), unconformities (hachured), and inferred temporal relationships between Middle to Upper Jurassic units in south-central Utah (San Rafael Swell region), north-central New Mexico, and the central Wyoming region. Modified from Cather et al. (2013). Note that Dickinson (2018) interpreted the depicted unconformities as diachronous, time-transgressive surfaces between prograding or laterally migrating depositional systems. Age constraints are: **A**– 156.84±0.59 Ma (northeastern Utah) and 156.77±0.55 (southeastern Utah) $^{40}Ar/^{39}Ar$ ash ages in basal Morrison Formation (Tidwell Member; Trujillo and Kowallis, 2015); **B**– early Oxfordian age of lower Curtis Formation based on dinoflagellate cysts (*Wanea fimbriata*, *Stephanelytron redcliffense*) and the ammonite *Quenstedtoceras* (Pavloviceras) (Wilcox and Currie, 2006; Wilcox, 2007); **C**– ash ages as young as 168.25±0.64 Ma in upper Carmel Formation (modified from Kowallis et al., 2001, using the 28.201 Ma standard for Fish Canyon sanidine of Kuiper et al., 2008 (B.J. Kowallis, written commun., 2013)); **D**– ca. 158 Ma maximum depositional age from detrital zircon analysis of Bluff Sandstone (Dickinson and Gehrels, 2009); **E**– biostratigraphic control of Bathonian ages of marine beds in Sundance Formation (Imlay, 1980). Fish symbols are non-age-diagnostic fossil fishes *Hulettia americana* and *Caturus dartoni*, which occur in both the Todilto Formation and the lower Sundance Formation. Timescale is GSA 2012 (Walker et al., 2012). Bajo. – Bajocian, Bath. – Bathonian, Callo. – Callovian, Tith. – Tithonian.

Alternatively, the Curtis Formation of central Utah may be younger than the Todilto. If so, this presents problems for models (e.g., Lucas et al., 1985; Kirkland et al., 1995; Lucas and Anderson, 1997) that interpret Todilto deposition to have occurred *during* the Oxfordian Curtis maximum transgression, rather than before it. If the Curtis/Summerville contact of central Utah is indeed younger than the Todilto/Summerville contact of New Mexico, it would lend support to the age interpretations by stratigraphers of the USGS, who use the term Beclabito Member of the Wanakah Formation in lieu of the Summerville Formation.

Although the term Summerville Formation has been used in recent quadrangle mapping in New Mexico (e.g., Cather et al., 2002; Kelley et al., 2005; Cather, 2011), I suggest the term Beclabito, here raised to formation rank, is the preferable term for these beds. If the Todilto and the Curtis formations are not correlative (a distinct possibility), then use of the term Summerville in New Mexico is questionable. From a genetic perspective, it seems inadvisable to apply the name Summerville both to a siltstone-dominated, marginal marine succession in Utah and a sandier, marginal salina succession in New Mexico. If future research shows the Beclabito Formation is indeed equiv-

alent to the Summerville Formation of Utah, the correlation can simply be noted. But if the two units are not correlative, much confusion will be avoided if the term Summerville does not become further entrenched in New Mexico geologic maps and reports. It is always easier to correlate units retroactively than it is to uncorrelate them, especially when erroneous terms appear on geologic maps that typically have a decades-long shelf life. It thus seems prudent to employ the local stratigraphic term Beclabito Formation rather than to rely on the disputable regional correlation to the Summerville Formation.

MORRISON FORMATION
Bluff Sandstone and Recapture Members

The Morrison Formation in northwestern New Mexico has traditionally been divided into the Bluff Sandstone, Recapture, Westwater Canyon, and Brushy Basin Members (Gregory, 1938). Some workers (Rapaport et al., 1952; Craig et al., 1955; Anderson and Lucas, 1995 and 1997; Dickinson, 2018), however, have argued that the eolian Bluff Sandstone Member should be removed from the base of the Morrison and become a formation within the underlying, mostly eolianite San Rafael Group.

Removal of the Bluff Sandstone Member from the Morrison has not been accepted by some workers (e.g., Turner and Peterson, 2004; Hintze and Kowallis, 2009; O'Sullivan, 2010b; Kirkland et al., in press). The ongoing controversy about the affinity of the Bluff Sandstone, however, need not be a major issue for mappers. As long as it is mapped separately and contact relationships are adequately defined (placement of contacts varies significantly among workers; see summaries in Anderson and Lucas (1995, 1997) and O'Sullivan (2010b)), the Bluff Sandstone can be assigned to either the Morrison Formation or the San Rafael Group at a later date when consensus is achieved. For now, I tentatively consider the eolian Bluff Sandstone (=Junction Creek Sandstone in Colorado) as the upper formation in the mostly eolian San Rafael Group. An added benefit of considering the Bluff Sandstone a formation (rather than a member of the Morrison Formation) is that it allows the Bluff to be divided into members, should the need arise.

The eolianites above the Beclabito have been divided into various units: the Bluff Sandstone (*sensu* O'Sullivan, 2010b), the Cow Springs Sandstone, the Horse Mesa Member of Wanakah Formation, and the Sandstone at Mesita (Harshbarger et al., 1957; Condon and Peterson, 1986; Condon, 1989). I follow Lucas and Heckert (2003) and Dickinson (2018) in thinking these units should be subsumed within a broadly defined Bluff Sandstone (Fig. 2; see below). I agree with Dickinson (2018) that the various terms applied to the Bluff Sandstone (as here broadly defined) are based on expectable lithologic variations within an erg system, and that such variations should not be the basis for formal lithostratigraphy. Such lithologic variations are best accommodated *within* a formation, as members or sedimentary lithofacies.

Anderson and Lucas (1995, 1997) argued that sabkha and eolian deposits in the basal 12–17 m of Gregory's (1938) Re-

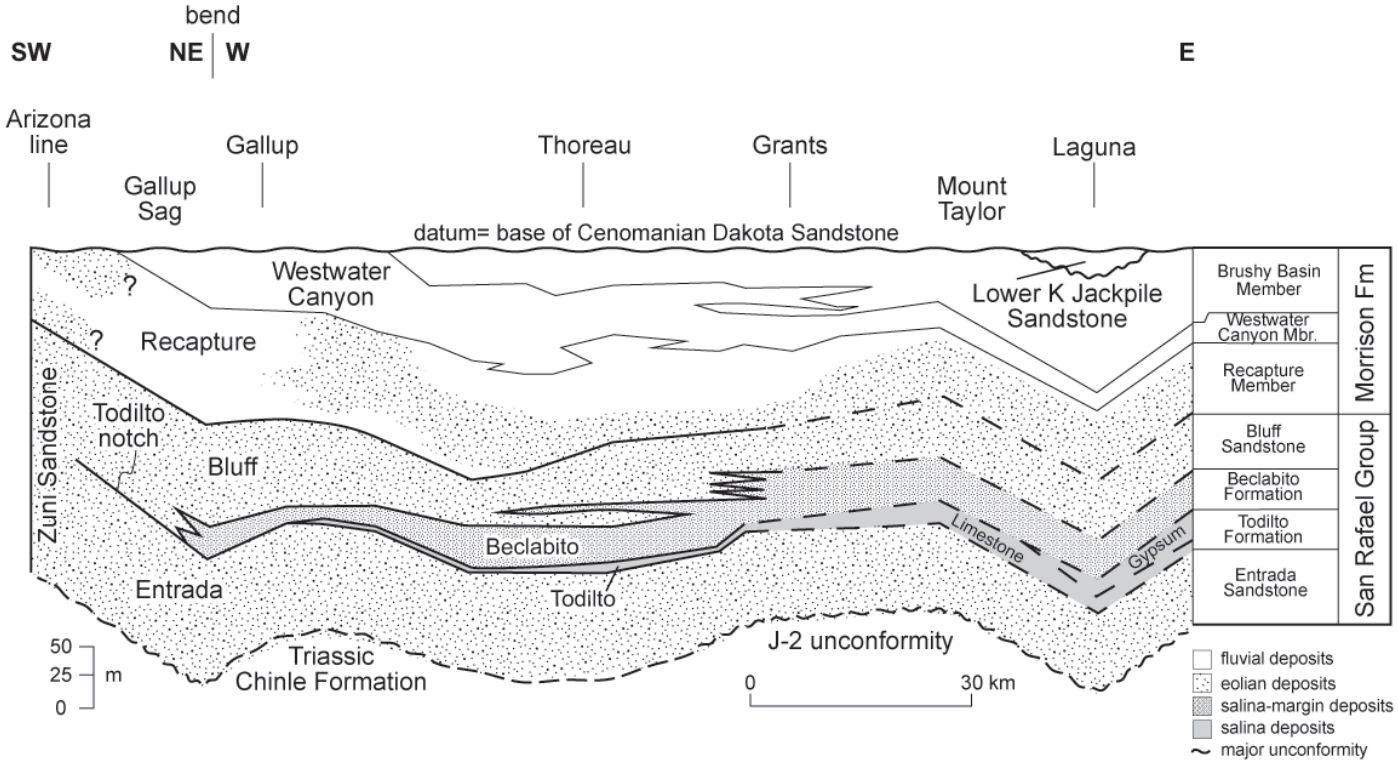

FIGURE 2. Correlation and suggested nomenclature for Jurassic strata in the southern San Juan Basin along the I–40 corridor from the Arizona line to near Laguna, New Mexico. Dashed lines indicate inferred subsurface contacts. Redrawn from Condon (1989, his fig. 2). See Condon (1989, his fig. 1) for locations of control points.

capture Member should also be included in the upper part of the San Rafael Group (this interval became their Recapture Member of the Bluff Sandstone of the San Rafael Group). The remainder of Gregory's Recapture Member, above their interpreted position of the J-5 unconformity, they assigned to the mostly fluvial Morrison Formation (the lower part of their revised Salt Wash Member; see below). The eolian component of the Gregory's Recapture Member, however, is not limited to its basal part, but interfingers with fluvial deposits at many stratigraphic levels within the Recapture (Fig. 2; Condon, 1989). Moreover, the proposed contact lies within a recessively weathering sedimentary succession and, thus, is of questionable mappability.

The presence of eolian facies in the Recapture Member, a fine-grained, southern fan complex that is equivalent to the Salt Wash Member, is an expectable consequence of the northward Jurassic drift of Laurentia, as the southern part of the Morrison depositional system was the last to leave the desert latitudes (Dickinson, 2018). Dickinson (2018) kept the entire Recapture Member (*sensu* Gregory, 1938) within the Morrison Formation, a decision with which I concur. The basal contact of the Morrison Formation should be placed at the top of the uppermost ledge of the Bluff Sandstone. This contact is a disconformity that represents a short lacuna (at most ~ 2 my; Fig. 1), likely related to the diachronous progradation of the basal Morrison fluvial systems across the Bluff erg (Dickinson, 2018).

Westwater Canyon Member

The Westwater Canyon Member (Gregory, 1938) of the Morrison Formation overlies the Recapture Member and is overlain by, and grades northward into, the Brushy Basin Member (Dickinson, 2018). Anderson and Lucas (1995, 1997) argued that the term Westwater Canyon Member is a junior synonym for the Salt Wash Member (Lupton, 1912; Gilluly and Reeside, 1928) and should be abandoned because of priority. Studies of regional stratigraphy, paleocurrents, detrital zircon analysis, and petrology, however, have all demonstrated that the Salt Wash and Westwater Canyon members were deposited by overlapping megafans with differing source regions (e.g., Craig et al., 1955; Hurd et al., 2006; Dickinson and Gehrels, 2008; Dickinson and Gehrels, 2010; Dickinson, 2018; Kirkland, *in press*). Most workers restrict the Salt Wash Member to southeastern Utah and southwestern Colorado, where it interfingers southward with the Recapture Member. The term Westwater Canyon Member is thus valid and should be retained.

Jackpile Sandstone

The Jackpile Sandstone has been regarded by most workers as the uppermost member of the Morrison Formation in the Mount Taylor area of New Mexico (e.g., Freeman and Hilpert, 1956; Owen et al., 1984; Lucas, 2018). Aubrey (1992), however, argued that the Jackpile is probably equivalent to the Lower Cretaceous Burro Canyon Formation, a unit that occupies a stratigraphic position similar to the Jackpile but is Lower Cretaceous (Barremian?–Albian, based on palynomorphs and a zircon fission-track age of 125±10 Ma from a bentonite; Craig, 1982; Tschudy et al., 1984).

The interpretation that the Jackpile is part of the Morrison is partly based on the local gradational basal contact of sandstones of the Jackpile with underlying, fine-grained deposits. The basal contact of the Burro Canyon Formation, however, in places occurs *within* the fine-grained deposits beneath its basal prominent sandstone (Turner and Peterson, 2010, p.11). Thus, it seems possible that the basal disconformity of the Jackpile may locally also lie within the underlying, fine-grained deposits.

Unlike sublitharenitic sandstones of the underlying Brushy Basin Member (Dickinson, 2018), sandstones of the Burro Canyon and the Jackpile are quartzose and contain widespread kaolinite cement. Correlation of the Jackpile to the Burro Canyon is further supported by their nearly identical detrital-zircon age distributions and the dissimilarity of their zircon populations to the rest of the Morrison Formation (Dickinson and Gehrels, 2010). The Jackpile Sandstone should be removed from the Morrison Formation (Cather et al., 2013; Dickinson, 2018) and mapped separately as Lower Cretaceous Jackpile Sandstone, or simply as Burro Canyon Formation.

SUMMARY

Of the stratigraphic terms discussed in this report, it is interesting to note that only the Brushy Basin Member of the Morrison Formation has escaped nomenclatural controversy. It is perhaps expectable that subdivision of vast Jurassic depositional systems of the southwestern United States into named units is not straightforward. Some of this controversy derives from differing concepts of how formations should be named. Should a formation be defined primarily on its lithologic characteristics (which reflect its depositional environment)? Or should nomenclature hinge more upon factors such as lateral correlation of bounding unconformities that serve to divide similar lithofacies or bound ones that are lithologically dissimilar? I suggest the former approach is better.

Since the 1980s, some workers have emphasized the role of unconformities and lateral correlations in naming formations. This can be problematic because regional correlations of Jurassic units are seldom unambiguous (the Summerville/Beclabito controversy is a good example of this) and, as noted by Dickinson (2018), unconformities are not everywhere traceable and are likely time-transgressive. Moreover, the stratigraphic position of some unconformities is disputed. For example, Anderson and Lucas (1995) placed the J-5 unconformity within Gregory's (1938) Recapture Member, but O'Sullivan (2010b) placed the J-5 within the underlying eolianites, at the base of his Bluff Sandstone Member of the Morrison Formation.

An example of the disadvantage of relying upon unconformities to define formations is the Bluff Sandstone. In southeastern Utah, geologists of the USGS consider the eolian Bluff Sandstone Member to overlie an unconformity (their J-5), which is developed on another eolianite, the Horse Mesa Member of the Wanakah Formation (e.g., O'Sullivan, 2010a; Turner and Peterson, 2010, p. 16). It seems possible to me that

this unconformity is simply a major intra-erg erosion surface (an eolian super-surface; Kocurek, 1988) within a fundamentally eolian succession. A similar intra-eolianite unconformity, however, is not present in the San Juan Basin region. Because of this, the USGS regards the entire eolianite above the Beclabito in the southeastern San Juan Basin as Horse Mesa Member (e.g., Condon, 1989). I agree with Anderson and Lucas (1996) and Dickinson (2018) that the whole eolianite above the Beclabito (their Summerville) should be regarded as Bluff Sandstone, the uppermost formation of the San Rafael Group.

Another example of overemphasis on unconformities (in this case, to broaden the content of a formation) is the eolian Moab Member of Utah, formerly part of the Entrada Sandstone, but now considered part of the Curtis Formation (e.g., Doelling, 2002). This reassignment was based on the presence beneath both the Curtis and the Moab of the J-3 unconformity, which serves to divide them from the underlying Entrada Sandstone.

Inclusion of the Moab as a member of the Curtis, however, creates a formation that ranges in its genesis from shallow marine to eolian, which is contrary to the definition of a formation, "A formation should possess some degree of internal lithic homogeneity..." [North American Stratigraphic Code (NASC), North American Commission on Stratigraphic Nomenclature, 2005, p. 1567]. Because the Stratigraphic Code allows unconformities within formations ("a formation...may include breaks in deposition"; NASC, p. 1567), it would be best to regard the Moab Member as part of the mostly eolian Entrada Sandstone [see Dickinson (2018, his Table 10) for a similar opinion], or to map it separately as a formation.

Formation-rank stratigraphic nomenclature based on depositional environments (i.e., dominantly erg, salina, salina-margin, or fluvial; Fig. 2) offers more reproducibility than does a nomenclature based on lateral correlation or interpretive subdivision of depositional systems using unconformities. A similar approach was advocated by Dickinson (2018). Within a nomenclatural scheme based on depositional environment, unconformities and facies characteristics can be used to subdivide formations into members or lithofacies.

The synthesis presented above will not resolve all issues concerning the Jurassic stratigraphic nomenclature of the San Juan Basin region. My intent is to propose a workable nomenclature for field mapping that may begin to heal some of the major schisms in the stratigraphic nomenclature of New Mexico.

ACKNOWLEDGMENTS

Field work was supported by the New Mexico Bureau of Geology and Mineral Resources and the STATEMAP program (Mike Timmons, Associate Director). I benefited from discussions with Spencer Lucas, Doug Sprinkel, and the late Bill Dickinson. Stephanie Chavez drafted the figures. The manuscript was improved by reviews from Jim Kirkland and Kate Zeigler.

REFERENCES

Anderson, O.J., and Lucas, S.G., 1995, The base of the Morrison Formation, Jurassic, of northwestern New Mexico and adjacent areas: New Mexico Geology, v. 17, p. 44–53.

Anderson, O.J., and Lucas, S.G., 1996, Stratigraphy and depositional environments of Middle and Upper Jurassic rocks, southeastern San Juan Basin: New Mexico Geological Society, Guidebook 47, p. 205–210.

Anderson, O.J., and Lucas, S.G., 1997, The Upper Jurassic Morrison Formation in the Four Corners region: New Mexico Geological Society, Guidebook 48, p. 139–155.

Aubrey, W.M., 1992, New interpretations of the stratigraphy and sedimentology of uppermost Jurassic to lowermost Upper Cretaceous strata in the San Juan Basin of northwestern New Mexico: U.S. Geological Survey, Bulletin 1808-J, p. 1–17.

Burbank, W.S., 1930, Revision of geologic structure and stratigraphy in the Ouray district of Colorado and its bearing on ore deposition: Colorado Scientific Society Proceedings, v. 12, p. 151–232.

Cather, S.M., 2011, Preliminary geologic map of the Dos Lomas 7.5-minute quadrangle, Cibola and McKinley Counties, New Mexico: New Mexico Bureau of Geology and Mineral Resources, Open-File Geologic Map OF-GM 219, scale 1:24,000.

Cather, S.M., Connell, S.D., Lucas, S.G., Picha, M.G., and Black, B.A., 2002, Preliminary geologic map of the Hagan 7.5-minute quadrangle, Sandoval County, New Mexico: New Mexico Bureau of Geology and Mineral Resources, Open-File Geologic Map OF-GM 50, scale, 1:24,000.

Cather, S.M., Zeigler, K.E., Mack, G.H., and Kelley, S.A., 2013, Toward standardization of Phanerozoic stratigraphic nomenclature in New Mexico: Rocky Mountain Geology, v. 48, p. 101–124.

Condon, S.M., 1989, Revisions of Middle Jurassic nomenclature in southeastern San Juan Basin, New Mexico: U.S. Geological Survey, Bulletin 1808-E, p. 1–21.

Condon, S.M., 1993, The Middle Jurassic Summerville Formation, northern New Mexico–a reply to Anderson and Lucas, 1992: New Mexico Geology, v. 15, p. 33–37.

Condon, S.M., and Peterson, F., 1986, Stratigraphy of Middle and Upper Jurassic rocks of the San Juan basin: Historical perspective, current ideas, and remaining problems, *in* Turner-Peterson, C.E., Santos, E.S., and Fishman, N.S., eds., A Basin Analysis Case Study: The Morrison Formation, Grants Uranium Region, New Mexico: American Association of Petroleum Geologists, Studies in Geology, v. 22, p. 7–26.

Craig, L.C., 1982, Uranium potential of the Burro Canyon Formation in western Colorado. U.S. Geological Survey, Open-File Report 82-222, 25 p.

Craig, L.C., Holmes, C.N., Cadigan, R.A., Freeman, V.L., Mullens, T.E., and Weir, G.W., 1955, Stratigraphy of the Morrison and related formations, Colorado Plateau region: A preliminary report: U.S. Geological Survey, Bulletin 1009-E, p. 125–168.

Craigg, S.D., 2001, Geologic framework of the San Juan structural basin of New Mexico, Colorado, Arizona, and Utah, with emphasis on Triassic through Tertiary rocks: U.S. Geological Survey, Professional Paper 1420, 70 p.

Dickinson, W.R., 2018, Tectonosedimentary relations of Pennsylvanian to Jurassic strata on the Colorado Plateau: Geological Society of America, Special Publication 533, 184 p.

Dickinson, W.R., and Gehrels, G.E., 2009, Use of U-Pb ages of detrital zircons to infer maximum depositional ages of strata: A test against a Colorado Plateau Mesozoic database: Earth and Planetary Science Letters, v. 288, p. 115–125.

Dickinson, W.R., and Gehrels, G.E., 2010, Implications of U-Pb ages of detrital zircons in Mesozoic strata of the Four Corners region for provenance relations in space and time: New Mexico Geological Society, Guidebook 61, p. 135–146.

Doelling, H.H., 2002, Geologic map of the Fisher Towers quadrangle, Grand County, Utah: Utah Geological Survey, Map 183, 22 p., 2 plates, scale 1:24,000.

Dutton, C.E., 1885, Mount Taylor and the Zuni Plateau: U.S. Geological Survey, 6th Annual Report, p. 105–198.

Freeman, V.L., and Hilpert, L.S., 1956, Stratigraphy of the Morrison Forma-

tion in part of northwestern New Mexico: U.S. Geological Survey, Bulletin 1030-J, p. 309–334.

Gilluly, James and Reeside, J.B., Jr., 1928, Sedimentary rocks of the San Rafael Swell and some adjacent areas in eastern Utah, *in* Shorter contributions to general geology, 1927: U.S. Geological Survey, Professional Paper 150-D, p. D61–D110.

Gregory, H.E., 1917, Geology of the Navajo Country – a reconnaissance of parts of Arizona, New Mexico and Utah: U.S. Geological Survey, Professional Paper 93, 161 p.

Gregory, H.E., 1938, The San Juan Country: U.S. Geological Survey, Professional Paper 188, 123 p.

Harshbarger, J. W., Repenning, C. A. and Irwin, J. H., 1957, Stratigraphy of the uppermost Triassic and Jurassic rocks of the Navajo country: U. S. Geological Survey, Professional Paper 291, 74 p.

Hintze, L.F., and Kowallis, B.J., 2009, Geologic history of Utah: Brigham Young University, Geology Studies Special Publication 9, 225 p.

Hurd, O.V., McGraw, J.L., and Dickinson, W.R., 2006, U-Pb ages of detrital zircons in the Morrison Formation (Salt Wash and Westwater Canyon members) of the Four Corners region, southwest USA: Geological Society of America, Abstracts with Programs, v. 38, p. 34.

Imlay, R.W., 1980, Jurassic paleobiogeography of the conterminous United States in its continental setting: U.S Geological Survey Professional Paper 1062, 134 p.

Kelley, S.A., Lawrence, J.R., and Osburn, G.R., 2005, Preliminary geologic map of the Youngsville 7.5-minute quadrangle, Rio Arriba County, New Mexico: New Mexico Bureau of Geology and Mineral Resources, Open-File Geologic Map OF-GM 106, scale 1:24,000.

Kirkland, D.W., Denison, R.E and Evans, R., 1995, Middle Jurassic Todilto Formation of northern New Mexico and southwestern Colorado: marine or nonmarine?: New Mexico Bureau of Mines and Mineral Resources, Bulletin 147, 37 p.

Kirkland, J.I., DeBlieux, D.D, Hunt-Foster, R.K., Foster, J.R., Trujillo, K.C., and Finze, E., *in press*, The Morrison Formation and its bounding strata on the western side of the Blanding Basin, San Juan County, Utah: Utah Geological Association, Geology of the Intermountain West.

Kocurek, G., 1988, First-order and super bounding surfaces in eolian sequences—Bounding surfaces revisited: Sedimentary Geology, v. 56, p. 193–206.

Kowallis, B.J., Christiansen, E.H., Deino, A.L., Zhang, C., and Everett, B.H., 2001, The record of Middle Jurassic volcanism in the Carmel and Temple Cap Formations of southwestern Utah: Geological Society of America Bulletin, v. 113, p. 373–387.

Kuiper, K.F., Deino, A., Hilgen, F.J., Krijgsman, W., Renne, P.R., and Wijbrans, J.R., 2008, Synchronizing rock clocks of Earth history: Science, v. 320, p. 500–504.

Lee, W. T., 1902, The Morrison shales of southern Colorado and northern New Mexico: Journal of Geology, v. 10, p. 36–58.

Lucas, S.G., 2004, The Triassic and Jurassic systems in New Mexico, in Mack, G.H., and Giles, K.A., eds., The Geology of New Mexico: A Geologic History: New Mexico Geological Society, Special Publication 11, p. 137–152.

Lucas, S.G., 2014, Lithostratigraphy of the Jurassic San Rafael Group from Bluff to the Abajo Mountains, southeastern Utah: Stratigraphic relationships of the Bluff Sandstone: Volumina Jurassica, v. 12, p. 55–68.

Lucas, S.G., 2018, The Upper Jurassic Morrison Formation in north-central New Mexico—Linking Colorado Plateau stratigraphy to the stratigraphy of the High Plains: Utah Geological Association, Geology of the Intermountain West, v. 5, p. 117–129.

Lucas, S.G., and Anderson, O.J., 1993, Upper Triassic stratigraphy in southeastern New Mexico and southwestern Texas: New Mexico Geological Society, Guidebook 44, p. 231–235.

Lucas, S.G., and Anderson, O.J., 1997, The Jurassic San Rafael Group, Four Corners region: New Mexico Geological Society, Guidebook 48, p. 115–132.

Lucas, S. G. and Anderson, O. J., 1998, Jurassic stratigraphy and correlation in New Mexico: New Mexico Geology, v. 20, p. 97-104.

Lucas, S.G., and Heckert, A.B., 2003, Jurassic stratigraphy in west-central New Mexico: New Mexico Geological Society, Guidebook 54, p. 245–262.

Lucas, S.G., Kietzke, K.K.., and Hunt, A.P., 1985, The Jurassic System in east-central New Mexico: New Mexico Geological Society, Guidebook 36, p. 213–243.

Lupton, C.T, 1912, Oil and gas near Green River, Grand County, Utah: U.S. Geological Survey, Bulletin 541, p. 115–133.

North American Commission on Stratigraphic Nomenclature, 2005, North American stratigraphic code: American Association of Petroleum Geologists Bulletin, v. 89, p. 1547–1591.

O'Sullivan, R.B., 1980, Stratigraphic sections of Middle Jurassic San Rafael Group from Wilson Arch to Bluff in southeastern Utah: U.S. Geological Survey, Oil and Gas Investigations Chart OC-102, 1 sheet.

O'Sullivan, R.B., 2003, The Middle Jurassic Entrada Sandstone in northeastern Arizona and adjacent areas: New Mexico Geological Society, Guidebook 54, p. 303–308.

O'Sullivan, R.B., 2010a, Correlation of the upper part of the Middle Jurassic San Rafael Group in northeast Arizona, northwest New Mexico, and southeast Utah: New Mexico Geological Society, Guidebook 61, p. 91–100.

O'Sullivan, R.B., 2010b, The lower and upper contacts of the Upper Jurassic Bluff Sandstone Member of the Morrison Formation in southeastern Utah: New Mexico Geological Society, Guidebook 61, p. 101–106.

Owen, D.E., Walters, L.J., Jr., and Beck, R.G., 1984, The Jackpile Sandstone Member of the Morrison Formation in west-central New Mexico – a formal definition: New Mexico Geology, v. 6, p. 45–52.

Peterson, F., 1994, Sand dunes, sabkhas, streams, and shallow seas: Jurassic paleogeography in the southern part of the western interior basin, *in* Caputo, M.V., Peterson, J.A., and Franczyk, K.J., eds., Mesozoic Systems of the Rocky Mountain Region, USA: Denver, Rocky Mountain Section, SEPM (Society for Sedimentary Geology), p. 233–272.

Pipiringos, G.N. and O'Sullivan, R.B., 1978, Principal unconformities in Triassic and Jurassic rocks, Western Interior, U.S.: A preliminary survey: U.S. Geological Survey Professional Paper 1035-A, 29 p.

Rapaport, I., Hadfield, J.P., and Olsen, R.H., 1952, Jurassic rocks of the Zuni Uplift, New Mexico: U.S. Atomic Energy Commission, RMO-642, 49 p.

Schaeffer, B., and Patterson, C., 1984, Jurassic fishes from the western United States, with comments on fish distribution: American Museum Novitates, no. 2796, 86 p.

Schultze, H.-P., and Enciso, G., 1983, Middle Jurassic age of the fish-bearing horizon in the Cañon City embayment, Colorado: Journal of Paleontology, v. 57, p. 1053–1060.

Sprinkel, D.A., Doelling, H.H., Kowallis, B.J., Waanders, G., and Kuehne, P.A., 2011, Early results of a study of middle Jurassic strata in the Sevier fold and thrust belt, Utah: Utah Geological Association, Publication 40, p. 151–172.

Trujillo, K.C., and Kowallis, B.J., 2015, Recalibrated legacy $^{40}Ar/^{39}Ar$ ages for the Upper Jurassic Morrison Formation, Western Interior, U.S.A.: Utah Geological Association, Geology of the Intermountain West, v. 2, p. 1–8.

Tschudy, R.H., Tschudy, B.D., and Craig, L.C., 1984, Palynological evaluation of Cedar Mountain and Burro Canyon Formations, Colorado Plateau: U.S. Geological Survey, Professional Paper 1281, 24 p.

Turner, C.E., and Peterson, F., 2004, Reconstruction of the Upper Jurassic Morrison Formation extinct ecosystem — A synthesis: Sedimentary Geology, v. 167, p. 309–355.

Turner, C.E., and Peterson, F., 2010, First-day road log from Cortez, Colorado, to Bluff, Utah, and return via the Four Corners: New Mexico Geological Society, Guidebook 61, p. 1–23.

Walker, J.D., Geissman, J.W., Bowring, S.A., and Babcock, L.E., compilers, 2012, Geologic Time Scale v. 4.0: Geological Society of America.

Wilcox, W.T., 2007, Sequence stratigraphy of the Curtis, Summerville, and Stump Formations, Utah and northwest Colorado [M.S. thesis]: Oxford, Miami University, 101 p.

Wilcox, W.T., and Currie, B.S., 2006, Depositional age and sequence stratigraphy of the Jurassic Curtis, Summerville, and Stump Formations, Utah and Colorado: Geological Society of America, Abstracts with Programs, v. 38, no. 7, p. 388.

Zuchuat, V., Sleveland, A.R.N., Sprinkel, D.A., Rimkus, A., Braathen, A., and Midtkandal, I., 2019, New insights on the impact of tidal currents on a low-gradient, semi-enclosed, epicontinental basin—The Curtis Formation, east-central Utah, USA: Utah Geological Association, Geology of the Intermountain West, v. 5, p. 131–165.

New Mexico Geological Society, Special Publication 14, Geology of the Mount Taylor Area, 2020, p. 153-166.

CLUES FROM THE SANTA FE GROUP FOR OLIGOCENE-MIOCENE PALEOGEOGRAPHY OF THE SOUTHEASTERN COLORADO PLATEAU NEAR GRANTS, NEW MEXICO

Daniel J. Koning[1], Matthew Heizler[1], and Andrew Jochems[2]

[1]New Mexico Bureau of Geology and Mineral Resources, 801 Leroy Place, Socorro, NM 87801; dan.koning@nmt.edu
[2]New Mexico Environment Department, 1190 St Francis Dr., P.O. Box 5469, Santa Fe NM 87502

Abstract—Progressive erosion of the southeastern Colorado Plateau during Miocene deposition shed notable amounts of sediment into the western Albuquerque basin, where it constitutes the Santa Fe Group. We use gravel compositions, clast ages, and paleoflow data from the middle Santa Fe Group to infer the Oligocene-Miocene paleogeography of the southeastern Colorado Plateau. This paper focuses on gravelly strata in the Cerro Conejo Formation (Santa Fe Group) mapped in the central Rio Puerco valley (within 25 km north of I–40), which are assigned to a new informal unit called the Benavidez member (14-8 Ma). These gravelly strata interfinger eastward with the Navajo Draw Member (Arroyo Ojito Formation) and the main, non-gravelly body of the Cerro Conejo Formation. The Benavidez member can be divided into three gravel-based petrosomes: volcanic-dominated, chert-dominated (≤5% volcanics), and mixed volcanic-chert (5-50% volcanics). Minor quartzite, quartz, and Proterozoic metarhyolites are found with the chert gravel. Only the chert-gravel petrosome is present north of latitude 35°9'N. To the south, the volcanic-gravel petrosome lies at the base of the Benavidez member, with stratigraphically higher Benavidez strata consisting of interfingering mixed-gravel and chert-gravel petrosomes. Paleocurrent data from the volcanic-gravel and mixed-gravel petrosomes are slightly more easterly (medians of 112 and116°) than the chert-gravel petrosome (median of 138°), supporting a more northerly source for the latter. $^{40}Ar/^{39}Ar$ radiometric analyses of four ignimbrite clasts in the volcanic-gravel petrosome returned ages and K/Ca values matching the Vicks Peak Tuff (28.77±0.01 Ma) and the La Jencia Tuff (29.00±0.01 Ma)—consistent with lithologic similarities observed in hand samples. Based on the spatial distribution of the Benavidez petrosomes and their associated paleocurrents, we interpret that a volcaniclastic apron sourced from the Mogollon-Datil volcanic field extended northward to ~35°20' N in the Oligocene, coinciding with the northern edge of the younger Mount Taylor volcano (Plio-Pleistocene). This apron interfingered with the Chuska Sandstone and chert-rich gravel derived from the Zuni uplift. During the Pliocene through Pleistocene, exhumation caused a progressive southward retreat of the northward extent of the volcaniclastic sediment, culminating with its complete removal north of the Rio Salado.

INTRODUCTION

One of the fascinating aspects of geology is the reconstruction of past landscapes. This reconstruction is most readily accomplished through recognition of depositional facies in sedimentary rocks where such rocks have been preserved, commonly within a basin. The sedimentary record in a basin, particularly sediment composition and paleoflow indicators, can also offer clues about the nature of the source area(s). This sedimentary record is particularly important for older (typically pre-Quaternary) deposits, where time intervals are significantly long to allow modification of the source area through exhumation or tectonic processes.

In addition to refining our understanding of past landscapes, understanding the original extent of volcaniclastic aprons and ignimbrites is imperative given the recent popularity of using detrital zircon and detrital sanidine methods to understand regional uplift, exhumation, and river history. Intermediate-felsic volcanic complexes can generate particularly large volcaniclastic aprons that have been documented to extend 100 km or more from the source vents. Examples include the volcaniclastic apron on the southwestern flanks of the Latir volcanic field (Abiquiu and Los Pinos formations; Smith, 2004) and the volcaniclastic sediment extending south from the eastern Mogollon Datil field (Thurman Formation, see Seager and Mack, 2003, fig. 13). Likewise, ignimbrites can travel 100-200 km, particularly if "funneled" through paleovalleys (e.g., Chapin and Lowell, 1979). Due to subsequent erosion, the original extent of volcaniclastic aprons can be difficult to establish, and researchers using detrital methods can misinterpret data if these original extents are not recognized.

This paper uses sedimentological and stratigraphic evidence in the Cerro Conejo Formation (Santa Fe Group) to interpret the source of gravel shed into the western Albuquerque basin between ~14 and 8 Ma. The studied gravel is located in the middle Santa Fe Group in the Rio Puerco Valley within 25 km north of I–40 (study area outlined in Fig. 1). Over the past decade, the geology in this part of the Rio Puerco Valley has been mapped at 1:24000 scale by the New Mexico Bureau of Geology and Mineral Resources (Cikoski et al., 2012; Koning and Jochems, 2014; Koning and Rawling, 2017; Rawling and Koning, 2019, in prep), and the data for this paper were collected during this STATEMAP-funded mapping. The generalized geology of the study area is shown in Figure 2. Four tuff-gravel samples were collected for $^{40}Ar/^{39}Ar$ radiometric dating of sanidine to determine if the volcanic gravels were derived from the San Juan or Mogollon-Datil volcanic fields.

Literature on the paleogeography of the southeastern Colorado Plateau includes Cather et al. (2003, 2008, 2012, 2019,

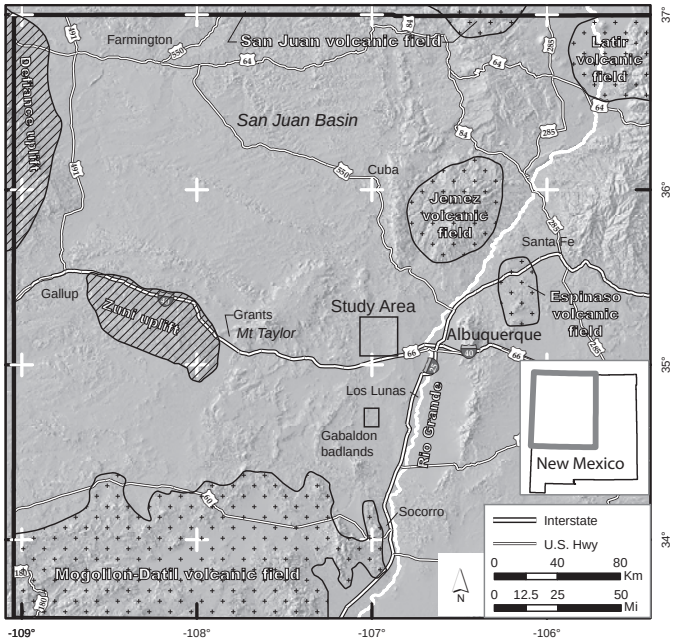

FIGURE 1. Geography of northwest New Mexico depicted on a hillshade DEM. The Rio Puerco Valley study area and Gabaldon Badlands are denoted by black squares. Eighty kilometers to the west lies Mount Taylor and Grants. Beyond 100 km to the south-southwest is the Mogollon-Datil volcanic field. Other volcanic fields are located to the north and northwest of the study area. Laramide uplifts on the southeastern Colorado Plateau are illustrated by diagonal-line patterns.

and references therein). Notable previous stratigraphic work on the Santa Fe Group along the western margin of the Albuquerque basin includes Bryan and McCann (1937, 1938), Wright (1946), Galusha (1966), Gawne (1973, 1981), Kelley (1977), and Lozinsky and Tedford (1991). Richard Tedford spearheaded studies on the paleontology and stratigraphy of the lower to middle Santa Fe Group along the eastern slopes of the Rio Puerco Valley (Tedford, 1981, 1982; Tedford and Barghoorn, 1997, 1999; Tedford et al., 1987). Connell et al. (1999) and Connell (2008a) revised Santa Fe Group stratigraphy and provided related age control. This revised stratigraphy was applied to the east edge of the study area in the geologic map of Connell (2008b). Previous work most applicable to constraining the age of the studied gravelly strata are in the synthesized magnetostratigraphic, paleontological, and radiometric data of Tedford and Barghoorn (1999) together with the focused paleontological work by Morgan and Williamson (2000, 2007) on the Cerro Conejo Formation.

METHODS

Details of mapping methodology are given in the reports for the aforementioned STATEMAP projects. Petrographic analyses were performed on 30-µm thin sections from Middle Miocene Santa Fe Group strata of the Benavidez Ranch quadrangle; those from the Cerro Conejo Formation are presented in this paper. Grain size is predominately medium to coarse grained. Thin sections were analyzed using a polarizing microscope with a 0.1-mm-precision stage caliper. Grid spacings were set larger than the maximum grain size for each thin section. Random point counts of 100-150 grains were conducted. Grains were analyzed in both plane and crossed-polarized light and were subsequently binned into quartz-feldspar-lithic (QFL) classes, with additional notes on texture and the composition of feldspar and lithic grains (Koning and Jochems, 2014).

$^{40}Ar/^{39}Ar$ analysis was conducted on four individual gravel clasts at the New Mexico Geochronology Research Laboratory. Sanidine crystals were concentrated using standard heavy liquid, Franz magnetic, and hand-picking techniques. The separates were irradiated in a machined aluminum tray for 16 hours at the USGS TRIGA facility, using neutron flux monitor Fish Canyon Tuff sanidine (FC-2, assigned age of 28.201 Ma; Kuiper et al., 2008). Following irradiation, sanidine grains were loaded into an ultrahigh vacuum chamber and individual grains were fused with a CO_2 laser to extract the argon. Argon isotopic compositions of the crystals were measured on an Argus VI mass spectrometer. Dates were calculated using a ^{40}K total decay constant of 5.463E-10/a (Min et al., 2000) and ages of clasts are the weighted inverse variance of the crystals deemed to define a population. Uncertainties are reported at 1 sigma and errors are increased by the square root of the MSWD when MSWD is greater than one.

STRATIGRAPHY

Based on observations during the course of geologic mapping, gravelly sand tongues interfinger eastward with the sand-dominated Cerro Conejo Formation in the northeastern study area (Fig. 3). Such gravel tongues are shown in the upper part of the magneostratigraphic section of Tedford and Barghoorn (1999, fig. 3), at stratigraphic heights >250 m above the base of the Cerro Conjeo Formation (column A, Fig. 3). However, to the southwest pebbly sediment occurs lower in the Cerro Conejo Formation (column C, Fig. 3). Sandy strata of the Cerro Conejo Formation near these gravelly intervals are lithologically similar to the sand within the gravelly tongues, including where gravelly strata dominate the section (e.g., cross section E-E' in Fig. 2). Thus, it is reasonable to include these gravelly strata with the Cerro Conejo Formation.

We apply the informal name "Benavidez member" to tabular-bedded, tan to reddish yellow sand that contains ≥1% gravel beds. The Benavidez member is relatively well-exposed near cross section E-E' in Figure 2, but these exposures are on the To'hajiilee Reservation and not publicly accessible. Publicly accessible gravelly strata assigned to the Benavidez member are found in I–40 roadcuts, at a distance 3 km west of the Rio Puerco.

The Cerro Conejo Formation overlies the Zia Formation and underlies the Navajo Draw Member of the Arroyo Ojito Formation (Figs. 4, 5; see Appendix 1 for more detail on these stratigraphic units). Along the Ceja del Rio Puerco, north of the study area depicted in Figure 2, gravelly sands occupy a transitional, 12- to 18-m-thick interval between the Cerro Conejo and Navajo Draw Member of the Arroyo Ojito Formation (Koning and Rawling, 2017). In the northern study area, the lower contact intertongues with the Cañada Pilares Member of

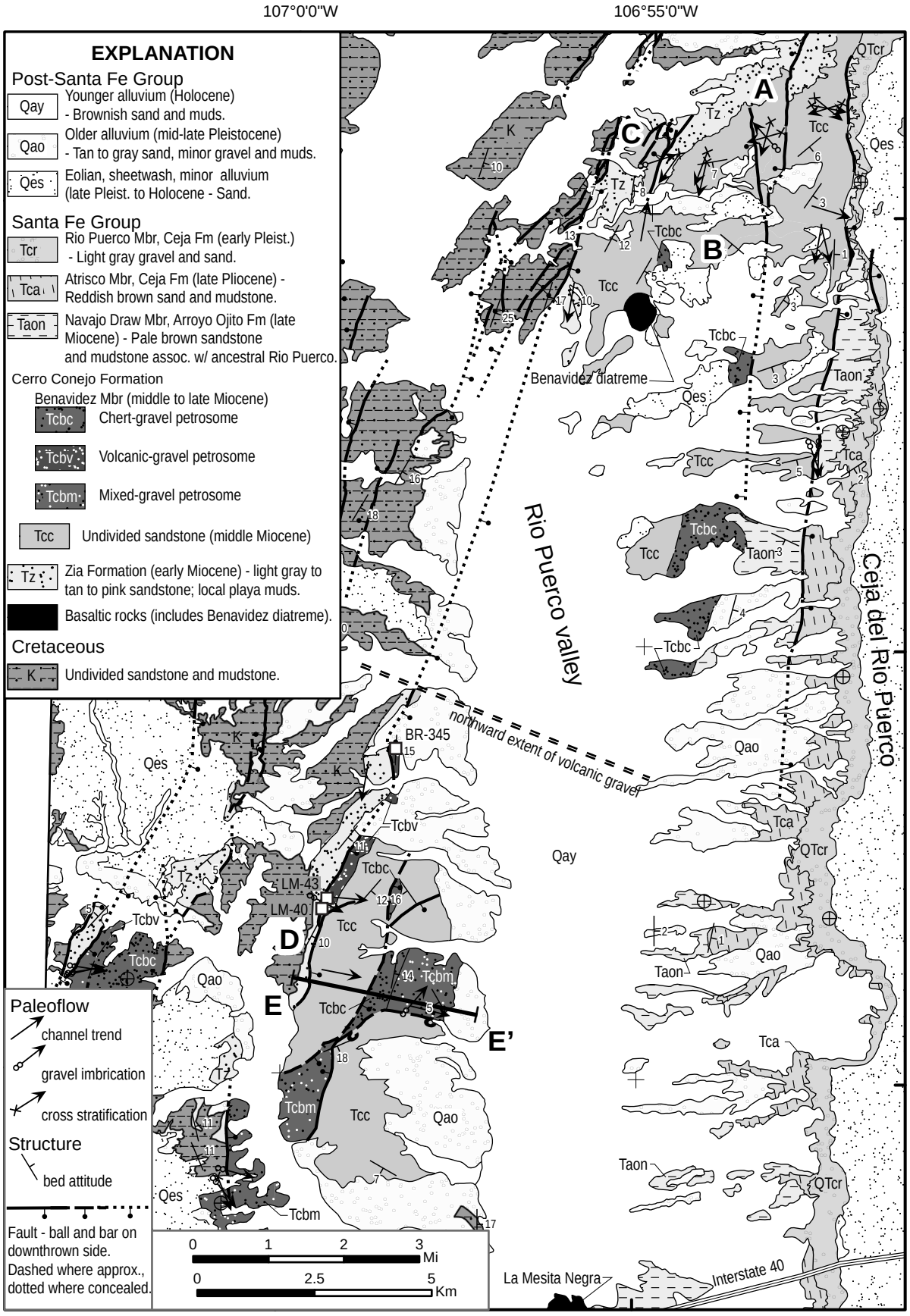

FIGURE 2. Geologic map of the studied Rio Puerco area. Modified from Williams and Cole (2007) according to Connell et al. (2008b) and recent STATEMAP work (Cikoski et al., 2012; Koning and Jochems, 2014; Koning and Rawling, 2017; Rawling and Koning, 2019, in prep). Letters A through D depict the locations of the stratigraphic columns of Figure 3. The white squares are locations of dated graveel samples. Paleocurrent arrows for gravel imbrication is the mean value at a site.

the Zia Formation (Koning and Rawling, 2017). However, this mudstone-rich unit is not present to the south, and there the Cerro Conejo directly overlies tan to pink sands of the upper Zia Formation (Figs. 3, 4, Tzu and Tz respectively). In the southern study area, basal strata of the Cerro Conejo Formation consist of a reddish gravelly sand (Tcblv, Figs. 3, 4), with a gravel fraction that is mostly volcanic in composition. The base of this volcaniclastic tongue is not exposed due to normal faulting. The volcaniclastic gravelly sand is overlain by 70-80 m of sand, locally cross-stratified and inferred to be eolian, interbedded with minor mudstone (Tccu, Figs. 3, 4).

In the northeastern study area, the piedmont lithofacies assemblage has prograded eastward over basin floor assemblages (Tcc4 overlying Tcc2-3, column B in Fig. 3), and lower in the section these basin floor deposits interfinger westward with piedmont deposits (compare columns B and C, Fig. 3). The piedmont lithofacies assemblage throughout the Cerro Conejo Formation is characterized by medium to thick, tabular-bedded, pink to light brown to reddish yellow sandstones. These beds are either massive or laminated (mostly horizontal-planar). There are minor (1-5%) clayey, very fine- to fine-grained sandstone beds and clay-dominated mudstones. The sand is subangular to rounded, and the grain size is mostly fine to medium with minor, scattered coarse to very coarse sand grains composed of quartz, chert, and volcanic lithic grains. The Benavidez member, occupying the gravelly, more medial parts of the aforementioned piedmont lithofacies assemblage, thickens from 100 to 250 m between the northeast and southwest parts of the study area (not including the basal volcaniclastic tongue) along with an increase in the proportion of gravel beds.

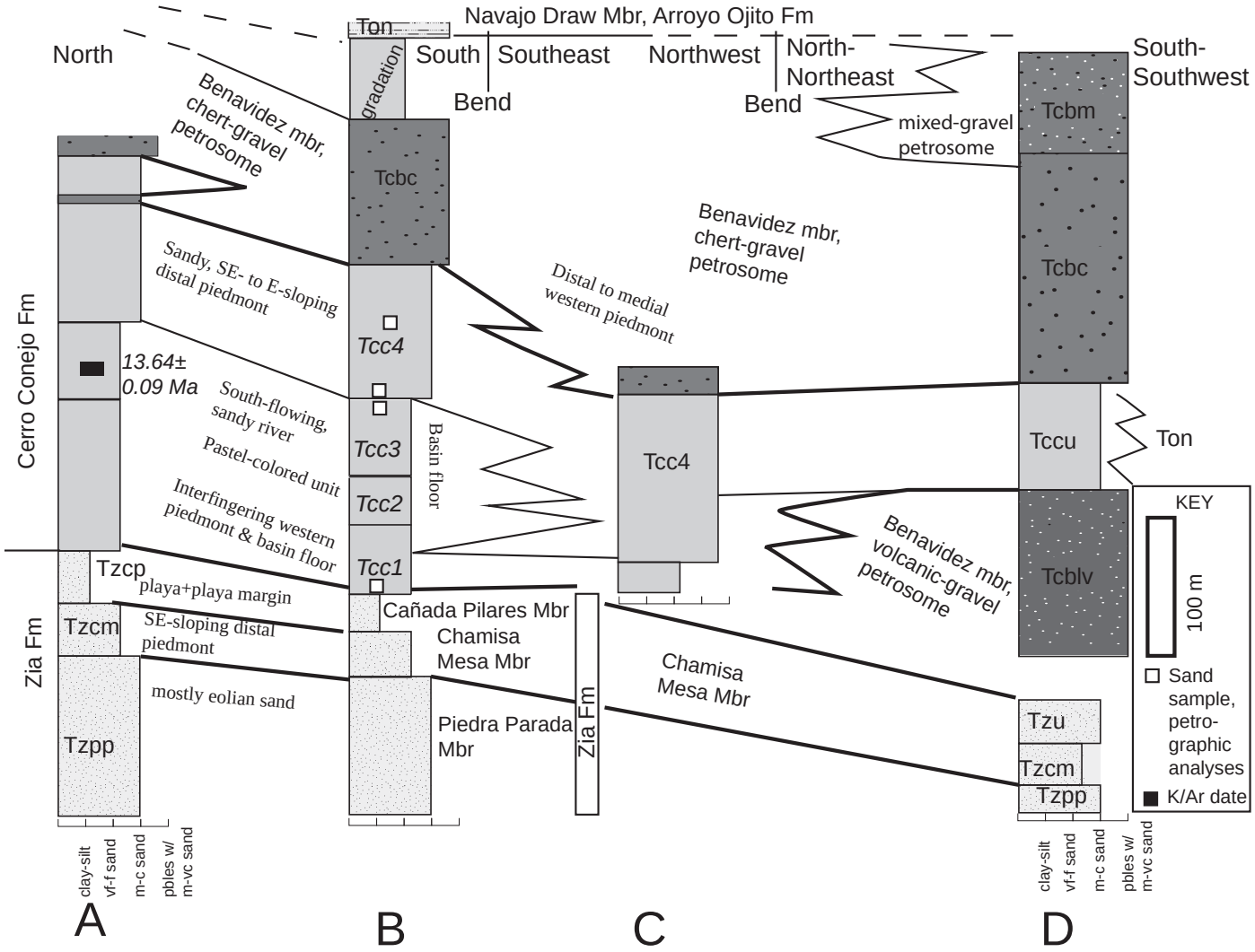

FIGURE 3. Stratigraphic fence diagram illustrating lower to middle Santa Fe Group stratigraphic relations along the studied reach of the Rio Puerco Valley, including the Benavidez member and its associated petrosomes. The locations of Columns A through D are shown in Figure 2. Open squares are the stratigraphic position of petrographic sand samples, taken within 5 km of the Benavidez diatreme. The black rectangle in Column A is the stratigraphic position of the K/Ar sample of Tedford and Barghoorn (1999). Tcc1 through Tcc4 are the subunits of the Cerro Conejo Formation mapped in Koning and Jochems (2014). Abbreviations for members of the Zia Formation: Tzpp = Piedra Parada, Tzcm = Chamisa Mesa, Tzcp = Cañada Pilares. Abbreviations for Benavidez member petrosomes: Tcbc = chert-dominated gravel, Tcbm = mixed gravel, Tcblv = volcanic-dominated gravel. Other abbreviations: Tzu = Upper Zia Formation; Ton = Navajo Draw Member of Arroyo Ojito Formation. Note that we designate the Cerro Conejo Formation base at the top of the playa facies of the Cañada Pilares Member, following Koning and Jochems (2014; cf., Tedford and Barghoorn, 1999).

In the Benavidez member, gravelly intervals occupy 1-25% of the piedmont lithofacies assemblage and are dominated by pebbles with <5% cobbles. Gravel occurs in intervals 1-5 m thick, and the individual gravel beds are mostly very thin to thin and tabular to lenticular; pebbly sand is typically horizontal-planar laminated (Fig. 5). Maximum clast size is commonly 5-7 cm.

Gravel Petrosomes

The Benavidez member can be subdivided into three petrosomes (Figs. 2-4). A petrosome is an informal stratigraphic unit (body of sediment) recognized solely by composition; in our study, we use gravel compositions (Figs. 2-4). The chert-gravel petrosome has ≤5% volcanic clasts and the dominant clast type is chert. The volcanic-gravel petrosome has 50-100% volcanic clasts, with the remainder of the gravel being chert, lesser quartzite and quartz, and trace petrified wood. More variable proportions of chert vs. volcanics (i.e., chert with 5-50% volcanics) are assigned to the mixed-gravel petrosome. The volcanic-gravel petrosome is only found in the lower Benavidez member west of the Rio Puerco (Tcblv, Figs. 2-4).

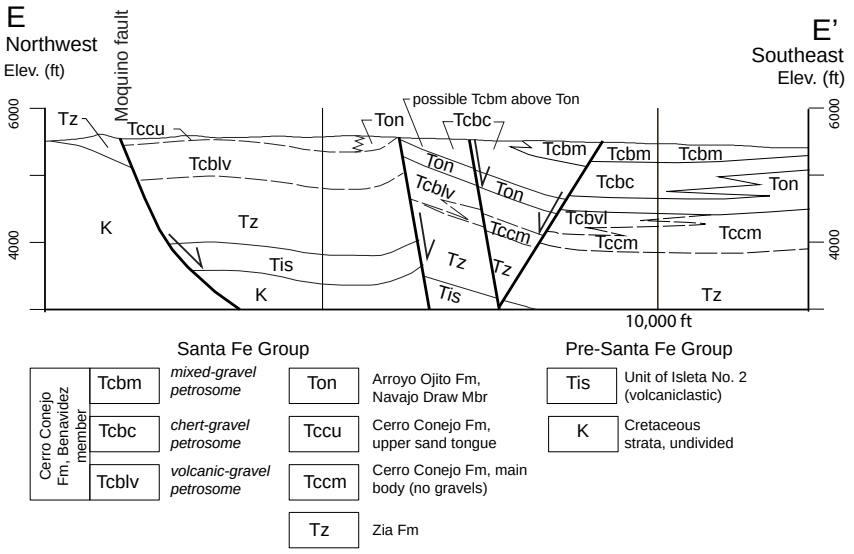

FIGURE 4. Cross section E-E' illustrating stratigraphic and thickness relations in the southwest part of the study area (cross section location given in Figure 2). Slightly modified from Cikoski et al. (2012).

Age

The age of the Benavidez member is ca. 14 to 8 Ma. The minimum age of 8 Ma is based on the age of the interfingering Navajo Draw Member (Arroyo Ojito Formation) in the southwestern study area, which has a lava flow dated at 8.11±0.05 Ma (La Mesita Negra in Fig. 2; Maldonado et al., 2006, table 1). The maximum age is obtained from the following observations in the northeastern study area. Fossils in the Cerro Conejo Formation have primarily been recovered from the basin floor deposits (Tcc2-3, Fig. 3) and are interpreted as being 14-12 Ma (Tedford and Barghoorn, 1999; Morgan and Williamson, 2000, 2007). This age range is consistent with a 13.64±0.09 Ma ash (Tedford and Barghoorn, 1999) found 130 m above the base of the formation (Fig. 3). Comparing the stratigraphic distance of the lowest pebbles to the west (column C, Fig. 3) relative to this dated ash (column A, Fig. 3), the Benavidez member has a maximum age of 13.5 Ma in the northern study area (columns A-C, Fig. 3). However, it is likely older (14-15 Ma?) in the southern study area, considering the stratigraphically low position of the volcanic-gravel petrosome (column D, Fig. 3).

RESULTS
Sedimentological Data

Sand composition in main body of Cerro Conejo Formation

In order to characterize the source area of the Benavidez member, we conducted sand petrographic analyses of the Cerro Conejo Formation. Samples were taken from units Tcc1, Tcc3, and Tcc4 (Fig. 3; Appendix 2). Of particular interest are the two samples from Tcc4, interpreted as a distal piedmont equivalent of the chert-gravel petrosome of the Benavidez Member. In Figure 6, a quartz-feldspar-lithic ternary diagram is used to compare these data with the sand composition of the Arroyo Ojito and Ceja formations (Brandes, 2002) and the Chuska Sandstone (Wright, 1956; Trevena, 1979; Cather et al., 2003; Dickinson et al., 2010).

The sand composition is variable within the Cerro Conejo Formation. For three of the four Cerro Conejo samples, quartz is the most abundant constituent at 42-50%, followed by 14-35% feldspar (plagioclase and potassium feldspar), and 23-36% lithic and mafic grains (Fig. 6). The lithic grains are composed

FIGURE 5. Photograph illustrating gravelly beds associated with the Benavidez member, taken in the southwest part of the study area.

of volcanics, chert, and siltstone to fine-grained sandstone (Appendix 2). One sample that contrasts with this generalization is Tcc4-lower, which has notably higher quartz and lower lithic proportions: 70% quartz, 19% feldspar (dominated by potassium feldspar), and 12% lithic grains consisting of very fine- to fine-grained sandstone and siltstone (Fig. 6, Appendix 2). Sample Tcc4-upper is slightly coarser-grained than the other samples (range of medium to very coarse, with very minor granules up to 7 mm). This coarser texture might account for the higher lithic content of that sample compared to Tcc4-lower—which would be consistent with hand-sample observations elsewhere. The quartz-feldspar-lithic composition of Tcc4-lower compares favorably with the Narbona Member of the Chuska Sandstone and the western piedmont facies of the Arroyo Ojito and Ceja formations (Fig. 6), in addition to its high ratio of potassium feldspar vs. plagioclase (cf. Dickinson et al., 2010, table 2). Higher in the piedmont lithofacies assemblage and closer (stratigraphically) to the gravel tongues, the sand composition (Tcc4-upper) is 44% quartz, 29% feldspar (slightly more potassium feldspar than plagioclase), and 25% lithic grains that contain quartzose sandstone, carbonate, and chert (Appendix 2). This sample, in addition to Tcc1, contains more lithic grains and less quartz than previously reported for the Chuska Sandstone (Fig. 6).

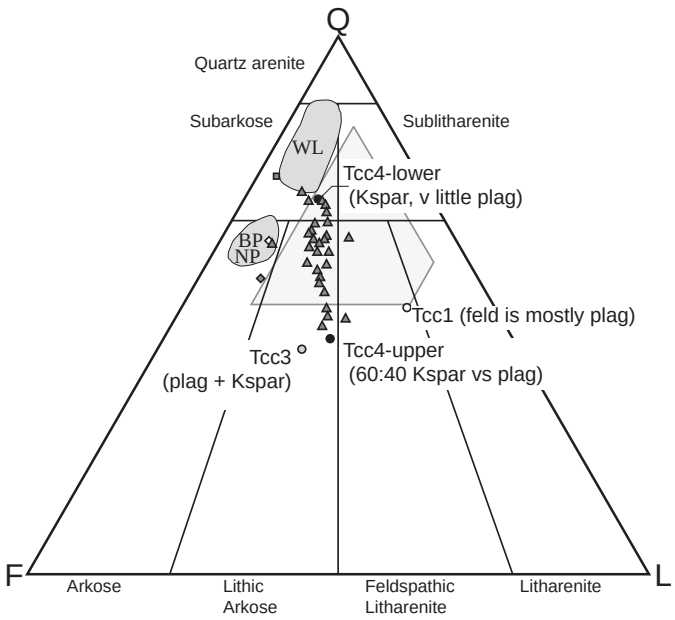

Cerro Conejo Fm, this work
- ● Upper western piedmont facies (Tcc4)
- ○ Sandy, south-flowing fluvial facies, main body (Tcc3)
- ○ Interfingering, lower western piedmont and basin floor facies (Tcc1)

Arroyo Ojito and Ceja Fm (Brandes, 2002)
- ▲ Western piedmont facies

Chuska sandstone
- ▫ Wright (1956)
- ◇ Deza Mbr -- Trevena (1979)
- ◆ Narbona Pass Mbr -- Trevena (1979)

Light-gray shade: values from Cather et al. (2003).
Medium-gray shade: values from Dickinson et al. (2010).
BP & NP = Buffalo and Narbona Pass; WL = Whiskey Lake.
Quartz values adjusted to reflect total quartz.

FIGURE 6. Ternary plot depicting the total quartz-feldspar-lithic (QFL) sand composition of the Cerro Conejo Formation and the Chuska Sandstone. Of particular interest in this study are samples Tcc4-lower and Tcc4-upper from the piedmont lithofacies assemblage. Upslope on this paleopiedmont would be the gravelly sediment associated with the Benavidez member, so the sand composition of these samples would reflect that of the Benavidez member. Shown for comparison is a sandy, south-flowing fluvial facies in the Cerro Conejo Formation (sample Tcc3) and interfingering basin floor-western piedmont lithofacies at the base of the Cerro Conejo Formation (sample Tcc1).

Gravel composition in Benavidez Member

The composition of gravels in the Benavidez member petrosomes was determined by clast counts and visual estimates (Tables 1-2, Appendices 3-4) conducted over the course of mapping. The visual estimates have an estimated error of 3% (for 0-10% ranges), 5% (for 10-15% ranges), and 10% (for 20-50% ranges).

Table 2 presents a detailed list of volcanic gravel compositions at one site in the volcanic-gravel petrosome (LM-43-cc in Table 1); associated photographs are shown in Appendix 3. Of the gravel types, 35% were felsic volcanic and 28% were intermediate-felsic volcanic types; cherts are 21% of the total gravel. The felsic volcanic gravel is mostly a similar, light gray, crystal-poor tuff (20% of total gravel) that has 1-3% phenocrysts dominated by sanidine. Other felsic types include a eutaxitic, reddish brown tuff (2%) and a crystal-rich tuff (5%) with >30% crystals (0.2-1.5 mm in size) composed of quartz, clear feldspar (sanidine + plagioclase), and 1-10% mafics. The intermediate volcanic rocks are mostly a light gray, porphyritic dacite with >15% phenocrysts composed of plagioclase, hornblende, and local biotite. Other intermediate types include relatively fine-grained and darker andesite and basaltic andesite. These same types of volcanic clasts were typically observed in the mixed-gravel petrosome as well.

Stratigraphically above the volcanic petrosome, the Benavidez member consists of the chert-gravel petrosome, which is overlain by (or intertongues with) the mixed-gravel petrosome south of latitude 35°9'N. The chert-gravel petrosome is dominated by chert clasts and has ≤5% volcanic gravel. Locally, intraformational sandstone and reworked calcium carbonate nodules are notable constituents of the gravel (e.g., LM-85, Table 1). Relatively minor gravel components include metarhyolites, quartz, and quartzite—each being ≤15%. Tan to brown sandstone clasts occur locally but are ≤7%. The composition of the mixed-gravel petrosome is relatively similar to that of the chert-gravel petrosome, except that the percentage of volcanic types is as high as 23%. Granite and Pedernal Chert clasts are typically not seen except in the stratigraphically highest parts of the Benavidez member (e.g., upper part of the mixed-gravel unit, eastern part of cross-section E-E', Fig. 4). There, Pedernal Chert is observed in trace amounts, but granite is slightly higher—typically trace to 1% and as much a 15% in LM-85 (Table 1). Pedernal Chert is found in the northern Nacimiento Mountains (Kelley et al., 2013; Vazzana and Ingersoll, 1981; Moore, 2000; Timmer, 1976), and presumably the granite is derived from the western front of the Nacimiento Mountains since this is the closest bedrock source to the Pedernal Chert (NMBGMR, 2003).

Table 1. Gravel composition according to petrosome in the Benavidez member of the Cerro Conejo Formation (values in percent).

	Chert gravel-petrosome (≤5% volcanics)																
	SF-344D	**BR-509**	**BR-136**	**BR-524**	**LM-75**	**LM-79**	**LM-82-cc**	**LM-83**	**LM-85**	**H-578**	**H-581**	**H-583**	**H-585b**	**H-588a**	**H-593**	**H-598**	**H-602**
Int volc	0	0	0	0	0		3	tr	0	0	0	0	0	0	0.5	0	0
Felsic volc$^{\Omega}$	1-3	0	0	0	0	1	2	0	0	0	0	0	0	0	0	0	0
Volcanic, undivid	1-3	0	0	0	0	1	5	0	0	0	0	0	0	0	0.5	0	0
Chert (approx)	95	85	70	90	85	95	56	90	33	80	80	70-75	80	80	75	70-75	90
Quartz	1-2	1-5	10	5-7	3-5	3	9	5-7	0	5	5-10	5-10	3	5	10	7-10	5
Quartzite	xxx	1-5	10	1-3	3-4	3	8	3	0	10	5-7	10	5	1	5	5	1-3
Metarhyolite	xxx	1-5	xx	xx	5	xx	15	tr-1	0	5	5	10	10	10-15	10	10	xx
Petrified wood	1	1	0	1	0.5	0	tr	0	0	tr	1-2	0	0.5-1	0	0	0	1
Granite	0	0	7-10	0	0	0	0	0	15	0	0	0	0	0	0	0-tr	0
Pedernal Chert	0	0	0	0	0	0	0	0	0.5	0	0	tr	0	0	0	tr	0
Other	0	0	0	0	0	0	1 lm, 7 ss	tr, ss	0	0	tr lm		0	0	0	0	0
IntraFm ss & $CaCO_3$	0	0	0	0	0	0	0	0	50	0	0	0	1	0	0	0	0

	Volcanic gravel		*Mixed gravel-petrosome*												
	BR-345-cc	**LM-43-cc**	**LM-74**	**LM-77**	**LM-87**	**LM-88**	**LM-126**	**LM-133**	**LM-140-cc**	**H-495**	**H-496**	**H-498**	**H-500**	**H-502**	**H-624**
Int volc	33	28	0	1-3	0	3-5	0	3	4						1-2
Felsic volc	43	35	1	5-8	7-10	3	10-20	20	24						3-4
Volcanic, undivid	94	63	5-8	8-10	7-10	6-8	10-20	23	28	15	15	15	15	10	n/a
Chert (approx)		21	75		85-90		40	45	39	65	75	75	70	80	90
Quartz	1	4	7-10	7-10**	3	3-4	5-10	5	1	10	10**	10-15**	15**	10**	5
Quartzite		1	5	**	3	3	5-10	0	3	10	**	**	**	**	1-2
Metarhyolite	1	8	5-7	xx	xx	xx	xx	xx	8	xx	xx	xx	xx	xx	xx
Petrified wood		0.5	0.5	tr	0.5	0	tr	0	1	2-3	0	0	0	0	0
Granite		0	0	1	0	1	0	0	0	0	0	0	0	0	0
Pedernal Chert		0	0	0	0	0	tr	0	0	0	0	0	0	0	0
Other	1 ss	0.5 ss	0	0	0	0	0	0	1 ss	1-5, ss	0	0	0	0	0
IntraFm ss & CaCO3		2.5	1	5	0	1-3	20	20-25	25	0	0	0	0	0	0

Abbreviations:
int = intermediate
volc = volcanic
lm = limestone
ss = sandstone
intrafm = intraformational

Notes: "-cc" indicates that sample underwent a clast count; otherwise, percentages are based on visual estimation. Locations of all samples are in Appendix 4.

** quartzite lumped with quartz; xx = probable metarhyolite that was lumped with cher; and **Ω** = includes extrusives and tuffs.

TABLE 2. Differentiation of volcanic gravel types, Site LM-43.

Gravel type	*Count*	*Percent*	*Comments*
Cenozoic volcanic – intermediate to mafic	**47**	**28%**	
Basaltic andesite	10	6%	Dark gray and commonly vesicular. Mostly fine-grained (crystal size <1 mm) and slightly porphyritic; phenocrysts are pyroxene and plagioclase.
Andesite	8	5%	Medium-gray and fine-grained. Mostly fine-grained and slightly porphyritic; phenocrysts are plagioclase and non-biotite mafics (probably hornblende or pyroxene).
Dacite	29	17%	Light gray and notably porphyritic. >15% phenocrysts (as large as 3 mm) composed of plagioclase, hornblende, ± biotite. Lacks quartz.
Cenozoic volcanic – felsic	**58**	**35%**	
Reddish brown tuff	3	2%	Eutaxitic with 1-10% phenocrysts (vitreous and mafic types) up to 1 mm long.
Light gray, crystal-poor tuff	33	20%	Monolithic; 1-3% phenocrysts (up to 3 mm long) composed of sanidine and very minor quartz. Local fiamme.
Aphanitic rhyolite	12	7%	
Crystal-rich tuff	9	5%	>30% crystals (0.2-1.5 mm) composed of quartz, sanidine + plagioclase, 1-10% mafics; similar to Hells Mesa Tuff.
Miscellaneous tuffs	1	0.5%	
Metamorphic	**15**	**9%**	
Metarhyolite	13	8%	Resinous luster; variable flow foliations; mostly aphanitic.
Quartzite	2	1%	Individual crystals seen, typically ~1 mm in size.
Chert and quartz	**42**	**21**	
Quartz	7	4%	No individual quartz crystals seen.
Chert	35	21%	Range in color from yellow, brown, red, and black.
Sedimentary	**6**	**3.5%**	
Very fine-grained, brown sandstone	1	0.5%	Inferred to be Mesozoic in age.
Reworked Santa Fe Group	3	2%	Sand is fine- to coarse-grained, quartz-rich, and contains chert lithic grains.
$CaCO_3$ nodule	1	0.5%	
Petrified wood	1	0.5%	

Total count: 168. Volcanic rock identification is via hand lens.

Paleocurrent data

We took 471 measurements of paleocurrent indicators for the Benavidez member, which are plotted on a rose diagram per petrosome (Fig. 7) and generalized on the geologic map (Fig. 2). The measurements consist primarily of clast imbrications, with only a few from measurement of channel trends. The average paleocurrent vector is to the southeast, but ranges from northeast to southwest. The mean and median values for the volcanic-gravel and mixed-gravel petrosomes are within 99-116°. However, the mean and median for the chert-gravel petrosome are more southerly at 138-144°, implying a slightly more northern source area.

Sampled Gravel

Lithologic description

West of the Rio Puerco, four samples of volcanic clasts from the volcanic-gravel petrosome (plotted as white squares in Fig. 2) were radiometrically dated using the $^{40}Ar/^{39}Ar$ method. The gravel are of two types. The first is a reddish brown (2.5YR 5/3) tuff having 1-10% phenocrysts dominated by sanidine (up to 4 mm) with very minor quartz (samples LM-40, LM-43red, BR-345). The second (LM-43gray) is a light gray, crystal-poor tuff having <3% phenocrysts of sanidine and very minor quartz. These samples correlate to the reddish brown tuff and light gray, crystal-poor tuff identified in the detailed LM-43 clast count (Table 2). Both types of tuff have minor fiamme and the reddish brown tuff is locally eutaxitic, supporting an interpretation that they represent welded tuffs.

Radiometric data

Sanidine was dated from the four clasts described above, and a summary of the results are presented in Figure 8. Details of the analyses are given in Appendix 5. Between 10 and 18 crystals were dated from each clast, and overall the individual dates define age populations with minor scatter. Of the total of 57 grains dated, three were omitted as being anomalously old and are thought to be xenocrysts. One sanidine grain was relatively young and omitted due to suspected argon loss (Appendix 5). The reddish brown tuff clasts returned ages of 28.96±0.02, 29.00±0.03, and 29.06±0.03 Ma (1σ error). The sanidines have associated K/Ca values (derived from the measured $^{37}Ar/^{39}Ar$ ratio) ranging from ~5 to 25, with mean values ~15±5. The light gray, crystal-poor tuff returned a distinctly younger age of

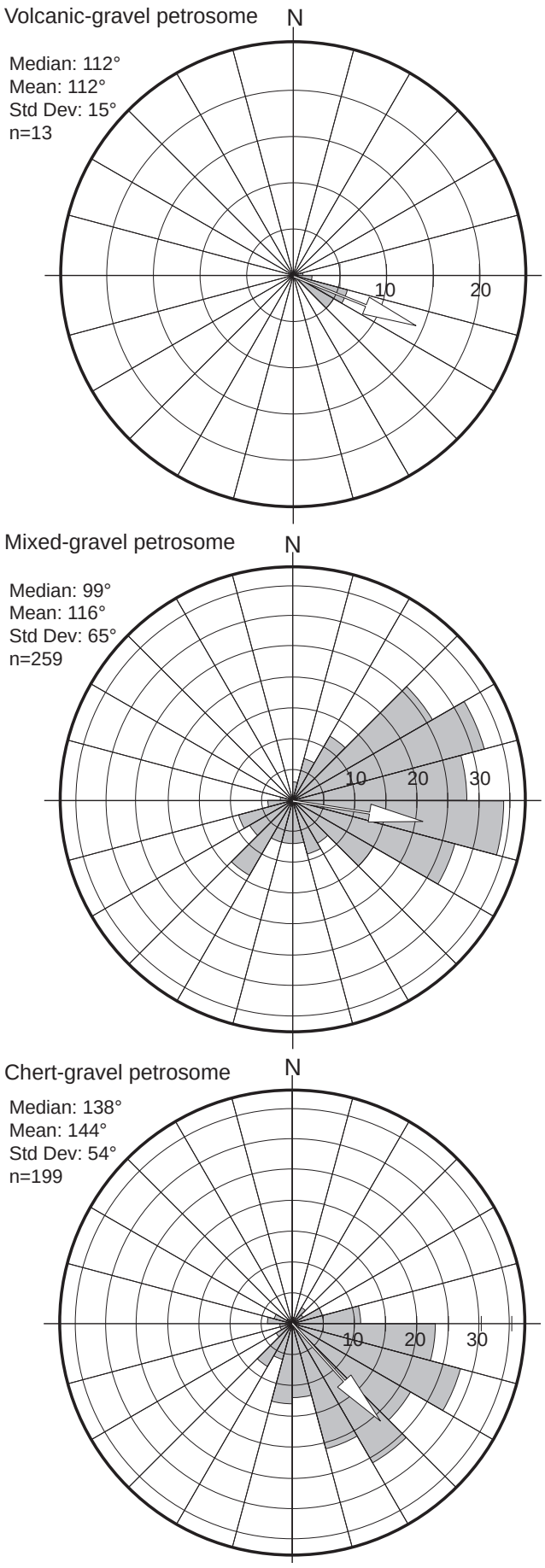

28.76±0.06 Ma; it had much higher K/Ca values, ranging from 50 to 100 and a mean at ~65±20. Thus, the reddish brown clasts (LM-40, LM-43red, BR-345) have sanidines with distinctively different age and K/Ca compared to those of the gray clast (LM-43gray; Fig. 8).

Correlation

The clast eruption ages and their individual sanidine dates and K/Ca results are compared to those of regional ignimbrites of similar age from both the San Juan and Mogollon-Datil volcanic fields (Fig. 8). Age-correlative ignimbrites from the Mogollon-Datil field include the La Jencia and Vicks Peak tuffs. The comparative age data for these two tuffs are taken from Cather et al. (in press). The ages and K/Ca ratios of the reddish brown tuff clasts generally overlap the age range of the La Jencia Tuff sanidines whereas sanidine of the gray clasts results are in good agreement with data of the Vicks Peak Tuff sanidines, both in age and K/Ca.

We also compare our $^{40}Ar/^{39}Ar$ data to ignimbrites from the San Juan volcanic field. Possibly age-correlative tuffs from the southwestern San Juan volcanic field include the Dillian Mesa, Blue Mesa, and Ute Ridge tuffs; the associated sanidine data for these units are taken from Lipman (2007). These units have individual sanidine dates ranging from 28.5-29.3 Ma that overlap the sanidine ages of our sampled clasts (Fig. 8). The San Juan tuff dates are relatively imprecise and, based on age alone, cannot be distinguished from the clast data. However, the K/Ca values of the San Juan volcanic field tuffs are for the most part distinctly different from those of the clast data (Fig. 8). The South Fork and Ra Jadero tuffs from the southeast San Juan Mountains are also possible age-equivalent correlatives to the sampled clasts (Lipman et al., 1996; note these data are not shown in Fig. 8). The sanidines from these tuffs have similar K/Ca composition to the reddish brown sampled-tuff clasts; however, their ages are ~29.2 Ma and distinctly older than the clasts. Thus, based on age there is a poor correlation of the South Fork and Ra Jadero tuffs to the reddish brown tuff clasts. Additionally, the east-southeast paleocurrents in the Benavidez member make a southeast San Juan Mountain source unlikely, considering that the southeastern San Juan Mountains are north-northeast of the study area. Thus, there is no likely correlation between the sampled clasts and the San Juan Mountain tuffs based on age, K/Ca, and paleocurrent data.

Macroscopic features of these gravel samples corroborate the radiometric data in assigning the reddish brown tuff (BR-345, LM-40, LM-43red) to the La Jencia Tuff and the light gray, crystal-poor tuff (LM-43gray) to the Vicks Peak Tuff. The La Jencia Tuff is notably eutaxitic and has 3-7% sanidine phenocrysts and minor amounts of small, rounded quartz phe-

FIGURE 7. Rose diagram showing gravel imbrication data for the Benavidez member, divided according to petrosome (volcanic-, mixed-, and chert-gravel). The associated data primarily represent clast imbrication, with only a few paleochannel trends. The arrow shows the median value of the data. Note that the chert-gravel petrosome has a more southeasterly paleoflow direction than the mixed-gravel petrosome, consistent with a more northerly source area. Total number of measurements is 471.

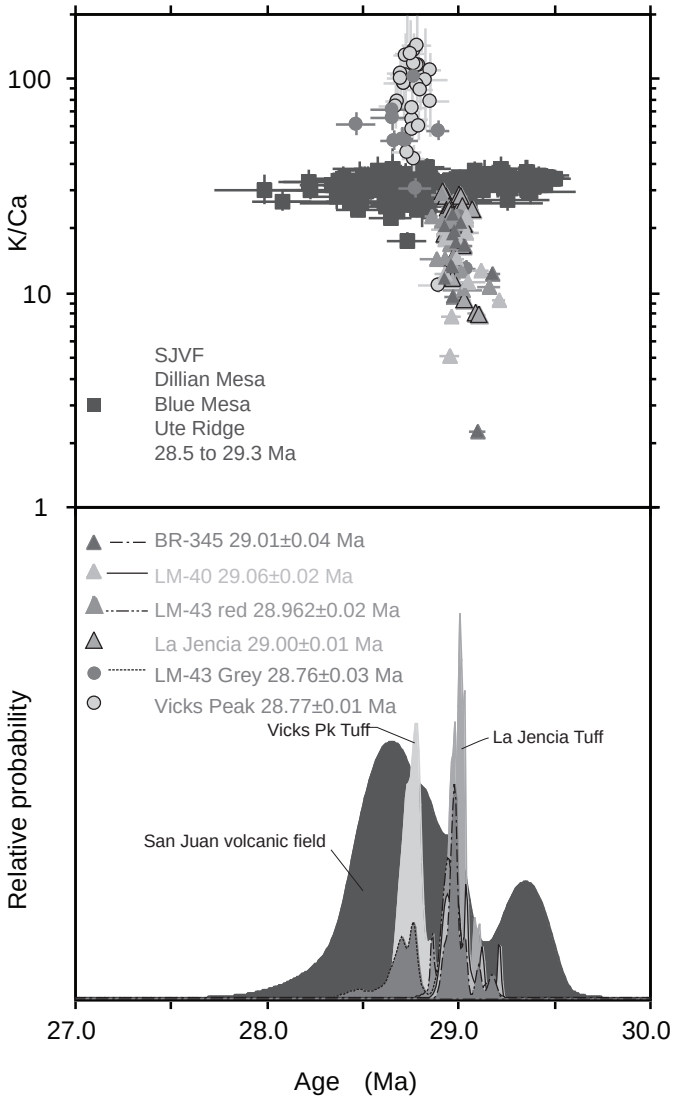

Figure 8. **Top**) K/Ca and age data for clast-derived sanidines, plotted with 1σ error bars. These are compared to ignimbrite data from the Mo-gollon-Datil (i.e., Vicks Peak and La Jencia Tuffs) and southwestern San Juan volcanic fields (Dillian Mesa, Blue Mesa, Ute Ridge tuffs). **Bottom**) Various shades illustrate the age probability distributions for the four Benavidez samples (whose shades are outlined with various line types) and the comparative samples (whose shades are not outlined). The reddish-brown clasts (BR-345, LM-40, LM-43red) show a strong age and composition correlation with sanidine from the La Jencia Tuff, whereas the gray clast (LM-43gray) overlaps with sanidine data from the Vicks Peak Tuff. Although there is age overlap with San Juan sanidines, there is generally poor K/Ca agreement. Therefore, we interpret that the Benavidez clasts were derived from the Mogollon-Datil volcanic field.

nocrysts (Osburn and Chapin, 1983). Where visited by the senior author, outcrops of the La Jencia Tuff near the Datil Mountains are reddish brown and very similar to the reddish brown tuff samples in the Benavidez member. The Vicks Peak Tuff in the Datil and western Gallinas Mountains is light gray, crystal-poor, and contains 1-3% sanidine phenocrysts together with trace amounts of quartz, biotite, clinopyroxene, and plagioclase (Osburn and Chapin, 1983) — very similar to the macroscopic appearance of sample LM-43 and the light gray, crystal-poor tuffs described in Table 2.

DISCUSSION

Source Area for Benavidez Member

Our initial hypothesis for the source area of the Benavidez member was reworking of a volcaniclastic apron shed from the southwestern San Juan volcanic field; such a large, southwest- to south-sloping fan had been previously interpreted by Cather et al. (2003, 2008). This initial inference was based on the southeast average paleoflow trend, the Late Miocene age (younger than the late Eocene-early Oligocene age of the San Juan volcanic field), and the mixed intermediate-felsic composition of the gravel in the Benavidez member. Although the Mogollon-Datil contains intermediate and felsic volcanic rocks, including many ignimbrites, this field is to the south, contrary to the paleoflow directions. The Latir volcanic field (Fig. 1) is a possible candidate, given that its volcaniclastic apron may have extended to the northern part of the Nacimiento Mountains (Smith, 2004, fig. 7), but that extent is still east of the northwest projection of the streams depositing the Benavidez member and no Amalia Tuff clasts were observed. The Mount Taylor volcanic field did not exist until the middle Pliocene (3.74 Ma; Goff et al., 2019), so it can be ruled out as a volcanic source area. Other than Oligocene mafic intrusions and diatremes associated with the Navajo volcanic field (Semken, 2001), there are no other volcanic centers upstream (northwest) of the Rio Puerco valley study area. The western San Juan volcanic field is the right age and more directly upstream from the study site than these other potential sites and would be expected to have both intermediate volcanic rocks and ignimbrites.

However, the ages and K/Ca ratios of the four volcanic gravel clasts correlate better to the La Jencia and Vicks Peak Tuffs of the Mogollon-Datil field rather than to tuffs from the San Juan volcanic field. Furthermore, sedimentologic and stratigraphic work to the south of our study area supports a source area ultimately derived from the Mogollon-Datil volcanic field. In the Late Miocene Popotosa Formation in the Gabaldon badlands, located 25 m southwest of Los Lunas (Fig. 1), gravelly sediment is interpreted as being deposited on a piedmont-slope that graded downstream into alluvial flats (Lozinsky and Tedford, 1991). The gravel composition of the conglomerates is predominately composed of volcanic types, where rhyolites and ash flow tuffs greatly outnumber basalts, and no andesite was recognized (Lozinsky and Tedford, 1991, p. 22, table 2). Moreover, G.R. Osburn, an expert on the volcanic stratigraphy of the northern Mogollon-Datil field, identified some of these felsic clasts as being La Jencia Tuff or Vicks Peak Tuff (based on hand-sample identification; Lozinsky and Tedford, 1991, p. 12). Sand petrographic analyses indicated a source area dominated by intermediate volcanic rock types with lesser amounts from a sedimentary terrane, probably Cretaceous strata. Similar to our study area, paleoflow in the Gabaldon badlands also averaged southeast. The upstream projection of these streams, then, would have been near Grants. This is significantly farther north than what is typically recognized as the northern extent of the Mogollon-Datil field (e.g., Chapin et al., 2004). In the southwestern corner of the Albuquerque basin, western-sourced

alluvial fan deposits of Miocene age also are commonly composed of volcaniclastic fanglomerate (Machette, 1978).

Given the southeasterly paleoflow data in our study area and the Gabaldon badlands (Lozinsky and Tedford, 1991), a Mogollon-Datil source for the volcanic gravel in the Benavidez member (and correlative Popotosa strata in the Gabaldon badlands) would involve three possibilities: (1) fluvial reworking of an older (Eocene-Early Miocene), gravelly volcaniclastic apron shed northward from the Mogollon-Datil volcanic field, (2) erosion of in-situ Vicks Peak and La Jencia Tuffs that were emplaced as far north as Grants, or (3) a Middle to Late Miocene paleoriver that flowed north (west of the Rio Grande rift) for 120-130 km and then doglegged back into the rift. We favor the first option for four reasons. One, although the La Jencia and Vicks Peak Tuffs could have been emplaced as ignimbrite flows far north of the Mogollon-Datil field, the diverse mixture of other felsic and intermediate volcanic gravel types with clasts of the La Jencia and Vicks Peaks Tuff indicate that such flows would have been interbedded within heterolithic sands and gravels of volcanic origin. Two, the long north-south extent of the Middle-Late Miocene, piedmont-slope depositional environments along the western margin of the Albuquerque basin (>100 km) is more consistent with exhumation of an older volcaniclastic apron than a paleo-river dog-legging back into the rift at a relatively fixed point. In addition, such a northward paleoflow immediately west of the rift margin would be opposite that of the southerly paleoflow within most of the northwestern Albuquerque basin (Connell et al., 1999). Three, the older volcaniclastic apron correlates lithologically and chronologically with the unit of Isleta No. 2 (Lozinsky, 1994), which in the southern Albuquerque basin is inferred to be sourced from the Mogollon-Datil volcanic field (Cather et al., 2008). Lastly, rift-flank exhumation would be expected during active tectonism of the Rio Grande rift in the Miocene (House et al., 2003).

We interpret that the volcaniclastic apron interfingered with the age-equivalent Chuska Formation and chert-rich gravels shed from the Zuni uplift. The Chuska Sandstone consists of sand that blanketed the southeastern Colorado Plateau in the Early Oligocene (Cather et al., 2003, 2008). The pre-rift, volcaniclastic apron was likely shed during or shortly after the 40-24 Ma volcanic activity of the Mogollon-Datil field (age from Chapin et al., 2004), and thus its middle-upper parts are time-correlative to the Chuska Sandstone.

We infer that the chert-rich gravel was eroded from the Zuni uplift (Laramide age), probably from gravel-bearing Mesozoic units (e.g., basal Dakota Formation, Jackpile Sandstone, and the Shinarump Member of the Chinle Formation). The general lack of Pedernal Chert negates a source from the Nacimiento Mountains, and the gravel deposited in south-flowing paleo-rivers of the San Jose Formation is purported to contain more quartzite and quartz clasts compared to chert clasts, with other minor lithologies including granite, sandstone, mudrock rip-ups, and volcanic rock (Baltz, 1967, p. 48, 51; Smith and Lucas, 1991, p. 19). The Zuni uplift-derived gravels are inferred to have been transported northward into the San Juan Basin in Paleogene time, where they may have partly interfingered with the San Jose Formation south of the preserved extent of the latter (note that Nacimiento stratigraphic units with northward paleoflow into the San Juan Basin only contain sandstone and siltstone gravel; Cather et al., 2019). Continued gravelly deposition into the Early Oligocene would have resulted in interfingering of the chert-dominated gravels with the Chuska Formation and the Mogollon-Datil volcaniclastic apron.

Sand petrographic results from our Cerro Conejo Formation samples are consistent with sand derived from a Chuska Sandstone source area mixed with chert- and volcanic-detritus from the Zuni uplift and Mogollon-Datil volcanic fields. In the QFL plot of Figure 6, one of our samples (Tcc4-lower) is compositionally similar with the Chuska Sandstone. The other three samples (Tcc1, Tcc3, and Tcc4-upper) have more lithic grains and plagioclase than the Chuska Sandstone. These samples may define a mixing relation between the Chuska Sandstone and a more plagioclase- and lithic-rich source; this mixing may also be reflected in the linear compositional trend of stratigraphically higher data of Brandes (2002; Fig. 6). The lithics in Cerro Conejo Formation sand are predominately chert and volcanic (hand lens inspection in Koning and Jochems, 2014; Koning and Rawling, 2017). Thus, one could explain the QFL composition of samples Tcc1, Tcc3, and Tcc4-upper by mixing of a Chuska Sandstone source with chert detritus from the Zuni uplift and volcanic- and plagioclase-rich detritus from the Mogollon-Datil field.

Given our interpretation of reworking of a volcaniclastic apron shed northward from the Mogollon-Datil field, stratigraphic relations coupled with paleoflow data indicates that the apron extended approximately as far north as what is now the north flank of Mount Taylor (35°20'N latitude). There is no volcanic gravel within any stratigraphic level of the Benavidez member north of about 35°9'N latitude. But volcanic gravel is found in the Benavidez member south of that latitude, and the proportion of volcanic gravel increases further south in the Gabaldon badlands (Lozinsky and Tedford, 1991). A straight-line projection from the northern boundary of the volcanic-bearing petrosomes (35°9'N latitude), using a representative paleoflow of 115° (from the volcanic- and mixed-gravel petrosomes, Fig. 7), extends to 35°20'N latitude (Fig. 9).

In summary, we propose an Oligocene paleogeographic model of a Datil-Mogollon volcaniclastic apron interfingering with the Chuska Sandstone eolianite and a chert-dominated sandy gravel up to about 35°20'N latitude (Fig. 9). The chert-dominated gravel unit extended perhaps 60-80 km further north (from 35°20'N) into the San Juan Basin, where it interfingered with the Chuska eolianite (Fig. 9). Since chert is less abundant in the Gabaldon Badlands compared to our study area, presumably the chert-dominated gravel was located north of where the majority of that volcaniclastic sediment was derived—consistent with the slightly more southerly paleocurrent direction associated with the chert-gravel petrosome of the Benavidez member.

Moreover, we interpret the following paleogeographic scenario for the southeastern Colorado Plateau near the town of Grants. First, Paleocene-Eocene (Laramide) erosion of the Zuni Uplift produced a northeast-sloping piedmont containing chert-dominated gravel that extended into the southern

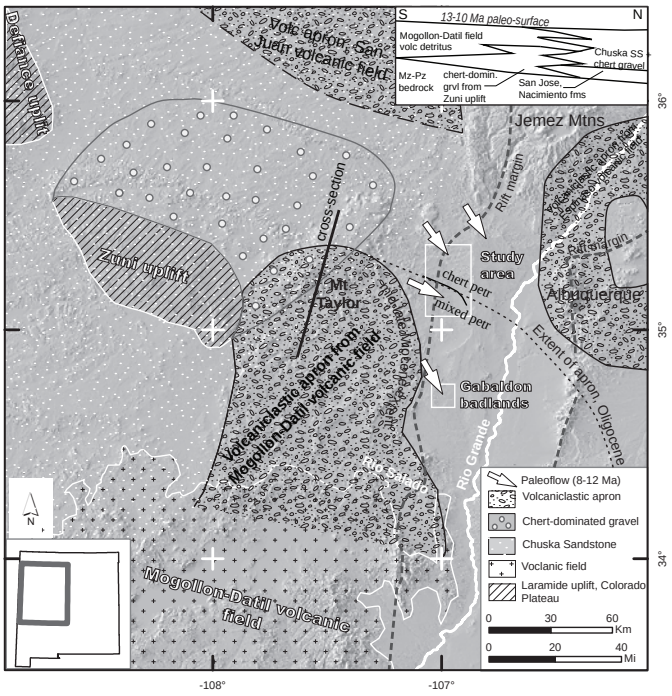

FIGURE 9. Paleogeographic map showing the northward extent of the volcaniclastic apron derived from the Mogollon-Datil volcanic field. To the northwest was chert-dominated gravel inferred to be eroded from the Zuni uplift. Tongues of the Chuska Sandstone interfingered with the chert gravel and the northern Mogollon-Datil volcaniclastic apron. To the north, the Chuska Sandstone also interfingered with the distal part of the volcaniclastic apron of the San Juan volcanic field (Cather et al., 2008). In the upper-right of the figure, a schematic north-south cross-section across the Mount Taylor region depicts the inferred geology ca. 13-10 Ma. Note that the Zuni uplift may possibly have been completely buried by the Chuska Sandstone ca. 27 Ma (Cather et al., 2008), although Dickinson et al. (2010) thought the Zunis persisted as a paleotopographic high. Post-Chuska exhumation may have caused deposition of thin chert gravels overlying various erosional surfaces (not shown in the cross-section).

San Juan Basin. Second, during Late Eocene-Early Oligocene time, a volcaniclastic apron sourced from the Mogollon-Datil volcanic field extended northward to about ~35°20'N, following a northward paleotopographic gradient created by uplift of the Mogollon-Datil volcanic field (Cather et al., 2012). This volcaniclastic apron interfingered northward with a mixture of chert-dominated gravel (from the Zuni uplift) and arkosic to subarkosic sand of the Chuska Formation. The Vicks Peak and La Jencia Tuffs were either in the source area of this volcaniclastic apron, consistent with their stratigraphically high position in the northern Datil and Gallinas Mountains (e.g., Osburn and Chapin, 1983), and/or emplaced as ignimbrite flows on the volcaniclastic apron. Eolian sand tongues of the Chuska Sandstone may have extended far across the volcaniclastic fan. During the Middle to Late Miocene (and probably the Early Miocene), exhumation of the aforementioned sedimentary package occurred. Assuming a wedge-shaped geometry of the volcaniclastic apron (thinning to the north), spatially constant rates of exhumation would have caused a progressive southward retreat of the preserved northward extent of the volcaniclastic sediment with time. By the early Pleistocene, this erosion and southward recession of the Oligocene-age volcaniclastic fan remnants culminated in complete removal of the volcaniclastic sediment north of the Rio Salado (see Fig. 9 with NMBGMR, 2003). Thin, chert- and quartz-rich gravels and sands locally lie beneath the Pliocene lava flows of the Mount Taylor volcanic field (Shari Kelley, written communication, March 30, 2020). These likely are late to middle Pliocene in age, but if they are late Eocene-early Oligocene then it would indicate that the volcaniclastic apron existed immediately east of Mount Taylor.

Implications for regional uplift and detrital studies

Previous studies, particularly Cather et al. (2012), have interpreted pulses of uplift and exhumation of the southeastern Colorado Plateau during the Oligocene-Early Miocene (25-15 Ma) and again after 6 Ma. The pause in the Middle Miocene and early Late Miocene is largely inferred based on the presence of the ~250 m thick Bidahochi Formation (Cather et al., 2008) near the border of Arizona and New Mexico (extending southeast into New Mexico as the Fence Lake Formation). However, our study shows that the Bidohochi Formation did not extend further east than about Gallup. Rather, the Colorado Plateau was being exhumed in the Grants and Mount Taylor area during 14 Ma through 8 Ma (age of Benavidez member) and likely as early as 20 Ma (age of basal Zia Formation; Tedford and Barghoorn, 1999), consistent with thermochronologic interpretations of the Lucero uplift (40 km west of Los Lunas) by Ricketts et al. (2016). This exhumation along the rift margin may be driven, in part, by rift shoulder or mantle-driven uplift associated with the Rio Grande rift. In other words, the "Alvarado Ridge" seen in modern topography (Eaton, 1987) may have been occurring as early as ca. 14 Ma. One cannot rule out uplift along the Jemez lineament as a possible driver (McCann, 1938), although previous studies infer that this uplift occurred after ca. 8 Ma (Wisniewski and Pazzaglia, 2002; Nereson et al., 2013; Channer et al., 2015).

Lastly, our study should be useful for future detrital zircon and detrital sanidine studies. The source area for zircons and sanidines associated with the Mogollon-Datil field can be found as far north as latitude 35°20'N. Furthermore, these grains were recycled into the northwestern Albuquerque basin. Therefore, the presence of these grains in Neogene-Quaternary sediment does not necessarily imply a source area coinciding with what is strictly the Mogollon-Datil volcanic field.

CONCLUSIONS

Gravelly strata composed mainly of chert and volcanic rock types interfinger with the sand-dominated Cerro Conejo Formation as well as the Navajo Draw Member of the Arroyo Ojito Formation. We informally refer to these gravelly strata as the Benavidez member of the Cerro Conejo Formation. Three gravel-based petrosomes can be recognized in the Benavidez member: chert-gravel, volcanic-gravel, and mixed-gravel. Volcanic gravel is not present north of 35°9'N, and south of this latitude volcanic gravel is most abundant in the lowest parts

of the Benavidez member. $^{40}Ar/^{39}Ar$ analyses of four volcanic clasts from the volcanic-gravel petrosome indicate correlation with the La Jencia and Vicks Peak Tuffs of the Mogollon Datil field. We thus infer that the volcanic gravel was derived from erosion of a volcaniclastic apron that extended north of the Mogollon-Datil field. Using a representative paleoflow of 115° measured in the mixed- and volcanic-gravel petrosomes of the Benavidez member, and considering the northern extent of the volcanic gravel in the Benavidez member, we conclude that the northern extent of the Oligocene-age volcaniclastic apron was about 35°20'N — coinciding approximately with what is now the northern flank of Mount Taylor.

ACKNOWLEDGMENTS

We are grateful for the reviews provided by Richard Lozinsky and Steven Cather, as well as comments by Sean Connell and John Hawley. Shari Kelley and Kate Zeigler provided an editorial review. We also thank the To'hajiilee Navajo Chapter and Laguna Pueblo for access to their lands in the Rio Puerco valley.

REFERENCES

Baltz, E.H., 1967, Stratigraphy and regional tectonic implications of part of upper Cretaceous and Tertiary rocks, east-central San Juan basin, New Mexico: U.S. Geological Survey, Professional Paper 552, 101 p.

Brandes, N.N., 2002, Lithostratigraphy and petrography of Upper Santa Fe Group deposits in the northern Albuquerque Basin, New Mexico [M.S. thesis]: Socorro, New Mexico Institute of Mining and Technology, 208 p.

Bryan, K., and McCann, F.T., 1937, The Ceja del Rio Puerco: A border feature of the Basin and Range Province in New Mexico. I. Stratigraphy and structure: Journal of Geology, v. 45, p. 801-828.

Bryan, K., and McCann, F.T., 1938, The Ceja del Rio Puerco: A border feature of the Basin and Range Province in New Mexico. II. Geomorphology: Journal of Geology, v. 46, p. 1-16.

Cather, S.M., Heizler, M.T., and McIntosh, W.C., in press, Middle Eocene to Pliocene volcanic, volcaniclastic, and intrusive rocks of the Quebradas Region: New Mexico Bureau of Geology and Mineral Resources, Memoir 51.

Cather, S.M., Peters, L., Dunbar, N.W., and McIntosh, W.C., 2003, Genetic stratigraphy, provenance, and new age constraints for the Chuska Sandstone (upper Eocene-lower Oligocene), New Mexico-Arizona: New Mexico Geological Society, Guidebook 54, p. 397-412.

Cather, S.M., Connell, S.D., Chamberlin, R.M., McIntosh, W.C., Jones, G.E., Potochnik, A.R., Lucas, S.G., and Johnson, P.S., 2008, The Chuska erg: Paleogeomorphic and paleoclimatic implications of an Oligocene sand sea on the Colorado Plateau: Geological Society of America Bulletin, v. 120, no. 1/2, p. 13-33; doi: 10.1130/B26081.1.

Cather, S.M., Chapin, C.E., and Kelley, S.A., 2012, Diachronous episodes of Cenozoic erosion in southwestern North America and their relationship to surface uplift, paleoclimate, paleodrainage, and paleoaltimetry: Geosphere, v. 8, no. 6, p. 1177-1206; doi: 10.1130/GES00801.1.

Cather, S.M., Heizler, M.T., and Williamson, T.E., 2019, Laramide fluvial evolution of the San Juan Basin, New Mexico and Colorado: Paleocurrent and detrital –sanidine age constraints from the Paleocene Nacimeinto and Animas formations: Geosphere, v. 15, no. 5, p. 1641-1665, https://doi.org/10.1130/GESO2072.1.

Channer, M.A., Ricketts, J.W., Zimmerer, M., Heizler, M., and Karlstrom, K.E., 2015, Surface uplift above the Jemez mantle anomaly in the past 4 Ma based on $^{40}Ar/^{39}Ar$ dated paleoprofiles of the Rio San Jose, New Mexico, USA: Geosphere, v. 11, no. 5, p. 1384-1400.

Chapin, C.E., and Lowell, C.E., 1979, Primary and secondary flow structures in ash-flow tuffs of the Gribbles Run paleovalley, central Colorado, *in* Chapin, C.E., and Elston, W.E., eds., Ash-flow tuffs: Geological Society of America, Special Paper 180, p. 137-154.

Chapin, C.E., McIntosh, W.C., and Chamberlin, R.M., 2004, The Late Eocene-Oligocene peak of Cenozoic volcanism in southwestern New Mexico, *in* Mack, G.H., and Giles, K.A., eds., The Geology of New Mexico: A Geologic History: New Mexico Geological Society, Special Publication 11, p. 271-293.

Cikoski, C.T., Koning, D.J., and Connell, S.D., 2012, Geologic map of the La Mesita Negra quadrangle: New Mexico Bureau of Geology and Mineral Resources, Open-file Geologic Map 223, scale 1:24,000.

Connell, S.D., 2008a, Refinements to the stratigraphic nomenclature of the Santa Fe Group, northwestern Albuquerque Basin, New Mexico: New Mexico Geology, v. 30, no. 1, p. 14-35.

Connell, S.D., 2008b, Geologic map of the Albuquerque-Rio Rancho metropolitan area, Bernalillo and Sandoval Counties, New Mexico: New Mexico Bureau of Geology and Mineral Resources, Geologic Map GM-78, scale 1:50,000, 2 plates.

Connell, S.D., Koning, D.J., and Cather, S.M, 1999, Revisions to the stratigraphic nomenclature of the Santa Fe Group, northwestern Albuquerque Basin, New Mexico: New Mexico Geological Society, Guidebook 50, p. 337-353.

Dickinson, W.R., Cather, S.M., and Gehrels, G.E., 2010, Detrital zircon evidence for derivation of arkosic sand in the eolian Narbona Pass Member of the Eocene-Oligocene Chuska Sandstone from Precambrian basement rocks in central Arizona: New Mexico Geological Society, Guidebook 61, p. 125-134.

Eaton, G.P., 1987, Topography and origin of the southern Rocky Mountains and Alvarado Ridge: Geological Society of London, Special Publications, v. 28, p. 355-369.

Galusha, T., 1966, The Zia Sand Formation, new early to medial Miocene beds in New Mexico: American Museum Novitates, no. 2271, 12 p.

Gawne, C.E., 1973, Faunas and sediments of the Zia Sand, medial Miocene of New Mexico [Ph.D. dissertation]: New York, Columbia University, 354 p.

Gawne, C.E., 1981, Sedimentology and stratigraphy of the Miocene Zia Sand of New Mexico: Summary: Geological Society of America Bulletin, v. 92, p. 999-1007.

Goff, F., Kelley, S.A., Goff, C.J., McCraw, D.J., Osburn, G.R., Lawrence, J.R., Drakos, P.G., and Skotnicki, S.J., 2019, Geologic map of the Mount Taylor area, New Mexico: New Mexico Bureau of Geology and Mineral Resources, Geologic Map 80, scale 1:36,000.

House, M.A., Kelley, S.A., and Roy, M., 2003, Refining the footwall cooling history of a rift flank uplift, Rio Grande rift, New Mexico: Tectonics, v. 22, no. 5, p. 14-1–14-18.

Kelley, V.C., 1977, Geology of the Albuquerque Basin, New Mexico: New Mexico Bureau of Mines and Mineral Resources, Memoir 33, 60 p.

Kelley, S.A., Kempter, K.A., McIntosh, W.C., Maldonado, F., Smith, G.A., Connell, S.D., Koning, D.J., and Whiteis, J., 2013, Syndepositional deformation and provenance of Oligocene to Lower Miocene sedimentary rocks along the western margin of the Rio Grande rift, Jemez Mountains, New Mexico, *in* Hudson, M.R., and Grauch, V.J.S., eds., New Perspectives on Rio Grande Rift Basins: From Tectonics to Groundwater: Geological Society of America Special Paper 494, p. 101-123, doi: 10.1130/2013.2494(05).

Koning, D.J., and Jochems, A.P., 2014, Geologic Map of the Benavidez Ranch 7.5-Minute Quadrangle, Bernalillo and Sandoval Counties, New Mexico: New Mexico Bureau of Geology and Mineral Resources, Open-file Geologic Map 234, scale 1:24,000.

Koning, D.J., and Rawling, G., 2017, Geologic map of the San Felipe Mesa 7.5-minute quadrangle, Sandoval County, New Mexico: New Mexico Bureau of Geology and Mineral Resources, Open-file Geologic Map 266, scale 1:24,000.

Kuiper, K.F., Deino, A., Hilgen, F.J., Krijgsman, W., Renne, P.R., and Wijbrans, J.R., 2008, Synchronizing rock clocks in Earth history: Science, v. 320, p. 500-504.

Lipman, P.W., 2007, Incremental assembly and prolonged consolidation of Cordilleran magma chambers: Evidence from the Southern Rocky Mountain volcanic field: Geosphere, v. 3, no. 1, p. 42-70; doi: 10.1130/GES00061.1.

Lipman, P.W., Dungan, M.A., Brown, L.L., and Deino, A.L., 1996, Recurrent eruption and subsidence at the Platoro Caldera complex, southeastern San Juan volcanic field, Colorado; new tales from old tuffs: Geological

Society of America Bulletin, v. 108, issue 8, p. 1039-1055.
Lozinsky, R.P., 1994, Cenozoic stratigraphy, sandstone petrology, and depositional history of the Albuquerque Basin, central New Mexico: Geological Society of America Special Paper 291, p. 73-82.
Lozinsky, R.P., and Tedford, R.H., 1991, Geology and paleontology of the Santa Fe Group, southwestern Albuquerque Basin, Valencia County, New Mexico: New Mexico Bureau of Geology and Mineral Resources, Bulletin 132, 35 p. and 3 sheets.
Machette, M.N., 1978, Geologic map of the San Acacia quadrangle, Socorro County, New Mexico: U.S. Geological Survey, Map GQ-1415, scale 1:24,000.
Maldonado, F., Budahn, J.R., Peters, L., and Unruh, D.M., 2006, Geology, geochronology, and geochemistry of basaltic flows of the Cat Hills, Cat Mesa, Wind Mesa, Cerro Verde, and Mesita Negra, central New Mexico: Canadian Journal of Earth Sciences, v. 43, no. 9, p. 1251-1268.
McCann, F.T., 1938, Ancient erosion surface in the Gallup-Zuni area, New Mexico: American Journal of Science, v. 36, p. 260-278.
Min, K., Mundil, R., Renne, P. R. and Ludwig, K. R., 2000, A test for systematic errors in $^{40}Ar/^{39}Ar$ geochronology through comparison with U–Pb analysis of a 1.1 Ga rhyolite: Geochimica et Cosmochimica Acta, v. 64, p. 73–98.
Moore, J.D., 2000, Tectonics and volcanism during deposition of the Oligocene-Lower Miocene Abiquiu Formation in northern New Mexico [M.S. thesis]: Albuquerque, University of New Mexico, 144 p.
Morgan, G.S., and Williamson, T.E., 2000, Middle Miocene (late Barstovian) vertebrates from the Benavidez Ranch local fauna, Albuquerque Basin, New Mexico: New Mexico Museum of Natural History and Science Bulletin No. 16, p. 195-207.
Morgan, G.S., and Williamson, T.E., 2007, Middle Miocene (late Barstovian) mammal and bird tracks from the Benavidez Ranch local fauna, Zia Formation, Albuquerque Basin, Sandoval County, New Mexico: New Mexico Museum of Natural History and Science Bulletin 42, p. 319-330.
Nereson, A., Stroud, J., Karlstrom, K., Heizler, M., and McIntosh, W., 2013, Dynamic topography of the western Great Plains: Geomorphic and $^{40}Ar/^{39}Ar$ evidence for mantle-driven uplift associated with the Jemez Lineament of NE New Mexico and SE Colorado: Geosphere, v. 9, no. 3, p. 521-545, https://doi.org/10.1130/GES00837.1.
New Mexico Bureau of Geology and Mineral Resources, 2003, Geologic Map of New Mexico: New Mexico Bureau of Geology and Mineral Resources, scale 1:500,000.
Rawling, G.C., and Koning, D.J., 2019, Geologic map of the Herrera 7.5-minute quadrangle, Sandoval and Bernalillo Counties, New Mexico: New Mexico Bureau of Geology and Mineral Resources, Open-file Geologic Map 273, scale 1:24,000.
Rawling, G.C., and Koning, D.J., in preparation, Geologic map of the Canoncito School 7.5-minute quadrangle, Bernalillo County, New Mexico: New Mexico Bureau of Geology and Mineral Resources, Open-file Geologic Map XX, scale 1:24,000.
Ricketts, J.W., Kelley, S.A., Karlstrom, K.E., Schmandt, B., Donahue, M.S., and van Wijk, J., 2016, Synchronous opening of the Rio Grande rift along its entire length at 25-10 Ma supported by apatite (U-Th)/He and fission-track thermochronology, and evalution of possible driving mechanisms: Geological Society of America Bulletin, v. 128, no 3/4, p. 397-424; doi:10.1130/B31223.1.
Osburn, G.R., and Chapin, C.E., 1983, Nomenclature for Cenozoic rocks of northeast Mogollon-Datil volcanic field, New Mexico: New Mexico Bureau of Mines and Mineral Resources, Stratigraphic Chart 1.
Seager, W.R., and Mack, G.H., 2003, Geology of the Caballo Mountains, New Mexico: New Mexico Bureau of Geology and Mineral Resources Memoir 49, 136 p.
Semken, S.C., 2001, The Navajo volcanic field, *in* Crumpler, L.S., and Lucas, S.G., eds., Volcanology of New Mexico: New Mexico Museum of Natural History and Science Bulletin, p. 79-83.
Smith, G.A., 2004, Middle to late Cenozoic development of the Rio Grande rift and adjacent regions in northern New Mexico, *in* Mack, G.H., and Giles, K.A., eds., The Geology of New Mexico, A Geologic History: New Mexico Geological Society, Special Publication 11, p. 331-358.
Smith, L.N., and Lucas, S.G., 1991, Stratigraphy, sedimentology, and paleontology of the lower Eocene San Jose Formation in the central portion of the San Juan Basin, northwestern New Mexico: New Mexico Bureau of Geology and Mineral Resources, Bulletin 126, 44 p.
Tedford, R.H., 1981, Mammalian biochronology of the late Cenozoic basins of New Mexico: Geological Society of America Bulletin, Part 1, v. 92, p. 1008-1022.
Tedford, R.H., 1982, Neogene stratigraphy of the northwestern Albuquerque basin: New Mexico Geological Society, Guidebook 33, p. 273-278.
Tedford, R.H., and Barghoorn, S., 1997, Miocene mammals of the Española and Albuquerque basins, north-central New Mexico: New Mexico Museum of Natural History and Science Bulletin No. 11, p. 77-95.
Tedford, R.H., and Barghoorn, S., 1999, Santa Fe Group (Neogene), Ceja del Puerco, northwestern Albuquerque basin, Sandoval County, New Mexico: New Mexico Geological Society, Guidebook 50, p. 327-335.
Tedford, R.H., Skinner, M.F., Fields, R.W., Rensberger, J.M., Whistler, D.P., Galusha, T., Taylor, B.E., Macdonald, J.R., and Webb, S.D., 1987, Faunal succession and biochronology of the Arikareean through Hemphillian interval (late Oligocene through earliest Pliocene epochs) in North America, *in* Woodburne, M.D., eds., Cenozoic mammals of North America, geochronology and biostratigraphy: Berkeley, University of California Press, p. 153-210.
Timmer, R.W., 1976, Geology and sedimentary copper deposits in the western part of the Jarosa and Seven Springs quadrangles, Rio Arriba and Sandoval Counties, New Mexico [M.S. thesis]: Albuquerque, University of New Mexico, 151 p.
Trevena, A.S., 1979, Studies in sandstone petrology: Origin of the Precambrian Mazatzal Quartzite and provenance of detrital feldspar [Ph.D. dissertation]: Salt Lake City, University of Utah, 316 p.
Vazzana, M.E., and Ingersoll, R.V., 1981, Stratigraphy, sedimentology, petrology, and basin evolution of the Abiquiu Formation (Oligo-Miocene), north-central New Mexico: Summary: Geological Society of America Bulletin, v. 92, Part I, p. 990-992, Part II, p. 2401-2483.
Williams, P.L., and Cole, J.C., 2007, Geologic map of the Albuquerque 30' X 60' Quadrangle, north-central New Mexico: United States Geologic Survey, Scientific Investigations Map 2946, scale 1:100,000.
Wisniewski, P., and Pazzaglia, F.J., 2002, Epeirogenic controls on Canadian River incision and landscape evolution, Great Plains of northeastern New Mexico: Journal of Geology, v. 110, p. 437-456, doi: 10.1086/340441.
Wright, H.E., Jr., 1946, Tertiary and Quaternary geology of the lower Rio Puerco area, New Mexico: Geological Society of America Bulletin, v. 57, p. 383-456.
Wright, H.E., Jr., 1956, Origin of the Chuska Sandstone, Arizona-New Mexico: A structural and petrographic study of a Tertiary eolian sediment: Geological Society of America Bulletin, v. 67, p. 413-434, doi: 10.1130/0016-7606(1956)67[413:OOTCSA]2.0CO;2.

Supplemental data can be found at http://nmgs.nmt.edu/repository/index.cfml?rid=2020005

New Mexico Geological Society, Special Publication 14, Geology of the Mount Taylor Area, 2020, p. 167-175.

HORIZONTAL SHORTENING OF THE LARAMIDE ZUNI ARCH, WEST-CENTRAL NEW MEXICO: A PRELIMINARY STUDY

Jacob O. Thacker

New Mexico Bureau of Geology and Mineral Resources, 801 Leroy Place, Socorro, NM 87801; jacob.thacker@nmt.edu

Abstract—The Zuni Mountains are an anticlinal Laramide arch with marked asymmetry along its southwestern forelimb (Nutria monocline), a low-elevation basement-involved range crest, and a gentle northeast-dipping backlimb (Chaco Slope). However, the range exhibits considerable along-strike complexity at odds with this simplistic framework. In the northwest Zuni arch, folds are southwest vergent, and the two dominant reverse faults, the Stinking Springs and McGaffey faults, strike north to northwest and exhibit east to northeast dips. In the southeast Zuni arch, the dominant fold pattern is northeast vergent and the Sedgwick reverse fault is largely north-northwest striking and exhibits a west to southwest dip. Minor fault data (strike-slip, conjugate strike-slip, and thrust) from these northwest and southeast domains show that early horizontal shortening preceded significant folding and faulting, as suggested by restoring bedding to horizontal, and both domains share similar geometric and kinematic results despite opposing fault polarities and variably-striking (i.e., E-W or N-S) beds from which minor faults are documented. Similarly, both domains and the range record WSW-ENE directed shortening (051–073° azimuth; 061° mean azimuth) that is consistent with estimates of shortening on numerous other Laramide arches in the Colorado Plateau and Rocky Mountains. Comparable shortening azimuths suggest that deformational processes between the Colorado Plateau and Rocky Mountain regions during the Late Cretaceous–Paleogene were similar, and therefore ENE horizontal shortening is the likely means by which the Zuni arch deformed during Laramide orogenesis. These results and interpretations are not in accord with previously suggested models for Zuni arch formation by mass transfer and/or Eurasian-style extrusion tectonics.

INTRODUCTION

The Zuni Mountains (Fig. 1), located between Gallup, Ramah, and Grants, New Mexico, are a structural arch (the "Zuni arch") that formed during the Cretaceous–Paleogene Laramide orogeny (Kelley, 1967). The range is in part a reactivated portion of the earlier and likely larger Zuni-Defiance uplift that formed during the Pennsylvanian–Permian Ancestral Rocky Mountains orogeny (Ross and Ross, 1986). Although the Zuni arch comprises one of the classic Laramide structures of the Colorado Plateau, its deformation history and structural characteristics have received comparatively little attention. Complex deformation is observed throughout the range in the form of (1) opposing reverse fault polarities at either end of the range, (2) a sinuous range crest, and (3) numerous faults of variable orientation. The preliminary dataset presented herein seeks to address some of this complexity by analyzing the geometry and kinematics of a handful of minor faults in post-Pennsylvanian (post-Ancestral Rocky Mountains) rocks across the Zuni Mountains. Many fault kinematic studies have been conducted in both the Colorado Plateau (e.g., Bump and Davis, 2003; Bump, 2004) and the Rocky Mountains (e.g., Erslev and Koenig, 2009; Weil and Yonkee, 2012; Singleton et al., 2019) and provide a base by which to analyze the Zuni arch with similar methods and to compare the results with a regional dataset. Such work has implications for Laramide deformation on the Colorado Plateau, the connection (in space, time, and style) of Colorado Plateau Laramide arches to their larger Rocky Mountain counterparts, and, overall, the tectonic processes responsible for intracontinental strain that formed Laramide arches of the interior western United States.

Past studies on the Zuni arch have evoked markedly different interpretations than those presented in this paper, warranting future research on the range. For example, Anderson et al. (2003) suggested initial vertical uplift via mid- to lower-crustal mass transfer followed by later horizontal shortening for the northwestern Zuni Mountains, an idea that is tested in this paper through structural analysis. Additionally, Chamberlin and Anderson (1989) also utilized fault slickenline data at a number of locations around the range to suggest that the Zuni Mountains formed by Eurasian style extrusion tectonics related to a rigid mid-crustal mafic anomaly south of the south-central Zuni arch. Chamberlin and Anderson (1989) postulated that this mafic "indenter" pushed the southeast Zuni Mountains up north/northeastward and laterally extruded the northwest Zuni Mountains westward, as expressed through numerous strike-slip and reverse faults within the range. This kinematic model is tested in this paper. Mafic crustal anomalies are of interest in other parts of the Laramide foreland (e.g., Bighorn arch, Wyoming: Worthington et al., 2016), and their role in localizing upper crustal strain warrants consideration. This paper builds on these previous works with an expanded dataset on a diverse array of fault types in different parts of the range and comes to a different conclusion for the tectonic processes that formed the Zuni arch.

In short, two objectives are addressed in this paper:

1. What is the structural framework of the Zuni Mountains (fault geometries and kinematics), and what might be the cause of structural complexity observed?
2. What was the shortening direction responsible for deformation? Is it consistent at each end of the range? How does it compare to other Laramide arches and what does it imply for the tectonic processes that drove deformation?

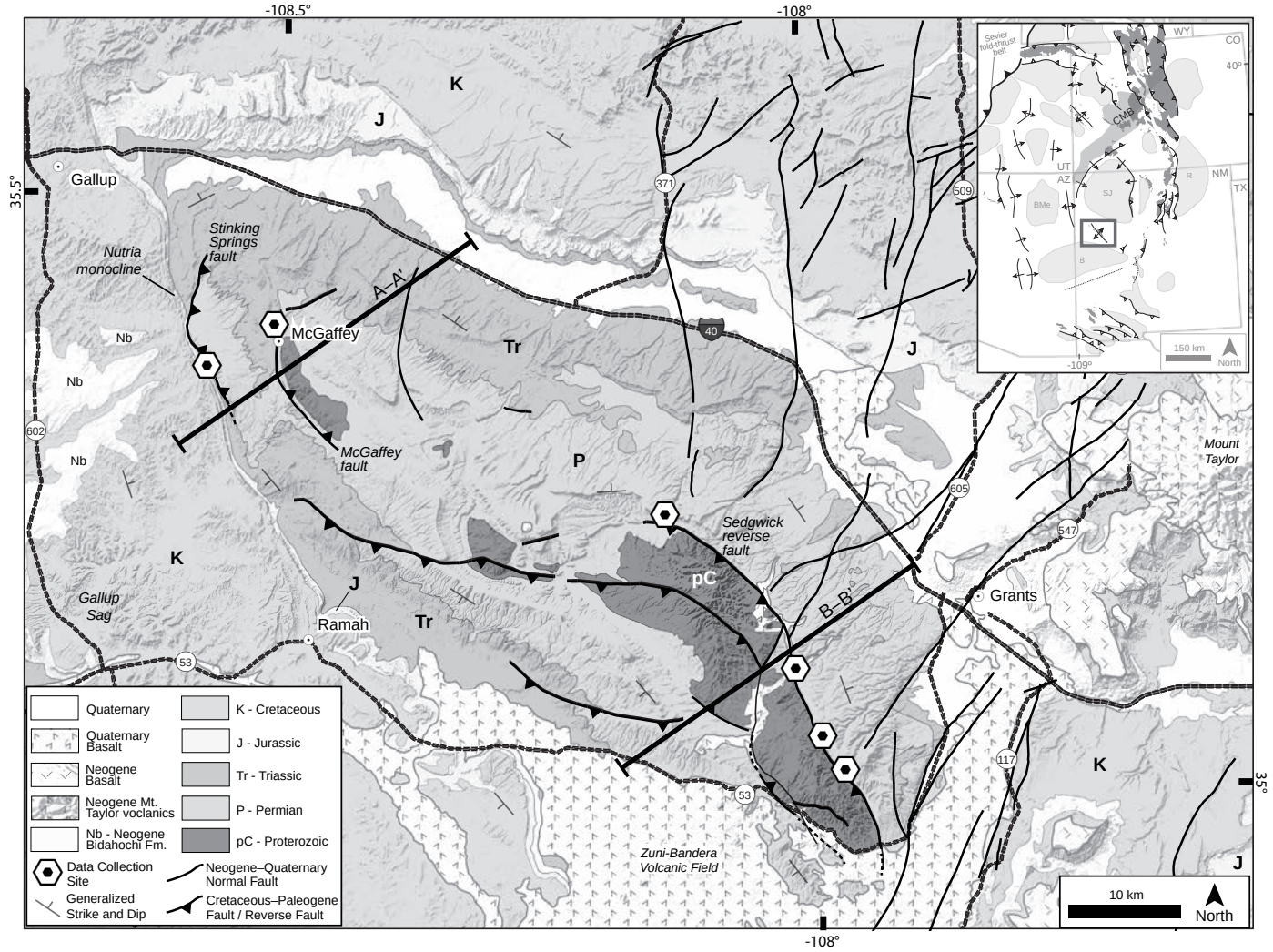

FIGURE 1. Simplified geologic map of the Zuni Mountains showing cross section locations (Fig. 2) and data collection sites. Inset map shows relative position of the Zuni arch in the southern Laramide foreland region. B – Baca basin; BMe – Black Mesa basin; R – Raton Basin; SJ – San Juan Basin; CMB – Colorado Mineral Belt. Geologic map data modified from Green and Jones (1997).

To address these questions, preliminary geometric and kinematic data and paleostrain analyses are presented in order to characterize fault geometries and to infer the orientation of Laramide shortening. Zuni arch data show characteristic fault geometries and a mean shortening azimuth of 061°. The estimated shortening direction is consistent with other Laramide arches across the Colorado Plateau and Rocky Mountain regions from Montana–South Dakota to Arizona–New Mexico, and suggests of a common deformational process that was pervasive throughout the entire Laramide foreland. Lastly, the structural data is used to address some of the complex deformation exhibited by the Zuni arch, namely opposing reverse fault polarities at each end of the range. It is hypothesized that a zone of sinistral displacement transfer accommodated strain between these two opposing domains (northwest and southeast), although there are currently insufficient data to fully make this claim. Future work will help to test this hypothesis, as well as other unanswered structural questions related to the Zuni arch.

GEOLOGIC SETTING AND LARAMIDE STRUCTURAL FRAMEWORK

The Zuni Mountains are situated on the southeastern Colorado Plateau and form the southwestern margin of the San Juan Basin, the northern margin of the Baca basin, and the eastern margin of the Gallup sag (Fig. 1; Cather, 2004). Proterozoic basement rock is exposed at four localities and, within the southeastern Zuni Mountains, is dated at ca. 1630 and ca. 1430 Ma (Strickland et al., 2003). Basement rock in the region was uplifted and exposed during the Pennsylvanian–Permian Ancestral Rocky Mountains orogeny as part of the larger Zuni-Defiance Uplift (Ross and Ross, 1986) and was subsequently buried by late Paleozoic through Mesozoic sedimentation. Western Interior Cretaceous Seaway sedimentation started with deposition of the Upper Cretaceous Dakota Sandstone. Structural partitioning of the San Juan Basin took place in the Late Cretaceous–Paleogene Laramide orogeny and resulted in a change to localized Paleocene–Eocene basin-fill sedimentation (Cather, 2004).

Commonly considered to be the result of flat slab subduction of the Farallon plate (Coney and Reynolds, 1977; Dickinson and Snyder, 1978), the Laramide orogeny was responsible for the formation of large basement involved ("thick skinned") arches and deep intermontane basins throughout the interior western United States, as presently exposed from Montana–South Dakota to southern Arizona–New Mexico. In west-central New Mexico, Laramide deformation may have commenced ca. 80–75 Ma, based on northeast-directed paleoflow indicators that suggest a paleohighland developing in the vicinity of the Defiance Mountains (Arizona–New Mexico state line) and Zuni Mountains (Cather, 2004). Inversely modeled apatite fission-track and apatite (U-Th)/He thermochronology data similarly suggest deformation of the Zuni arch commenced ca. 84–77 Ma (Thacker et al., unpubl. data).

Structurally, the Zuni arch encompasses a greater area than the present physiographic expression of the Zuni Mountains. The arch forms an overall NW-SE–striking, basement-involved, doubly plunging anticline with sharp forelimb asymmetry to the southwest along the Nutria monocline (Figs. 1, 2A; Darton, 1928; Edmonds, 1961) and a gentle northeast-dipping backlimb (Chaco Slope). The Zuni range crest is sinuous, and trends northwesterly in the northwest, easterly in the central part of the range, and again northwesterly in the southeast part of the range (Fig. 1). Although the overall structure is that of a southwest-facing asymmetric arch, the Zuni Mountains display marked along-strike complexity. Range-scale cross sections (Figs. 2A, B) and the simplified geologic map (Fig. 1) display a clear change in reverse fault polarity and fold vergence from the northwestern to southeastern Zuni arch. In the northwest, northeast-dipping reverse faults at the range front and near the town of McGaffey, New Mexico (Stinking Springs and McGaffey faults, respectively) create a southwest-facing asymmetric anticline with a more gently dipping backlimb (Fig. 2A). In the southeast, asymmetry is to the northeast via the southwest-dipping Sedgwick reverse fault (Fig. 2B; as shown by Goddard, 1966 and Timmons and Cikoski, 2012), although smaller-scale northeast-dipping reverse faults core southwest-vergent folds on the southwest side of the range here (Figs. 1, 2B). The central Zuni arch is characterized by easterly-striking faults, consistent with the easterly-trending range crest (Fig. 1). Numerous faults and folds are present (e.g., Hackman and Olson, 1977) that are attributable to Laramide deformation and make for a dense and complex array of faults throughout the range.

Late Cenozoic normal faults are evident in the study area, dominantly on the eastern part of Zuni arch (Fig. 1). These faults may represent the western extreme of the Rio Grande rift, Jemez Lineament volcanism and/or igneous intrusions, or some combination of each, but the structures are more likely reactivated Laramide faults related to the northern Hickman fault zone (Cather, 1990). Normal faults are approximately N-S to NNE-SSW striking. Extensional faults have not significantly affected the range, though notable exceptions do occur (e.g., near Zuni Canyon; Fig. 2B). Faults in the southeastern part of the range are coincident with Cenozoic basalt flows and cinder cone volcanoes of the Zuni-Bandera volcanic field.

METHODS

Geometric and kinematic structural data were collected dominantly from brittle minor faults (strike-slip, conjugate strike-slip, and thrust) and fractures in Permian Abo Formation through Upper Cretaceous Gallup Sandstone in the northwest-

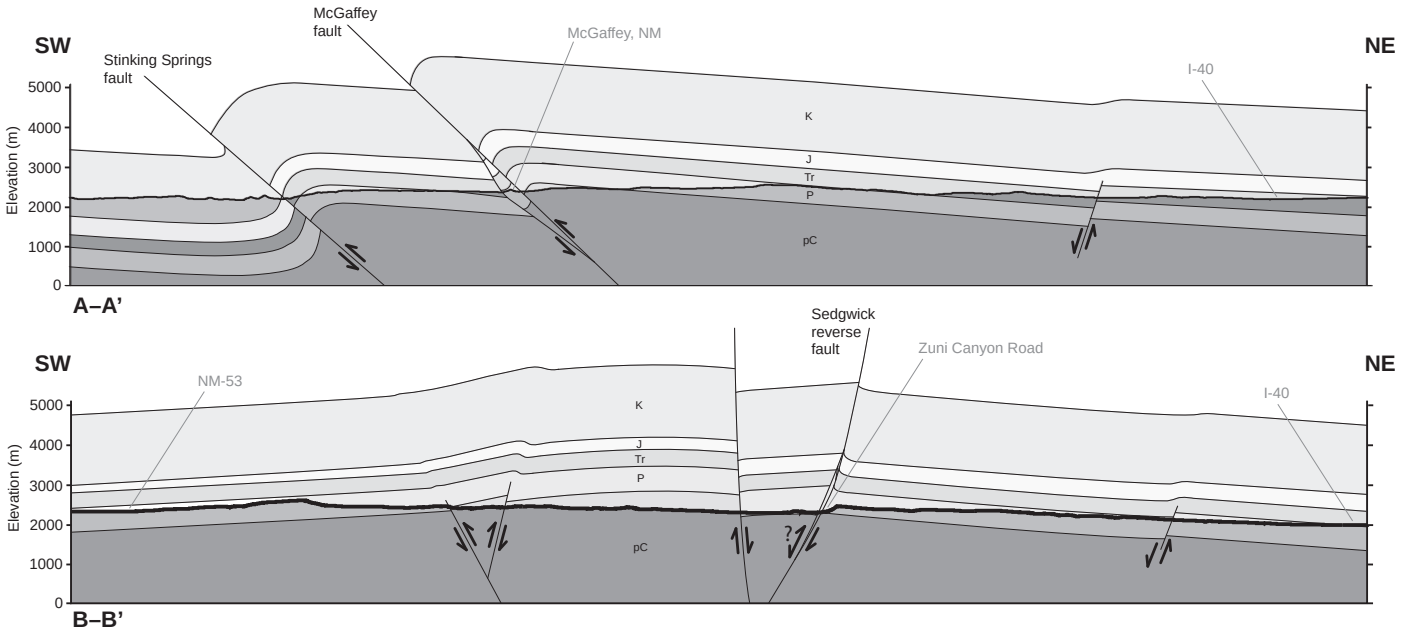

FIGURE 2. Admissible range-scale cross sections (locations shown in Fig. 1) of the Zuni Mountains (no vertical exaggeration). **A**) Northwest Zuni Mountains. Note range asymmetry to southwest. **B**) Southeast Zuni Mountains. Note complexity in deformation compared to northwest Zuni Mountains and change in dominate thrust polarity along the Sedgwick reverse fault.

ern and southeastern parts of the range (Fig. 1). Most minor fault data were collected near map-scale faults (Fig. 1). Pennsylvanian (and possibly older) units were largely stripped from the range during the Ancestral Rocky Mountains orogeny; minor faults in Pennsylvanian units are exposed in select localities throughout the range (Bursum Formation; Timmons and Cikoski, 2012) but were excluded to avoid collecting data from faults that formed during this earlier contractional episode. All post-Pennsylvanian minor faults were considered to have formed during the Late Cretaceous because of a lack of contractional tectonism for the region between the late Permian–Early Cretaceous. Bedding orientations were measured at every data collection site for retrodeformation of minor fault data and ranged between 15°–68° dip and N-S to E-W strike. Minor fault slip sense was determined using kinematic criteria outlined by Petit (1987) or through observable outcrop displacements (Fig. 3). In many instances, conjugate fault and fracture sets were observed that lacked slip-sense criteria, although their relative slip sense could be assumed based on their geometry (e.g., conjugate) and/or nearby conjugate faults of comparable orientation that exhibited positively identifiable slip-sense criteria.

The programs Stereonet (Allmendinger et al., 2012; Cardozo and Allmendinger, 2013) and FaultKin (Marrett and Allmendinger, 1990; Allmendinger et al., 2012) were used to process and analyze structural data. For geometric data (Fig. 3), Stereonet was used to calculate a cylindrical best fit from poles to planes in order to determine statistically significant populations and mean planes from eigenvalue statistics (Vollmer, 1990), as well as the acute bisector (σ_1: maximum shortening direction) for restored conjugate fault populations. Kamb contours were calculated from restored poles to planes using a contour interval of 2σ and a significance level of 1σ. For kinematic data (Fig. 4), FaultKin was used to invert restored minor fault data to model paleostrain axes from eigenvalue statistics on P- and T-axes (Marrett and Allmendinger, 1990). Separate paleostrain analyses are presented that both exclude and include the assumed slip-sense data discussed above. Shortening azimuth results (Table 1) were plotted as a rose diagram to show a mean shortening azimuth from all Zuni minor fault data (Fig. 5).

STRUCTURAL ANALYSIS

Geometric Analysis

Structural data are presented for the northwest and southeast domains and for the range as

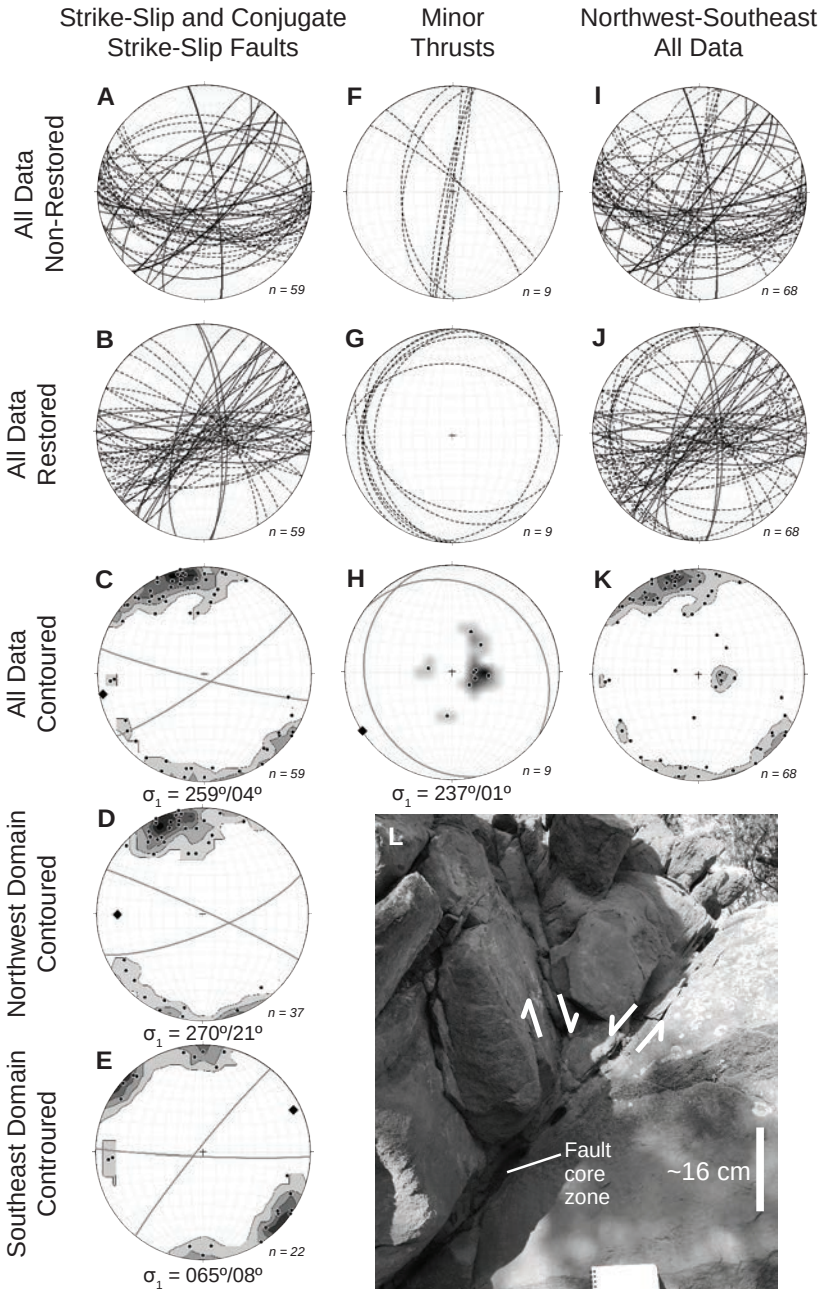

FIGURE 3. Preliminary geometric data and contoured poles to planes on lower hemisphere equal area stereonets. Dashed lines represent northwest domain; solid lines represent southeast domain. **A–E**) Conjugate strike-slip and strike-slip minor fault data. **A**) Non-restored (raw) data. **B**) Data restored to horizontal. **C**) Kamb contoured stereonet, mean planes (gray lines), and acute bisector (black diamond) of all restored conjugate strike-slip and strike-slip minor fault data for the entire Zuni Mountains. **D**) Kamb contoured stereonet, mean planes (gray lines), and acute bisector (black diamond) of restored conjugate strike-slip and strike-slip minor fault data from the northwest domain. **E**) Kamb contoured stereonet, mean planes (gray lines), and acute bisector (black diamond) of restored conjugate strike-slip minor fault data from the southeast domain. **F–H**) Minor thrust-fault data. **F**) Non-restored data. **G**) Restored data. **H**) Kamb contoured stereonet, mean planes (gray lines), and acute bisector (black diamond) of restored minor thrust data points. **I–K**) All data from both domains. **I**) Non-restored data. **J**) Restored data. **K**) Kamb contoured stereonet of all restored data. **L**) Example conjugate fault set used for data collection: looking up at small displacement conjugate fault set in Abo Formation sandstone in the southeast Zuni Mountains.

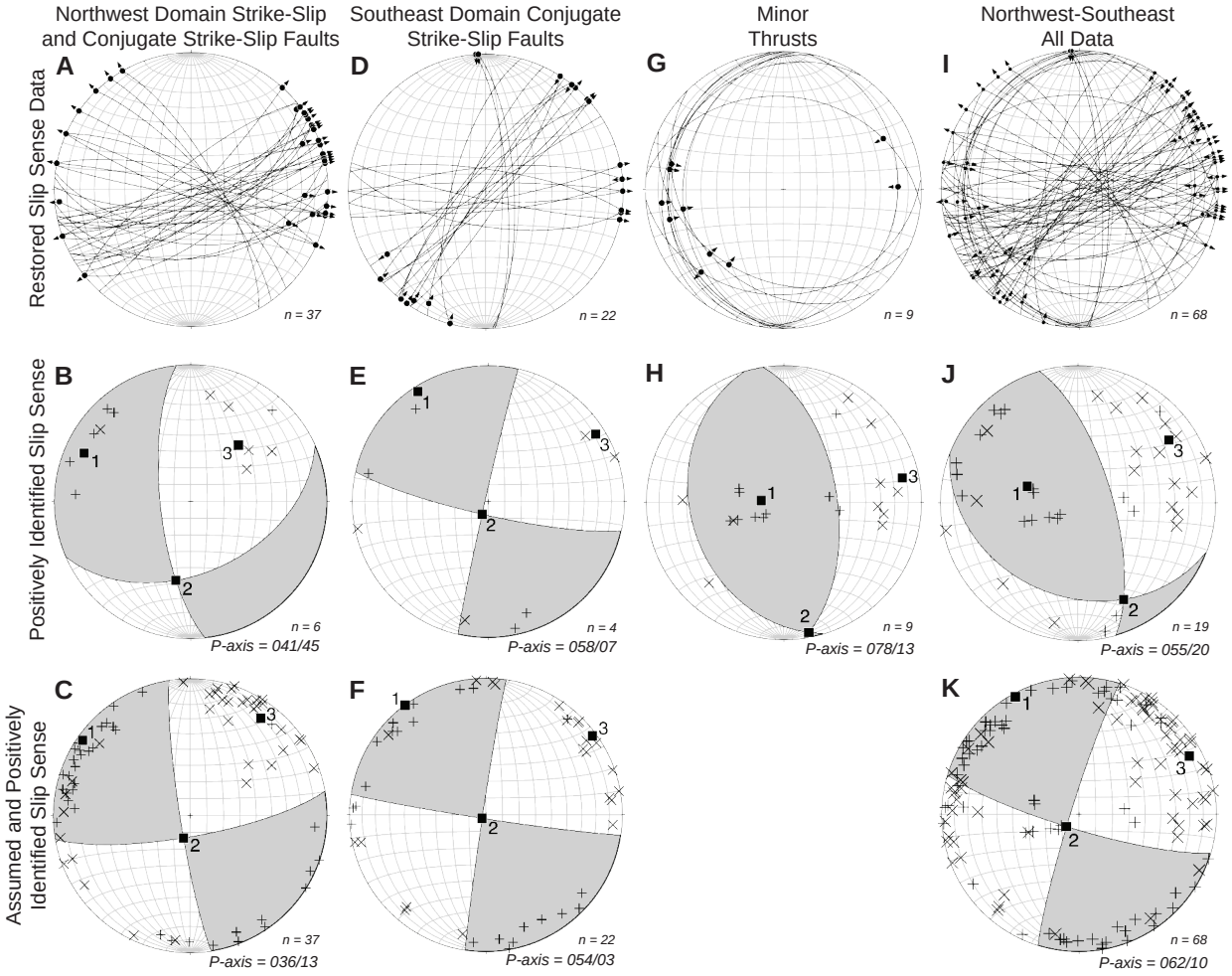

FIGURE 4. Preliminary kinematic data and paleostrain analyses. Arrows show hanging wall slip direction. Crosses (Xs) represent P (compressional) axes; pluses (+s) represent T (dilational) axes. **A–C**) Strike-slip and conjugate strike-slip minor fault data from the northwest domain. **A**) Restored kinematic data. **B**) Paleostrain analysis for only data with positively identified slip sense. **C**) Paleostrain analysis for data with positively identified slip sense and with assumed slip sense. **D–F**) Conjugate strike-slip fault data from the southeast domain. **D**) Restored kinematic data. **E**) Paleostrain analysis for only that data with positively identified slip sense. **F**) Paleostrain analysis for data with positively identified slip sense and with assumed slip sense. **G–H**) Minor thrust data from the northwest domain. **G**) Restored kinematic data. **H**) Paleostrain analysis for minor thrust data (all positively identified slip sense). **I–K**) Data from both domains and for all faults. **I**) Restored kinematic data. **J**) Paleostrain analysis for data with positively identified slip sense. **K**) Paleostrain analysis for data with positively identified slip sense and with assumed slip sense.

a whole in Figure 3 (geometric data) and Figure 4 (kinematic data and paleostrain analyses). All structural data required retrodeformation to a horizontal datum. In all cases, unrestored data displayed an incoherent geometry, whereby restoration to pre-deformation horizontal resulted in coherent fault/fracture geometries (e.g., conjugate), suggesting that these faults formed early in the deformation history prior to considerable strain accumulation (folding and faulting).

The majority of data were collected on strike-slip and conjugate strike-slip minor faults and fractures (Figs. 3A, B). Two dominant pole populations for all strike-slip data are observed that give mean planes of 055°, 83°SE and 104°, 86°S with an acute bisector of trend/plunge (T/P) = 259°/04° (Fig. 3C). Separating conjugate strike-slip faults and fractures into domains produces similar results. Northwest domain strike-slip and conjugate strike-slip minor faults and fractures were collected from Permian and Triassic units within a fault sliver near McGaffey (Figs. 1, 2A). The contoured plot exhibits mean planes of 068°, 76°SE and 295°, 87°NE with an acute bisector of T/P = 270°/21° (Fig. 3D). Southeast domain conjugate strike-slip minor faults and fractures were collected dominantly from the Permian Abo Formation, with mean planes oriented 219°, 86°NW and 092°, 87°S with an acute bisector of T/P = 065°/08° (Fig. 3E).

Minor thrust-fault data (Figs. 3F, G) comprise a small amount of the dataset (n = 9) and were collected only from the northwest domain near McGaffey in the Permian Glorieta Sandstone and Triassic units, as well as at the range front along Forest Service Road 10 within the Cretaceous Gallup Sandstone (Fig. 1). The contoured stereonet results in mean planes oriented 307°, 19°NE and 165°, 20°SW with an acute bisector of T/P = 237°/01° (Fig. 3H).

All data collected for the entire range (Figs. 3I, J) includes strike-slip, conjugate strike-slip, and minor thrust faults. The contoured stereonet in Figure 3K displays seven populations

TABLE 1. Summary table of all shortening azimuths estimated from geometric and kinematic minor fault data (shown in Figs. 3–4). NW: northwest; SE: southeast.

Dataset	Trend	Plunge	Value Type	Analysis Type
All Conjugate Faults (NW and SE Domains) – Fig. 3C	259	04	Acute bisector	Geometric
NW Domain Strike-slip/Conjugate Strike-slip Faults – Fig. 3D	270	21	Acute bisector	Geometric
SE Domain Conjugate Strike-slip Faults – Fig. 3E	065	08	Acute bisector	Geometric
Minor Thrust Faults – Fig. 3H	237	01	Acute bisector	Geometric
NW Domain Strike-slip/Conjugate Strike-slip Faults (Positively Identified Slip Sense) – Fig. 4B	041	45	P-axis (e3*)	Kinematic
NW Domain Strike-slip/Conjugate Strike-slip Faults (With Assumed Data) – Fig. 4C	036	13	P-axis (e3)	Kinematic
SE Domain Conjugate Faults (Positively Identified Slip Sense) – Fig. 4E	058	07	P-axis (e3)	Kinematic
SE Domain Conjugate Faults (With Assumed Data) – Fig. 4F	054	03	P-axis (e3)	Kinematic
Minor Thrust Faults – Fig. 4H	078	13	P-axis (e3)	Kinematic
All Data (Positively Identified Slip Sense) – Fig. 4J	055	20	P-axis (e3)	Kinematic
All Data (With Assumed Data) – Fig. 4K	062	10	P-axis (e3)	Kinematic

* Eigenvector e3 from calculated kinematic P-axes

of poles to planes. These populations are consistent with conjugate fault geometries (two dominant populations with pole populations at north/south and NW/SE), low-angle fault geometries (central population of poles), and high-angle fault geometries (pole populations at west and southwest). A σ_1 estimate is not provided for these data given the variety of fault types.

Kinematic and Paleostrain Analyses

Minor faults with positively identified slip sense comprise ~28% of kinematic data. However, at many locations slip sense could be assumed based on systematic geometries (i.e., conjugate) and/or positively identified slip sense on nearby conjugate faults of similar orientation. Results for data with both positively identified slip sense and assumed slip sense are presented separately for comparison to check the suitability of these assumptions (Fig. 4). In the rotated data in Figure 4, most data with slip lineations along the primitive (outside) circle are assumed with an idealized plunge of 00°.

Strike-slip and conjugate strike-slip minor faults from the northwest domain (Fig. 4A) make up the majority of the currently-available dataset. A paleostrain analysis for positively identified slip-sense data (Fig. 4B) results in a strike-slip fault plane solution with significant oblique slip, and a P-axis oriented T/P = 041°/45°. The paleostrain plot that includes assumed slip-sense data results in a strike-slip fault plane solution with minor oblique slip and a P-axis oriented T/P = 036°/13° (Fig. 4C). Southeast domain conjugate strike-slip minor faults display a clear conjugate geometry (Fig. 4D). Positively identified conjugate strike-slip faults from the southeast domain were collected from bedding with an average orientation of 288°, 50°N, and result in a strike-slip fault plane solution with a P-axis oriented T/P = 058°/07° with minimal oblique slip (Fig. 4E). The southeast domain fault plane solution that includes assumed slip-sense data is strike-slip with a P-axis of T/P = 054°/03° (Fig. 4F). In both the northwest and southeast domains, paleostrain results from positively identified (non-assumed) slip-sense data and assumed slip-sense data produce similar P-axes within 005° azimuth, although appreciable variability in plunge is observed. P-axes compared to acute bisectors from geometric data are markedly different for the northwest domain, although southeast domain P-axis and geometric acute bisector estimates are similar.

Minor thrust-fault data collected from the northwest domain comprises 13% of the overall dataset (Fig. 4G). All kinematic data collected were observed at the outcrop (i.e., no assumed data). Paleostrain analysis results in a thrust-fault plane solution with negligible to very minor oblique slip and a P-axis oriented T/P = 078°/13° (Fig. 4H). The kinematic results show moderate variance with the geometric estimate for shortening (Fig. 3H).

Data from both the northwest and southeast domains include minor strike-slip, conjugate strike-slip, and thrust minor faults (Fig. 4I). Data with positively identified slip sense (Fig. 4J) produce an overall thrust-fault plane solution – given the large amount of thrust-fault data – with marked oblique slip

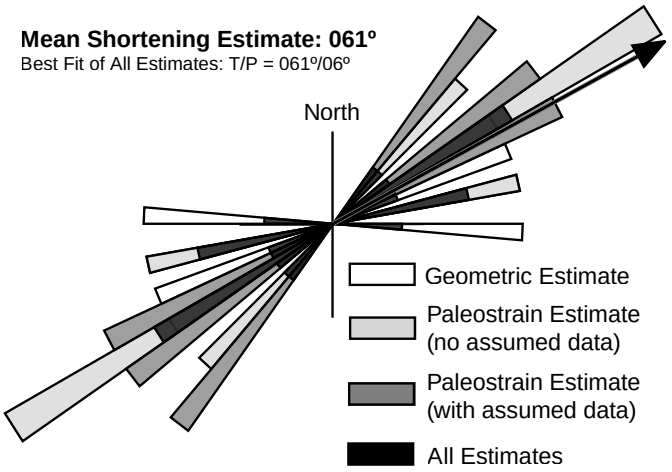

FIGURE 5. Rose diagram showing all shortening azimuths from Table 1 (and text), color-coded by data type. Petals are in 5° increments and scaled to 50% of total perimeter. The mean shortening azimuth (black arrow) is 061°; unique datasets ranged between 051–073° azimuth. A cylindrical best fit of all lineations is trend/plunge (T/P) = 061°/06°.

and a P-axis oriented T/P = 055°/20°. Using both assumed and positively identified slip-sense data produces a strike-slip fault plane solution with minor obliquity (Fig. 4K) – given the large amount of strike-slip fault data – and a P-axis oriented T/P = 062°/10°. Similar P-axis trends are observed for both assumed slip-sense and observed slip-sense data.

DISCUSSION

Laramide Horizontal Shortening and Zuni Arch Formation

Despite opposing reverse-fault polarities between the northwest and southeast domains, preliminary geometric and kinematic data from both parts of the range produce similar results when restored to pre-deformation horizontal. Geometrically, minor strike-slip and conjugate strike-slip faults display ~NE-SW and E-W to ESE-WNW strikes and near-vertical dips (Figs. 3C, D, E). Kinematically, NE-SW and E-W striking planes equate to dextral and sinistral slip, respectively, as shown by paleostrain analyses (Figs. 4B–C, E–F, J–K) that are consistent with field observations. Minor thrust faults show overall N-S and WNW-ESE strikes, although it is important to note the shallow dips of these data (~20°). Given the shallow dip, minor thrust data may actually represent Riedel R or P minor faults rather than true thrust faults, although similarly shallow conjugate thrust faults have been documented in other Laramide deformation studies (e.g., Singleton et al., 2019). Kinematic analysis of minor thrust data shows NNW-SSE striking dip slip low- and moderate-angle nodal planes (Fig. 4H). Continued data collection will produce a more robust mean estimate for all faults, especially minor thrust faults, and will give preference to minor faults that exhibit shear sense criteria. Overall, it is notable that minor fault geometries are similar between the northwest and southeast domains and for the range as a whole.

Shortening directions are geometrically estimated from the acute bisector ($\sigma 1$) of conjugate strike-slip minor faults in all geometric data (Fig. 3) and kinematically estimated from P-axes utilizing both positively identified slip-sense data and assumed slip-sense data (Fig. 4). Shortening azimuths from both geometric and kinematic datasets show similar results, as synthesized in Table 1. A rose diagram of all geometric and kinematic shortening estimates (Fig. 5) produces a mean shortening azimuth of 061°. A cylindrical best fit to all shortening lineation estimates is T/P = 061°/06°. The mean shortening estimate for each data type ranges between 051–073° azimuth. Collection of these data from NNE-SSW, N-S, NNW-SSE, and ENE-WSW striking beds shows that the shortening estimate does not reflect preferential sampling and further suggests that results record early horizontal shortening that preceded significant strain accumulation (i.e., formed prior to significant folding and faulting). Continued data collection will likely diminish the spread shown by the Figure 5 rose diagram. However, the shortening azimuth provided here from preliminary data is consistent with early suggestions of 060° shortening for the southern San Juan Basin and Zuni arch (Smith, 1957).

WSW-ENE shortening has been documented on a variety of Laramide structures throughout the Colorado Plateau and Rocky Mountain regions from Montana–South Dakota to northern Arizona–New Mexico (Bump and Davis, 2003; Bump, 2004; Erslev and Koenig, 2009; Weil and Yonkee, 2012; Singleton et al., 2019). It is interesting to note the remarkable similarity in average shortening azimuths across the entire expanse of the Laramide foreland region as exemplified by an array of researchers, methods, and datasets, although some variability has been mentioned (e.g., ~N-S shortening: Craddock and van der Pluijm, 1999). This is especially true when comparing the results herein with shortening estimates from the most distal Laramide arch, the Black Hills in South Dakota–Wyoming, and its documented mean shortening azimuth of ~068° (Singleton et al., 2019). Similar Late Cretaceous–Paleogene mean shortening directions for numerous Laramide arches suggests (1) a consistent regional shortening direction for the entire Laramide foreland and (2) that Laramide structures, although variably oriented, likely formed from pervasive WSW-ENE-directed shortening. Perseverance of this shortening direction across the Colorado Plateau and Rocky Mountain regions also, by extrapolation, suggests similar formational processes for Laramide structures in both of these distinct provinces, despite marked structural differences (namely less accumulated strain on Colorado Plateau structures).

Other mechanisms cited for formation of the Zuni arch are less attractive in light of a regionally consistent shortening direction and observation of early horizontal shortening. The structural complexity called upon by Chamberlin and Anderson (1989, Fig. 3) as evidence for Eurasian style extrusion tectonics is more likely attributable to variable reactivation of older faults from Proterozoic extension and/or contractional orogenesis related to the Ancestral Rocky Mountains. Reactivation would have been within a simple WSW-ENE shortening direction. Furthermore, similar fault geometries and shortening estimates from both ends of the range are not consistent

with westward extrusion of the northwest Zuni Mountains, as different shortening estimates would be expected for each part of the range (e.g., west-oriented P-axes in the northwest and north- to northeast-oriented P-axes in the southeast). However, this does not negate the role that the interpreted mafic crustal anomaly (Chamberlin and Anderson, 1989) may have played on localizing upper crustal strain here. Preliminary results do, however, negate early vertical uplift followed by later horizontal shortening (Anderson et al., 2003). Early horizontal shortening was likely established prior to significant folding and faulting, as clear fault geometries are noted when data is restored to pre-deformation horizontal (Figs. 3B, G, J).

Hypothesized Role of Sinistral Faulting Within the Laramide Zuni Arch

East-striking faults mapped by Goddard (1966) at scale 1:31,680 and Hackman and Olson (1977) at scale 1:250,000 are coincident with the central portion of the range. Taking into consideration the kinematic results (Fig. 4) and WSW-ENE directed shortening (Fig. 5), east-striking faults in the Zuni arch would have been susceptible to sinistral slip during Laramide contraction. Sinistral slip between two oppositely directed reverse faults in the northwest (southwest-directed) and southeast (northeast-directed) domains is kinematically feasible, and would suggest that the central Zuni arch deformed via sinistral displacement transfer as strain from the northwest transferred to the southeast (or vice versa). Such kinematics have been suggested for the Laramide Beartooth arch in southwest Montana by impingement of the shallow crustal ultramafic-mafic Stillwater Complex along its north-central margin (Wise, 2000). Similar to the Zuni range, the northwest Beartooth arch is characterized by southwest-directed folds and faults (near Gardiner, Montana), while northeast-directed folds and faults characterize the southeast Beartooth arch (e.g., Red Lodge, Montana). Both ends are connected by a discrete structure, the Mill Creek-Stillwater fault zone, which may have localized sinistral displacement transfer. The similar structural framework and the possible role of mafic "indenters" (Stillwater Complex and El Morro Gravity High of Chamberlin and Anderson, 1989) suggest a potential commonality between Zuni and Beartooth arch formation whereby crustal heterogeneity may have localized and/or deflected upper crustal strain.

However, kinematic evidence in support of sinistral displacement transfer for the central domain is thus far lacking. The major easterly striking fault in the central portion of the Zuni Mountains (Fig. 1) was originally mapped by Goddard (1966) as a fault zone with silicified breccia and slickensided planes of 40° oblique dextral slip. This "fault" is actually a (Proterozoic?) pegmatite dike with no associated breccia zones or fault surfaces, based on field examination of this feature in the summer of 2019. More east to east-southeasterly striking faults are mapped by Goddard (1966) as sinistral within the central domain and in the southeast domain near New Mexico State Route 53. Additionally, Chamberlin and Anderson (1989) suggest that numerous easterly striking faults are sinistral on their Zuni Mountains tectonic map. Furthermore, northerly striking dextral faults (including the Sedgwick reverse fault) are kinematically viable considering the results presented in this study (e.g., Fig. 4K). Given these mapped structures and the preliminary results of this work, future studies will focus on easterly striking structures in the Zuni arch, especially within the central domain, to test the hypothesis of sinistral displacement transfer.

FUTURE WORK

The preliminary work presented here outlines a structural framework for the Zuni arch that can be expanded upon by future studies. Of first order importance is the accumulation of a larger and more comprehensive structural dataset that will better characterize fault geometries and kinematics and produce a robust estimate of Late Cretaceous–Paleogene shortening for the range. Secondly, the character of deformation and its kinematics in the central domain are of utmost interest for deciphering how strain transferred between the NE-dipping Stinking Springs and McGaffey reverse faults and the SW-dipping Sedgwick reverse fault. Inherently and in accord, distinct intra-range structural complexities are in need of attention to better understand both Laramide and Ancestral Rocky Mountains deformation.

The southeast Zuni Mountains highlight a key question: what is the role of the southwest dipping Sedgwick reverse fault? The pervasive dip of the Chaco Slope deep into the San Juan basin (e.g., Cather, 2004) would suggest that the controlling structure for the Zuni arch is a NE-dipping reverse/thrust fault. Therefore, it is possible that the Sedgwick reverse fault was a backthrust off a main thrust at depth (the "Zuni thrust"). Particularly interesting is the observation that the northwest Zuni Mountains are relatively more shortened, via the Nutria monocline bounding the Gallup sag, but are lower topographically, while the southeast Zuni Mountains are less shortened but more uplifted via the Sedgwick reverse fault, as shown by the expansive basement outcrop in the southeast and the topographic highpoint of Mt. Sedgwick. Assuming a northeast-dipping master thrust, a backthrusted Sedgwick reverse fault would have exploited an initially high structural level that then, through progressive deformation, produced a structurally higher although minimally deformed block via the Sedgwick reverse fault. Alternatively, the observed disparity could be related to warping related to the elevated temperatures along the Jemez lineament. These hypotheses can be tested through cross-section balancing and forward kinematic modeling.

CONCLUSIONS

Characteristic minor fault geometries and kinematics are documented in the Zuni arch that include NE-SW and E-W striking strike-slip and conjugate strike-slip faults and N-S to NNW-SSE striking reverse and thrust faults. Horizontal shortening was established early in the deformation history prior to significant folding and faulting. Fault geometries and kinematics are similar for both the northwest and southeast Zuni Mountains, despite marked differences in the structural style at both ends of the range. Geometric and kinematic analyses produce a

WSW-ENE-directed shortening estimate (061° mean azimuth) that is attributed to reflect the orientation of horizontal shortening responsible for formation of the Zuni arch, and is consistent with most shortening estimates from numerous Colorado Plateau and Rocky Mountain Laramide arches. Therefore, it seems likely that Laramide arches throughout the entire interior western U.S.A. formed from similar tectonic processes, and not from special and localized mechanisms that have been previously proposed for the Zuni arch (extrusion tectonics and vertical uplift). The structural framework and shortening azimuth may have been conducive for a zone of sinistral displacement transfer within the central part of the arch during Laramide deformation. Future work will address this hypothesis, as well as other aspects of the range's structural complexity.

ACKNOWLEDGMENTS

A portion of a UNM GPSA grant supported a portion of the fieldwork costs. This paper benefited from reviews by Dr. Jason Ricketts (UTEP), Dr. Steve Cather (NMBGMR), and Dr. Karl Karlstrom (UNM), and by the editors Drs. Shari Kelley and Kate Zeigler. Dan Young, Katie Holleron, and Shoshone-Nizhoni (Shoni) Dog were of great help in the field.

REFERENCES

Allmendinger, R.W., Cardozo, N., and Fisher, D.M., 2012, Structural Geology Algorithms: Vectors and Tensors: Cambridge, Cambridge University Press, 302 p.

Anderson, O.J., Maxwell, C.H., and Lucas, S.G., 2003, Geology of Fort Wingate quadrangle, McKinley County, New Mexico: New Mexico Bureau of Geology and Mineral Resources Open-File Report 473, scale 1:24,000, 15 p.

Bump, A.P., 2004, Three-dimensional Laramide deformation of the Colorado Plateau: Competing stresses from the Sevier thrust belt and the flat Farallon slab: Tectonics, v. 23, https://agupubs.onlinelibrary.wiley.com/doi/10.1029/2002TC001424.

Bump, A.P., and Davis, G.H., 2003, Late Cretaceous–early Tertiary Laramide deformation of the northern Colorado Plateau, Utah and Colorado: Journal of Structural Geology, v. 25, p. 421–440.

Cardozo, N., and Allmendinger, R.W., 2013, Spherical projections with OSX-Stereonet: Computers & Geosciences, v. 51, p. 193–205.

Cather, S.M., 1990, Stress and volcanism in the northern Mogollon-Datil volcanic field, New Mexico: Effects of the post-Laramide tectonic transition: Geological Society of America Bulletin, v. 102, p. 1447–1458.

Cather, S.M., 2004, Laramide orogeny in central and northern New Mexico and southern Colorado, *in* Mack, G.H., and Giles, K.A., eds., The Geology of New Mexico, A Geologic History: New Mexico Geological Society Special Publication 11, p. 203–248.

Chamberlin, R.M., and Anderson, O.J., 1989, The Laramide Zuni uplift, southeastern Colorado Plateau: A microcosm of Eurasian-style indentation-extrusion tectonics?: New Mexico Geological Society, Guidebook 40, p. 81–90.

Coney, P.J., and Reynolds, S.J., 1977, Cordilleran Benioff zones: Nature, v. 270, p. 641–644.

Craddock, J.P., and van der Pluijm, B.A., 1999, Sevier–Laramide deformation of the continental interior from calcite twinning analysis, west-central North America: Tectonophysics, v. 305, p. 275-286.

Darton, N.H., 1928, "Red beds" and associated formation in New Mexico, with an outline of the geology of the state: U.S. Geological Survey, Bulletin 794, no. 3, 298 p.

Dickinson, W., and Snyder, W.S., 1978, Plate tectonics of the Laramide orogeny: Geological Society of America, Memoir 151, p. 355-366.

Edmonds, J.R., 1961, Geology of the Nutria monocline, McKinley County, New Mexico [M.S. thesis]: Albuquerque, University of New Mexico, 100 p.

Erslev, E.A., and Koenig, N.V., 2009, Three-dimensional kinematics of Laramide, basement-involved Rocky Mountain deformation, USA: Insights from minor faults and GIS-enhanced structure maps, *in* Kay, S.M., Ramos, V.A., and Dickinson, W.R., eds., Backbone of the Americas: Shallow Subduction, Plateau Uplift, and Ridge and Terrane Collision: Geological Society of America, Memoir 204, p. 125–150.

Goddard, E.N., 1966, Geologic map and sections of the Zuni Mountains fluorspar district, Valencia County, New Mexico: U.S. Geological Survey, Miscellaneous Investigations Map I-454, scale 1:31,680.

Green, G.N. and Jones, G.E., 1997, The digital geologic map of New Mexico in ARC/INFO format: U.S. Geological Survey Open-File Report 97-0052, 9 p.

Hackman, R.H., and Olson, A.B., 1977, Geology, structure, and uranium deposits of the Gallup 1 degree x 2 degree quadrangle, New Mexico and Arizona: Washington, D.C., U.S. Geological Survey, Miscellaneous Investigations Series I-981, scale 1:250,000, 2 sheets.

Kelley, V.C., 1967, Tectonics of the Zuni-Defiance region, New Mexico and Arizona: New Mexico Geological Society, Guidebook 18, p. 28–31.

Marrett, R.A., and Allmendinger, R.W., 1990, Kinematic analysis of fault-slip data: Journal of Structural Geology, v. 12, p. 973–986.

Petit, J.P., 1987, Criteria for the sense of movement on fault surfaces in brittle rocks: Journal of Structural Geology, v. 9, p. 597–608.

Ross, C.A., and Ross, J.R.P., 1986, Paleozoic paleotectonics and sedimentation in Arizona and New Mexico, *in* Peterson, J.A., ed., Paleotectonics and Sedimentation in the Rocky Mountain Region, United States: Tulsa, American Association of Petroleum Geologists, Memoir 41, p. 653–668.

Singleton, J.S., Mavor, S.P., Seymour, N.M., Williams, S.A., Patton, A.I., Ruthven, R.C., Johnson, E.P., and Prior, M.G., 2019, Laramide shortening and influence of Precambrian basement on uplift of the Black Hills, South Dakota and Wyoming, U.S.A.: Rocky Mountain Geology, v. 54, p. 1–17.

Smith, C.T., 1957, Geology of the Zuni Mountains, Valencia and McKinley Counties, New Mexico: Four Corners Geological Society, Guidebook, p. 53–61.

Strickland, D., Heizler, M.T., Selverstone, J., and Karlstrom, K.E., 2003, Proterozoic evolution of the Zuni Mountains, western New Mexico: Relationship to the Jemez lineament and implications for a complex cooling history: New Mexico Geological Society, Guidebook 54, p. 109–117.

Timmons, J.M., and Cikoski, C.T., 2012, Geologic map of the San Rafael quadrangle, Cibola County, New Mexico: New Mexico Bureau of Geology and Mineral Resources, Open-file Geologic Map 232, scale 1:24,000.

Vollmer, F.W., 1990, An application of eigenvalue methods to structural domain analysis: Geological Society of America Bulletin, v. 102, p. 786–791.

Weil, A.B., and Yonkee, W.A., 2012, Layer-parallel shortening across the Sevier fold-thrust belt and Laramide foreland of Wyoming: Spatial and temporal evolution of a complex geodynamic system: Earth and Planetary Science Letters, v. 357–358, p. 405–420.

Wise, D.U., 2000, Laramide structures in basement and cover of the Beartooth Uplift near Red Lodge, Montana: American Association of Petroleum Geologists Bulletin, v. 84, p. 360–375.

Worthington, L.L., Miller, K.C., Erslev, E.A., Anderson, M.L., Chamberlain, K.R., Sheehan, A.F., Yeck, W.L., Harder, S.H., and Siddoway, C.S., 2016, Crustal structure of the Bighorn Mountains region: Precambrian influence on Laramide shortening and uplift in north-central Wyoming: Tectonics, v. 35, p. 208–236.

New Mexico Geological Society, Special Publication 14, Geology of the Mount Taylor Area, 2020, p. 177-188.

CONTINUOUS SOIL-MOISTURE MEASUREMENTS TO ASSESS FRACTURE FLOW IN INSCRIPTION ROCK AT EL MORRO NATIONAL MONUMENT, NEW MEXICO: IMPLICATIONS FOR THE DETERIORATION OF INSCRIPTIONS

B. Talon Newton and Shari A. Kelley

New Mexico Bureau of Geology and Mineral Resources, 801 Leroy Place, Socorro, NM 87801, talon.newton@nmt.edu

Abstract—Inscription Rock, the main attraction at El Morro National Monument, is a 70-m-high sandstone monolith that documents a long history of human activity. The Atsinna Pueblo ruins sit on top of the monolith above steep cliff walls that exhibit thousands of signatures carved into the sandstone by Spanish explorers and American emigrants. One of the primary goals of the National Park Service in managing the monument is the preservation of the historic inscriptions, which are deteriorating largely due to natural weathering processes that are driven by the presence of water. The loss of inscriptions is particularly noticeable on the northeastern-most point on the cliff at El Morro, where lichen is obscuring inscriptions. The experiment described here was part of a larger hydrogeologic study with the objective of identifying water sources and mechanisms by which water comes in contact with the inscriptions.

This experiment compared fluctuations in soil moisture at the base of the cliff in different areas to soil moisture fluctuations at "control points" away from the cliff, where local precipitation that falls on the surface is most likely the only source of soil moisture. Continuous soil moisture data at depths of 10 and 30 cm were collected between April 27 and October 5, 2017. Soil moisture data for sites in close proximity of the cliff showed evidence of additional soil moisture sources in areas where the cliff face was perpendicular to the northeasterly strike of the primary joint system, providing evidence of water percolating relatively quickly through these fractures. Water that is stored in these fractures that are close to the wall surface can potentially move slowly through the sandstone matrix, mainly driven by capillary action and a water potential gradient resulting from the evaporation of water that reaches the rock surface. We hypothesize that this process is occurring on the north side of Inscription Rock, where lichen growth is greatly impacting inscriptions.

INTRODUCTION

El Morro National Monument is located in northwestern New Mexico approximately 40 mi southwest of Grants and south of the Zuni Mountains (Fig 1). This national monument features the cliffs of El Morro, which served as a prominent landmark and water source (the historic pool at the base of the cliff) for Puebloan people, Spanish explorers and American settlers for hundreds of years. Inscription Rock, a 70-m-high sandstone monolith (composed of Jurassic Zuni Sandstone; Fig. 2), documents a long history of human activity, with the Atsinna Pueblo ruins on the cliff top, and rock art that includes thousands of symbols and signatures carved into the cliff walls by Native Americans, Spanish explorers and American emigrants. One of the primary management goals of El Morro National Monument, which was established in 1906, is the preservation of these historic inscriptions, which are deteriorating due to natural and anthropogenic processes. The loss of inscriptions is particularly noticeable on the north side of Inscription Rock in the vicinity of North Point, the northeastern-most point on the cliff at El Morro, where lichen is obscuring inscriptions (Burris, 2007). Much research has been conducted to understand the natural erosional processes that contribute to the deterioration of these inscriptions in order to identify possible methods to mitigate the eventual loss of the inscriptions. Important weathering processes that contribute

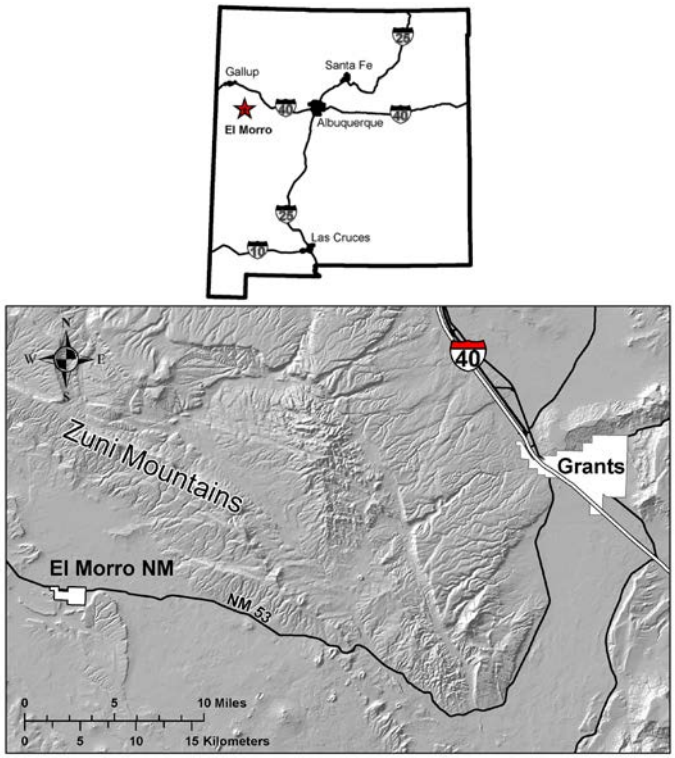

FIGURE 1. Index map showing the location of El Morro National Monument, New Mexico.

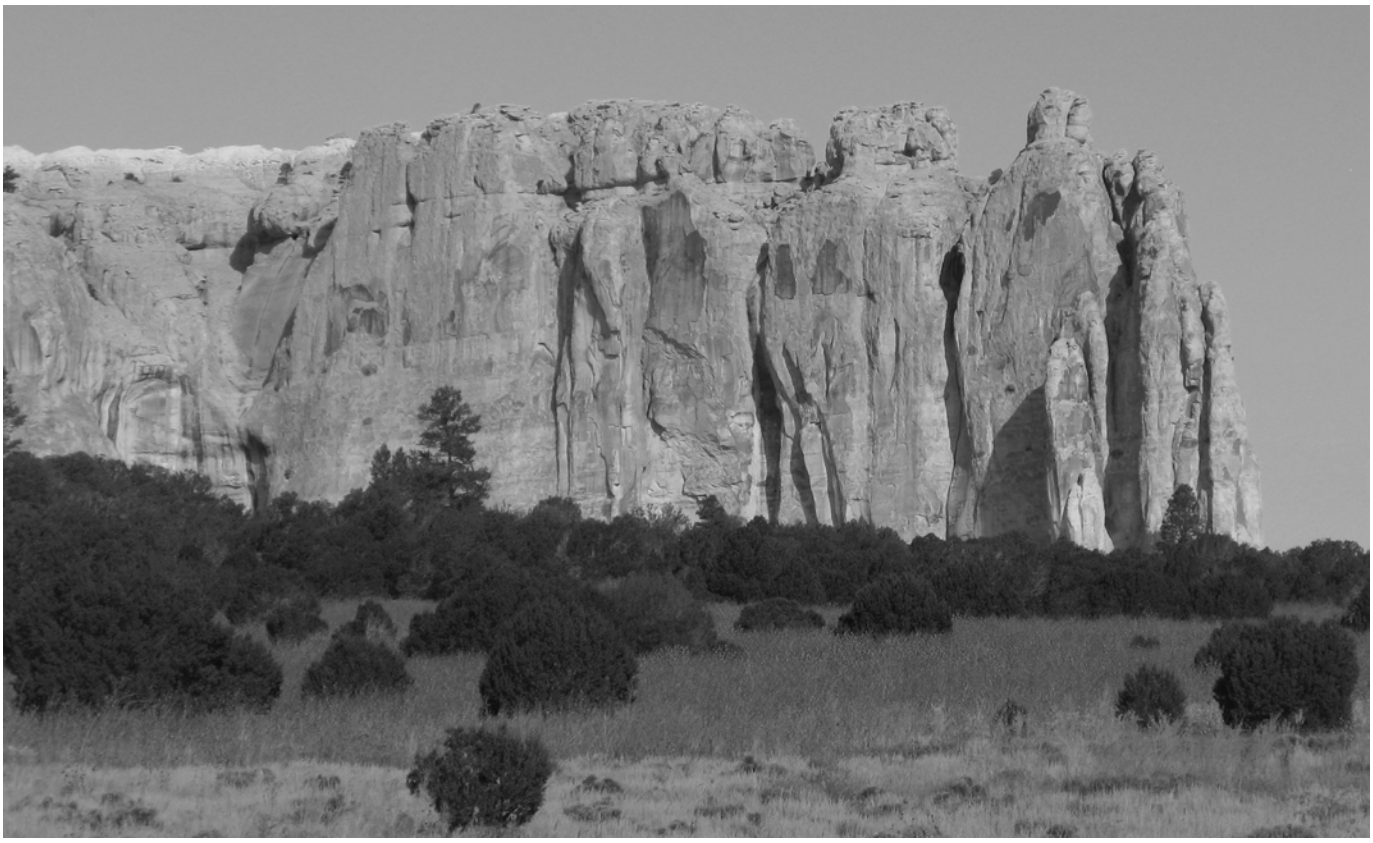

FIGURE 2. Photograph of Inscription Rock at El Morro National Monument in New Mexico. The part of the Zuni Sandstone cliff at the far right is called North Point. The view is from the road to the visitor's center, looking north.

to the deterioration of the inscriptions include (Padgett, 1992; Cross, 1996; Pranger, 2002):

- Granular disintegration — the separation of individual grains or clumps of grains by physical removal due to pelting rain or water flow over the cliff face or by freezing and thawing of water in pores and in fractures;
- Rockfall — the detachment of coherent blocks;
- Spalling — the shedding of small, relatively thin flakes of rock by alternating wetting and drying or from capillary rise from wet soil at the base of a cliff;
- Biological factors — insect borings or lichen growth.

The presence of water drives many of these weathering processes. Research focused on the local hydrogeology has made progress toward the identification of surface and subsurface water sources that contribute to weathering processes (Padgett, 1992; Cross, 1996; Pranger, 2002; Van Dam and Hendrickx, 2007). However, there are significant questions about the hydrogeologic system that need to be answered before mitigation techniques to help preserve the inscriptions can be assessed. A recent hydrogeologic study conducted by the New Mexico Bureau of Geology and Mineral Resources aimed to construct a more complete hydrogeologic conceptual model at El Morro National Monument (Newton and Kelley, 2019). This paper describes an experiment within that study that focused on the use of continuous soil moisture measurements to assess mechanisms by which water flows through the Zuni Sandstone cliffs of El Morro and the role that these mechanisms may play in the deterioration of the inscriptions.

As mentioned above, inscriptions on the north side of Inscription Rock are deteriorating particularly fast compared to other areas on Monument. Lichen growing on the north side of the promontory accelerates the chemical and mechanical weathering processes that result in the deterioration of the inscriptions in this area. At North Point, the sharp boundary between lichen covered rock and non-lichen covered rock is remarkable (Fig. 3). St. Clair and Knight (2001) identified 43 different species of lichen, mostly on the north side of Inscription Rock and observed significant encroachment by the lichen from the rock surface into the sandstone matrix. They attributed the presence of this lichen to shading by woody vascular plant vegetation around and near Inscription rock, which slows water evaporation and reduces mean summer temperature.

Van Dam and Hendrickx (2007) studied the local hydrogeology at El Morro, using hydrologic and geophysical techniques. They installed shallow piezometers in the vicinity of the historic pool and near North Point and observed an ephemeral shallow water table near the historic pool, with isotopic evidence that this shallow groundwater had likely resided in the cliff for some amount of time before being pushed out by a recent precipitation event. The absence of water in the piezometers near North Point for the duration of the study and electromagnetic induction measurements suggested that an ephemeral water table, similar to that observed near the pool, does not exist in

FIGURE 3. North Point of Inscription Rock. Note the sharp boundary between rock without lichen (left) and rock covered with lichen (right), marked by a vertical fracture. The fence rail in the foreground is about 10 cm thick.

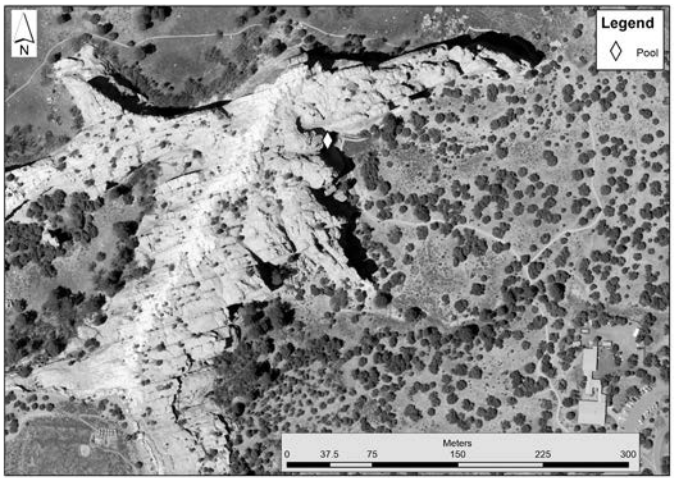

FIGURE 4. Aerial view of Inscription Rock with North Point at the far northeastern end. The primary joint system can easily be seen, striking to the northeast. The location of the pool is marked with a white diamond.

the vicinity of North Point. However, the electromagnetic induction data also showed an increase in soil moisture towards the cliff both near the pool and North Point. With no shallow groundwater in the vicinity of North Point, Van Dam and Hendrickx (2007) suggested that the rapid deterioration in this area is due to either unique physical and chemical properties of the rock in this area or to a source of water from the top of the cliff.

The very well defined northeast-striking joint system is a prominent feature of the Inscription Rock and has hydrologic implications (Fig. 4). While these fractures are filled with sediment to some extent, they nevertheless must be conduits that provide a relatively quick transport of rain and snow melt from the top of the cliff, downward to the subsurface (Hendrickx and Flury, 2001). Here, we describe an experiment that uses continuous soil moisture data to provide direct evidence of water movement through these preferential flowpaths within the cliff, with implications for processes that lead to the severe deterioration of the inscriptions on the north side of Inscription Rock.

DESCRIPTION OF THE STUDY AREA

Regional and local geology

El Morro, located on the southwestern flank of the Zuni Mountains, is an impressive outcrop made of Middle to Late Jurassic (155 to 165 my) Zuni Sandstone capped by Late Cretaceous (~95 to 96 my) Dakota sandstone and shale. The yellowish-green to tan Zuni Sandstone is composed of well-sorted, angular quartz grains with minor feldspar, cemented primarily by kaolinite. As a consequence of the cementation by clay, the sandstone is soft, easy to carve, and is easily eroded. Large-scale cross-bedding is common in the Zuni Sandstone. The grain sorting and the cross-bedding are characteristic of sand dunes that were part of a dune field that covered much of northwestern New Mexico, northeastern Arizona, southeastern Utah, and southwestern Colorado about 150 Ma ago. Cross (1996) measured the permeability of the Zuni Sandstone at several locations on the monument. Permeability ranged from 0.01 to 204 millidarcies, which correlates to hydraulic conductivities ranging from $1x10^{-10}$ to $2.3x10^{-6}$ m per day.

A Proterozoic-basement cored uplift that formed during Laramide compressional deformation about 75 to 50 my ago, the Zuni Mountains include a pronounced fracture (joint) system that cuts both the Jurassic and the Cretaceous sandstones in the area. The most prominent set strikes NE (65-70°) with relatively regular spacing of 10 to 15 m between fractures. The weaker joint set strikes NW (305-330°). These fractures likely play an important role in the local hydrogeology, specifically in the movement of precipitation downward through the sandstone cliffs.

Although the base of the Zuni Sandstone is not exposed in this area, this unit overlies fine-grained sandstones of the Upper Triassic Rock Point Member of the Chinle Group, which in turn rests on siltstones and mudstones of the Petrified Forest Member of the Chinle Group (NMBGMR, 2003). An apron of younger Quaternary colluvium (rocks block eroded from the cliffs), alluvium (water-lain deposits in arroyos), and windblown silt surround the sandstone cliffs.

Hydrogeology

The surface water and groundwater systems considered in this study are local in scale with the primary water source being

local precipitation. Annual precipitation on the Monument averages between 35 and 40 cm (Salas and Bolen, 2010). Within the monument, the only perennial surface water is in the historic pool located in an alcove on the south side of Inscription Rock. This pool has been historically documented and appears to have been a stable water source for early Puebloan inhabitants as far back as the 1200s, explorers who visited the area since the early 1600s (West and Baldwin, 1965), and the Monument until 1961. Padgett (1992) describes the history of the pool and how it has changed due to natural and anthropogenic causes. Currently, the pool stores, on average, approximately 757 m^3 (200,000 gallons). Several studies have concluded that most, if not all, of the water in the pool is from surface runoff that cascades off the top of the cliff during rain events (West and Baldwin, 1965; Van Dam and Hendrickx, 2007; Newton and Kelley, 2019). The cliffs surrounding the pool provide shade, especially in the afternoon, which reduces evaporation.

As mentioned above, there is evidence that shallow perched aquifers sometimes exist near the cliff in the vicinity of the pool. Van Dam and Hendrickx (2007) installed six piezometers on the monument, four in the pool area and two near North Point. Depths of the piezometers range from five to 10 ft below the surface. These piezometers are still in place and being used by the Southern Colorado Plateau Network (SCPN) to monitor water levels (Soles and Monroe, 2012). Van Dam and Hendrickx (2007) state that groundwater was not observed during the drilling of the wells, but the moisture content was observed to increase significantly with depth. The observation wells were dry most of the time. However, it was reported that water was present in two wells near the pool on three occasions in August 2006 after rainfall events. Water was observed in one well near North Point on August 8, 2006, after a heavy rainfall. Soles and Monroe (2012) detected water in three of the wells near the pool on different occasions during 2011. Monroe and Soles (2015) noted water in two of the wells near the pool several times in 2012 and 2013. Observed groundwater levels near the pool are all below the pool water surface. Van Dam and Hendrickx (2007) concluded that these shallow perched aquifers were likely ephemeral, existing during wet periods, and were recharged from precipitation on the top of the cliff. Geochemical data indicates that these shallow groundwater systems are not hydrologically connected to the historic pool (Van Dam and Hendrickx, 2007). In addition to the geochemical data, fast groundwater level responses to precipitation events suggest that groundwater recharge to these ephemeral perched aquifers is likely local precipitation that flows from the cliff top through fractures in the Zuni Sandstone (Newton and Kelley, 2019).

Geophysical surveys near North Point and the pool area showed a significant increase in apparent moisture content closer to the cliff (Van Dam and Hendrickx, 2007). Geophysical surveys also showed a larger difference in moisture content between dry conditions in July 2004 and wetter conditions in August 2004 the closer the surveys were to the cliff. While Van Dam and Hendrickx (2007) stated that "the presence of the cliff has a significant impact" on moisture content in the shallow subsurface, they did not discuss what processes cause these observed trends in moisture content. We hypothesize that this increase in moisture in proximity to the cliff is mainly due to water flowing from the top of the cliff through prominent joints. The soil moisture experiment described in this paper was designed to test this hypothesis.

METHODS

On April 26, 2017, we installed ECH_2O-ECTM soil moisture instruments, made by Decagon Services, at nine different sites (Fig. 5, SM3 – SM11). SM10 was located on top of the cliff. All other soil moisture sites were located at the bottom of the cliff in different areas. At each site an instrument was installed at 10- and 30-cm depth. To install these instruments, we dug a small hole (~30 cm in diameter) to the desired depth and laterally inserted prongs in the side of the hole at a specific depth to minimize disruption of the soil. The sensors at each site were connected to a Campbell data logger, which was programmed to log soil moisture and temperature data every 15 minutes. We removed all instruments on October 5, 2017.

These probes indicate volumetric soil moisture (volume of water/ total volume of soil) by measuring the dielectric permittivity (the ability of a substance to hold an electric charge) of the surrounding medium. Because the dielectric permittivity of water is much greater than other constituents of soil, a change in dielectric permittivity is directly related to a change in water content. Prior to installing these instruments, we collected soil samples from each site and calibrated each instrument to the specific soil associated with each site. Instrument calibration in the lab entailed correlating raw millivolt outputs to known volumetric water contents. Average raw millivolt readings were recorded for different known water contents, beginning with a dry soil sample and subsequent incremental increases in water content. The resulting linear regression for each instrument was then used to calculate volumetric soil moisture at each instrument site. As will be seen in the discussion about these data below, for reasons unknown, some instruments pro-

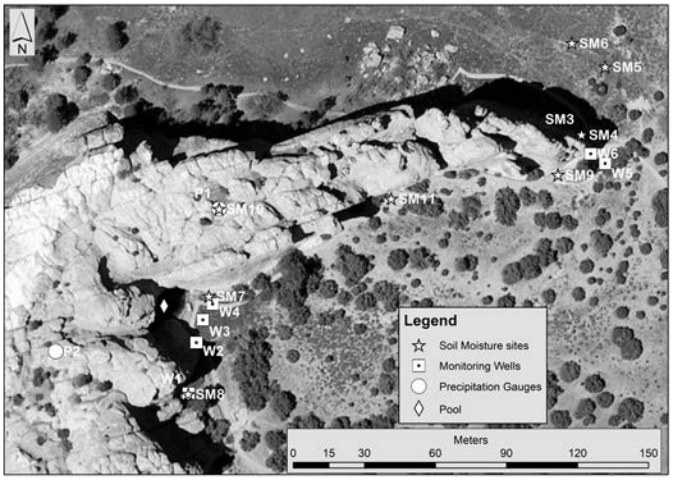

FIGURE 5. Locations of piezometers (W1–W6), soil moisture sites (SM3–11), and a precipitation gauge and collector (P1 and P2). Soil moisture sites 3 and 4 are only about six meters apart.

duced somewhat noisy data sets with fairly large fluctuations from measurement to measurement. Fortunately, seasonal trends and responses to rain events can still be identified in the time series datasets that are discussed below.

The storage and movement of water in soils is largely controlled by soil characteristics, such as grain-size distribution, bulk density, organic content, etc. We conducted wet sieve analyses to characterize the grain-size distribution, and we measured the soil bulk density using the core method (Al-Shammary et al., 2018). We did not measure organic content. A precipitation collector was installed near the soil moisture site on top of the cliff and daily precipitation readings were collected from the weather station run by the National Park Service on the monument.

RESULTS

Continuous soil-moisture data were collected at all locations between April 27 and October 5, 2017. This experiment aimed to compare fluctuations in soil moisture at areas near the base of the cliff to soil-moisture fluctuations at control points, thus to some degree indicating the processes by which water is introduced to the soil. Table 1 shows site descriptions and sieve-analysis results for each soil-moisture site.

Sites SM5 and SM6 are located tens of meters away from Inscription Rock to the northeast of North Point. Based on the assumption that all soil moisture comes from local precipitation that falls directly on the soil surface or local surface runoff from the surrounding topography, these sites, far from Inscription Rock, were designated control sites. The vegetation was primarily the low-growing Winterfat Dwarf shrub (*Krascheninnikovia lanata*; Salas and Bolen, 2010); thus, these sites are exposed to the sun most of the day. SM-6 was located on a shallow slope out in the open, and SM5 was located at the bottom of a shallow depression or channel that may have accumulated some surface runoff during large rain events. The highest water content was observed at 10-cm depth in response to precipitation events in late April and early May while antecedent soil moisture was relatively high, likely due to cumulative infiltration of winter rain and snowmelt with low evaporation rates. This high antecedent soil moisture during April and May was observed for almost all sites. The May rain event produced peak soil moisture values at 10 cm of about 0.36 and 0.23 for SM5 and SM6, respectively (Fig. 6). Soil moisture at ten centimeters depth then decreased gradually to about 0.05 at both sites due to increasing temperatures. Monsoon storms beginning in July resulted in an increase in water content with peak values of 0.2 and 0.16. Subsequent drying was observed from August through late September when another storm caused values to increase to about 0.15 for both sites (Fig. 6). For both sites, soil moisture at 30-cm depth mostly shows a drying trend with very little response to precipitation events. For SM5, this drying trend is more drawn out over time and there are small responses to some of the bigger storm events. Soil moisture data for the SM10 (Appendix 1), located on the top of the cliff, were very similar to those for SM6. These data strongly suggest that most soil water is lost to evapotranspiration, with very little infiltration past 10 cm for most precipitation events during the monsoon season.

SM7 was located very close to the cliff near the historic pool, and SM8 was located close to the cliff in an alcove just south of the pool. Piezometers have shown evidence of an ephemeral water table that develops during periods of heavy rainfall at both of these sites. Soil moisture data at these two sites show very different responses to precipitation than those observed at the sites further away from the cliff and on top of the cliff. Figure 7 shows soil moisture fluctuations for SM7 and SM8. Missing data for SM8 is due to technical issues with

Table 1. Site descriptions and wet-sieve grain-analysis data.

Site number	Site description	% medium sand	% fine and very fine sand	% silt and clay	Soil Texture
SM3	North Point – east side of fracture at base of cliff	3.3	81.3	15.4	Loamy very fine sand
SM4	North Point – west side of fracture at base of cliff	1.3	85.6	13.1	Loamy very fine sand
SM5	Drainage north of North Point >10 m from the cliff	1.6	74	24.4	Very fine sandy loam
SM6	West of EM-9005 on grass-covered slope >10 m from the wall	4.4	85.5	10.1	Fine sand
SM7	Near monitoring well EM-0003, below pool proximal to cliff wall	1.1	83	15.9	Loamy, very fine sand
SM8	In alcove just south of the pool at base of cliff	0.6	88.6	10.8	Very fine sand
SM9	South side of North Point below Arran Lopez inscription at base of cliff	1.7	80.9	17.4	Loamy very fine sand
SM10	At top of cliff in shallow depression	2.5	82.8	14.7	Loamy fine sand
SM11	At interpretation point 10 along inscription trail, beneath overhanging cliff wall	1.2	82.1	16.8	Loamy fine sand

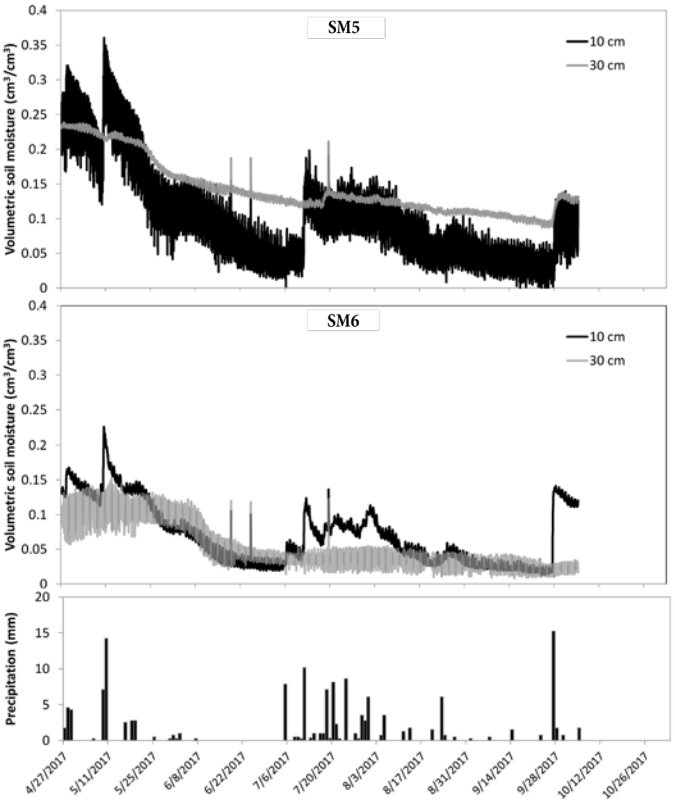

FIGURE 6. Soil moisture time series for SM5 and SM6. The bottom graph shows local precipitation amounts. Although soil moisture datasets for SM5 at 30-cm depth and for SM6 at 10-cm depth show considerable noise, which is likely related to the specific instruments, the signal/noise ratio is still good enough to identify seasonal trends and correlations between soil moisture and precipitation events.

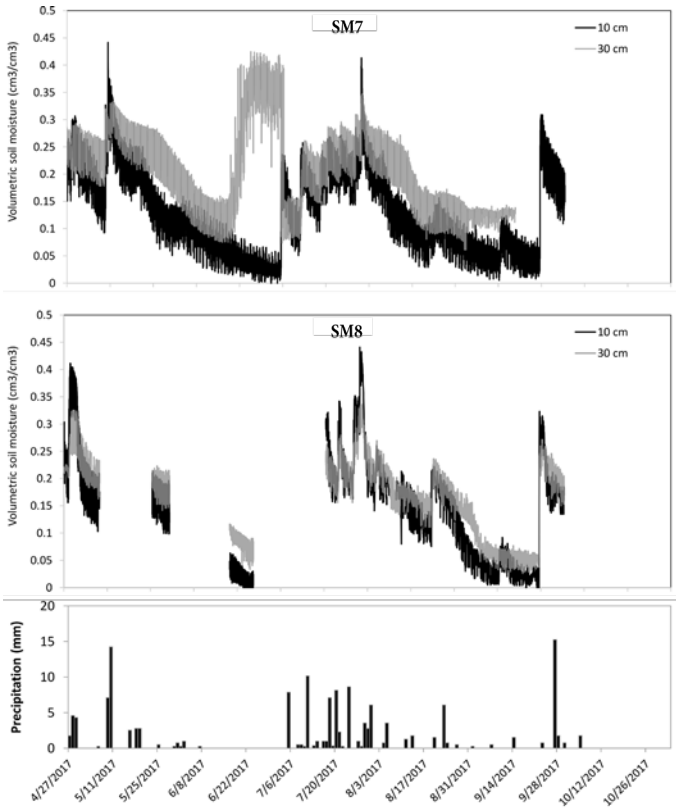

FIGURE 7. Soil moisture time series for SM7 and SM8. The bottom graph shows local precipitation amounts.

the data logger. Initial trends at 10-cm depth were similar to those seen for control sites but with slightly higher peak values for April and May storm events (>0.4). Subsequent drying resulted in soil moistures decreasing to levels less than 0.1 at the shallow depths by early July. We do not have an explanation for the anomaly observed at 30-cm depth for SM7 where the soil moisture abruptly increases to values as high as 0.45 in mid-June and remains high through early July. We speculate that this is related to an event where water from the pond was diverted to test a nearby newly built drainage structure. However, we have not been able to confirm with Monument staff that this actually happened. During the monsoon season at both of these sites, soil moisture at 10-cm depth responded very quickly to some individual storms but also showed a cumulative increase with maximum values occurring in late August as the monsoons began to wane. Soil moisture during the monsoon season at the shallow depths climbed to values higher than 0.40, which is much higher than those observed during this time period for sites discussed previously. Interestingly, unlike the sites discussed above, soil moisture at 30-cm depth for SM7 and SM8 responded to rain events during the monsoon season almost identically to the responses observed at 10 cm, both in terms of timing and magnitude.

SM9 was located near the trail going east just before North Point, within one meter of the cliff wall. Soil moisture fluctuations at this site were almost identical to those observed for SM6, which is the control site out in the open. Soil moisture at both depths decreased during May and June due to increasing temperatures (Fig. 8). Monsoon rains significantly increased soil moisture at 10-cm depth but had little effect on soil moisture at 30-cm depth. Soil moisture at both depths never rose above 0.2 (Fig. 8). It appears that for this site, the close proximity to the cliff did not affect soil moisture fluctuations.

Soil moisture site SM11 was located along the Inscription Rock trail within one meter of the cliff, underneath a small overhang. This overhang significantly decreases the amount of rain that reaches the ground surface. There was no significant change in soil moisture for the duration of this study (Appendix 2), and soil moisture data at this site at both depths did not go above 0.03.

We placed soil moisture instruments SM3 and SM4 within one meter of the cliff wall at North Point, shown in Figure 2, in the area where the wall is bare and where the wall is covered with lichen, respectively (Fig. 9). These sites are within three meters of each other, and the first two months of soil moisture fluctuations are almost identical with the typical high initial values and gradual decrease going into summer months (Fig. 10). However, soil moisture fluctuations exhibited different characteristics during the monsoon season. At both sites the first two large storms in July resulted in soil moisture increases at 10-cm depth but not at 30 cm. For storms that occurred during late July and early August, soil moisture at 30 cm did increase at both sites but to a much larger extent for SM4, located

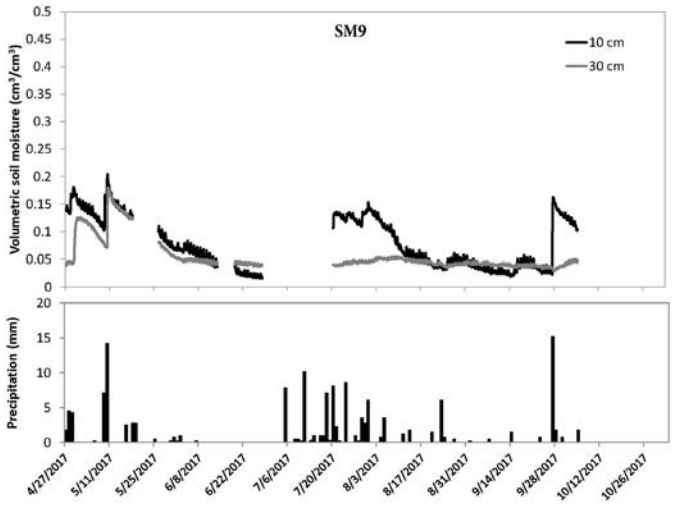

FIGURE 8. Soil moisture time series for SM9. The bottom graph shows local precipitation amounts.

adjacent to the lichen-covered wall. At SM4, soil moisture values at 30 cm were of the same magnitude as values observed at the shallow depth, and similar to what was observed for SM7 and SM8 near the pool. The soil moisture responses observed at 30-cm depth for SM3, located adjacent to the bare wall, were slightly delayed and at a much smaller magnitude with respect to the response seen at 10-cm depth. The soil moisture fluctuations observed for SM3 were similar to those of SM6, where the only source of soil moisture was local precipitation that fell directly on the surface (Figs. 6, 10). The 30-cm response to the large storm in September was also much more pronounced for SM4 than for SM3 (Fig. 10). These data suggest that different mechanisms control soil moisture conditions at these two locations, which are in close proximity to each other.

After almost two months of continuous dry conditions, a major precipitation event of 15 mm occurred on September 27. The sudden change or absence of change in response to this storm at each soil moisture sensor provides more support for our conceptual hydrologic model discussed in the next section. The soil textures indicate that the soil water holding capacities of the soils are between 10 and 20 volume percent. A storm of 15 mm could increase the moisture in the top 10 cm of the soil by about 15 volume percent but wouldn't significantly affect soil moisture at 30-cm depth. Observed soil moisture changes due to the September 27 storm were analyzed to estimate the amount of water that infiltrated into the soil due to the storm. The change in volumetric water content at 10-cm depth was assumed to represent the total amount of infiltration in the top 10 cm of soil. The observed change in soil moisture at 30-cm depth was assumed to represent the total amount of infiltration between 0- and 30-cm depth. The amount of water that infiltrated between 10- and 20-cm depth was estimated by linear interpolation. Results of these calculations are shown in Table 2. The location description in Table 2 includes the orientation of the cliff wall with respect to strike of the primary joint system (perpendicular or parallel). The significance of this relationship will be discussed in the next section.

FIGURE 9. Site SM3 is under the rock in the foreground close to the wall with little or no lichen. SM4 is located under the rock in the background next to the wall that is covered by lichen. Graduate student, Kylian Robinson is seen finishing up instrument installation.

For the control sites SM5 and SM6, we estimated total infiltration to be 16.5 and 18 mm respectively, slightly larger than the total amount of precipitation. We are likely overestimating actual total infiltration, and therefore the total amount of infiltration in both control points is likely equal to the total precipitation amount (15 mm). For the two sites close to the pool, SM7 and SM8, which are located close to the cliff wall and are perpendicular to the joints, total infiltration was estimated to be much greater than precipitation. Total infiltration for SM8 was estimated to be 75 mm, about five times that of total precipitation. The total amount of infiltration to 30-cm depth for SM7 could not be estimated due to technical issues with the instruments. However, we estimated the amount of water infiltrating into the top 10 cm to be 26 mm, and the total infiltration to 30-cm depth is likely comparable to that estimated for SM8. For SM9, located close to the wall, which is parallel to joint strike,

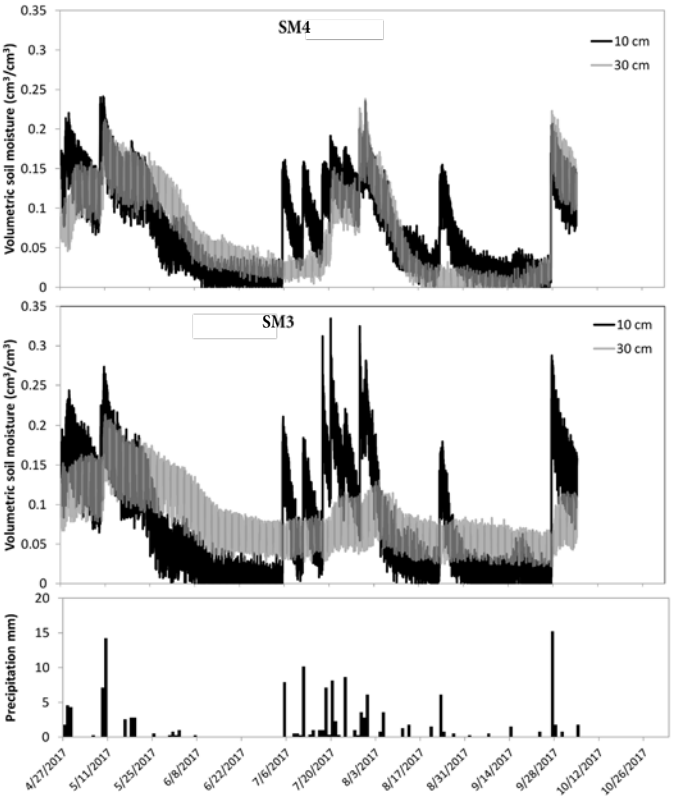

FIGURE 10. Soil moisture time series for SM3 (Northpoint near bare wall) and SM4 (North Point near lichen-covered wall). The bottom graph shows local precipitation amounts.

we estimated total infiltration to be 19.5 mm, which is similar to estimates for the control sites, suggesting that total infiltration equal total precipitation. We estimated total infiltration to be almost zero (about 1 mm) for SM11, located near the wall (parallel to joint strike) under a small overhang. For SM3 and SM4, located at North Point where the wall is perpendicular to joint strike, we estimated total infiltration to the depth of 30 cm to be 45 and 57 mm respectively. As was observed at sites near the pool (SM7 and SM8) both of these estimates of total infiltration are much larger than total precipitation. Interestingly, infiltration estimated for SM4, adjacent to the lichen-covered wall was larger than infiltration estimated for soil near the bare wall. For SM10, located on the top of the cliff in a small sediment-filled depression, total infiltration was estimated to be 43.5 mm. This large infiltration amount indicates that significant runoff accumulates in this depression.

DISCUSSION

Hydrogeologic Conceptual Model

Van Dam and Hendrickx (2007) observed an increase in soil moisture as they moved closer to the cliff in the vicinity of the pool and near North Point. Similarly, we observed average soil moisture values near the cliff in the vicinity of the pool (SM7 and SM8) and near North Point (SM3 and SM4) to be significantly higher than those observed at control points away from the cliff (SM5 and SM6), especially during monsoon season. However, sites SM9 and SM11, which were also in very close proximity to the cliff wall, did not exhibit higher soil moisture value compared to the control points. Figures 11 and 12 show that sites SM7, SM8, SM3 and SM4 are all located in areas where the cliff face is perpendicular to the strike of the primary joint system, and SM9 and SM11 are located along the northeast trending cliff wall that is parallel to the joint strike. This observation strongly suggests that additional soil moisture observed near the cliff in some of these sites is due to the percolation of water from the top of the cliff downward through the vertical fracture that defines the primary joint system. Figure 13 shows our conceptual model of the local cliff hydrogeologic system. Most precipitation and snowmelt at the top of the cliff either runs off the side of the cliff (in this case filling the historic pool) or into the large fractures at the surface. Water is stored in the pores of the sediments that partially fill these fractures. With the addition of runoff from monsoon precipitation, hydraulic head in the fractures increases, causing water to

FIGURE 11. Satellite photograph of Inscription Rock in the vicinity of the pool (white diamond), SM7, and SM8. SM10 is on top of the cliff in a small depression filled with sediment (gray patch north of the SM10 site on this image). Joints that likely transport water downward through the cliff to the subsurface near the base of the cliff are clearly visible in this image.

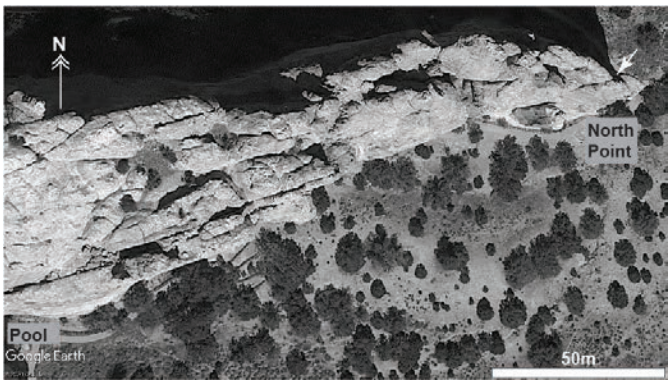

FIGURE 12. Google Earth image of Inscription Rock within the vicinity of North Point. The white arrow denotes the fracture that is in between SM3 and SM4.

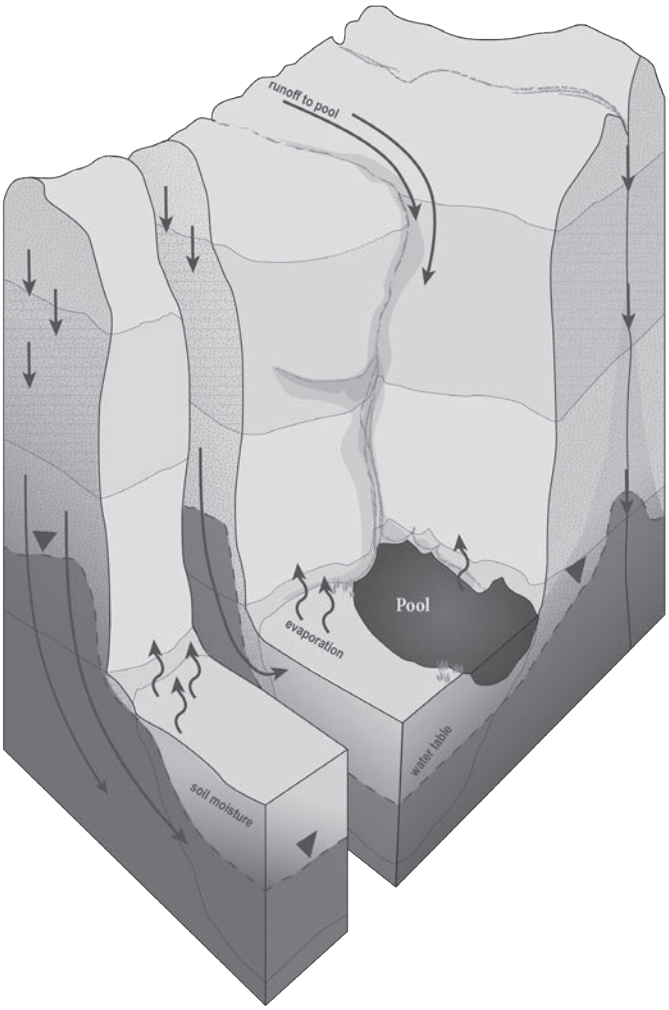

FIGURE 13. Conceptual model illustrating hydrogeologic processes at El Morro National Monument near the historic pool. Most precipitation and snowmelt at the top of the cliff either runs off the side of the cliff (in this case filling the historic pool) or into the large fractures at the surface. Water stored in sediment that partially fills fractures can be mobilized by an increase in the head gradient due to the addition of water by large snowmelt or storm events. The water percolates downward through fractures to contribute to soil moisture and may sometimes provide enough water to form an ephemeral shallow perched aquifer (dashed water table) at the base of the cliff.

percolate downward. This water contributes to soil moisture at the base of the cliff, as evident by the observed soil-moisture increases at 30-cm depth. During very wet periods, enough water will accumulate to form a shallow perched aquifer as is observed near the pool. The apparent absence of an ephemeral perched aquifer near North Point is discussed below.

Soil Moisture Responses at North Point

Soil moisture fluctuation data described above provide direct evidence of the movement of water from the top of the cliff to unconsolidated sediments at the base of the cliff via northeast-southwest trending joints. Soil moisture time series datasets for sites SM3 and SM4 (Fig. 10) and estimated infiltration volumes for these sites (Table 2) indicate that water from the top of the cliff is moving through these fractures and contributing to soil moisture at the base of the cliff at North Point, where lichen is impacting inscriptions (Fig. 3). The soil moisture trends observed for SM3 and SM4, which are only three meters apart, have implications for the presence of lichen and increased deterioration rates of inscriptions on the north side of Inscription Rock near North Point. Similar soil moisture values and responses to precipitation events in May for both SM3 and SM4 (Fig. 10) at both measurement depths indicate similar volumetric contributions from fracture flow to soil moisture at both sites. However, for subsequent precipitation events in late July and on September 27, fracture flow contributions to soil moisture for SM4 (near lichen-covered wall) were significantly higher than those observed for SM3 (near bare wall). This observation indicates that under some conditions, more water is flowing though fractures above the lichen-covered wall than those above the bare wall. This difference in apparent fracture flow volumes at these two sites may be due to different water supply volumes to fractures and/or differences in water loss or depletion rates from the fractures.

Although we think that the observed differences in soil moisture fluctuations for SM3 and SM4 are due to factors that control the transport of water through fractures and the sandstone matrix in the cliff, which are discussed below, other possibilities should also be considered. Grain-size analyses showed similar distributions for both sites (Table 1), and therefore, we would expect to see similar soil moisture trends if local precipitation was the only source of soil moisture. However, as seen in Figure 9, vegetation at these sites is quite different. With more sun exposure, the area adjacent to the bare rock wall (SM3) is characterized by mostly bare ground with scattered small shrubs. For the area adjacent to the lichen covered wall (SM4), less sun exposure due to the northern aspect of the wall and shade by nearby trees, results in the ground being mostly covered with grasses and other low-lying plants. It is possible that interactions between the vegetation and soil may significantly affect soil water parameters, including infiltration rates. More research should be done to assess these ecohydrological processes.

Controls on water supply volume to fractures

The amount of water that flows through fractures from the top of the cliff to sediments at the base of the cliff is likely related to characteristics of fractures within the cliff and how they influence water flowpaths. Fractures on top of the cliff near North Point (Fig. 12) are not as well defined and continuous as those above the pool area (Fig. 11). This difference alone can explain why there appears to be more water flowing through fractures and contributing to soil moisture near the pool (SM7 and SM8) compared to the area near North Point (SM3 and SM4). In addition to limiting the volume of fracture flow near North Point, the poorly defined fractures may also exhibit lower vertical permeability compared to the better defined fractures above the pool area. Therefore, not only might there be less water flowing through fractures at North Point compared to those above the pool, water may also move at

TABLE 2. Estimated infiltration amounts for the 15-mm rainfall during the September 2017 storm event, based on volumetric soil moisture measurements before and after the storm.

			Volumetric water content (%)			*Estimated infiltration (mm)*			
Site	**location**	**Depth (cm)**	**Pre-storm**	**Post-storm**	**Difference**	**0 - 10 cm**	**10 - 20 cm**	**20 - 30 cm**	**Total**
SM3	Near cliff at North Point, bare wall, perpendicular to joints	10	2%	27%	25%	25	15	5	45
		30	4%	9%	5%				
SM4	Near cliff at North Point, lichen covered wall, perpendicular to joints	10	2%	20%	18%	18	19	20	57
		30	2%	22%	20%				
SM5	> 10 m from cliff, control site, shallow depression	10	3%	10%	7%	7	5.5	4	16.5
		30	9%	13%	4%				
SM6	> 10 m from cliff, control site, gentle slope	10	2%	14%	12%	12	6	0	18
		30	2%	2%	0%				
SM7	Close to pool, near cliff, perpendicular to joints	10	3%	29%	26%	26	NA	NA	> 26
		30	NA	NA	NA				
SM8	Close to pool, near cliff, perpendicular to joints	10	2%	31%	29%	29	25	21	75
		30	4%	25%	21%				
SM9	Close to cliff, parallel to joints	10	2%	15%	13%	13	6.5	0	19.5
		30	3%	3%	0%				
SM10	Top of cliff, shallow depression	10	2%	20%	18%	18	14.5	11	43.5
		30	4%	15%	11%				
SM11	Close to cliff, under overhang, parallel to joints	10	0%	1%	0%	0.7	0.35	0	1.05
		30	1%	1%	0%				

slower velocities in fractures at North Point compared to those above the pool area.

Further examination of fractures at North Point can help to explain differences in apparent supply volumes to fractures associated with SM3 versus those associated with SM4. The fracture that appears to be in between soil moisture sites SM3 and SM4 (Fig. 12) exists as a fracture in a very small section of rock near the tip of North Point and a section of the cliff just east of the pool. In between these two sections of cliff, the inner wall of this joint is exposed as the cliff face (facing south). The small extent of this joint at North Point greatly limits the amount of precipitation that can be diverted to it and any small fractures to the south that may contribute to soil moisture at SM3. Fractures to the north are more extensive and may be connected to other fractures to the west. These fractures can potentially transport more precipitation that falls on the top of the cliff to the subsurface near the base of the cliff near SM4.

Depletion of water stored in fractures

The fact that apparent fracture flow contributions to soil moisture at SM3 and SM4 changed with time indicates that water stored in sediments that partially fill the fractures can be depleted. Fracture flow in early May for SM4 is indicated by a soil moisture increase at 30-cm depth. Water was apparently depleted from storage within the fractures during the dry period between May and July, as the fracture flow contribution to soil moisture at 30 cm was not apparent in early July when the monsoon season began. Early monsoon rains apparently replenished water being stored in fractures, and the fracture flow contribution to soil moisture was once again observed for precipitation events in late July and early August as significant increases in soil moisture at 30-cm depth. Water in these fractures was apparently depleted fairly quickly with a decrease in the frequency of storms, as we observed a soil moisture response to a storm in late August at 10 cm but not at 30-cm depth. The large storm in late September appears to have refilled the fractures and transported water to the soil at the base of the cliff. This temporal trend in soil moisture was observed for SM3 (the site near the bare wall at North Point) but with much smaller fracture flow contributions to soil moisture for late monsoon rains and the late September event.

After precipitation events, which drive water to percolate downward through sediments that fill fractures, the volume of water that is stored in these sediments is controlled by the water-holding capacity, which is probably similar to that for sediments at the base of the cliff (10 to 20 volume percent). Depletion of this stored water may be due to evaporation from

the sediment surface within the fractures, transpiration by trees that have roots in the fractures, and lateral movement of water into the adjacent sandstone matrix. Evaporation of pore water from sediments will only significantly deplete water from the top 30 cm or so of the fracture-filling sediments. As seen in Figure 4, vegetation is scarce on top of the cliff, limiting the effects of transpiration on the volume of water stored in the fractures. Lateral movement of water into the sandstone matrix is a slow process driven by diffusion due to a water potential gradient.

The apparent depletion of water from storage in fractures was not observed at sites near the pool (SM7 and SM8) where all precipitation events showed fracture-flow contributions to soil moisture. So, why do we see significant depletion of stored water in fractures at North Point and not in fractures near the pool? We think the depletion of water stored in fractures above North Point is mostly due to the lateral movement of water from sediments in fractures through the adjacent sandstone matrix to the surface of the cliff wall. The reason this process may lead to significant depletion of water stored in fractures at North Point and not in fractures above the pool is related to the total storage volume in fractures (smaller water supply to these fractures and smaller, less developed fractures as discussed above), vertical permeability in fractures (lower fracture-flow velocities as discussed above), and the proximity of the stored water to the vertical surface of the cliff wall. Water that moves through the sandstone matrix and reaches the cliff wall surface quickly evaporates. If the stored water is in close proximity to the wall surface, continuous evaporation from the wall surface and near-surface pores may result in a sufficient water potential gradient to transport a large enough volume of water relative to the stored volume to significantly deplete water stored in these fractures during dry and hot periods. Because both sides of the arm of the cliff that forms North Point are essentially fracture faces, diffusive transport of water through the matrix from nearby parallel fractures will draw water to the cliff wall surface. In contrast, diffusive transport of water stored in fractures near the pool moves water into the massive sandstone matrix and not towards the cliff wall surface. Higher evaporation rates on the bare wall surface above SM3 due to more sun exposure compared to the adjacent lichen covered wall help to explain the smaller fracture-flow contribution to soil moisture for SM3 compared to SM4.

CONCLUSIONS

Soil moisture data shows strong evidence that the presence of the cliff affects the amount of water infiltrating into the soil in some areas. At control sites away from the cliff where local precipitation that falls on the surface is the only source of soil moisture, volumetric water content increased at 10-cm depth in response to individual storms with little or no soil moisture response at 30 cm. Total estimated infiltration for a storm in September 2017 at control sites was roughly equal to the total amount of precipitation. In areas near the cliff where the cliff face is perpendicular to the strike of the primary joint system (northeast-southwest), soil moisture increased significantly (by similar magnitudes) at both 10- and 30-cm depth as responses to large storms or groups of storms with total estimated infiltration for the September storm greatly exceeding the total precipitation amount. This additional soil moisture was not observed at sites near the cliff in areas where the cliff face is parallel to joint strike. This additional source of soil moisture observed at sites near the cliff where the cliff wall is perpendicular to the primary joint strike is direct evidence of water moving from the top of the cliff through fractures to unconsolidated sediments at the base of the cliff. Water is stored in the pores of sediment that partially fills fractures. During a precipitation event, water runs off into fractures, increasing hydraulic head in the fractures, causing water to move downward into unconsolidated sediments at the base of the cliff. We observed this fracture flow contribution to soil moisture at two sites near the pool and at two sites near North Point. These data were used to construct the hydrogeologic conceptual model shown in Figure 13.

At North Point, soil moisture was measured at two sites within three meters of each other on either side of a vertical fracture in the cliff that defines a boundary with lichen covering the wall on one side and bare rock and no lichen on the other side. Both sites exhibited evidence for fracture-flow contribution to soil moisture, although to a smaller degree than was observed at sites near the pool. The site adjacent to the wall with lichen showed higher fracture flow contributions to soil moisture than the site near the bare wall. Fracture-flow contributions to soil moisture at both of these sites changed with time, indicating water was being depleted from storage in sediments within the fractures during periods of no precipitation and high temperatures. Storage depletions were not observed at sites near the pool. These apparent depletions from storage in the fractures were observed to be higher for soil near the bare wall. Analysis of fractures in aerial photographs (Figs. 11 and 12) suggests that fracture characteristics (development, size, connectivity, etc.) likely control the amount of water that is stored in fractures and how quickly it moves through the fractures to underlying sediments. Apparent depletions from storage in fractures observed at sites near North Point are likely due to water moving laterally through the sandstone matrix to the nearby surface of the cliff face where it quickly evaporates. Higher evaporation rates on the bare wall due to higher sun exposure causes the observed higher storage depletion rates.

Water moving downward from the cliff top through fractures to the unconsolidated sediments at the base of the cliff is likely an important mechanism by which water ultimately comes in contact with the inscriptions in certain areas. It appears that in some locations, such as the area near the pool, percolation of water through fractures contributes a significant amount of water to the unsaturated soil, and at times of high snow melt or rainfall, these fractures can transmit enough water to develop a shallow perched aquifer in the alluvium. Water may move upward through the sandstone matrix of the cliff by capillary action from the ephemeral water table or from the soil to come in contact with inscriptions. However, the more important mechanism by which water reaches the inscriptions, specifically related to the cliff face on the north side of Inscrip-

tions Rock near North Point, likely involves the movement and storage of water moving in fractures that are close to the wall surface. This water can potentially move slowly through the sandstone matrix mainly driven by capillary action and a water potential gradient resulting from the evaporation of water that reaches the rock surface. Along the arm of the cliff that forms North Point (Fig. 12), fractures are not as well defined and continuous as observed in other areas such as the area above the pool. Water may not be transported downward as easily, and therefore the amount of water that does make it to the bottom of the cliff is insufficient to form an ephemeral perched saturated zone in the alluvium at the base of the cliff. Much of this water may be "trapped "in dead-end fractures in the rock, where it is diffusively transported through the rock matrix to the cliff face. The combination of these processes and lower evaporation rates due the northern aspect and shade by nearby trees likely makes the area on the north side of Inscription Rock more hospitable to lichen that is currently contributing to the deterioration of inscriptions in the area.

ACKNOWLEDGMENTS

We thank the following entities and individuals for their valuable contributions to this project: the University of New Mexico, Colorado Plateau Cooperative Ecosystems Study Unit, the National Park Service (NPS), El Morro National Monument, New Mexico Bureau of Geology and Mineral Resources (New Mexico Tech), Mitzi Frank (NPS, Superintendent, El Malpais and El Morro National Monuments), and Richard Greene (NPS,Branch Chief of Cultural Resources, El Malpais and El Morro National Monuments).

We would also like to thank Angelyn Bass (UNM, project PI) and Doug Porter (University of Vermont) for initiating this collaboration and for providing assistance and guidance for this study. This study would not be possible without the help of Steve Baumann (NPS, Chief of Resources Manager, El Malpais and El Morro National Monuments) and Calvin Chimoni (NPS, Preservation Masonry Specialist, El Malpais and El Morro National Monuments), who spent many hours working with local tribes and other stakeholders to obtain permission to work on the Monument. We also appreciate their assistance with many of our experiments for this study. We thank Ellen Soles (NPS) and Steve Monroe (formerly from NPS) for adjusting the measurement frequency for data loggers in piezometers to accommodate our study needs. We also thank NMBGMR Aquifer Mapping Program team members, including Stacy Timmons, Dr. Trevor Kludt, Scott Christenson, Kitty Pokorny, Brigitte Felix, and Kylian Robinson (currently at Hydrofluency, Taos, NM) for their help on fieldwork, data management, and report preparation. And a big thank you to Dr. Jan Hendrickx (NM Tech) and Dr. Geoffery Rawling (NMBGMR) for their very helpful reviews of this paper.

REFERENCES

Al-Shammary, A.A.G., Kouzani, A.Z., Kaynak, A., Khoo, S.Y., Norton, M., and Gates, W., 2018, Soil Bulk Density Estimation Methods: A Review: Pedoshpere, v. 28, no. 4, p. 581-596, ISSN 1002-0160/CN 32-1315/P.

Burris, C.A., 2007, The analysis of sandstone deterioration at the northeast point of Inscription Rock at El Morro National Monument, [M.S. thesis]: Philadelphia, University of Pennsylvania, 174 p.

Cross, A., 1996, Stratigraphy, sedimentology, and surface water quality at El Morro National Monument: Report prepared for the National Park Service, 104 p.

Hendrickx, J.M.H., and Flury, M., 2001, Uniform and preferential flow mechanisms in the vadose zone, *in* Feary, D.A., ed., Conceptual models of flow and transport in the fractured vadose zone: Washington, D.C., National Research Council, National Academy Press, p. 149-187.

Monroe, S.A., and Soles, E.S., 2015, Hydrologic monitoring in El Morro National Monument Water Years 2012 through 2014: Natural Resource Data Series NPS/SCPN/NRDS – 2015/805, 10 p.

Newton, B.T., and Kelley, S., 2019, Hydrogeologic Investigation at El Morro National Monument: New Mexico Bureau of Geology and Mineral Resources, Report submitted to University of New Mexico, 68 p.

NMBGMR, 2003, Geologic Map of New Mexico: New Mexico Bureau of Geology and Mineral Resources, scale 1:500,000.

Padgett, A., 1992, Assessment of deteriorative factors affecting the inscriptions, El Morro National Monument, New Mexico with recommendations for their preservation: Santa Fe, Report to the National Park Service, Southwest Regional Office, 47 p.

Pranger, H., 2002, Trip Report - May 29, 2001 - site visit and technical report - Hydrogeology and geology of Inscription Rock and site management recommendations, El Morro National Monument (ELMO): Denver, Memorandum to the Superintendent, El Morro National Monument. National Park Service, Geologic Resources Division, 15 p.

Salas, D., and Bolen, C., 2010, Vegetation classification and distribution mapping report, El Morro National Monument: Fort Collins, Natural Resource Technical Report. NPS/SCPN/NRTR–2010/365, National Park Service, 122 p.

Soles, E.S., and Monroe, S.A., 2012, Hydrologic Monitoring for the Historic Pool in El Morro National Monument: 2010–2011 summary report: Fort Collins, Natural Resource Data Series NPS/SCPN/NRDS—2012/356. National Park Service, 17 p.

St. Clair, L.L., and Knight, K.B., 2001, Impact of microflora (lichens) on the condition of the sandstone and inscriptions at El Morro National Monument, Ramah, New Mexico: Ramah, Final Report submitted to National Park Service, 22 p.

Van Dam, R.L.V., and Hendrickx, J.M.H., 2007, Hydrological investigation at El Morro National Monument: New Mexico Institute of Mining and Technology, Final Report-664176 to National Park Service, 46 p.

West, S.W., and Baldwin, H.L., 1965, The water supply of El Morro National Monument: U.S. Geological Survey, Water-Supply Paper 1766, 32 p.

Appendices can be found at http://nmgs.nmt.edu/repository/index.cfml?rid=2020006

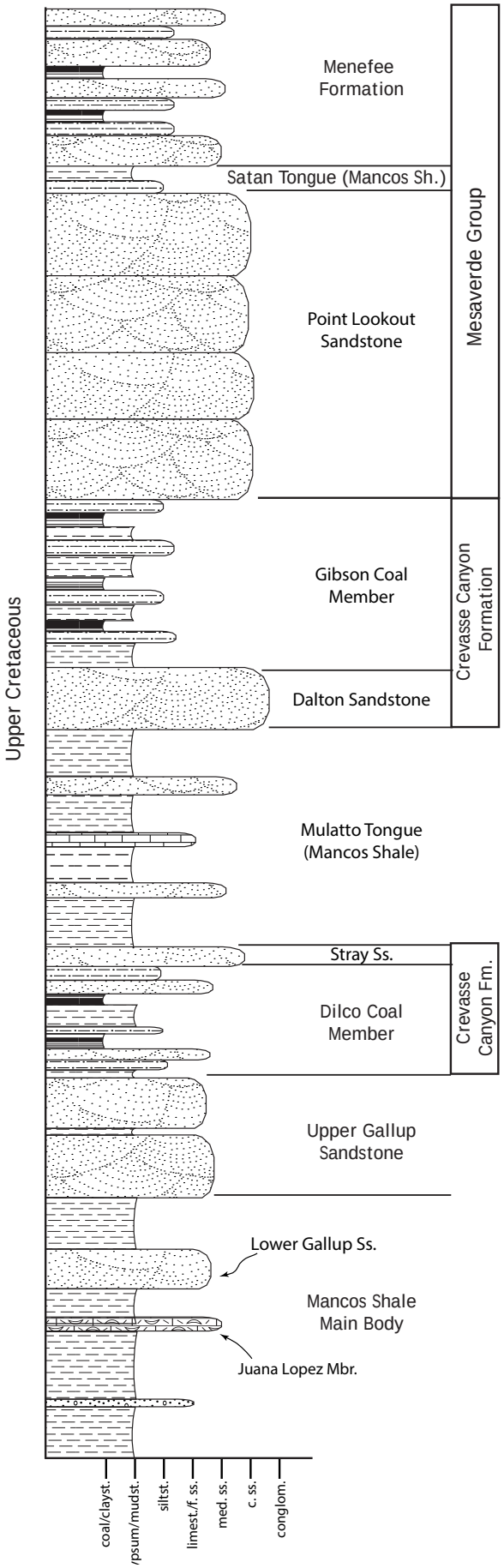

Composite Schematic Stratigraphic Column For the Mesozoic of the Mount Taylor Area

K.E. Zeigler

Compiled and modified from: Molenaar (1983, 1989), Ferguson and McCraw (2010), Cather (2011), Dickinson (2018), Cather (2020).

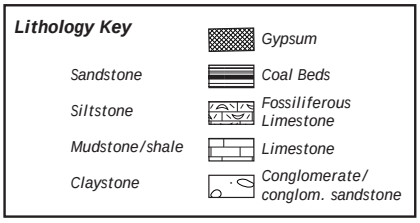

30.5 m
(100 ft)

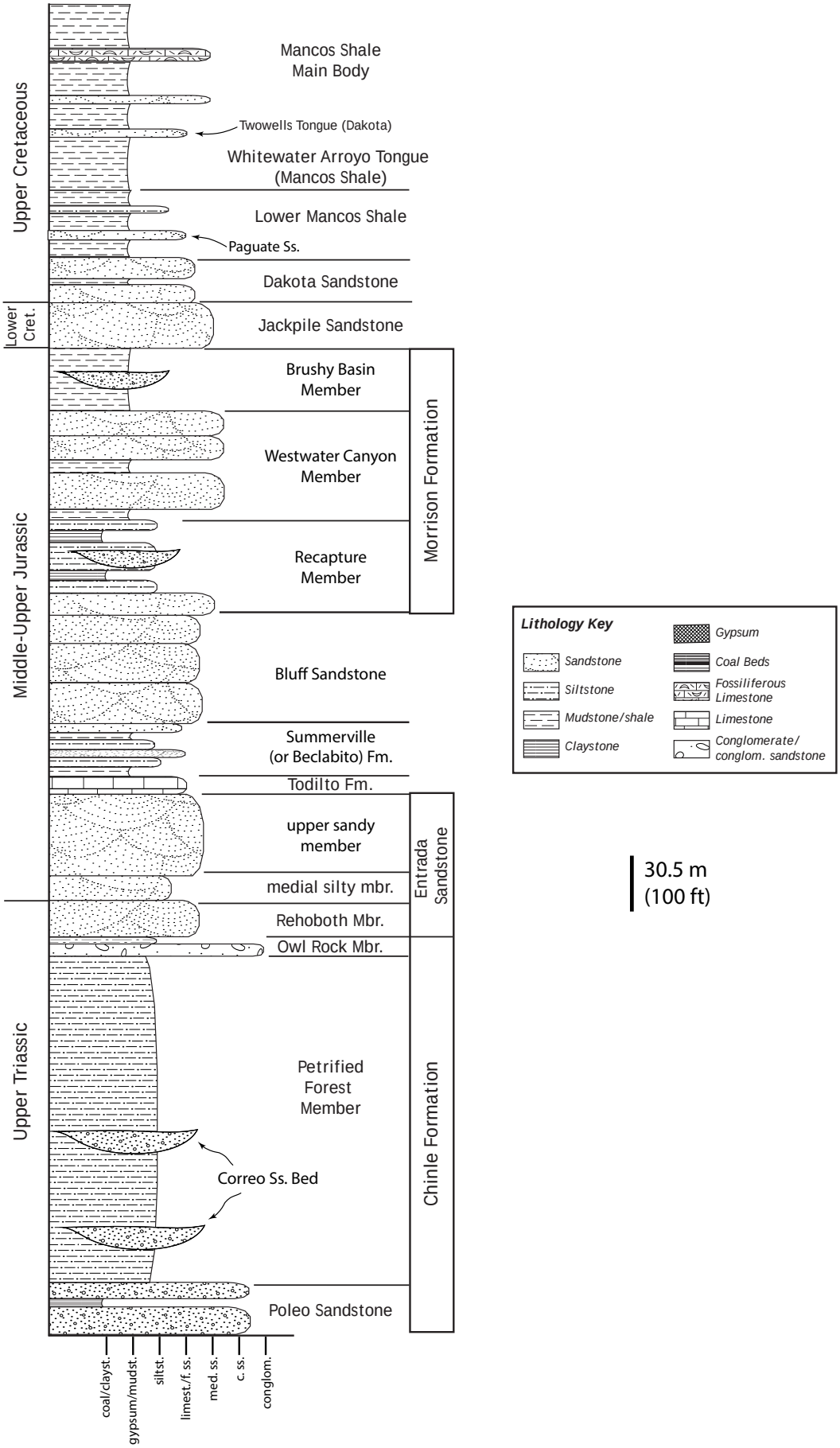
Upper Cretaceous
Middle-Upper Jurassic
Upper Triassic
Lower Cret.
Mancos Shale Main Body
Twowells Tongue (Dakota)
Whitewater Arroyo Tongue (Mancos Shale)
Lower Mancos Shale
Paguate Ss.
Dakota Sandstone
Jackpile Sandstone
Brushy Basin Member
Westwater Canyon Member
Recapture Member
Morrison Formation
Bluff Sandstone
Summerville (or Beclabito) Fm.
Todilto Fm.
upper sandy member
medial silty mbr.
Rehoboth Mbr.
Entrada Sandstone
Owl Rock Mbr.
Petrified Forest Member
Correo Ss. Bed
Chinle Formation
Poleo Sandstone
coal/clayst.
gypsum/mudst.
siltst.
limest./f. ss.
med. ss.
c. ss.
conglom.
Lithology Key
Sandstone
Siltstone
Mudstone/shale
Claystone
Gypsum
Coal Beds
Fossiliferous Limestone
Limestone
Conglomerate/ conglom. sandstone
30.5 m
(100 ft)

The Mount Taylor area occupies a crossroad where geologic history, human history, and societal impacts intersect. Situated on the eastern edge of the Colorado Plateau and flanking the transition zone to the Rio Grande rift, Mount Taylor is a late Pliocene stratovolcano located on the Jemez Lineament, an enigmatic NE-trending alignment of late Cenozoic volcanic centers. Mount Taylor lies along the southeast margin of the San Juan Basin bounded by the Zuni (south) and Nacimiento (east) uplifts. Mount Taylor also has some of the richest uranium deposits in the United States.

The human history of the Mount Taylor region is no less compelling. Indigenous communities lived here for thousands of years despite Spanish conquest and the establishment of land grants. In the 1800s, settlement of this U.S. territory came, as did the railroad and timber industries, and later the uranium boom and its lasting legacy. Corridors of commerce opened with Route 66, succeeded by Interstate 40. The designation of Mount Taylor as a Traditional Cultural Property recognizes the mountain's importance to Native, Spanish and U.S. cultures.

The papers in this online volume, NMGS Special Publication 14, were written for the 2020 NMGS fall field conference guidebook. The field conference was postponed to 2021, due to the Covid-19 pandemic. The papers in this volume cover a spectrum of topics, ranging from geologic studies and mining history to the effects of mining on the population and the environment today.

NMGS Special Publication 14

These volumes provide a comprehensive library of geologic literature for New Mexico.